Aspects of the Biogenesis of Cytochrome c Oxidase in Human Cells

PhD Thesis

Siôn Llewelyn Williams

Royal Free and University College Medical School,
University College London, 2004.

ProQuest LLC
789 East Eisenhower Parkway
P.O. Box 1346
Ann Arbor, MI 48106-1346

ACADEMIC REGISTRAR
ROOM 261
UNIVERSITY OF LONDON
SENATE HOUSE
MALET STREET
LONDON WC1E 7HU

For Taid and Nain, Grandma and Granddad, Eluned, Auntie Winnie and Sparky.

ACKNOWLEDGEMENTS

Thanks to my supervisors Jan-Willem Taanman and Tony Schapira and also Mark Cooper for their guidance and support. Special thanks to Michelle Smith, Kate Holden-Dye, Hannah Tucker and Cassy Williams for keeping me going and to my brothers and Martin & the boys for getting me to stop occasionally. Extra special thanks are due to my parents, Prasad "the disco" and Seema without whose selfless support, assistance and encouragement this thesis would never have been written.

ABSTRACT

Cytochrome c oxidase (COX) is a component of the mitochondrial oxidative phosphorylation system (OXPHOS) which is the principal source of ATP for the majority of human tissues. The COX holo-complex is a homodimer of 13 different subunits, encoded by both the nuclear and mitochondrial genomes (mtDNA), and contains metal ions and haem A prosthetic groups. Disrupted biogenesis of the holo-complex is the most common cause of COX deficiency. As genetic manipulation of human cells is difficult, cells derived from patients with COX deficiency provide a valuable resource for improving our understanding of COX biogenesis and COX deficiency.

This thesis is a comparative study of COX deficient fibroblasts derived from seven patients with mitochondrial disorders of undetermined genetic origin, normal controls and disease controls carrying mutations in mitochondrial tRNA genes or the COX assembly factors *SCO1* and *COX10*. The project was designed to answer two questions:

i) What are the molecular mechanisms behind the enzyme deficiency in the patient cells?
ii) What can this tell us about the biogenesis of the COX holo-complex?

Phenotyping of the cultures revealed distinct patterns of OXPHOS subunit expression and confirmed that the COX defects were caused by disrupted biogenesis of the holo-complex. Genotyping excluded the involvement of mtDNA and sequencing of the COX assembly factor *SURF1* identified mutations in four of the patients. Blue-native polyacrylamide gel electrophoresis found that COX sub-complexes, which resembled known assembly intermediates, accumulated in *SURF1* and *SCO1* mutant cells but not those with *COX10* mutations. This suggests that SURF1 and SCO1 function at a similar point in COX biogenesis and supports the view that COX10 functions early in COX assembly. The results are discussed in the context of our current understanding of COX biogenesis and the causes of COX deficiency with emphasis on the molecular pathology of *SURF1* mutant cells.

TABLE OF CONTENTS

TABLES

FIGURES

ABBREVIATIONS

aA	amino acid
bp	base pair
CES	control by epistasis of synthesis
CSF	cerebrospinal fluid
LDH	lactate dehydrogenase
LM	lauryl-maltoside
mRNP	mRNA-ribonucleoprotein
MSR	mitochondrial stress response
NMD	non-sense mediated decay
nt	nucleotide
PDH	pyruvate dehydrogenase
RNC	ribosome-mRNP complex
ROS	reactive oxygen species
RRF	ragged-red fibres
UTR	untranslated region

HUGO Gene Nomenclature Committee (HGNC) gene names have been used throughout. Proteins are given in uppercase and genes or mRNAs in uppercase italics, e.g. "levels of COX4I1" refers to the levels of COX4I1 protein and "expression of *COX4I1*" refers to the expression of *COX4I1* mRNA. Yeast genes expressed on plasmids are given in square brackets. Components of protein complexes are separated by dots but the order the proteins are listed in does not necessarily infer direct binding, e.g. MTCO1•COX4I1 denotes a protien complex containing MTCO1 and COX4I1.

INTRODUCTION

PREFACE

This thesis deals with the biogenesis of cytochrome c oxidase (COX) and how disruption of this process leads to COX deficiency. To place COX in a functional context, Section 1 describes the OXPHOS. Section 2 provides an overview of the structure and function of human COX. The biogenesis of COX is absolutely dependent on mtDNA gene expression and mitochondrial protein import and these are covered in Sections 3 and 4. What is known of the assembly of the COX holo-complex is covered in Section 5 along with a description of *control by epistasis of synthesis* as a model of protein-complex assembly. Finally, the causes and incidence of COX deficiency are covered in Section 6.

1 THE OXIDATIVE PHOSPHORYLATION SYSTEM (OXPHOS)

Mitochondria are the major metabolic organelles of eukaryotic cells. Processes which depend upon them include amino acid synthesis, dNTP synthesis, haem synthesis, Fe-S synthesis, lipid synthesis and steroid synthesis. In addition they are involved in apoptotic signalling cascades and Ca^{2+} signalling. One of the most important functions of mitochondria is the synthesis of ATP via an aerobic process called oxidative phosphorylation which is the major source of ATP for most human cell types. Oxidative phosphorylation describes the coupling of electron transfer, from NADH and $FADH_2$ to O_2, with the phosphorylation of ADP to generate ATP. The oxidative phosphorylation system (OXPHOS), which carries out this function, is defined as a series of five integral inner-membrane enzyme complexes and two associated mobile electron carriers (table 1). Under the strictest definition of the OXPHOS, electrons enter from either the matrix pool of NADH via complex I or from the tricarboxylic acid cycle (TCA) via complex II-bound $FADH_2$[1] (figures 1A & 1B). They are then transferred through the redox centres of these complexes to free co-enzyme Q in the mitochondrial inner membrane. Complex III accepts electrons from reduced co-enzyme Q (QH_2) and transfers them to free cytochrome c in the IMS. The oxidation of reduced co-enzyme Q in the inner-membrane is dependent on complex III which couples this activity to proton pumping as part of the *Q-cycle*[1,2]. Cytochrome c oxidase (COX, complex IV) oxidises reduced cytochrome c at

its IMS face and in the final electron transfer step, transfers electrons to O_2 forming H_2O. The phosphorylation of ADP is coupled to the electron transfer chain via a chemiosmotic proton circuit[3]. The free energy (ΔG) of exergonic electron transfer between redox centres within complexes I, III, and COX is harnessed to pump protons "uphill" out of the mitochondrial matrix creating a proton gradient (ΔpH) across the inner membrane. In the physiological environment of the cell, this creates an proton-electrochemical gradient across the inner-membrane ($\Delta\tilde{\mu}_{H+}$). The electrical potential across the inner-membrane ($\Delta\psi$) which is a component of $\Delta\tilde{\mu}_{H+}$ drives complex V[4] that acts as a conduit to allow proton flow "downhill" back into the matrix. The energy released by the dissipation of $\Delta\tilde{\mu}_{H+}$ is harnessed by complex V to synthesise ATP from ADP and P_i.

Table 1 Components of the OXPHOS.

Complex	Enzyme name and EC* number	Respiratory chain redox centres
Complex I	NADH dehydrogenase (EC 1.6.5.3)	FMN, 6-8[Fe-S] centres
Complex II	Succinate dehydrogenase (EC 1.3.99.1)	FAD, 3[Fe-S] centres
Complex III	Ubiquinol-cytochrome c oxidoreductase (EC 1.10.2.2)	2 haem B, Rieske Fe-S centre, haem C
Complex IV	Cytochrome-*c* oxidase (EC 1.9.3.1)	2 haem A, 2 copper centres
Complex V	F_1F_o-ATP synthase (EC 3.6.1.34)	---

Mobile carrier	Location	Respiratory chain redox centre
Co-enzyme Q	Mitochondrial inner membrane	Quinoid
Cytochrome c	Intermembrane space (IMS)	Haem C

Key: * Enzyme Commission (International Union of Biochemistry)

The first four complexes and the mobile electron carriers of the OXPHOS constitute the *respiratory chain*[1]. This is a chain of around 20 redox centres distributed between the various components which transfer electrons from reducing equivalents to O_2. The redox centres of the respiratory chain can be divided into two groups i) quinoid structures such as protein-bound FMN and FAD moieties and co-enzyme Q, and ii) transition metal complexes such as haems A, B and C, iron-sulphur clusters and copper ions. The direction of transfer of electrons through the respiratory chain is determined by the overall difference in redox potential between centres and the movement of electrons from one centre to another is described by an aspect of quantum mechanics called *electron tunnelling*[5]. An important consequence of electron tunnelling in terms of OXPHOS structure, is that the distance travelled between redox centres is always less than 14 Å. At distances greater than this, electron transfer rapidly becomes too slow to sustain the physiological redox reactions which donate electrons to the respiratory chain. Electron tunnelling is more or less impervious to changes in the intervening protein

Figure 1A

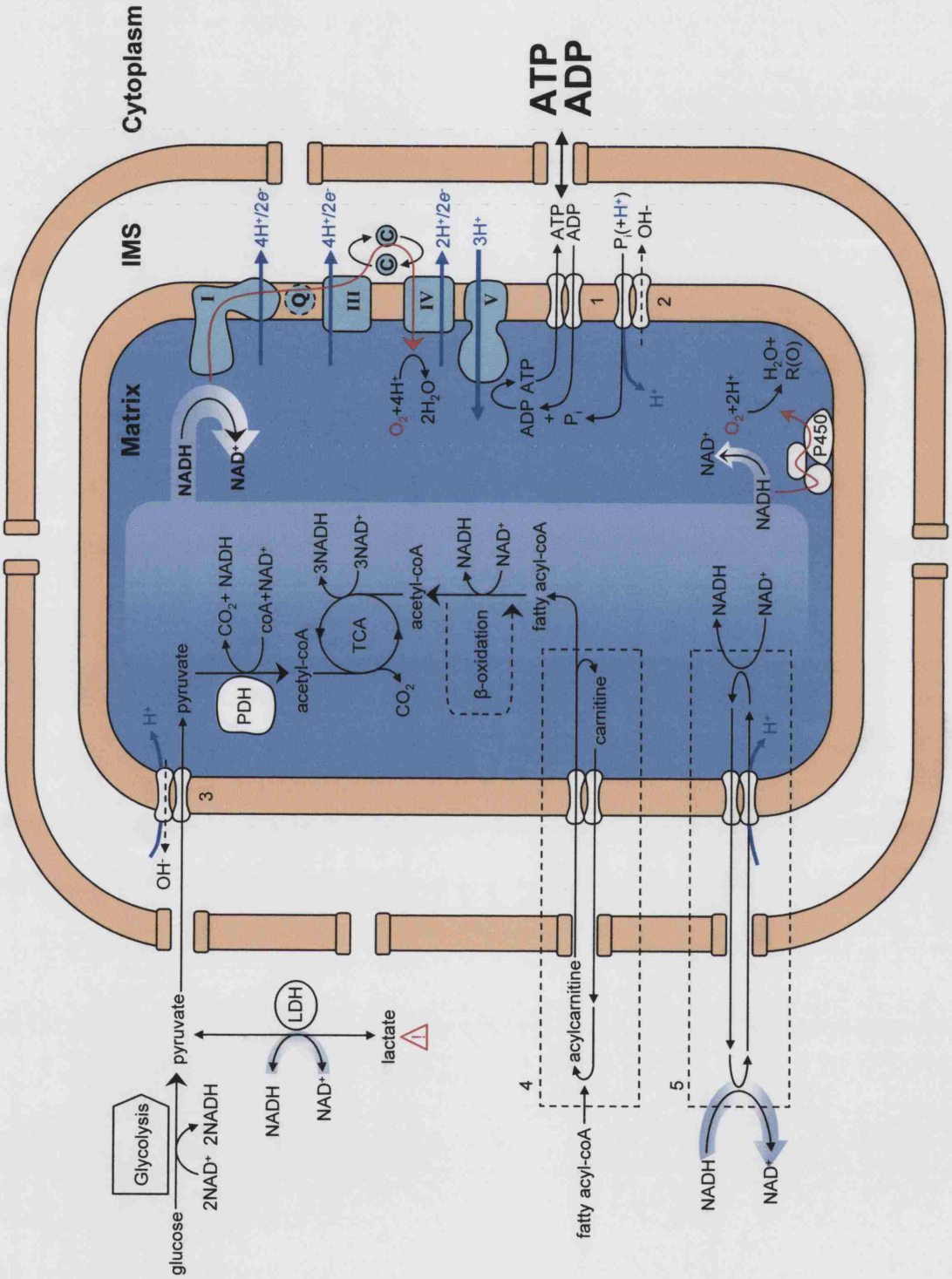
Cytoplasm
IMS
Matrix
ATP
ADP
4H+/2e-
2H+/2e-
3H+
I
III
IV
V
Q
C
1
2
3
4
5
NADH
NAD+
O2+4H+
2H2O
ADP ATP
+
Pi
Pi(+H+)
OH-
H+
O2+2H+
H2O+
R(O)
P450
pyruvate
PDH
CO2+ NADH
coA+NAD+
acetyl-coA
TCA
3NADH
3NAD+
CO2
β-oxidation
fatty acyl-coA
carnitine
acylcarnitine
Glycolysis
glucose
2NAD+ 2NADH
LDH
lactate

Figure 1A The principal sources of NADH supplying electrons to the OXPHOS via complex I. Components of the OXPHOS are coloured pale green and denoted using Roman numerals; C, is cytochrome-c; Q, represents co-enzyme Q and the Q-cycle. The metabolite-permeant outer-membrane and impermeable inner-membrane are coloured orange and the matrix in blue. Important membrane translocases and shuttles are numbered as follows: 1, adenine nucleotide transporter (ANT); 2, phosphate carrier (P_iC); 3, pyruvate carrier; 4, carnitine shuttle; 5, malate-aspartate shuttle -simplified to a single cycle. Electron transfer from NADH to O_2 is shown in red. Proton pumping out of the matrix by complexes I, III and COX is shown in blue as is proton flow into the matrix via complex V and proton symport by 2, 3 and 5. Important cytosolic sites of NADH oxidation are highlighted in blue. Mitochondrial P450 systems are denoted in the bottom of the figure, representing a form of non-respiratory oxygen consumption and a minor source of NAD^+. Abbreviations: PDH, pyruvate dehydrogenase complex; LDH, lactate dehydrogenase complex; TCA, tricarboxylic acid cycle; β-oxidation, mitochondrial β-oxidation pathway; co-A, co-enzyme-A.

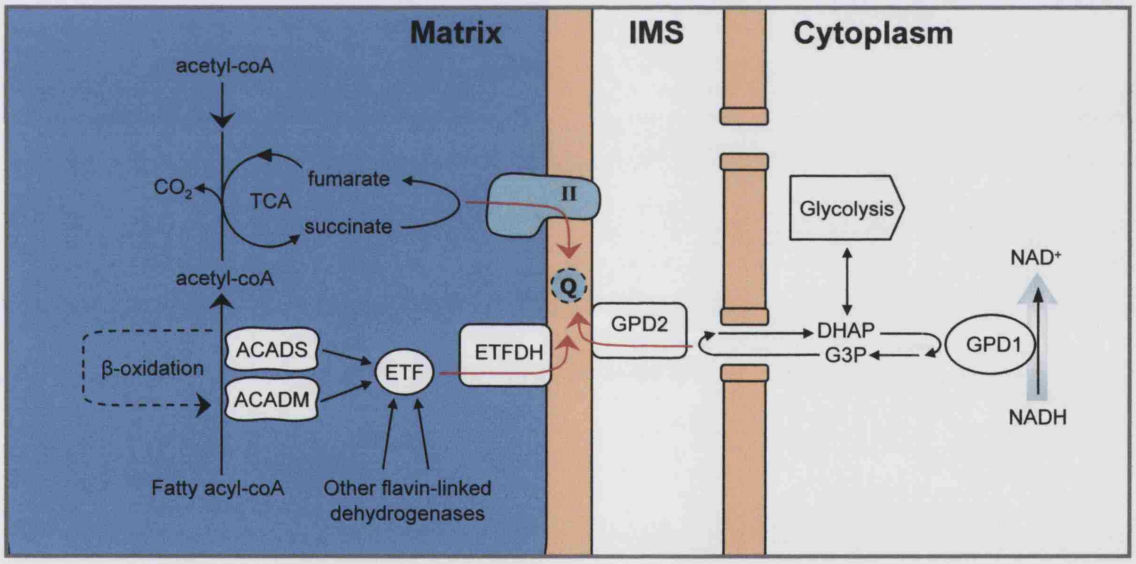

Figure 1B Pathways of electron entry into the OXPHOS from FAD-linked sources. Colouring is as in figure 1A. Pathways of electron transfer from FAD to co-enzyme Q are shown in red. Cytosolic NADH oxidation by the glycerol phosphate shuttle is highlighted in blue. HGNC names: ACADM, medium-chain Acyl-coA dehydrogenase; ACADS, short-chain acyl-coA dehydrogenase; EFT, electron transferring flavoprotein; ETFDH, electron transferring flavoprotein:quinol-oxidoreductase; GPD2, mitochondrial glycerol-3-phosphate dehydrogenase; GPD1, soluble glycerol-3-phosphate dehydrogenase. Chemical abbreviations: DHAP, dihydroxyacetone phosphate; G3P, glycerol-3-phosphate.

structures. Hence this "evolution tolerant" phenomenon has provided a rugged platform for the diversification of electron transfer systems[5].

The classical five complex definition of the OXPHOS is very much a product of the research style of the 70s and 80s, the object of which was the fragmentation and subsequent reconstruction of the minimum inner-membrane components of electron transfer and ATP-synthesis. It provides an incomplete picture of electron transfer *in vivo* and fails to take into account physiologically relevant associations between complexes. Although complex II is the only FAD-linked source of electrons in the classical definition of the OXPHOS, there are two other FAD-linked enzymes which transfer electrons to co-enzyme Q (figure 1B). These are the electron-transfer flavoprotein dehydrogenase[1] (*ETFDH*; 1.1) and the mitochondrial glycerol-phosphate dehydrogenase (*GPD2*), which is part of the glycerol phosphate shuttle (1.2).

1.1 TRANSFER OF ELECTRONS FROM ETF

ETFDH is a 64 kDa protein that localises to the matrix face of the inner membrane. It contains an FAD and an Fe-S cluster redox centres[6] and accepts electrons from a free heterodimeric complex called the electron-transfer flavoprotein (ETF; *ETFA*, *ETFB*). ETF is also FAD-linked and accepts electrons from at least nine FAD-linked dehydrogenases found in the matrix[7]. The most notable of these are the medium and short-chain acyl-coA dehydrogenases involved in β-oxidation (*ACADM*, *ACADS*). As each round of the mitochondrial β-oxidation cycle[8] results in the production of one NADH which is oxidised by complex I and an ETF-linked $FADH_2$, ETFDH is a very significant source of electrons for the OXPHOS. This is especially true in tissues such as cardiac muscle where β-oxidation is a major source of energy[9].

1.2 MAINTENANCE OF THE CYTOPLASMIC NAD^+/NADH POOL

NADH generated from glycolysis and other cytosolic pathways cannot be oxidised directly by complex I because the matrix NAD^+/NADH pool is distinct from the cytosolic pool and there are no mechanisms for transport of NADH across the mitochondrial inner membrane[10]. Two mechanisms exist for maintaining cytosolic NAD^+/NADH ratios via electron transfer to the OXPHOS; the malate-aspartate shuttle and the glycerol-phosphate shuttle, both of which are linked to glycolysis. The malate-aspartate shuttle is a complex system composed of a pair of substrate-linked inner-membrane antiporters,

the α-ketoglutarate/malate antiporter and the aspartate/glutamate antiporter[11] (figure 1A). Cytosolic and mitochondrial forms of malate dehydrogenase and aspartate-amino transferase complete two interlinked cycles of oxidation and reduction resulting the recycling of NAD^+ in the cytosol and oxidation of NADH in the matrix. The glycerol-phosphate shuttle transfers electrons from cytosolic NADH to the respiratory chain at co-enzyme Q[11] (figure 1B). The shuttle is composed of two glycerol phosphate dehydrogenases, one cytosolic (*GPD1*) and another on the outer-face of the inner-membrane (*GPD2*). In most tissues, including brain, liver, skeletal and cardiac muscle, the glycerol-phosphate shuttle does not play an essential role in ATP synthesis[12,13]. In these tissues the malate-aspartate shuttle is the predominant mechanism for maintaining cytosolic NAD^+/NADH ratios.

1.3 MOLECULAR ORGANISATION OF THE OXPHOS

The mitochondrial matrix is extremely protein rich[14], containing an estimated 800 mg of protein per ml. Such a crowded molecular environment tends to stabilise protein associations and decrease the effectiveness of diffusion in protein-protein interactions[15-18]. Large associations between OXPHOS complexes and associations between OXPHOS complexes and matrix enzymes have both been identified.

1.3.1 Matrix enzyme associations

Saturable and specific binding of the PDH complex, NAD^+-linked dehydrogenases from the TCA cycle and the malate-aspartate shuttle to complex I have been demonstrated using extracts of pig heart mitochondria[19]. Similarly, the saturable binding of enzymes from β-oxidation to pig heart mitochondrial inner-membrane has also been demonstrated[20]. Binding between redox enzymes and the OXPHOS is believed to increase the kinetics of enzyme turnover by improving the rate of re-oxidation of NADH and $FADH_2$. This is supported by experiments examining the disruption of mitochondria on the turnover of enzymes involved in β-oxidation[21]. Biochemical and immunological analysis of ETF-containing complexes isolated using DEAE-cellulose chromatography has tentatively identified ACADM•ETF•ETFDH•III* and ETF•ETFDH•II•III complexes[22]. The ACADM complex clearly fits the electron transfer pathway from β-oxidation to cytochrome-c (figure 1B).

---

* Roman numerals denote respective OXPHOS complexes.

1.3.2 OXPHOS super-complexes

From the early work on the OXPHOS based on a *solid state* model, supported by some biochemical studies[23], the view of the OXPHOS has shifted to a *liquid state* model where individual complexes moved freely in the plane of the inner-membrane independently. This view in turn has now been challenged by a *partially solid state* model supported by the existence of OXPHOS super-complexes composed of multiple OXPHOS complexes. OXPHOS super-complexes have been identified in bacterial[24-26], yeast[27,28], plant[29] and mammalian[28,30] systems.

OXPHOS super-complexes have been primarily characterised using blue-native poly-acrylamide gel electrophoresis (BN-PAGE), a technique suited to the resolution of membrane protein complexes[31-34]. As with all native separation techniques, the degree of disruption of samples influences the associations observed. Using BN-PAGE, all complexes with the exception of complex III, can be isolated as intact functional monomers using high detergent concentrations[35,36]. Intermediate solubilisation conditions enable the isolation of super-complexes containing variable ratios of the OXPHOS complexes. By examining the spectrum of super-complexes isolated under different conditions and using a ratio of OXPHOS complexes[30] of 1:1½:3:6:3 (I:II:III:IV:V), two major classes of OXPHOS super-complex have been proposed to exist in bovine heart samples under steady-state conditions, $I•III_2•IV_4$ and $III_2•IV_4$[36]. They are thought to be present at a ratio of 2:1[36]. As with the matrix enzyme associations described above, OXPHOS super-complexes match electron transfer pathways of the OXPHOS, $I•III_2•IV_4$ being sufficient for the entire electron transfer from matrix NADH to O_2 and $III_2•IV_4$ from the co-enzyme Q to O_2. No super-complexes containing either complex II or complex V have been identified in any organisms using BN-PAGE[36] and while $I•III_2$ and $I_2•III_4$ have been identified in plants they do not contain COX[29]. The stabilisation of yeast OXPHOS super-complexes requires cardiolipin[37,38] although super-complexes can still assemble in its absence[38]. Given that III•IV-type complexes have been isolated from bacteria which do not have homologues of the mammalian nuclear-encoded subunits[24-26] there is speculation that binding between complex III and COX may be a feature of the core subunits of each complex[38]. Furthermore, in yeast deletion strains, super-complex formation is not dependent on the presence of exposed subunits from complex III[27], cytochrome c nor COX[38*]. Supercomplexes may also play a role in stabilising constituent OXPHOS complexes as complex I appears to be stabilised by the formation of super-

---

* Human homologues complex III: UQCRFS1, UQRCH, HSPC051 and UQCR; COX: COX8A, COX6B and COX6A1.

complexes in *Paracoccus denitrificans*[26] and human cells[41]. There is also evidence that mutations affecting the stability of complex III impact on the stability of complex I in human and murine cells[860], an observation that can be explained by a failure to assemble stable supercomplexes.

1.3.2.1 Substrate channelling and respirasomes

Given the theoretical and empirical of evidence for the existence of both matrix enzyme associations and OXPHOS super-complexes, it seems very likely that *in vivo,* massive *respirasomes* composed of both types of association exist. A function of respirasomes may be to enable tight substrate channelling between the component enzymes. In yeast neither cytochrome-c nor co-enzyme Q exhibit pool behaviour providing evidence for tight substrate channelling[39]. Biochemical evidence also exists for substrate channelling in mammalian systems between β-oxidation and the OXPHOS[21] and between complex I and complex III but not complex III and COX[40].

2 HUMAN CYTOCHROME C OXIDASE

Cytochrome-c oxidase[1] (COX) is the terminal component of the OXPHOS respiratory chain (figure 1A). It is a member of the haem-copper terminal oxidase superfamily that are present in all aerobic organisms. COX catalyses the transfer of electrons from cytochrome-c to O_2, producing H_2O. The overall reaction of the enzyme is:

$$4\ \text{cyt-c}(Fe^{2+}) + O_2 + 8H^+_{(matrix)} \rightarrow 4\ \text{cyt-c}(Fe^{3+}) + H_2O + 4H^+_{(IMS)}$$

where cyt-c is cytochrome-c. Unlike the majority of the electron transfer events in the OXPHOS, this reaction is irreversible[42] and as such serves, in part, to maintain the overall directionality of transfer by clearing electrons from one end of the system.

2.1 BASIC STRUCTURE

The human COX holo-complex is a homodimer of two 13-subunit heteromers each with a total M_r of ~205 kDa[43] (figures 2A & 2B). Each monomer is composed of three mtDNA-encoded subunits and ten nuclear-encoded subunits (table 2) and contains two haem A moieties, haem-a and haem-a_3, two copper centres, CuA and CuB, a magnesium ion, a sodium ion, a zinc ion and two cardiolipin molecules. As with the other OXPHOS enzyme

complexes, comparison of COX crystal structures and biochemical evidence has demonstrated a high degree of conservation between enzymes from different organisms[44]. The following description is based on data from crystal structures of bovine and bovine-human chimeric* enzymes[45-48] that are good models of the human enzyme.

The core of each monomer is made up of single copies of each of the three mtDNA-encoded subunits MTCO1, MTCO2 and MTCO3. MTCO1 is composed of 12 membrane spanning helices, the peptide backbones of which are arranged in three arcs. When viewed along an axis perpendicular to the inner membrane, the space between these arcs forms three pores which enclose the majority of the functional side chains of the protein (figure 3B and tables 3A & 3B). Pore A contains the side-chains and trapped water molecules which form the D-channel, involved in proton translocation (2.3). A second proton conducting channel, the K-channel (2.3), is located in pore B which also contains the haem-a_3-CuB binuclear centre and a magnesium ion coordinated by ligands both from MTCO1 and MTCO2. Pore C contains haem-a and a sodium ion, residues adjacent to which form the putative proton exit channel termed the H-channel (2.3). Crystal structures have revealed a covalent bond between Tyr244 at the top of the K-channel, and His240, one of the ligands of CuB. This is believed to be involved the catalytic activity of the enzyme[49]. MTCO2 is composed of a C-terminal β-barrel bound to the IMS face of MTCO1, and two N-terminal helices which are embedded in the inner-membrane contacting the side of MTCO1. The β-barrel domain of MTCO2 encloses the two copper ions of the binuclear CuA centre and the IMS-exposed face of MTCO2 forms the majority of the cytochrome c binding-patch. The ligand provided by MTCO2 for the magnesium ion is adjacent to those which coordinate the CuA centre (table 3). MTCO3 also binds MTCO1 but has only minimal contact with MTCO2. It has 7 membrane spanning helices which are connected by short loops and no major extra-membrane regions. MTCO3 does not contain any prosthetic groups.

The ten nuclear-encoded subunits form a "cage" around the core of each monomer, binding to the IMS, matrix and membrane-exposed faces of the mtDNA-encoded proteins† (figure 2A & table 2). COX6B binds the IMS face of each monomer and there are extensive contacts between the COX6B subunits of each monomer in the holo-complex. COX6A1 also makes contact between the intermembrane regions of both monomers. Biochemical as well as crystallographic studies have shown that these two

---

* Cytochrome c oxidase purified from HeLa cells expressing bovine MTCO1.
† As this thesis is based on observations of human fibroblast COX, ubiquitously expressed isoforms of the nucelar subunits have be discussed (2.5).

subunits contribute to the association between the monomers[50]. COX5A and COX5B bind to the matrix face of the complex and do not have any membrane integral domains. A zinc ion is coordinated by COX5B but it is not believed to be involved in the catalytic activity of the enzyme. The remaining nuclear-encoded subunits, COX4I1, COX7A2, COX7B, COX7C and COX8, bind to the exposed face of each monomer, each forming a single inner membrane-spanning helix. The location of the cardiolipin molecules within the holo-enzyme remains to be determined although chemical labelling studies place the hydrocarbon tails in contact with either COX7A2, COX7B, COX7C or COX8[51].

Table 2 Reference table of COX subunits.

Subunit	M_r (kDa)	Description and location	Mitochondrial localisation signal	Membrane topology
MTCO1	57.0	12 membrane spanning α-helices [hemes a and a_3, CuB (Cu^{2+}), Na^{2+}, *Mg^{2+}]	--	N_{matrix}-C_{matrix}
MTCO2	25.6	2 membrane spanning α-helices, β-barrel IMS domain [CuA ($2Cu^{1.5+}$), *Mg^{2+}]	--	N_{IMS}-C_{IMS}
MTCO3	30.0	7 membrane spanning α-helices.	--	N_{matrix}-C_{matrix}
COX4I1	17.2	Single membrane spanning α-helix, short IMS and matrix domains.	N-terminal, 22aA	N_{matrix}-C_{IMS}
COX4I2	20.0	Assumed similar to above, putative internal S-S bond.	N-terminal, unknown	N_{matrix}-C_{IMS}
COX5A	12.5	4 α-helix bundle, matrix face.	N-terminal , 41aA	-
COX5B	10.6	Globular, matrix face. [Zn^{2+}]	N-terminal , 31aA	-
COX6A1	9.5	Single membrane spanning α-helix.	N-terminal, 12aA	N_{matrix}-C_{IMS}
COX6A2	9.6	Single membrane spanning α-helix.	internal	N_{matrix}-C_{IMS}
COX6B	10.1	3 α-helix bundle, IMS face.	internal	-
COXVIB2	10.5	Assumed similar to above	assumed internal	-
COX6C	8.6	Single membrane spanning α-helix.	uncleaved N-terminal helix	N_{matrix}-C_{IMS}
COX7A1	6.7	Single membrane spanning α-helix.	N-terminal , 21aA	N_{matrix}-C_{IMS}

Subunit	M_r (kDa)	Description and location	Mitochondrial localisation signal	Membrane topology
COX7A2	6.7	Single membrane spanning α-helix.	N-terminal , 21aA	N_{matrix}-C_{IMS}
COX7B	6.4	Single membrane spanning α-helix.	N-terminal, 32aA	N_{matrix}-C_{IMS}
COX7C	5.4	Single membrane spanning α-helix.	N-terminal, 16aA	N_{matrix}-C_{IMS}
COX8A	4.9	Single membrane spanning α-helix	N-terminal, 18aA	N_{matrix}-C_{IMS}
COX8C	4.7	Single membrane spanning α-helix	N-terminal, 29aA	N_{matrix}-C_{IMS}

Key: *single ion is coordinated by ligands from both subunits; ‡coding region boundaries

2.2 ELECTRON TRANSFER AND PROTON PUMPING

COX accepts electrons one at a time from cytochrome-c. Evidence from the crystal structure of yeast complex III bound by Cyc1p[52]; computer modelling of the interaction between bovine COX and equine cytochrome c[53]; and biochemical investigation of COX binding by cytochrome c in *Rhodobacter sphaeroides*[54,55], has suggested that a common, ringed binding-patch mediates binding between cytochrome c and its redox partners. A central region of hydrophobic residues surrounds the haem cleft on cytochrome c and binding-patches on CYC1 (complex III) and MTCO2. These regions are believed to participate in non-polar planar stacking interactions between each protein. The hydrophobic patch is in turn surrounded by a ring of weak, long-range, electrostatic interactions involving conserved lysines on the surface of cytochrome c and acidic residues present on complex III and COX.

Cytochrome-c binding to dimeric COX is cooperative, nevertheless in contrast to complex III[56,57], there is currently no evidence of interaction between monomers during redox cycling or proton pumping. Electron transfer[43,44] proceeds from the haem of cytochrome-c to the binuclear CuA centre (figures 3A & 3B). From CuA, electrons are passed to haem-a and finally to the binuclear haem-a_3-CuB centre which is the site of O_2 reduction. Each cycle of the enzyme consumes four electrons from the IMS and four protons from the matrix side of the enzyme in the reduction of one O_2. This is coupled to the pumping of an additional four protons across the inner-membrane from the matrix side. There remain uncertainties surrounding proton translocation concerning the energetic and temporal positioning of the movement of protons during the redox cycle and with the channels used by protons consumed in O_2 reduction and those pumped

across the inner membrane[45,46,58-62] (2.3). It should also be noted that the model above represents an ideal and that slippage (decreased H^+/e^- stoichiometry) and leakage (backflow of protons) of occur *in vivo*[63].

Table 3 MTCO1 and MTCO2 functional residues

Function	MTCO1 functional residues
Coordination of haem a Fe^{3+}	His61, His378
Coordination of haem a_3 Fe^{3+}	His376
Coordination of CuB	His240, His290, His291
Coordination of Na^+	Glu40, Gly45, Ser441
Coordination of Mg^{2+}	His368, Asp369
D-channel	Tyr19, Asn80, Asp91, Asn98, Ser101, Ser156, Ser1157, Asn163, Thr167, Glu242
K-channel	Tyr244, Ser255, Thr316, Lys319
H-channel	Lys440, Ser441, Asp51

Function	MTCO2 functional residues
Predicted CYCS biding patch	hydrophobic: His102, Gly103,Trp104, Tyr105; electrostatic: Glu109, Asp119, Asp139, Glu157, Asp158
Coordination of CuA	His161, Cys196, Cys200, His204
Coordination of Mg^{2+}	Glu198
K-channel	Glu62
H-channel	Ser205

2.3 THE D-, K- AND H-CHANNELS

Analysis of crystal structures and mutagenesis studies have identified two channels, termed the D-channel and the K-channel, extending inwards from the matrix face of the MTCO1, which are thought to be involved in proton conduction[44,64]. The D-channel starts at Glu91 and extends to Glu242 and the K-channel starts at Ser255 and extends to Tyr244, very close the haem-a_3-CuB centre (figure 3A; tables 3A & 3B). H-bonded water molecules and exposed side chains of the helices bounding the channels are believed to act as conduits for protons[44,62]. A third proton conducting channel, the H-channel extends from haem-a to the IMS face of the enzyme[44-46]. It incorporates Lys440, Ser441 and Asp51 of MTCO1 and Ser205 of MTCO2. Mutagenesis and crystallographic studies of human-bovine chimeric COX have implicated the H-channel and in particular shuttling of Asp51 between an internal and an IMS-exposed position, in redox coupled proton transfer from haem-a to the IMS[46].

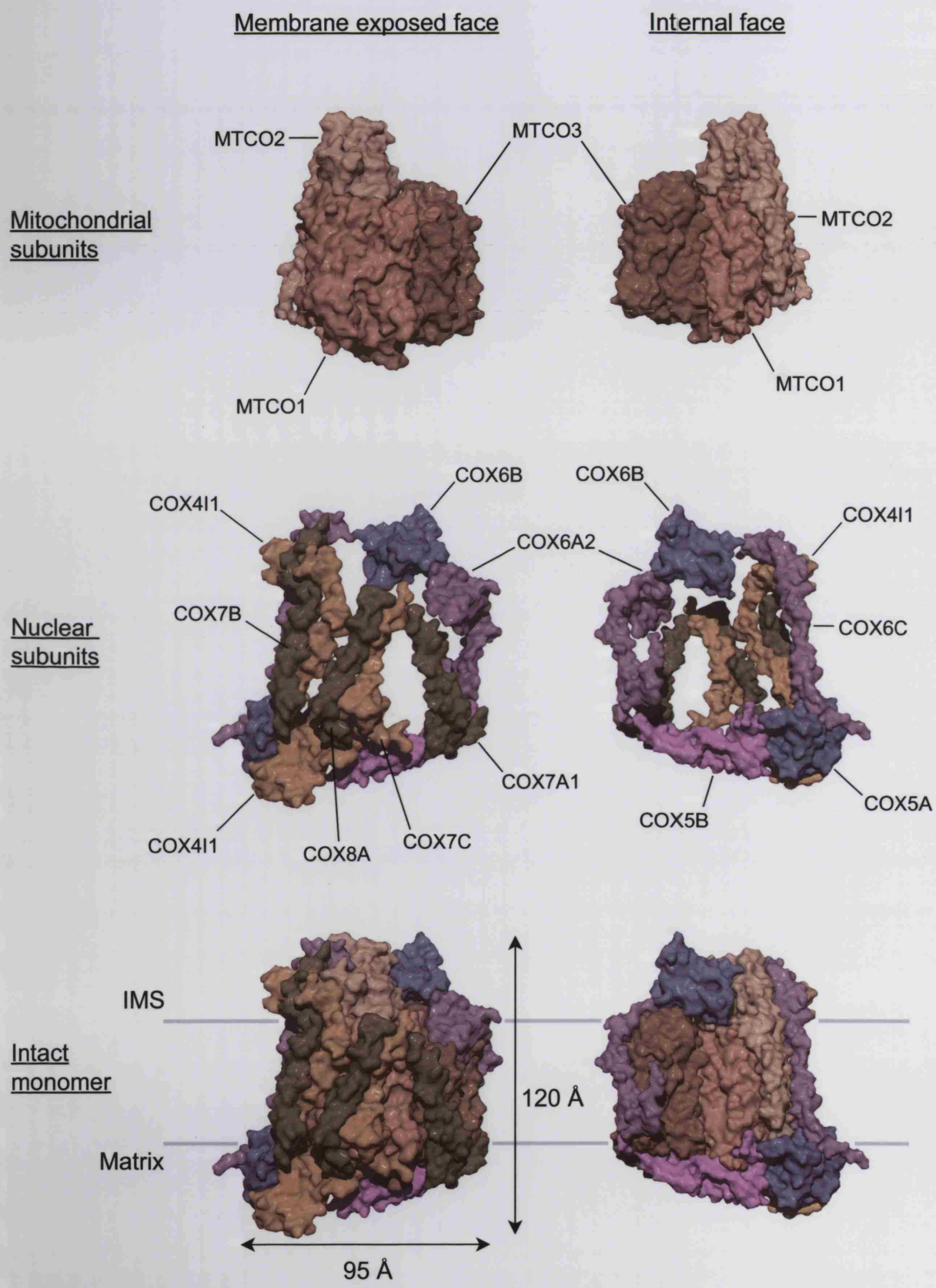

Figure 2A Surface rendered models of COX subunits built from the crystal structure of the bovine heart enzyme (PDB code 1OCC). Surfaces represent 1.4 Å radii for all atoms. Colours have been selected arbitrarily to identify chains. Approximate membrane boundaries are shown in grey. Subunit names are HGNC names for human heart subunits.

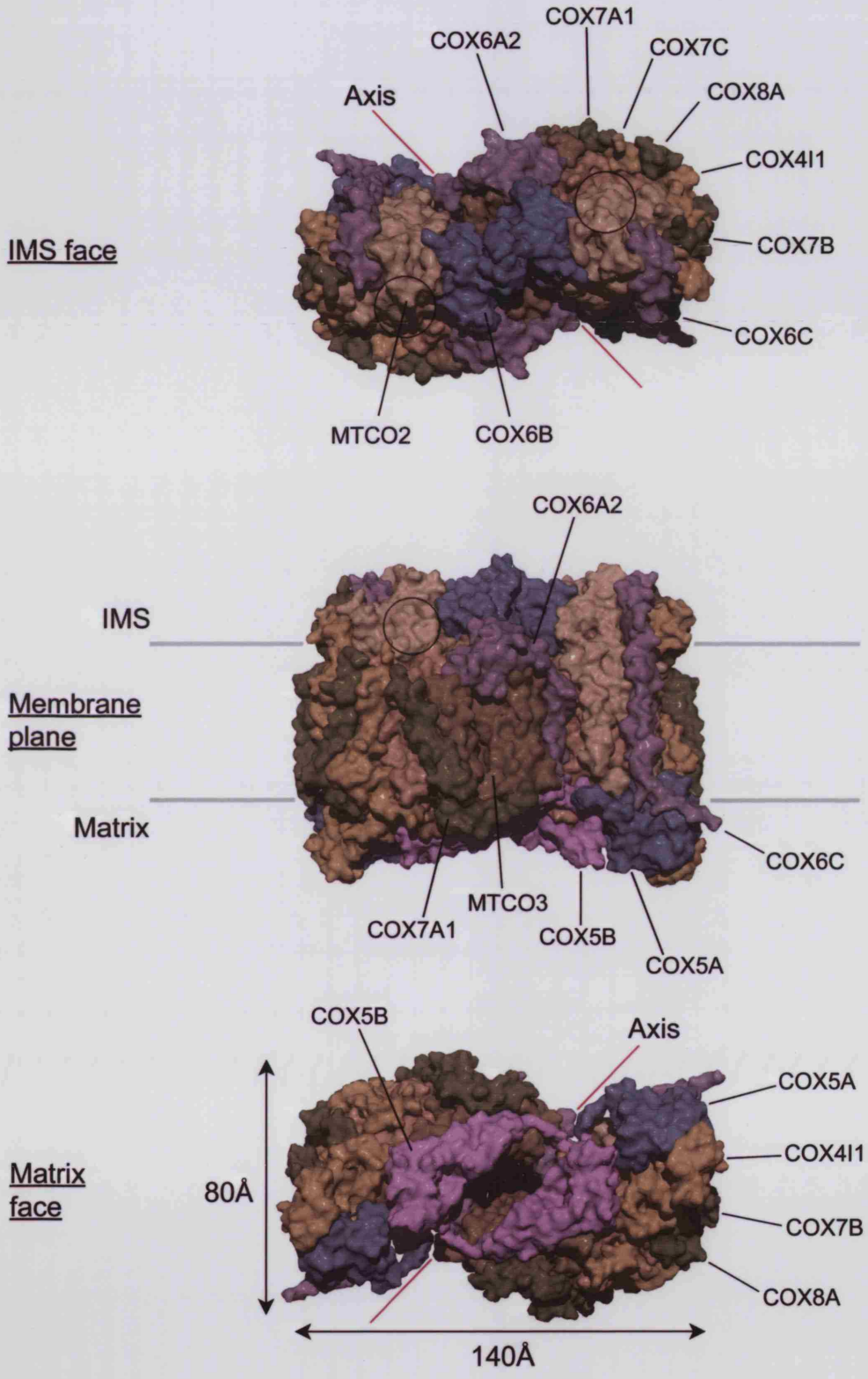

Figure 2B The structure of the dimeric COX holo-complex. Colouring and nomenclature is as in 2A. The axis of symmetry of the dimer is indicated along with a circle marking the cytochrome c binding patch. Surfaces in both figures were generated using Deep View 3.7 and rendered with POV-Ray 3.5.

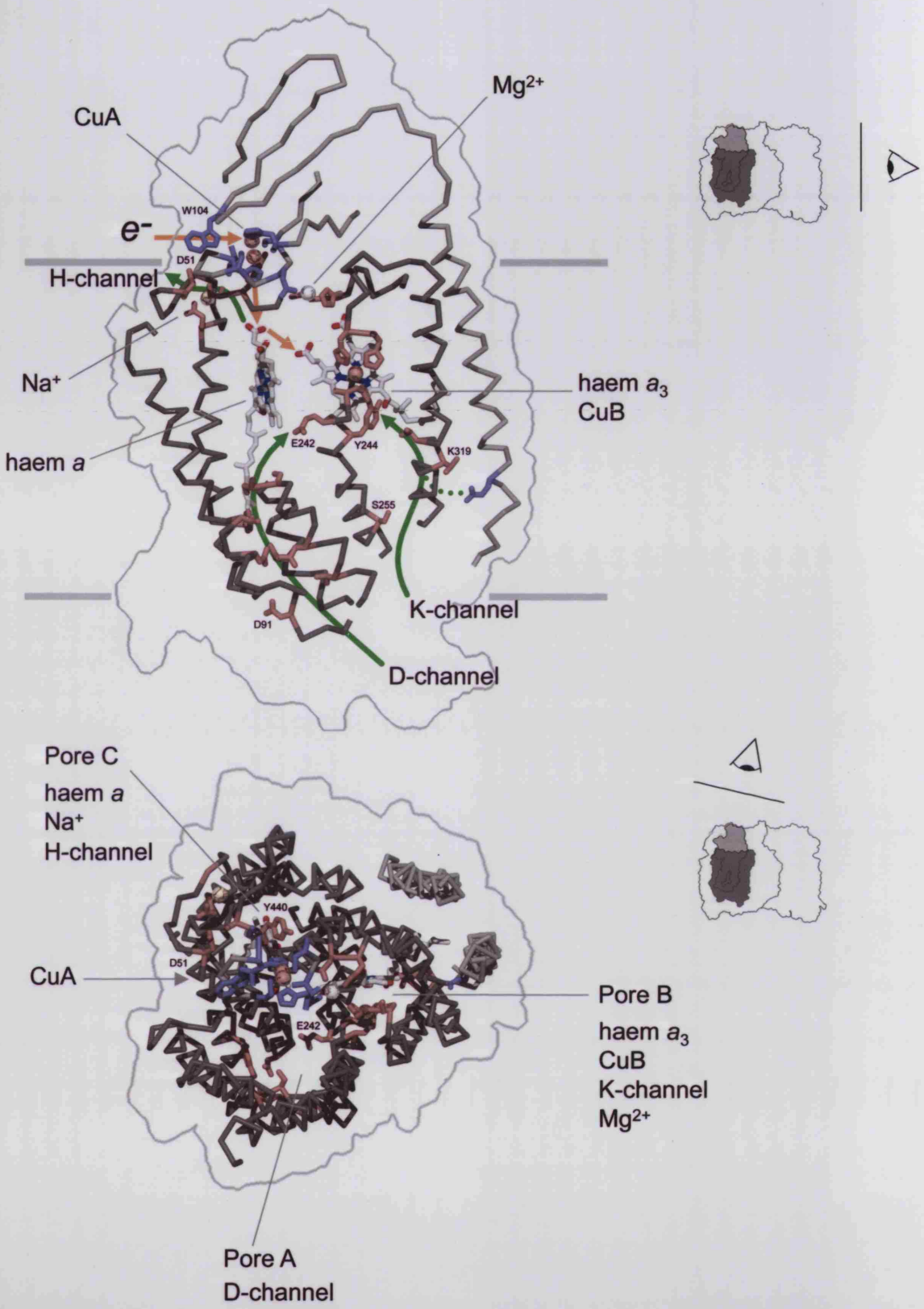

Figure 3A A model showing the relative positions of key residues of MTCO1 in pink and MTCO2 in blue derived from the crystal structure of the fully oxidised bovine enzyme (PDB code 1OCO). Key residues are labelled using single letter code, see also table 3A and 3B. The α-carbon trace for regions of MTCO1 is shown in dark grey and MTCO2 in light grey. The outline is that of bound MTCO1 and MTCO2. The pathway of electron transfer is shown in orange and proton movement within the D-, K- and H-channels in green. The dotted line into the K-channel indicates an alternative start for the channel at MTCO2 Glu62. The cartoon shows the angle of view. **3B** A view of the model shown in figure 3A from the IMS face. All the transmembrane helices of MTCO1 and MTCO2 are shown. Colouring and labelling as in figure 3A. Pores A, B and C and associated prosthetic groups are indicated. Models were generated using Deep View 3.7 and rendered with POV-Ray 3.5.

2.4 IN VIVO HETEROGENEITY OF COX

Attributing function to the nuclear-encoded subunits of COX has proved difficult. As the catalytic properties of simple COX from bacteria are similar to those of the more complex mammalian enzymes, it is assumed that the nuclear-encoded subunits do not play a significant role in the basic catalytic cycle of the enzyme. Instead they are believed to be involved in assembly and regulation of enzyme function[63]. This is supported by the existence of differentially expressed isoforms of some of the nuclear-encoded subunits (table 2; 2.5) and the identification of nucleotide-binding sites and phosphorylation sites on COX (2.6). An important consequence of this is that *in vivo* the COX pool of a cell is heterogeneous in terms of both subunit composition and phosphorylation/nucleotide-binding state.

2.5 ISOFORMS OF THE NUCLEAR-ENCODED SUBUNITS

In humans four COX subunits have differentially expressed isoforms all of which are encoded by separate genes. *COX4I1* is ubiquitously expressed and the *COX4I2* isoform is detectable in foetal muscle and lung and at high levels in adult lung[65]. *COX6A1* is also ubiquitously expressed, whereas *COX6A2* is only detectable in heart and skeletal muscle. Similarly *COX7A2* is ubiquitously expressed and *COX7A1* is only expressed in heart and skeletal muscle. Isotype switching from the major species being the ubiquitously expressed isoform to the major species being heart and skeletal muscle-specific isoforms, has been observed for both *COX6A1*/*COX6A2*[66,67] and *COX7A1*/*COX7A2*[68] in foetal tissue. Genomic evidence suggests that a second isoform of *COX8A* exists[69], termed *COX8C* and that a testes-specific isoform of *COX6B*, *COXVIB2* is also present[70].

2.6 ALLOSTERIC CONTROL VIA NUCLEOTIDE BINDING AND PHOSPHORYLATION

Nucleotide-binding sites and phosphorylation sites have been localised to some COX subunits. Both functions have been shown to be involved in allosteric control of enzyme function. Nucleotide-binding sites have only been partially characterised and there is still debate as to the exact consequences of nucleotide binding. This is primarily due to the complexities of respiratory control and differences in the characteristics of COX purified from different tissues and using different procedures. However, it is universally agreed

that COX activity responds to changes ATP/ADP levels on both sides of the inner membrane[63]. On the IMS face of the complex, nucleotide-binding sites have been localised to both COX6A1, COX6A2[71] and COX4I1[63] (no data is available for COX4I2). On the matrix face there is evidence of nucleotide binding to COX4I1 and possibly COX5A[63].

Metabolic labelling studies have demonstrated that MTCO1[72], MTCO2[72,73], COX4I1[74,75], and COX5B[63,73] can be phosphorylated *in vivo* or when components of purified holo-complex. Conserved canonical cAMP-dependent phosphorylation sequences are present in MTCO1[76] and the COX4I1 N-terminal mitochondrial localisation signal[74,75]. A functional role for cAMP-dependant phosphorylation of COX in the matrix is supported by the specific binding of the protein kinase A (*PKA**) regulatory subunit PRKAR1A to COX5B[77]. In addition to cAMP-dependent phosphorylation, COX4I1 may also be phosphorylated via cAMP-independent mechanisms[75]. The phosphorylation state of COX modulates allosteric control by high matrix ATP:ADP ratios[73]. Phosphorylation of the solubilised enzyme turns on inhibition of COX activity by high ATP levels. Conversely Ca^{2+}-dependent de-phosphorylation turns off this inhibition. Potential roles for COX subunit phosphorylation *in vivo,* include hormonal control of both holo-complex assembly[74] and regulation of COX activity[63,72].

3 MITOCHONDRIAL GENE EXPRESSION

As MTCO1, MTCO2 and MTCO3 that form the core of the COX holo-complex are encoded by mtDNA, mitochondrial gene expression is essential for the biogenesis of the COX holo-complex.

3.1 MTDNA

3.1.1 Structure and organisation

Human mtDNA (mtDNA) is a closed circular molecule of 16.6 kbp[78]. The gene content, gene order and compact nature of human mtDNA is typical for a mammalian mitochondrial genome[79]. It carries protein coding genes for 13 subunits of four of the five OXPHOS complexes and the 2 rRNAs and 22 tRNAs[78] necessary for mitochondrial

* PKA is regulated by cAMP

translation (figure 4). In contrast to lower eukaryotes, mammalian mtDNA does not contain any introns or significant UTRs. The only significant non-coding region of human mtDNA is a region referred to as the D-loop between *MTTF* and *MTTP* which contains many of the *cis*-elements including the transcriptional start sites.

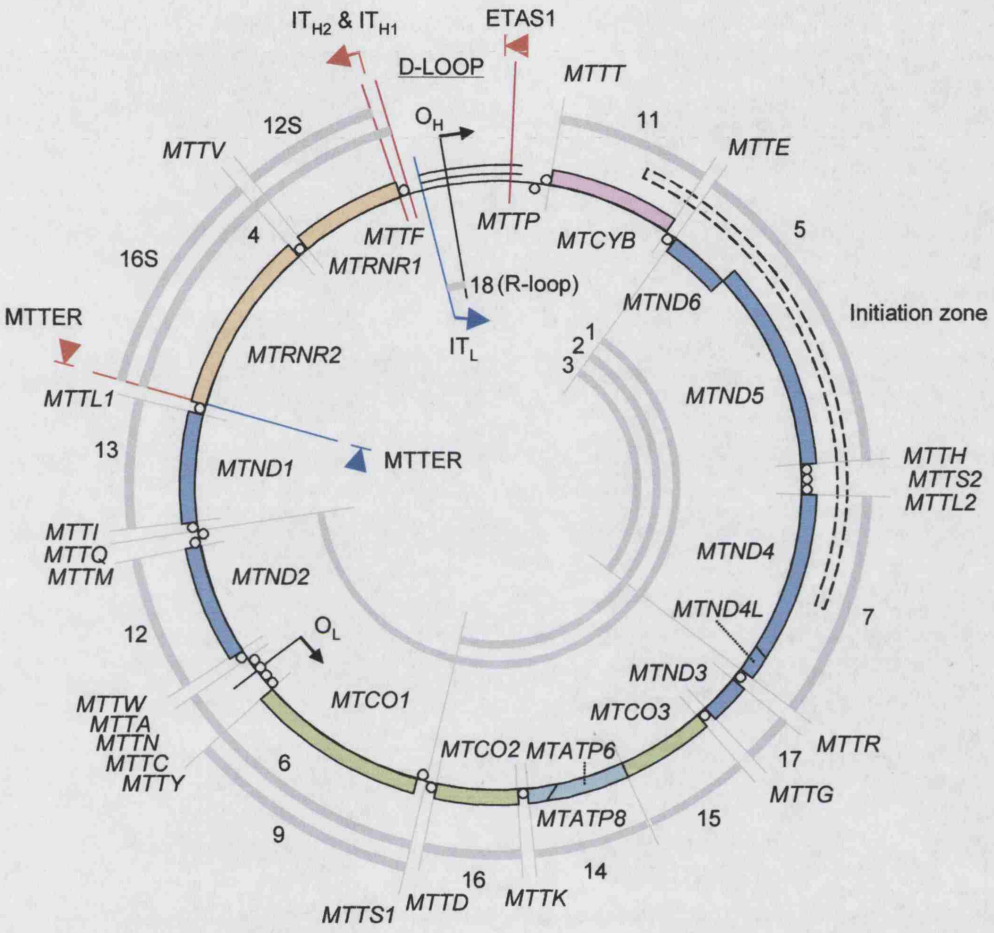

Figure 4 A map of the human mtDNA. A map of the human mtDNA. HGNC names are given for all genes. Genes for complex I subunits are coloured blue; complex III pink; COX green; complex V cyan and mitochondrial rRNAs orange. tRNAs are shown as circles. Genes transcribed in the L-strand orientation are on the inner circle, those transcribed in the H-strand orientation on the outer circle. Initiation (arrows) and termination (blocked arrows) sites for H-strand (red) and L-strand (blue) transcripts are indicated. The origins of heavy (O_H) and light strand (O_L) replication for the asynchronous model of replication are given in black. The approximate extent of the initiation zone for the synchronous model of replication is shown as a dashed box. The 18 mitochondrial mRNAs, abundant processing intermediates and rRNAs are shown as grey bars. RNAs 8 and 10 are low abundance processing intermediates of the rRNAs and are not shown. Transcript cleavage sites are shown as radial lines at the boundaries of mRNAs.

All mitochondrial genomes use a genetic code distinct from the respective nuclear genome. In mammalian mtDNA, TGA is used as a tryptophan codon rather than as a

stop codon, AGR and UAR* specify stop codons and AUA codes for methionine instead of isoleucine[80]. Mitochondrial translation is achieved with only 22 tRNAs as opposed to the >50 or so tRNAs expressed as multigene families in the nucleus. This is accomplished by some tRNAs using a modified tRNA wobble base interaction and others recognising pairs of codons which differ only in the third position[81]. Further reduction is enabled by the use of the same tRNA for initiating formyl-methionine as well as internal methionine residues. Early work with CsCl gradient centrifugation of denatured mtDNA resolved the two strands of the molecule based on nucleotide content. The acronyms H and L, for heavy and light-strand, are now used as a convention to describe transcript orientation.

A characteristic of mtDNA recently returned to prominence is the realisation that the majority, if not all, mtDNAs in mammalian cells are chimeric molecules which contain regions of RNA/DNA base pairing[82-88]. Estimates have put the number and size of such regions between 8-30 regions of at least 4 consecutive RNA/DNA base pairs per molecule[82-84,88]. These regions are believed to originate from the persistence of RNA primers from synchronous replication however this has not been confirmed and no function has been attributed to them as yet.

3.1.1.1 The polymorphic nature of mtDNA

Loci or populations of hypothetically identical mtDNA are referred to as homoplasmic and mixed loci or populations as heteroplasmic. Despite persistent use of the term homoplasmic to describe non-pathological mtDNA populations, evidence suggests that mtDNA is highly polymorphic and that *in vivo,* wild-type mtDNA populations are rarely, if ever, homoplasmic. mtDNA varies in both structure and sequence within individuals to a far higher degree than nuclear DNA. Between 1-10% of mtDNA within cells appears to exist as non-clonal, deleted, circular forms termed sublimons[89]. The abundance of sublimons varies between tissues with skeletal and cardiac muscle having the highest levels. It is unclear whether sublimons are transcriptionally active or not, although they do not appear to be associated with disease or aging[90,91]. Single cell PCR has shown that low levels of mtDNA recombination occur in human cells[92]. The high copy number and polyclonal nature of mtDNA replication also means that sequence variation exists within cells and tissues. Up to 6% of the mtDNAs from normal human synaptosomes have been found to carry D-loop sequence polymorphisms[93]. The existence of clonal

---

* R =purine

expansion of somatic polymorphisms *in vivo* has also been clearly demonstated[94]. Intercellular differences in clonal expansion of background sequence variation creates distinct patterns of polymorphisms between wild-type cells and it is thought that *in vivo* normal cells may contain hundreds of different mtDNA sequences[95,96].

The creation of cells without mtDNA has played an important role in mitochondrial genetics. Cells without mtDNA are referred to as ρ^0 and those with mtDNA as ρ^+. ρ^0 cells can be created using chemical inhibitors of mtDNA replication such as ethidium bromide[97] or genetically, via ectopic overexpression of dominant negative POLG, the catalytic subunit of mitochondrial DNA polymerase[98]. When fused with sources of ρ^+ mitochondria, such as whole cells, enucleated cells or platelets, ρ^0 cells can be repopulated with novel ρ^+ mitochondria.

3.1.1.2 Mitochondrial nucleoids and mtDNA-binding proteins

Cells from most human tissues contain between 10^3 and 10^4 copies of mtDNA although over 10^5 are found in oocytes[81]. mtDNA resides within the matrix of the organelle as negatively supercoiled, protein-coated, membrane-anchored nucleoids. Nucleoids have an abundance in the region of 2.3±0.4 per mitochondria in cultured simian cells[99*], although the diversity of mitochondrial morphology suggests this figure varies widely. Human nucleoids contain 6-10 copies of mtDNA[100,101] in accordance with their role as part of the minimal heritable unit of mitochondria that is lower than the abundance of mtDNA[102-104].

The principle DNA-binding protein found in nucleoids[99,100] is the HMG[†] protein[105] TFAM which is present at sufficiently high quantities to coat mtDNA[106], binds mtDNA non-specifically[107] and has characteristics similar to the bacterial histone HU[106], suggesting a similar role in mitochondria. An ssDNA-binding protein, SSBP1, is also present[99,100] and is likely to be important for the protection of replicating mtDNA and the maintenance of structural isoforms of the D-loop region[106]. Proteins required for replication, repair and transcription are also components of mitochondrial nucleoids. The mitochondrial DNA polymerase γ and the helicase PEO1[‡] are both present[99] and the mtDNA repair protein Mgm101p has been detected in yeast[108,109]. The hsp60 chaperonin[110,111] (4.3.1.2), the yeast hsp70 Ecm10p[112,113] (4.3.1.1) and the Lon protease[114] (4.3.2.4) are also present,

---

[*] COS7, *Cercopithecus aethiops*, African green monkey kidney cells (SV40 transformed).
[†] High mobility group.
[‡] non-HGNC name TWINKLE.

consistent with the role of chaperones and proteases in modulation of mtDNA-binding proteins. In this respect, direct interaction between Lon and both the mitochondrial DNA polymerase* and PEO1 have been demonstrated *in vivo*[114,115]. TCA cycle enzymes have also been found in nucleoids although their function remains unknown[110].

Nucleoids appear to be anchored to both mitochondrial membranes via proteins which are intimately linked with the mitochondrial fission/fusion apparatus which is in turn required for nucleoid transfer during cell division[101,116-118] (figure 5). In yeast, the membrane-bound, DNA-binding protein Yhm2p is likely to act as an anchor along with Mmm2p[119] and Mmm1p[109,120,121] that is inserted into both mitochondrial membranes and spans the IMS. Two-membrane-structures (TMS) have been visualised in yeast and have been found to persist in the absence of associated mtDNA[109]. The non-random distribution of nucleoids and their association with mitochondrial kinesin and tubulin[101] has confirmed that their distribution is key to the segregation of the mitochondrial mass of cells during division. Fusion, fission[99] and movement[100,101] of nucleoids has been observed *in vivo*. The intimate association of nucleoids with nascent mitochondrial RNA, the mitochondrial protein import machinery and cytosolic ribosomes in human cells provides a basis for models coupling mitochondrial protein import, transcription and translation[101,122].

3.1.1.3 7S mtDNA and the D-loop

In vivo, a minority of mtDNA molecules(<1-10%) contain displaced loops of DNA in the D-loop region. In these molecules the H-strand is displaced by an 800 base pair chimeric RNA/DNA called the 7S mtDNA which is bound to the L-strand. Very little is known about the role played by this structure, although a connection with replication is generally accepted. The RNA component of the 7S mtDNA, termed the R-loop RNA, originates from the initiation site of transcription of the L-strand transcripts[78]. The RNA/DNA duplex formed is a highly structured species. It is thought to contain Holliday junctions[123] and only a very short region forms a linear RNA/DNA duplex[124]. The position of the switch from RNA to DNA within the 7S mtDNA varies over a short conserved region of the D-loop and processing is mediated via RNase-MRP[78]. The 3' boundary of the 7S mtDNA is also variable but lies in close proximity to a conserved region called ETAS1[125] which is believed to be important for processing. It is not known whether any of the *cis*-elements in the D-loop region require triplex formation for function. While the *cis*-acting elements

* POLG and POLG2 subunits.

are conserved, the remainder of the D-loop region is the most variable region of the human mitochondrial genome[78].

3.1.2 Transcription

3.1.2.1 Mitochondrial RNA polymerase and transcription factors

Despite the fact that mtDNA is smaller than many nuclear genes our understanding of mitochondrial transcription remains somewhat cloudy. Transcription is carried out by the mitochondrial RNA polymerase POLRMT which shows homology to single subunit bacteriophage RNA polymerases[126] and contains[122] two N-terminal PPR domains[127]. Transcription requires the mtDNA packaging protein TFAM and either of the transcription factors TFB1M and TFB2M[128,129]. TFB1M and TFB2M interact directly with TFAM[130] and POLRMT but with differing abilities to promote transcription[128] (TFB2M>TFB1M) and they both show homology to bacterial RNA methyltransferases[128,129]. TFB1M binds *S*-adenosylmethionine[129] and is believed to methylate the mitochondrial 12S rRNA[131]. Following their discovery, a recombinant *in vitro* transcription system can now be reconstituted with POLRMT, TFAM and TFB1M or TFB2M as minimum components[128].

3.1.2.2 Transcripts and transcript processing

mtDNA is transcribed from two promoters which are located tail-tail within 150 bp of each other in the D-loop region[78,81]. One directs transcription in the H-strand orientation the other in the L-strand orientation (figure 4). They both contain a pentadecamer consensus sequence and have been shown to function independently[132]. Four primary transcripts are constitutively expressed in human cells[78,81]. Two long transcripts which encompass almost the entire molecule in each orientation, a short H-strand transcript terminating after the mt-rRNA genes and a short L-strand transcript providing the R-loop RNA. With the exception of the R-loop RNA, transcripts are processed to provide the mature mRNA, tRNA and rRNA pools.

Detailed examination of the kinetics of transcript turnover has suggested that the two H-strand transcripts have different initiation sites[133] separated by *MTTF*. IT_{H1} acts as an initiation site for the long H-strand transcript which includes *MTTF*, while a downstream initiation site, IT_{H2}, is the start site for the short H-strand transcript. Transcription of the short H-strand transcript terminates around a cis-element called MTTER and transcription of the long transcript is thought to terminate around ETAS1 in the D-loop

region[125]. The short H-strand transcript is transcribed at around 50-fold higher levels than the long transcript and constitutes the source of the mt-rRNA pool[133-135]. The long H-strand transcript is in turn processed to provide 10 mRNAs and 14 tRNAs. The long L-strand transcript is transcribed at levels ~20-30 fold higher than the long H-strand transcript[136]. The vast majority of this transcript is turned over. It encodes only a single mRNA, *MTND6* which is present at extremely low steady-state levels[136,137], and the remaining 8 mt-tRNAs. The transcription start site for the long L-strand transcript (IT_L) is the same as that used for the R-loop RNA and L-strand transcription terminates at MTTER which functions bi-directionally[138]. The relative rates of synthesis of mtDNA transcripts is to a certain extent dynamic and responds to ATP levels[134] and stimuli such as thyroid hormone[139]. There is evidence that this may be due to both alterations in the relative rates of transcription initiation at the various start sites[139] and via modulation of MTTER-binding complexes[140-142]. Therefore, like nuclear and prokaryotic gene expression, mitochondrial gene expression is regulated at multiple points.

3.1.2.3 mRNA and rRNA processing

Excluding the two rRNAs, 16 abundant RNAs can be resolved from mitochondria under steady-state conditions, most of which correspond to mature mRNAs[143] (figure 4). Despite originating from a single transcript the steady-state levels of H-strand mRNAs vary over a 6-fold range and although transcribed at far higher levels than the H-strand mRNAs, steady-state levels of the single L-strand mRNA are around 20-fold less than the most abundant H-strand mRNAs[136]. Thus, in common with nuclear RNA turnover[144], there is a high degree of degradation of transcripts during processing[136]. The majority of mRNA boundaries correspond to tRNA genes[145] and a model of mitochondrial transcript processing, termed the *tRNA punctuation model*, has emerged whereby mRNA processing is dependent on tRNA excision[143]. Mitochondrial RNA processing is rapid *in vivo* and occurs co-transcriptionally in a similar fashion to nuclear RNA processing[146]. Mitochondrial mRNAs are not 5' capped[147] and they do not contain conventional poly-A signals. Mammalian mitochondrial mRNAs are poly-adenylated with about 55 nucleotides[148] in a process which is not dependent on the presence of stop codons[140]. Poly-adenylation appears to increase the stability of human mitochondrial mRNAs as is also the case in the cytosol[149,150] although is not known whether mitochondrial mRNAs adopt a circular conformation enabling communication between 3' and 5' as occurs with cytosolic mRNAs[151]. Mitochondrial rRNAs are methylated[152] and also adenylated during processing, the 16S rRNA receives 10 residues and the 12S rRNA is mono-adenylated[153].

3.1.2.4 *tRNA excision , processing and charging*

Following the tRNA punctuation model of mRNA processing tRNA excision is an important process in mitochondrial gene expression. 5'-excision is carried out by a multimeric RNase-P which also functions in 5'-cleavage of nuclear mRNAs and is related to RNase-MRP[154]. 3'-cleavage of mitochondrial tRNAs is carried out by an RNase Z encoded by *ELAC2*[*] which like RNase P is also found in the nucleus[155]. 3'-cleavage of mt-tRNAs is dependent on prior 5'-cleavage[155,156]. Following 3'-cleavage a CCA triplet that will receive the charging amino acid is added to the 3' end of the tRNA by TRNT1[†][157]. Before becoming fully active, up to 10% of tRNA bases are modified. In particular, modification often occurs in the wobble position of the tRNA with the addition of taurinomethyl and thio-groups[158]. tRNA charging is carried out by a complex and diverse set of around 20 mitochondrial tRNA-aminoacyl transferases[159-162]. Formylation of initiator f-Met-tRNA^{Met} occurs after tRNA charging and is mediated via the recognition of the charging methionine which enables the use of a single *MTTM* gene for both initiator and internal codons[163].

3.1.2.5 *mRNA-binding proteins*

Numerous mRNA species-specific, mitochondrial mRNA-binding proteins have been identified in yeast and counterparts of some of these have been identified in humans (5.2.3.3). Such proteins are not well conserved[164] and it is likely that many orthologues of yeast mRNA-binding proteins remain to be identified[122]. In accordance with the membrane localisation of nucleoids and mitochondrial ribosomes, many mitochondrial mRNA-binding proteins are membrane bound[164]. A set of proteins which bind *MTCO2* mRNA have been identified in bovine samples, although none of them appear to be specific for *MTCO2* mRNA[164]. Among them a high-affinity, 15 kDa, inner-membrane protein and a novel 74 kDa, PPR motif protein[‡] (5.2.3.2) were identified. The identities of the other proteins remain to be confirmed, however, based upon molecular weight, mitochondrial localisation and proven mRNA binding capability, the following are thought to be candidates: the DNA/RNA helicase SUPV3L1[165], glutamate dehydrogenase (*GLUD1*) which also binds cytosolic COX subunit mRNAs[166-168] and the β-oxidation pathway enzyme enoyl-CoA hydratase[169] (*ECH1*).

---

[*] Drosophila homologue JHI-1.
[†] Mitochondrial ATP(CTP)-tRNA-specific nucleotidyltransferase.
[‡] Matching hypothetical protein FLJ20758.

Two mitochondrial mRNA-binding proteins, LRPPRC and HNRNPK, have been positively identified both of which are also components of nuclear/cytosolic mRNP* particles. LRPPRC (5.2.3.3) binds mitochondrial mRNAs non-specifically *in vivo*[170], although mutation analysis suggests a specific role in COX biogenesis[171]. HNRNPK is an hnRNP† which interacts with many proteins, DNA and RNAs[172,173]. A pool of HNRNPK has been identified in mitochondria and it binds most human mtDNA transcripts *in vivo*[173]. Based on known cytosolic and nuclear functions, HNRNPK has been proposed to function widely in signal transduction as a interface between diverse stimuli and nucleic acid processes regulating gene expression[172-174]. Central among these, HNRNPK act as a phosphorylation-dependent translational silencer[175]. Although interaction has not been investigated in mitochondria, LRPPRC is a component of certain HNRNPK-containing mRNP particles[176].

3.1.2.6 Steady-state patterns of OXPHOS subunit gene expression‡

The range of expression of 14 OXPHOS subunit genes has been found to vary over at least two orders of magnitude in murine tissues with mtDNA-encoded genes consistently expressed at higher levels than nuclear genes[137]. However, the ratios of expression of mitochondrial mRNAs to each other and those of nuclear mRNAs to each other, are more or less constant[137]. As mitochondrial mRNAs originate from only two transcripts this implies that the relative rates of mitochondrial RNA processing and turnover are invariant. When compared between different tissues, the abundance of mitochondrial mRNAs is more variable than that of nuclear mRNAs and cultured cells have consistently lower levels mitochondrial mRNAs than tissues[137]. Over the physiological range of mtDNA:nDNA ratios, there does not appear to be a correlation between mtDNA abundance and mitochondrial mRNA abundance[137].

3.1.2.7 OXPHOS gene expression levels do not respond to stress

While evidence from the function of OXPHOS-related transcription factors such as the nuclear respiratory factors§ and co-regulators such as PGC-1 proteins**, demonstrates coordination between increases in expression of nuclear and mitochondrial OXPHOS

---

* mRNA-ribonucleoprotein.
† Heterogeneous ribonucleoprotein.
‡ Throughout this thesis "gene expression" refers to steady-state mRNA expression levels and not protein levels.
§ NRF1 (*NRF1*) and NRF-2 (*GABPA*, *GABPB1* and *GABPB2*).
** PPARG [Peroxisome proliferator-activated receptor-γ] co-activator-1α *(PPARGC1A)*, PPARG co-activator-1β (*PPARGC1B)* and PPARGC1-related co-activator (*PPRC1).*

genes[177,178], chemically or genetically induced mtDNA depletion does not lead to alterations in steady-state expression of nuclear-encoded OXPHOS genes[137,179-181]. This implies that while signalling pathways[182-184] and expression levels of mitochondrial chaperones[185] respond to mitochondrial insult (4.3.4), there is no associated compensatory increase in OXPHOS subunit gene expression. The independence of nuclear and mitochondrial gene expression has also been demonstrated in cells treated with thiamphenicol (TAP) which dysregulates mitochondrial gene expression by inhibiting mitochondrial translation and increasing the abundance of mitochondrial mRNAs. In cells treated with TAP the increase in mitochondrial mRNAs is not coupled to any alteration in the abundance of nuclear OXPHOS mRNAs[186]. Similarly, in a mouse cell genetic model with a heteroplasmic premature termination codon in *MTND5*, no alterations in total *MTND5* mRNA (RNA 5) were seen in response to decreases in the proportion of wild-type mtDNA to <10% normal levels[187]. Analysis of the RNA 5 pool in these cells found that the proportion of wild-type RNA 5 correlated exactly with the proportion of wild-type mtDNA[187], indicating that there was no difference in stability between wild-type and mutant transcripts.

3.1.3 Turnover and replication

mtDNA turnover is a relatively slow process. In cultured murine tumour cells, mtDNA molecules turnover in around 10 days[188] and *in vivo* rat muscle mtDNA has a half-life ($t_{½}$) of 12-24 months[189]. Replication is independent of the cell cycle[190] and occurs in both quiescent and enucleated cells[191]. As such, the cellular mass of mtDNA remains constant in replicating and non-replicating cells[192]. mtDNAs appear to be selected for replication randomly[190] and DNA synthesis has been visualised throughout the mitochondrial network of cells[101,191]. It is estimated that replication of an entire mtDNA takes 1.5-2 hours[193-195]. Recent work with yeast has shown that mtDNA replication occurs only in membrane bound nucleoids[109]. A minimal, mammalian, *in vitro* dsDNA replication system requires the mitochondrial DNA polymerase γ (POLG & POLG2 subunits), the ssDNA-binding protein SSBP1 and the helicase PEO1[195].

3.1.3.1 Mechanisms of mtDNA replication

The mechanism of mtDNA replication is currently the focus of fierce debate[196-198]. During the 70's and 80's, Vinograd and Clayton proposed a strand asynchronous mechanism of replication in which the origins of replication of the H- and L-strands were separated both temporally and spacially[188,199]. According to this model, replication of the H-strand

originates at O_H and only when replication had progressed to O_L does synthesis of the L-strand commence (figure 4). Thus, in this model, both stands are synthesised continuously, requiring maintenance of a huge loop of ssDNA. Recently work by Holt and co-workers[82,200,201] has seriously questioned the strand asynchronous model. They have proposed a strand-synchronous model in which replication proceeds through the advancement of standard "Y" shaped replication forks, similar to the mode of chromosomal DNA replication, in which the leading strand is synthesised continuously and the lagging strand is synthesised discontinuously[82,200,201]. According to Holt's model, replication starts at any point within an initiation zone between *MTND4* and *MTCYB,* and initially proceeds bi-directionally producing a theta replication bubble[200]. Progression of the D-loop proximal replication fork then arrests within ~500 bp of O_H which acts as a replication fork barrier. Subsequently replication proceeds only in the D-loop distal direction until the complete mtDNA has been replicated.

Discussion of the basis for each model is beyond the scope of this thesis although it is worth noting that the synchronous model proposed by Holt and co-workers fits well with known mechanisms of DNA replication, unlike the asynchronous model which appears to be restricted to mammalian mtDNA. Prior to Holt's work, standard mtDNA replication forks, as required for synchronous replication, had been identified in yeast[202], sea urchins[203] and *Plasmodium*[204]. In addition, Holt's model is tolerant of, and possibly accounts for, the presence of RNA tracts and the D-loop[82,200]. During the early 1970s prior to the cementing of the asynchronous model of replication in the field, evidence for synchronous mtDNA replication had been presented[205] and RNA tracts in mtDNA had been examined using exactly the same sets of RNases[88] as employed by Holt. Interestingly, the overwhelming majority of clinically relevant mtDNA deletions result in molecules that remove the initiation zone from retain both O_H and O_L[573]. Prior to Holt's work this was taken as evidence for the importance of O_H and O_L in mtDNA maintenance[107]. Holt has interpreted the loss of the initiation zone as evidence that *cis* elements within the initiation zone are not required for mtDNA replication and that molecules with stalled replication forks at the replication fork barrier at O_H and the partial barrier at O_L are favoured substrates for recombination or deletion[200].

3.2 MITOCHONDRIAL PROTEIN SYNTHESIS

3.2.1.1 Mitochondrial ribosomes

Mitochondrial ribosomes are found in the matrix of the organelle. They are related to prokaryotic ribosomes although they have diverged considerably during evolution. Mammalian mitochondrial rRNAs are around 40-50% shorter and have fewer modifications[152] than their prokaryotic counterparts. Proteomic studies have identified what is thought to be the full complement of bovine mitochondrial ribsomal proteins[206-209] (MRPs) and many human homologues[210,211]. Homologues of around 30 prokaryotic ribsomal proteins are absent from mammalian ribosomes which contain 34 novel, eukaryote-specific proteins[210]. As a result of the divergence in protein and RNA content,

mammalian mitochondrial ribosomes are larger, heavier but less dense than prokaryotic ribosomes. Although the structure of essential domains are conserved, the overall organisation of mitochondrial ribosomes is distinct from that of prokaryotic and cytosolic ribosomes and it does not appear that eukaryotic MRPs have physically replaced absent RNA structures[212]. Many protein-protein and protein-RNA bridges are present in mammalian mitochondrial ribosomes which are absent in prokaryotic ribosomes[210]. These are proposed to function in binding and communication between subunits.

Proteomic studies have identified novel characteristics for certain MRPs. In particular three homologues of prokaryotic S18 are present in mammals, MRPS18A, MRPS18B and MRPS18C[209,213]. As only a single copy is present per small subunit, mammalian mitochondrial ribosome pools may be heterogeneous. Moreover bacterial S18 is changes conformation upon mRNA binding, suggesting that differences in the kinetics of mRNA handling may exist[209]. Cardiac-specific isoforms of other MRPs[214] have been identified along with others that also function in apoptotic signalling[215].

At least half the mammalian *MTRNR1* pool of is bound to the inner membrane-independent of the presence of nascent chains[216]. In yeast, mitochondrial translation appears to be exclusively associated with the inner membrane[217,218]. As all mtDNA-encoded proteins are inner-membrane proteins, mitochondrial translation is generally accepted as occurring concurrent with membrane insertion. Both translating and inactive ribosomes bind the OXA1 membrane insertion complex (4.2.6.2) and the identification of membrane-resident chaperones (4.3.1.3) and mRNA-binding proteins (5.2.3.2;5.2.3.4) supports models whereby the entire mitochondrial gene expression process, from transcription to translation, occurs at the inner membrane[101,122] (figure 5).

3.2.1.2 Translation

The components and cycle of mammalian mitochondrial translation are homologous to those of prokaryotes[219], although there are some important differences possibly related to alterations in ribosomal structure. In contrast to prokaryotes, mammalian mitochondrial start codons are thought to be located by non-specific mRNA binding followed by 5' scanning[220,221] without the need for auxiliary factors[222]. In prokaryotes, three initiation factors IF1, IF2 and IF3 are required for assembly of an initiation complex composed of the ribosomal small subunit, mRNA and f-Met-tRNA^{Met}. Human mitochondrial homologues of IF2 and IF3 have been identified (*MTIF2*[223-225], *MTIF3*[226]) while functional homologues of IF1 appear not to be required in mammals[226]. Following large subunit

binding, three elongation factors EF-Tu, EF-Ts and EF-G, are required in prokaryotes for correct recruitment of charged tRNAs, tRNA transfer between the ribsomal A-, P- and E-sites and displacement of uncharged-tRNAs during chain elongation. Homologues of all three are present in human mitochondria, including two constitutively expressed isoforms of EF-G, (*TUFM*[227], *TSFM*[228], *EFG1*[229], *EFG2*[230]). In common with prokaryotic EF-Tu, there is evidence that the phosphorylation state of TUFM is a regulator of mitochondrial translation[231]. Structural[232] and kinetic[233] data from bovine mitochondrial elongation factors suggests that the mechanics of elongation in mitochondria is similar to that in prokaryotes. Termination of translation and ribosome recycling in prokaryotes requires four termination factors, RF1, RF2, RF3 and RRF. To date homologues of RF1 and RRF (*MTRF1*, *MRRF*) are the only termination factors identified in humans[234].

3.2.1.3 mRNA turnover

There is evidence that similar to cytosolic mRNAs, concentric rounds of mitochondrial translation lead to shortening of mRNA poly-A tails which marks mRNAs for degradation[149] ($<A_{11}$). In yeast mitochondria, a 160 kDa ribosome-associated RNA degradosome has been identified composed of a helicase, Suv3p, and an RNase II, Msu1p*. A homologue of Suv3p, SUPV3L1, has been identified in humans yet it appears to be a matrix protein with a preference for dsDNA substrates[165]. No homologue of Msu1p has been found. Yeast mitochondrial mRNAs are not poly-adenylated thus different systems may well operate in mammals[150]. The RNases involved in turnover of mammalian mitochondrial mRNAs and processing intermediates remain to be identified experimentally[140,149,150]. In prokaryotes and chloroplasts, PNPases† are components of RNA degradosomes[150] and it has been speculated that in humans the mitochondrial PNPase, PNPT1‡[235,236], may be involved in mRNA turnover. No PNPase-like proteins are present in yeast genomes which may account for the differnce[150,236].

4 PROTEIN TARGETING TO MITOCHONDRIA AND BIOGENESIS OF THE MITOCHONDRIAL PROTEOME

Only 13 of the ~1000 proteins of the human mitochondrial proteome[237,238] are encoded by mtDNA, corresponding to around 10% of mitochondrial protein mass[239]. Hence, a vast array of proteins with widely varying physical characteristics and expression profiles are

---

* ssRNA 3'-5' exoribonuclease, also known as Dss1p.
† Polynucleotide phosphorylase, *in vivo* 3'-5' exonuclease.
‡ Non-HGNC name hPNPase[old-35].

imported into the mitochondrial compartments. The following section provides a summary of the mechanisms of protein targeting to mitochondria and the biogenesis of the mitochondrial proteome.

4.1 CYTOSOLIC EVENTS

There are two principal routes for protein import to mitochondria, co-translational import, which predominates for prokaryotic components[240] of the mitochondrial proteome, and post-translational import, which predominates for proteins of eukaryotic origin[241].

4.1.1 The localisation RNCs to mitochondria for co-translational import

Mitochondrial protein targeting is absolutely dependent on the global gene expression machinery (figure 5). Many of the cytosolic events that influence mitochondrial targeting are indistinguishable from those of non-mitochondrial proteins. In particular many ubiquitous cytosolic chaperones are required for mitochondrial protein targeting.

Translationally active ribosome-mRNP complexes (RNCs) encoding proteins destined for mitochondrial compartments have long been know to associate with mitochondria[242] (figure 5). It is also clear that certain proteins can only be imported co-translationally[243]. Verification of the extent of the association of RNCs with mitochondria has been provided by genomic screens of yeast in which around 500 mRNAs were identified as components of RNCs predominantly localised to mitochondria[241], a figure that represents at least half the predicted yeast mitochondrial proteome. The only common feature among the proteins encoded by the localised mRNAs was that they tended to be prokaryotic in nature[240]. Contrary to previous assumptions, there was no evidence that co-translational import favoured hydrophobic proteins[241].

Under steady-state conditions, whether or not particular RNCs accumulate on the outer membrane is thought to be dependent on regulation of the window during which the emerging nascent chain can interact with TOM complex receptors (4.2.1), while still a component of the RNC[244,245]. This in turn is dependent on the stability of the RNC, the kinetics of translation and the presentation of the emerging nascent chain[244,245]. Control of the kinetics of translation, including stalling, is likely to be mediated via *cis* elements in mRNAs. There is good evidence of a role for 3'UTRs in mitochondrial localisation[246] and for the binding of translational inhibitors to mRNAs localised to mitochondria[247]. Attachment of RNCs to the outer membrane is via electrostatic interaction between

ribsomal components and outer membrane proteins[248]. It requires GTP and intact ribosomes and is stabilised by the presence of an emerging mitochondrial localisation signal[249]. Whether or not the mitochondrial proteins involved in RNC attachment are known components of the TOM complex (4.2.1; 4.2.2) remains to be determined.

Examples of proteins known to influence the association of RNCs with mitochondria include yeast homologues of mammalian SR proteins*[250,251] which are components of mRNPs[252] and homologues of β-karyopherins[253] which function as nucleo-cytosolic shuttles[252]. Both have been implicated in RNC localisation to mitochondria though their direct and indirect ability to control the stability of RNCs in the cytosol. *In vitro* studies have also shown that two ribosome-associated chaperone complexes, the ribosome-associated complex[254] (RAC) which is an hsp70/hsp40 pair† present only in yeast, and the nascent polypeptide-associated complex[255-257] (NAC), promote the interaction of RNCs with mitochondria. Both complexes are required for correct presentation of emerging mitochondrial targeting signals. A role for free cytosolic hsp70s in presentation of emerging targeting signals from mitochondria-localised RNCs can also be inferred from early work examining the import of proteins such as ATP2p[258‡] in yeast which is now known to be imported co-translationally[241].

4.1.2 The role of cytosolic chaperones in post-translational import

The primary role of cytosolic chaperones in post-translational mitochondrial protein import is to maintain nascent proteins in an *import competent* state, i.e. to block collapse of the protein into stably folded forms, and to facilitate reading of targeting signals[244,245] (figure 5). The cytosolic chaperones involved in this process are components of the global gene expression machinery which is designed to enable the correct reading of multiple cellular localisation signals and to facilitate the entrance of nascent proteins into appropriate assembly pathways[244,245]. The interaction of mitochondria-targeted proteins with cytosolic chaperones is dependent on the intrinsic properties of the cargo protein and varies according to the availability of cytosolic chaperones. Studies of the ubiquitous hsp70 HSPA8[259,260§], 14-3-3 proteins**[264,265] and hsp90s[260] have shown that different proteins rely on specific chaperones to different extents and that certain proteins require

---

* serine-argenine rich.
† Ssz1p and Zuo1p.
‡ human homologue, ATP5B, non-HGNC name F_1-β.
§ Non-HGNC names, Hsc70, Heat shock cognate 70, Hsp73.
** The 14-3-3 dimer YWHAE•YWHAZ has previously been referred to as mitochondrial import stimulating factor (MSF). This titla has not been used here as 14-3-3 proteins, including YWHAE and YWHAZ function in many aspects of cell biology[261-263].

members of multiple chaperone families for mitochondrial import[266]. Alterations in the abundance of different chaperones leads to import of cargo proteins via different cytosolic chaperones as has been demonstrated for HSPA8 and 14-3-3s[265]. Neither HSPA8 nor 14-3-3s show any preference for interaction with cargo proteins containing internal targeting sequences or N-terminal presequences[264,265], however, the phospho-serine-binding characteristics of 14-3-3s may play a part in regulation of import of proteins with phosphorylation sites within mammalian mitochondrial import sequences[74]. In support of this, pre-sequence phosphorylation-dependent trafficking by 14-3-3 dimers complexed with hsp70 has been confirmed in plants for both mitochondrial and chloroplast localisation[267]. Hsp90 has primarily been associated with the import of proteins with internal targeting sequences[260]. The PPIase* AIP has recently been shown to be required for the import of a model protein with an N-terminal import pre-sequence via binding close to the import sequence[268].

HSPA8 and 14-3-3s[264,265,269] are required for the ATP-dependent transfer of certain mitochondrial cargo proteins to outer membrane TOM complex receptors (figure 5; 4.2.1). Transfer of cargo proteins from these chaperones has been demonstrated to both TOMM70A and TOMM20[264,265,269]. AIP is also involved in the delivery of cargo proteins to TOMM20 and may cooperate with HSPA8[268]. When bound to cargo proteins, HSPA8[266], 14-3-3s[264] and hsp90[266,270] can all bind TOMM70A, providing an interface between the TOM receptors and cargo proteins. The same may be true for AIP which contains TPR domains that interact with TOMM20 and possibly also HSPA8[268]. TOMM70A also contains TPR domains[271] and these are proposed to be involved in HSPA8 and hsp90 binding[266]. As TOMM70A does not have any chaperone-like activity[272], an important function of hsp70 and hsp90 chaperones in respect to TOMM70A binding, is that they probably facilitate both the reading of internal targeting signals by the TOM receptors and cargo transfer to binding-patches within the TOM complex by maintaining cargo proteins in a quasi-unfolded state while attached to the outer membrane[266].

It should be noted that hsp70[273] and hsp90[274] chaperones are dependent on zone-specific co-factors and co-chaperones for function and that these proteins are therefore also involved in mitochondrial protein import. As would be expected given the prominent role of hsp70s in mitochondrial import, the cytosolic hsp40 co-chaperone Ydj1p is required for mitochondrial import in yeast[275]. Interestingly, Ydj1p contains a C-terminal

---

* Peptidyl-propyl *cis-trans* isomerases (*syn.* cyclophilins) catalyse the isomerisation of propyl peptide bonds enabling twisting of peptide backbones at proline residues.

farnesyl moiety that has been speculated to be involved in anchoring the it to the mitochondrial outer membrane[276,277]. Of the few human hsp40s that have been studied, DNAJA1* and DNAJA2† appear to be required for mitochondrial import as cytosolic partners of HSPA8[278].

4.1.3 The role of proteolysis in mitochondrial localisation

An important backdrop to the import of mitochondrial proteins is that accurate mitochondrial *localisation* is achieved in part by the constant degradation of unimported or mis-localised proteins. Un-imported mitochondrial proteins, for instance cytosolic forms with intact presequences, are notoriously unstable *in vivo*. Under conditions where mitochondrial protein import is inhibited, cytosol-resident mitochondrial proteins are rapidly degraded[279,280] as has been confirmed specifically for nascent COX4I1[181], although proteins which are imported co-translationally are somewhat spared[243]. Furthermore, ectopic overexpression of mitochondrial genes which can be detected at the mRNA level, is generally not manifest as increased cytosolic forms of the proteins[281,282].

The direct transfer of chaperone-bound cargo proteins to the proteasome‡ as a function of either *kinetic partitioning*[283] or *cradle to grave*[284] models of nascent protein turnover[285], provides an explanation for the extremely low steady-state levels of mitochondrial proteins in the cytosol. Without the constant clearing of cytosolic pools of mitochondrial proteins, the accurate localisation of the mitochondrial proteome necessitates an unrealistic, hyperefficient, error-free model of import. Consideration of the role of proteolysis in protein localisation is especially important given the wide spectrum of proteins which are imported into mitochondria *in vivo*, variations in the strength of mitochondrial import signals and the cell-type specific variation in expression of components of the global gene expression machinery required for mitochondrial import.

---

* Non-HGNC name dj2.
† Non-HGNC names dj3, cpr3.
‡ In the context of this thesis, *proteasome* refers to the total protease component of the proteome and is not a specific reference to the 26S proteasome.

Figure 5

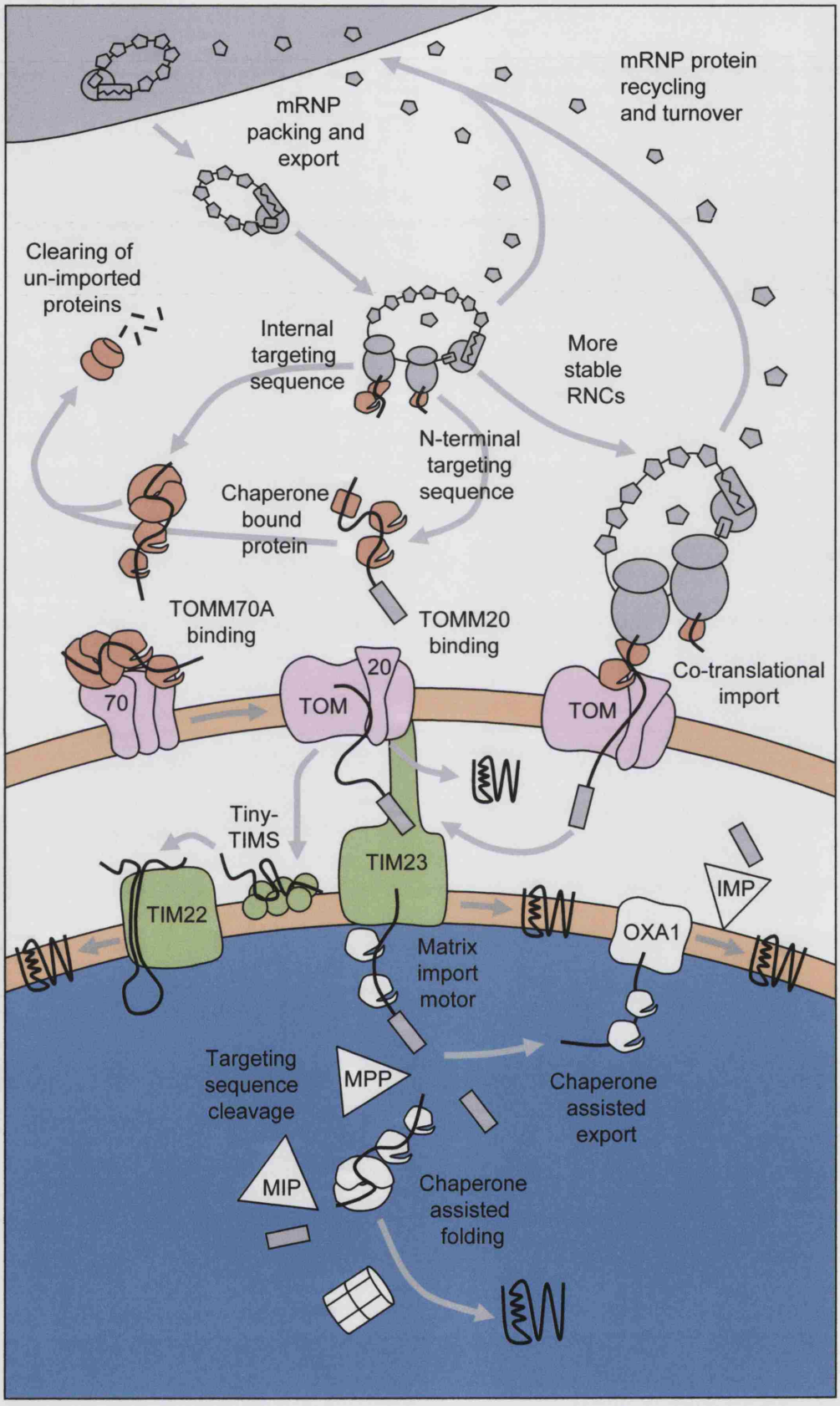
mRNP protein recycling and turnover
mRNP packing and export
Clearing of un-imported proteins
Internal targeting sequence
More stable RNCs
N-terminal targeting sequence
Chaperone bound protein
TOMM70A binding
TOMM20 binding
70
20
TOM
TOM
Co-translational import
Tiny-TIMS
TIM23
TIM22
IMP
OXA1
Matrix import motor
Targeting sequence cleavage
MPP
Chaperone assisted export
MIP
Chaperone assisted folding

Figure 5 Pathways of mitochondrial protein import. Cytosolic aspects of mRNA export, the nucleus, mRNP protein re-cycling and translational control are shown in grey. Cytosolic chaperones such as hsp70s and hsp90s are shown in orange as is the cytosolic proteasome. N-terminal mitochondrial import signals are depicted as grey boxes. The TOM machinery, including GIP complex and TOMM70A and TOMM20 receptors are in pink. The TIM23 complex and TIM22 complex are coloured green along with a membrane associated Tiny-TIM complex. The mitochondrial matrix is coloured blue and matrix proteins involved in handling of the nascent mitochondrial proteome in white. OXA1, OXA1 complex; MPP, matrix processing peptidase; MIP, mitochondrial intermediate peptidase; IMP, mitochondrial IMS peptidase.

4.2 MITOCHONDRIAL PROTEIN IMPORT

Whether imported co-translationally or post-translationally, proteins destined for the mitochondrial compartments appear to translocate the outer membrane via a single outer-membrane translocase called the TOM complex. For IMS-resident proteins, import halts at this point. However, for the majority of the mitochondrial proteome, import continues across the inner-membrane via one of two translocases, the TIM22 complex or the TIM23 complex. Subsequently, cleavable targeting signals are removed by peptidases and export of matrix-resident proteins destined for the inner-membrane is mediated by inner-membrane complexes, including the OXA1 complex. Details of these events are given below.

4.2.1 The TOM complex receptors

The outer membrane translocase (TOM) complex can be functionally divided into two parts, the general import pore (GIP) complex and the receptor proteins[286-288] (figure 5). The receptor proteins recruit mitochondrial targeted proteins at the cytosolic face of the outer membrane and direct them to the GIP complex for membrane translocation. In yeast Tom70p, Tom20p and Tom22p are the principle receptors of the TOM complex[289*]. Studies of Tom70p and TOMM70A have shown that it forms homodimers and primarily recognises chaperone bound cargo proteins with internal targeting sequences[290]. Upon cargo delivery, multiple TOMM70A dimers bind a single cargo protein[290]. Mitochondrial proteins with internal targeting sequences are generally hydrophobic inner-membrane proteins and it is believed that multimerisation of TOMM70A and retention of cytosolic chaperones precludes aggregation in an environment containing an abundance of unfolded proteins[290]. Cargo proteins with N-terminal presequences and certain proteins without, are recognised by Tom20p/TOMM20[290]. It contains a hydrophobic grove in its cytosolic domain that interacts with the hydrophobic face of amphipathic mitochondrial

* Human homologues, TOMM70A, TOMM20 and TOMM22.

targeting sequences[291]. Tom22p is the universal receptor and forms part of the GIP complex. It accepts cargo proteins from the other TOM receptors and directs them through the translocation pores. In contrast to TOMM70A, TOMM20 and TOMM22 have a degree of intrinsic chaperone-like activity which probably contributes to maintaining cargo proteins in an import competent state during interaction with the TOM complex[272].

4.2.2 The TOM complex general import pore (GIP)

The yeast GIP complex component of the TOM complex has a molecular weight of around 400 kDa and is formed by a non-stoichiometric assembly of Tom40p, Tom22p and Tom7p* and a number of smaller proteins[286-288]. Cargo bound receptor proteins are also transiently recruited to the GIP complex during cargo transfer. The core of the GIP complex is composed of Tom40p and Tom22p which from a triple pore structure[292]. The pores have a diameter of around 20 Å and are capable of accommodating α-helices or loops of unfolded cargo proteins. This enables the transfer of proteins with internal targeting sequences mid-section first as opposed to linearly. Cargo proteins are transferred through the pores via a series of interactions of increasing affinity with receptor protein binding-patches on both the cytosolic and IMS faces of the GIP complex, in particular the universal receptor Tom22p. This mechanism of transfer is described as the *binding chain theory* of translocation[293]. Human homologues of most components of the yeast TOM complex have been identified and functional studies in mammalian cells suggest that the general mechanisms of the TOM complex are the same in humans and yeast[294]. Cargo proteins remain bound to TOM receptors on both faces of the outer membrane during translocation. Before translocation is complete, cargo proteins destined for the matrix and inner-membrane are bound by components of either of the two inner-membrane translocases the TIM22 complex and the TIM23 complex[287,288].

4.2.3 The TIM22 complex and the tiny-TIMS

The TIM22 complex is required for the import of polytopic inner-membrane proteins with hydrophobic, internal mitochondrial targeting sequences that are principally components of the eukaryotic component of the mitochondrial proteome[287,288]. It requires $\Delta\Psi$ for function but not matrix ATP. Following import of matrix resident domains, all cargo proteins imported via the TIM22 complex are transferred laterally into the inner-membrane without fully entering the matrix (figure 5).

---

* Human homologues, TOMM40, TOMM22 and TOMM7.

The transfer of cargo proteins between the TOM complex and the inner-membrane components of TIM22 complex is mediated by multimeric complexes of 8-13kDa proteins referred to as the tiny-TIMS. All tiny-TIMs contain conserved $CX_3CX_{11-16}CX_3C$ motifs[295]. These residues are required for function and structural integrity, although discussion remains as to whether they are required for Zn^{2+}-binding or S-S formation. In yeast, free tiny-TIM complexes bind cargo proteins at hydrophobic transmembrane regions as they emerge from the TOM complex[296]. Binding to TOM complex-resident cargo proteins is dependent on $\Delta\psi$ and is necessary and sufficient to stimulate release of the cargo proteins from the TOM complex binding-chain[287,288]. In human cells, all tiny-TIMs appear to be attached to the inner-membrane and to be components of two complexes, one of 70 kDa which is thought to be a hetero-hexameric tiny-TIM complex and another of 450 kDa which appears not to contain any other components of the TIM22 complex[297]. Although the mechanism of transfer of cargo proteins from the TOM complex to the tiny-TIMs is unknown in human cells, they are also believed to function as chaperones binding hydrophobic regions of cargo proteins prior to transfer to the TIM22 complex.

There are three principle membrane components of the TIM22 complex (300 kDa) in yeast, Tim22p, Tim18p and Tim54p. Homologues of Tim18p and Tim54p do not appear to be present in mammalian genomes[287,288,294]. The yeast TIM22 complex contains two import pores[298] formed by Tim22p[299]. Gating of the pores is dependent on $\Delta\psi$, is stimulated by internal mitochondrial targeting signals and is unresponsive to N-terminal targeting signals which stimulate the TIM23p complex[299]. The two pores of each complex function cooperatively and gating of one pore induces closure of the unoccupied pore[298]. Each pore is 18Å in diameter and is wide enough to accommodate two α-helices, enabling the import of internal loops of cargo proteins into the matrix prior to lateral transfer into the inner membrane. While there are likely to be structural difference between the TIM22 complex in yeast and human cells, the overall function of the complex is believed to be conserved.

4.2.4 The TIM23 complex

The import of proteins via the TIM23 complex is the best characterised of the mitochondrial import systems[287,288] (figure 5). The majority of proteins imported via this pathway carry amphipathic α-helical import signals which are predominantly N-terminal and cleaved on import but can also be internal or C-terminal. Cargo proteins for the

TIM23 complex are both eukaryotic and prokaryotic in origin. Import requires both $\Delta\Psi$ and ATP on the matrix side of the inner membrane.

The yeast TIM23 complex is around 400 kDa in size and is composed of approximately equimolar associations of Tim23p, Tim17p, Tim44p and Tim50p[287,288]. The core of the complex is formed by two subunits of Tim23p and two of Tim17p. The C-termini of Tim23p form the import pore[300] and the N-terminal section extends across the IMS and through the outer membrane[301]. This structure is believed to restrict the TIM23 complex to the inner boundary membrane. The TIM23 import pore is 14 Å in diameter[300] which is very similar to the diameter of the ribosomal exit pore. It is able to accommodate a single α-helix and an extended chain. The gating of the pore is very fast and is stimulated by the binding of positively charged peptides to the IMS face of Tim23 in the presence of $\Delta\Psi$[300]. If a membrane potential is maintained across the channel for extended periods it closes, this mechanism is expected to act *in vivo* to stop the collapse of $\Delta\Psi$. Tim17p shares some homology with Tim23p and is involved in stimulation of channel gating by signal peptides[300]. It is not known whether Tim17p is also able to form pores. Tim50p extends into the IMS and binds TOM complex resident cargo proteins[302,303]. It is believed to act as a receptor for the TIM23 complex and to direct cargo proteins to binding-patches on Tim23p. As with transfer to the TIM22 complex, cargo proteins remain bound to the TOM complex during initial interaction with the TIM23 complex and careful disruption of cells enables isolation of 600 kDa, cargo-bound TOM•TIM23 complexes[304]. The binding of cargo proteins to Tim23p causes opening of the conductance channel which leads to passage of the positively charged cargo protein presequence through the inner-membrane into the negatively charged matrix. Once cargo proteins begin to emerge into the matrix, they are either bound by the matrix import motor which facilitates transfer into the matrix[305-307] (4.2.4.1) or, if "stop transfer" signals are present, they are transferred laterally into the inner-membrane without transfer into the matrix (4.2.6.1). As with the TOM complex, homologues of most of the components of the yeast TIM23 complex have been identified in the human genome and there is no evidence of major functional differences.

4.2.4.1 Membrane translocation and the matrix import motor

The translocation of proteins into the matrix via the TIM23 complex requires unfolding of cytosol-resident domains of cargo proteins and pulling of the protein into the matrix. This is achieved by the electrophoretic effect of $\Delta\Psi$ and the activity of the matrix import motor (figure 5). The extent to which each is involved is dependent on the intrinsic properties of

the cargo protein and the characteristics of its N-terminal presequence[308,309]. Proteins with short presequences which only marginally enter the matrix prior to protein unfolding are dependent on $\Delta\Psi$ to catalyse unfolding until a sufficient portion of the protein is inside the matrix to interact with the matrix import motor[309]. Proteins with long presequences are able to recruit the assistance of the import motor earlier and are to a certain extent free from the requirement of $\Delta\Psi$ for unfolding and pulling[309]. Conversely cargo proteins with high positive charges can rely more on $\Delta\Psi$ in the initial stages of import[309]. Both $\Delta\Psi$ and the matrix import motor act to trap the unfolding of the external domains of cargo proteins as they are imported[308,309]. Although there has been much debate[310], it is now accepted that the matrix import motor acts as a Brownian ratchet[311,312], trapping positive moment of cargo proteins into the matrix, rather than using a "power stroke" to pull cargo proteins into the matrix.

The matrix import motor is composed of mitochondrial hsp70 and specific co-factors which function in tandem with the TIM23 complex during import[287,288,313]. In yeast the matrix hsp70 chaperone Ssc1p is precisely positioned to receive emerging cargo proteins via interaction with Tim44p[314]. It functions in concert with the hsp40 co-chaperone Pam18p[315], the scaffold protein Pam16p[316] and the GrpE nucleotide exchange factor Mge1p[317]. The concerted action of these proteins enables ATP-dependent cycling of Ssc1p binding to Tim44p and repeat interaction with cargo proteins during membrane translocation[287,288,311,313]. Homologues of all the components of the matrix import motor are found in human cells[294,315,316], although in contrast to yeast, a pool of soluble TIMM44 also exists in the mammalian matrix[318]. To date no function has been attributed to this pool.

The rate of import of fully translated, prefolded matrix proteins through the TIM23 complex is estimated to be 9-13 amino acids per second[319]. Nascent proteins emerge from ribosomes at around 4 amino acids per second, thus whether they do so post-translationally or co-translationally, cargo proteins entering the matrix face the same disparity between the slow rate of emergence of unfolded domains and the rapid rate of protein folding. For this reason mitochondrial chaperones (4.3.1) are extremely important for the maturation of imported mitochondrial proteins.

4.2.5 Mitochondrial processing peptidases

Mitochondria contain three processing peptidases responsible for the removal of the majority of cleavable mitochondrial import signals (figure 5).

4.2.5.1 MPP

The mitochondrial processing peptidase (MPP) is the matrix resident, Zn^{2+}-dependent peptidase responsible for the cleavage of canonical N-terminal import signals recognised by the TIM23 complex[320]. It is a heterodimer of PMPCA which is thought to be required for substrate recognition and PMPCB which is the catalytic subunit. Both subunits have homology to the complex III CORE subunits, UQCRC1 and UQCRC2. Prediction of MPP cleavage sites remains rather inaccurate. Currently only about 65% of sites fall into predictable motifs which have the following characteristics: an overall positive charge, a predicted amphipathic α-helix structure and one of four motifs specified by the position of argenine residues relative to the cleavage site (R-2, R-3, R-10 and R-none). There is also evidence that the structural characteristics of substrate proteins in the region of N-terminal import sequences contribute to substrate recognition and the complexity of MPP substrate interaction.

4.2.5.2 MIPEP

The mitochondrial intermediate peptidase (*MIPEP*) is a monomeric matrix peptidase required for N-terminal cleavage of certain proteins following cleavage by MPP[320]. MIPEP activity is Mn^{2+} and thiol-dependent and MIPEP sequences show homology to thiol-dependent TOP* family metalloproteases. Predicable substrates for MIPEP all have R-10 MPP cleavage sites and cleavage by MIPEP removes an octa-peptide. As with MPP, structural features C-terminal to MIPEP cleavage sites may influence substrate specificity. *MIPEP* expression is highest in heart, skeletal muscle and brain.

4.2.5.3 IMP

The mitochondrial IMS peptidase (IMP) cleaves IMS resident substrates including those exported from the matrix[320]. In yeast IMP is composed of two subunits Imp1p and Imp2p which are anchored to the IMS face of the inner-membrane via N-terminal anchors. Another potential subunit, Som1p, has also been identified. Catalytic domains of Imp1p and Imp2p are C-terminal Ser/Lys dyads and activity is dependent on the presence of acidic phospholipids. Som1p does not have any homology with either Imp1p or Imp2p. Determinants of IMP substrate specificity remain unclear. In humans only a single IMP subunit gene has been identified[321], *IMMP2L*, which retains the N-terminal transmembrane topology of yeast IMP subunits.

---

* Thimet oligopeptidase, IRP001567.

4.2.6 Inner-membrane insertion

As mentioned above, insertion of TIM22 complex cargo proteins always occurs laterally directly into the membrane. Insertion of TIM23 complex cargo proteins and those encoded by mtDNA occurs via different pathways.

4.2.6.1 "Stop-transfer" insertion

Like the TIM22 complex, import via the TIM23 complex can lead to lateral transfer via a mechanism called "stop-transfer" insertion[322] (figure 5). Proteins inserted in this way are transferred laterally between the protein domains forming the import pores of the complex. Stop-transfer can either result in a conventional N_{matrix}-C_{IMS} topology or the reverse N_{IMS}-C_{matrix} topology. This second form is achieved via import of a single internal loop mediated by an internal amphipathic import signal which is directly C-terminal to the eventual transmembrane domain[323,324]. A defining marker for all stop-transfer inserted proteins is that they have a single transmembrane domain. Cleavable N-terminal targeting signals are processed normally. Proteins inserted into the inner-membrane using stop-transfer are thought to be exclusively the eukaryotic in origin.

4.2.6.2 The OXA1 complex

The OXA1 complex is required for the export of matrix proteins into the inner membrane[322,325] (figures 5 & 6). It has been best studied in yeast and *Neurospora crassa* and in both organisms it is a homo-oligomeric complex, most likely a tetramer, of Oxa1p[326-328]. OXA1 complex cargo proteins are bound directly by Oxa1p[329,330] and are exclusively prokaryotic in origin including mtDNA-encoded proteins and nuclear-encoded proteins imported via TIM23[322]. All nuclear-encoded OXA1 cargo proteins achieve a final N_{IMS}-C_{matrix} topology[322]. mtDNA-encoded cargo proteins achieve either N_{IMS}-C_{IMS} or N_{matrix}-C_{matrix} topologies[330], although the OXA1 complex is not thought to be necessary for C-terminal tail export of mitochondrial N_{IMS}-C_{IMS} proteins[331,332]. Export of N-terminal tails by the OXA1 complex for N_{IMS}- topologies is dependant on the presence of $\Delta\psi$[322]. There remain some questions as to the role of the OXA1 complex in export of internal loops of polytopic proteins and it seems that the complex may play a redundant role, serving to optimise efficient export[322,333]. Whether or not $\Delta\psi$ is required for export of internal loops is also uncertain[322,330,333]. As with many of the questions regarding localisation of the mitochondrial proteome, these uncertainties are a reflection of the extremely small number of model cargo proteins which have been studied.

Mature Oxa1p is a 36 kDa protein which has 5 predicted transmembrane domains[334]. It is well conserved and the human homologue, *OXA1L,* is able to complement *Δoxa1* yeast[335]. Homology between OXA1L and bacterial and chloroplast proteins involved in transmembrane export suggests it represents an evolutionarily conserved membrane translocation mechanism[336-338]. The C-terminal region of Oxa1p forms a basic, coiled-coil domain. This domain is required for interaction with ribosomes[328] and ribosomal large subunits[339] in the region of the ribosomal exit pore. Although binding is higher in the presence of nascent chains, it is not dependent on their presence[328,339], suggesting that the OXA1 complex might be involved in the steady-state attachment of ribosomes or ribosomal large subunits to the inner membrane[216] (figure 5). The binding of ribosomes to the OXA1 complex clearly functions in co-translational export of mtDNA-encoded subunits. Oxa1p binding to mitochondrial nascent chains occurs prior to the completion of translation[330] and is maintained for between 30-60 minutes following translation[340]. Whether the C-terminal domain of Oxa1p also interacts with chaperones involved in the export nuclear-encoded proteins remains to be clarified although there is some evidence that this might be the case[339]. *OXA1L* is located at 14q11.2, it is composed of 10 exons spanning ~5 kb[341]. A single 2 kb transcript is expressed.

4.2.6.3 The OXA2 complex

An *OXA1* homologue has also been identified in *N. crassa* and humans termed *OXA2*[340*]. It appears to be an orthologue of yeast *COX18* which is required for C-terminal tail export of Cox2p[331,332] but is not present in most genomes including *N. crassa* and humans. Indeed, human OXA2 can compliment yeast *Δcox18* strains[340]. Oxa2p forms homo-oligomeric complexes that are similar to but distinct from the OXA1 complex. Homology between Oxa1p and Oxa2p is restricted to the central region and the presence of five predicted transmembrane domains. Oxa2p does not contain the C-terminal ribosome-binding domain present in Oxa1p and it associates with nascent Cox2p and Cox3p (but not Cox1p) for around 1 hour following translation which suggests it functions downstream of the OXA1 complex. Disruption of the OXA2 complex appears to have a specific effect on the assembly of COX and it may represent a COX assembly factor as opposed to a general export complex.

---

* NCBI hypothetical protein FLJ38991.

4.2.6.4 *Other membrane insertion mechanisms*

Despite the important role of the OXA1 and OXA2 complexes in export of inner-membrane proteins, this aspect of mitochondrial biology remains poorly understood. For instance, it is still unknown whether Oxa1p is actually a receptor, a chaperone or a pore forming protein[325]. Genetic studies in yeast have indicated that the OXA1 and OXA2 complexes may not be the only means by which matrix proteins are exported into the inner membrane. While some proteins such as Cox2p are dependent on the OXA1 complex for export, other model cargo proteins appear to show variable degrees of dependence upon it[322]. *OXA1* appears to be dispensable for the insertion of some polytopic nuclear-encoded N_{matrix}-C_{matrix} orientated proteins[333]. Analysis of polytopic TIM23 cargo proteins has shown that they have an abundance of negatively charged amino acids in IMS-resident loops not seen in TIM22 cargo proteins[333]. Export of these proteins is dependent on the presence of $\Delta\psi$ thus spontaneous insertion of some proteins may occur. Furthermore, as many proteins including Oxa2p require Oxa1p for membrane insertion[340], *Δoxa1* strains are complex pleiotropic models of disrupted matrix export that may not provide clear evidence on the role of Oxa1p. In yeast, additional proteins involved in membrane insertion starting to be uncovered such as MBA1[325,327,342] but no homologues have yet been identified in mammals.

4.3 MITOCHONDRIAL CHAPERONES AND PROTEASES

4.3.1 Mitochondrial chaperones required for OXPHOS subunit expression

The nascent mitochondrial proteome contains two pools of unfolded proteins, those emerging from mitochondrial ribosomes and those entering the mitochondrial compartments from the membrane translocation complexes. Both pools of proteins need to fold vectorally and require protection from the crowded molecular environment of the matrix. This protection is provided by the chaperones comprising the mitochondrial foldasome*, members of which handle both pools of unfolded proteins.

4.3.1.1 *Mitochondrial hsp70, hsp40 and GrpE systems*

Mitochondrial hsp70s, hsp40s and GrpE nucleotide exchange factors are best studied in yeast in which a number of distinct systems have been described, typical of the discreet

---

* In the context of this thesis foldasome refers to the entire chaperone system of mitochondria required for handling proteins prior to their maturation.

zones of function apparent for cytosolic chaperone systems[343]. The matrix import motor, described above (4.2.4.1), is a prominent role for these proteins. It comprises pools of the hsp70 Ssc1p[317], the GrpE Mge1p[317,344] and the hsp40, Pam18p[315]. Ssc1p has also been demonstrated to be important for correct folding and maturation of newly imported proteins[345] in a similar manner to cytosolic hsp70 chaperones. In this context, it functions with Mge1p[344] and a different hsp40 called Mdj1p[317]. Two other mitochondrial hsp70s have been identified in yeast, Ssq1p* and Ecm10p. Ssq1p is present at levels around 1000-fold lower than Ssc1p and appears to have a specific function in Fe-S formation[346,347]. Like Ssc1p, it is also thought to use Mge1p as a GrpE, although it utilises a distinct hsp40, Jac1p[347]. Ecm10p has a very high degree of homology to Ssc1p yet is unable to compensate in *Δssc1* strains[348]. It has been identified as a component of nucleoids[112,113] inferring a role in modulation of mtDNA-binding proteins.

To date only a single mitochondrial hsp70, termed HSPA9B† has been identified in humans. This is likely to change however, as many Hsp70s are present in the human genome and cellular localisation data tends to lag genomic and proteomic data. Also, in rodents two isoforms of HSPA9B are expressed[349]. In common with much of the mitochondrial proteome, HSPA9B is also present outside the mitochondria. Detailed analysis has localised it to the plasma membrane, cytoplasmic vesicles[350] and the ER[351] and it has been implicated in cytoplasmic events during transformation[349]. Three putative mitochondrial hsp40s have been identified DNAJA1, DNAJA2[278], DNAJA3[352] although only DNAJA3 has been confirmed as an interacting partner of HSPA9B[352]. Extra-mitochondrial functions have been identified for DNAJA1[353], DNAJA2[354] and DNAJA3[355]. Splice variants of DNAJA2[354] and DNAJA3[352] are expressed leading to very complex patterns of expression for these proteins and, as with mitochondrial hsp70s, it is possible that more hsp40s will be localised to mitochondria. In contrast to the large numbers of hsp70s and hsp40s in the human genome, only two GrpE homologues, *GRPEL1*[356] and *GRPEL2*[357], have been identified, both of which appear to be mitochondrial‡[273,358]. The lack of cytosolic GrpE proteins reflects differences the reaction cycles of cytosolic and mitochondrial hsp70s. All GrpEs interact with hsp70s as dimers[273,359,360]. The complex patterns of hsp70, hsp40 and GrpE expression and localisation evident from what little is known about these systems in mammalian mitochondria suggest that the roles of these proteins in humans are much more complex than those in yeast. While homologous roles in the formation of the matrix import motor and folding of imported proteins can safely be

---

* Also called Ssc2p and Ssc3p respectively.
† Non-HGNC names mt-Hsp70, mHsp70, mortalin.
‡ GrpE Interpro domain IPR000740.

inferred, the well defined roles of these proteins in apoptosis, proliferation and differentiation creates a more complicated picture of their biology in humans.

4.3.1.2 The Hsp60 chaperonin

The mitochondrial hsp60 chaperonin is a member of the group I chaperonin family which includes the bacterial GroEL/GroES complex* and is related to the cytosolic group II chaperonin TRiC†. hsp60 is composed of two stacked, heptameric rings of HSPD1‡ which interacts with a heptameric cap of HSPE1§[273,361,362]. The heptameric rings of group I chaperonins form barrel-like structures which provide protective lumens that enable and enhance the of folding of substrate proteins[273,361-363]. The function of the hsp60s is ATP-dependent and ATP binding and hydrolysis influences interaction with HSPE1 caps[273,361,362].

Like cytosolic chaperones mitochondrial chaperones are highly processive[348]. In yeast, hsp60 acts sequentially with newly imported proteins after their interaction with Ssc1p[364,365]. Other work in yeast has shown that only a subset of the mitochondrial proteome requires hsp60 for folding[366] and that substrates have molecular weights of between 15-90 kDa[367]. The substrate proteins identified for yeast hsp60 can be classified into two main groups, those that require only Hsp60p for folding and those that require both Hsp60p and Hsp10p for folding[367], establishing that there are diverse modes of interaction with hsp60 *in vivo*. Aside from roles in protein maturation and stress responses[368] (4.3.4) and as a component of nucleoids[110,111] in the matrix, hsp60 is involved in apoptotic signalling[369-372] and as with HSPA9B, in human fibroblasts around 15-20% of the total cellular HSPD1 pool is present in the cytosol[373]. The human *HSPD1* and *HSPE1* genes are aligned head to head at 2q33.1 and share a single bidirectional promoter[374]. Basal expression of *HSPD1* is around twice that of *HSPE1* and following heat shock expression of both genes raises around 12-fold[374].

4.3.1.3 Prohibitins

The yeast prohibitins, Phb1p and Phb2p, form a large 1-2 MDa complex[375-377] in the mitochondrial inner boundary membrane[378,379] (figure 5). A homologous complex has

---

* *E. coli* Cpn60 and Cpn10 gene products.
† TCP-1 [tailless complex polypeptide-1] ring complex.
‡ Non-HGNC name HSP60.
§ Non-HGNC name HSP10.

also been identified in human cell extracts[376], composed of PHB and REA* the human Phb1p and Phb2p homologues. Sequence analysis has identified a low level homology between Phb1p and Phb2p and *E. coli* GroEL[376], suggesting a possible structural model for the prohibitin (PHB) complex, in agreement with functional data. The PHB complex is not thought to contain any other proteins[375-377] and cross-linking studies indicate an alternating structure of Phb1p and Phb2p[380]. One model which would satisfy these observations is that of an alternating barrel of Phb1p and Phb2p[380] reminiscent of the Anfinsen cage formed by group I chaperonins and the ring structures proposed for AAA+ proteases (4.3.2.2;4.3.2.4). Assuming a of 1 MDa this would require at least 14 copies of each subunit per complex. The structural association of both proteins has been confirmed genetically whereby deletion strains for one prohibitin gene result in extremely low steady-state levels of the remaining prohibitin protein without alteration in mRNA levels[375,378]. Protease digestion of mitoplasts has indicated that the PHB complex is tightly folded and extends from the IMS face of the inner membrane[375].

A role for the PHB complex in COX biogenesis was determined following the discovery of a molecular association between the PHB complex and the *m*-AAA protease but not the *i*-AAA protease[375]. Using strains overexpressing *[PHB1/PHB2]* or a *Δcox4*† model of aberrant COX assembly, it was demonstrated that the PHB complex stabilises proteins digested by the *m*-AAA such as Cobp and Cox3p and therefore may act as a chaperone for such proteins[375]. This is supported by evidence of transient interaction between nascent, unincorporated Cox3p and the PHB complex[376] and an increase in steady-state levels of the PHB complex in both *mss1* mutants[376] (5.2.3.2) and *Δshy1* mutants[381] (5.2.3.1) which have aberrant COX assembly. The presence of the PBH complex had no effect on the stability of Cox2p in *Δcox4* cells[375] despite evidence that it does bind Cox2p[376]. No data are available regarding interaction between Cox1p and the PHB complex, although nascent Cox1p levels are not increased in *[PHB1/PHB2]* overexpressing cells which have in increased levels of nascent Cobp and Cox3p/Atp6p‡[376]. Evidence for a wide ranging role for the PHB complex in OXPHOS biogenesis comes from recent work with human cells which identified a sub-complex of complex I containing PHB[382].

---

* *PHB* is the HGNC name for the human *PHB1* homologue. *REA* (repressor of oestrogen receptor activity) is the HGNC interim name for the human *PHB2/BAP37* homologue. To avoid confusion the alternative nomenclature proposed independently by Nijtmans *et al*[377] will not be used.
† Homologue of human COX5B.
‡ Cox3p and Atp6p signals were not resolved.

4.3.1.4 *Other mitochondrial chaperones*

In yeast and *N. crassa* mitochondrial PPIases* are required for optimal protein folding in mitochondria[383] and interact with hsp60[384] and hsp70s[385]. Due to their specific function in catalysing conformational change, human PPIases are probably required for optimal biogenesis of the OXPHOS. To date the most prominent human mitochondrial PPIase, *PPID*†, has principally been studied in terms of its role in conformational change of ANT in formation of the mitochondrial permeability transition pore and intermembrane junctions in apoptosis[386].

A single hsp90, TRAP1, has been identified in human mitochondria[387,388]. As with other mitochondrial chaperones it localises to cytosolic locations[388] and specific roles in regulating cytosolic signalling cascades have been demonstrated[389]. TRAP1 is dimeric and appears structurally similar to other hsp90s, although turnover of its ATPase is around 100-fold higher than cytosolic hsp90s[390]. In common with cytosolic hsp90s and hsp60, it is likely to be involved in the folding of imported proteins after their initial interaction with HSPA9B.

4.3.2 Mitochondrial proteases required for OXPHOS subunit expression

Proteases are essential for the assembly of the OXPHOS and mitochondrial biogenesis. They are involved in the turnover of assembly-intermediates of many complexes, maintenance of the appropriate steady-state levels of mitochondrial proteins and in the proteolytic activation or deactivation of specific substrates. As with mitochondrial chaperones members of many different protease families are present in mitochondria.

4.3.2.1 *The AAA+ super family*

The somewhat loosely titled AAA domain (ATPases associated with a number of cellular activities) is an ancient domain present in a large number of proteins in most forms of life[391,392]. There are currently at least 49 AAA domain proteins identified in the human genome‡. The AAA domain is about 220 residues long and contains Walker A and Walker B ATPase motifs. It is believed to function as a Zn^{2+}-binding, ATP-dependent, protein clamp[391]. Hence AAA domains are found in proteins with chaperone and/or protease activities. The AAA+ super family encompasses conserved AAA domain

---

* *Cpr3* and *CyP20* genes respectively.
† Non-HGNC name cyclophilin D.
‡ Interpro Domain IPR003959, AAA domain central region.

proteins and the related Clp/hsp100 family which contain more degenerate AAA domains. AAA+ family members are classified on the basis of the number of AAA domains present. Class I proteins contain two distinct AAA domains, separated by a variable linker and a undefined N-terminal region, related to the specific functions of the protein. Class II AAA+ proteins only have a single AAA domain. Many AAA+ proteins form hepta- or hexameric ring complexes which often associate as larger complexes.

4.3.2.2 Biology of the m-AAA and i-AAA in yeast

In yeast, two inner membrane-anchored class II AAA+ protease complexes, the *m*-AAA protease which faces the matrix and the *i*-AAA protease which faces the IMS, are involved in degradation of OXPHOS subunits[393-395]. Both complexes have been shown to degrade unfolded proteins[396], unincorporated subunits[397,398] and to be involved in the cleavage and activation of specific substrates[399,400]. The *m*-AAA protease is believed to be a heteromer of Afg3p and Rca1p[393,401] and the *i*-AAA a homomer of Yme1p*[393], although other proteins may be required for function of this complex[402]. The exact stoichiometry of the *m*-AAA and *i*-AAA complexes remains to be established[394]. Structural data is available for the related membrane AAA-protease FtsH from *E. coli* which forms flexible, hexameric ring-like structures[403,404], although chromatographic data suggests that yeast *m*-AAA[401] and *i*-AAA[393] complexes may be larger at around 1 MDa corresponding to 12-14 subunits. In common with other AAA+ proteins, oligomerisation of FtsH is essential for function[405].

Little is currently known about the mechanism of action of the *m*-AAA and *i*-AAA complexes. Deletion mutants have confirmed that the transmembrane domains of Afg3p and Rca1p are required for the extraction of membrane embedded substrates by the *m*-AAA[406]. Langer and co-workers have suggested that both complexes are able to extract proteins from the inner-membrane irrespective of the presence of substrate domains on the opposing side of the membrane[396]. However, this work was based on the naive assumption that the *m*-AAA and *i*-AAA protease are the only proteases present in the inner-membrane and that in *m*-AAA or *i*-AAA loss of function strains no other proteases would digest model substrates[396]. An expanding number of proteases have been shown to have substrate specificities which overlap those of the *m*-AAA and *i*-AAA[407,408]. Moreover, recent work by Langer's group has demonstrated that in *m*-AAA loss of

---

* Also referred to as Yta10p, Yta12p and Yta11p respectively.

function strains Oma1p (4.3.2.7) is able to compensate for *m*-AAA loss of function[409] seriously questioning their original work.

Chaperone activity has also been attributed to the *m*-AAA[401] and *i*-AAA[410] complexes. While there is no doubt that expression of these complexes is required for OXPHOS complex assembly[401,411,412], evidence for actual chaperone activity, in the sense of aiding protein folding, remains elusive. *In vitro* studies of the chaperone-like activity of activity of the Yme1p AAA domain by Langer's group[410] are somewhat questionable. The assay for chaperone activity used in this study was based on the prevention of aggregation of unfolded, solubilised substrate proteins. The "chaperone-like" activity of Yme1p AAA domain was only detectable with at least a 3-fold molar excess of AAA domain in the absence of ATP[410]. In the same paper, depletion of ATP was shown to enable to stable binding to unfolded substrate but to inhibit proteolysis[410]. Given the recent identification of a role for the *m*-AAA in import signal clipping of the ROS-scavenger Ccp1p[400*] and the confirmation of a role of the *m*-AAA complex in mitochondrial mRNA maturase maturation[413†], it is entirely possible that roles in OXPHOS assembly attributed to the *m*-AAA and *i*-AAA complexes may simply reflect the wider roles in the activation of essential OXPHOS assembly factors. A wide role for the *i*-AAA in mitochondrial biogenesis is clear from the morphological phenotypes of *Δyme1* strains which are unable to maintain a reticular mitochondrial network[414] resulting in increased autophagy of abnormal mitochondria[415].

The first evidence that AAA+ proteases might be involved in the degradation of COX subunits came from work looking at the effect of Zn^{2+} and ATP depletion on turnover of metabolically labelled mtDNA-encoded proteins[416]. Since their discovery the *m*-AAA and *i*-AAA proteases have been shown to preferentially degrade particular substrates. Loss of Afg3p function led to reduced turnover of *in vitro* translated nascent Cox1p, Cox3p, Cobp, Atp6p and Atp8p in an isolated mitochondria model of aberrant OXPHOS biogenesis[397]. Cox2p turnover was not significantly affected in this model. In a *Δcox4* model of aberrant COX assembly, turnover of nascent Cox2p was dependent on three genes, one of which was identified as *YME1*[402]. A role for Yme1p in nascent Cox2p turnover has also been demonstrated in *Δcyc1/Δcyc7*[‡] model of aberrant COX assembly[398]. The redundancy of the *m*-AAA and the *i*-AAA proteases in terms of steady-

---

* Cytochrome c peroxidase. No human homologue.
† Mitochondrial mRNA maturases are involved in removal of introns from mitochondrial transcripts. Introns are not present in mammalian mtDNA.
‡ Cytochrome c is required for cytochrome c oxidase assembly in yeast[417].

state COX subunit turnover has been demonstrated using an *Δoxa1* model of aberrant OXPHOS biogenesis[418]. While *Δoxa1/Δyme1* double deletion strains had increased steady-state levels of complex V subunits compared to *Δoxa1* strains, steady-state levels of COX subunits were not increased in *Δoxa1/Δyme1, Δoxa1/Δafg3 or Δoxa1/Δrca1* double deletion strains relative to *Δoxa1* strains.

4.3.2.3 The m-AAA and i-AAA proteases in humans

Mitochondrial AAA+ proteases are highly conserved. Both the human[419] and *N. crassa*[420] homologues of *YME1* are able to rescue *Δyme1* yeast and the pea* *m*-AAA subunit homologue is able to complement *afg3p*, *rca1* and *afg3/rca1* yeast strains[421]. The human homologues of the *AFG3* and *RCA1* pair are *AFG3L2*[422] and *SPG7*[423], although based on sequence data alone it is not possible to assign individual homology. Co-expression of [*AFG3L2/SPG7*] restores respiratory competence to *Δafg3/Δrca1* yeast and immunoprecipitation has confirmed that SPG7 and AFG3L2 form part of the same ~1 MDa complex confirming that they are homologous to the yeast *m*-AAA subunits[424]. Expression patterns for *AFG3L1*[422] and *SPG7*[423,425] are very similar with highest expression in heart and skeletal muscle. A second *AFG3*-like gene, *AFG3L1*[227], is also expressed in many human tissues, although the ubiquitously expressed form of *AFG3L1* does not contain an ORF and is therefore thought to be translationally silent[426]. A clearer homology exists for *Yme1* than the *m*-AAA subunits and a single human homologue encoding a mitochondrial protein has been identified termed *YME1L*[427]. *YME1L1* expression is typical of for an OXPHOS-related protein with highest expression in heart, liver, kidney and skeletal muscle[427]. All human *m*-AAA[422-424] and *i*-AAA[427] subunits have been localised to mitochondria.

The high degree of conservation mentioned above and the fact that mutations in *SPG7* are a cause of hereditary spastic paraplegia (HSP) with OXPHOS dysfunction[423] (6.1.3) indicate that the *m*-AAA and *i*-AAA are intimately involved in OXPHOS biogenesis in humans. Fibroblasts from patients with mutations in *SPG7* are sensitive to oxidative stress, have reduced growth in galactose-based medium and reduced complex I activity, although activities of complexes II, III, V and COX are normal[424]. In keeping with a role for the *m*-AAA in OXPHOS biogenesis, the reduction of complex I activity was caused by reduced abundance of the complex[424]. *Spg7*$^{-/-}$ mice have provided a model of *SPG7*-associated HSP and have shown that disrupted synaptic mitochondrial morphology is

---

* *Pisum sativum.*

early feature of the disease[428]. YME1L1 has been found to interact with the presenilins PSEN1 and PSEN2 suggesting an involvement in neuronal development[399*]. These functions underline the role of *m*-AAA and *i*-AAA in a far wider sphere of human biology than simply OXPHOS biogenesis.

4.3.2.4 The biology of the Lon protease in yeast

The matrix-localised Lon protease is highly conserved class II AAA+ protease with a C-terminal peptidase domain and an N-terminal coiled-coil domain required for substrate recognition. Based on work with the yeast Lon subunit, Pim1p[429], Lon is believed to be a flexible, heptameric, ring-like structure *in vivo*[430]. Lon assembly in yeast is a multi-step process which requires autocatalytic processing of Pim1p subunits following assembly of the Lon complex[431].

A number of findings have implicated Lon in OXPHOS biogenesis. At the simplest level the proteolytic and ATPase functions of Pim1p are required for respiration[431,432]. More specifically, overexpression of proteolytically active Pim1p can rescue *Δafg3*, *Δrca1*, *Δafg3/Δrca1* yeast strains[407†] suggesting some overlap of function with the *m*-AAA complex. As with the *m*-AAA protease, Lon has been implicated in the activation of mitochondrial mRNA maturases, however, proteolytically active Lon is also required for the translation of Cox1p-independent of this function[433].

4.3.2.5 Mammalian mitochondrial Lon protease

Lon protease subunits are highly conserved and proteolytically active murine Lon subunit PRSS15 is able to complement *Δpim1* yeast[434]. Metabolic labelling studies of murine PRSS15 suggest that it follows a maturation pathway similar to that described for yeast Pim1p and has a $t_{½}$ of around 24 hours[434]. Human PRSS15[‡] contains a conserved N-terminal Lon domain[§], a C-terminal Lon-C[**] domain and a central AAA domain. Mitochondrial Lon has been shown to degrade mis-folded[435] and oxidatively damaged[436] mitochondrial proteins and the high degree of conservation of PRSS15 suggest that these are universal substrates relevant for human Lon. Overexpression of *PRSS15*

---

[*] YME1L1 referred to by the authors as PAMP.
[†] Subsequent work by Langer *et al*[431] suggests that the form of Pim1p used in this study[407] may have been proteolytically active when fully processed *in vivo*.
[‡] Protease, serine-15. Non-HGNC name hLON.
[§] Interpro domain IPR003111.
[**] Interpro domain IPR008269.

increases association of MTCO1 and MTCO2 *in vivo*, implying a role for Lon in promoting COX assembly[437].

Expression of *PRSS15* in mice is highest in liver with significant expression also seen in heart and kidney, expression in skeletal muscle is surprisingly low[438]. In rat liver, expression of *PRSS15* and steady-state levels of PRSS15 increase following administration of thyroid hormone (T3)[439] which induces mitochondrial biogenesis. PRSS15 expression is also raised in rat hepatoma cells relative to normal liver and *PRSS15* is constitutively expressed during murine embryogenesis suggesting that Lon protease expression is increased under conditions of rapid mitochondrial biogenesis and increased cell division[439]. PRSS15 is component of mitochondrial nucleoids[114] and binds single-stranded DNA[114,434] and RNA[114] at GT and GU rich sequences in a protein substrate-stimulated, ATP-inhibited manner[114]. PRSS15 may bind mtDNA near the L-strand and H-strand promoters in the D-loop region[438] or alternatively at G-rich tracts which occur around once every 100 bp[114,434]. It has been proposed that such interactions may be involved in the regulation of mtDNA/RNA-binding proteins which is a known function of bacterial Lon[114].

4.3.2.6 The mammalian mitochondrial ClpXP protease

The ClpXP protease is a1.2 MDa*, barrel shaped mitochondrial protease which is structurally homologous to many prokaryotic proteases and the cytosolic 26S proteasome. It is composed of multiple copies of two subunits, *CLPP*[442,443] and *CLPX*[441,444]. CLPP is a serine peptidase which is unrelated to other Clp proteins. CLPX is Clp/hsp100, class II AAA+ chaperone. Two stacked, hexameric rings of CLPP form the central barrel of the complex[440,445]. Heptameric rings of CLPX bind both ends of this via their N-terminal domains. They determine substrate specificity for the peptidase and unfold substrate proteins[445]. Thus unlike Lon, in which the AAA and protease domains are part of the same subunit, in ClpXP these domains are resident in two separate subunits. The *in vivo* substrates of mammalian CLPX remain to be determined but are known to have different characteristics from those of bacterial ClpX[445]. The steady-state expression profiles of *CLPP*[442] and *CLPX*[444] are the same with highest expression in skeletal muscle, heart and liver in good agreement with roles in mitochondrial function. A single *CLPP* mRNA is expressed where as two *CLPX* mRNAs are ubiquitously expressed.

---

* Calculated mature protein molecular weigh based on 26 kDa CLPP[440] and 62.5 kDa CLPX[441].

Homologues of the prokaryotic ClpXP protease are present in the chloroplasts and/or mitochondria of many organisms with the exception of fungi which only contain a CLPX homologue (Mcx1p), hence this protease has been very much overlooked relation to mitochondrial biogenesis. Like Lon, ClpXP appears to be predominantly a matrix resident complex. However, immuno-localisation has determined that a significant proportion of ClpXP is associated with the inner membrane[440]. Chloroplast ClpXP has been implicated in degradation of the cytochrome b_6f holo-complex and assembly-intermediates (5.3.1) but not unassembled subunits, suggesting it may play a role in the latter stages of complex assembly and maintenance of holo-complex levels[446]. Although the majority of known substrates for prokaryotic ClpXP are soluble proteins, it has also been implicated in the degradation of some membrane proteins[447]. Similarly the 26S proteasome is involved in degradation of ER proteins following retrograde transport and the AAA+ chaperones of the complex are thought to provide the driving force for membrane export of some substrates[448-450]. Adaptor proteins which modify the substrate specificity of AAA+ proteins, including ClpX, have been identified for a number of AAA+ proteins in different organisms including eukaryotes[451]. Whether such proteins exist in mitochondria remains to be determined.

4.3.2.7 Other mitochondrial proteases

Studies of *Δafg3* yeast recently lead to the discovery of Oma1p a mitochondrial metalloprotease with substrate specificity overlapping that of the *m*-AAA[409]. Like the *m*-AAA the proteolytic centre of Oma1p is matrix exposed and it forms large complexes in the inner membrane[409]. However, Oma1p shows no homology to Afg3p or Rac1p, it does not contain a AAA domain and proteolysis is ATP independent[409]. A role for Oma1p in OXPHOS biogenesis has not yet been examined, however, it can be implied from the overlapping substrate specificity and redundant nature of many protease-substrate interactions, that Oma1p is very likely to be involved. Prior to the discovery of *OMA1*, the human homologue *MPRP-1*[*] had been identified in database screens for metalloprotease motifs[452]. Expression of *MPRP-1* is typical for that of a mitochondrial protein and matches that of the *m*-AAA subunit genes with highest expression in heart, muscle kidney and liver[452]. To date, immuno-localisation indicates MPRP-1 is present in the ER[452].

[*] HGNC interim name.

Another IMS protease, PRSS25*, has recently been described which shows homology to bacterial HtrA2 proteases involved in removal of unfolded and misfolded proteins[453-455], a substrate specificity which would suggest an involvement in OXPHOS biogenesis. PRSS25 is widely expressed in human tissues with highest expression found in kidney and liver[456]. Mutations in *PRSS25* have recently been found in the murine motor neurone disease-2 loci (*mnd2*)[457] and the crystal structures of PRSS25 homologues are well defined[453-455]. To date much of the work regarding PRSS25 has concentrated on its interaction with caspases following release from mitochondria during apoptosis[458,459] and there is no data relating to OXPHOS components.

4.3.3 Kinetic partitioning of the nascent mitochondrial proteome

Based on the close relationships between mitochondrial chaperones and proteases, *kinetic partitioning* of the nascent mitochondrial proteome (which includes un-folded imported proteins and those translated *in situ*) has been proposed by a number of groups[408,460]. In yeast, the *m*-AAA[408] and Lon[408,435] proteases require Ssc1p, Mdj1p and Mge1p for activity indicating that these systems are functionally associated. In addition, optimal degradation of newly imported proteins by Lon requires the chaperone Hsp78p†[461] and as mentioned above, the PHB complex associates with the *m*-AAA[375]. Studies using mammalian mitochondria have demonstrated that mutant ACADM[462] and ACADS[463] interact transiently with HSPA9B during import but are subsequently retained in complex with hsp60. Retention of ACADM in complex with hsp60 can also be induced by limiting the abundance of FAD which is a component of mature ACADM[464]. Subsequent transfer of hsp60-retained ACADS to the mitochondrial proteasome has been confirmed using metabolic labelling[463]. These associations mirror the functional relationship between the cytosolic foldasome and the proteasome and draw further parallel between the handling of nascent proteins emerging from cytosolic ribosomes and the handing of "nascent" mitochondrial proteins emerging from both mitochondrial import pathways and mitochondrial ribosomes. Accordingly, proteins which are able to transit the mitochondrial foldasome rapidly are thought to avoid transfer to the mitochondrial proteasome whereas proteins which are retained within the foldasome due to repeated misfolding or lack of stable binding-partners have a higher likelihood of being transferred to the mitochondrial proteasome[408,460].

---

* Non-HGNC names Omi, HtrA2.

† Hsp78p is a ClpB homologue and a member of the hsp100 class I AAA+ super family. There do not appear to be any ClpB homolgues in mammalian mitochondria.

4.3.4 Mitochondrial stress response (MSR)

Hoogenraad and co-workers[465] coined the term MSR as an extension of the cytosolic and ER stress responses to describe the upregulation of mitochondrial chaperones and proteases in response to disruption of nascent mitochondrial proteome. They found that in response to expression of a mutant, aggregation-prone form of OTC*, expression of the chaperones *HSPD1*, *HSPE1* and *DNAJA3* and the proteases *CLPP* and *PRSS15* were upregulated in simian cells†. Importantly in this model, *HSPA9B* and *CLPX* were not upregulated and neither were specific cytosolic (*HSPA1A*‡, *HSPA8*) and ER (*HSPA5*§) stress-response chaperones. A similar disparity between the involvement of *HSPD1* and *HSPE1* and the absence of a *HSPA9B* response has also been seen in comparisons of ρ^0 and ρ^+ cells[466]. However, other groups have found different patterns of chaperone and protease involvement in similar forms of mitochondrial stress. Levels of mitochondrial chaperones are upregulated in *Caenorhabditis elegans* in an MSR caused by RNAi-induced reduction in expression of subunits from complex I (*NDUFB7*), complex III (*UQCRB,CYC1*) and COX (*COX5B*)[185]. In each case, subunit loss can safely be assumed to lead to aberrant biogenesis of the respective OXPHOS complex. Chaperones involved in this response include homologues of HSPA8 and HSPA9B[185] (hsp60 was not investigated). The involvement of cytosolic and mitochondrial hsp70s in this MSR show it is distinct from that described by Hoogenraad. MSR can also be induced by blockage of cytosolic protein synthesis caused by either direct inhibition or secondary to ER stress which itself causes a reduction in cytosolic protein synthesis. Components involved in this response include *HSPA9B*, *PRSS15*, *YME1L* and *HSPA5* but not *HSPD1*[437] which is also different to the response described by Hoogenraad. In addition, murine cells expressing mutant *PRSS25* have increased sensitivity to ER stress[457] suggesting it may also be involved in this form of MSR. These examples demonstrate that cells respond to disruption of the mitochondrial proteome and that the spectrum of involvement in such responses appears to stimulus-specific.

---

* Ornithine carbamoyltransferase.
† COS7, *C. aethiops*, African green monkey kidney cells (SV40 transformed).
‡ Non-HGNC name Hsp72.
§ Non-HGNC names BiP, GRP78.

5 ASSEMBLY AND MAINTENANCE OF CYTOCHROME C OXIDASE

5.1 FEATURES OF COX HOLO-COMPLEX ASSEMBLY

Over the past 30 years progress has been made in defining a pathway of assembly for the COX holo-complex. The following sections contain a summary of some of the key findings.

5.1.1 Nascent subunits associate with the holo-complex at different rates

5.1.1.1 mtDNA-encoded subunits

Metabolic labelling combined with immuno-precipitation or enzyme purification have demonstrated that nascent MTCO1 is incorporated into the holo-complex more slowly than nascent MTCO2 and MTCO3. In 1972 Weiss[467] noted that in *N. crassa*, labelled Cox3p could be precipitated as a component of the purified holo-complex following 5 minutes of labelling and that both nascent Cox3p and Cox2p could be precipitated following 10 minutes of labelling. Significant incorporation of labelled Cox1p required around 40 minutes of labelling. Subsequently, Nelson *et al*[468,469] demonstrated that a staggered association of the mtDNA-encoded subunits also occurred in rat hepatocytes, implying that this pattern of association of subunits is a universal feature of COX assembly. In whole cells, only labelled MTCO2 and MTCO3 could be immuno-precipitated as components of the holo-complex following 60 minutes of labelling in the presence of cycloheximide* despite the presence of labelled MTCO1 in mitochondrial membranes derived from the same cells[468]. Following 120 minutes of labelling under the same conditions, MTCO1 could be immuno-precipitated along with MTCO2 and MTCO3, indicating that significant quantities of the nascent protein had associated with nascent MTCO2 and MTCO3[468]. Similar results were also achieved in the absence of cycloheximide with nascent MTCO1 detectable in all complete samples but absent from the holo-complex at 30[469] or 60[468] minute time points yet present at 120[468] or 180[469] minutes. Using well characterised polyclonal antibodies against the N- and C-termini of MTCO2 which precipitate un-incorporated and total MTCO2 respectively, Attardi *et al*[470] confirmed the previous work of Weiss and Nelson using metabolic labelling of human tumour cells† in the presence of emetine‡.

---

* Reversible inhibitor of cytosolic protein synthesis.
† HeLa, cervical carcinoma.
‡ Irreversible inhibitor of cytosolic protein synthesis.

5.1.1.2 Nuclear-encoded subunits

Data on the association of the nuclear-encoded subunits of COX is rather sparse. This is no doubt due in part to the very small size and hence low methionine content of many of the small COX subunits*. Nelson *et al* found that in samples from rat hepatocytes antibodies against MTCO2 could immuno-precipitate nascent *subunit VI*† with nascent MTCO2 and MTCO3 following 30 minutes of labelling[469]. As mentioned above, nascent MTCO1 does not immuno-precipitate with MTCO2 and MTCO3 at this time point. This suggests therefore that subunits composing the *subunit VI* signal, associate with nascent MTCO2 and MTCO3 faster than the incorporation of nascent MTCO1 into the holo-complex pool. This result correlates well with crystallographic data in that COX6C predominantly binds MTCO2 while COX6A1 and COX6B predominantly bind MTCO3.

In addition, it can be inferred from work with yeast, that Cox7p‡ probably binds Cox3p prior to its association with Cox1p and Cox2p. Under aerobic conditions when COX biogenesis is elevated, specific antisera raised against Cox6p§ and Cox7p[471] or antisera against the *small COX subunits*"[472], precipitate nascent Cox1p, Cox2p and Cox3p. Under anaerobic conditions when COX biogenesis is restricted, the same antisera only precipitate nascent Cox3p[471,472] despite nascent Cox1p and Cox2p being present in whole mitochondria[471]. This provides strong evidence that under anaerobic conditions in yeast, COX biogenesis is restricted at a point downstream of association of nascent Cox3p with Cox7p but upstream of association of Cox3p•Cox7p with Cox1p and Cox2p.

Although somewhat limited, these examples provide a foundation for the following assumptions, nascent nuclear-encoded subunits probably associate with nascent MTCO2 and MTCO3 faster than nascent MTCO1 associates with nascent MTCO2 and MTCO3 and nascent nuclear-encoded subunits probably associate with nascent MTCO2 and MTCO3 before these two subunits associate to form the holo-complex.

---

* Number of methionine residues in mature subunits: Rat: MTCO1 30; MTCO2 14; MTCO3 7; COX4I1 5; COX5A 1; COX5B 4; COX6A1 3; COX6B unknown; COX6C 3; COX7A2 4; COX7B 0; COX7C unknown; COX8L unknown. Human: MTCO1 32; MTCO2 10; MTCO3 11; COX4I1 7; COX5A 1; COX5B 3; COX6A1 3; COX6B 3; COX6C 5; COX7A2 1; COX7B 1; COX7C 1; COX8A 1.

† Nomenclature as in original paper.

‡ Homologue of human COX7A2.

§ Homologue of human COX5A.

" Subunit bands IV, V and VI, potentially composed of COX4I1, COX5A, COX5B, COX6A1, COX6B, COX6C.

5.1.2 The availability of haem A influences COX assembly

The availability of haem A has been found to influence holo-complex assembly in a number of studies. In 1978 Saltzgaber-Müller and Schatz[473] demonstrated that *hem1*[*] yeast, deficient in global haem synthesis, have normal Cox2p and Cox3p synthesis but reduced synthesis of Cox1p. Despite the presence of significant quantities of the mtDNA-encoded subunits, antibody against Cox6p (which was detectable in the *hem1* cells[279,473]) failed to immuno-precipitate labelled mitochondrial translation products, indicating that residual subunits were not assembled in these mutants. Steady-state levels of the nuclear-encoded subunits Cox4p[†], Cox5ap[‡] and Cox7p were very low in *hem1* cells. *Cox4* and *Cox7* mRNA levels were also reduced[279], suggesting that feedback systems are present which suppress expression of certain subunit genes when holo-complex biogenesis is suppressed and/or that non-COX haem is required for the optimal expression of certain subunits.

A subsequent classic work by Wielburski and Nelson[474] examined the effects of addition of haems A or B to isolated, radiolabelled rat liver mitochondria. Immuno-precipitation with antibody against Cox1p precipitated nascent Cox1p, Cox2p and Cox3p following addition of haem A but only Cox1p in samples treated with haem B or controls. Antibody against Cox2p immuno-precipitated nascent Cox1p, Cox2p and Cox3p following addition of haem A and both Cox2p and Cox3p in samples treated with haem B and controls. As the samples were pulsed, chased and incubated with haem over a total period of 90 minutes the lack of association of Cox1p with Cox2p and Cox3p in the absence of haem A was in agreement with previous work characterising the staggered association of nascent mtDNA-encoded subunits. The association of Cox1p with the other subunits in the presence of haem A within 90 minutes proved that haem A can stimulate the association of pools of unassembled nascent Cox1p with nascent Cox2p•Cox3p and is therefore likely to be rate-limiting for the incorporation of nascent MTCO1 into the holo-complex.

5.1.3 The composition of COX assembly-intermediates

In 1972 metabolic labelling studies by Weiss *et al* suggested the presence of at least two pools of nascent Cox1p in *N. crassa*[467] on the basis of a sigmoid pattern of ^{35}S-Met

---

[*] Hem1p is 5-aminoluvelinate synthase, homologue of human *ALAS1*. Original work was with strain GL1-38 which is 5-aminoluvelinate synthase deficient.
[†] Homologue of human COX5B.
[‡] Homologue of human COX4I1.

incorporation. A similar pattern was later identified in rat hepatocytes[475]. By 1990 it was generally accepted that stable *assembly-intermediates*, sub-complexes composed of nascent subunits, were present in the COX assembly pathway[476].

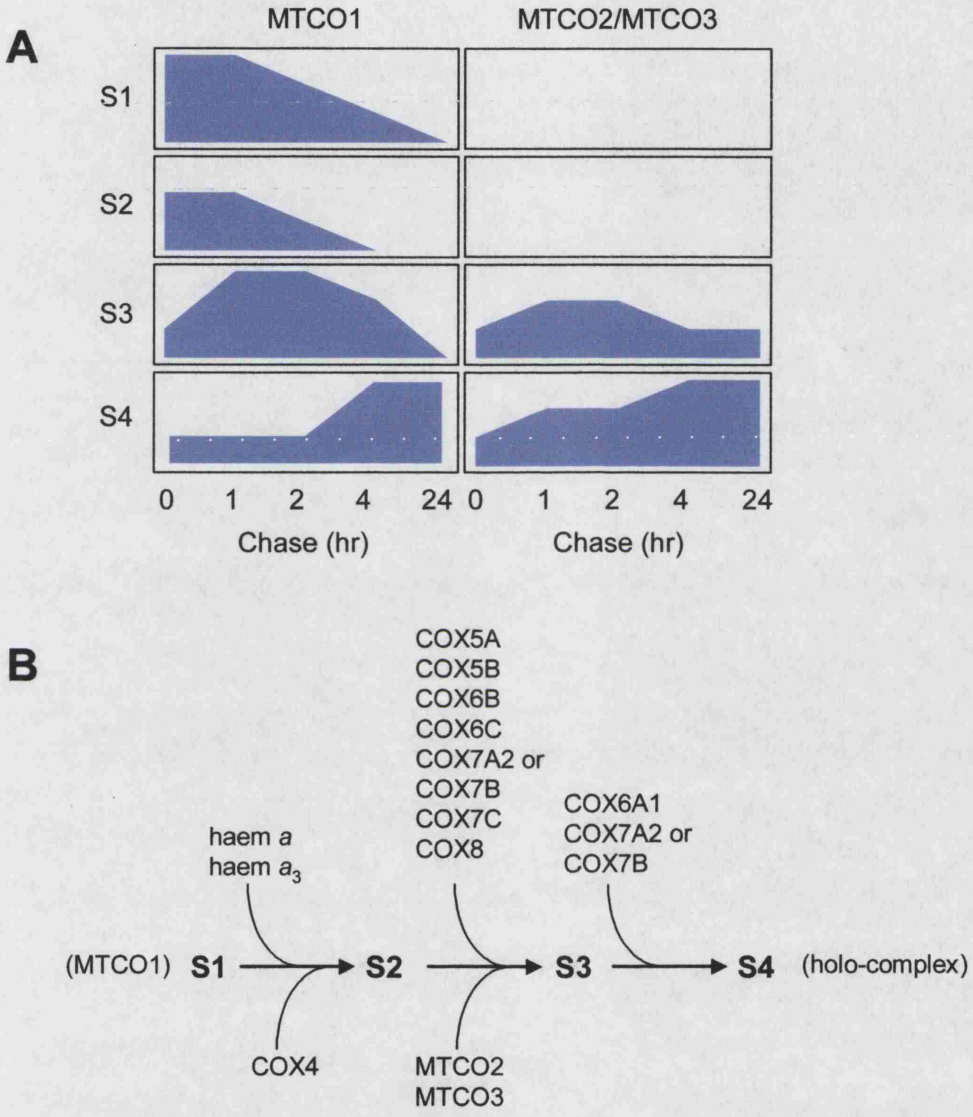

Figure 6A A summary of the 2D BN-PAGE data from Nijtmans *et al*[477]. The figure shows the relative abundance of MTCO1 and MTCO2/MTCO3 signal (arbitrary units) in spots corresponding to assembly intermediates S1-S4 in MOLT-4 human leukemic cells. **6B** The scheme of cytochrome c oxidase assembly proposed by Nijtmans.

The seminal work defining COX assembly-intermediates was published in 1998 by Nijtmans *et al*[477] (figures 7A & 7B). In this work the COX holo-complex monomer, termed S4, and three sub-complexes, termed S1-S3, present in LM-solubilised samples were resolved using blue-native PAGE. Western blotting indicated that S1 contained *at least* MTCO1 and S2 was composed of *at least* MTCO1 and COX4. S3 was found to be composed of many subunits but was nevertheless smaller than the holo-complex

monomer. Using metabolic labelling in the presence of cycloheximide, MTCO1 signal was detectable in S1 and S2 following 1 hour of labelling and persisted during a chase of around 4 hours. MTCO1 signal was clearly detectable in S3 following 1 hour of labelling and a 1 hour chase and then declined slowly over the following 3 hours. MTCO2/MTCO3* signal was detectable in S3 following 1 hour of labelling and peaked following an additional 1 hour chase and subsequently declined over the following 24 hours. MTCO2/MTCO3 signal was also detectable in S4 following 1 hour of labelling and this signal continued to increase over the following 24 hours (figure 6A). The results of Nijtmans study led to the scheme of COX assembly shown below in figure 6B. It is worth noting that none of the assembly-intermediates identified by Nijtmans correspond directly to a complex of nascent MTCO2 and MTCO3 predicted by Nelson and co-workers[469].

5.1.4 Nascent COX subunits turnover during assembly

Metabolic labelling studies have demonstrated that the mtDNA-encoded subunits of COX are subject to high levels of turnover in the first few hours following synthesis. This time period corresponds to the maturation of subunits and assembly-intermediates and their incorporation into the final pool of holo-complex. In yeast, large reductions in the nascent MTCO2 and MTCO3 signal(s) and smaller reductions in nascent MTCO1 signal can be seen in the first 1.5-2 hours following synthesis in respiratory competent cells[402,417,478-480]. Decay of the nascent MTCO2 signal during the window between synthesis and incorporation into the holo-complex has also been noted in normal human tumour cells†[470]. Quantification of the decay of nascent MTCO1, MTCO2 and MTCO3 signals in normal human tumour cells‡ indicates that MTCO2 and MTCO3 signals fall by around 50% in the first 2 hours following synthesis and then decay more slowly, stabilising at around 25% of the t=0 intensity by 20 hours[481]. Concurrent with the drop in MTCO2 and MTCO3 signals, the MTCO1 signal drops by around 10% in the first 2 hours and continues to decay at the same rate, stabilising at around 50% of the t=0 value by 20 hours. The high level of turnover of mtDNA-encoded subunits during maturation is not surprising given the requirement of AAA+ proteases for normal COX biogenesis. Turnover of nascent subunits during synthesis is also entirely compatible with kinetic partitioning of the nascent mitochondrial proteome (4.3.3).

---

* These subunits are not resolved using the tris-tricine second dimension employed by Nijtmans.
† HeLa, cervical carcinoma.
‡ 143B, osteosarcoma.

5.1.5 The half-life of the COX holo-complex

Surprisingly, there is very little data regarding the $t_{½}$ of the COX holo-complex. ^{35}S-Met labelling studies by Kurup[482,483] have calculated a $t_{½}$ of 5.4 days corrected for methionine reuptake from an absolute $t_{½}$ of 10.8 days. A similar $t_{½}$ of 5.7 days was also determined by Ip and co-workers[484] using [^{14}C]-$NaHCO_3$ which is incorporated into arginine, an amino acid with low levels of re-cycling. In the same study Ip also determined a $t_{½}$ for COX-associated haem of 5.7 days indicating that haem A is turned over with the holo-complex and is not recycled[484]. This is in agreement with previous work by Aschenbrenner *et al* which established a $t_{½}$ for haem A of 5.6 days[485].

A study using 2D electrophoresis of labelled extracts from non-proliferating* hepatocytes established that inner-membrane proteins turnover at different rates[486]. Using dual isotope labelling separated by a 44 hour chase period, subunits from COX and complex V were found to be the most persistent proteins with a $t_{½}$ in excess of 100 hours, whereas some components of other complexes turned over with a $t_{½}$ as short as 24 hours[486]. This demonstrates that OXPHOS complexes are differentially targeted for proteasomal turnover in normal cells and that COX is one of the longest lived OXPHOS complexes. The above values are thought to primarily represent proteasomal turnover of mitochondrial components[486]. In addition to this process, lysosomal autophagy of whole mitochondria also occurs, although it is thought not to play a significant role in mitochondrial turnover in normal cell cultures. No data is available regarding the $t_{½}$ of the holo-complex in COX deficient patient cells or any models of defective OXPHOS biogenesis.

5.2 FACTORS REQUIRED FOR THE BIOGENESIS OF COX

Genetic analysis of yeast mutants and patient-derived cells has enabled the identification of an expanding number of COX assembly factors required for haem A synthesis, construction of the copper centres and expression and maturation of the subunits.

5.2.1 Factors required for haem A synthesis

Haem synthesis and breakdown are highly controlled aspects of cellular metabolism due to the potential oxidant properties of haems and their derivates[487]. Synthesis of haem B, which is a component of many proteins, takes place in all cell types. Porphyrin rings are

* Serum deprived.

synthesised via six enzymatic steps from 5-aminolevulinic acid which is principally synthesised in liver mitochondria and exported. The terminal stages of haem synthesis, closing of the porphyrin ring and incorporation of Fe^{2+} by ferrochelatase (*FECH*), take place in mitochondria of all cells. Haem A differs from haem B, in that it has a farnesyl group in place of a vinyl group at C2 and a formyl instead of a methyl group at C8 (figure 7, page 86). Haem A is synthesised from haem B via a stable intermediate, haem O, which is farnesylated but retains a methyl group at C8.

5.2.1.1 COX10

The farnesylation of haem A is carried out by COX10 which is a haem A:farnesyl transferase (EC 2.5.1.-)[488,489]. Farnesyl diphosphate is used as a substrate which is synthesised by farnesyl diphosphate synthase (*FDPS*), a component of the isoprene synthetic pathway responsible for the synthesis of cholesterol, ubiquinone and other non-sterol metabolites. COX10 sequences show homology to other prenyltransferases involved in isoprene synthesis and conservation of COX10 is high. Human *COX10* can compliment yeast *Δcox10* strains[490]. Comparison with the related E.coli enzyme (*cyoE*) suggests that the active sites reside in hydrophilic loops on the matrix equivalent face of the protein[491].

Human COX10 is 443 amino acids long. It is predicted to contain 7-9 transmembrane domains*[490,492] and is assumed to be an integral inner-membrane protein†. The human *COX10* gene is located at 17p11.2-p12, it contains seven exons spread over 135 kb[493]. The promoter region has the characteristics of a house-keeping gene[493] and a single mRNA is ubiquitously expressed with highest expression is seen in heart, skeletal muscle and testis.

5.2.1.2 COX15

COX15 is essential for the conversion of haem O to haem A. Yeast Cox15p localises to the inner-membrane and proteolysis indicates a substantial portion of the protein is membrane embedded[494]. COX15 sequences are well conserved, although they do not have any clear homology to other protein families. Differences in the sedimentation behaviour of native Cox10p and Cox15p have ruled out the possibility of these proteins acting as part of a single complex[495]. Genetic and biochemical screens in yeast have

---

* HMMTOP, http://www.enzim.hu/hmmtop/index.html
† There is currently no published data on the localisation of COX10.

confirmed that Cox15p functions in association with the Arh1p-Yah1p electron transport chain[496,497] which acts as an electron carrier for several mitochondrial cytochrome P450 systems[498]. Yah1p contains an Fe_2-S_2 centre and accepts electrons from Arh1p, an FAD-linked inner-membrane protein which in turn accepts electrons from NADH or $NADPH_2$[498]. The Arh1p-Yah1p system* is also known to be involved in Fe-S synthesis, although the terminal electron acceptor has not yet been identified[499,500]. In *Bacillus subtilis* the *cta*A gene product is required for the conversion of haem O to haem A[488]. CtaA contains a haem B redox centre and has a low level of homology to COX15. Three histidine residues are conserved among all known COX15 sequences and these have been proposed as potential haem coordinating ligands[496]. The reaction mechanism of *COX15* is unknown but is thought to proceed via electron transfer[501] analogous to P450 systems. Formylation of haem O by CtaA is O_2 dependent[502] yet the oxygen of the resulting haem A formyl group is derived from H_2O[501].

Human *COX15* is located at 10q25[503], it contains 9 exons extending over 22 kb. Three splice variants have been identified, termed *COX15.1 COX15.2* and *COX15.3*[503]. *COX15.1* contains a different terminal exon to *COX15.2* and *COX15.3*. *COX15.2* and *COX15.3* differ in the use of alternative poly-adenylation signals for the terminal exon[503] resulting in mRNAs with 3'UTRs of 462, 153 and 1570 bases, respectively. All three splice-variants are ubiquitously expressed with highest expression in heart and skeletal muscle[503]. *COX15.2* and *COX15.3* encode identical proteins of 388 amino acids. The *COX15.1* ORF diverges at residue 367 and encodes a protein of 410 amino acids[503]. Both human isoforms of COX15 are predicted to contain five transmembrane regions. Electrophoretic mobility-shift assays predict a cleaved N-terminal import sequence of 31-32 amino acids and *in vitro* import assays of an unspecified human COX15 isoform has confirmed mitochondrial localisation[503].

5.2.1.3 Control of haem A synthesis in yeast

Examination of yeast Cox-assembly mutants by Tzagoloff and co-workers has provided evidence that haem A synthesis may be regulated by downstream events at two stages. With the exception of *Δcox10* strains, yeast Cox-assembly mutants accumulate haem O relative to controls but have very low levels of haem A[478,495,504]. However, *[COX15]* or *[COX15/YHA1]* overexpressing *cyc3*† null strains[495,497] and *COX15* overexpressing human fibroblasts[505] can accumulate haem A. Haem spectra and the very low levels of

---

* Human homologues: *FDX1* and *FDXR* respectively.
† Cytochrome *c* haem lyase. Cytochrome c is required for cytochrome c oxidase assembly[417].

Cox1p in *cyc3/[COX15]* strains confirm that the predominant haem A environments in these cells are not native holo-enzyme[495]. Tzagoloff and co-workers propose that this capacity to accumulate haem A, not associated with Cox1p, implies that the low levels of haem A in Cox-assembly mutants are unlikely to be caused by haem A degradation and instead may be caused by a down-regulation of haem A synthesis[495]. They propose that as most Cox-assembly mutants accumulate haem O, a component of the down-regulation of haem A synthesis acts at the level of conversion of haem O to haem A[495].

Despite accumulating haem O, *Δcox15* yeast strains have lower haem O levels than most Cox-assembly mutants[495,497]. If strains deleted for single COX assembly factors are also made *Δcox15*, haem O levels drop close to that of single deletion *Δcox15* strains[495]. Generally, overexpression of *[COX10]* in COX-assembly mutants increases haem O levels, the exceptions being strains with a *Δcox15* background where no increase haem O levels is seen[495]. The dominant negative effect of *Δcox15* on haem O levels suggests that Cox15p or a haem O-A intermediate is required for optimal activity of the preceding farnesylation of haem B[495]. In addition, based on the observation that *imp2*/ρ^0 mutants accumulate less haem O than *imp2*/ρ^+ mutants, Tzagoloff has also suggested that haem A synthesis may be regulated by COX assembly-intermediates[495]. These findings imply that haem A synthesis is very tightly controlled and that synthesis and incorporation are a single interlaced system.

5.2.2 Factors required for assimilation of copper

Being a potent oxidant, copper ions are extremely toxic and their movement within cells is very restricted. Eukaryotic cells have a massive overcapacity to bind copper which ensures that the existence of free copper is minimised[506,507]. Copper is generally transported bound to proteins in its reduced state, Cu^+, as opposed to the more catalytically active, oxidised state, Cu^{2+}, generally present in reaction centres. Studies have indicated that there is less than one free copper ion per cell in the cytosol[508]. In contrast, a large pool of non-proteinaceous copper has recently been found in yeast mitochondria[509]. The identity of the copper ligand remains to be determined although the copper pool is accessible to matrix metalloproteins and responds to the abundance of cytosolic Cu^+. It is unknown whether such a pool exists in mammalian cells. Copper entry into human cells is mediated by the ubiquitous plasma membrane carrier SLC31A1[506,507]. Cu^+ bound by SLC31A1 is transferred to specialised metallochaperones in the cytoplasm for transport to target proteins and from the proteins currently identified, it seems that cytoplasmic metallochaperones are dedicated to specific cellular targets.

5.2.2.1 COX17

COX17 is a soluble 8 kDa protein which localises to the IMS and cytosol[510]. COX17 sequences are well conserved in their central regions and do not show homology to any other protein families. Yeast Cox17p exists a tetrameric complex within the IMS and tetramerisation appears to be required for function[511]. The cytosolic form is thought to be dimeric[511]. Binding studies have indicated a stoichiometry of 3 Cu^+ per Cox17p monomer[512] which is unaltered by oligomerisation[511]. Poly-Cu^+ binding is via a conserved CCXC motif which is also required for oligomerisation[511,512]. An amphipathic C-terminal helix is also required for function, possibly through oligomerisation or interaction with other proteins[513]. Cox17p-bound Cu^+ is not solvent exposed, consistent with the role of metallochaperones in shielding copper from interaction with other proteins[511]. The dual localisation of COX17 had previously suggested that it may act as a Cu^+ shuttle between the cytosol and the IMS, however recent work demonstrating that Cox17p function is only required in the IMS[513] and is not required for accumulation of mitochondrial copper[509], has dispelled this hypothesis. Recently, direct transfer of Cu^+ from Cox17p to Cox11p and Sco1p has been confirmed in yeast[514] demonstrating that Cox17p is probably involved in the synthesis of both CuA and CuB.

COX17 is located at 3q13.33 and has three exons spread over 29 kb. A basal housekeeping promoter has been identified upstream of the murine gene[515] and in murine tissues a single mRNA is ubiquitously expressed. mRNA levels are highest in heart, kidney, brain and endocrine tissues[516] (no data are available for skeletal muscle). The mRNA expression pattern which is mirrored by immunohistochemistry, suggests that COX17 may also function in Cu^+ delivery to proteins other than COX[516].

5.2.2.2 SCO1 and SCO2

SCO1 (30 kDa) and SCO2 (25 kDa) are transmembrane proteins located in the mitochondrial inner membrane[517]. Although not all organisms contain two *SCO1*-like genes, SCO1 and SCO2 sequences are highly conserved and where present, both proteins show a high degree of homology and are structurally very similar. They each have a single, equivalently located, transmembrane helices and are orientated in an N_{matrix}–C_{IMS} manner[518] and both have cleavable, N-terminal mitochondrial targeting sequences of around 40 residues. The C-terminal, IMS resident[519] domains of SCO1 and SCO2 contain a conserved CXXXC motif* and a conserved histidine* ($CXXXC(X)_nH$)

---

* SCO1, Cys133-Cys137; SCO2, Cys169-Cys173.

required for Cu^+ binding[520,521]. A similar CXXXC motif coordinates CuA in MTCO2 (table 3). SCO1 shows limited homology to peroxiredoxins and some bacterial thiol:disulphide oxidoreductases which led to an early proposal of a role for SCO proteins in the reduction of the cysteines coordinating CuA although this is now not thought to be the case[521].

Genetic studies indicate that SCO1 and SCO2 have non-overlapping, cooperative functions in human cells possibly dictated by their N-terminal, matrix-resident tails which are the most divergent regions of the proteins[519]. Distinct roles have also been confirmed in yeast as *Δsco1* strains are respiratory deficient *Δsco2* strains are not[522]. The two genes are thought to have originated independently in mammals and fungi are they are not believed to be direct functional homologues[523]. In humans[519,521] and yeast both proteins have been shown to form homomers and Cu^+-independent, Cox2p binding by Sco1p and Sco2p has been confirmed in yeast[518,524]. Overexpression of *COX17* partially rescues *SCO2* mutant cells but not *SCO1* mutant cells and mutations in either *SCO1* or *SCO2* appear to be dominant negative in cells expressing the other SCO protein[519]. Therefore, the current model for SCO1 and SCO2 function is that the IMS domains of SCO2 homomers accept Cu^+ from COX17 tetramers and transfer Cu^+ to CuA in a SCO1-dependent mechanism during MTCO2 incorporation[519]. The mechanism of oxidation of Cu^+ during the synthesis of CuA remains undetermined. It is also worth considering that CuA is removed safely from degraded COX and subunits turned over during normal assembly and it may be that SCO1 and/or SCO2 also function in this capacity.

SCO1 is located at 17p12-p13 around 3.4 Mb from *COX10*. It contains 6 exons spread over 17 kb. A single 1.7 kb mRNA is expressed ubiquitously with the highest steady-state levels in heart, skeletal muscle, liver, kidney and brain[503,523]. *SCO2* is located at 22q13.33. It comprises just two exons and is 2 kb in size. A single 0.9 kb mRNA is ubiquitously expressed with an expression pattern matching that of *SCO1*[523]. Comparisons of signal strength from northern blots indicates that *SCO1* is expressed at higher levels that *SCO2*[523].

5.2.2.3 COX11

COX11 was first implicated in COX assembly in yeast models[525]. It encodes a 28 kDa protein which localises to the mitochondrial inner membrane[525]. As with many COX

---

* SCO1, His260; SCO2, His224.

assembly factors, COX11 sequences are well conserved and do not show homology to other protein families. COX11 contains a single predicted transmembrane helix and is oriented N_{matrix}–C_{IMS}[526]. A role for COX11 in metal ion delivery to COX was initially determined from studies of *Rhodobacter sphaeroides Δcox11* strains[527]. Overexpression of the aa_3 oxidase in these cells results in synthesis of an oxidase lacking CuB and with only 15-30% occupancy of the Mg^{2+} binding site. Recent functional data from yeast Cox11p supports these findings[526] and a role for COX11 in the synthesis of CuA has been excluded in complementation studies of *SCO2* mutant human cells[519]. The IMS domain of COX11 is composed of a unique immunoglobulin-like fold[528] and contains the conserved CFCF motif necessary for Cu^+ binding and another cysteine* thought to possibly be involved in disulphide bond formation[528] during dimerisation[519,526]. A conserved methionine† is also implicated in Cox11p function *in vivo* but not Cu^+ binding *in vitro* and it is thought that it may be involved in copper transfer to MTCO1[526]. The matrix-exposed N-termini of *Schizosaccharmyces pombe* Cox11p shows significant homology to *S. cerevisiae* Rsm22p[526]. Rsm22p is a mitochondrial ribosomal protein and this fusion implies a putative functional association. Based on this finding and the fact that the COX holo-complex can assemble "around" Cox1p lacking CuB in *Δcox11* strains of *Rh. sphaeroides*[527], an attractive model is that Cu^+ delivery to CuB by COX11 occurs co- or para-translationally, prior to association of MTCO1 with MTCO2 and MTCO3. The synthesis of CuB in intact or partially assembled COX is not a popular model given the location of the CuB-haem a_3 centre. Human *COX11* is located at 17q22 and has 4 exons spread over 6 kb. Two transcripts of 1.6 and 2.6 kb are ubiquitously expressed with slightly elevated expression in muscle, heart, brain and kidney[503].

5.2.3 Factors specifically required for COX subunit expression and maturation

5.2.3.1 SURF1

SURF1 encodes a 34 kDa protein which localises to the mitochondrial inner-membrane[504]. A 42 residue, N-terminal targeting sequence is cleaved on import to give a mature protein of 30 kDa[529]. SURF1 sequences are fairly well conserved in organisms with aa_3-type COX complexes and show no homology to any other protein families[530]. Predicted N- and C-terminal transmembrane helices have been reported[504,530], although such results are algorithm-dependent[531] and strongly influenced by the presence of

---

* Cys121, Cys117 and Cys119.
† Met233.

mitochondrial import signals[532]. Certain tools only predict the presence on a N-terminal transmembrane domain*, consistent with a stop-transfer insertion. Proteinase K digestion has indicated that the central region of the protein is resident in the IMS[533].

SURF1 null human cells and *Δshy1* yeast strains† have around 10-40% of wild-type COX activity[478,504,534-537] which is mirrored by reduced cytochrome aa_3 signal[478,504] and haem A/O ratios[495]. This suggests that SURF1 activity is to a certain extent redundant. The haem B, A, O profiles of *Δshy1* yeast strains[495] and *SURF1* null human cells[492] are consistent with SURF1 not being required for haem A synthesis and no known metal binding motifs are present[530]. The functional domains of SURF1 have been examined in both yeast[504] and human cells[529,533] using truncated proteins, although no useful information has emerged as only extremely short truncations of the C-terminal region of the protein are tolerated. *SURF1* null cells have reduced steady-state levels of all COX subunits[478,504,534-537]. In particular, levels of MTCO2 are very low while MTCO1 and COX4I1 are less affected[533,534,538]. The residual MTCO1 and COX4I1 in such cells are components of complexes similar to S1 and S2 and are therefore thought to reflect the presence of stalled assembly-intermediates[529,539,540].

In both human and yeast cell extracts, SURF1 runs as part of a 250 kDa complex and two smaller complexes using BN-PAGE[381] and there is evidence for presence of MTCO2 in the 250 kDa SURF1 complex[381]. Ultracentrifugation of extracts from yeast cells confirm the existence of the 250 kDa complex but find a single 95 kDa complex instead of two smaller complexes[478]. Metabolic labelling has implicated Shy1p in maintaining nascent core subunit levels during COX assembly[381,478]. Direct interaction between Shy1p and nascent Cox1p can be excluded on the basis of GST-pull-down experiments[480] and the different sedimentation characteristics of complexes containing Shy1p and the nascent Cox1p-binding protein Mss51p[478] (5.2.3.4). *Δshy1* strains have reduced rates of translation of Cox1p and reduced stability of Cox2p and Cox3p[478], although *COX1* reporter gene studies have shown that Shy1p is not essential for Cox1p translation[541], suggesting that the reduction in expression is a response to the *Δshy1* genotype. *Δshy1* strains can be partially rescued by overexpression of *[MSS51]* or by expression of *mss51* mutants which increase translation of Cox1p, Cox2p and Cox3p[478]. There are no comparable data regarding translation of MTCO1, MTCO2 and MTCO3 in human cells, although Tiranti *et al* refer to unpublished findings that loss of SURF1 has

---

* e.g. N-terminal only: BROMPT, http://www.jenner.ac.uk/bprompt/ Both: MEMSAT, http://bioinf.cs.ucl.ac.uk/psipred/psiform.html

† *SHY1* is the yeast homologue of *SURF1*.

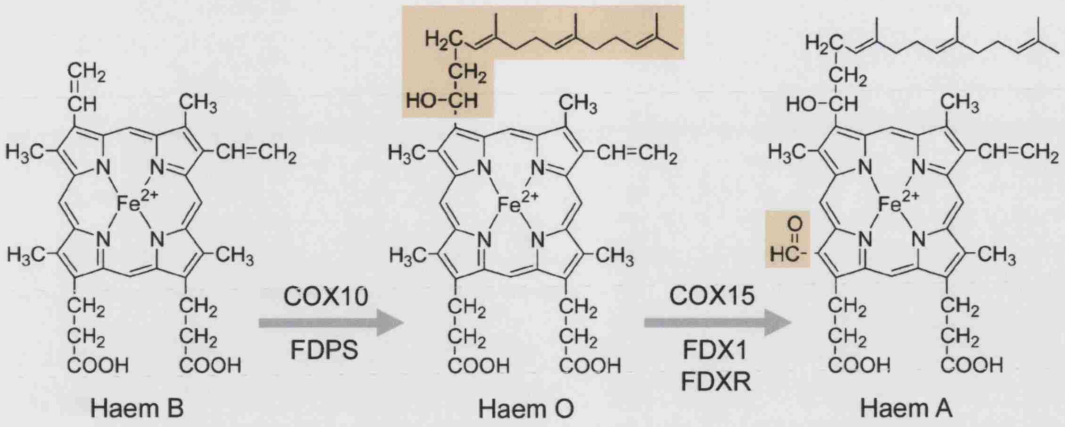

Figure 7 The structures of haems B, O and A. Modifications are highlighted in orange. COX10 and FDPS are required for the farnesylation of haem B at C2 and COX15 and the FDX1•FDXR electron transport chain are responsible for the subsequent formylation of haem O at C8 to give haem A.

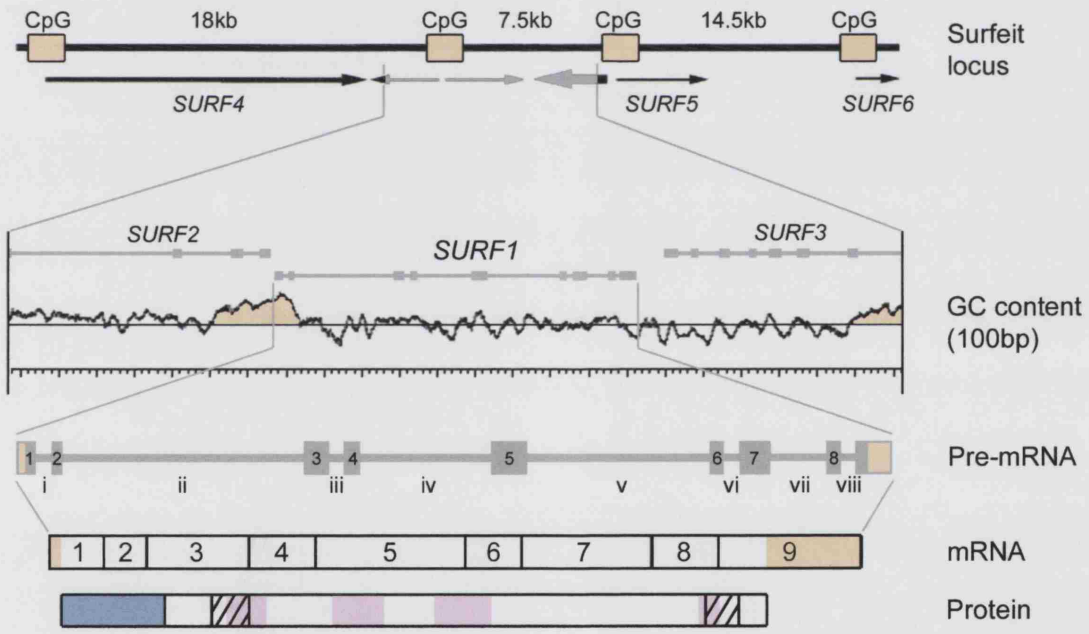

Figure 8 *SURF1* and the surfeit locus. Upper map shows entire surfeit locus with the position and orientation of *SURF1-SURF6*. Yellow boxes mark CpG islands. Central graphic is a C+G trace of *SURF1* (100 bp window) and flanking regions showing the position of CpG island and exons. Lower maps are the *SURF1* primary transcript, mRNA and protein. 5' and 3'UTRs are coloured yellow on the pre-mRNA and mRNA, exons are numbered in Arabic numerals and introns in Roman numerals. On the protein the mitochondrial import sequence is blue, predicted transmembrane domains are cross-hatched and conserved regions are coloured pink.

no effect[529]. A role for SURF1 in assembly of the protein subunits of COX is supported by the increased expression of the PHB complex in Δ*shy1* yeast[381] and a 3-4 fold increase *OXA1* mRNA levels in *SURF1* null cells[542] both of which imply an increase in the handling of nascent proteins in the absence of SURF1.

SURF1 is a member of the surfeit housekeeping gene cluster at 9q34.2 which contains six unrelated genes spread over 60 kb[543] (figure 8). Five of the genes are arranged in alternating orientations with very short intergenic regions of 100-400 bp. The gene order and compact nature of the surfeit locus is conserved among vertebrates. As is typical for many housekeeping genes, the 5' end of each gene is marked by a CpG island. *SURF1* shares a TATA-less bi-directional promoter with *SURF2*. The directionality of expression is regulated by transcription factor binding[544-547] yet expression in the *SURF1* direction alone responds rapidly and transiently to stimuli such as serum, probably via the MAP kinase cascade[548]. *SURF1* contains 9 exons spread over 6 kb. A single 1 kb transcript is ubiquitously expressed with highest steady-state expression in liver, heart and pancreas, intermediate levels in skeletal muscle and kidney and very low levels in brain[533].

5.2.3.2 PET309

Pet309p (106 kDa) is required for maintaining stability of intron containing *COX1* mRNA and wild-type levels of translation of *COX1* in yeast[549] although translation of a *COX1* reporter gene does occur in *Δpet309* strains[541]. Overexpressed *[PET309]* is an integral inner-membrane protein[550]; however, evidence in wild-type cells questions this finding, suggesting instead that it may be peripheral to the inner membrane[551]. BN-PAGE has shown that Pet309p is part of a 900 kDa inner-membrane complex composed of at least 8 proteins including Cpb1p which regulates translation of Cobp* and a protein thought to be the mRNA-binding protein Nam1p[551]. Interaction between Nam1p and Pet309p has previously been demonstrated using immunoprecipitation[552]. Two-hybrid screens have identified binding between Pet309p and the *COX3* expression factors Pet54p (a *COX3* mRNA binding factor) and Pet122p (a ribosome interacting translational regulator of *COX3*[552]). The temporal and stoichiometric features of these interactions remain unknown. Pet309p contains approximately 8 copies of the pentatricopeptide repeat (PPR) motif. PPR† motifs are around 35 amino acids long and are related to TPR domains[127]. They are thought to be composed to two anti-parallel helices and currently have no confirmed function although roles in protein-protein and/or protein-RNA

---

* Homologue of MTCYB.
† Pentatricopeptide repeat, Interpro domain IPR002885.

interactions are inferred. In plants in particular, a growing number of PPR motif proteins are being implicated in organellar RNA metabolism[122,127,164].

5.2.3.3 LRPPRC

LRPPRC is a 157 kDa protein* which contains at least 10 copies of the PPR motif[170,553,554]. Although the homology is extremely low†, LRPPRC is the reciprocal best match of yeast Pet309p[555]. LRPPRC is a component of mRNP particles[176] and binds nuclear and mitochondrial mRNAs *in vivo*[170] and single-stranded, cytosine-rich microsatellite DNA *in vitro*[554]. mRNA binding is mediated via a C-terminal domain which does not show homology to any known RNA binding motifs. Under steady-state conditions, LRPPRC localises to the mitochondrial inner-membrane and smaller pools are also found in the nucleus and cytoplasm[170,553]. In accordance with such a complex pattern of molecular interaction and cellular distribution, LRPPRC contains a canonical N-terminal mitochondrial localisation signal[170] and numerous N-terminal nuclear shuttle signals, protein-protein interaction motifs and transcription factor-binding signals[556]. It is therefore debatable whether LRPPRC is a true COX assembly factor or a protein with pleiotropic functions required for COX biogenesis.

A disease-associated missense mutation[555] (A345V) causes increased cytoplasmic residence of the protein concurrent with reductions in nuclear and mitochondrial abundance[171]. Reductions in steady-state *MTCO1*, *MTCO2* and *MTCO3* mRNA levels and nascent MTCO1 and MTCO3 levels are also seen, while expression of other mtDNA genes appears unaffected. The mechanism by which LRPPRC is involved in COX biogenesis remains to be determined but it may play an orthologous role to Pet309p in maintaining mRNA stability. Tissue distribution is typical for that of an OXPHOS related mitochondrial protein with highest mRNA levels in heart and skeletal muscle, and significant levels in kidney and liver[556]. The C-terminal domain of LRPPRC interacts with a novel MTCO1- and MTND1-binding protein VCY2IP1‡[553,556] (112 kDa) that has significant homology to microtubule-associated proteins[557] (MAPs). *VCY2IP1* maps to 19p13.11 and its expression differs from that of LRPPRC in that a single transcript is expressed at almost uniform levels in all tissues[556] but with highest expression in testes[557].

---

* Apparent molecular weight 130 kDa. Non-HGNC name LRP130.
† Blastp E=0.037, i.e. far too high to be considered non-random.
‡ Previously C19ORF5.

5.2.3.4 *MSS51 and COX14*

Mss51p[558] (50 kDa) and Cox14p[559] (8 kDa) are both peripheral, matrix-face, inner-membrane proteins[480,560], involved in the regulation of translation of Cox1p in yeast. Mss51p is a positive regulator, that functions independently of Pet309p[541]. It interacts with *COX1* mRNA UTRs and coding regions and binds nascent Cox1p within the first 30 minutes following translation[480,541]. Cox14p appears to be a negative regulator of Mss51p function and binds nascent Cox1p post-translationally[480]. The association of Mss51p with Cox1p is not Cox14p dependent[480] yet nearly all nascent Cox1p appears to be bound by Cox14p during the first 30 minutes following translation[480]. Both Mss51p and Cox14p[559] can be isolated as components of >150 kDa complexes that account for around 50% of the abundance of each protien[480]. Examination of *cox14/(COX assembly factor)* double mutants has suggested functional interaction between Cox14p and both Pet309p and Oxa1p[480].

Barrientos and co-workers[480] have proposed a model whereby the initiation and elongation of translation of Cox1p is dependent on the interaction of Mss51p with *COX1* mRNA and nascent Cox1p. Subsequently, Cox1p•Mss51p joins a large complex containing Cox14p that binds Cox1p. The Cox14p•Cox1p•Mss51p complex serves to sequester Mss51p and prevents further stimulation of translation. As assembly proceeds, Mss51p is released from the complex to initiate further translation while Cox14p possibly remains bound to Cox1p. In assembly mutants, Mss51p is not released form the Cox14p•Cox1p•Mss51p complex and translation of Cox1p is down regulated. To date, no human proteins have been identified that show homology to Mss51p or Cox14p, although there are no data regarding low level matches such as that between pet309p and LRPPRC.

5.2.3.5 *Other yeast factors involved in COX biogenesis*

A large number of yeast factors specifically involved in expression of Cox1p, Cox2p and Cox3p have been described. A detailed account of all such factors was felt to be beyond the scope of this thesis for the following reasons:

i) None of the factors omitted from this thesis show any clear homology to mammalian proteins.

ii) Yeast mtDNA contains introns and 5'UTRs and historically a number of factors involved in yeast mtDNA expression have been implicated to function, at least in part, in intron removal or 5'UTR binding.

iii) Yeast Cox2p has an N-terminal presequence that is cleaved on inner-membrane insertion and factors involved in Cox2p expression may be required for this process.

iv) There is only very vague data on the function of most of these factors and generally each factor has only been studied by one or two labs. Hence peer review tends to be rather poor and proposed functions of these factors often change.

v) Under suitable environmental conditions, yeast are able to switch from oxidative phosphorylation to fermentation and are therefore likely to have some differences in the control of expression of OXPHOS subunits.

5.3 CONTROL BY EPISTASY OF SYNTHESIS (CES) AS A MODEL OF ORGANELLAR MEMBRANE PROTEIN COMPLEX ASSEMBLY

Over the past 6 years, evidence has emerged that the assembly of COX may follow a control by epistasis of synthesis (CES) model, as first described by Wollman and co-workers[561-566]. This relatively unexplored aspect of COX assembly is covered in the discussion (17.1.4) and the following sections aim to provide some background on CES.

CES is a universal biological strategy for ensuring the controlled assembly of protein complexes. It describes the inter-dependence of the synthesis of certain subunits on the presence of other subunits[561,563,565]. The concept of CES is widely recognised in chloroplast protein complex assembly and CES-based mechanisms have been demonstrated to control the assembly of the cytochrome b_6f complex, the CF1 portion of the chloroplast ATP synthase, rubisco, the photosystem I reaction centre I (RCI), and photosystem II[561,563,565]. The concept of CES was developed over around a decades work on the assembly of the cytochrome b_6f complex of *Chlamydomonas reinhardtii* by Wollman and co-workers[561-566].

5.3.1 The C. reinhardtii cytochrome b_6f complex

The cytochrome b_6f complex is present in all thylakoid membranes and is functionally and structurally analogous to mitochondrial complex III[567-569]. It exist as a dimer[32] and in *C. reinhardtii* each monomer is composed of eight subunits. The three core subunits, petA (cytochrome *f*)*, petB (cytochrome *b*) and petD (SUIV) are encoded by the chloroplast DNA (cpDNA). The remaining subunits, petC (Reiske), petG, petL, petM and petN are nuclear-encoded and each is present as a single copy per monomer[567]. In the photosynthetic electron transfer chain, cytochrome b_6f lies between photosystem II which reduces co-enzyme Q and photosystem I which accepts electrons from plastocyanin. Cytochrome b_6f transfers electrons from the thylakoid membrane pool of reduced co-enzyme Q to the soluble electron carrier plastocyanin in the thylakoid lumen. Electron transfer is coupled to proton pumping across the thylakoid membrane into the thylakoid lumen via a Q-cycle-like mechanism and direct pumping by the protein complex.

5.3.2 CES of cpDNA encoded subunits

In pulse-chase experiments examining the synthesis of the chloroplast DNA (cpDNA)-encoded subunits, Wollman and co-workers noted that the rate of synthesis of petA was dependent on the presence of the petB and petD subunits[564]. In the absence of either petB or petD, the rate of synthesis of petA dropped, although the protein remained stable for 180 minutes. Conversely, in the absence of petA, the synthesis of petB and petD remained normal yet the proteins were degraded within 15-60 minutes[564]. This pattern of interdependence of synthesis was described as *control by epistasy of synthesis,* CES[561,563,565], i.e. the steady-state levels of petA were controlled by an epistasy of *synthesis*, whereas the steady-state levels of petB and petD were determined by an epistasy of *stability*. Using the terminology of Wollman and colleagues, the subunits dependent on the presence of others for epistasy of synthesis are called CES subunits, in this case petA, and those subunits influencing the synthesis others are called dominant subunits, in this case petB and petD. To date, all CES systems where analysis has been possible have been found to be regulated at the level of initiation of translation of the CES subunit(s)[561,563,565].

---

* For simplicity *C. reinhardtii* cytochrome b_6f subunits are referred to by their gene names and not subunit numbering. Genetic components are referred to here in italics and proteins are in regular font. It is acknowledged that this is not a convention used by plant biologists.

5.3.3 The genetic basis of CES of the C. reinhardtii cytochrome b_6f complex

Analysis of CES mutants found that the 5'UTR of *petA* mRNA was required for CES along with a short patch of the C-terminal region of petA[562,566]. As part of the C-terminal region of petA required for CES is buried in the thylakoid membrane and the exposed residues required for CES do not have mRNA-binding characteristics[566], it was deemed unlikley that petA interacted with the *petA* 5'UTR directly. This suggested the existence of ternary effectors, capable of regulating petA translation in response to levels of unincorporated petA. Genetic screens of *C. reinhardtii* mutants with aberrant petA expression identified only two genes that were specifically required for petA synthesis: *MCA1*, was required for the maturation and stability of *petA* mRNA[570], and *TCA1*, was required for accumulation of normal levels of *petA* mRNA and petA translation[571]. Both *MCA1* and *TCA1* interact genetically with the *petA* 5'UTR[570,571]. As assembly of the cytochrome b_6f complex is insensitive to large decreases in cpDNA transcript levels, it is not thought that regulation of *petA* mRNA levels is a major effector of CES[561]. Steady-state levels of petA are disrupted in *tca1* mutants and such cells do not have the same CES response to deletion of the C-terminal region of *petA* or deletion of *petD* as wild-type cells[571]. This led to the proposal that TCA1 acts as the major effector, inhibiting petA translation when the C-terminal region of unincorporated petA is exposed[563,565,571], though the exact molecular mechanisms underlying the interactions between the petA C-terminus, *petA* 5'UTR, *MCA1* and *TCA1* remain to be determined[561].

6 CYOCHROME C OXIDASE AND DISEASE*

6.1 CAUSES OF COX DEFICIENCY

COX deficiency, either as an isolated defect or part of multiple OXPHOS defects, is a common feature of mitochondrial disorders[574-578]. Greater clinical awareness and improvements in diagnostic techniques over the past 20 years have led to a massive expansion in the spectrum of mitochondrial disorders. In view of this, a detailed description of the clinical spectrum associated with the numerous forms COX deficiency is beyond the scope of this thesis. The following is a summary of the most prominent mitochondrial disorders of which COX deficiency is a feature and those diseases associated with an isolated COX deficiency.

---

* Unless otherwise stated all information in this section is taken from references [572] & [573].

Table 4 Disorders with a COX deficiency associated with mtDNA lesions.

Disorder	Features	mtDNA lesions	Gene	Function
MELAS	Mitochondrial Encephalomyopathy, Lactic Acidosis and Stroke-like episodes	tRNA point mutation, 3243A-G in *MTTL1* (>80%)	-	-
MERRF	Myoclonus, Epilepsy and Ragged Red Fibres	tRNA point mutation, 8344A-G in *MTTK* (>80%)	-	-
NARP	Neurogenic muscle weakness, Ataxia and Retinitis Pigmentosa	Point mutations 8993T-G and 8993T-C in *MTATP6* (>80%)	-	-
Maternally inherited Leigh's syndrome	Characteristic bilateral symmetrical necrotic lesions of brainstem and thalamus	Point mutations in *MTATP6* (~18%)	-	-
PEO	Progressive External Ophthalmoplegia, ptosis, myopathy	Clonal single deletions (40-70%)	-	-
ad/ar-PEO	As above	Multiple deletions (15%[579])	*ANT1*[580]	adenine nucleotide transporter
			PEO1[115]	mitochondrial helicase
			POLG[581,582]	mitochondrial DNA polymerase
Alpers' syndrome	Refractory seizures, neurodegeneration and liver disease	mtDNA depletion	*POLG*[583]	mitochondrial DNA polymerase
Kearns-Sayer syndrome (KSS)	PEO with severe multisystemic disorder	Clonal single deletions (80%)	-	-
MNGIE	Mitochondrial NeuroGastroIntestinal Encephalomyopathy, PEO	Multiple deletions with or without mtDNA depletion	*ECGF1*[584]	thymidine phosphorylase
mtDNA depletion syndrome	Hepatic failure, seizures	Drastic reduction in mtDNA abundance	*TK2*[585]	thymidine kinase
			DGUOK[586]	deoxyguanosine kinase
Congenital nephrotic syndrome (Finnish type)	Severe proteinuria	mtDNA depletion in kidney	*NPHS1*[587,588]	plasma membrane receptor, function undefined

Key: Disorder: ad/ar, autosomal dominant/autosomal recessive. mtDNA lesions: lesions described are the forms most often associated with each disease, percentages in brackets refer to approximate incidence among patients.

Table 5 Mutations in COX assembly factors.

Gene	Function	Mutation classes	Clinical features
COX10	haem O synthesis	Single patient homozygous for N204K/N204K[589].	Fatal infantile leukodystrophy and proximal tubulopathy
		Single patient compound heterozygous for T196K/P225L[492].	Fatal infantile hypertrophic cardiomyopathy and anaemia
		Single patient compound heterozygous for D336V/D336G[492].	Leigh's syndrome and anaemia
COX15	haem A synthesis	Single patient compound heterozygous for R217W and a deletion inducing NMD[505].	Fatal infantile hypertrophic cardiomyopathy
		Single patient homozygous for R217W[590]	Leigh's syndrome
SCO1	Cu^+ chaperone	Single patient compound heterozygous for P174L and 363delGA which induced mRNA instability through NMD[591].	Fatal infantile hepatic failure and encephalopathy
SCO2	Cu^+ chaperone	Six patients compound heterozygous for E140K and either Q53X, R90X, R173W, S225F[523,592].	Fatal infantile hypertrophic cardiomyopathy with encephalopathy
		Two cases[593,594] compound heterozygous for E140K and C133Y/dup1312-1321	Spinal muscular atrophy type-1
		Three patients homozygous for E140K[595].	Severe Leigh's-like syndrome, Neurogenic muscular atrophy and hypertrophic cardiomyopathy
		Index patient compound heterozygous for E140K and Q53X	Undetermined number of spontaneous abortions and foetal wastage.
SURF1	unknown	>40 mutant alleles described, the vast majority of which induce mRNA instability through NMD[536,596].	Leigh's syndrome although rare cases of atypical Leigh's-like disease have been reported
LRPPRC	mRNA biding protein	22 cases are known, among them a single C1277X allele, all other mutant alleles are A345V.	French-Canadian Leigh's syndrome[555]

Regardless of the clinical presentation, in over 75% of cases, COX deficiency is manifest as a failure to maintain normal steady-state levels of COX subunits[538,597]. Importantly this implies that, aberrant biogenesis of the holo-complex is the major cause of COX deficiency as opposed to loss of function of fully assembled forms of the enzyme. The dual genetic origin of COX subunits and the complexity of holo-complex assembly dictates that COX deficiency due to aberrant biogenesis can be caused by a very wide variety factors. Despite the screening of large numbers of samples worldwide, mutations in the nuclear-encoded COX subunit genes have never been documented[598,599] and mutations in mtDNA-encoded genes are very rare[488,578].

6.1.1 COX deficiency caused by mtDNA lesions

There are two principle forms of mtDNA lesions, clonal populations of mutant mtDNA which are inherited maternally and mixed populations of mutant molecules which follow an autosomal pattern of inheritance[573]. Clonal mtDNA lesions are generally heteroplasmic. Our understanding of the molecular mechanisms by which offspring inherit pathological mutant loads of mutant mtDNAs from their mothers remains incomplete[600,601] and it is likely that drift towards high mutant loads during both oogenesis and early embryonic development play a role. Maternally inherited, clonal, mutant mtDNAs can take many forms e.g. point mutations, deletions alone and topologically-related deleted and duplicated forms[573]. Rare cases of sporadic, clonal mtDNA mutations have been also described which also fall into this category[573]. Autosomally inherited mtDNA lesions are generally the result of mutations which impact on mtDNA maintenance. In such instances mutant mtDNA populations are non-clonal and can be detected as mixed populations of multiple deleted and occasionally duplicated forms. A drastic reduction in mtDNA abundance, termed mtDNA depletion syndrome, is also inherited autosomally[585,586,602] and also falls into this category. The relationships between mtDNA genotype and clinical presentation are very poor for most forms of mtDNA lesion whether they be clonal or non-clonal (table 4).

6.1.1.1 Clonal mtDNA lesions affecting mitochondrial protein synthesis

Defects of mitochondrial protein synthesis are generally accepted as the primary cause of the OXPHOS dysfunction seen in cells carrying high mutant loads of mt-tRNA mutations[603]. Large deletions also invariably cause multiple OXPHOS defects due to disruption of mitochondrial translation[603] in addition to the loss of expression of deleted OXPHOS subunit genes because of the distribution of mt-tRNA genes throughout the

mitochondrial genome (figure 4; table 4). The pathophysiology of mt-tRNA point mutations remains elusive and is likely to be heterogeneous[603,604]. There is emerging evidence that in the case of 3243A-G (*MTTL1*) and 8344A-G (*MTTK*), translation is impaired by disrupted maturation of the mutant tRNA[605,606] leading to reduced abundance and charging of mature tRNA[607]. In the case of some other mt-tRNA mutations aberrant excision of the nascent tRNA and disrupted mRNA processing are also thought to be involved[603,604].

Table 6 Mutations in mtDNA-encoded COX subunit genes

Gene	Mutation	Consequence	Clinical features
MTCO1	5920G-A	W6X	Myoglobinuria[608]
	6015del5	42X	Amyotrophic Lateral Sclerosis (ALS)[609]
	6489C-A	L196I	Epilepsia partialis continua[610]
	6721T-C	M273T	Sideroblastic anaemia[611]
	6742T-C	I280T	Sideroblastic anaemia[611]
	6930G-A	G343X	Myopathy[612]
MTCO2	7587T-C	M1T	Encephalomyopathy[613]
	7671T-A	M29K	Myopathy[614]
	7706G-A	A41T	Alpers-Huttenlocher-like disease[615]
MTCO3	9379G-A	W58X	Childhood myopathy and lactic acidosis[616] with recovery[617]
	9480del15	F94-Δ5	Myoglobinuria[618]
	9537insC	P111X	Leigh's syndrome[619]
	9952G-A	W249X	Encephalomyopathy[620]
	9957T-C	F250L	MELAS[621]

Key: 42X, frame-shift induced stop codon at residue 42; F94-Δ5, five amino acid deletion from residue 94.

6.1.1.2 Clonal mutations in MTCO1, MTCO2 and MTCO3

Clonal mutations in the mtDNA-encoded COX subunit genes are extremely rare[578,599,622]. Over the last decade 14 mutations have been identified (table 6) and in contrast to point mutations mt-tRNA genes, many *MTCO1*, *MTCO2* and *MTCO3* mutations are sporadic. All mutations have been heteroplasmic and resulted in severe reductions in COX activity in cells or tissues with high mutant loads. Where data are available, COX biogenesis and steady-state levels of numerous COX subunits are affected. As is typical for mtDNA-associated disease, clinical features of patients with *MTCO1*, *MTCO2* or *MTCO3* mutations are predominantly neuromuscular and show no clear genotype-phenotype correlations. Onset of disease is generally in late childhood or adulthood.

6.1.1.3 *Non-clonal mtDNA lesions caused by nuclear mutations*

Non-clonal mtDNA deletions, duplication or depletion of mtDNA can all be caused by nuclear mutations (table 4). As is the case for clonal mtDNA lesions, non-clonal mtDNA lesions induced by nuclear mutations generally cause multiple OXPHOS defects via disturbance of mitochondrial protein synthesis. The majority of nuclear genes associated with mtDNA lesions are directly involved in maintenance of mtDNA. *ANT1*[580], *ECGF1*{[580,584-586], *TK2*[585] and *DGUOK*[584] are all required for synthesis/maintenance of mitochondrial dNTP pools. Indeed, it has recently been shown that mtDNA depletion can be prevented in cells with *DGUOK* mutations by supplementation of dNTP pools[623]. *PEO1** and *POLG* are both required for mtDNA replication[579,624]. In contrast, *NPHS1* is not thought to be involved in mtDNA maintenance as it encodes a cell-membrane protein expressed in renal glomeruli[625]. Most mutations identified in *NPHS1* lead to accumulation of mutant NPHS1 in the ER[626]. The accumulation of aberrant cell-membrane proteins in the ER is a recognised consequence of disrupted cell-membrane protein maturation[627] and even though mitochondria respond to ER stress[437], the relationship between mutations in *NPHS1* and loss of mtDNA is likely to be complex.

6.1.2 Mutations in COX assembly factors

Mutations in COX assembly factors are responsible for causing COX deficiency in a growing number of patients (table 5).

Mutations in *COX10*[492,589] fall either; within the predicted second transmembrane domain potentially affecting the topology of an adjacent matrix resident active site identified in the *E.coli* enzyme[491] (T196K, N204K) or, within predicted matrix-resident loops thought to be required for farnesyl diphosphate binding[628] and haem B stability[491] (P225L, D336G/V). HPLC analysis of mitochondrial haems has demonstrated that all mutant *COX10* alleles are loss of function alleles[492]. Despite this apparent homogeneity mutations in *COX10* are associated with a number of clinical presentations.

Two patients have been identified with mutations in *COX15*. The first was compound heterozygous for a null allele induced by nonsense mediated decay (NMD) and a missense allele which altered a conserved argenine to tryptophan (R217W) in an extramembrane loop between predicted transmembrane domains 3 and 4[505]. As with

* Non-HGNC name TWINKLE.

COX10 mutations, HPLC analysis showed that this mutation created a loss of function allele. The second patient was homozygous for R217W[590].

Mutations in *SCO1* have also only been identified in a single patient[589]. They carried a null allele and a missense mutation (P174L) immediately adjacent to the Cu^+ binding motif. The most common mutations in *SCO2* also fall in the vicinity of the Cu^+ binding motif (E140K, C133Y, S225F). Detailed biochemical analysis of $SCO2_{E140K}$ and $SCO2_{S225F}$ has shown that they both adopt different structures to the wild-type protein and that while $SCO2_{E140K}$ bound less Cu^+ than the wild-type, $SCO2_{S225F}$ bound more[629]. Moreover, cells derived from patients expressing $SCO2_{N140K}$ have increased Cu^+ uptake but normal Cu^+ retention[521]. Thus the pathophysiology of clinically relevant *SCO1* and *SCO2* mutations appears rather complex, this is mirrored by the finding that mutations in *SCO2* are associated with a number of different clinical presentations.

Mutations in *SURF1* were first identified in patients with COX deficient Leigh's syndrome in 1998[535,537] and mutations in *SURF1* appear to exclusively associated with this biochemical form of the disease. The vast majority of mutations in *SURF1* create premature stop codons which induce NMD, hence the majority of mutant *SURF1* alleles are null alleles. Missense mutations in conserved regions of the protein are also observed, although at much lower frequency.

Mutations in *LRPPRC* were recently identified in 22 patients with French-Canadian Leigh's syndrome[555], making it a significant cause of Leigh's syndrome. French-Canadian Leigh's syndrome is restricted to kindreds originating from the Saguenay-Lac-Saint-Jean region of north-eastern Quebec[630,631]. It is characterised by the presence of an isolated defect in COX activity which is particularly severe in brain and liver but less so in kidney and skeletal muscle. The most common mutant *LRPPRC* allele is the missense mutation A345V[555], the cellular consequences[171] of which are described above (5.2.3.3).

6.1.3 Other nuclear mutations associated with defects in OXPHOS biogenesis

A number of disease loci have been mapped for hereditary spastic paraplegia (HSP). Mutations in the *SPG7* disease locus have been mapped to *SPG7*[423]. SPG7 is a component of the *m*-AAA protease and patients with *SPG7* mutations have decreased OXPHOS function. *Spg7*$^{-/-}$ mice develop a neuropathology very similar to that of HSP patients, the first features of which are an accumulation of abnormal mitochondria in

spinal neurons[428]. Since the identification of mutations in *SPG7*, mutations in the *SPG4* locus have been mapped to *SPG4*. It also encodes an AAA+ protease though the protein does not localise to mitochondria and there is no evidence of OXPHOS defects in patients with *SPG4* mutations[632,633]. Mutations in the mitochondrial hsp60 subunit gene *HSPD1* were identified at the *SPG13* locus[634]. As yet there are no details on the effect of *HSPD1* mutations on COX function.

TIMM8A is a tiny-TIM required for TIM22 complex function. Mutations in *TIMM8A* have been associated with autosomal recessive deafness dystonia syndrome[635,636]. Cells from such patients have defects in the assembly of the TIM23 complex which requires TIM22 function for import[637]. Defects in the function of both import complexes is believed to lead to pleiotropic mitochondrial dysfunction.

6.2 MITOCHONDRIAL DISORDERS RELEVANT TO THIS THESIS

6.2.1 MELAS

Mitochondrial Encephalomyopathy, Lactic Acidosis and Stroke-like episodes is the most common maternally inherited mitochondrial disease[572] (table 4). It is a progressive disorder with a mean age at death of 34 years and is defined by encephalopathy characterised by dementia or seizures, or both; stroke-like episodes; RRF; and lactic acidosis in CSF or blood, or both. Vascular involvement along with other features have led to the hypothesis that MELAS may be an angiopathy. MELAS has been associated with a number of mtDNA lesions. *MTTL1* seems to be a hotspot for point mutations associated with the disease and 3243A-G accounts for around 80% of all cases. In general mutant loads in muscle from MELAS patients exceed 80%.

6.2.2 Leigh's syndrome

Leigh's syndrome is a paediatric subacute necrotising encephalomyopathy that was first described in 1951. The neuropathology is defined by bilateral symmetrical focal necrotic lesions of the thalamus, extending into the pons, inferior olives and spinal chord[638]. The clinical features of Leigh's syndrome are of psychomotor retardation, hypotonia, failure to thrive, respiratory abnormalities, oculomotor disturbance, optic atrophy, seizures and lactic acidosis[638]. Leigh's-like disease is a term used to describe atypical Leigh's syndrome where certain diagnostic features may be absent[638].

Biochemical abnormalities in Leigh's syndrome include PDH deficiency, isolated disruption of OXPHOS complexes I, II and COX and combined OXPHOS deficiencies such as I+IV defects[639]. Leigh's-like diseases has been associated with a similar spectrum of biochemical defects and in addition biotinidase deficiency. This spectrum of abnormalities has lead to the conclusion that a major cause of Leigh's syndrome is defective mitochondrial ATP production. There do not appear to be any relationships between the biochemical defects and the spectrum of features seen in patients with Leigh's syndrome[639]

Clonal mutations in mt-tRNA genes and mtDNA protein coding genes have both been associated with Leigh's syndrome[573]. Disruption of mtDNA integrity such as clonal mtDNA deletions[640] and mtDNA depletion[639] have also been found. The 8993T-C or 8993T-G mutations in *MTATP6* are of particular interest as when present at mutant loads of >75% carriers present with NARP (table 4), whereas when present at mutant loads of >95% carriers present with Leigh's syndrome[641]. The majority of Leigh's syndrome cases are caused by nuclear mutations. Mutations in nuclear-encoded subunits of complex I[642,643] and complex II[644,645], the mRNA-binding protein *LRPPRC*[555] and the COX assembly factors, *SURF1*[535,537], *SCO2*[595], *COX10*[492] and *COX15*[590] have all been identified (table 5). Of the nuclear mutations found to date mutations in *SURF1* and *LRPPRC* are the most frequently encountered.

6.2.2.1 The incidence of mtDNA mutations

In spite of the fact that many mitochondrial disorders have been associated with mutations in mtDNA[572,573] there remains little epidemiological information. A study covering a 10 year period in the North-East of England[646] found a prevalence of disease attributable to mtDNA of 6.57 per 100,000* among the adult population†. According to this figure, mtDNA-associated disease among adults has a prevalence comparable to neurological disorders such as Huntington's disease and motor neuron disease (6.4 and 6.2/100,000 respectively) and is more common than neuromuscular disorders like myotonic dystrophy and Duchenne muscular dystrophy (5 and 3.2/100,000 respectively)[646]. In the same study a minimum prevalence of asymptomatic carriers and affected individuals among all those under 60 years of age was calculated to be 12.48 per 100,000‡. While these data suggests mtDNA lesions may be a relatively common

---

* 95% CI = 5.30-7.83
† Total UK population 58,781,914 in 2001: http://www.statistics.gov.uk/census2001/profiles/uk.asp
‡ 95% CI = 10.75-14.23, mid-year period 1997.

cause of neuromuscular disease in the population as a whole, the incidence of disease due to mtDNA lesions among paediatric patients appears much lower. A population-based study of infants under 6 years of age from Western Sweden covering a 14 year period[575] found an incidence of mitochondrial encephalomyopathies of 8.9 per 100,000* infants and the point prevalence of mtDNA lesions among the under 16s was 1.1 per 100,000†.

6.2.2.2 The incidence of Leigh's syndrome

Despite its prominence in mitochondrial medicine, Leigh's syndrome is a rare paediatric disorder. In the Swedish study described above[575] the incidence of Leigh's syndrome was 3 per 100,000‡ infants. A similar study of the Australian population found an incidence of Leigh's syndrome of 1.3 per 100,000 births and Leigh's syndrome plus Leigh's-like disease had a combined incidence of 2.5 per 100,000 births[638]. To place these figures in context, the total number of live births in the UK in 2001 was 594,634§.

6.2.2.3 The incidence of mtDNA mutations in Leigh's syndrome

Screening large numbers of whole mtDNA genomes has only been feasible in recent years[647]. Nevertheless the seemingly restricted association of a small number of mtDNA mutations with Leigh's syndrome has enabled relatively comprehensive determination of the incidence of clonal mtDNA mutations in Leigh's syndrome using RFLP mapping. Of the 32 patients with mitochondrial encephalomyopathy comprising the Swedish study group[575], only a single case of the eight diagnosed with Leigh's syndrome was found to carry a mtDNA mutation (*MTATP6*, 8993T-C). All patients in the study were screened for 3243A-G[648], 8993T-C, 8993T-G and 8344A-G[649,650], all of which have been associated with Leigh's syndrome[573].

A Japanese study of 100 Leigh's syndrome patients covering a 20 year period, found 18% of cases were due to mtDNA mutations all of which fell within *MTATP6* (8993T-C, 8993T-G, 9176T-C)[651]. In the majority of these cases, the course of the disease was typical with onset in the first year. Another study of 67 Australian Leigh's syndrome or Leigh's-like patients identified over a 17 year period and estimated to include >75% of such patients from South-Eastern Australia during this window, also identified mtDNA

---

* 95% CI = 5.3-14.0
† 95% CI = 0.3-2.9, 1st January 1999.
‡ 95% CI = 1.1-6.5
§ http://www.statistics.gov.uk/CCI/nugget.asp?ID=369&Pos=6&ColRank=1&Rank=224

lesions in 18% of cases[638]. In agreement with the Japanese cohort, mutations in *MTATP6* predominated, accounting for 15% of cases overall. Other mtDNA lesions identified included a mtDNA deletion and a mutation in a mitochondrial tRNA gene, 8344A-G (*MTTK*). Contrary to both the Australian and Japanese studies, examination of 66 Leigh's syndrome patients identified over a 12 year period at Great Ormond Street Hospital, Guy's Hospital and the Department of Neurology University of Newcastle upon Tyne, 25% of whom were non-European, found mtDNA lesions in only 6% of patients[639]. This group was composed of two patients with an *MTATP6* mutation (8993T-C), one with a tRNA mutation (8344A-G, *MTTK*) and a case of mtDNA depletion. 92% of patients in the British study were screened for 8993T-C and 8993T-G confirming the low prevalence of these mutations in this cohort[639].

6.2.2.4 The incidence of SURF1 mutations in Leigh's syndrome and other disorders

According to Tiranti *et al*[536] around 75% of Leigh's syndrome patients with an isolated COX deficiency are thought to carry *SURF1* mutations and Pecina *et al* found that mutations in *SURF1* are present in around a third of all patients with an isolated COX deficiency[652]. Due to the historical nature of the majority of patients reported with *SURF1* mutations, the relatively small numbers of patients involved and international variation in diagnosis of mitochondrial disorders, these figures remain uncertain. Nevertheless it appears that among Leigh's syndrome patients with an isolated COX defect, mutations in *SURF1* are present in the majority of cases[573]. *SURF1* mutations have also been reported in very rare cases without the specific pattern of brain lesions required for a definitive diagnosis of Leigh's syndrome[534,653].

7 THE OBJECTIVES OF THIS THESIS

Given its indispensable role in aerobic metabolism, an improved picture of the biogenesis of COX is an important goal in our understanding of human cell biology. Furthermore, COX deficiency caused by aberrant biogenesis of the holo-complex is a common feature of many paediatric mitochondrial disorders and better knowledge of the biogenesis of COX would improve diagnosis and genetic counselling. To date, much of what we know about the biogenesis of COX has been determined from yeast models. Production of human cell models, particularly of uncharacterised systems, is far more difficult thus patient cells provide a valuable resource for investigating the causes of COX deficiency and improving our understanding of the biogenesis of the COX holo-complex.

This thesis is a comparative study of COX deficient fibroblasts derived from seven patients with mitochondrial disorders of undetermined genetic origin, control fibroblasts and disease control fibroblasts carrying mutations in mitochondrial tRNA genes or the COX assembly factor genes *SCO1* or *COX10*. The objectives of the study were to:

i) Determine as fully as possible the causes of the enzyme deficiency in the patient cells.
ii) To use these cells as models to investigate the biogenesis of the COX holo-complex.

The characterisation and phenotyping of the patient cells is presented in Section 10 and genetic analysis is presented in Section 11. The involvement of mtDNA was excluded in all cultures and mutations in *SURF1* were identified in four of the cultures. The OXPHOS subunit signatures of the *SURF1* mutant cells suggested the presence of stable COX sub-complexes. Section 12 covers the investigation of COX sub-complexes in the patient cells and disease controls using blue-native PAGE (BN-PAGE). The Results are discussed in Sections 13 to 18.

CLINICAL DETAILS AND MATERIALS & METHODS

8 CLINICAL DETAILS

8.1 TERMINOLOGY

The patient fibroblast cultures examined in this study are designated the letter "P" followed by a number. The patients from which they were derived are referred to using the same numbering but without any prefix e.g. P1 was derived from patient 1. The suffix "s" denotes siblings of patients or cell cultures derived from these patients and where necessary multiple siblings are also numbered e.g. P1s1 was derived from patient 1s1, the sibling of patient 1. Amniocytes from patient 6s are denoted by the suffix "a", P6sa. Control fibroblast cultures are numbered and have the prefix "C".

8.2 PATIENT 1

Patient 1 was born to healthy unrelated parents. She presented with hypertrichosis, lactic acidemia, hypotonia and ataxia. Nystagmus was noted from 2.5 years. A muscle biopsy, taken 3 months later, showed normal morphology. CT scan was normal. She had delayed bone age, was never able to walk independently, suffered from excessive sweating with polyuria and there was a progressive loss of motor and mental achievements. The patient died at the age of 3.3 years from respiratory insufficiency. Autopsy was not performed. A younger sister, patient 1s1, also presented with hypertrichosis and died of a similar illness. Three other siblings, 1s2, 1s3 and 1s4 were unaffected. Biochemistry for patient 1 is given in table 7.

Table 7 Biochemical data from P1-5 and muscle derived from the same patients.

	Fibroblasts (nmol•min^{-1}mg^{-1} protein)			Muscle (•min^{-1}g^{-1} tissue)									
Patient (fibroblast culture)	Cytochrome c oxidase (IV)	Succinate-cytochrome c oxidoreductase (II+III)	IV/II+III	IV (k)	II+III (U)	NADH oxidase (I; U)	Succinate dehydrogenase (II; mU)	PDH (mU)	2KGDH (mU)	CTP1 (mU)	CTP2 (mU)	CK (U)	Protein (mg)
1 (P1)	0.00	5.77	0.000	5	1.20	1.00	269			75	72	158	134
2 (P2)	0.00	1.57	0.000	5	0.33	0.74		136	305			132	88
3 (P3)	0.28	16.7	0.017	3	1.47	0.77	188	471		63	98	162	112
4 (P4)	0.15	11.7	0.013	4	1.20	0.88	412	411					166
5 (P5)	0.00	25.8	0.000	0	0.34	0.75		234				131	131
controls	2.29	13.8	0.2	95	5.2	3.66	723	759	988	77	96	307	174
SD	0.51	2.8	0.04										
range min/max	0.72-5.66	3.03-27.8	0.062-0.460										

Key: Carried out in the laboratory of Dr HR Scholte.

Table 8 Biochemical data from patient 6.

Tissue	Biochemical data					
Muscle	COX/CS	Complex I/CS	Complex II+III/CS	Complex II/CS	Succinate dehydrogenase/CS	Complex III/CS
	31 (100±13)	87 (76±24)	676 (368±55)	439 (282±40)	789 (271±71)	134 (88±72)
P6 fibroblasts (controls)	COX	PDH (native)	PDH (activated[a])	pyruvate carboxylase	II+III	lactate/pyruvate ratio
	2.82±0.34 (6.63±1.2)	1.12±0.04 (1.02±0.51)	1.36±0.15 (1.28±0.28)	0.34 (0.91)	4.90±0.46 (n/a)	104±42 (19±3)

Key: Muscle biochemistry carried out in the laboratory of Dr Nancy Kennaway. Fibroblast biochemistry carried out by Dr Brian Robinson and is given as nmol•min-1mg-1 protein. [a] = activated by dichloroacetate; n/a = data not available.

8.3 PATIENT 2

Patient 2 had no antenatal problems but fed poorly at birth and rapidly developed a metabolic acidosis with profound lactic acidemia. He failed to gain skills and died aged 7 months. A muscle biopsy revealed a marked type-IIb fibre atrophy with accentuated T-tubules but no other abnormalities. A male sibling had severe intrauterine growth retardation, was born with a gross lactic acidemia, hypotonia and hypospadias, and died at 27 h of age. Biochemistry for patient 2 is given in table 7.

8.4 PATIENT 3

Patient 3 was born to healthy unrelated parents after a normal pregnancy (37/40). A heart murmur was noted at 6 weeks and a right divergent squint from 1.25 years. He was first admitted to a hospital at 1.5 years with a viral infection. On arrival, the patient was shocked, poorly perfused and drowsy and blood lactate was raised. CT brain scan was normal and EMG showed no evidence of peripheral neuropathy. Echocardiogram revealed hypertrophic cardiomyopathy and pericardial effusion. A renal tubular defect was also noted. The patient died aged 2.4 years. Post-mortem examination established a diagnosis of Leigh's syndrome. Two older siblings had also died, one a stillbirth and the other a sudden death after a mild upper respiratory tract infection at the age of 1.5 years. A third sibling was 9 years old and well at the time of admission of patient 3. Biochemistry for patient 3 is given in table 7.

8.5 PATIENT 4

Patient 4 was the first child of healthy, unrelated parents following a normal pregnancy (2700 g). After an initial normal development, he presented with vomiting at 8 months, by 1.2 years showed failure to thrive and subsequently developed progressive cerebellar ataxia, nystagmus, hypotonia and developmental regression. No optic atrophy or peripheral retinopathy was noted and muscle biopsy showed normal complex IV histochemistry but increased lipid. Plasma lactate was elevated. EMG showed mixed peripheral neuropathy, CT brain scan was normal but MRI of the brain showed lesions consistent with Leigh's syndrome. Subsequently there was a progressive deterioration leading to death (age at death was unclear as the patient died at home). A subsequent

child died of a similar disorder but was not investigated. Biochemistry for patient 4 is given in table 7.

8.6 PATIENT 5

The clinical details and some biochemical findings of patient 5 have been reported[654]. The patient was born to unrelated parents and early development was uneventful but by 6 months the infant was failing to thrive. By of 1 year age he presented with metabolic acidosis and was diagnosed with proximal renal tubular acidosis. The patient continued to thrive poorly and developed hypotonia and intermittent nystagmus. At 1.4 years, MRI of the brain and an EEG were both normal. Later, the patient developed increased tremor and ataxia with indications of further renal tubular damage. A second MRI showed demyelination in the cerebellum, basal ganglia and medulla oblongata. The child died aged 2.5 years. Post-mortem examination confirmed a diagnosis of Leigh's syndrome. Biochemistry is given in table 7.

8.7 PATIENT 6

Patient 6 was induced at term although intrauterine growth retardation had been noted from 26 weeks. On day 1 she had metabolic acidosis with a pH of 7.1 which persisted and was due to elevated lactate that rose to a maximum of 34 mM (controls 1.0-1.8 mM). She was treated with bicarbonate and a "vitamin cocktail" under total parental nutrition. A mild facial dysmorphism was noted with simple ears and broad nasal bridge. Brain MRI was normal but MRS showed a marked elevation of lactate. Muscle and skin biopsies were performed on day 8. She remained stable until day 9 when she underwent rapid desaturation, requiring intubation. Her condition continued to deteriorate and she died later that day. At autopsy the liver was markedly abnormal with micro- and macrovesicular steatosis, cholestasis, pseudoacinar formation, bile duct proliferation and marked deposition of iron. Kidneys also showed lipid accumulation. Neuropathology was indicative of a developmental problem with bilateral porencephaly, microcephaly and dysgenesis of cingulated gyri. A sibling, patient 6s was induced at 24 weeks following evidence of intrauterine growth retardation from week 22. The baby died 45 minutes after birth. Amniocentesis had been performed at week 17. Autopsy of patient 6s was normal except for excess stainable iron in hepatocytes. Biochemistry for patient 6 is given in table 8.

Table 9 Biochemical data from patient 7.

Tissue	COX (nmol•min^{-1}mg^{-1} protein)	Citrate synthase (CS; nmol•min^{-1}mg^{-1} protein)	CS/COX (all controls 0.5-2.5)
P7 fibroblasts	2.9	92	31.7
Lymphocytes	8.6	80.6	9.4
Muscle (PM)	33	232	7

Key: Carried out in the laboratory of Dr J Houštěk.

Table 10 Biochemical data from patient 8.

	Activities (nmol•min^{-1}mg^{-1} protein)					Ratios				
Tissue	Complex I	Complex II	Complex III	II+III	COX (IV)	IV/I	IV/II	IV/III	III/II	IV/II+III
Liver	28 (11-31)	79 (76-194)	150 (95-246)		17 (84-245)	0.6 (8.2±2.3)	0.2 (1.6±0.2)	0.1 (2.4±0.2)	1.9 (2.4±0.2)	
Muscle				30 (19-37)	0.5 (94-196)					0.2 (4.7±1.3)

Key: Carried out in the laboratory of Dr P Rustin[591].

8.8 PATIENT 7

The course of the disease in patient P7 was typical for Leigh syndrome with symmetrical lesions of the basal ganglia noted on brain MRI. Failure to thrive, growth retardation, hypertrichosis and strabismus developed from 6 months, followed in the second year with progressive hypotonia and clinical symptoms of severe cerebellar disturbances. Wrist X-ray showed diffuse osteoporosis. Laboratory investigations revealed raised blood and cerebrospinal fluid (CSF) lactate levels (B-lactate 2.55-4.9 mmol/l; control values < 1.8 and CSF-lactate 4.1 mmol/l; control values < 2.1) with increased blood lactate/pyruvate ratios (20-30; control values 12-18). CSF-alanine was increased (79 µmol/l; control values < 35), although urinary organic acids profile and free and total carnitine levels in blood were normal. Spectrophotometric measurements of enzyme activities in isolated lymphocytes, fibroblasts and muscle tissue revealed a severe deficiency of COX relative to citrate synthase. The girl died of bronchopneumonia at 34 months. Biochemistry is given in table 9.

8.9 PATIENT 8

Patient 8 has been previously described[591]. He was born to unrelated, healthy parents at term (2700 g) and was hypotonic, lethargic and required immediate assistance for respiratory distress at birth. He had severe metabolic acidosis (pH 7.19, plasma bicarbonate 7.7 mM, lactate 12.7 mM, controls <2.5 mM) with high urinary lactate, fumarate and succinate. Hepatocellular dysfunction was noted at day 4 but recovered thereafter. Severe axial hypotonia, hypoglycaemia and hyperlactatemia (3.5 mM) persisted and liver enlargement was observed. He continued to present with recurrent episodes of apnoea and bradycardy and died aged 2 months. At post mortem, histopathology of liver showed swollen hepatocytes with microvesicular lipid vacuoles and panlobular steatosis. Accumulation of lipid droplets was also noted in muscle. A year later a second boy was born at 34/40 (1750 g). He presented with severe neurological distress and metabolic acidosis and died aged 5 days. Biochemistry for patient 8 is given in table 10.

8.10 PATIENT 9

Patient 9, a male born to consanguineous parents has been previously described[589,655]. Two siblings have also been described: An older sister died aged 5 years from a mitochondrial encephalopathy ascribed to COX deficiency[655] and a younger sister died of a similar condition to patient 9 aged 3 years[656]. Patient 9 was born full term after an uneventful pregnancy and had an unremarkable development until 18 months. At 18 months he presented with ataxia and his neurological condition worsened over the following 6 months. At 2 years he presented with poor eye contact, severe muscle weakness, hypotonia, ataxia, ptosis, pyramidal syndrome and status epilepticus. Heart ultrasound was normal. Blood and CSF lactate were elevated (3.8 and 3.1 mmol/l, respectively), and urinary amino acids, lactate and Krebs cycle intermediates could be detected, indicative of a renal tubulopathy. An isolated COX defect was identified in muscle, lymphocytes (47 $nmol \cdot min^{-1} mg^{-1}$ protein, controls 72-203[589]) and fibroblasts[655]. He died at 2 years of age.

8.11 CONTROLS

8.11.1 Normal controls

C1 and C2 were both primary dermal fibroblast cultures. C1 was derived from a 1.5 year old male patient admitted for orchidoplexy and C2 was derived from a healthy 1.5 year old female.

8.11.2 MELAS disease control

The disease control MELAS primary dermal fibroblast culture was derived from an adult patient diagnosed with MELAS. A 79% mutant load of the 3243A-G *MTTL1* mutation was determined by Dr Mei Gu (Neurosciences, RFUCMS) via quantitative RFLP.

9 MATERIALS AND METHODS

9.1 PHENOTYPIC ANALYSIS

9.1.1 Establishment of primary cultures used in this study

All the fibroblast cultures used in this study were derived from skin biopsies and were established out of house using standard procedures. P1-P5 were sent from Dr HR Scholte (COEUR, Erasmus University Rotterdam, Rotterdam, Netherlands), P6 was a gift from Dr NG Kennaway (Oregon Health & Sciences University, Portland OR, USA) and P7 was a gift from Dr J Houštěk (Academy of Sciences of the Czech Republic, Prague, Czech Republic).

9.1.1.1 A549 cells

The A549 ρ^+ and A549 ρ^0 cultures* used in this study were a gift from Dr Ian Holt (Dunn School Cambridge UK). The A549 cell line was originally derived from a lung carcinoma of a 58 year old Caucasian male. As with many tumour cell lines, A549 cultures have an abnormal karyotype. Analysis ECACC suggest that they are hypotriploid with around 8% polyploidy.

9.1.1.2 Primary amniocytes

Primary amniocytes were obtained by amniocentesis and cultured as described[657] in media containing a 1:1 mix of Ham's F10 (Invitrogen, 31550-23) and Chang's (Irvine Scientific, T101-019) base media. Aside from the different media, all maintenance was as for primary fibroblast cultures (9.1.2).

9.1.1.3 Generation of tsT-fibroblast lines

Cells from P1, P3, P5, P6 and the control culture C1 were transduced with a retroviral vector conferring *Neo*^{r} and a temperature sensitive isoform of SV40 large-T antigen. The ability of this vector to influence the growth properties of human primary dermal fibroblasts has been previously documented[658]. When grown at 35°C proliferation of transduced fibroblasts was higher than that of controls and when grown at 39°C, in contrast to controls, transduced cells did not proliferate. Transduction was carried out by

---

* Specific ρ^0 clone was A549.B2.

Dr Mike O'Hare of the Ludwig Institute UCL. The vector used, pZIP-NeoSV(X)1, was constructed from Moloney murine leukaemia virus (MMLV) and the pBR322 plasmid, to enable propagation of the vector in *E. coli*[659]. It contained MMLV 3'- and 5'-LTRs*, the pBR322 and SV40 origins of replication, an MMLV 3' splice site and *Neo*^{r} from the transposon Tn5†. The isoform of SV40 large-T antigen (*Tag*) inserted into the 3' splice site in this instance contained the *tsA58* mutation conferring temperature sensitivity, and the *U19* mutation blocking DNA binding[660,661]. Prior to being given to Dr O'Hare, all of the cell cultures were treated for 14 days ciprofloxacin (1 mg/ml) to remove potential mycoplasma infection. Treatment was halted 7 days before transduction. Vials of cells selected for transduction were all between passages 6-10 when defrosted. Transduction of the fibroblasts by Dr O'Hare was as described in Xu *et al*[658] except that two rounds of infection were used. Transduced tsT-fibroblast cultures were not cloned and were used as mixed clones throughout this study. All tsT-fibroblast cultures were grown at 33°C in accordance with advice from Dr O'Hare. The use of these cells was enabled on the basis of, and was in accordance with, Royal Free & University College Medical School, Genetically Modified Organism application RF99-2.

9.1.2 Cell culture

All primary dermal fibroblast cultures, tsT-fibroblast cultures, A549 ρ^0 and ρ^+ cultures, and fibroblast-A549 synkaryons were maintained under identical conditions. The base medium used was a high glucose DMEM (25 mM glucose) with Glutamax I (l-alanyl-l-glutamine; Invitrogen, 61965-026) to which the supplements were added to the proportions indicated; 10% (v/v) γ-irradiated FCS (BioWest, 5096551800/100), 0.2 mM uridine (Sigma, U3003), 1 mM sodium pyruvate (Invitrogen, 58636), 50 U/ml penicillin and 50 µg/ml streptomycin (Invitrogen, 15140-122). Cultures were grown in Heraeus or Nuare DH autoflow tissue culture incubators with 8% CO_2 and 90% humidity at 37°C, except for tsT-fibroblast cultures which were grown at 5% CO_2 and 90% humidity at 33°C. Phosphate buffered saline (PBS) for use in tissue culture was made from 10x concentrate and sterilised in house. Cultures were always dissociated for passaging using trypsin solution (Invitrogen, 25090-28) diluted 1/25 in Versene EDTA solution (Invitrogen, 15040-066) and stopped using full culture media. For routine cell culture,

---

* Long terminal repeats.

† The sequence for the (related) vector pZIP-NeoSV(Tag), containing SV40 large-T antigen which has been constructed from component sequences is available from the NCBI as accession Z93724. The pZIP-NeoSV(X)1 sequence deposited at the NCBI (accession M18803) contains only the pZIP-NeoSV(X)1 5'-LTR which differs slightly from that of pZIP-NeoSV(Tag) and is suitable only for vector screening.

stopped trypsin was not washed off cell suspensions prior to re-plating. Fibroblast cultures were generally passaged every 2-4 days and generally split 1 in 3. Small quantities of cells were routinely grown in 90 mm diameter Nunc culture dishes (57 cm^2; Nunc, 150350). When larger quantities of cells were required, cultures were expanded in triple-layered culture flasks (500 cm^2; Nunc, 132913). Nunc coated 35 and 60 mm dishes and 96 well plates were used as required for specialist applications (Nunc, 153066, 150288 & 161093).

9.1.2.1 Freezing and thawing of cells

Identical techniques were used for the freeze/thawing of fibroblasts, A549 ρ^0 and ρ^+ cultures, and fibroblast-A549. Generally, cells from one confluent plate were frozen for storage in 600 µl normal culture medium with 10% (v/v) DMSO. Vials of cells were slow frozen in polystyrene boxes -70°C (assumed to provide a temperature drop of ~1°C/minute) and then transferred to liquid nitrogen for long term storage. Vials of cells were rapidly defrosted in a water bath at 37°C. Freezing media was removed by centrifugation and cells were initially seeded onto no more than 2 plates.

9.1.2.2 Collection of cell pellets for nucleic acid purification

For DNA/RNA purification cells were trypsinised and resuspended in a 10x volume of full medium. Suspensions were pelleted at 1000 rpm using a Sorvol T6000D bench top centrifuge and washed in an equal volume of PBS. Pellets were resuspended in 1 ml PBS and pelleted at 6500 rpm using a Heraeus Biofuge fresco refrigerated mini-fuge, in standard, free-standing, 1.5 ml tubes (screw cap, o-ring), aspirated and stored at -20°C until required. Pellets for DNA purification were generally prepared from 2-5 plates of cells of between 70-100% confluence (0.6-4.0 $x10^6$ cells). Pellets for RNA purification were prepared from proliferating cultures of no more than 70% confluence.

9.1.3 COX activity stains

The histochemical COX activity stain employed in this study was based on the widely applied diaminobenzidine (DAB) stain described by Seligman and co-workers[662]. The stain is based on the oxidation of an effectively electroneutral "off the shelf" cytochrome c solution by COX which in turn enables the oxidation and polymerisation of DAB, forming a brown precipitate in the vicinity of the enzyme. Unlike TMPD-based reactions used in polarography[663,664], this reaction requires repeated binding and release of cytochrome c from the enzyme.

Cells were seeded on uncoated, 22 mm, glass coverslips at around 50% confluence and left to proliferate to around 90-100% confluence under standard culture conditions (9.1.2). For staining, coverslips were washed 3x in PBS with 0.5 mM $MgCl_2$ and 0.9 mM $CaCl_2$, drained and air dried for around 10 minutes. When dry, coverslips were soaked for around 1 hour at 37°C in a tissue culture incubator in an aqueous staining solution containing 50 mM sodium phosphate buffer (pH 7.4), 0.5 mg/ml DAB·4HCl, 1 mg/ml horse heart cytochrome c (Roche, 103888; formerly Boehringer Mannheim) and 2 µg/ml catalase (Sigma, C9322). Coverslips were then washed once in PBS and soaked in Zymed DAB Enhancer (00-2021) at room temperature for 15 minutes. They were then washed again in PBS, counterstained using a standard Mayer's haematoxylin stain[665], dehydrated using 3x 30 second washes in ethanol followed by xylene, and mounted using DPX mountant (BDH 360294H).

9.1.4 Spectrophotometry

Spectrophotometric analysis of freeze-thawed cells was carried out under the guidance of Dr Brigitte Meunier at the Galton laboratory, UCL. Cells pellets were collected as those for nucleic acid analysis (9.1.2.2) except that around 10^7 cells were frozen per pellet. Thawed cell pellets were resuspended in 200 µl chilled suspension buffer (50 mM tris·HCl, 10% ficoll (BDH, 43709 3T) on ice. Analysis was carried out using a single beam instrument built in house. Readings were standardised to total cellular protein using the BCA protein assay kit (9.1.5.3).

9.1.4.1 Whole-cell visible spectra

60 µl of each cell suspension was reduced by the addition of a small quantity of solid sodium dithionite. Absolute reduced spectra were recorded against a baseline of milk solution which has similar light scattering properties to cell suspensions in the 520-650 nm region. Readings were taken using a cuvette with a 45 µl chamber volume and a light path of 3 mm. Quadratic baseline correction (QBC) was used to correct for imperfect matching of the synthetic baseline[666]. An estimation of the *c*-type cytochrome content of the samples was obtained from A550-A542 nm using a molar extinction coefficient[667] of ε=18 $mM^{-1}•cm^{-1}$. The *b*-type cytochrome content was determined from A563-A579 nm using ε=27 $mM^{-1}•cm^{-1}$. The cytochrome aa_3 content was determined from A604-((A594-A614)x0.5) using an extinction coefficient[667,668] of ε=14 $mM^{-1}•cm^{-1}$. Following the addition of cyanide (CN; 10 mM final) to the reduced samples, the CN-binding cytochrome a_3

content was determined from absolute, reduced, QBC-corrected spectra using A592-A610 nm with an extinction coefficient[667,668] of ε=18.7 $mM^{-1} \bullet cm^{-1}$.

9.1.4.2 Whole-cell CO laser-flash photolysis

A 100 µl aliquot of each cell suspension was diluted to 500 µl with suspension buffer (9.1.4) and reduced by the addition of solid sodium dithionite. Cellular membranes were permeabilised by the addition of LM to a final concentration of 1 mM. CO ligation and saturation was achieved by bubbling CO through the samples for 2-4 minutes at room temperature. Room temperature photolysis of CO-ferrohaem a_3 was achieved with short actinic laser light pulses of a frequency doubled Nd-YAG laser (10 ns half peak width; 532 nm; >100 mJ/pulse). Signals were recorded at 430 and 445 nm and 20-50 transients were signal-averaged at each wavelength. The CO-binding cytochrome a_3 content of the samples was determined from the amplitude of the difference spectra (A430-A445 nm) of CO re-ligation following photolysis using a molar absorption coefficient[667] ε=113 $mM^{-1} \bullet cm^{-1}$. The haem a_3 environment of the samples was investigated by determining the rate of CO ligation[666]. First order decays were fitted by eye to the difference spectra to give an observed rate constant (κ_{obs}).

9.1.5 Denaturing gel electrophoresis and western blotting of lauryl maltoside protein extracts

Denaturing SDS-urea polyacrylamide gel electrophoresis (PAGE) was carried out using Bio-Rad Mini Protean II or Mini Protean 3 mini-gel systems (10 cm) more or less as described previously[669,670].

9.1.5.1 Collection of pellets for protein extraction

Cell pellets for protein extraction were prepared in much the same way as those for nucleic acid purification (9.1.2.2) except that they were collected into standard conical bottomed, flip cap 1.5 ml tubes and the second wash to pellet the cells used cold PBS with the following protease inhibitors, 1 µg/ml leupeptin, 1 µg/ml pepstatin and 1 µM PMSF* (Sigma, L5811, P5318 & P7626). For protein purification, cells were harvested from proliferating cultures of between 70-90% confluence and pellets were used immediately without freezing prior to use.

---

* Phenylmethylsulfonyl fluoride.

9.1.5.2 *Preparation of lauryl maltoside protein extracts*

Lauryl maltoside* protein extracts (LM extracts) were prepared from whole cells[669,670] using a PBS/LM solution containing protease inhibitors. Cell pellets (9.1.5.1) were resuspended and solubilised in PBS containing, 27 mM LM (equivalent to 1.35% w/v; Anatrace, D310), 4.5 µg/ml leupeptin, 4.5 µg/ml pepstatin and 10 µg/ml PMSF for 30 minutes on ice. The volume of solubilising solution added was estimated by eye according to an approximation of 200 µl per average single plate pellet. Samples were centrifuged using a mini-centrifuge at 13,000 rpm for 20 minutes at 4°C, the supernatant was decanted into a clean tube and stored at -80°C until required.

9.1.5.3 *Balancing of LM extracts*

The protein content of LM extracts was determined using the BCA Protein Assay kit from Pierce (23225) read using a Hitachi U3210 spectrophotometer. The kit is based on the biuret reaction, the reduction of Cu^{2+} to Cu^{+} by peptide bonds and cysteine & cystine, tryptophan and tyrosine in alkaline solutions, that is coupled to the colorimetric detection of Cu^{+} using a bicinchonic acid compound. For the purposes of this study, the manufacturers 37°C protocol was used with each sample and protein standard read in triplicate and equivalent volumes of LM extraction buffer diluted in protein standards. Half volume (1 ml) reactions were used with a fixed volume of 5-10 µl of each LM extract diluted into the 50 µl sample volume of each reaction. Protein concentrations were generally in the range 1-1.6 µg/µl and were diluted with LM extraction buffer such that each of the set of samples required for a series of western blots were the same concentration as the most dilute original sample.

9.1.5.4 *Sample preparation*

Balanced LM extracts were dissociated by the addition of an appropriate volume of a 5x buffer concentrate to give final concentrations of 140 mM SDS† (equivalent to 4% w/v; BDH, 108073J), 50 mM Tris-HCl (pH 6.8), 12% (v/v) glycerol, 5 mg/ml Bromophenol blue (BDH, 200152E) in addition to extraction buffer components (9.1.5.2). Samples were reduced by the addition of 2% (v/v) β-mercapto-ethanol (Sigma, M6250) and incubation at 40°C for 30 minutes. Samples were stored at -80°C.

---

* n-Dodecyl-β-D-maltopyranoside also known as n-dodecyl-β-D-maltoside, DDM.
† Sodium dodecyl sulphate.

9.1.5.5 *Gels and electrophoresis*

Denaturing SDS-urea PAGE gels with discontinuous pH gradients were used to resolve samples[669,670]. 10% gels were used for the resolution of MTCO1, SDHA, ATP5A1 and VDAC1; 12.5% gels for MTCO2, COX4I1, SDHB, UQCRC2 and NDUFA9; 15% gels for MTCO3, COX5A, COX5B, COX6A1 and COX6B. 10%, 12.5% or 15% gel solutions were prepared for separating gels: [the appropriate volume of] 37.5:1 acrylamide-bis solution (Bio-Rad, 161-0148), 6 M urea, 375 mM Tris·HCl (pH 8.6) and 0.5% (w/v) amonium persulphate. Prior to pouring, gel solutions were filtered through 0.2 µm hydrophobic filters to remove particulates and polymerisation was catalysed by the addition of a 0.001% volume of TEMED*. 3% stacking gels were prepared using Bio-Rad 37.5:1 acrylamide-bis solution, 6 M urea, 50 mM Tris·HCl (pH 6.8) and 0.5% (w/v) amonium persulphate. Stacking gels were filtered and polymerised as for separating gels. Gels were poured such that there was around 1 cm of stacking gel between the bottom of sample wells and separating gels. All gels used were 0.75 mm thick and manufacturers standard combs with 10-12 spacers were used. Molecular weight standards and buffer blanks were added to non-sample lanes as appropriate. Sample loading was fixed for each blot at 8-10 µg per lane. Gels were run using a standard denaturing running buffer of 25 mM Tris·HCl (pH 8.6), 192 mM glycine, 35 µM SDS (0.1% w/v). Running voltages were set at 90 V until samples had entered the separating gel (~30 minutes) and then were run at a constant voltage between 120-200 V until blue sample buffer ran out of the gel (~60-120 minutes).

9.1.5.6 *Western blotting*

Gels were blotted onto Millipore Immobilon-P PVDF membrane (IPVH 000 10) using the Bio-Rad Protean systems, Whatman 3MM paper (Fisher, CJF-240-190R) and Towbin's buffer (25 mM Tris-base (pH ~8.3), 192 mM glycine, 20% (v/v) methanol) as directed by manufacturers. Prior to blotting, gels were left in chilled Towbin's buffer for <10 minutes to dehydrate and equilibrate. Blotting voltage was set at 100 V for 1 hour and blotting was done with chilled buffer, mixed using a magnetic stirrer during blotting.

9.1.5.7 *Probing and development of denaturing gel western blots*

Wet blots taken direct from blotting tanks were washed in ddH_2O and then PBS prior to probing. Air-dried blots were wetted briefly in methanol and washed in ddH_2O then PBS.

---

* N,N,N',N'-Tetramethylethylenediamine.

In the following section, all steps were carried out either in dishes (~12x8 cm) on a shaker or blocked, 50 ml polythene blood tubes on a rotator. Wetted blots were blocked for 1-2 hours in PBS with 10% (w/v) non-fat milk powder (Marvel). They were then washed for 2 minutes in PBS and then 5 minutes in PBS-Tween (All PBS-Tween solutions 0.3% (v/v) Tween 20, Sigma, P5927). Blots were then probed with primary antibody or antibody cocktails (9.1.6) diluted in PBS-Tween for 2 hours. Unadsorbed primary was diluted with 3x 5 minute washes in PBS-Tween and blots were then probed with secondary antibody (9.1.6) diluted in PBS-Tween for 1 hour. Unadsorbed secondary antibody was removed with 3x 5 minute washes in PBS-Tween and then 2x 5 minute washes in PBS. Blots were developed using the Western Lightening Western Blotting Reagent Plus kit (Perkin Elmer, NEL105001EA, formerly Renaissance kit NEN-Dupont). For a standard ~6x10 cm blot 7 ml of solution was used. Saran wrap (Fisher, SEL-360-500Q) covered blots were then exposed to Hyperfilm ECL (Amershem, RPN3103H) film in an exposure cassette for various times between 5 seconds and 8 minutes. Film was developed using a standard, manual development protocol.

9.1.6 Antibodies

All primary antibodies against OXPHOS subunits were developed and verified by Drs Jan-Willem Taanman and Michael Marusich in the laboratory of Dr Roderick Capaldi (Eugene, Oregon; table 11). Although the stocks used in this study were original preparations of varying purity, all of the OXPHOS subunit antibodies are also available from Molecular Probes (Eugene, Oregon). The dilutions of primary antibody used for probing gel blots and in immunofluorescence were all chosen to on the basis of a wealth of experience in the use of this antibody set in the afore mentioned laboratory.

Primary antibodies against VDAC1, HSPD1, HSPA9B and CYCS(2x) were all purchased from commercial suppliers (Calbiochem, 529538; Neomarkers, MS-120-P; Alexis, ALX-804-077; Pharmingen, 556433; Santa Cruz, sc-7159, respectively). Various secondary antibodies were employed: for western blotting HRP-conjugated, affinity purified, anti-mouse IgG antibodies (B-E, figures 56, 58 & 59) were from Bio-Rad (B & C, goat, two different stocks of 172-1011), Dakocytomation (D, rabbit, P 0260) and Jackson (E, goat, 115-065-164); Anti-rabbit IgG was from BioRad (goat, 172-1019); HRP-conjugated anti-HRP tertiary antibody (PAP) was also from Dakocytomation (A, mouse monoclonal, P0850); for immunofluorescence an Alexa Fluor 488-conjugated anti-mouse IgG antibody from Molecular Probes was used (A-11001). All secondary and tertiary antibodies were used in accordance with manufacturers instructions, except for the

increased concentrations of secondary antibody used for western blots of 2D BN-PAGE mentioned below and the application of PAP antibody as a tertiary layer for western blotting (9.3.3.3).

Table 11 Primary antibodies.

Target	Source	Type	Clone(s)
MTCO1	Dr RA Capaldi	Mouse monoclonal	1D6E1A8
MTCO2	Dr RA Capaldi	Mouse monoclonal	12C4F12
MTCO3	Dr RA Capaldi	Mouse monoclonal	DA5
COX4I1	Dr RA Capaldi	Mouse monoclonal	10G8D12C12 20E8C12
COX5A	Dr RA Capaldi	Mouse monoclonal	6E9B12D5
COX5B	Dr RA Capaldi	Mouse monoclonal	16H12H9
COX6A1	Dr RA Capaldi	Mouse monoclonal	14A3AD2BH4
COX6B	Dr RA Capaldi	Mouse monoclonal	3F9D3D11
COX6C	Dr RA Capaldi	Mouse monoclonal	3G5F7G3
NDUFA9	Dr RA Capaldi	Mouse monoclonal	20C11B11B11
SDHA	Dr RA Capaldi	Mouse monoclonal	2E3GC12FB2AE2
SDHB	Dr RA Capaldi	Mouse monoclonal	21A11AE7
UQCRC2	Dr RA Capaldi	Mouse monoclonal	13G12AF12BB11
ATP5A1	Dr RA Capaldi	Mouse monoclonal	7H10BBD4
VDAC1	Calbiochem	Mouse monoclonal	89-173/045
HSPD1	Neomarkers	Mouse monoclonal	LK1
HSPA9B	Alexis	Mouse monoclonal	JG1
CYCS A	Pharmingen	Mouse monoclonal	7H8.2C12
CYCS B	Santa Cruz	Rabbit polyclonal	H-104

9.1.7 Immunofluorescent stains

Immunofluorescent staining was carried out as previously described[670] with the following modifications: Mitotracker staining was not carried out; cells were permeabilised in acetone at -20°C as opposed to methanol; the nuclear counter-stain DAPI* was added to a final concentration of 200 ng/ml to the mountant in place of the addition of bis-benzimide to primary antibody incubations. For SDHA stains, coverslips were incubated in 10 mM sodium citrate (pH 6.0) at 90°C for 20 minutes between fixing and permeabilisation.

* 4',6-Diamidino-2-phenylindole.

9.1.8 MTS growth assays

The growth of fibroblast cultures was measured using the MTS* tetrazolium-based CellTiter 96 AQ_{ueous} cell proliferation assay from Promega (G5421), read using a BioRad 2550 ELISA plate reader. Using this kit the growth of cultures is measured as change in absorbance at 490 nm due to the reduction of MTS tetrazolium to formazan by cellular dehydrogenases. Initial testing of the kit, using serial dilutions of cells plated 24 hours prior to reading, found that incubation with MTS reagent for 2 hours gave good signal strength and range (figure 9). Experiments were generally seeded at 500 cells per well to enable detection of decreases in cell number and to provide a low enough initial signal to allow for large increases in cell number. All cultures used were passages and all were a similar passage number in each experiment. Cells were harvested, counted and seeded in triplicate onto 96 well plates in 200 µl of culture medium on day 0. The first readings were recorded on day 1. To avoid cell death due to prolonged handling, cell suspensions were kept on ice throughout the seeding procedure and were rapidly aliquoted using an repeater pipette. Medium was changed every 5 days throughout experiments and a separate plate was seeded for each day readings were required. Readings were taken as directed by the manufacturer. Details of the media used in the different experiments and other variations are given below.

9.1.8.1 Sugar substitution study

Glucose medium: DMEM with 4 mM glutamine and no glucose (Invitrogen, 11966-025) supplemented with 25 mM glucose and, 10% FBS, 0.2 mM uridine, 1 mM sodium pyruvate, 50 U/ml penicillin and 50 µg/ml streptomycin. Galactose medium: As for glucose but with 25 mM galactose (Sigma, G0750).

9.1.8.2 Pyruvate and uridine restriction study

Full medium: DMEM with 25 mM glucose and 4 mM glutamine, 10% dialysed FCS (PAA A15-205), 0.2 mM uridine, 1 mM sodium pyruvate, 50 U/ml penicillin and 50 µg/ml streptomycin. Restricted medium: As for full medium but without pyruvate and uridine.

9.1.8.3 RPMI study

Full glucose medium: RPMI 1640 with 4 mM glutamine (Invitrogen, 11879-020) supplemented with 25 mM glucose (Sigma, D9559), 10% dialysed FCS, 0.2 mM uridine,

---

* 3-(4,5-dimethylthiazol-2-yl)-5-(3-carboxymehtoxyphenyl)-2-(4-sulfophenyl)-2H-tetrazolium.

1 mM sodium pyruvate, 50 U/ml penicillin and 50 µg/ml streptomycin. Restricted glucose medium: As for full glucose medium but without pyruvate and uridine. Full galactose medium: As for full glucose medium but with 25 mM galactose in place of glucose. Restricted galactose medium: As for restricted glucose medium but with 25 mM galactose in place of glucose.

tsT-fibroblast study

All plates of cells in this study were cultured at 33°C to enable expression of SV40 large-T (9.1.1.3). This experiment was seeded at 250 cells per well. Incubation with MTS was carried out at 37°C as directed by the manufacturer. Full glucose medium: As for full medium above (9.1.8.1) but with dialysed FCS. Restricted glucose medium: As for restricted medium above (9.1.8.2). Full galactose medium: As for galactose medium above (9.1.8.1) but with dialysed FCS. Restricted galactose medium: As for restricted glucose medium but with 25 mM galactose in place of glucose.

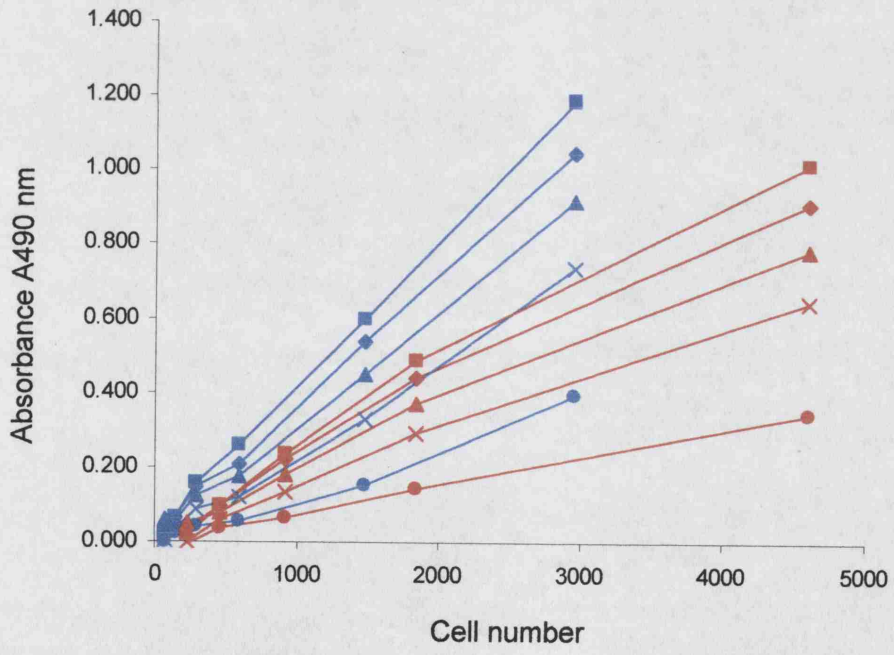

Figure 9 Testing of the MTS growth assay. Absorbance of serial dilutions of P4 and C1 cells at different incubation times using the Promega CellTiter 96 AQ_{ueous} Non-radioactive cell proliferation assay. Two cultures were chosen to represent the likely spectrum of behaviours of the cultures under study, the patient fibroblast culture P4 and the control culture C1.Results for P4 are shown in blue and those for C1 in red. Incubation times in minutes are as follows: ■ = 180, ◆= 120, ▲= 90, x = 75, ● = 30.

9.2 GENETIC ANALYSIS

9.2.1 Strategy for mtDNA sequencing

Nuclear pseudogenes can be a problem when amplifying mtDNA and have in the past led to erroneous results when screening mtDNA[671,672]. Of particular relevance to the mt-tRNA and COX subunit genes screened in this study are the processed pseudogenes of *MTCO1* and *MTCO2* at 10q22.1*, that of *MTCO3* at 10p12.31†, and the 5.8 kb nuclear-mtDNA fragment linked to D1S243 at 1p36.33[673]. This fragment is an ancestral hominid translocation of mtDNA spanning *MTND1* to *MTCO3* (3914-9755; figure 4) and therefore includes pseudogenes for 11 mt-tRNAs, *MTCO1*, *MTCO2* and *MTCO3*. It was not felt that DNA purification from isolated mitochondria would provide a suitable source of mtDNA as extraction would be labour intensive and require large numbers of cells. Instead long-range PCR was used to amplify almost the entire mtDNA as a pseudo-purification (9.2.1.5). Product from these amplifications was cleaned enzymatically (9.2.1.7) avoiding DNA fragmentation caused by matrix binding and aliquots were resolved on 0.6-0.8% agarose TAE slab gels (9.2.2.1) to verify that a single product of the appropriate size had been amplified. Cleaned, long-range PCR product was then used as a template for a further standard PCR amplification of sequencing fragments of around 500 bp (9.2.1.6). These were cleaned using kits employing silica-based columns (9.2.1.7) and aliquots were resolved on 3% agarose TAE slab gels to check that single products of the appropriate size had been amplified. Column cleaned products (9.2.1.7) were then sequenced using either fluorescent dye-primer or dye-terminator kits (9.2.1.8;9.2.1.9), or in a some cases a manual radiolabelled-terminator kit (9.2.1.10).

Trace files (.abi) from fluorescent sequencing were assembled into contigs and aligned against the NCBI human mtDNA sequence NC_001807, using Lasergene '98 Seqman II (v3.61). All conflicts were screened by visual inspection of trace files and those in regions of poor quality data at the ends of runs or in the region of "dye blobs" were discarded. All sequencing reactions were repeated until high quality traces were obtained over the entire length of genes of interest. In most instances sequencing traces were obtained in both orientations over genes of interest, although in some instances (*MTTE*, *MTTK*, *MTTR*, *MTTV*) technical constraints caused by the physical position of primers meant that this could not be achieved for all samples. Base changes resulting from genuine conflicts were screened against Mitomap version 3.0 to determine whether

---

* Ensembl Vega-genes OTTHUMG00000018387 and OTTHUMG00000018389 respectively.
† Ensembl Vega-gene OTTHUMG00000017783.

they had been previously described and whether data existed on pathogenicity. The strategy for verification of manual sequencing data is given below (9.2.1.10).

9.2.1.1 Total DNA purification

High grade, whole-cell DNA was purified using the Nucleon BACC1 genomic DNA extraction kit from Amersham (RPN8501; formerly Scotlab SL-8501). This kit was used to obtain high quality, large fragment length, genomic DNA as it does not require DNA binding to any form of matrix during the purification. Purified genomic DNA from frozen pellets (9.1.2.2) was resuspended by incubation at 60°C in 30-150 µl TE buffer (10 mM Tris, 1 mM EDTA, pH 8.4) and stored at -20°C.

PCR grade whole-cell DNA was rapidly purified using the Qiamp DNA purification kit from Qiagen (51304). This kit is based on DNA binding to a silica matrix and selective washing through of contaminants by centrifugation. Samples purified from ~3 plates of cells (1.5-3x10^6 A549 cells or 0.9-2.4x10^6 fibroblasts) were resuspended in 50 µl of TE and stored at -20°C.

9.2.1.2 Total RNA purification

Total cellular RNA was extracted from fibroblasts as described previously[670] using a modified version of the protocol devised by Chomczyski and Sacchi[674] employing LiCl to selectively precipitate RNA. For long-term storage, RNA extracts were stored in 70% ethanol, 120 mM sodium acetate at -70°C. Prior to use the concentration of RNA recovered from each sample was determined from the absorbance at 280 nm using an extinction coefficient of ε=25 $mg^{-1} \bullet cm^{-1}$. The proximity of the ratio of A260/A280 nm to an ideal of 2.0 was used as an indicator of protein contamination and scans from A210 to A310 nm were inspected to exclude humps indicative of protein or detergent contamination. Visual inspection of total RNA samples resolved on 0.8% agarose TAE slab gels was also undertaken to check for degraded samples. Samples with low intensity signals for the nuclear rRNAs, a deviation for an approximate ratio of intensity 2:1 for the same signals or a high abundance of high mobility non-specific signal were discarded.

9.2.1.3 Verification of DNA purity and concentration

All BACC1-purified DNA samples and selected PCR samples were screened for purity and quantified using spectrophotometric scanning of A210-A310 nm. Samples were

diluted to 500 µl in ddH_2O and read against a water baseline using a Hitachi U3210 spectrophotometer. Typically 2-5 µl of BACC1 DNA and 10 µl of PCR product was read. Wavelength scans were visually inspected for humps characteristic of protein or detergent contamination and an estimate of purity was attained from the proximity of the A260/A280 ratio to an ideal of 1.8. DNA concentration was determined from A280 nm using an extinction coefficient of ε=20 $mg^{-1} \bullet cm^{-1}$, BACC1 DNA samples were generally in the range 0.8-1.8 µg/ml. Where samples contained little DNA and were therefore noisy, readings at A259-261 nm and A279-281 nm were averaged.

9.2.1.4 PCR consumables and hardware

All PCR reactions and other reactions requiring thermal cycling were carried out using 200 µl thin-walled PCR tubes bought from a variety of suppliers which were purchased and used either as strips of up to 8 tubes or as single tubes. Thermal cycling was achieved using either a Perkin Elmer GeneAmp 2400 PCR system, an MJ Research PTC-200 DNA engine fitted with an ALS-1296 96-well alpha-unit.

9.2.1.5 Long-range PCR of mtDNA

Long-range PCR of almost the entire mtDNA was carried out using the method of Cheng *et al*[675] using two inverted primers in *MTCYB*, TGAGGCCAAATATCATTCTGAGGGGC and TTTCATCATGCGGAGATGTTGGATGG (5' bases L15149 and H14841, respectively). PCR was carried out using the GeneAmp XL kit from Perkin Elmer (N808-0192) employing the "hot start" cycle shown below, in which recombinant *Tth* (*Thermus thermophillus*) polymerase supplied by the manufacturer was added to each sample during an 80°C hold following the initial denaturation step. As this protocol was not used as a qualitative or quantitative assay, 1 µl of BACC1 purified DNA (9.2.1.1) was used as template in all reactions.

	Denaturation	Hold	Cycles 1-35		Termination	Hold
Temperature (°C)	94	80	94	69	72	4
Time (s)	90	-	35	840	600	∞

Table 12 Primer pairs used for mtDNA sequencing fragment generation and fragment sequencing.

Target gene	Position	3' base L-strand primer	3' base H-strand primer	Primer sequences (L over H, 5'-3')
MTTF	577-647	L336	H706	AACACATCTCTGCCAAACC GGATGCTTGCATGTGTAATC
MTTV	1602-1670	L1360	H2202	GGGCTACATTTTCTACCCCA CAACCAGCTATCACCAGGCT
MTTL1	3230-3304	L3130(n)	H3353(n)	AGGACAAGAGAAATAAGGCC GCGATTAGAATGGGTACAATGA
MTTI, MTTQ, MTTM	4263-4469	L4215	H4643	ATATGTCTCCATACCCAT CTTGATGGCAGCTTCTGTGG
MTTW, MTTA, MTTN, MTTC, MTTY	5512-5891	L5465	H5931(n)	TACCACGCTACTCCTACCT AGAGAATAGTCAACGGTCGGC
MTCO1	5904-	L5866	H6485	CCAATGCCTCACTCAGC TAGGACTGCTGTGATTAGGA
MTCO1	-	L6426	H6968	GCCATAACCCAATACCAAACG GCCAGTCAGGCCACCTAC
MTCO1	-	L6799	H7196	AGACACACGAGCATATTTCA GAGAAAGTGTTGTGGGAAGA
MTCO1	-7445	L7115	H7650	CCTAGACCAAACCTACGC GTGATAAGCTCTTCTATGAT
MTTS1, MTTD	7445-7585	as above	-	–
MTCO2	7586-	as above	-	–
MTCO2	-	L7588	H7992	GGCACATGCAGCGCAAGTAG GGAGTCGCAGGTCGCCTG
MTCO2	-8262	L7865	H8445	AGACGAGGTCAACGATCC TTTAGTTGGGTGATGAGGAA
MTTK	8295-8364	L8196	H8726	ACAGTTTCATGCCCATCGTC GTTCGTCCTTTCGTGTTGTG
MTCO3	9207-	L9151	H9744	ATCCAAGCCTACGTTTTCAC CTGAGGCTTGTAGGAGGGTA

Target gene	Position	3' base L-strand primer	3' base H-strand primer	Primer sequences (L over H, 5'-3')
MTCO3	-9990	L9638	H10107	CACCTGAGCTCACCATAGTC GTAGTAAGGCTAGGAGGGTG
MTTG	9991-	as above	-	–
MTTG	-10058	L9983	H10452	AGGGTCTAACTCTTTTAG CATAATTTAATGAGTCGAAATC
MTTR	10405-10469	L10362	H10724	CTGGCCTATGAGTGACTA ATATGTGTTGGAGATTGA
MTTH, MTTS2, MTTL2	121-38-12336	L12069	H12395	TGTTCATACACCTATCCCCCAT AGGATGGGGGGAATTAGG
MTTE	14674-14742	L14595	H14883	AATAGGAGAAGGCTTAGAAG ACCGTGATTTGGAGGATCAGGCA
MTTT, MTTP	15888-15953	L15875	H16345	CTCAAATGGGCCTGTCCTTG TGTAATGTGCTATGTACGGT

Key: Numbering indicates first 5' base of primer excluding M13 tags where present. (n) = no M13 tag. M13 sequences are given above (9.2.1.6).

Table 13 Primer set designed by Tiranti and co-workers for amplification of *SURF1* genomic fragments.

Fragment (exons)	Length (bp)	Position	Primers (forward above reverse)	T_m (°C)	Buffer, final concentrations.
1+2	297		ATGCAGATGCTTCCTGCGTC CAGACAGCAGGTGGCTCTGC	56	Expand High Fidelity PCR buffer with 1.2M betaine (Sigma B0300), 1.2% (v/v) PCR grade DMSO (Sigma D9170).
3+4	380		TTCGAGGGCTTCTGGCTCCA AAGTAAAACAGGCCCTAGG	59	Advanced Biotechnologies buffer IV plus 10% (v/v) PCR grade DMSO.
5	275		CAAACCTTGCTCGGCCACTG TCTGCCAGGACAGCCAGCTC	57	Advanced Biotechnologies buffer IV plus 10% (v/v) PCR grade DMSO.
6+7	389		CCACCTGAAGTAGCACTTTC AGCTACTTGTTCCGAGATGG	59	Advanced Biotechnologies buffer IV
8+9	318		AGAGGCTGGCAGGCCAGTAG CTGCATTATCCAGGGACAGGG	61	Advanced Biotechnologies buffer IV

9.2.1.6 PCR of mtDNA sequencing fragments

Templates for mtDNA sequencing were generated using Advanced Biotechnologies Red Hot thermoprime plus *Taq* DNA polymerase systems using buffer IV-based reaction mixtures (20 mM $(NH_4)_2SO_4$, 75 mM Tris-HCl (pH 8.8), 0.01% (v/v) Tween 20, 1.5 mM $MgCl_2$; final concentrations). Hundreds of such reactions were carried out using either separate components (: AB-1406), 0.9x Reddy-Load master mix (AB-0575LD/a) or 10x Reddy-Load master mix (AB-0816) and no influence on the data presented in this thesis could be attributed to the choice of buffer IV-mix system used. Reddy-Load master mixes contained unspecified dyes and precipitants to enable direct loading of PCR products onto agarose gels without addition of loading dye (9.2.2). In addition to the standard buffer IV composition given above, Reddy-Load master mixes also contained final concentrations of 1.25 U *Taq* (*Thermus aquaticus*) DNA polymerase (per 50 µl final volume) and 0.2 mM of each dNTP. When individual components were used the following final reaction mixture was made up: 0.2 mM each dNTP, 1.5 mM $MgCl_2$, 1.5 U Red Hot *Taq* polymerase (per 50 µl final volume). In all cases primers were added to a final concentration of 0.5 µM. 50 µl reaction volumes were used as required and no influence on sequence data could be attributed to alterations in reaction volume.

The vast majority of sequencing fragments were generated using M13-tagged primer pairs designed and validated by Dr Isobel Nelson[620,676] (Institute of Neurology, London; table 12). The -21M13 tag TGTAAAACGACGGCCAGT, was added to the 5' end of all primers for L-strand synthesis and the M13Rev tag GGTCATAGCTGTTTCCTG, was added to the 5' end of all primers for H-strand synthesis (both sequences 5'-3'). The following PCR cycle with a fixed T_m (melting temperature) of 56°C was used for all M13 tagged primers regardless of the calculated T_m of individual primers. M13 tagged fragments were used for both dye-primer and dye-terminator sequencing.

	Denaturation	Cycles 1-25			Termination	Hold
Temperature (°C)	94	94	56	72	72	4
Time (s)	300	30	30	32	600	∞

Sequencing fragment amplifications using primers without M13 tags were amplified using the following cycle:

	Denaturation	Hold	Cycles 1-25			Termination	Hold
Temperature (°C)	94	80	94	T_m	72	72	4
Time (s)	300	-	30	30	40	600	∞

Where T_m was the melting temperature which was set at 50°C for all fragments with the exception of the L5476-H5931 fragment where a T_m of 56°C was used. Fragments without M13 tags were only used for manual radiolabel-terminator sequencing.

9.2.1.7 PCR cleanup

Standard PCR products were cleaned using the Promega Wizard PCR cleanup (A7170) or the Qiagen PCR cleanup (28106) kits unless otherwise specified. Both kits are based on DNA binding to silica columns and the selective washing through of unwanted components of the PCR reaction. Reactions were eluted from columns into 50 µl of TE. According to manufacturers datasheets the Promega kit recovers 96-99% of DNA in the 300-1.5k bp fragment range, ≥60% in the 200-3.2k bp range and ≤3% in the 75-50 bp range, the Qiagen kit recovers fragments of 100-10,000 bp and removes those smaller than 40 bp.

Long-range PCR products and other specified PCR products were enzymatically cleaned using the ExoSAP-it kit from Amersham (US78200). Heat-labile shrimp alkaline phosphatase and exonuclease I were added to completed PCR reactions and incubated at 37°C for 15 minutes to digest unincorporated deoxynucleotides and ssDNA with exposed 3' ends. Both enzymes were subsequently inactivated by incubation at 80°C for 15 minutes. This cleanup protocol does not remove residual polymerase or buffer components from PCR reactions.

9.2.1.8 Dye-Primer sequencing

Dye-primer sequencing was carried out using ABI Prism -21 M13 and M13 Rev dye-primer Ready Reaction kits with AmpliTaq DNA Polymerase FS from Perkin Elmer (402111 & 402109, respectively). A, C, G and T reaction mixes were prepared at half the manufactures recommended volumes (A & C = 2.5 µl, G & T = 5 µl final) and thermal cycling was carried out in the absence of oil overlay using a Perkin Elmer GeneAmp 2400 PCR system according to manufactures cycle. 0.5 µl of column-cleaned sequencing fragment was used template for A and C reactions and 1.0 µl was used for G and T reaction mixes (9.2.1). Completed A, C, G and T reactions were pooled using 40 µl of 99% ethanol, precipitated for 30 minutes at 4°C, pelleted for 20 minutes at 13,000

rpm using a bench-top centrifuge, aspirated and air dried for 15 minutes at room temperature. Pellets were stored at -20°C and resuspended and loaded according to manufacturers instructions by sequencing technicians. Samples were resolved using either Perkin Elmer ABI Prism 373A or Perkin Elmer ABI Prism 310 genetic analysers maintained as a core facility. Sequence output files were analysed as described above (9.2.1).

9.2.1.9 Dye-Terminator sequencing

Dye-terminator sequencing was carried out using ABI Prism BigDye terminator cycle sequencing kits with Amplitaq DNA polymerase FS from Perkin Elmer (4303149). Sequencing reactions were carried out at half manufacturers recommended volumes (10 µl final volume) using 1 µl of column-cleaned sequencing fragment was used as template (9.2.1). Sequencing reactions in each orientation were prepared using the same primers used to generate sequencing fragments (table 12). Thermal cycling was as recommended by manufacturer. Products were precipitated using half volumes of the ethanol/sodium acetate precipitation protocol specified by the manufacturer. Samples were resuspended using 20 µl of the manufacturers template suppression reagent (TSR) following the recommended protocol and analysed using a Perkin Elmer ABI Prism 310 genetic analyser maintained as a core facility. Sequence output files were analysed as described above (9.2.1).

9.2.1.10 Radiolabelled manual sequencing

Radiolabelled manual sequencing was carried out using the Thermo Sequenase radiolabelled-terminator cycle-sequencing kit and [α-^{33}P]-labelled ddNTP terminators from Amersham Life Sciences (US79750 & AH9539, respectively). 2 µl of enzymatically cleaned (9.2.1.7) sequencing fragment was used as template for all manual sequencing reactions which were prepared, cycled (at T_m = [primer T_m] +7°C) and terminated as recommended by the manufacturer. dGTP and dITP termination master mixes supplied by the manufacturer were used as required to overcome compressions. 3 µl of each terminated sample was resolved using a Life Technologies BRL model S2, vertical electrophoresis system. Glycerol tolerant, 6% acrylamide, 7.5 M urea sequencing gels were prepared for all samples as per manufactures instructions. Gels were pre-run at 80 W for 45-60 minutes to reach a temperature of around 55°C before loading and run briefly between the loading of each 4-lane sample to prevent lateral diffusion. Gels were run at 65-80 W to maintain a temperature of around 55°C. To facilitate the collection of good data, runs of around 2 and 5 hours were carried out for each primer of each

sequencing fragment to enable reads proximal and distal to primers. Following runs, gels were soaked in 20% methanol, 5% acetic acid for <5 minutes and transferred to Whatman 3MM paper (Fisher, CJF-500-050X) and the exposed side of the gel was covered with Saran wrap. Gels mounted in this way were then dried at 80°C for 15 minutes using a BioRad model 583 gel dryer. Saran wrap was removed from dried gels and the exposed face of the gel was placed against 35x43 cm Kodak BioMax MR film (856 7232) in a development cassette overnight at room temperature before the film was developed using a standard autorad development protocol. Sequences were checked visually by screening for differences in the banding pattern between samples. Any differences were identified using the original Cambridge sequence[145] and then checked against Mitomap version 3.0 to determine originality and pathogenicity.

9.2.2 Agarose gel electrophoresis

Nucleic acids were resolved using agarose gels of varying densities in two different buffer systems. Standard molecular biology grade agarose was sourced from Sigma (A5095) and for separation of certain short fragments with limited size differentials, high grade agarose from Boehringer Mannheim was used (1816578). Agarose gels were run using Pharmacia GNA100 or GNA200 gel tanks.

9.2.2.1 Agarose TAE slab gel electrophoresis

A standard TAE buffer system (Tris-base 40 mM, pH 8.2; 20 mM acetic acid; 1 mM $[Na_2]$EDTA -final concentrations) made from 10x concentrate (made in house) was used to resolve all routine samples such as sequencing fragments. 5 µl of 10mg/ml ethidium bromide solution (Sigma, E1510) was added to each 100 ml gel solution prior to pouring. TAE-buffered gels were run between 90-120 V, corresponding to 10 Vcm^{-1}±0.2. For loading, samples were mixed with appropriate volumes of either Promega 6x Blue/Orange loading dye (G1881), Fermentas loading dye (R0611) or Sigma 6x ChromaTrack loading dye (C8468). The migration of coloured loading dyes and periodic visualisation of ethidium bromide stained samples using UV trans-illumination during runs was used to determine run times.

9.2.2.2 Agarose TBE slab gel electrophoresis

A standard TBE buffer system (Tris-base 90 mM, pH 8.2; 90 mM boric acid; 2 mM $[Na_2]$EDTA -final concentrations) made from 5x concentrate (made in house) was used to resolve samples containing short fragments with small size differentials. Generally

TBE-buffered gels were prepared using high grade agarose (9.2.2). The addition of ethidium bromide, use of loading dyes, running voltages were as described for TAE systems above (9.2.2.1).

9.2.3 RFLP of 6852G-A

The presence of 6852G-A was investigated using *Msp* I which cleaves the palindromic sequence C^CGG symmetrically leaving a 2 bp overhang on the opposing strand. The 6852G-A transition identified in P2 abolished the *Msp* I recognition sequence at 6850-6853 (figure 27). *Msp* I was obtained from Promega (R6401) and used with buffer B without acetylated BSA. 20 µl reactions were set up using 10 units of *Msp* I, 10 µl of column cleaned (9.2.1.7) L6799-H7196 sequencing fragment (9.2.1.6; table 12) and appropriate volumes of ddH_2O and buffer concentrate. Digests were incubated for 2 hours at 37°C. As the sequencing fragment contained 18 bp M13 tags 5' and 3' full length fragment was 433 bp and cleavage resulted in fragments of ~364 and ~69 bp. Subsequently 18 µl of each digest was resolved on a 3% high grade agarose TAE gel (9.2.2.1).

9.2.4 Whole-cell fusion and selection of synkaryons

The fusion protocol used for fusion of primary dermal fibroblasts and A549 *Neo*^{r} tumour cells was similar to that published by Cassio[677] except that cells on coverslips were moved between dishes of solutions as opposed to solutions being changed in dishes of adherent cells. Briefly, 2 days prior to fusion fibroblasts were plated out at around 50-70% coverage in dishes containing 4x 13 mm diameter Thermanox coverslips (Nunc, 174950). On the day of the fusion, coverage of the fibroblasts was around 70-100%. A549 cells were then plated out into the same dishes as the fibroblasts at around 80-90% coverage and left for a few hours to adhere. Fusion was carried out using the following procedure: Plates containing both cell types were aspirated and washed once and then flooded with high glucose DMEM with penicillin and streptomycin (9.1.2). Coverslips were then remove individually and dipped through sterile 35 mm or 60 mm culture plates containing the following solutions: 1 minute in 50% polyethylene glycol 1500 (NSB, 00-1480-6/B), 5% DMSO (Sigma, D1435), 45% high glucose DMEM; washed 2x in high glucose DMEM with 10% DMSO; washed 3x in high glucose DMEM and then placed into 35 mm dishes with full high glucose DMEM culture medium (9.1.2). All solutions used, without exception, were aliquoted into plates and maintained at 37°C in an cell culture incubator prior to use and all were disposed between fusions. On day 4,

plates containing the coverslips were trypsinised and the cells were plated back into the same 35 mm dishes with selective medium containing G418 (400 µg/ml; PAA, P27-011), without pyruvate or uridine supplementation (standard high glucose DMEM (9.1.2); 10% dialysed FCS, penicillin, streptomycin). It was noted at this stage that multinuclear cells could be seen in all cultures. G418 selection was maintained for 20 days until day 24, sufficient to kill all cells not maintaining *Neo*[658,660]. Pyruvate and uridine was restricted until day 78 (figure 30). Cultures were stained for COX activity (9.1.3) on days 21, 49 and 77, and cell pellets were frozen on day 82 for DNA extraction (9.1.2.2). As a precaution synkaryons were frozen down periodically throughout the experiment to enable rescue should there be any problems (9.1.2.1).

9.2.4.1 RFLP of 6852G-A in A549 synkaryons

A similar *Msp* I digest as was used for screening primary fibroblasts was used to screen for 6852A-G in fibroblast-A549 synkaryons (9.2.3). The major differences being that 25 µl reactions were used, a shorter fragment was amplified for digestion using the L6799 and H6968 sequencing primers (table 12) and that template DNA for this amplification was PCR grade DNA (9.2.1.1) purified from cell pellets (day 82; 9.2.4). In this instance the full length fragment was 205 bp (including M13 tags) and cleavage resulted in fragments of ~136 and ~69 bp. Following digestion 25 µl of each digest was resolved on a 3.5% high grade agarose TBE gel (9.2.2.1).

9.2.4.2 RFLP of poly-CA tract in A549 synkaryons

As previously described[670] a rare CA deletion in a $[CA]_5$ tract at 514-523 found in A549 mtDNA was used to confirm the absence of A549 mtDNA in the fibroblast-A549 synkaryon cultures. The 371-535 fragment was amplified using the H-strand orientated primer CTAACACCAGCCTAACCAGA and the L-strand orientated primer GGTTAGCAGCGGTGTGTGAG that introduces an *Alu* I restriction site (AG˅CT blunt ended) due to the mismatched A, in the absence of a terminal [TG] when combined with the adjacent downstream [CT] (described in L-strand orientation). Amplification was carried out using a standard Red Hot *Taq* PCR mix (9.2.1.6) with 0.25 µl of synkaryon (day 82; 9.2.4) or 0.5 µl of control fibroblast PCR grade DNA as template using the following cycle:

	Denaturation	Cycles 1-25			Termination	Hold
Temperature (°C)	94	94	53	72	72	4
Time (s)	240	60	60	30	600	∞

28 µl of column-cleaned product was digested in a 32 µl reaction with 5 units of Alu I, 1/100 dilution of acetylated BSA in buffer B, all sourced from Promega (R6281). Digests were resolved on a 3% high-grade agarose TBE gel (9.2.2.2). Wild-type undigested fragment was 173 bp in length (including M13 tags), A549 undigested fragment was 171 bp and digested fragments were 147 and 24 bp in length.

9.2.5 Southern Blotting

Southern blotting was carried out as previously described[670] using *Pvu* II digestion of total DNA to linearise mtDNA via cleavage at 2562 (*MTRNR1*, figure 4) and to excise a 12 kb fragment of the nuclear rRNA repeat unit encompassing the 18S rRNA DNA*. Cleavage thus enabled resolution of mtDNA as a single band and provided a similar sized marker of nuclear DNA abundance for comparison of nuclear DNA mtDNA ratios.

Briefly, 8 µg of BACC1-purified total DNA (9.2.1.1) was digested in 50 µl using 30 units of *Pvu* II (Fermentas, Lithuania; ER0631; CAG˅CTG, blunt ended) using buffer G supplied by the manufacturer. Digestion was carried out at 37°C for 4.5 hours and a 1 µg aliquot was resolved on a 0.8% agarose TAE slab gel to ensure that digestion had been successful and all samples ran as long smears. 3 µg of digested DNA was resolved using a 0.8% agarose TAE slab gel and blotted onto Hybond-N membrane (Amersham RPN203N). Blots were hybridised with [α-^{32}P]dCTP-labelled, random-primed, dsDNA probes generated against the entire mtDNA and the 18S rDNA (9.2.5.1). Blots were hybridised with the mtDNA probe alone in the first instance, to enable screening for mtDNA deletions and secondly with both probes to screen for depletion of mtDNA. Blots were not stripped between hybridisations. Results were visualised by both exposure to film (Kodak BioMax MS, 829 4985; Fuji RX, 106270; Amersham, Betamax Hyperfilm RPN9) developed using a standard manual procedure and exposure to a general purpose (GP) cassette-mounted phosphor screen using a Storm model 860 imaging system (both from Amersham; formerly Molecular Dynamics, screen 63-0034-82).

* Fragment corresponds to a pseudo-circular restriction fragment originating from tandem repeats of the rDNA repeat unit. It is composed of the "last" 861 bp of one unit and the "first" 11194 bp of the next unit as mapped using the NCBI deposited sequence U13369. >300 copies of this repeat are present in the human genome.

Exposure times for film were typically 18 hours and for phosphor screens 6.5 hours corresponding to peak counts of ~200 cps on blots.

9.2.5.1 Probes for Southern blotting

Probes were generated using [α-^{32}P]dCTP and the Rediprime DNA labelling kit from Amersham (AA0065-250μCi & RPN1633, respectively). Entire mtDNA, isolated from placenta, was used as a template for the mtDNA probe and a cloned 5.8 kb *Eco*R 1 fragment of the 45S rDNA repeat unit encompassing the 18S transcript[678] was used as a template for the 18S probe (kindly supplied by Dr Ian Holt of the Dunn School, Cambridge, UK). Quantities of template DNA and [α-^{32}P]dCTP used for probe synthesis and quantities of probe used for hybridisation were as recommended by the manufacturer (25 ng & 5 μl per 50 μl reaction mix and 14 μl per 5 ml hybridisation buffer, respectively)

9.2.6 Strategy for sequencing of *SURF1* genomic fragments

Five *SURF1* genomic fragments spanning all 9 exons were amplified and sequenced using the primer set devised by Tiranti and co-workers[535] (table 13). As described below (9.2.6.1) different PCR conditions to those given by Tiranti were used as published conditions did not result in clean sequencing fragments. Sequencing fragments from P1-P7 were amplified from BACC1-purified DNA, those of P1 and P7 family members were amplified from column-purified DNA (9.2.1.1). PCR conditions were as described below. 10 μl aliquots of all P1-P7 fragments were resolved on 2% agarose TAE slab gels to ensure amplification had been successful prior to sequencing. Sequencing fragments were cleaned using Qiagen PCR cleanup columns (9.2.1.7) and sequencing was carried out using half reaction volumes of the ABI Prism BigDye fluorescent dye-terminator sequencing kit as used for mtDNA sequencing (9.2.1.9). Sequences were determined using an ABI Prism 310 genetic analyser maintained as a core facility. All fragments were sequenced in both forward and reverse directions using the same primers used to amplify sequencing fragments. Sequences were assembled with the genomic sequence of *SURF1* taken from the Genbank contig AC002107 using Lasergene '98 Seqman II (v3.61). The context of all conflicts was checked carefully in original trace files to ensure they were present in regions of reliable sequence.

9.2.6.1 PCR of SURF1 genomic fragments

The following thermal cycle was used for all reactions:

	Denaturation	Cycles 1-25			Termination	Hold
Temperature (°C)	94	94	T_m	72	72	4
Time (s)	160	20	20	20	420	∞

Where T_m was as given in table 13 below. Standard Advanced biotechnologies Red Hot *Taq* PCR mixes (9.2.1.6) were used for amplification of most fragments with addition of 10% DMSO for certain fragments (table 13). In all reactions primer concentrations were 0.5 µM, dNTPs were 0.2 mM each and 1.5 units of polymerase was used per 50 µl reaction mix. Where used, 0.5 µl of BACC1 DNA or 1 µl of Qiamp DNA (9.2.1.1) was added per 50 µl reaction mix. The exon 1+2 fragment is particularly GC rich and so was amplified in the presence of 1.2 M betaine (trimethylglycine), 1.2% (v/v) DMSO[679] using the Expand High Fidelity PCR kit from Roche (1 732 650) with a reaction mix according to manufacturers instructions with thermal cycling as shown below.

	Denaturation	Cycles 1-10			Cycles 11-30			Termination	Hold
Temperature (°C)	93	93	56	72	92.7	56	72	72	4
Time (s)	180	30	20	20	20	30	30	420	∞

9.2.6.2 Resolution of exon 3+4 fragments from P1 family members

SURF1 exon 3+4 fragments amplified from Qiamp DNA (9.2.1.1) derived from blood or primary dermal fibroblasts of P1 family members were resolved using a 3.5% high grade agarose TBE slab gel (9.2.2.2) to screen for the presence of the 8 bp deletion due to 312del10insAT. Fragments were amplified as described above (9.2.6.3).

9.2.6.3 PAGE gel electrophoresis of SURF1 exon 1+2 fragment

SURF1 exon 1+2 fragments were amplified from BACC1 DNA (9.2.1.1) from P1-P7, ten disease controls and 3 normal controls as described above (9.2.6.1). 3 µl of each sample was resolved on a non-denaturing 8% polyacrylamide (19:1) gel with a standard TBE buffer (9.2.2.2) using a ATTO 15 cm vertical gel tank. Samples were run at room temperature at 300 V for 3 hours. The gel was developed using a standard silver staining procedure. The gel was fixed for 8 minutes in 10% ethanol, 0.5% acetic acid; washed in ddH_2O; soaked for 5 minutes in 10 mM $AgNO_3$; washed in ddH_2O; developed by eye in 375 mM NaOH, 0.0015% (v/v) formaldehyde; washed in ddH_2O and development was fixed in 140 mM Na_2CO_3. Following development, images of the wet gel were recorded.

9.2.7 Northern blotting

Northern blotting was carried out as previously described[670]. 5.8 µg of glyoxalated total RNA (9.2.1.2) was resolved per lane using a 1.4% agarose slab gel and a sodium phosphate buffer (pH 6.8). A single blot was prepared using Amersham Hybond-N membrane (RPN203N). It was probed sequentially in the following order with [α-^{32}P]-labelled probes, *SURF1* mRNA, *MTCO2/MTCO1*, the 18S rRNA and *MTRNR1/MTRNR2*. ^{32}P signal was left to decay on the blot between hybridisations and the blot was not stripped. A [α-^{32}P]dCTP-antisense-labelled, dsDNA probe was generated against *SURF1* mRNA as described below (9.2.7.1). Random, [α-^{32}P]dCTP-labelled, dsDNA probes were used for detection of the 18S rRNA, *MTCO1/MTCO2* and *MTRNR1/MTRNR2* (9.2.7.2) Following hybridisation with the *SURF1* probe, peak radioactivity of the blot was 1-3 cps and it was exposed to Kodak Biomax MS film (822-2648) at -70°C with an intensifier screen for 6 days. One week later (0.5 x $t_{½}$) the blot was hybridised with the *MTCO1/MTCO2* probe and peak counts were 80 cps. One month after the second hybridisation (2 x $t_{½}$) the blot was hybridised with the 18S probe and peak counts were >2000 cps. Four months (8.6 x $t_{½}$) after the third hybridisation the blot was hybridised with the *MTRNR1/MTRNR2* probe and peak counts were ~350 cps. For the *MTCO2/MTCO1*, 18S rRNA and *MTRNR1/MTRNR2* hybridisations images of the blot were recorded both by exposure to a Storm phosphor screen and via multiple exposures of Kodak Biomax MS film (9.2.5).

9.2.7.1 Synthesis of probe for northern blotting of SURF1 mRNA

A [α-^{32}P]dCTP-labelled, dsDNA probe labelled only in antisense (cDNA sense) was generated to detect *SURF1* mRNA in an attempt to minimise potential background signal in relation to the anticipated low-strength *SURF1* mRNA signal. Template for generation of the probe was amplified from control oligo-d(T)-primed cDNA (9.2.8.2) using the forward primer TGGAGGAGCGTCCTCAGGGTCT (73-94, exon 2) and a reverse primer originally designed for recombinant protein purification that introduced a C-terminal $[His]_6$ tag, ATGATGATGATGATGATGCACACCAGGTGTCCCACGTAGG (879-899+$[His]_6$, exon 9). A standard Red Hot *Taq* PCR mix was used (9.2.1.6) with 1 µl of cDNA as template with thermal cycling as given below.

	Denaturation	Cycles 1-35			Termination	Hold
Temperature (°C)	94	94	58	72	72	4
Time (s)	40	20	20	60	420	∞

10 µl of product was enzyme cleaned (9.2.1.7) and 1 µl of this along with the reverse primer above was used to generate labelled probe using the Thermo Sequenase kit (9.2.1.6) with [α-^{32}P]dCTP (Amersham, AA0065-250µCi) in place of [α-^{33}P]ddCTP using the following cycle:

	Cycles 1-30		
Temperature (°C)	94	58	72
Time (s)	20	30	240

The antisense-labelled probe was cleaned using the DNAprep resin purification steps of the NonaPrimer Kit I from Appligene Oncor (140014).

9.2.7.2 Templates and synthesis of random dsDNA probes for northern blotting

The 18S rRNA probe was generated using a cloned *Eco*R 1 fragment of the nuclear 45S rDNA repeat unit[678] as template as also used for Southern blotting[670] (9.2.5). The *MTCO1/MTCO2* probe was generated using a cloned *Xba* I fragment[670] as template encompassing mtDNA nucleotides 7441-8286, corresponding to 4 bases of *MTCO1*, *MTTS1*, *MTCO2* and 24 bases of the intergenic region between *MTCO2* and *MTTK* (8263-8295) as template. The *MTRNR1/MTRNR2* probe was generated using a PCR product of mtDNA nucleotides 660 to 3287 corresponding to *MTRNR1* minus the 12 most 3' bases, *MTTV*, *MTRNR2* and 57 bases of the 5' end of *MTTL1* as template. The template for the *MTRNR1/MTRNR2* probe was generated using a standard 50 µl Advanced Biotechnologies Reddy Load PCR (9.2.1.6) with 0.2 µl of enzyme-cleaned (9.2.1.7), long-range mtDNA PCR product (9.2.1.5) of control BACC1 DNA (9.2.1.1) as template. Thermal cycling was as shown below and the following M13 tagged primers were used: L660, CCTAGCCTTTCTATTAGC and H3287, GAACCTCTGACTGTAAAGTT, see 0 for tags.

	Cycles 1-35			Termination	Hold
Temperature (°C)	94	56	72	72	4
Time (s)	15	15	200	420	∞

Random primed dsDNA probes for northern blotting were generated using both [α-^{32}P]dCTP and the Rediprime DNA labelling kit from Amersham (AA0065-250µCi & RPN1633, respectively). In each instance quantities of template DNA and [α-^{32}P]dCTP used for probe synthesis (25 ng & 5 µl per 50 µl reaction mix, respectively) and the final

concentration of probe in the hybridisation buffer (14 µl per 5 ml ~2.8 ng/ml) were as recommended by the manufacturer.

9.2.8 cDNA synthesis

9.2.8.1 3' anchor-ligated cDNA

Anchor-ligated cDNA was synthesised using the 5'/3' RACE kit from Roche (cat.# 03 353 621 001; formerly Boehringer Mannheim (cat.# 1 734 792)) using the following oligo d(T)-primer to attach a 3' anchor to all cDNAs GACCACGCGTATCGATGTCGAC$[T]_{16}V^{*}$. The kit as originally purchased employed avian myeloblastosis virus reverse transcriptase. 1.3 µg of total RNA from each sample was used as template.

9.2.8.2 Oligo d(T)-primed cDNA

Oligo d(T)-primed cDNA was synthesised using the displayTHERMO-RT kit from Display Systems Biotechnologies (sample lot, 570-104-0998-1) employing a recombinant Moloney murine leukaemia virus (MMLV) reverse transcriptase engineered for activity at high temperature and devoid of RNase $H^{\dagger}$ activity. 0.75 µg of total RNA from each sample was used as template and synthesis was carried out at 55°C as directed by the manufacturer.

9.2.9 3' RACE PCR of *SURF1*

3' RACE PCR of *SURF1* cDNA was carried out with anchor-ligated cDNA (9.2.8.1) using a nested 3' anchor primer GACCACGCGTATCGATGTCGAC and the *SURF1* exon 7-specific internal primer GGAAGCTATGGCCAGAATCACAG (nucleotides 710-731) designed using Lasergene '98 Primer Select software (v3.11). PCR amplification of *SURF1* exon 7→5'-anchor fragments was carried out using the Advantage-HF2 AdvanTaq‡ PCR kit from BD Biosciences (k1914-1; formerly Clontech k1914-1). Products were amplified using the touchdown PCR protocol shown below.

---

* V = A, C or G.
† Degrades RNA present in a RNA:DNA duplex.
‡ AdvanTaq PCR system is a dual polymerase mix with a major 5'-exonuclease deficient *Taq* polymerase and a minor amount of the 5'-exonuclase capable enzyme. It also includes an anti-polymerase antibody which prohibits enzyme activity at ambient temperature providing a form of "hot start".

	Denaturation	Cycles 1-10			Cycles 11-35			Termination	
Temperature (°C)	94	95	68-61	72	94	61	68	68	4
Time (s)	15	15	7	15	15	5	20	180	∞

Samples were resolved using a 2% high grade agarose TAE slab gel (9.2.2.1) and extraction of individual ethidium bromide-visualised bands was carried out using the Qiagen Quick Spin gel extraction kit (28704). Extracted DNA was then amplified using a standard 25 µl reaction of the Advanced Biotechnologies Red-Hot Taq PCR protocol (9.2.1.6) using the cycle below.

	Denaturation	Cycles 1-35			Termination	
Temperature (°C)	94	94	61	68	68	4
Time (s)	15	15	5	20	180	∞

Amplified product was cleaned with the Qiagen PCR cleanup kit (9.2.1.7) and sequenced using fluorescent dye-terminator sequencing (9.2.1.9).

9.3 INVESTIGATION OF COX SUB-COMPLEXES BY BN-PAGE

9.3.1 Sample preparation

9.3.1.1 Purification of mitochondria

Rat heart mitochondria were prepared in the laboratory of Dr Thierry Letellier (INSERM EMI 9929, Universite Bordeaux 2, F-33076 Bordeaux Cedex, France.) and supplied as a frozen pellet. Human fibroblast mitochondria from P8 and P9 were supplied frozen by Dr Pierre Rustin (INSERM U-393, Hôpital Necker-Enfants Malades, Paris, France) and mitochondria from P7 were prepared by Dr Jan-Willem Taanman. Fibroblast mitochondria were purified by differential centrifugation of homogenised, freeze-thawed cell pellets as described by Rustin and co-workers[680].

9.3.1.2 Isolation of crude mitoplast fractions using digitonin

The preparation of crude mitoplast fractions using digitonin was based on the method devised by Klement *et al*[681]. Cells were harvested using trypsin as detailed previously (9.1.5.1) except that cell suspensions were counted. Chilled, 4 mg/ml digitonin (BDH, 007124399) in PBS with protease inhibitors was added to 200 µl per 10^6 cells and the cell pellets were resuspended using a micropipette. Suspensions were left on ice for 15

min before being pelleted in a desk-top microfuge at 13,000 rpm and 4°C for 1 min. The supernatant was removed and the pellet was re-suspended and washed once by centrifugation in ice cold PBS with protease inhibitors at 13,000 rpm and 4°C for 1 min. The remaining supernatant was removed and mitoplast pellets were frozen at -70 °C in aliquots suitable for varying-sized experiments.

9.3.1.3 Solubilisation of mitochondria

Purified mitochondria from rat heart and human fibroblasts were solubilised using the protocol devised by Schägger[34]. Per lanes-worth of mitochondria, the following quantities were used: a variable volume of purified mitochondria (0.5-50 µg <2 µl) was added to 15 µl of protein solubilising solution with protease inhibitors (1 M 6-aminohexanoic acid (Sigma, A7824), 50 mM bistris pH 7.0 (Sigma, B7535), 1 µg/ml leupeptin, 1 µg/ml pepstatin and 1µM PMSF) and mixed briefly. 5 µl of 200 mM LM* was then added and the sample was mixed again and left on ice for 15 minutes. Samples were then cleared by centrifugation at 13,000 rpm for 20 minutes at 4°C using a mini-centrifuge. Supernatant was removed to which 2.5 µl of loading buffer (1 M 6-aminohexanoic acid, 5% (w/v) Coomassie Brilliant Blue G250 (Serva, 35050.02)) was added and the sample was mixed by vortexing. Occasionally unused samples were stored at -70°C and used within 2 weeks.

9.3.1.4 Solubilisation of mitoplast fractions

Mitoplasts were solubilised as described by Coenen *et al*[40]. 10^6 cell equivalents of thawed, mitoplasts (9.3.1.2) were resuspended in 100 µl of protein solubilising solution with protease inhibitors (9.3.1.3). 20 µl of 200 mM LM was added and samples were mixed briefly and incubated on ice for 15 minutes. They were then cleared by centrifugation at 13,000 rpm at 4°C for 20 minutes in a mini-centrifuge. The supernatant was removed into a clean tube and 10 µl of loading buffer was added (9.3.1.3). Samples were mixed briefly and then used. Solubilised mitoplast samples were not stored prior to use.

---

* 10% (w/v).

9.3.2 BN-PAGE electrophoresis

9.3.2.1 Pouring BN-PAGE mini-gels

Gel solutions were made up as detailed by Schägger[33] using appropriate quantities of 48% acrylamide/3% bis-acrylamide (Sigma, A3553 & M7279) which had been cleaned using Amberlite MB-1 resin (BDH, 55007). 4% acrylamide stacking gels were used for all gels. Gel buffer contained final concentrations of 500 mM 6-aminohexanoic acid and 50 mM bistris pH 7.0. Linear gradients were formed using a Hoefer gradient maker (XPO77) mounted on a magnetic stirrer. Gels were poured into BioRad Mini Protean 3 gel cassettes using a Watson-Marlow peristaltic pump set at around 30% speed, fitted with 1.52 mm-bore silicone tubing (Watson Marlow, 982.0152.000). Equipment was cleaned thoroughly and assembled as detailed by manufacturers. Before use the glass plates, spacers and combs were cleaned with ddH_2O followed by 100% ethanol. The pump tubing and mixing chamber were rinsed immediately before use with ddH_2O and then with gel buffer. 0.75 mm spacers were used for all gels and 3.5 ml of total gradient gel solution was used per gel, creating a separating gel around 45mm long and leaving about 12 mm of stacking gel from the bottom of each well. Gels were poured with the tubes from the pump inserted into micro-pipette gel loading tips wedged into the top of the gel cassette with the high percentage (bottom) of the gel being poured first and the gradient being layered on top. To avoid handling small volumes, gels were poured in sets of 4. All gel solutions were filtered through 0.2 µm hydrophobic filters before use but were not degassed. Poured gradient gels were topped with ~80 µl of water-saturated butanol to encourage even polymerization. After about 15 minutes, once the gradient gels had set, the butanol was removed and the stacking gel was poured and a fitted with a 10-well comb. Gels were normally poured the day before use and once set, stored overnight at 4°C. Some gels were stored for 48 hours before use without any noticeable effect on quality.

9.3.2.2 Electrophoresis

Gel buffers were as described by Schägger except that the cathode buffer was not routinely exchanged for one with a low G250 content. Buffer components were as follows: Cathode buffer, 50 mM Tricine (Sigma, T0377), 15 mM bistris, 0.02% (w/v) G250 pH 7.0; Anode buffer, 50 mM bistris pH 7.0. 10-22 µl of sample was loaded per lane. Gels were run at a fixed current between 4-8 mA corresponding to a starting voltage ~100 V and an end voltage around 300 V. Electrophoresis was stopped once the loading dye had run off.

9.3.2.3 Blotting, probing and development of BN-PAGE 1D gels

BN-PAGE gels were blotted and probed exactly as for denaturing gels (9.1.5.6; 9.1.5.7) except that blotting was carried out for 90 minutes. Where blots were cut into strips they were probed using a purpose built, slotted tank and buffer volumes were adjusted accordingly. It was found that residual G250 interfered with blocking (12.1.4.2) so blots were routinely air dried and washed briefly in 100% methanol before blocking and probing. The choice of secondary antibody (9.1.6) was altered during the study (12.1.5.1), initially secondary antibody from BioRad was used (B) but this was subsequently switched in favour of one from Dakocytomation (D) and one from Jackson (E). For 1D blots, all secondary antibodies were used as directed by manufacturers. Development of BN-PAGE western blots was as for denaturing gel blots (9.1.5.7).

9.3.3 2D BN-PAGE/urea-SDS PAGE

9.3.3.1 Preparation and electrophoresis of 2D BN-PAGE/urea-SDS gels

The protocol for preparation and electrophoresis of 2D BN-PAGE/denaturing PAGE gels was based on those devised by Schägger[31-34,682,683] and Nijtmans[529,540,681,684-686] but with the use of discontinuous pH gradient urea-SDS PAGE as opposed to tris-tricine-SDS PAGE in the second dimension. Gel strips of first dimension lanes cut from BN-PAGE gels for 2D electrophoresis were either used fresh or were frozen flat in saran wrap at -20°C and thawed before use. Gel strips were equilibrated and reduced by soaking in reducing buffer (50 mM tris·HCl pH 6.8, SDS (1% w/v), 1% (v/v) β-mercapto-ethanol) and were then washed 2x in equilibrating buffer (50 mM tris·HCl pH 6.8, 1% (w/v) SDS). Initially gel strips were soaked for 45 minutes and washed twice for 10 minutes. Following investigation of the leaching of signal from strips (12.1.5.4), soaking was reduced to 15 minutes and washing to 2x 5 minutes. To pour second dimension gels, first dimension gel strips were dried briefly using Whatman 3MM paper and placed horizontally in gel cassettes in the region corresponding to the stacking gel such that their top side was around 5 mm from the top of the cassette. 12.5% or 13.5% acrylamide urea-SDS separating gels (pH 8.6), as used for denaturing gel electrophoresis (9.1.5.5), were then poured below the gel strips leaving around 10 mm between the bottom of the strip and the top of the separating gel. Separating gels were covered with ddH_2O to assist polymerisation and once set, a 3% stacking gel (pH 6.8) was poured around the first dimension strip and covered with water-saturated butanol to assist polymerisation. During the polymerisation of the stacking gel, gentle pressure was applied to the gel

cassette in the region of the gel strip to clear water which built up underneath it as a result of the polymerisation reaction. This ensured good contact between first dimension strips and the stacking gel.

9.3.3.2 Running second dimension gels

Second dimension gels were run exactly as denaturing gels (9.1.5.5) except that voltage was 160 V throughout. Electrophoresis was stopped once the front of residual dye from the first dimension strip had run off, ≤1 hour.

9.3.3.3 Blotting, probing and development of 2D BN-PAGE/urea-SDS page gels

2D gels were blotted and probed exactly as 1D BN-PAGE gels (9.3.2.3). Initially secondary antibody from BioRad (B; 9.1.6) was used, this was then switched for one from Dakocytomation (D) before a revised protocol employing three antibody layers was used (12.1.5.5). When three antibody layers were used, secondary antibody from Dakocytomation (D) was used at a 1/500 dilution in PBS-Tween and was left on blots for 45 minutes followed by 2x 5 minute washes in PBS-Tween before the tertiary peroxidase-anti-peroxidase (PAP) antibody from Dakocytomation (A) was added also at a 1/500 dilution in PBS-Tween and left on for 45 minutes. Blots were then washed 3x in PBS-Tween and once in PBS before development as for denaturing gel blots (9.1.5.7).

9.3.4 *In gel* enzyme activity stains

1D BN-PAGE gel strips for in gel activity staining were briefly washed in anode buffer to remove excess G250 and then rinsed in ddH_2O. Strips were placed in 7 ml tubes and incubated horizontally at 37°C in 1.5 ml of 200 mM sodium succinate, 200 mM potassium phosphate buffer (pH 7.4) and 1 mg/ml NBT*. Stains were left to develop for 1-5 hours until suitably strong signal could be seen. After staining strips were destained in either ddH_2O or 10% (v/v) acetic acid, 40% (v/v) methanol. COX activity staining was carried out exactly as for succinate dehydrogenase except that strips were incubate with 1.5 ml of COX activity stain solution as used for histochemical stains (9.1.3).

9.3.4.1 Purification of MTCO1

MTCO1 was purified by Dr Jan-Willem Taanman. Purified human heart COX (A gift from Dr AO Muijsers; University of Amsterdam) was dissociated using 3% SDS and resolved

---

* Nitroblue tetrazolium.

under denaturing conditions[687] on a BioRad Bio-Gel® P-60 gel-filtration column. To remove excess SDS, MTCO1-containing eluant was precipitated by the addition of 3 volumes of ethanol at room temperature. The protein pellet was washed once with 80% ethanol, dried, and dissolved in PBS, 3.5 mM SDS.

RESULTS

10 PHENOTYPING OF PATIENT CELL CULTURES

10.1 SELECTION OF PATIENT CELL CULTURES

Seven primary dermal fibroblast cultures were selected for study from archives of patient cells on the basis of expression of a severe COX deficiency in culture. All were derived from paediatric patients with severe mitochondrial dysfunction, including COX deficiency (8). Clinical details were not taken into account when selecting the cultures for study.

10.2 COX ACTIVITY AND ABUNDANCE

10.2.1 COX activity stains

The expression of a COX defect in culture was confirmed using a histochemical stain of COX activity.

10.2.1.1 P1-P7

No brown DAB precipitate was seen in P1, P3, P4, P5, P6 or P7 (figure 10). Some weak staining associated with mitochondria was present in P2. These experiments were repeated at least four times with consistent results. P3 cells maintained the large granular morphology seen in these stains throughout the entire study. Disease control fibroblasts derived from a patient with MELAS exhibit a mosaic staining characteristic of cultures with heteroplasmic mtDNA mutations[43]. This strong mosaic pattern was not observed in any of the patient cultures studied. In P3 and P6, a small number of mitotic cells stained positive for COX activity (figure 11). Close examination of the cells confirmed that the brown staining seen was not due to debris. Increased staining of mitotic cells was also noted in controls.

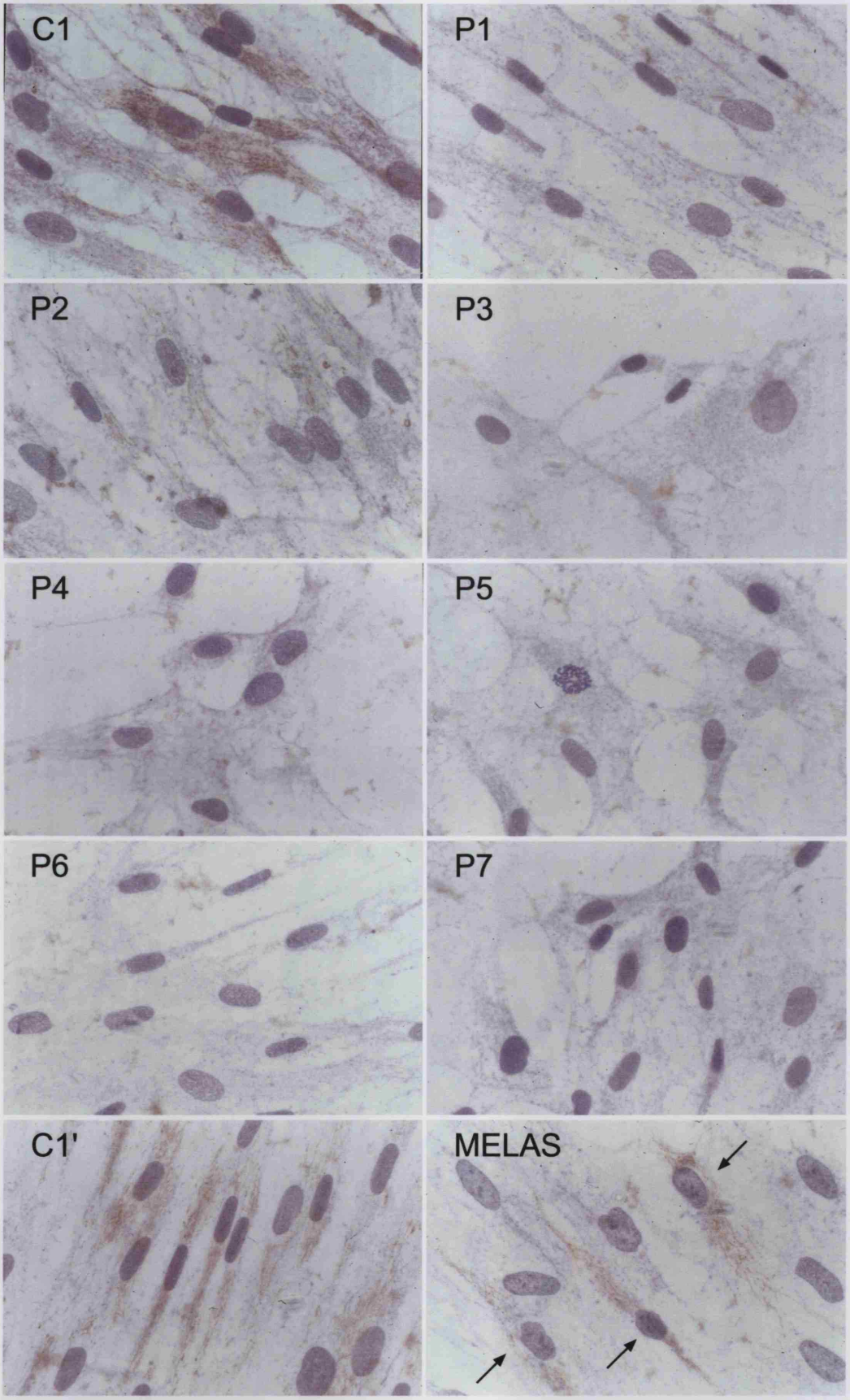

Figure 10 COX activity stains of P1-P7 and the control C1 stained in parallel. MELAS is a disease control primary fibroblast culture derived from a MELAS patient with a 79% mutant load of the mtDNA 3243G-A, *MTTL1* mutation. C1' is a control fibroblast culture stained in parallel with the MELAS culture. Arrows indicate COX positive cells. Magnification x330.

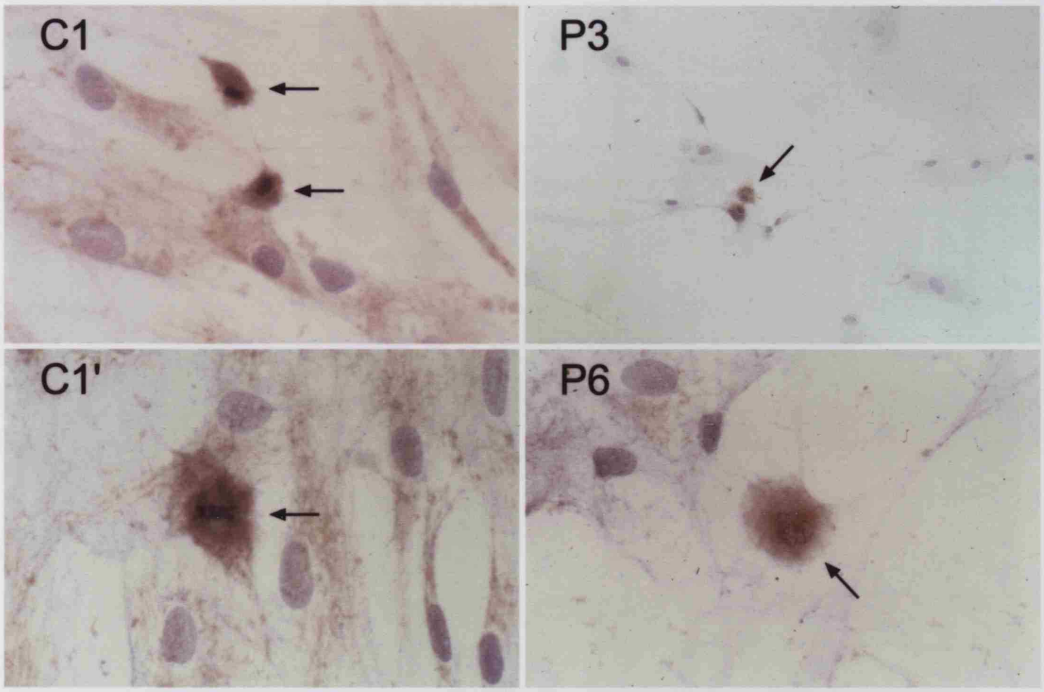

Figure 11 COX activity stains of C1, P3 and P6 showing COX positive mitotic cells, indicated with arrows. Top row: late telophase cells from C1 and P3. Bottom row: early prophase cells from C1 and P6. Magnification for both C1 images and P6 is x330, magnification of the P3 image is 66x.

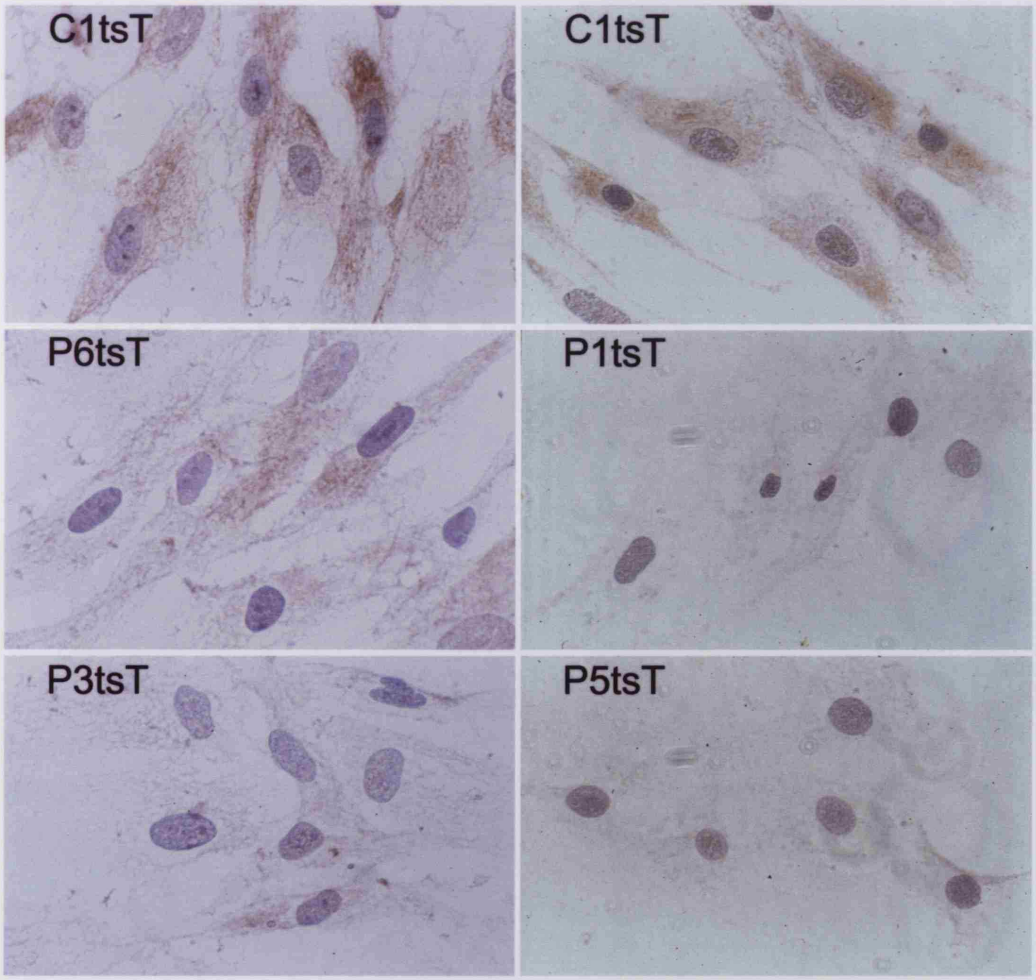

Figure 12 COX activity stains of C1tsT, P3tsT, P5tsT and P6tsT. Images in each column are from the same experiment. Magnification x330.

10.2.1.2 SV40 large-T antigen transduced cells

To facilitate genetic studies and increase the proliferative lifespan of the cells P1, P3, P5, P6 and the control primary fibroblast culture C1 were retrovirally transduced with a temperature sensitive form of the SV40 Large-T antigen (tsT). The COX negative phenotype of P1, P3 and P5 remained unchanged following transduction. However transduction rescued COX activity staining in P6 (figure 12). These stains were repeated at least twice with consistent results.

10.2.2 COX activity in P7 and the disease control cultures P8 and P9

Collaboration with Dr Pierre Rustin provided access to mitochondria from primary dermal fibroblasts derived from patients with known mutations in *SCO1* (P8) and *COX10* (P9). Spectrophotometric analysis of COX activity in mitochondria from P7, P8 and P9 was carried out by Dr Taanman. As expected patient mitochondria all had severely reduced COX activity relative to the mitochondrial marker citrate synthase (figure 20). The COX activities in the patient samples were all similar, ranging from 9.5%±1.1 in P9 to 14.0%±1.4 in P7.

10.2.3 Spectrophotometry of whole cell OXPHOS cytochromes

OXPHOS cytochromes were examined using spectrophotometry of freeze-thawed whole cells to avoid growing large quantities of primary cells and the possibility of the introduction of artefact from mitochondrial purification. Visible spectra were used to measure *a*, *b* and *c*-type cytochromes and CO laser-flash photolysis was employed examine cytochrome a_3. As cell suspensions have poor optical properties readings were only taken using fully reduced samples. This ensured redox homogeneity of the samples and avoided excessive manipulation of the cell suspensions which caused clumping. The protocols utilised in this section were devised and verified by Dr Brigitte Meunier and Prof Peter Rich of the Galton Lab, Department of Biology, UCL.

10.2.3.1 Visible spectra

An example of spectra for A549 ρ^+ and A549 ρ^0 cells is shown in figure 13. As ρ^0 cells have no mtDNA they do not contain complex III or COX cytochromes. As expected, the difference spectra shows a large peak around 604 nm corresponding to the cytochrome aa_3 signal. The peak around 562 nm corresponds to the complex III cytochrome *b*

component. The shoulder in this region on the ρ^0 spectra demonstrates the contribution of other *b*-type cytochromes to this signal. An example of the traces obtained with the patient cell suspensions obtained by Dr Meunier is given in figure 14. Due to the low cell density of the samples the signals are smaller than those of the ρ^0 vs ρ^+ samples. Combined with the poor optical properties of the cell suspensions, this hampered measurements of some samples (table 14). The difference spectra illustrates the isolated loss of the cytochrome aa_3 signal in P4. Although not all samples could be examined using visible spectra, the values obtained for the cytochrome aa_3 content are in good agreement with those of the CO laser-flash photolysis data (10.2.3.2). Very low levels of cytochrome aa_3 were seen in P7 but a milder deficiency was seen in P6. The *b*- and *c*-type cytochrome values for all patient cell samples for which measurements could be taken were normal.

Table 14 Mean cytochrome concentrations in whole cell samples given as pmol/mg total protein, the units for the observed rate constant for CO ligation (κ_{obs}) are s^{-1}.

	CO flash-photolysis				Visible spectra						
	Cytochrome a_3		κ_{obs}	a_3 as % control	*c*-type cytochromes		*b*-type cytochromes		Cytochrome $a+a_3$		ΔCN
Sample	pmol/ mg	SD	s^{-1}	%	pmol/ mg	SD	pmol/ mg	SD	pmol/ mg	SD	a_3
P1	0.87	0.42	65	10	26.72	1.5[r]	29.35	0.32[r]	nr		nr
P2	1.33	0.25	64	16	24.39		nr		nr		nr
P3	0.89	0.04[r]	65	11	nr		nr		nr		nr
P4	0.63	0.38	63	8	24.42		nr		nr		nr
P5	0.92	0.27	65	11	26.02		nr		nr		nr
P6	3.78	2.18	65	45	35.08	12.5	34.88	0.25[r]	3.17	0.14[r]	5.52
P7	1.48	0.07[r]	60	18	34.56	0.6	31.24	0.45[r]	1.18	0.69[r]	1.36
C1	7.52	1.64	56	90	32.56	6.3	25.81	0.78[r]	5.40	0.64[r]	nr
C2	9.18	1.36	59	110	31.84	0.8	34.17	0.58[r]	9.89	0.12[r]	7.53

Key: ΔCN a_3, cytochrome a_3 from CN difference spectra; nr, no reading, either sample was not available or clumping prohibited accurate reading; SD, standard error of three or more measurements; [r] value is range of two measurements. Data without errors are single measurements.

10.2.3.2 CO laser-flash photolysis

As clear cytochrome aa_3 signals could not be obtained for all samples using visible spectra, CO laser flash photolysis was employed to measure the abundance of cytochrome a_3 and to examine its haem environment. Figure 15 shows an example of a control trace and an overlay of a trace of P5 cells. Results of all the CO photolysis data are summarised in figure 16 and table 14. The cytochrome a_3 levels in the samples from P1-P5 and P7 were all consistently low, ranging from 0.63 pmol/mg to 1.48 pmol/mg corresponding to 8-18% of control mean. The cytochrome a_3 levels in P6 cells were

higher than those of the other six patient cultures, although these values have a large standard error. The observed rate constants (κ_{obs}) for CO ligation for all samples fell within the normal range[688*] of 50-70 s^{-1}. In addition, no biphasic behaviour was noted in any of the samples, excluding contamination of the signal by endogenous haemoproteins with faster rate constants[667] (e.g. haemoglobin >2000 s^{-1}).

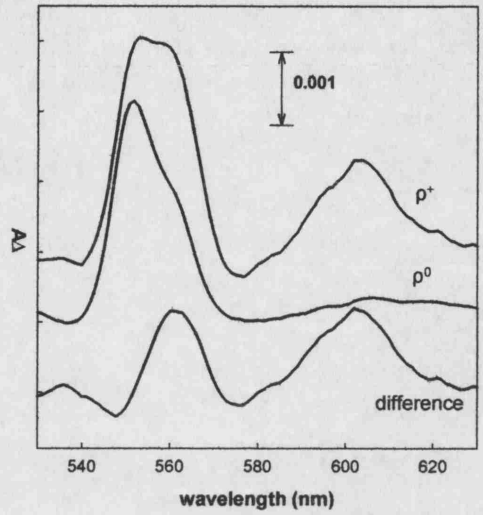

Figure 13 Examples of visible spectra A549 ρ^+ and A549 ρ^0 freeze-thawed cells. A549 ρ^+ and A549 ρ^0 cell pellets were resuspended to 25 and 12 mg of protein/ml, respectively. The two upper traces (ρ^+ and ρ^0) show the spectra of dithionite-reduced, freeze-thawed cell suspensions. The lower trace is the difference spectrum obtained by subtracting the signal of the ρ^0 cells from that of the ρ^+ cells.

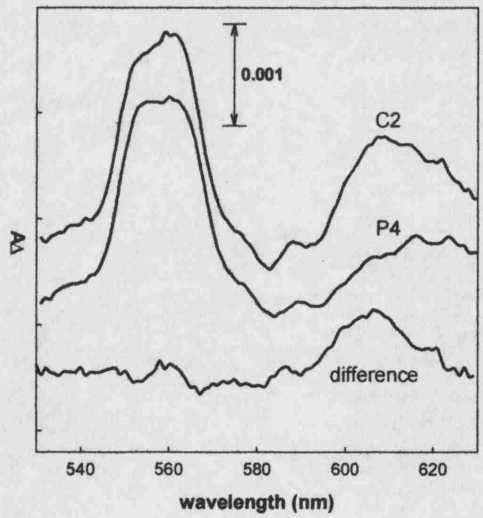

Figure 14 Examples of visible spectra of freeze-thawed control and patient fibroblast cells. The two upper traces are spectra of dithionite-reduced control (C2) and patient (P4) cells resuspended to 10 and 13 mg of protein/ml, respectively. The lower trace is the difference spectrum obtained by subtracting the signal of the patient trace from that of the control trace.

---

* Dr Brigitte Meunier personal communication.

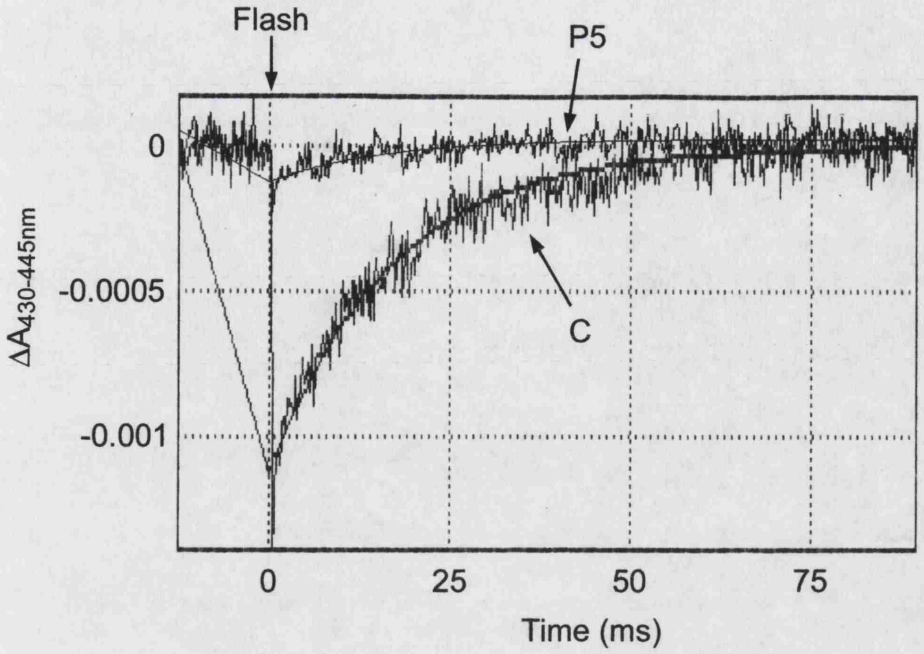

Figure 15 An example of the difference spectra obtained from CO laser-flash photolysis measurements. The time post-flash is shown across the bottom of the trace and the flash is indicated at the top of the figure. Traces from two freeze-thawed cell suspensions are overlaid, one from P5 and one from a control myoblast culture, C. (Fibroblasts and myoblasts have similar a_3 levels, this image is shown only as an example of the form of the data obtained.) Solid lines through the traces show first order decays fitted by eye to determine κ_{obs} and the amplitude of A430-A445 nm following flash-photolysis as described in the text. Cell suspensions were reconstituted to 2.6mg protein/ml for P5 and 3.6mg protein/ml for C. κ_{obs} was $65s^{-1}$ for P5 and $60s^{-1}$ for C and the cytochrome a_3 content of the samples was 1.1nM and 9.9nM respectively.

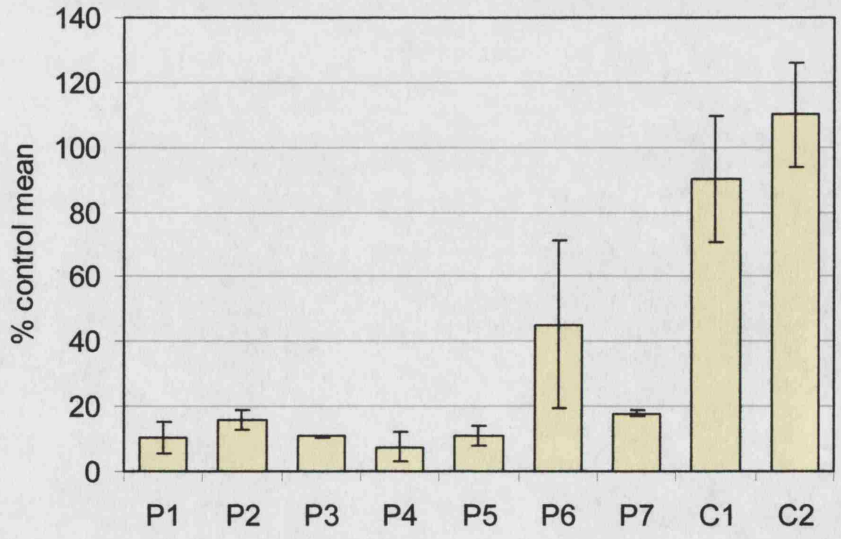

Figure 16 A bar chart of the cytochrome a_3 abundance of P1-P7 determined using CO laser-flash photolysis from table 7.

10.3 INVESTIGATION OF STEADY-STATE OXPHOS SUBUNIT LEVELS

10.3.1 Denaturing gel western blots of OXPHOS subunits in LM extracts

It was anticipated that examination of the steady-state levels of OXPHOS subunits would provide data on the extent to which the various complexes were affected in each of patient cell cultures. Results would also offer a means of phenotyping the cultures and act as a foundation for further studies. Denaturing urea-SDS PAGE gels were run using LM extracts and blots of the gels were probed with monoclonal antibodies against OXPHOS subunits. The outer membrane porin, VDAC1, was used as a marker for equivalent solubilisation and loading of samples.

10.3.1.1 P1-P5

P1-P5 were probed on the same sets of blots enabling comparison of antibody signals between all five cultures (figure 17). These blots also included samples from a disease control fibroblast culture derived from a patient with MELAS. This culture carried a 79% mutant load of the 3243A-G, *MTTL1* mutation. Three patterns of steady-state levels of OXPHOS subunit levels were seen in P1-5 and the MELAS culture, i) an isolated reduction of COX subunits, P1, P4 and P5; ii) a reduction of subunits from complexes containing proteins encoded by the mitochondrial genome, P3 and M; and iii) a generalised reduction in subunits from all OXPHOS complexes probed, P2. These western blots were repeated at least twice with two separate protein extracts for each sample. Consistent results were obtained and are summarised in table 15.

P1, P4 and P5 all had very low levels of MTCO2 and MTCO3 yet the signal for MTCO1 while reduced compared to controls but not so severely affected. Similar to the anti-MTCO1 signal, anti-COX4I1, anti-COX5A and anti-COX5B signals were also preserved relative to the MTCO2 and MTCO3 signals. Levels of NDUFA9, UQCRC2, SDHA, SDHB, ATP5A1 and VDAC1 were all normal. In P3 signals for MTCO1, MTCO2 and MTCO3 were all very low compared to controls. In particular, the MTCO1 signal was lower in P3 than any of the other samples. Similar to P1, P4 and P5, COX4I1 and COX5A seemed to be relatively preserved, while the COX5B signal was much lower in P3. P3 samples showed evidence of involvement of other OXPHOS complexes. Low signals were seen for NDUFA9 and UQCRC2. Signals for SDHA, SDHB, ATP5A1 and VDAC1 were normal. P2 had a reduction in steady-state levels of all OXPHOS subunits

probed. The reduction was generally not as severe as those seen in the other samples, examples being the MTCO2 and MTCO3 signals which, although lower than controls, were highest in samples from this culture. Uniquely, a reduction in the signals for ATP5A1 and VDAC1 was consistently present in samples from this culture.

10.3.1.2 P6, P6s, P6sa and P7.

Steady-state OXPHOS subunit levels were also probed in P6, P6s, P6sa and P7. Similar to P1, P3, P4, P5, steady-state levels of MTCO2 were very low in P7, P6, P6s and P6sa (figures 18 & 19). Signals for MTCO1 were also very low. As with P1-P5 the COX4I1 signal, although consistently lower than controls, was not reduced relative to controls to the same extent as the other COX subunits. Contrary to the biochemical data (table 8), there was some evidence of a reduction UQCRC2 levels in P6. SDHA levels were normal in all samples from P7, P6, P6s and P6sa. The similarity between the subunit signature of P6 and P6s indicated that both siblings were affected by the same disorder and blots of extracts from P6sa demonstrated that the defect was also expressed in amniocytes. Each of this set of blots was repeated at least once with consistent results. Results are summarised in table 15.

10.3.1.3 OXPHOS subunit levels in P7 and disease controls with mutations in SCO1 and COX10

The results obtained from P7 mitochondria compared favourably with the previous results using whole-cell LM extracts, although slightly stronger signals were obtained for MTCO1 and COX4I1 (compare figures 18 & 20). As with the previous results, no reduction in the SDHA signal was seen relative to controls. The steady-state OXPHOS subunit levels in the two disease controls P8 and P9 were identical. The steady-state subunit levels in P7 were similar to those of the disease controls although the MTCO1 signal was significantly higher in P7 than P8 or P9, and the COX6B signal was undetectable in P7, whereas an intermediate signal was detected in P8 and P9 (table 15). This series of blots was repeated once with independent mitochondrial samples and consistent results were obtained.

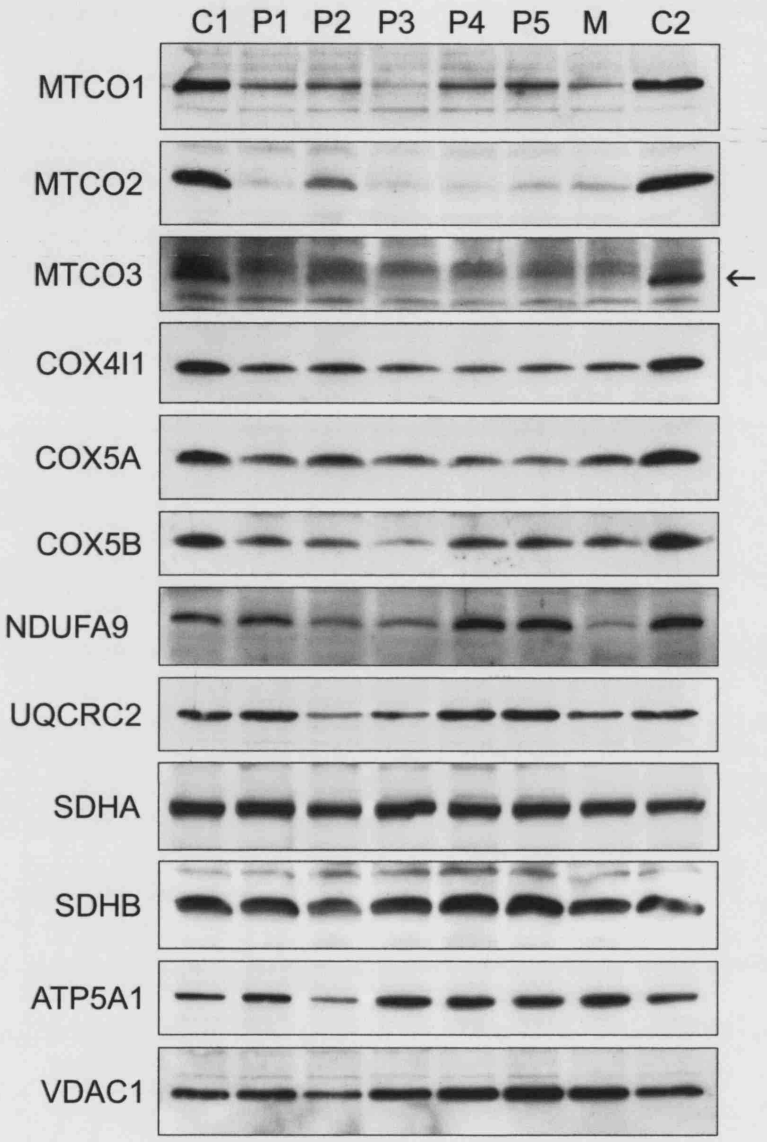

Figure 17 Denaturing gel western blots of LM extracts (10 µg per lane) from P1-P5 and the normal controls C1 and C2. "m" is a disease control MELAS culture with a 79% mutant load of the mtDNA 3243G-A, *MTTL1* mutation. Primary antibody targets are listed on the left. COX subunits, MTCO1, MTCO2, MTCO3 (arrow), COX4I1, COX5A, COX5B; Complex I, NDUFA9; Complex III, UQCRC2, Complex II, SDHA, SDHB ; complex V, ATP5A1. Antibody against the outer membrane porin, VDAC1, was used to determine the uniformity of loading.

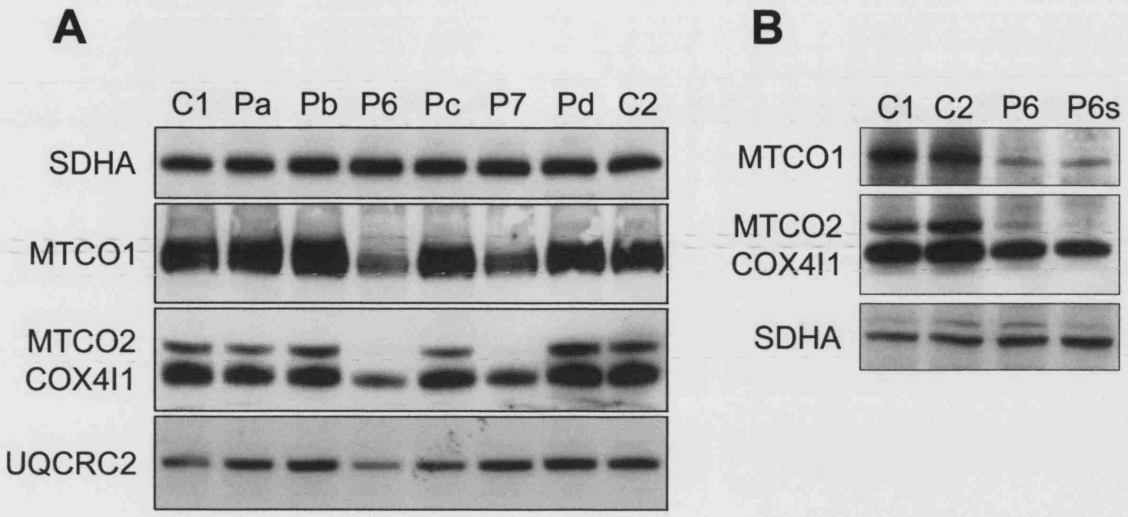

Figure 18A Denaturing gel western blots of LM extracts (9 µg per lane) from P6 and P7 and the normal controls C1 and C2. Pa-Pd are not discussed in this thesis. Primary antibody targets are listed on the right. COX subunits, MTCO1, MTCO2, COX4; Complex III, UQCRC2; Complex II, SDHA. **18B** Western blots of LM extracts from P6 and P6s, a fibroblast culture derived from an affected sibling of patient 6. C1 and C2 are normal controls. Primary antibody targets are listed on the right. COX subunits, MTCO1, MTCO2, COX4I1; Complex II, SDHA.

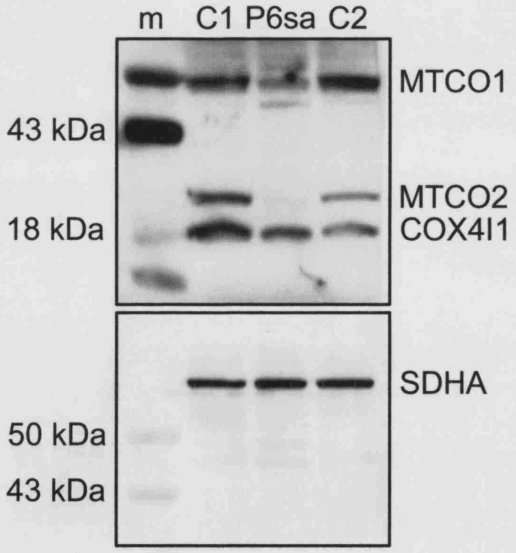

Figure 19 Denaturing gel western blots of LM extracts (10 µg per lane) from the amniocyte culture P6sa and two normal control amniocyte cultures, C1 and C2. Primary antibody targets are listed to the right of each panel. Upper panel, COX subunits, MTCO1, MTCO2, COX4; Lower panel complex II, SDHA. Molecular weights of protein markers are given on the left.

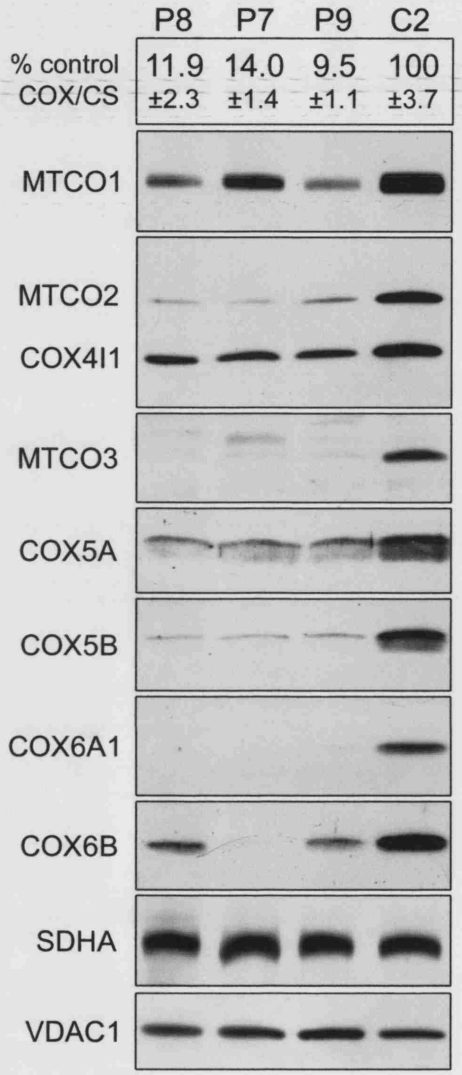

Figure 20 Denaturing gel western blots of mitochondria from P7, the disease controls P8 (*SCO1* mutant) and P9 (*COX10* mutant) and the normal control C2. Primary antibody targets are given to the left of each panel: COX subunits MTCO1, MTCO2, MTCO3, COX4I1, COX5A, COX5B, COX6A1, COX6B; complex II, SDHA. The outer membrane porin VDAC1 was probed to check uniformity of loading. Samples were balanced according to the signal for SDHA and then loaded according to a standard of 5 µg of C2. COX activity relative to citrate synthase is given in the top box as a percentage of the control ratio. n=4 for all values. The standard deviation is given below each value. All data in this figure was generated by Dr Jan-Willem Taanman.

Table 15 Summary of western blot data for P1-P9 from figures 17-20. Results are expressed relative to control cultures. C, reference control signal; M, MELAS disease control.

OXPHOS Antibody target		LM extracts									Purified mitochondria			
Complex	Subunit	P1, P4, P5	P2	P3	P6	P6s	P6sa	P7	M	C	P7	P8 (*SCO1*)	P9 (*COX10*)	C
COX	MTCO1	+	+	-	-	+	+	+	-	++	+	-	-	++
	MTCO2	-	+	-	-	-	-	-	-	++	-	-	-	++
	MTCO3	-	+	-	nd	nd	nd	nd	-	++	-	-	-	++
	COX4	+	+	+	+	+	++	+	+	++	+	+	+	++
	COX5A	+	++	+	nd	nd	nd	nd	+	++	+	+	+	++
	COX5B	+	+	-	nd	nd	nd	nd	+	++	-	-	-	++
	COX6A1	nd	nd	nd	nd	nd	nd	nd	nd	nd	-	-	-	++
	COX6B	nd	nd	nd	nd	nd	nd	nd	nd	nd	-	+	+	++
Complex I	NDUFA9	++	-	-	nd	nd	nd	nd	-	++	nd	nd	nd	++
Complex III	UQCRC2	++	-	+	-	nd	nd	++	+	++	++	++	++	++
Complex II	SDHA	++	+	++	++	++	++	++	++	++	nd	nd	nd	nd
	SDHB	++	+	++	nd	nd	nd	nd	++	++	nd	nd	nd	nd
Complex V	ATP5A1	++	-	++	nd	nd	nd	nd	++	++	nd	nd	nd	nd
---	VDAC1[a]	++	+	++	nd	nd	nd	nd	++	++	++	++	++	++

Key: ++, normal signal or close to normal signal; +, intermediate signal; -, very low signal; nd, not done. [a] VDAC1 is not a component of the OXPHOS but forms the voltage-dependent anion channel in the mitochondrial outer membrane.

Figure 21, part i.

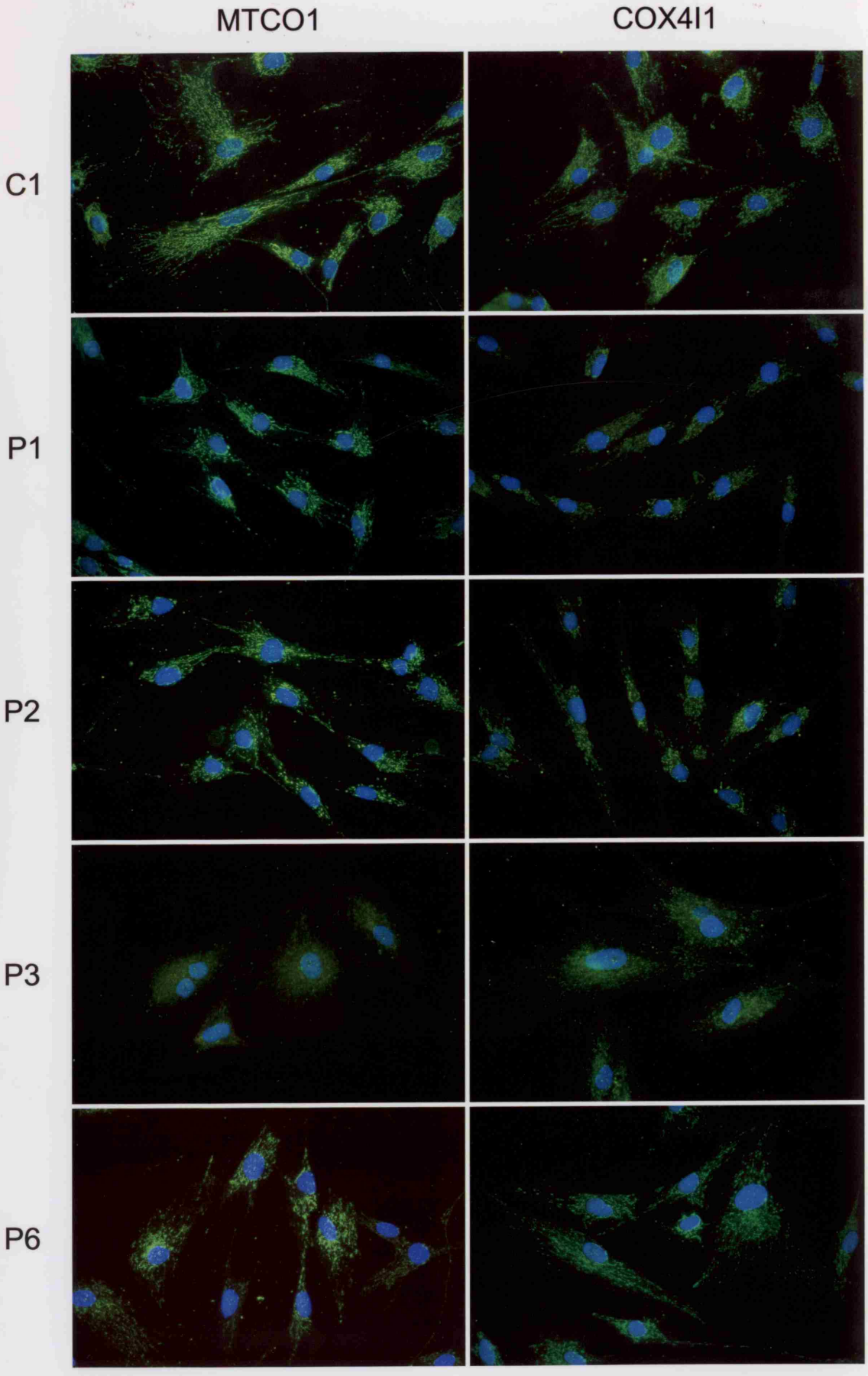

Figure 21, part ii.

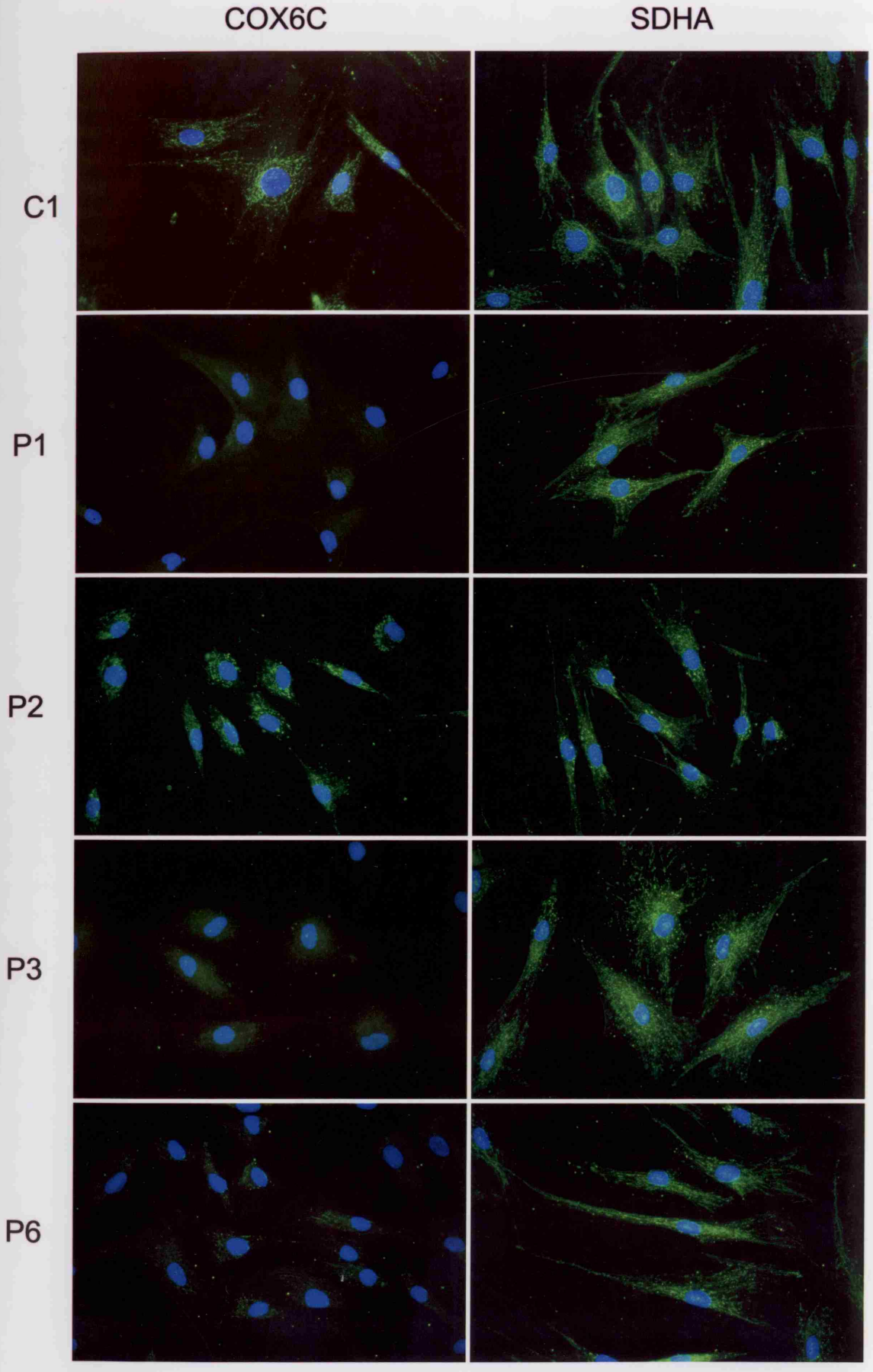

Figure 21 Immunofluorescent stains of P1, P2, P3 and P6 and the control C1. Monoclonal primary antibodies were detected using green fluorescent Alexa™ 488-conjugated secondary antibody. Nuclei were counter-stained blue using DAPI. Primary antibody targets are given at the top of each column. Part i, MTCO1 and COX4I1; part ii, COX6C and SDHA; part iii (this page), ATP5A1. Magnification x220.

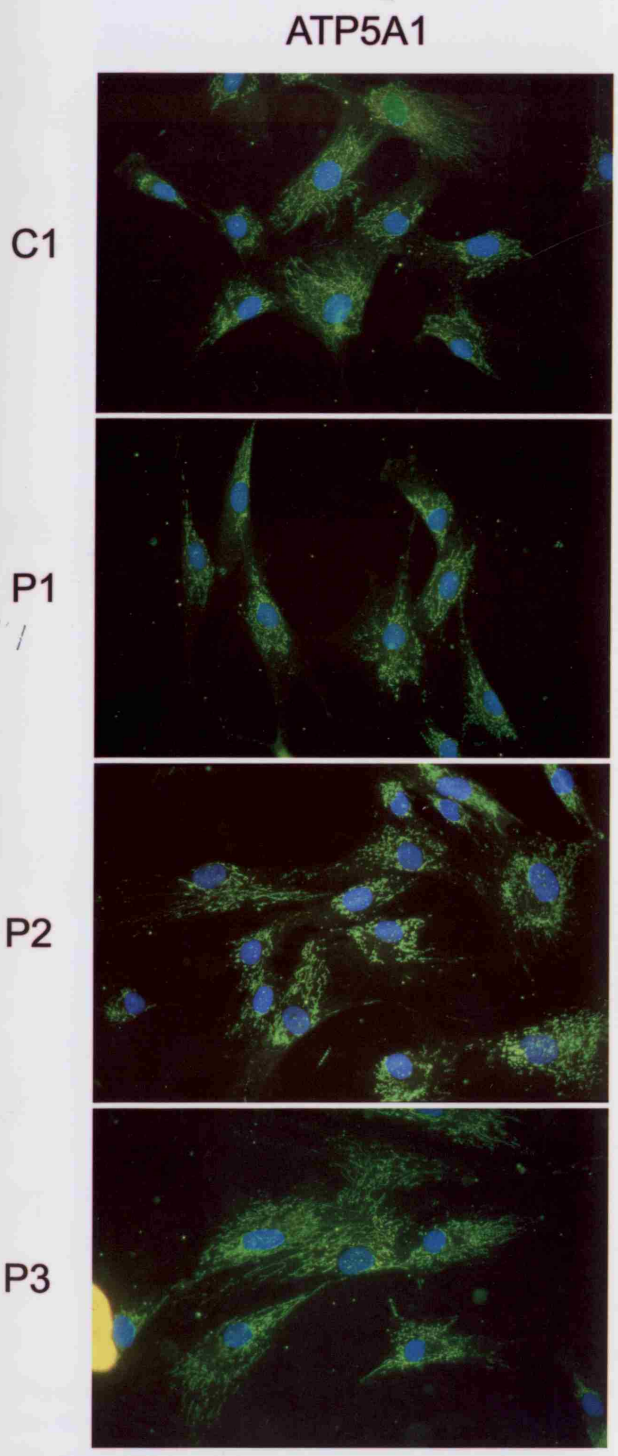

Figure 22 Immunofluorescent stains of the control C1 and fibroblasts derived from a patient with MELAS. The MELAS cells carry a 79% mutant load of the mtDNA 3243G-A, *MTTL1* mutation. Anti-MTCO1 was detected using a green fluorescent Alexa™ 488 conjugated secondary antibody. Two of the MTCO1 negative cells have been indicated in the MELAS culture with red arrows. Nuclei were counter stained blue using DAPI. Magnification x220.

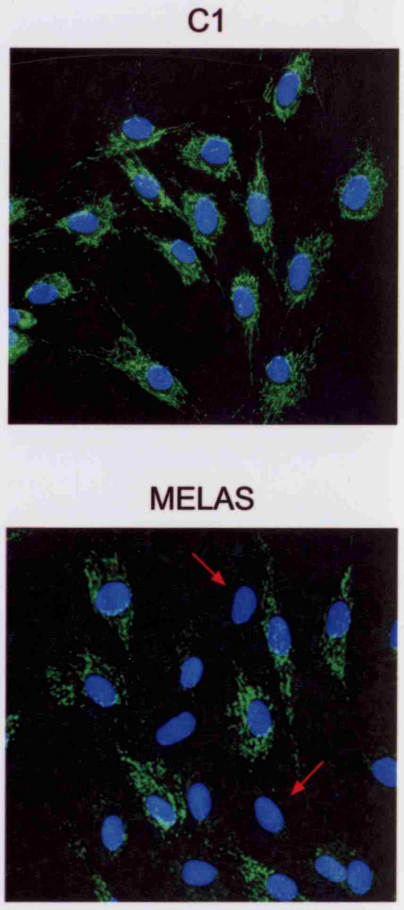

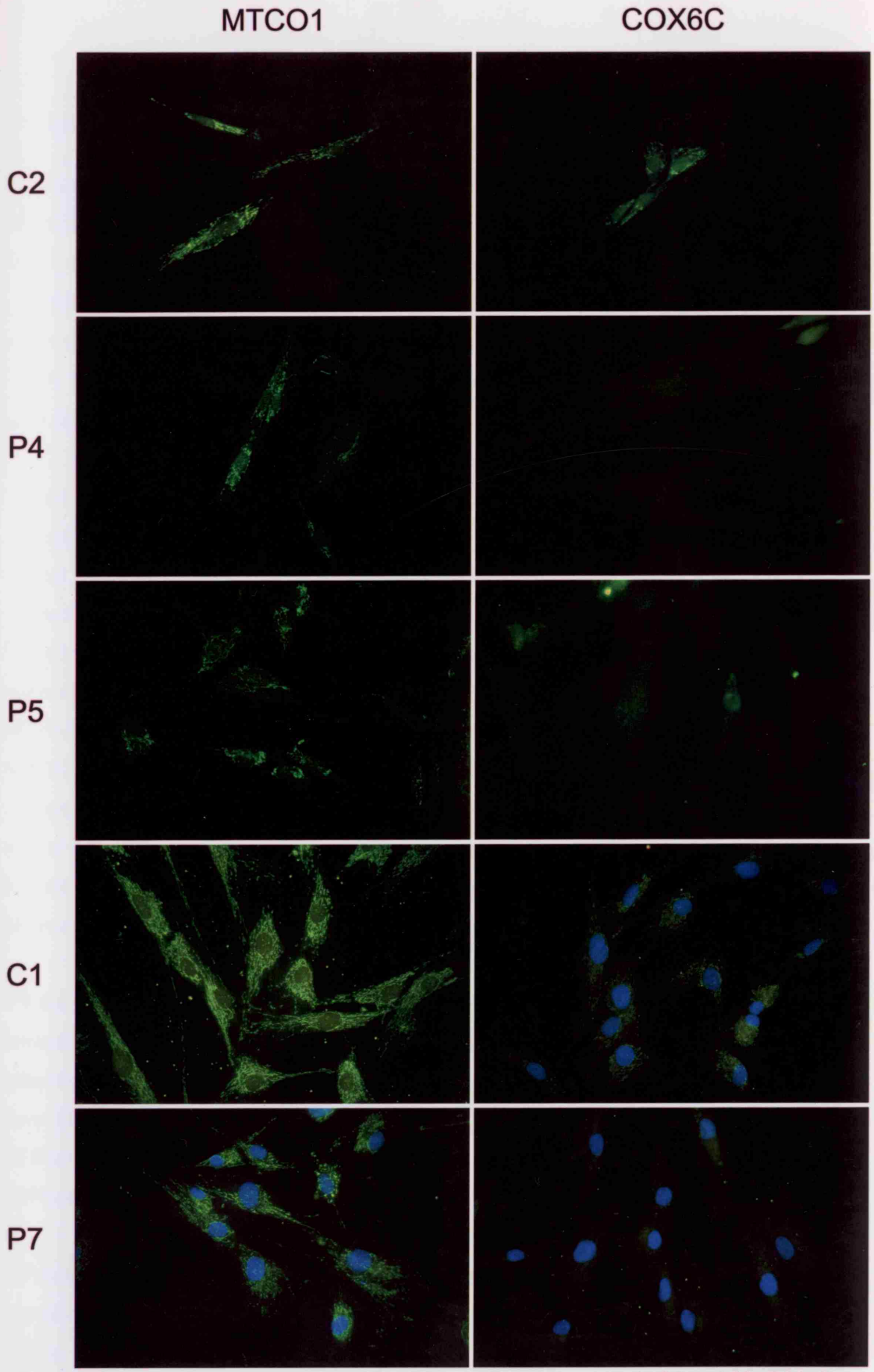

Figure 23 Immunofluorescent stains of P4, P5 and P7 and the controls C1 and C2. C2 is the control for the P4 and P5 stains, C1 is the control for the P7 stain. Primary antibodies were detected using a green fluorescent FITC-conjugated secondary antibody for C2, P4 and P5. Green fluorescent Alexa™ 488-conjugated secondary antibody for C1 and P7. Where coloured, nuclei were counter stained blue using DAPI. Magnification x220.

10.3.2 Immuno-fluorescent staining of OXPHOS subunits

Immuno-fluorescent staining was used to examine OXPHOS subunits *in situ*. Control fibroblast cultures and all patient fibroblast cultures were immuno-stained with monoclonal antibodies against COX subunits MTCO1, COX4I1 and COX6C, SDHA from complex II and ATP5A1 from complex V. Results of immuno-fluorescent staining of P1-P7 are summarised table 16 and representative images are given in figures 21 and 22. Each stain was repeated at least once with consistent results and all cultures used were of a similar passage number when stained.

Control cultures showed a finely branched cytoplasmic network consistent with a mitochondrial staining for all primary antibodies used. P1, P4, P5 and P7 all gave similar signal patterns (figures 21 & 23). Stains for MTCO1 and COX4I1 were the same as controls for each. In contrast, the anti-COX6C primary antibody gave a significantly lower signal in these cultures than controls and it was not possible to distinguish a mitochondrial network in these cells using this antibody. Antibodies to SDHA and ATP5A1 gave normal signals in agreement with western blotting data. The normal MTCO1 and COX4I1 intensities seen in P1, P4, P5 and P7 using immunohistochemistry reflects the greater sensitivity of western blotting to detection of subtle differences in signal strength. (As P1, P4, P5 and P7 all had the same staining patterns, images of the full set of antibodies are only shown for P1 in figure 21. Examples of the normal MTCO1 stain and the very low signal COX6B stain are given for P4, P5 and P7 in figure 23.

P3 stained very poorly with antibodies to MTCO1 and COX4I1 (figure 21). The staining intensity was lower than in controls and only a very poorly defined, punctuate mitochondrial network was could be seen. The antibody to COX6C again resulted in a very diffuse stain with no visible mitochondrial network. Antibodies to both SDHA and ATP5A1 gave good signals which matched those of controls and in particular the ATP5A1 antibody detected a clearly defined mitochondrial network.

P6 stained with a similar signal pattern to P1, P4, P5 and P7. MTCO1 and COX4I1 signals were equivalent to controls. The COX6C signal was however much less intense than in control cells, although in contrast to cells from P1, P3, P4, P5 and P7, a mitochondrial network could be deciphered (figure 21).

The staining intensity for all antibodies was the same as controls for cells from P2 (figure 21). The morphology of stains from this culture appeared slightly different from controls in that all antibodies resulted in a more punctuate staining pattern than was seen in control cells, although this was hard to quantify.

Cells from a MELAS fibroblast culture stained with a mosaic morphology, some having normal for MTCO1 signal and others being negative (figure 22). This mirrors the COX activity histochemistry which also showed a mosaic pattern (figure 10). A mosaic staining pattern was not found in any of the patient cultures.

Table 16 Summary of immunofluorescent stains using monoclonal antibodies against OXPHOS subunits. Results are expressed relative to appropriate control cultures.

OXPHOS complex	Subunit	P1, P4, P5, P7	P3	P6	P2
COX	MTCO1	++	+	++	++
	COX4I1	++	+	++	++
	COX6C	-	-	+	++
complex II	SDHA	++	++	++	++
complex V	ATP5A1	++	++	nd	++

Key: ++, staining similar to control cultures; + intermediate stain; -, no detectable mitochondrial network; nd, not done.

10.4 GROWTH ASSAYS

The results of the previous experiments in this section confirm that the patient fibroblast cultures express COX defects in culture and that there are differences in their molecular pathology. To demonstrate that the molecular pathology observed effected cellular fitness, growth was examined under conditions that created a reliance on the OXPHOS as the major source of ATP. When challenged with such media, cultures with low OXPHOS function generally show reduced growth that correlates with the severity of the OXPHOS defects present[689,690]. A colorimetric 96-well plate assay was used to assay cell numbers and results have been corrected to the day 1 value.

10.4.1 Growth in DMEM media

To optimise the growth of cells with mitochondrial dysfunction, all cultures in this study were routinely grown in high glucose DMEM supplemented with pyruvate and uridine at 37°C and 8% CO_2 (9.1.2). This medium was used as a base for experiments looking at the effect of replacing glucose with galactose and the restriction of pyruvate and uridine. Switching from glucose to galactose in standard DMEM led to a shift in the spread of

patient growth curves relative to those of controls (figures 24A & 24B). While all cultures expanded more slowly in galactose medium, the difference in the growth rates of control versus patient cultures was more pronounced in this medium compared to glucose medium. Disease control fibroblasts from a patient with MELAS (MELAS) and P3 were very severely affected by the change in sugars. By 150 hours, absorbencies for both of these cultures had declined to well below the 0 hour signal, indicating that the cultures were declining. P2 also showed very poor growth in galactose-based medium, with the absorbance dropping below the 0 hour signal over the course of the experiment. P1, P4 and P5 all showed increases in signal in galactose-based medium up to the 150 hour point indicating that these cultures were expanding, although this was far less than was seen in the glucose containing medium.

ρ^0 cells are unable to grow in medium without pyruvate or uridine[97]. Although ρ^0 cells constitute an extreme model of mitochondrial dysfunction, the effect of removal of these supplements was also examined in the patient fibroblast cultures. The removal of pyruvate and uridine from the standard DMEM medium had no effect on the growth of patient fibroblast cultures relative to control cultures. The results in figure 25 show that up to the 200 hour point, all cultures grew less well in the restricted medium, although there is no clear demarcation between the proliferation of patient and control cultures. Beyond the 200 hour point results were deemed unreliable as the signals plateaued presumably due to high cell densities. None of the cultures declined during this extended growth period.

10.4.2 Growth in RPMI-based media

The two separate experiments described above were replicated simultaneously in RPMI under the same culture conditions. RPMI contains lower levels of nutrients than DMEM. A direct comparison of the growth of cells in DMEM versus RPMI was not carried out. As in the DMEM experiments, patient and control cell cultures had overlapping signals for growth in glucose containing medium (figures 26A & 26C) and when galactose is used there was a clear demarcation between the growth of the control cultures and the patient cultures (figures 26B & 26D). There was a greater relative reduction in the growth of the control cultures when switching from glucose to galactose in RPMI than in DMEM. In the glucose containing RPMI, as with the glucose containing DMEM, there was no effect of restriction of these nutrients. This was also seen in the reciprocal experiment using RPMI with galactose.

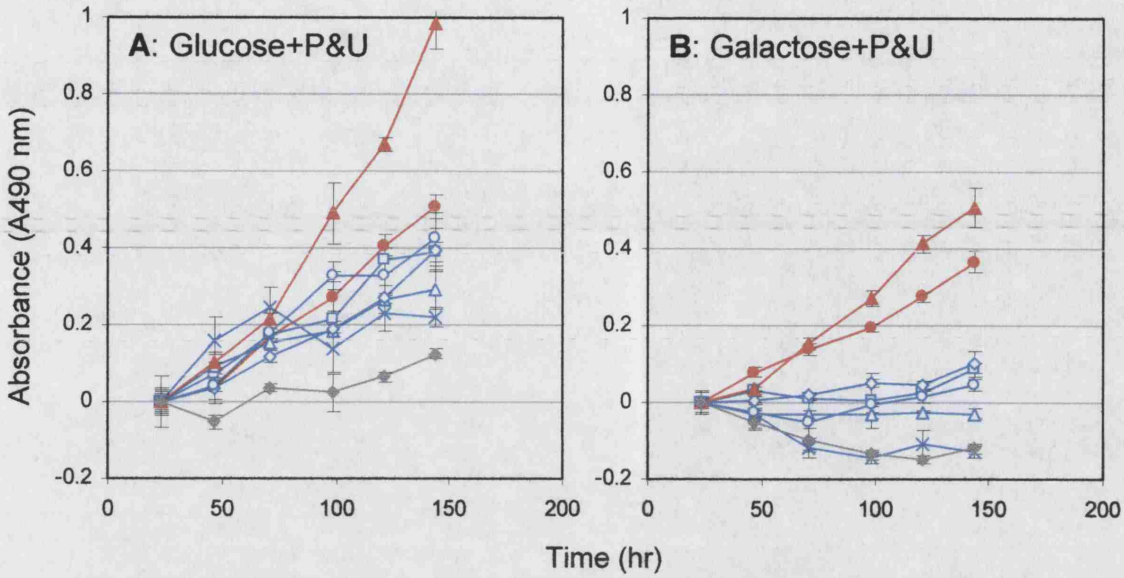

Figure 24 A comparison of growth patient and control fibroblasts in DMEM with glucose or galactose supplemented with 1 mM pyruvate and 0.2mM uridine (P&U). Patient cultures are shown in blue, control cultures in red. A) Glucose 25mM; B) Galactose 25mM. Each point represents mean of three values, error bars show standard error (P1, □; P2, △; P3, ×; P4, ◇; P5, ○; C1, ●; C2, ▲; MELAS, ◆).

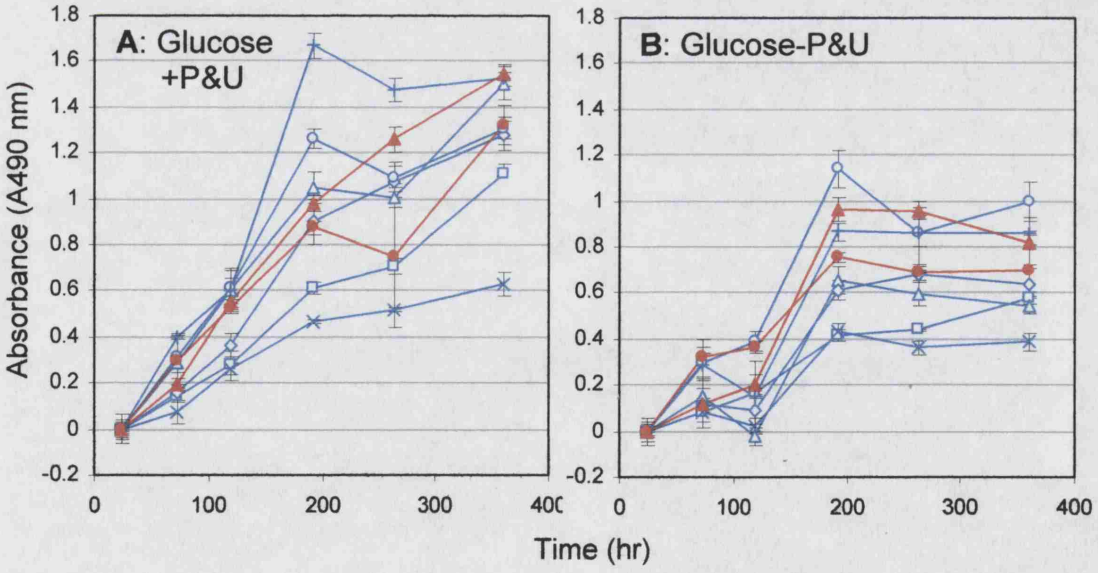

Figure 25 Growth of patient fibroblasts in DMEM with glucose and with or without 1 mM pyruvate and 0.2 mM uridine (±P&U). Patient cultures are shown in blue, control cultures in red. A) 25mM Glucose with pyruvate and uridine. B) 25mM Glucose without pyruvate and uridine. Each point represents mean of three values, error bars show standard error (P1, □; P2, △; P3, ×; P4, ◇; P5, ○; P6, +; C1, ●; C2, ▲).

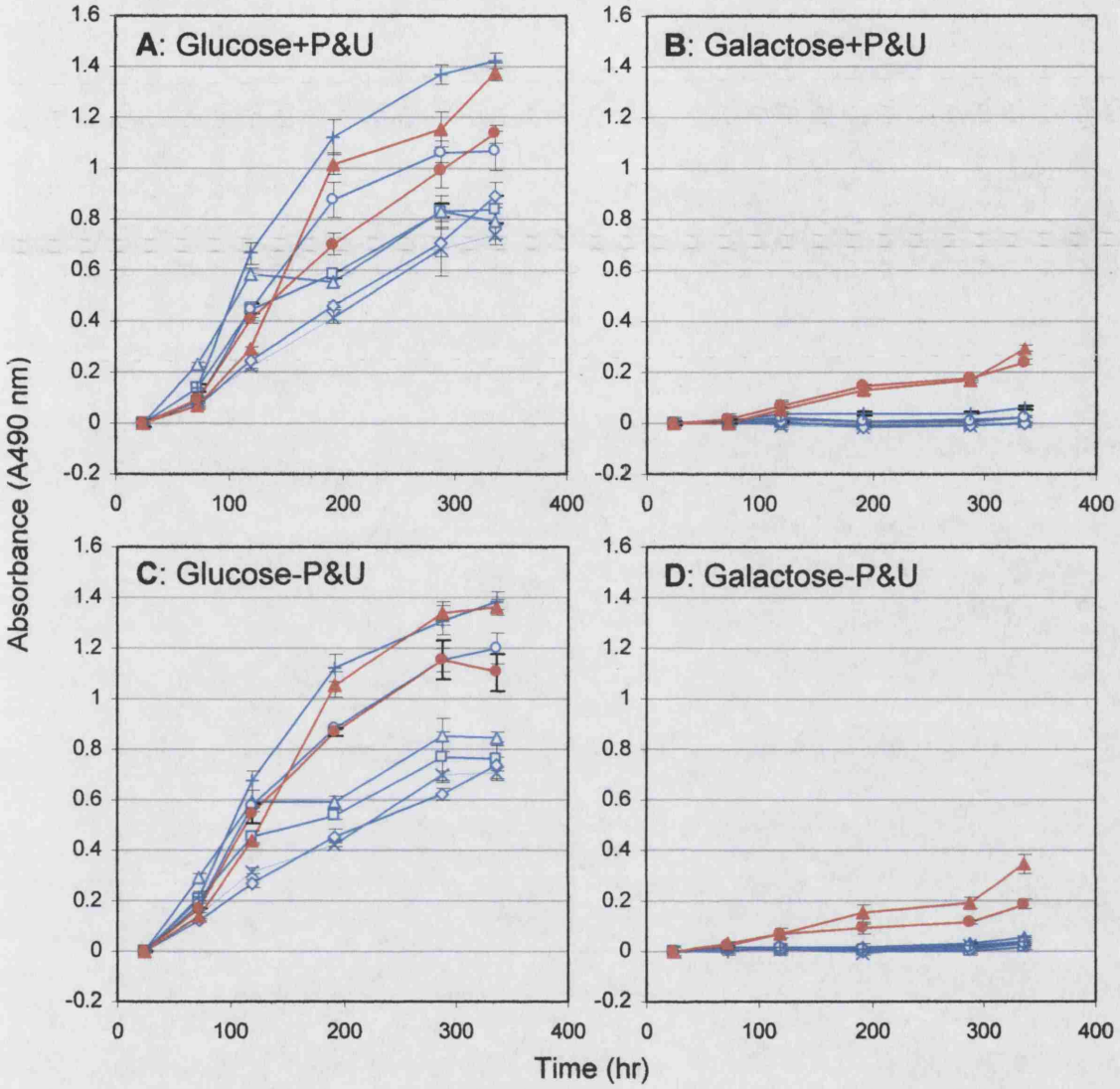

Figure 26 A comparison of the growth of patient and control fibroblast cultures in RPMI with glucose or galactose and with or without 1 mM pyruvate and 0.2 mM uridine (±P&U). Patient cultures are shown in blue, control cultures in red. A) 25mM Glucose with pyruvate and uridine. B) 25mM Galactose with pyruvate and uridine. C) 25mM Glucose without pyruvate and uridine. D) 25mM Galactose without pyruvate and uridine. Each point represents mean of three values, error bars show standard error (P1, □; P2,△; P3, ×; P4, ◇; P5, ○; P6, +; C1, ●; C2, ▲).

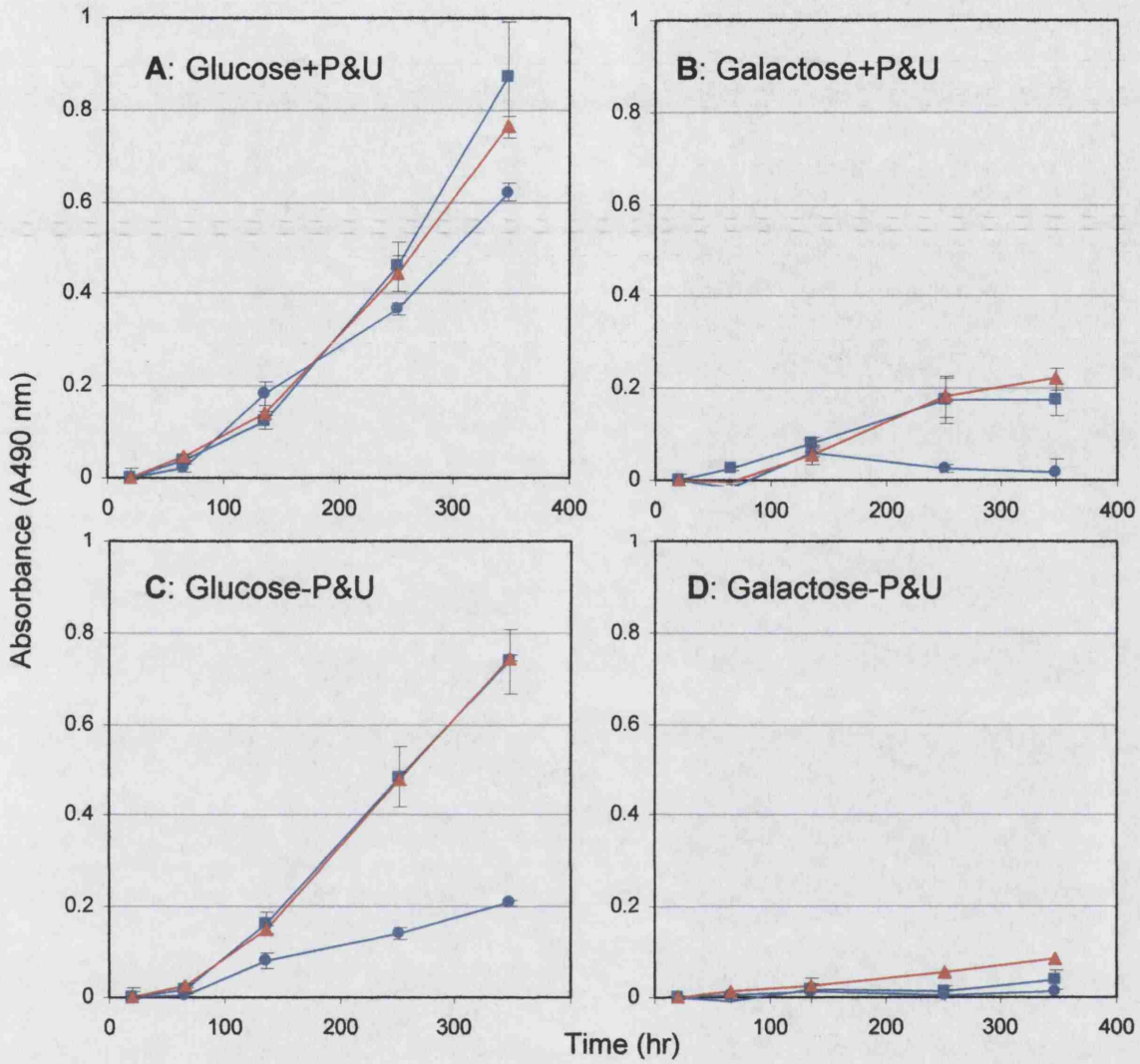

Figure 27 A comparison of the growth of patient and control tsT-fibroblast cultures at 33°C in DMEM with glucose or galactose and with or without 1 mM pyruvate and 0.2 mM uridine (±P&U). Patient cultures are shown in blue, control cultures in red. A) 25mM glucose with pyruvate and uridine. B) 25mM galactose with pyruvate and uridine. C) 25mM glucose without pyruvate and uridine. D) 25mM galactose without pyruvate and uridine. Each point represents mean of three values, error bars show standard error (P3tst, ●; P6tst, ■; C1tst, ▲).

10.4.3 Growth of tsT-fibroblast cultures

It was anticipated that the tsT-fibroblasts could be used in retroviral cDNA complementation experiments. For this to be effective, rescued cells would need to be selected under conditions that reduce the proliferation of non-rescued cells. It was hypothesised that conditions which slowed the growth of patient cells relative to that of control cells would be suitable for this type selection. Growth assays of these cells were carried out at 33°C and 5% CO_2. As with all the previous sets of experiments, all the tsT-fibroblast cultures grew better in glucose-based-medium than galactose-based-medium (figure 27A-D). The growth of the cultures in galactose medium was very poor due to the low seeding density of the experiment and as such it is not possible to determine whether the removal of pyruvate and uridine supplements from this medium had any differential effect on the growth of the patient cultures relative to the control.

Removing pyruvate and uridine supplements from the glucose medium had a drastic effect on the growth of P3tsT as seen in figure 27C. While the signal from C1tsT and P6tsT cultures was only marginally lower than in the full medium, P3tsT only achieved about 30% of the growth it had in full medium. This is interesting as there was no evidence from the results shown in figures 25 or 26 of P3 being uniquely affected when pyruvate and uridine are restricted. Non-transduced cells were not included in the experiment and so the role of the altered culture conditions on the pathology of P3 and P6 cannot be ruled out.

11 GENETIC INVESTIGATION OF PATIENT CELL CULTURES

11.1 EXAMINATION OF MTDNA

To determine whether the COX defects in the patient cell cultures were caused by mtDNA lesions number of complementary approaches were employed. Sequencing was used to screen the mitochondrial COX genes *MTCO1*, *MTCO2* and *MTCO3* in P1-P5 and P7. In addition, as a large proportion of mtDNA mutations associated with disease occur in tRNA genes, the full set of 22 mitochondrial tRNA genes were sequenced in P1-5. Large scale alterations in the integrity or abundance of mtDNA were screened for using Southern blotting and the steady-state levels of *MTCO1* and *MTCO2* mRNA were checked in P1-5 using northern blotting. Concurrent with these direct molecular

techniques, whole cell fusions between A549 ρ^0 cells and P1-6 were used to determine whether the COX defects could be transferred along with the patient mtDNA.

Table 17 mtDNA sequence polymorphisms identified in P1-5 and P7.

		Fibroblast culture						
Polymorphism	Gene	P1	P2	P3	P4	P5	P7	Comment
462 C-T	D-loop				+		ns	non-path
489 T-C	D-loop				+		ns	non-path
497 C-T	D-loop					+	ns	non-path
513 G-A	D-loop		+				ns	non-path
1438 A-G	*MTRNR1*	+	+	+	+	+	ns	non-path
1719 G-A	*MTRNR2*			+			ns	non-path
1811 A-G	*MTRNR2*		ns			+	ns	non-path
1888 G-A	*MTRNR2*		ns	+			ns	non-path
5894 A-G	*INT*		+					novel
6221 T-C	*MTCO1*	+						synonymous
6293 T-C	*MTCO1*						+	novel, synonymous
6776 T-C	*MTCO1*	+						synonymous
6852 G-A	*MTCO1*		+					novel, G317S
6908 T-C	*MTCO1*		+					novel, synonymous
7028 C-T	*MTCO1*		+	+	+	+	+	synonymous
7891 C-T	*MTCO2*				+			novel, synonymous
9477 G-A	*MTCO3*						+	V91I
9698 T-C	*MTCO3*					+		synonymous
10006 A-G	*MTTG*		+					non-path
10398 A-G	*MTND3*			+	ns	ns	ns	T114A
10463 T-C	*MTTR*			+			ns	non-path
10550 A-G	*MTND4L*					+	ns	synonymous
12133 C-T	*MTND4*		+				ns	novel, synonymous
12285 T-C	*MTTL2*		+				ns	non-path
12308 A-G	*MTTL2*					+	ns	non-path
12372 G-A	*MTND5*					+	ns	synonymous
14766 T-C	*MTCYB*	+					ns	I7T
14798 T-C	*MTCYB*				+	+	ns	F18L
15924 A-G	*MTTT*[a]					+	ns	non-path
15928 G-A	*MTTT*[a]			+			ns	non-path
15936 A-T	*MTTT*[a]				+		ns	novel
haplogroup		H3	?	T	J1	K1a	U5a	

Key: *INT* = intergenic region between *MTTY* and *MTCO1*; + = polymorphism present, blank cell = polymorphism absent; ns =not sequenced; non-path = confirmed as non-pathological according to Mitomap. Base changes not listed on Mitomap or in Herrnstadt *et al*[647] are listed as "novel". Amino acid changes are given in single letter code. Details from flanking regions of the genes of interest are shaded. Putative haplogroups are given for each sample at the bottom of the table.

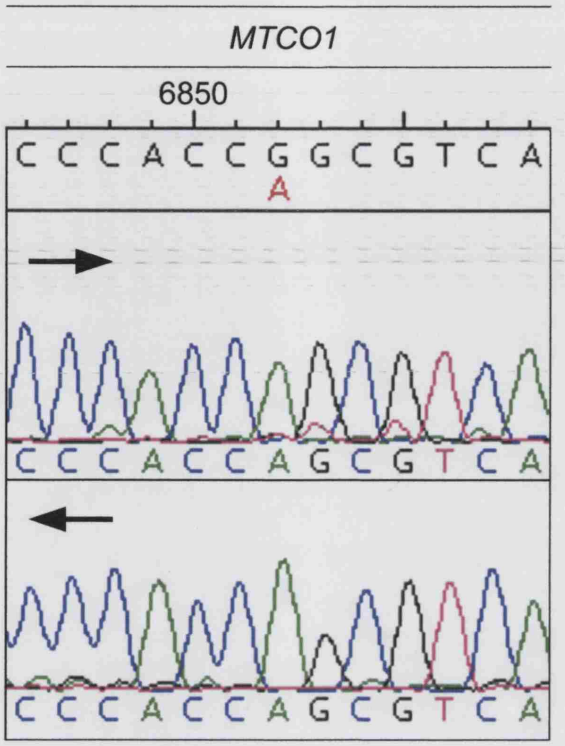

Figure 28 Electropherograms of the 6852G-A base change in *MTCO1* of P2. Arrows indicate the direction of sequencing. The revised Cambridge reference sequence is shown across the top with the conflict shown in red.

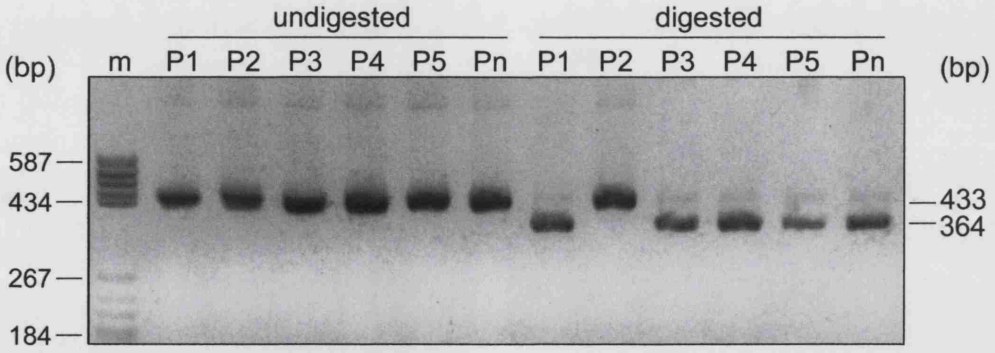

Figure 29 RFLP of 6852G-A in P1-P5. "m", indicates molecular weight markers, fragment lengths are shown on the left of the figure (bp). Patient samples are listed above respective lanes, Pn is not discussed in this thesis. Lengths of digest fragments are given on the right-hand side of the figure in bp. The image is an inverted scan of an ethidium bromide stained gel.

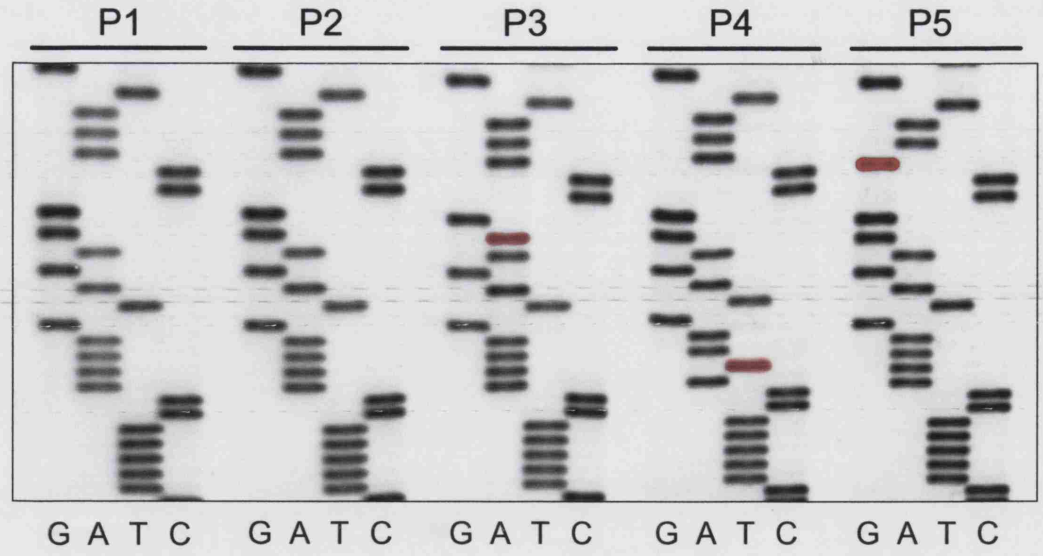

Figure 30 An image from a manual sequencing gel of P1-P5 spanning a region of *MTTT* from 15920 at the top to 15946 at the bottom. Polymorphisms are indicated in red, bases are listed at the bottom of each lane.

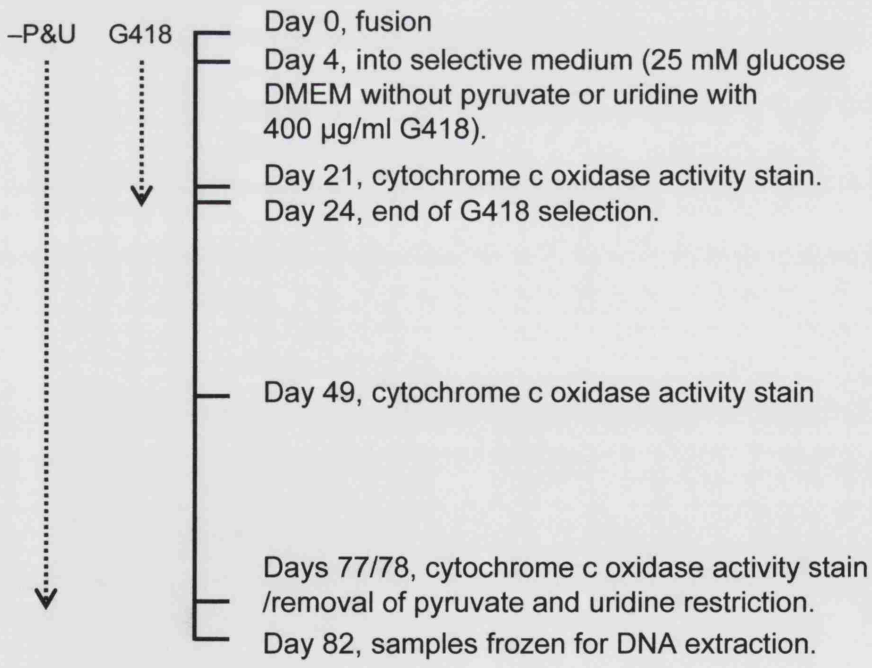

Figure 31 A timeline for the selection of synkaryons from the whole cell fusion of A549 ρ^0 cells with patient primary fibroblasts. Cytochrome c oxidase activity stains from day 21 are shown in figure 32 and those from day 77 in figure 33. "–P&U"=extent of pyruvate and uridine restriction, "G418"=extent of G418 selection.

11.1.1 mtDNA sequencing

Mitomap* was used as a searchable reference to verify the mtDNA sequencing results and to determine whether base changes have been previously described. Secondary to this, putative novel polymorphisms were manually checked against novel polymorphisms identified by Herrnstadt and colleagues[647] and also Finnilä and colleagues[691]. A summary of the base changes found in the mitochondrial COX genes, tRNA genes and flanking regions is given in table 17.

11.1.1.1 COX genes, MTCO1, MTCO2 and MTCO3

For all genes studied, sequences were compared to the NC_001807 sequence from the NCBI. This is a revised version of the original Cambridge reference sequence[145,692]. Importantly in terms of this work, the revised *MTCO1* sequence contains the correction 9559G-C which resulting in R118P. All the samples included in this study diverged from the original Cambridge sequence at this position. Known synonymous polymorphisms were found in the COX genes of every sample (table 17). Of particular prevalence was 7028T-C which was found in all but one of the samples. Three synonymous polymorphisms were found which have not previously been published, 6293T-C, 6908T-C, and 7891G-A. All were assumed to be homoplasmic according the electropherogram traces. P2 carried a novel homoplasmic polymorphism in the non-coding region between *MTTY* and *MTCO1*, 5894A-G. No function has been ascribed to this short region.

Two base changes were identified which lead to alterations in protein sequences. P7 carried 9477G-A, which is a known polymorphism in *MTCO3* resulting in the V91I primary sequence variant. A novel polymorphism was identified in *MTCO1* of P2, 6852G-A leading to G317S. An image from the electropherogram showing this base change in P2 is shown in figure 28. The presence of the 6852G-A base change was verified using RFLP demonstrating that the polymorphism was homoplasmic in P2 and that it was not present in any of the other samples (figure 29).

11.1.1.2 Sequencing of the 22 mitochondrial tRNA genes

Polymorphisms were found in mitochondrial tRNA genes of samples P2-5 but not in P1. None of the polymorphisms found in the tRNA genes of any sample have been linked

* http://www.mitomap.org/

with mitochondrial pathology according to Mitomap (table 17). Three known polymorphisms were found in *MTTT*, an image of the manual sequencing gel of this region is shown in figure 30.

11.1.1.3 mtDNA Haplotyping

Reduced-median-network analysis has been employed to refine the distinctions of the mitochondrial haplogroups[647]. Even with the relatively small amount of sequence data generated from COX and tRNA gene sequencing, it was possible to haplotype five of the six samples using these phylogenic networks. Samples have been compared to this in the first instance and to a network of European mitochondrial haplogroups devised by Finnilä and collegues[691] in the second.

Using polymorphisms identified in the COX genes, tRNA genes and flanking regions of both, the only sample that could not be haplotyped was P2 (table 17). The sample is of Asian origin but within the regions sequenced it carried none of the polymorphisms specific for any of the six Asian haplogroups currently defined (A, B, C, D, E, M). Polymorphisms that were identified in this sample were either uninformative and associated with many haplogroups (1438A-G, 7028C-T) or, although previously described, were too rare to feature in the Herrnstadt or Finnilä phylogenic networks (10006A-G, 12285T-C). The high number of novel polymorphisms identified in P2 tends to suggest that the sample belongs a relatively rare haplogroup. Detailed information on the ethnic origin of the sample was not available. The five samples that could be haplotyped were all of European origin and could all be assigned to haplogroups within the four major European haplogroup clusters, HV, UK, TJ and WIX[647,691]. Homoplasic polymorphisms were found in samples P1 and P3 but this is not unusual given the high variation in human mtDNA sequences. In both cases well defined haplogroup-specific polymorphisms were also present which permitted putative assignment of the samples to large haplogroups.

P1 can be assigned to haplogroup H3. Loss of 7028C-T only occurs in haplogroup H and P1 carries 6776T-C which is specific for haplogroup H3. A homoplasic polymorphism, 6221T-C, was found in P1 which was not present in 266 haplogroup H sequences identified by Herrnstadt[647] or 31 classified by Finnilä[691]. While this may seem to question the haplotyping of P1, homoplasic polymorphisms are very common in mtDNA[647] and simply reflect the high rate of variation between human mtDNAs of 1.7×10^{-3} substitutions per site for non-African sequences[693].

P3 can probably be assigned to haplogroup T as it carries the T-specific polymorphisms 10463T-C and 15928G-A. Although 10398A-G was not present 46 members of haplogroup T sequenced by Herrnstadt or 11 samples assigned to haplogroup T by Finnilä, this polymorphism is present in some members of the J haplogroup and as with the 6221T-C transition in P1, this is likely to be a homoplasic mutation.

P4 can be assigned to haplogroup J1. Both the Herrnstadt and Finnilä networks associate14798T-C is with haplogroups K and J. Therefore, the lack of K-specific polymorphisms places P4 in haplogroup J. In support of this, Finnilä places 462C-T and 489T-C in haplogroup J in a phylogenic network based on the D-loop region. D-loop sequences were not included in the analysis for the Herrnstadt networks. 14798T-C is associated with the J1 clade of haplogroup J, allowing further specificity within haplogroup J.

P5 can be unambiguously assigned to haplogroup K1a. The sample carries the U and K-specific 12308A-G and 12372G-A polymorphisms in addition to the K-specific 9698T-C and 10550A-G. 10398A-G is associated with haplogroup K1 and 15924A-G allows further specificity having been associated with K1a.

Surprisingly, even though only the COX genes were sequenced in P7 the sample can be assigned to haplogroup U5a1 according to Herrnstadt and Finnilä. It carries 9477G-A which is specific to all U haplogroups except U6. The other U haplogroups (U5a, U5b, U9 and U2) can be discounted because of the lack of clade-specific polymorphisms in the regions sequenced in this sample.

11.1.2 ρ^0 cell fusions

In conjunction with the sequencing work, cell fusions were used to screen for the influence of the patient mitochondrial genomes on COX activity. Whole cell fusions were carried out between P1-P6 plus two control cultures (C1, C2), and a ρ^0 clone of the A549 lung carcinoma cell line. The fusions were designed to provide information on the ability of the patient mtDNA to support mitochondrial function against a nuclear background which was normal with respect to OXPHOS function. Cell fusion is an unpredictable process that creates mixed cultures of hybrid cells with multiple nuclei which can be either heterokaryotic or homokaryotic. Continued culturing of such cells leads to nuclear fusion in a minority of hybrids that results in the formation of synkaryons, cells with a

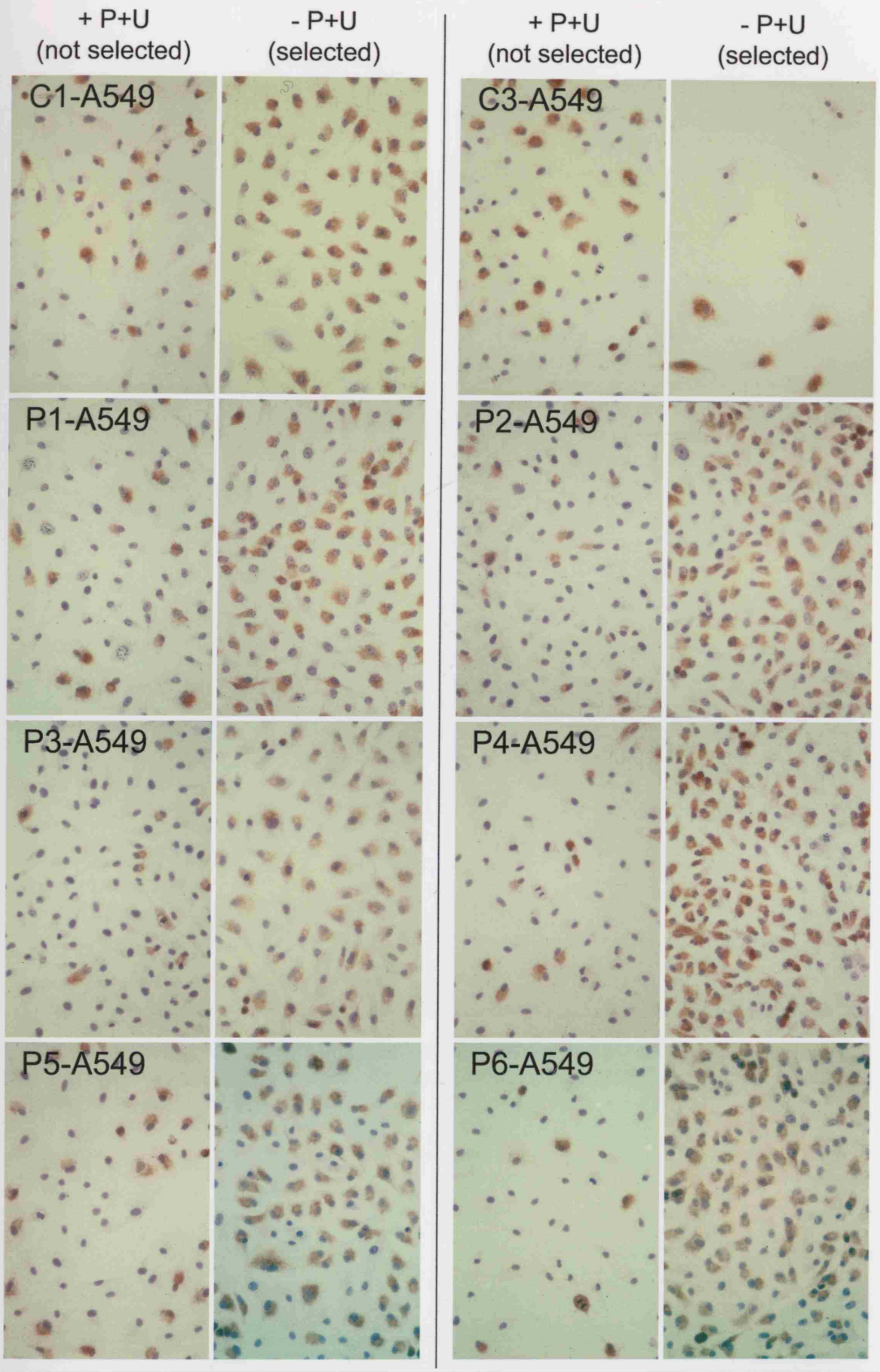

Figure 32 COX activity stains of fibroblast-A549 synkaryons on day 21 of selection. Pairs of images are shown for each culture which have either been selected by pyruvate and uridine restriction and G418 (- P+U) or expanded without pyruvate and uridine restriction but with G418 (+ P+U) as described figure 31.

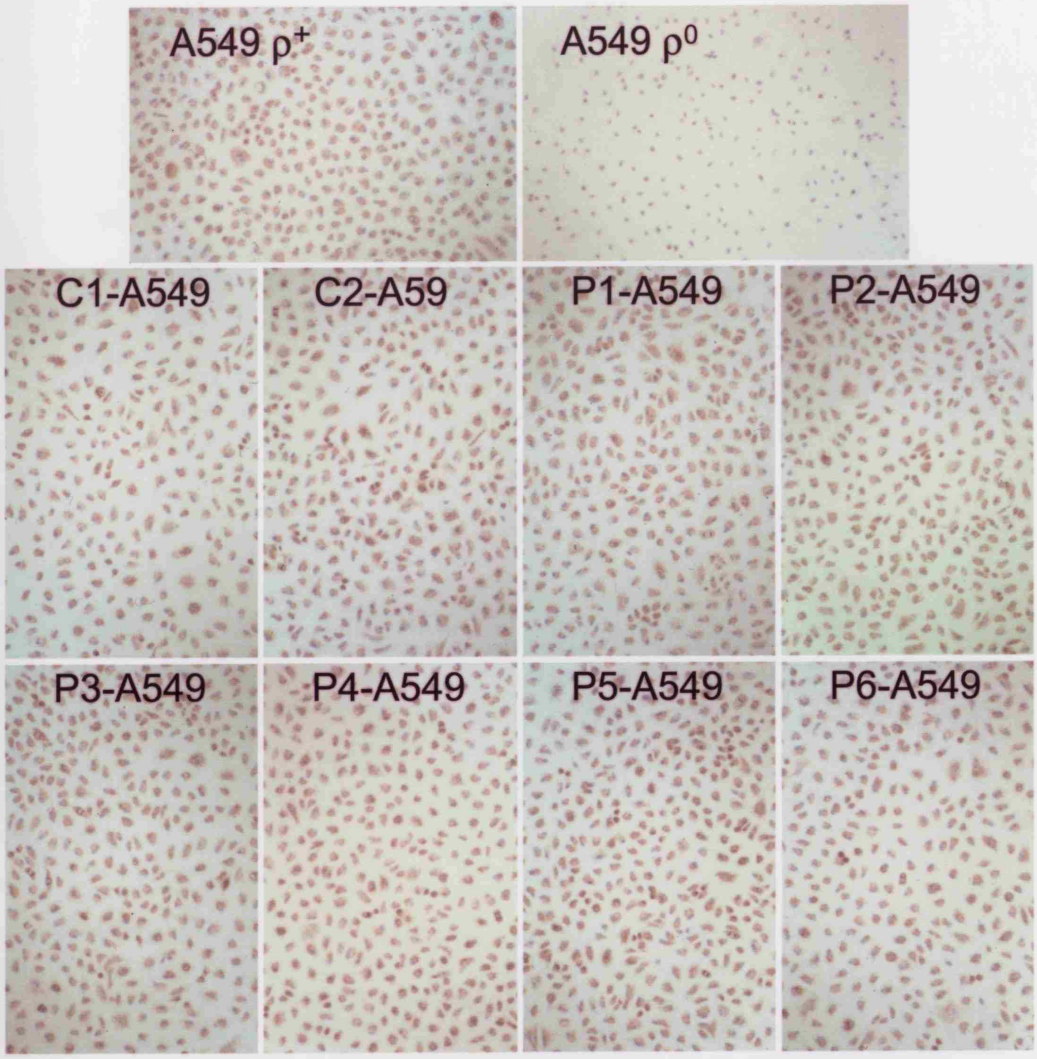

Figure 33 COX activity stains of fibroblast-A549 synkaryons at the end of selection on day 77. A positive control A549 ρ^+ culture and a negative control A549 ρ^0 culture stained in parallel are shown at the top of the figure.

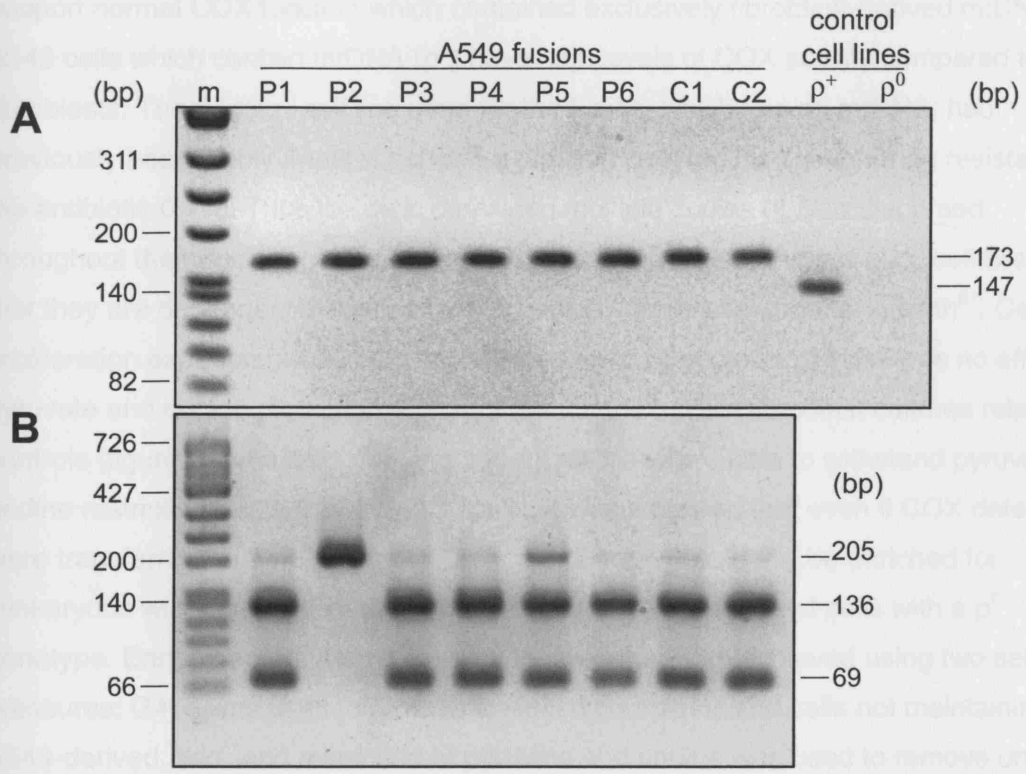

Figure 34 RFLP of P1-A549–P6-A549. Names of parental fibroblast cultures are given above each lane. "m" is molecular weight markers with fragment lengths listed on the left of each image (bp) and sizes of restriction fragments are listed on the right throughout. Images are inverted scans of ethidium bromide stained gels. **34A** Exclusion of the presence of A549 mtDNA in the synkaryons by screening for an A549-specific CA deletion. Undigested wild-type fragment is 173 bp and visible digest fragment from deleted A549 mtDNA is 147 bp. **34B** Analysis of 6852G-A. Undigested, polymorphic fragment is 205 bp and fragments resulting from cleavage of the wild-type sequence are ~136 bp and ~69 bp.

single nucleus carrying chromosomes from more than one parent cell. Selective pressure is generally required to increase the proportion of model synkaryons above that of uninformative cells, including residual un-fused parent cells.

The aim of this experiment was to produce cells with a karyotype that had the potential to support normal COX function which contained exclusively fibroblast-derived mtDNA. A549 cells which contain mtDNA (ρ^+) have high levels of COX activity compared to fibroblasts. The A549 ρ^0 cell line used for the fusion, which has no mtDNA, had previously been stably transfected with a plasmid carrying *Neo*^{r}, conferring resistance to the antibiotic G418. Thus the cells contained multiple copies of *Neo*^{r} dispersed throughout their nuclear genome. One of the defining characteristics of ρ^0 cell lines is that they are dependent on pyruvate and uridine supplementation for growth[97]. Cell proliferation experiments demonstrated that over a 14 day period there was no effect of pyruvate and uridine restriction on the growth of the patient fibroblast cultures relative to controls (figure 25). As cells carrying patient mtDNA were able to withstand pyruvate and uridine restriction better than A549 ρ^0 cells, it was assumed that even if COX defects were transferred with the patient mtDNA, the cultures would still be enriched for synkaryons with fibroblast-derived mtDNA via the selecting out of cells with a ρ^0 genotype. Enrichment for model synkaryons was therefore achieved using two selective pressures: G418 was used to remove un-fused fibroblasts and cells not maintaining A549-derived *Neo*^{r}, and restriction of pyruvate and uridine was used to remove un-fused A549 ρ^0 cells and cells not maintaining patient-derived ρ^+ mitochondria. Post-fusion cultures are referred to throughout using the strategy [specific parent cell culture]-A549, e.g. P1-A549 and P4-A549.

11.1.2.1 Selection and COX activity staining

Figure 31 shows a timeline for the selection process. G418 selection was removed on day 24 and restriction of pyruvate and uridine was maintained until day 77. Periodically throughout the experiment the cultures were stained for COX activity using a histochemical stain. This was used to determine whether residual un-fused A549 ρ^0 cells and fibroblasts had been selected out of the cultures. The COX activity stains on day 21 allowed a comparison of the cultures under full selection and those without nutrient restriction but with G418 selection (figure 32). They showed that there were still around 10-30% COX negative cells in each of the cultures under selection. In the cultures which received G418 but were not restricted for pyruvate and uridine there were far more COX negative cells. Hence, the nutrient selection was successfully reducing the number on

un-fused A549 ρ^0 cells in the cultures under full selection. Importantly, the stain also showed that similar proportions of COX negative cells were present in all cultures under each selection including controls.

Another set of COX activity stains was carried out on day 49 and less COX negative cells were found (<5%) but they were still easily identifiable in all cultures, including the two control fusions. As with the previous stains, there was no difference in the proportion of COX negative cells in each of the cultures. In order to produce good model cultures with very few contaminating ρ^0 cells, pyruvate and uridine restriction was continued. A third COX activity stain on day 77 found very low levels of COX negative cells, with less than one COX negative cell per 20x field of around 200-400 cells (figure 33). This was felt to be sufficient to remove selection and to extract DNA for analysis. The fact that all the cultures stained positive for COX activity following repopulation with patient mtDNA suggests that the patient cultures do not harbour mtDNA lesions that cause COX deficiency. Sadly a control experiment fusing cells with a known heteroplasmic mutation (such as the MELAS fibroblasts used a disease control in figures 17 & 22) with A549 ρ^0 cells could not be carried out due to insufficient abundance of cells. Had this experiment been possible it would have provided a good control for the fate of mutant mtDNA populations in this study.

11.1.2.2 RFLP of fibroblast-A549 synkaryons

The most effective test of the patient mtDNA in these cultures is to screen for polymorphisms of interest in the COX positive synkaryon cultures. An A549-specific CA deletion in a $[CA]_5$ tract from 514-523 was used to demonstrate the lack of A549 mtDNA in the synkaryon cultures[670] (figure 34A). The novel 6852G-A polymorphism in P2, was investigated using total synkaryon DNA extracted from day 82 cell pellets. Restriction digests shown in figure 34B, demonstrate that P2-A549 is homoplasmic for 6852G-A at the level of detection of this technique.

11.1.3 Southern blot analysis of mtDNA

Southern blotting enabled screening for large mtDNA deletions and reductions in the ratio of mtDNA to nuclear DNA. Samples were linearised with *Pvu* II and resolved on 0.8% agarose gels prior to blotting and hybridisation with radio-labelled, random-primed, dsDNA probes generated against the entire mtDNA and the nuclear 18S rRNA gene repeat unit. All samples were blotted and probed at least twice with consistent results. DNA samples from P1-P5 are shown in figure 35. There was no evidence of either deleted species migrating below the mtDNA signal or reductions in the cellular mtDNA content. Figure 36 shows results from the P6 and P7 cultures. Again, there was no evidence of abundant mtDNA lesions or reductions in the cellular mtDNA content.

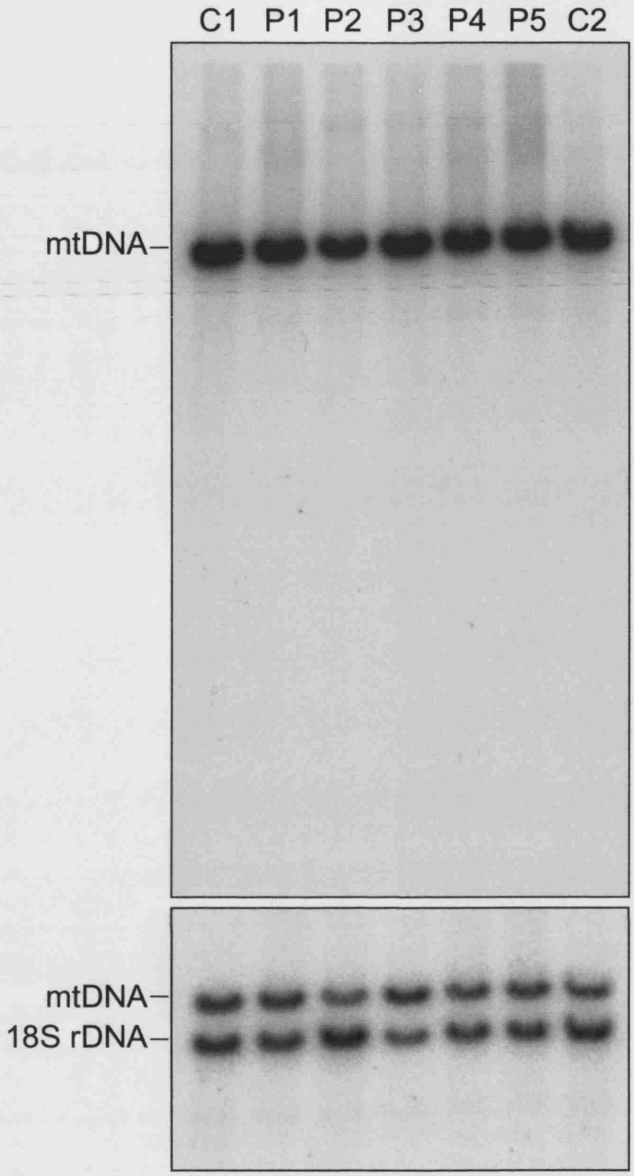

Figure 35 Storm phosphorimager pictures of Southern blots of total DNA (3 µg per lane) from P1-P5 and two controls, C1 and C2. Upper panel shows a blot probed with the mtDNA probe alone and the lower panel shows the same blot hybridised with probes to both mtDNA and the nuclear 18S rRNA gene repeat unit.

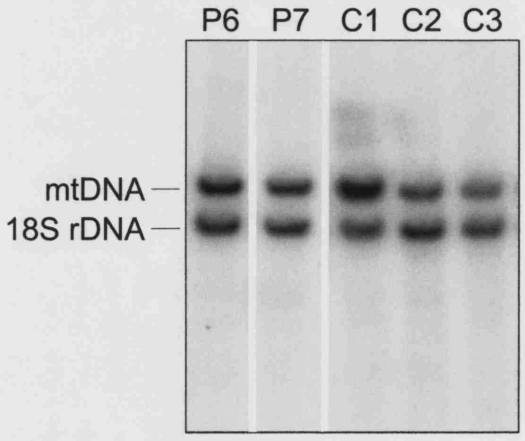

Figure 36 A composite image of a Southern blot of total DNA (3 µg per lane) from P6 and P7 and three controls C1, C2 and C3. The blot was hybridised simultaneously with probes to the mtDNA and the nuclear 18S rRNA repeat unit.

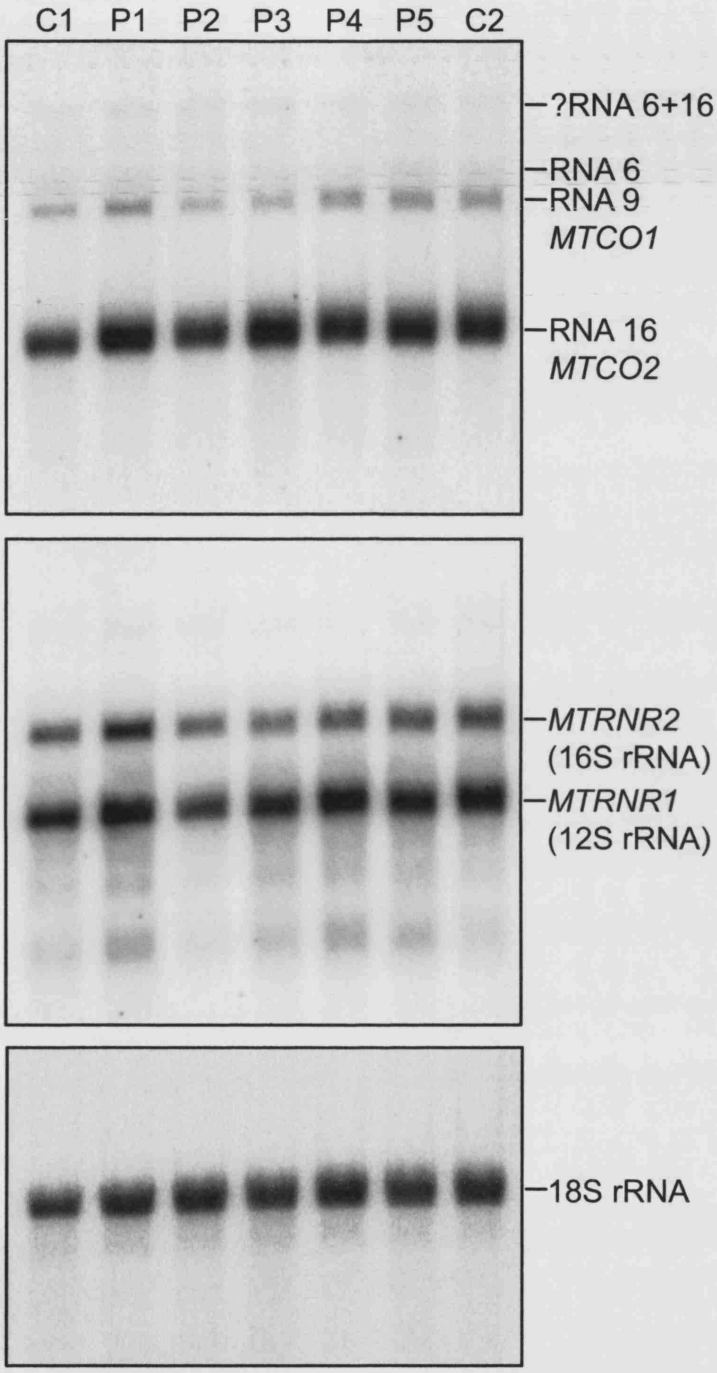

Figure 37 Storm phosphorimager pictures of northern blots of total RNA (5.8 µg per lane) from P1-P5 and two controls C1 and C2. The upper panel shows a blot hybridised with a probe encompassing RNA 6, RNA 9 and RNA 16 (figure 4). The middle panel shows the same blot hybridised with a probe spanning the mitochondrial rRNA genes. The lower panel shows the same blot hybridised with a probe for the nuclear 18S rRNA used to confirm equivalent loading of the samples. The single blot used for these images was probed over several months in the following order: upper panel 1st, lower panel 3rd and middle panel 2nd.

11.1.4 Northern blots of mitochondrial RNAs

Northern blotting was used to determine whether the COX defects in the patient cell cultures resulted from aberrant mitochondrial transcription or RNA instability. Blots were prepared from total cellular RNA from P1-P5 resolved on 1.4% agarose gels, and hybridised with probes against mitochondrial RNAs. Figure 37 shows images generated by a Storm phosphorimager of a single blot serially hybridised with a probe against *MTCO1/MTCO2* and another against *MTRNR1/MTRNR2*. The nuclear 18S rRNA was also probed and used as a marker to determine equivalent loading between samples.

The probe used to detect *MTCO1 and MTCO2* containing RNAs was generated using random primers from an *Xba* I fragment of human mtDNA[670,694] extending from 7441 to 8286. Although generated in both orientations, within the detection limits of this protocol, only L-strand transcripts were detected. The most prominent band was RNA 16 which is the *MTCO2* mRNA (figure 4). Although the probe only extends 4 base pairs into the *MTCO1* coding region (5904-7445), the *MTCO1* mRNA, RNA 9, was also detected because the H-strand orientated *MTTS1* tRNA gene is not cleaved from the 3' end of this RNA. *MTCO1*, *MTCO2* and *MTCO3* are expressed at similar levels in cultured cells[136] and the disparity between the *MTCO1* and *MTCO2* signals seen here is a reflection of the large difference in coverage of the probe over the two mRNAs. The RNA 9 precursor, RNA 6, which includes a 5' region corresponding to the H-strand orientated *MTTA*, *MTTN*, *MTTC* and *MTTY* tRNA cluster could also be seen. A larger RNA could also be detected. This is likely to be a precursor of RNA 6 plus RNA 16. Such an RNA would hybridise with the probe and have a size of ~2.7 kb which is in good agreement with the estimated size of the band visible on the blot. The same blot was subsequently hybridised with random-primed dsDNA probes generated from a PCR fragment extending from 660 to 3287 covering the *MTRNR1* and *MTRNR2* rRNA genes. Two bands were detectable, the 953 nt 12S rRNA encoded by *MTRNR1* and the 1558 nt 16S rRNA encoded by *MTRNR2* (figure 4). RNA 4, the partially processed transcript containing both rRNA genes and *MTTF* and *MTTV* was not detected. Probably due to the vast excess of mature rRNAs. Comparisons of the intensity of the signals from the *Xba* I probe and the mt-rRNA probe do not suggest any gross defects in steady-state levels of RNA 9, RNA 16 or either of the mt-rRNAs in samples P1, P3, P4 or P5 when compared to controls. There was also no evidence of truncation or mis-processing of any of the RNAs in samples from these cultures. Total RNA from P2 appeared to have slightly reduced mitochondrial RNA levels. This is clearest for the RNA 16 and 12S rRNA

signals. The nuclear 18S rRNA signal did not indicate any significantly lower loading of this sample.

11.2 EXAMINATION OF *SURF1*

During the course of this project mutations in *SURF1* were identified as a major cause of Leigh's syndrome with isolated COX deficiency[535,537]. Five of the fibroblast cultures, P1, P3, P4, P5 and P7, were obtained from patients diagnosed with Leigh's syndrome or Leigh's-like disease. Moreover, as shown in the previous section, P1, P4, P5 and P7 had an isolated reduction of steady-state COX subunit levels. It was therefore decided to sequence *SURF1* in all samples.

Table 18 Summary of *SURF1* analysis for P1-P7.

Sample	Intron 1 heptamers	Synonymous base changes	*SURF1* genotype	*SURF1* mRNA
P1	5 / 5	280T-C / 280T-C 573C-G / 573C-G	312del10insAT / 312del10insAT	-
P2	5 / 5	-	wt / wt	++
P3	5 / 4	-	wt / wt	++
P4	5 / 5	280T-C / 280T-C 573C-G / 573C-G	312del10insAT / 312del10insAT	-
P5	5 / 3	280T-C / wt 573C-G / wt	312del10insAT / 370G-A	+
P6	5 / 3	-	wt / wt	nd
P7	5 / 3	280T-C / wt 573C-G / wt	312del10insAT / 821del18	nd

Key: *SURF1* mRNA abundance: ++, similar to control levels; +, lower than controls; - , undetectable; nd, not done.

11.2.1 Screening of *SURF1* in patient samples

Five fragments were generated for sequencing spanning exons 1+2, 3+4, 5, 6+7 and 8+9 employing the primer set designed by Tirranti and colleagues[535]. Sequencing was carried out using a fluorescent dye-terminator reaction resolved on an automated ABI 310 single capillary sequencer. Sequences were compared to a genomic sequence of *SURF1* derived from the Genbank contig AC002107*. Mutations were identified P1, P4, P5 and P7 (table 18). No base changes were found in P2, P3 or P6. P1 and P4 were both homozygous for a common insertion-deletion at the 5' boundary of exon 4, 312del10insAT and two synonymous polymorphisms 280T-C and 573C-G. P5 was

* Now superseded by NT_017539.

compound heterozygous for the same insertion-deletion and polymorphisms as found in P1 and P4, and a missense transition in exon 5, 370G-A, leading to G124R. P7 was also compound heterozygous for 312del10insAT, 280T-C and 573C-G and in addition a novel 18 bp deletion in exon 8, 821del18. Electropherograms of the sequencing data spanning the mutations are shown in figures 38, 39 and 40.

Table 19 Summary of *SURF1* analysis of patient 1 and patient 7 family members.

Sample	Affected	Synonymous base changes	*SURF1* genotype
P1♀	no	280T-C / wt 573C-G / wt	312del10insAT / wt
P1♂	no	280T-C / wt 573C-G / wt	312del10insAT / wt
P1s1	yes	280T-C / 280T-C 573C-G / 573C-G	312del10insAT / 312del10insAT
P1s2[a]	no	-	312del10insAT / wt
P1s3[a]	no	-	312del10insAT / wt
P1s4[a]	no	-	wt / wt
P7♀	no	-	821del18 / wt
P7♂	no	280T-C / wt 573C-G / wt	312del10insAT / wt

Key: Sample codes as given in the text. [a] not sequenced, data from figure 45 only.

11.2.2 Screening of *SURF1* in patient family members

DNA was available from family members of patient 1 and patient 7. Sequencing confirmed that an affected sibling of patient 1, patient 1s1, was also homozygous for 312del10insAT, 280T-C and 573C-G and both parents were confirmed as carriers (figure 41). DNA was also obtained from three unaffected siblings of patient 1, patients 1s2, 1s3 and 1s4. Resolution of the exon 3+4 sequencing fragment demonstrated that 1s2 and 1s3 were carriers of 312del10insAT, 280T-C and 573C-G, and 1s4 was homozygous wild-type (figure 42). To examine the consistency of the immuno-fluorescence results from Section 1, fibroblasts from 1s1 and both parents were stained for COX6C and SDHA (figure 44). As expected P1s1 showed no signal for COX6C but normal signal for SDHA and cells from both parents stained normally for both proteins. Sequencing confirmed that the father of patient 7 carried 312del10insAT, 280T-C and 573C-G (figure 41) and the mother 821del18 (figure 43). The sequencing, immuno-staining and fragment length polymorphism data from patient 1 and patient 7 family members supports the recessive nature of the mutations identified in the probands. This data is summarised in table 19.

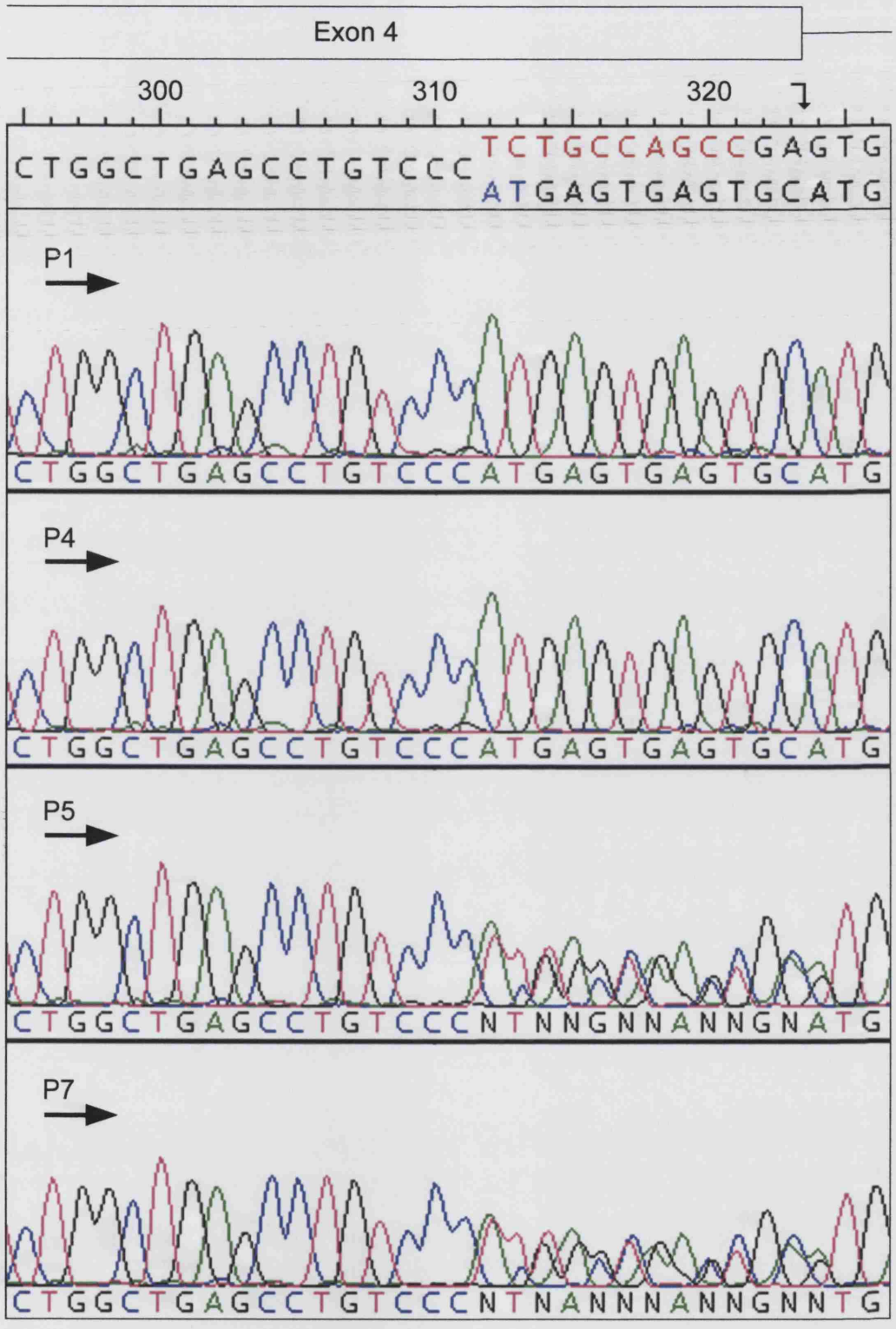

Figure 38 Electropherograms covering the 3' end of exon 4 of *SURF1* from P1, P4, P5 and P7. Arrows indicate the direction of sequencing. The *SURF1* genomic sequence is given across the top (uppermost sequences) along with a box showing the extent of exon 4. A vertical arrow indicates the intron 4 splice site. Bases deleted due to 312del10insAT are shown in red in the wild-type sequence and those inserted in blue in the divergent sequence resulting from the mutation (below).

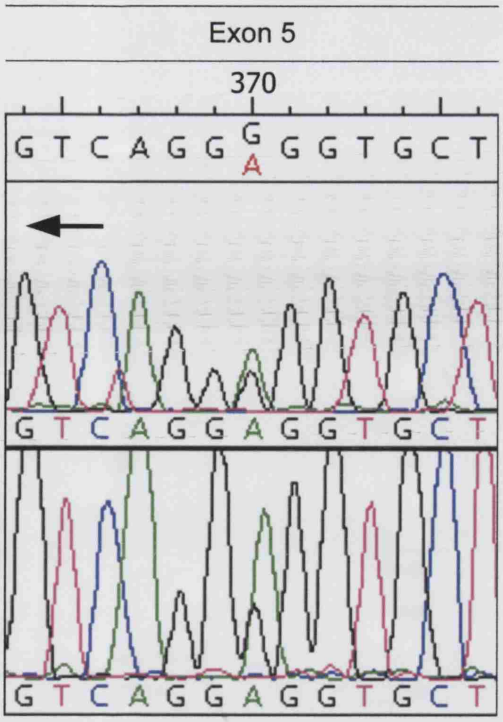

Figure 39 Electropherograms of part of exon 5 of *SURF1* from P5 including 370G-A. Wild-type sequence is given across the top with conflicts shown in red. Sequences are shown in both directions and the arrow indicates the direction of sequencing of the upper panel.

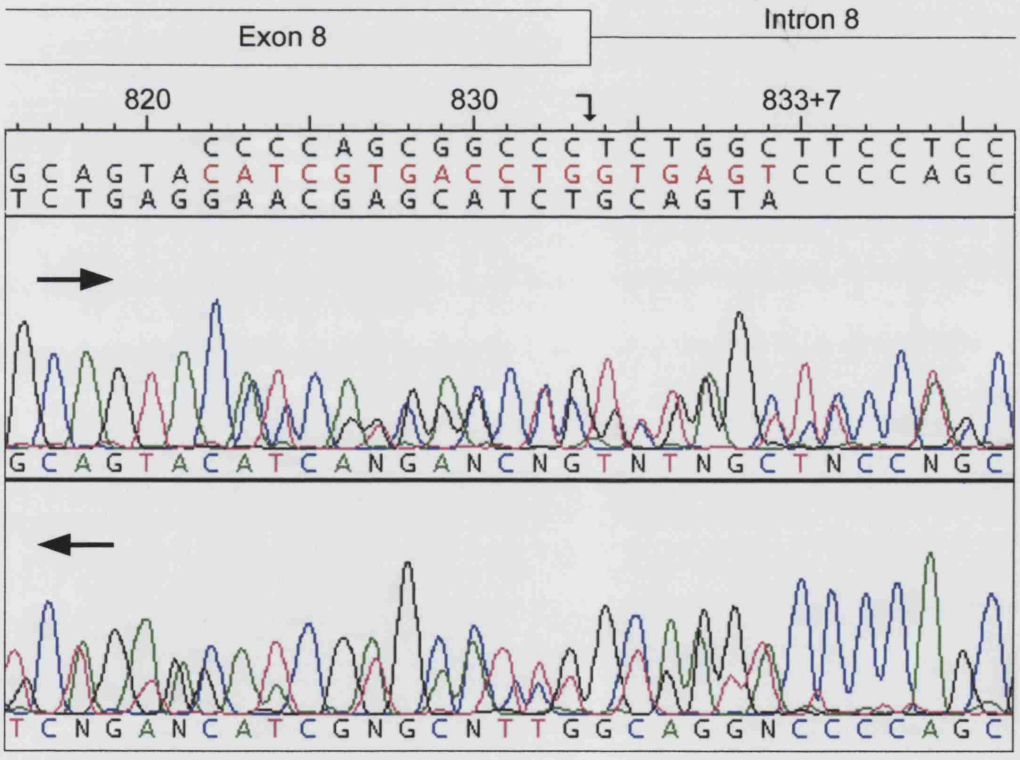

Figure 40 Electropherograms covering the 3' boundary of exon 8 of *SURF1* from P7. The middle sequence is the wild-type genomic sequence with the 821del18 deletion shown in red. The upper and lower sequences are those resulting from the deletion as read in opposing directions. The upper sequence is that read sequencing from left to right (top panel) and the lower sequence that read sequencing from right to left (bottom panel). The exon 8 boundary is indicated by the box at the top and the intron 8 spice site is marked with a vertical arrow.

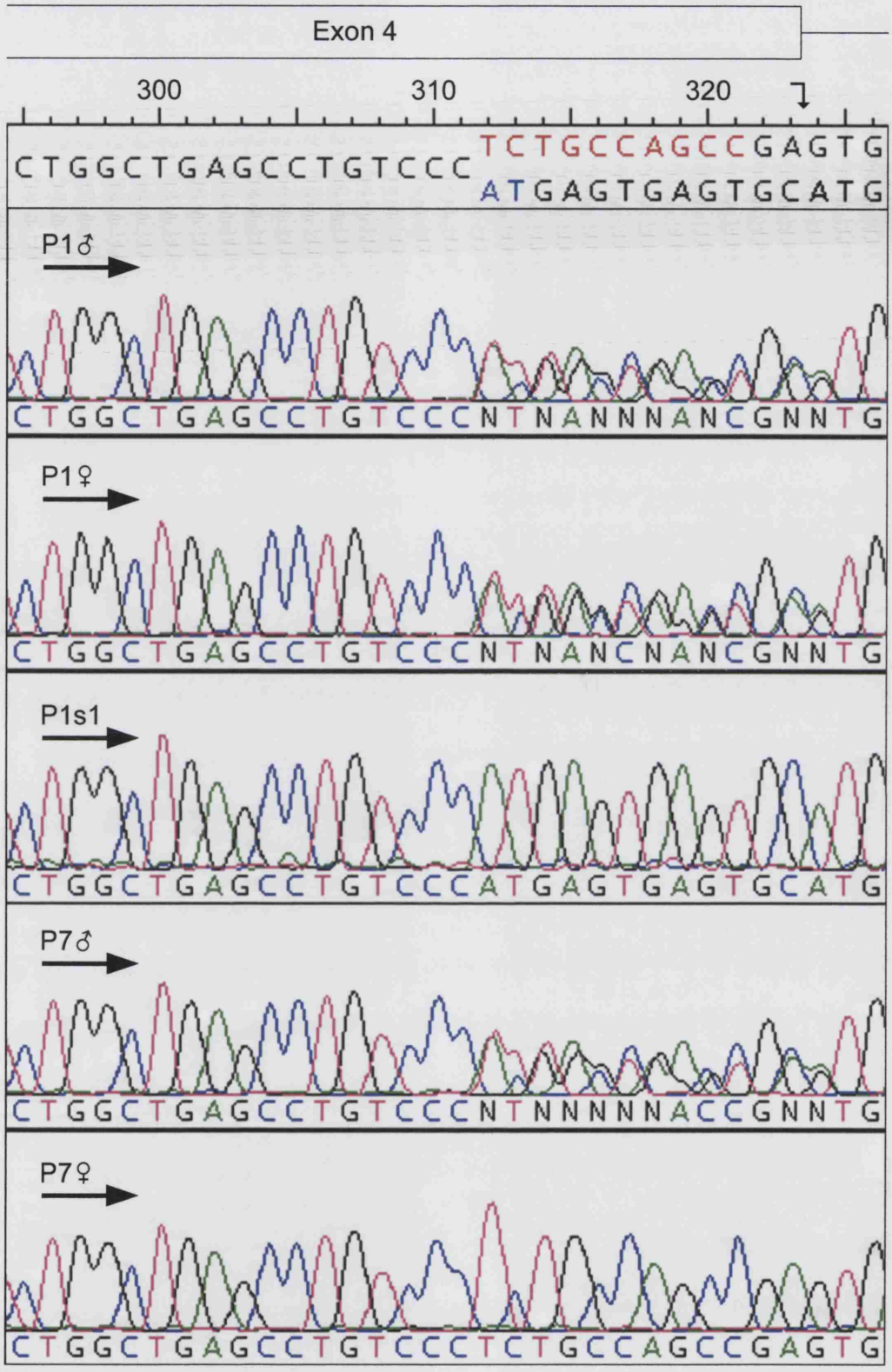

Figure 41 Electropherograms covering the 3' boundary of exon 4 of *SURF1* and the 312del10insAT mutation from family members of patient 1 and patient 7. Features and sequences shown above are as in figure 38. Arrows indicate the direction of sequencing.

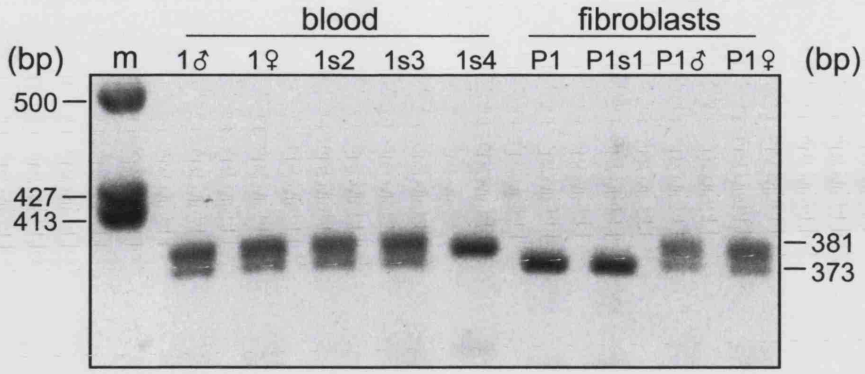

Figure 42 A high-resolution agarose gel of the exons 3+4 sequencing fragment of *SURF1* encompassing 312del10insAT from patient 1 and family members. "m" indicates marker lane with fragment lengths on the left (bp). The first five lanes are of DNA extracted from blood. Patient names are given above each lane, 1♂ & 1♀= parents; 1s2, 1s3 & 1s4 = siblings. The last four lanes are DNA obtained from primary fibroblast cultures. P1♂ & P1♀ = parents, P1s1 sibling. Lengths of fragments are given on the right-hand side of the gel. The image is an inverted scan of an ethidium bromide stained gel.

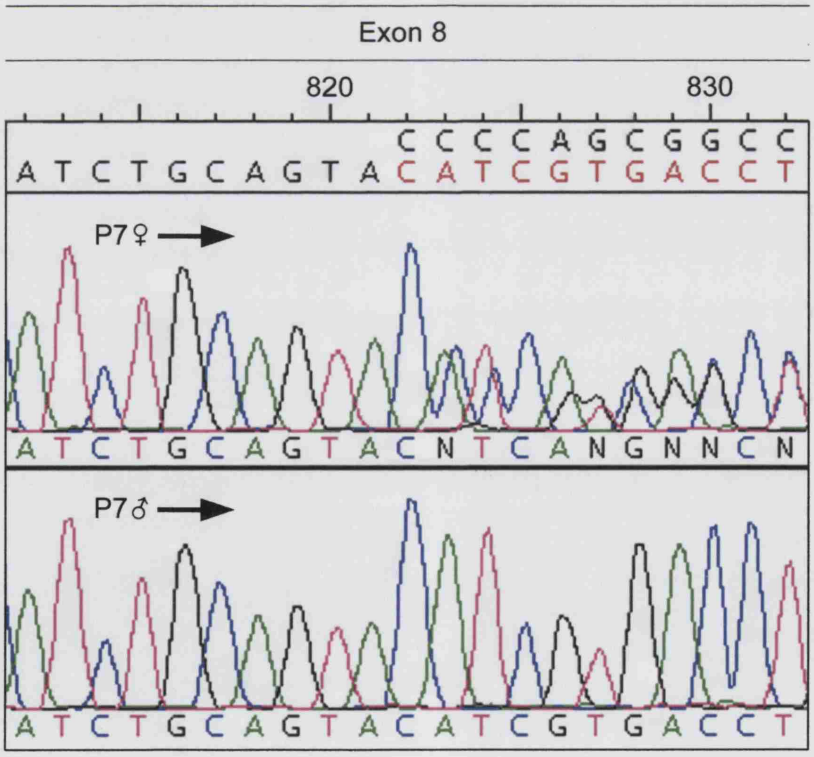

Figure 43 Electropherograms of the 3' end of exon 8 of *SURF1* from fibroblasts from the parents of patient 7. P7♂ and P7♀, father and mother respectively. Wild-type sequence is given across the top (lower sequence) with the 821del18 deletion in red. The upper sequence is that resulting from the deletion as read left to right. Direction of sequencing is indicated by the arrows.

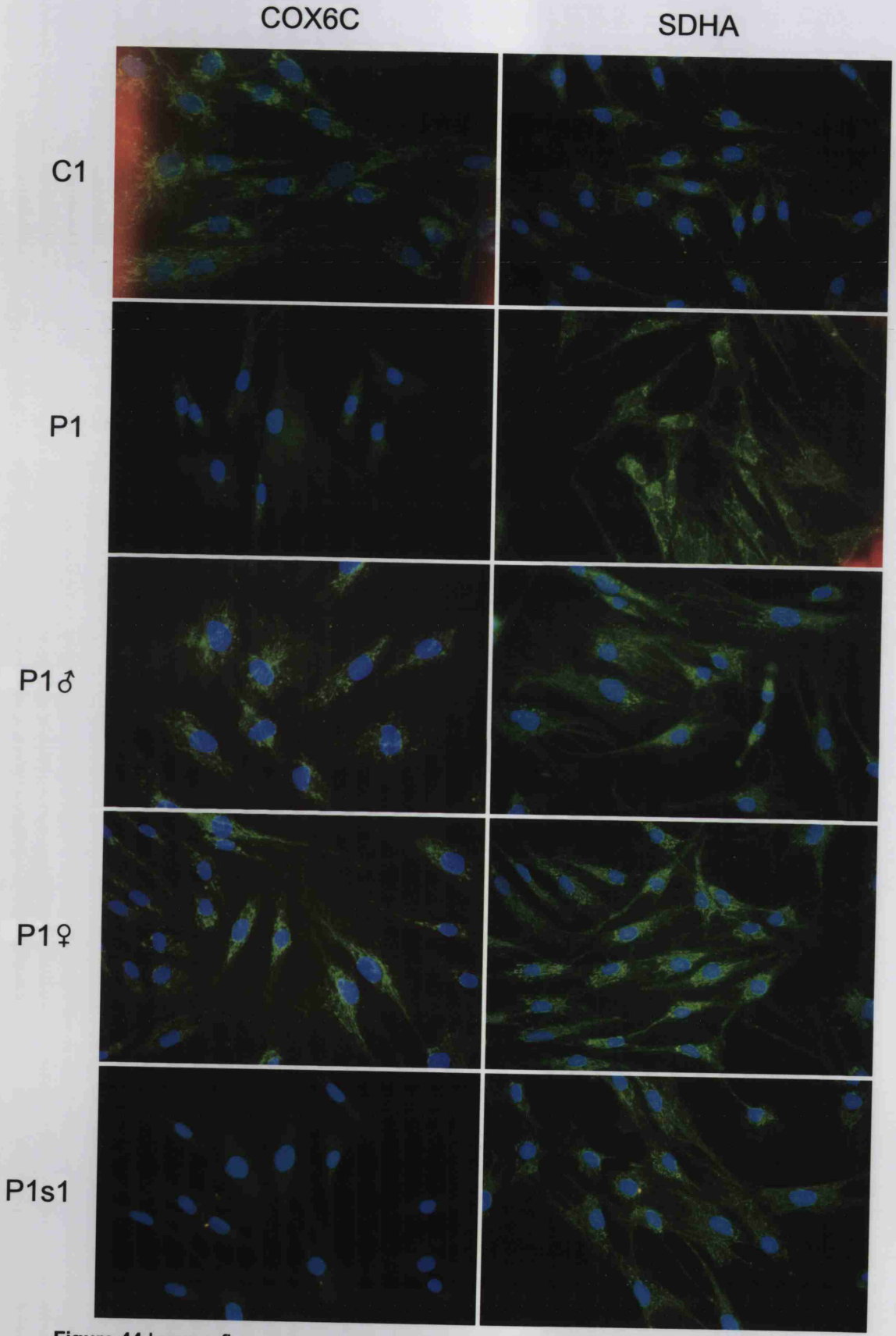

Figure 44 Immunofluorescent stains of P1 and fibroblasts from family members. C1=control, P1♂=father, P1♀=mother and P1s1 an affected sibling. Primary antibody targets are given at the top of each column. Primary antibodies were detected using green fluorescent Alexa™ 488 conjugated secondary antibody. Where coloured, nuclei have been counter stained blue using DAPI. Magnification x220.

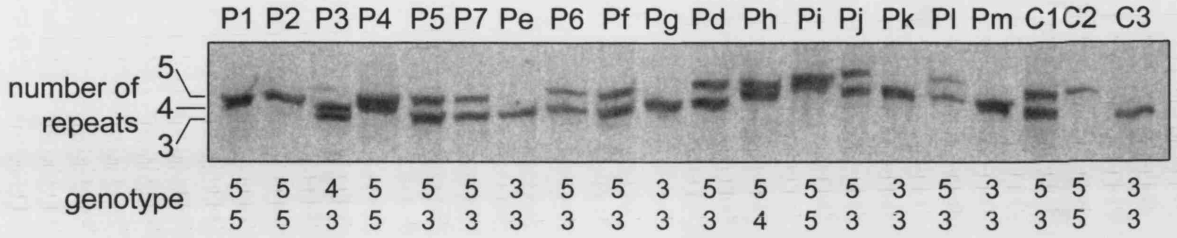

Figure 45 A silver stained 8% PAGE gel of the exon 1+2 *SURF1* sequencing fragment from P1-P7, ten disease controls (Pd-Pm) and three controls (C1-C3). Repeat numbers for the microsatellite repeat in intron 1 are given on the left-hand side of the gel with the number of repeats in each allele of each sample below each lane (genotype).

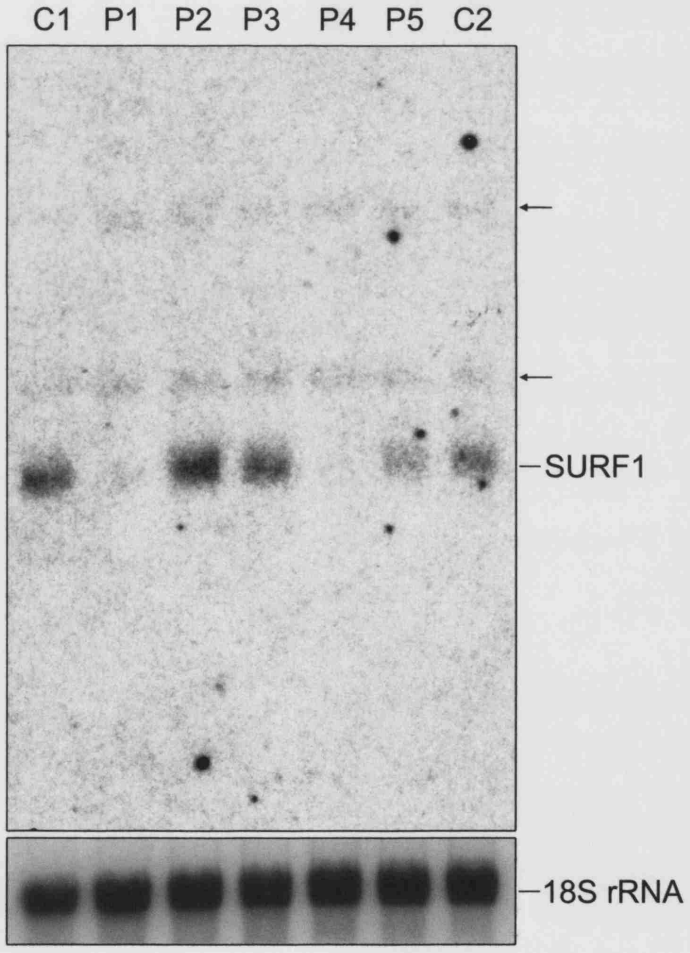

Figure 46 A northern blot of total RNA from P1-P5 (5.8 µg per lane) hybridised with a probe against *SURF1* mRNA. The *SURF1* signal is indicated on the right-hand side of the figure. Arrows indicate background signals, possibly from the 18S and 23S rRNAs. A section from the same blot hybridised with a probe against the 18S rRNA is shown at the bottom to confirm equivalent loading of samples. Due to the very low signal strength, the contrast in this image has been increased digitally resulting in the slightly speckled appearance of the image.

11.2.3 *SURF1* intron 1 microsatellite sequence polymorphisms

Intron 1 of *SURF1* is unusually short at only 86 bp (figure 8). Sequencing identified a microsatellite sequence with a variable number of heptameric repeats $[GGGTGCG]_{3-5}$ starting at 54+10. In every case the region was flanked at the 5' end by the related heptamer GGGCGCG. To examine the variability in this region and to see if repeat length could be used to identify carriers of mutant alleles, the sequencing fragment spanning exons 1+2 was amplified from DNA from P1-P7, ten disease control samples (Pd-Pm) and three controls (C1-C3). Products were resolved using PAGE and visualised using silver staining (figure 45). While 312del10insAT always segregated with 5 copies of the repeat, from the spread of the repeat lengths it can be seen that there is no reverse correlation of the two alleles. No repeats lengths larger or smaller than 3-5 copies were found in any of the samples.

11.2.4 Northern blotting of *SURF1* mRNA

Steady-state *SURF1* mRNA levels in P1-P5 were examined using northern blotting using the same blots as shown in figure 37*. A single major band was seen in control samples, assumed to be SURF1 mRNA (1019 nt). No signal was detectable in RNA from P1 and P4 and an intermediate signal was seen in P5 (figure 46). Two very faint bands could be seen above the *SURF1* signal band (see arrows). Given the weakness of the *SURF1* mRNA signal these probably correspond to cross-reaction with the 18S and 28S rRNAs (1900 nt and 4800 nt respectively).

11.2.5 Exon skipping as a result of 821del18

The novel deletion identified in P7, 821del18, removes the 3' boundary of exon 8 and the intron 8 splice donor site (figure 40). The two most frequent outcomes following the disruption of splice donor sites are skipping of the preceding exon or aberrant splicing due to the activation of cryptic splice donor sequences. 3'RACE was employed to examine whether the deletion caused any splice variants. cDNA with a ligated 3' anchor was generated from total fibroblast RNA and *SURF1* mRNA was amplified using a touch-down PCR protocol with a nested anchor primer and a specific primer in exon 7. PCR products were resolved using electrophoresis and sequenced.

---

* *SURF1* mRNA was probed before all other RNAs.

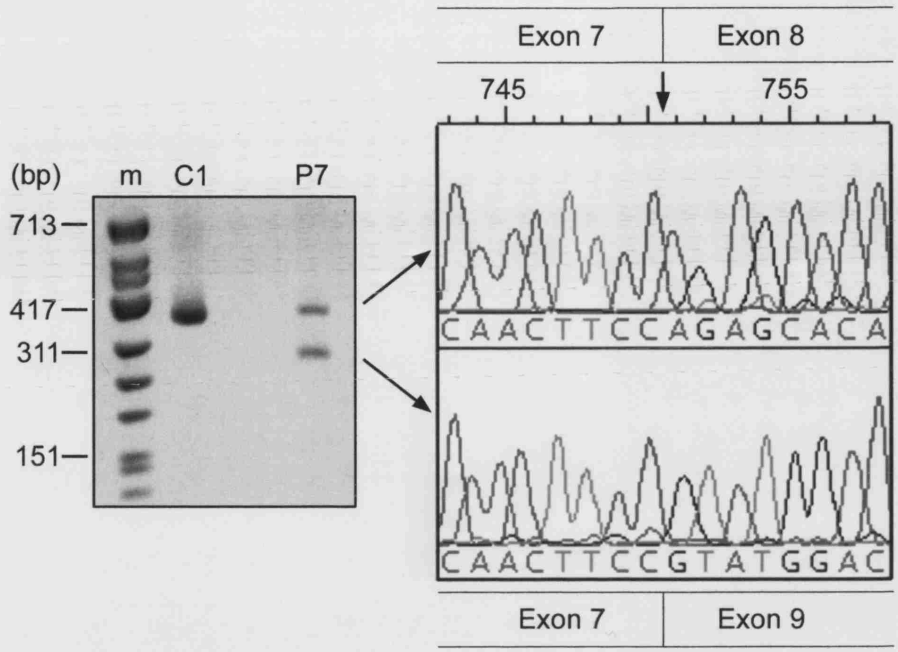

Figure 47 3'RACE of *SURF1* mRNA from P7 demonstrating skipping of exon 8. The left panel is an agarose gel of RACE fragments of *SURF1* mRNA amplified using a nested 3' anchor primer and a specific primer in exon 7. "m" is the marker lane with lengths of fragments given on the left (bp). The right-hand panel is electropherograms of cDNA eluted from the gel. The upper box is the wild-type sequence of the exon 7+8 boundary and the lower box is the exon 7+9 boundary resulting from skipping of exon 8. A vertical arrow indicates the splice junction.

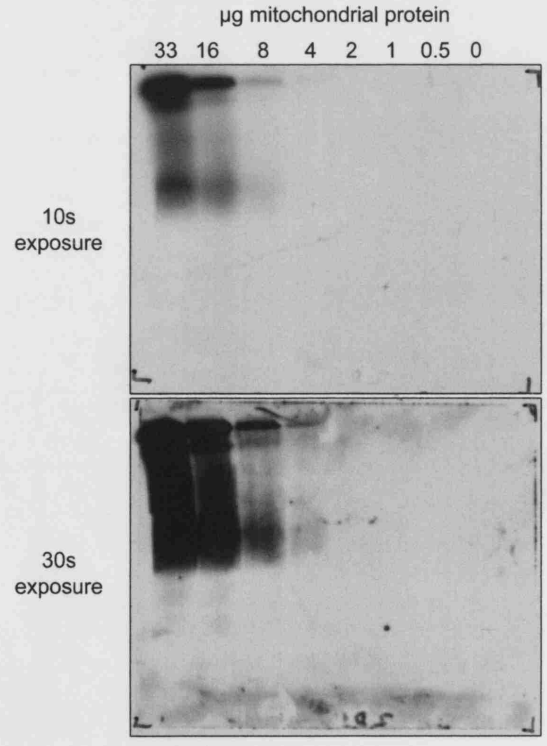

Figure 48 Two images of a single western blot of serial dilutions of rat heart mitochondria run to optimise loading. Samples were resolved using an 8% BN-PAGE gel and the blot was probed with anti-MTCO1. Exposure times are given to the left of each image. µg of protein loaded per lane according to the total protein content of the purified mitochondria are given above each lane.

A single *SURF1* mRNA fragment was amplified from the control, whereas two fragments were present in P7 (figure 47). Sequencing confirmed the loss of exon 8 in the smaller fragment from P7 which contained an exon 7+9 splice junction. The larger fragment was composed of exons 7+8+9. As P7 was heterozygous for 821del18 it is safe to assume that the 821del18 mutation in the maternal allele led to skipping of exon 8 and that the larger fragment corresponds to the paternal *SURF1*^{312del10insAT} allele.

11.2.6 Application of *in silico* splice site prediction tools to examine 312del10insAT

3'RACE PCR demonstrated that the complete loss of the intron 8 splice donor sequence led to skipping of exon 8 (figure 47). The 312del10insAT deletion ends at nt 321 which is only 2 bp from the intron 4 splice donor site GT at 323+1 (figure 38). It was thought that the mutation might interfere with splicing of intron 4. Despite trying multiple cDNA samples, different sets of primer pairs and PCR strategies, attempts to amplify cDNA spanning the exon 4 sequence from either mutant allele of P7 were unsuccessful. It was therefore not possible to determine whether 312del10insAT affected the function of the intron 4 splice donor sequence directly. Instead *in silico* analysis using splice site prediction software was employed to try and gain some insight into the effect of the mutation on the strength of the intron 4 splice donor sequence.

Correct identification of splice sites is an important aspect of gene finding and the massive increase in genomic data over the past decade has prompted the development of sophisticated tools for splice site prediction. A number of bioinformatics servers provide online splice site prediction tools. Three different tools were applied to the study of the *SURF1* genomic sequence retrieved from Ensembl*: GeneSplicer[695], available online from The Institute for Genome Research (TIGR)†; NetGene2[696], available online from the Technical University of Denmark Centre for Biological Sequence Analysis (CBS)‡ and SSPNN (Splice Site Prediction using Neural Networks)[697], available online form the Berkley Drosophila Genome Project (BDGP)§. Each of the tools uses a unique algorithm to analyse input sequences and they have each been trained using different data sets. All of the tools enabled the selection of algorithms optimised for screening human sequences and each was employed using default settings.

---

* ENSG00000148290, including full intron sequences and 50 bp flanking sequences 5' and 3'.
† http://www.tigr.org/tdb/GeneSplicer/gene_spl.html
‡ http://www.cbs.dtu.dk/services/NetGene2/
§ http://www.fruitfly.org/seq_tools/splice.html

The *SURF1* genomic sequence from Ensembl contains 6 copies of the intron 1 microsatellite repeat unit mentioned above. This number of repeats was not seen in any of the patients or controls sequenced (figure 45) and has never been documented[596]. It is very likely that the copy number of this repeat in the Ensembl sequence is an artefact introduced by the sequence analysis software used to compile the *SURF1* sequence. For the purposes of this study the Ensembl sequence was altered to provide a wild-type sequence that contained five copies of the repeat. Five copies of the repeat were also included in the 312del10insAT mutant sequence in accordance with the microsatellite sequence data above.

Table 20 *In silico* analysis of the *SURF1* intron 4 splice donor sequence using the GeneSplicer, NetGene2 and SSPNN online analysis tools.

NetGene2

SURF1 sequence	Intron 4 splice site score (1.0)	Splice donors identified	False +ve sites
wild-type	0.83	8 (0.63-0.93)	5 (0.32-0.55)
312del10insAT	0.93	8 (0.63-0.93)	5 (0.32-0.55)

GeneSplicer

SURF1 sequence	Intron 4 splice site score	Splice donors identified	False +ve sites
wild-type	6.46	7 (5.27-15.47)	7 (1.09-8.14)
312del10insAT	7.85	7 (5.27-15.47)	7 (1.09-8.14)

SSPNN

SURF1 sequence	Intron 4 splice site score (1.0)	Splice donors identified	False +ve sites
wild-type	0.98	8 (0.46-1.00)	20 (0.40-0.99)
312del10insAT	0.93	8 (0.46-1.00)	20 (0.40-0.99)

Key: Splice donors identified = the number of *in vivo* splice donor sites identified by each tool; False +ve sites = splice donor sites identified by each tool which do not correspond to those utilised *in vivo*. Ranges for *in vivo* splice donor site scores and false positive site scores for each of the *SURF1* sequences are given in brackets. All scores were returned using default parameters for the human sequence optimised algorithms for each tool.

There was some variation in the accuracy of each of the sets of results (table 20). The short length of *SURF1* introns is likely to have contributed to the false negative scores, in particular GeneSplicer contains a filter to return locally optimal splice donor sites within a 100 bp window. This led to a false negative call for the intron 1 splice donor site that could be corrected by increasing the length of intron 1. Using the default settings NetGene2 gave the most accurate results, followed by GeneSplicer and SSPNN. All of the tools gave a higher range of scores to the *in vivo* splice donor sites than the false positive sites and the number of false negatives called was consistently low. This confirms the suitability of these three tools for investigation of the *SURF1* splice donor

sequences. Each tool recognised the wild-type intron 4 splice donor site and returned a high score for it, demonstrating that the wild-type *SURF1* intron 4 splice donor site is part of a strong canonical splice donor sequence. When the 312del10insAT mutation and 280T-C and 573C-G polymorphisms were put into the wild-type sequence, all of the tools still predicted a high scoring splice donor site at the retained GA of the intron 4 splice donor site. Therefore, the 312del10insAT mutation is not predicted to adversely affect the strength of the canonical intron 4 splice donor sequence.

12 ANALYSIS OF PROTEIN COMPLEXES CONTAINING CYTOCHROME C OXIDASE SUBUNITS

The immunological analysis of P1-P7 demonstrated that they all expressed reduced steady-state levels of COX subunits and genetic analysis found *SURF1* mutations in P1, P4, P5 and P7. These cultures all had the same pattern of subunit loss with very low levels of MTCO2 and COX6C but only partially reduced levels of MTCO1 and COX4I1 (figures 17, 18 & 20; table 15). This suggested that some COX subunits may be stable in certain patient cells in the absence of normal biogenesis of the holo-complex. To examine whether these subunits persist as COX sub-complexes, blue-native polyacrylamide gel electrophoresis (BN-PAGE) was used to identify mitochondrial complexes containing COX subunits. As BN-PAGE is not a widely used technique, extensive studies were carried out to optimise a protocol for both 1D and 2D BN-PAGE gel western blotting.

12.1 DEVELOPMENT OF A WESTERN BLOTTING PROTOCOL FOR BN-PAGE ELECTROPHORESIS

12.1.1 Rat heart mitochondria

Preliminary experiments to optimise BN-PAGE were carried out using rat heart mitochondria kindly provided by Dr Thierry Letellier (Bordeaux). Samples were solubilised and run as described by Schägger *et al*[83] without modification.

12.1.2 Standard 1D BN-PAGE

Serial dilutions of rat heart mitochondrial protein from 33-0.5 µg per lane were used to optimise gel loading. These were resolved on an 8% gel and a blot was probed with a

monoclonal antibody against MTCO1 to identify COX. Results indicated that signal could be detected in lanes loaded with 4 µg per lane and above (figure 48, page 192).

The five dissociated OXPHOS complexes could be clearly distinguished using 5-13% linear gradient gels loaded with 33 µg of protein per lane and stained with residual G250 dye. Given the thorough work carried out by Schägger and co-workers in confirming the size of OXPHOS complexes resolved using BN-PAGE[32,35] no formal sizing of complexes was carried out. On 5-13% gels of rat heart mitochondria the three slowest migrating, G250-stainng bands corresponded to complexes I, III and V with apparent molecular weights of around 900, 600 and 500 kDa, respectively. In agreement with previous results, complex III migrated just below complex V as it is solubilised as a dimer. COX migrated below complex III, corresponding to an apparent molecular weight of 200 kDa and complex II migrated fastest of all the complexes, corresponding to an apparent molecular weight of 130 kDa. Assumed molecular weights of the complexes correlated well with their respective migrations (figure 49). In-gel activity stains of lanes loaded with 33 µg of protein confirmed the identity of the COX and complex II (succinate dehydrogenase) bands (figures 49 & 50). In both the activity stains and the G250 protein stains, the major COX signal appear as a close pair of bands (figure 50).

The identity of the OXPHOS complexes resolved on 5-13% gradient gels was confirmed using strips western blots of gels loaded with 4 µg of mitochondrial protein per lane (figure 49). On these blots the major COX subunit signals appeared as a broad band, substantiating the close pair double bands seen in the G250 and activity stains. In addition, a third faster migrating band could be seen (figures 49 & 51). This band was not active according to *in-gel* COX activity stains. Multiple bands were also found with antibodies against ATP5A1, UQCRC2 and SDHA. The monoclonal antibody to SDHA consistently cross-reacted with two bands. A lane probed only with secondary antibody confirmed that in the rat heart mitochondria samples all signals could be attributed to the primary antibodies (figure 51).

12.1.3 2D BN-PAGE/urea-SDS gels

A 2D BN-PAGE/denaturing PAGE protocol using the standard BN-PAGE first dimension followed by an urea-SDS second dimension was carried out to provide a preliminary verification of the technique (figure 52). The migration of the MTCO1 signal in the second dimension confirmed the identity of the signal however, a large number of non-specific spots could be seen when no primary antibody was present.

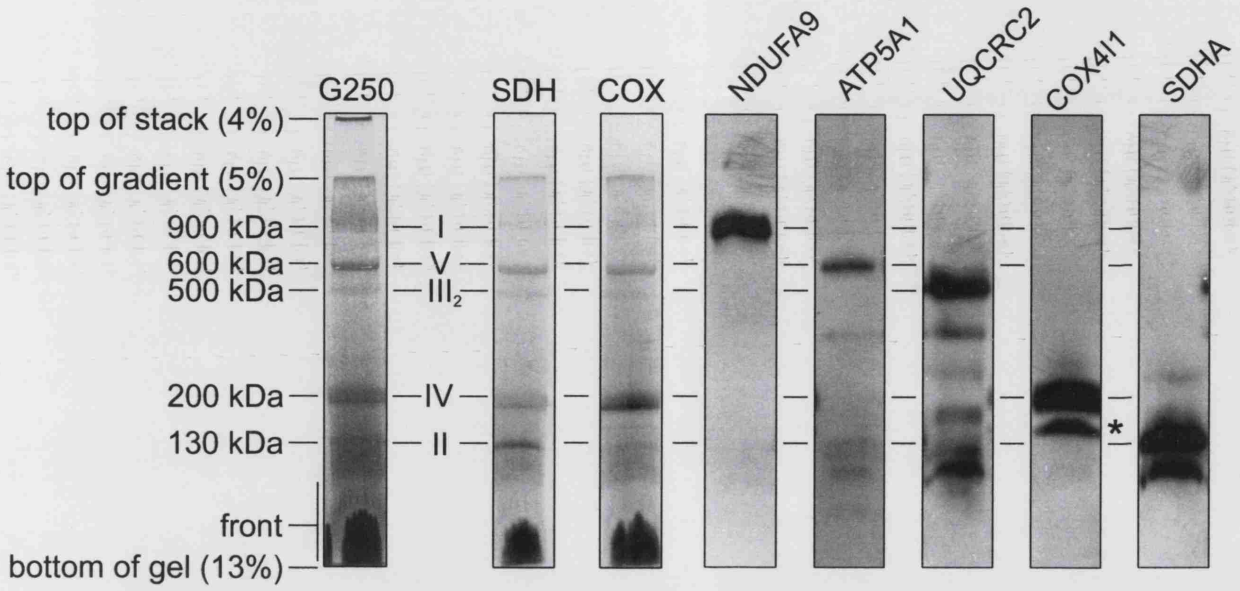

Figure 49 BN-PAGE gel electrophoresis of rat heart mitochondria. Aligned gel strips and blots from a pair 5-13% gradient gels poured and run in parallel. The strip on the far left (G250) is a Serva Blue-G250 stained gel slice loaded with 33 µg of mitochondrial protein. The positions of the gel boundaries and front are given on the left of the image. Roman numerals to the right denote the five major OXPHOS complexes and predicted molecular masses are given in kDa on the left. "SDH" and "COX" are *in-gel* activity stains for succinate dehydrogenase and COX activity respectively, again using lanes loaded with 33 µg of mitochondrial protein. The five strips to the right-hand side of the figure are western blots of lanes loaded with 4 µg of protein probed with monoclonal primary antibodies against the targets listed above each strip. NDUFA9, complex I; ATP5A1, complex V; UQCRC2, complex III; COX4I1, COX and SDHA complex II. The asterisk to the right of the COX4I1 blot indicates the fast migrating COX subunit signal.

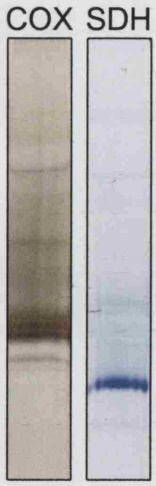

Figure 50 An image of *in-gel* activity stains of rat heart mitochondria. COX = cytochrome c oxidase activity, SDH = succinate dehydrogenase activity. The slices have been developed for longer than those in figure 49 allowing clear identification of the two major cytochrome c oxidase activity bands. Gel slices were destained following development of the activity stains.

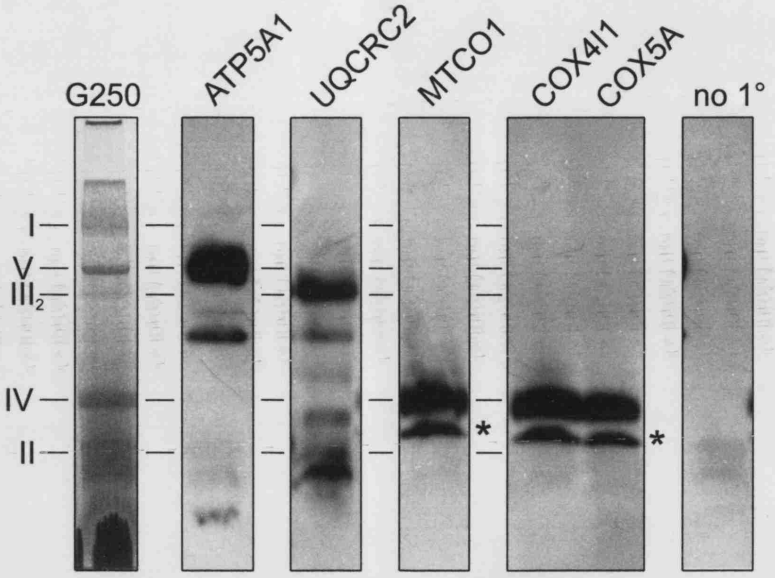

Figure 51 Western blots from the same gel as shown in figure 49. To aid orientation the left-hand lane shows the same G250 stain. Longer exposures of the complex V anti-ATP5A1 and complex III anti-UQCRC2 probed blots are shown. Blots probed with antibodies against MTCO1 and COX5A are shown in addition to the COX4I1 blot from figure 49. Asterisks to the right of the MTCO1 and COX4I1 & COX5A blots show the position of the fast migrating COX subunit signal. The far right-hand blot was only probed with secondary antibody (no 1°).

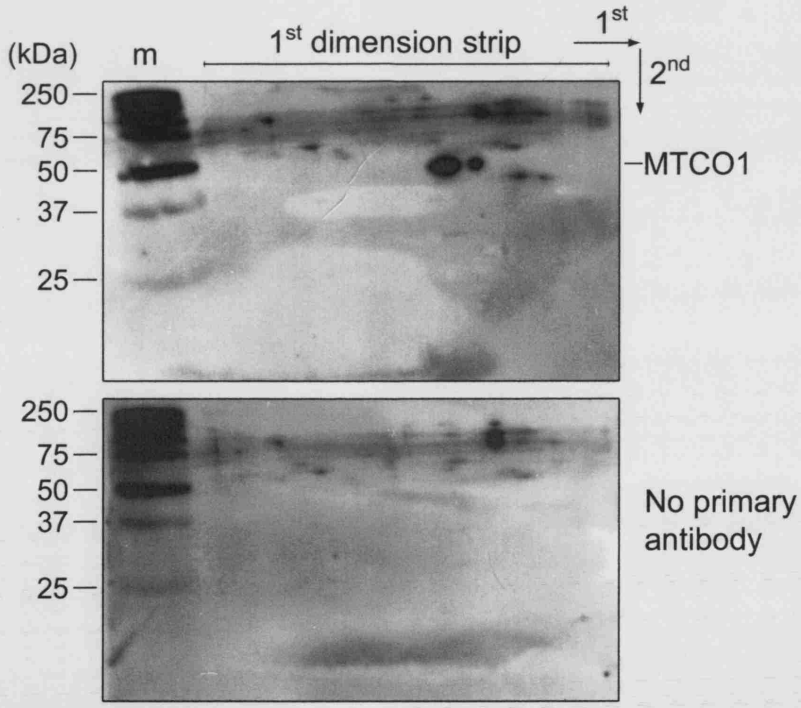

Figure 52 Western blots of 2D gels of rat heart mitochondria loaded with 4 µg protein per lane. The first dimension runs left to right and was cut from a 5-13% BN-PAGE gel similar to those in figures 49 and 51. The second dimension is a denaturing 12.5% urea-SDS PAGE gel running top to bottom. This orientation of gel dimensions is used for all subsequent 2D gel images. "m" indicates second dimension molecular weight markers with masses in kDa on the left. The blot in the upper panel was probed with primary antibody against MTCO1. The position of the MTCO1 signal in the second dimension is marked on the right-hand side. The double bands from the first dimension correspond to the large spot and the faster migrating third band to the smaller spot to the right. The blot in the lower panel was only probed with secondary antibody.

12.1.4 Preliminary work with human samples

12.1.4.1 1D BN-PAGE electrophoresis

Once the BN-PAGE electrophoresis protocols had been established using rat mitochondria they were applied to control human samples. Mitoplasts were prepared from fibroblasts using the protocol developed by Klement *et al*[681]. The rat samples had been run successfully for blotting at 1-4 µg of mitochondrial protein per lane. Human mitoplasts were run at an estimated 10 µg of mitoplast protein per lane. This corresponds to 1/10 of the 10^6 cell preparation described by Klement. It was reasoned that COX subunits accumulating in cells would form complexes smaller than the holo-complex dissociated by LM, therefore gel gradients were shifted from 5-13% to 8-16%.

12.1.4.2 Dye retention on PVDF membranes

The protocol used to run BN-PAGE gels for western blotting did not include a change of the cathode buffer to one with a low G250 content as suggested by Schägger[32-34]. Blotting gels without the buffer change, resulted in PVDF membranes which were heavily bound by G250 dye. During probing the dye was removed by washing in PBS-Tween (0.3%), however when blots were probed, a large area of non-specific signal was present (figure 53). This could be overcome by washing air-dried blots in methanol to remove residual G250 prior to probing.

12.1.4.3 Results with 8-16% gels

The altered gel gradient clearly influenced the migration of OXPHOS complexes (figure 54). Most strikingly, the anti-NDUFA9 signal demonstrated that complex I (900 kDa) was unable to migrate through the stacking gel. No signal could be detected for the complex V (600 kDa) subunit ATP5A1 and the UQCRC2 signal indicated that the complex III dimer (500 kDa) had barely entered the gel. As with the rat mitochondria, COX resolved as a pair of major bands in human samples. This was particularly clear on the strip probed with anti-COX5A. Below COX, two signals could be seen for the SDHA primary antibody. Both of these bands cross reacted with primary antibodies to SDHA and SDHB (figure 55). Antibodies to HSPD1* and HSPA9B† were also used on these strips. Anti-HSPD1 cross reacted with two bands below complex III. Anti-HSPA9B cross reacted

---

* Non-HNGC name HSP60
† non-HNGC name mtHSP70

with a prominent band towards the bottom of the blot assumed to be monomeric HSPA9B which has a molecular mass of 68.3 kDa.

12.1.4.4 Results with 10-16% gels

Increasing gel gradients further to 10-18% did not enable good migration of the COX holo-complex into the gel (figure 55). In addition it resulted in intense staining of the stacking gel even when probed with only secondary antibody, suggesting that a large amount of protein was not able to enter the separating gel.

12.1.4.5 Probing for cytochrome c

To examine the possibility that the close pair of COX signal bands may have been caused by the binding of residual cytochrome c to the holo-complex, strips of blots were probed with two different primary antibodies to cytochrome c. Two different primary antibodies were used, one which cross-reacted with the linearised protein and one which cross-reacted with the native protein (figure 56). The blot was repeated a number of times with increasing concentrations of antibody but no signal bands were detected in the region of COX or anywhere else on the blots. Although no positive controls were included in this study the antibodies used were known to function well on western blots and immunofluorescence staining, respectively.

12.1.4.6 2D BN-PAGE/urea-SDS electrophoresis

The aim of the development of a western blotting protocol for BN-PAGE electrophoresis was to enable the detection of COX sub-complexes. To this end, optimisation of a 2D native/denaturing gel resolution was important as it had the potential to provide information on the components of any sub-complexes identified.

As with the 2D rat mitochondria blots, there was a fairly poor signal to noise ratio in the initial 2D blots using human samples (figure 57). The MTCO1 signal was low and a lot of non-specific spots could be seen. In particular, a strong signal was generated by the cross-reaction of the secondary antibody with a species that migrated just below the COX major bands in the first dimension and above it in the second dimension (see arrows; figure 57). For this reason it was thought necessary to re-evaluate the secondary antibodies used.

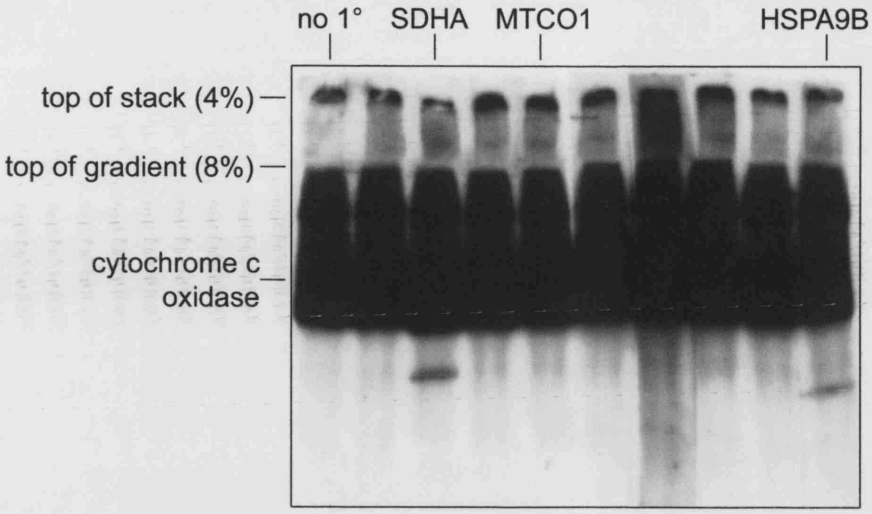

Figure 53 Strips cut from a single western blot of an 8-16% BN-PAGE gel of human control fibroblast mitoplasts. The massive signal resulting from G250 dye retained during blocking can be seen across the centre of all strips. Monoclonal primary antibody targets for some of the blot strips are given above including a control blot without primary antibody (no 1°). Labels on the left indicate the position of gel reference points and the approximate migration of the COX monomer bands.

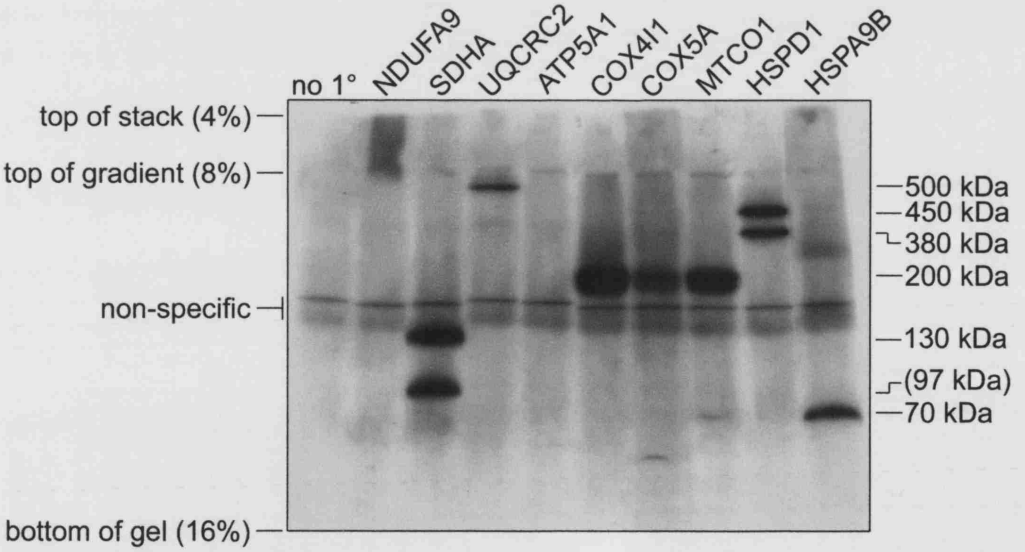

Figure 54 Scan of western blot strips from a 8-16% BN-PAGE gel run with control fibroblast mitoplasts. Mitoplasts equivalent to 10^5 cells were loaded per lane. Primary antibody targets are listed above each strip. A control without primary antibody is included (no 1°). Gel reference points are indicated on the left of the figure as is the position of a non-specific signal caused by the secondary antibody. Primary antibody targets are given above each lane; NDUFA9, complex I; SDHA, complex II; UQCRC2, complex III; ATP5A1, complex V; COX4I1, COX5A and MTCO1, COX; HSPD1 and HSPA9B, matrix chaperones. Apparent molecular weights are given on the right-hand side of the image according to the migration of the major OXPHOS complexes and matrix chaperones. (97 kDa) is the predicted molecular weight of an SDHASDHB dimer migrating as the lower SDHA signal band (figure 55).

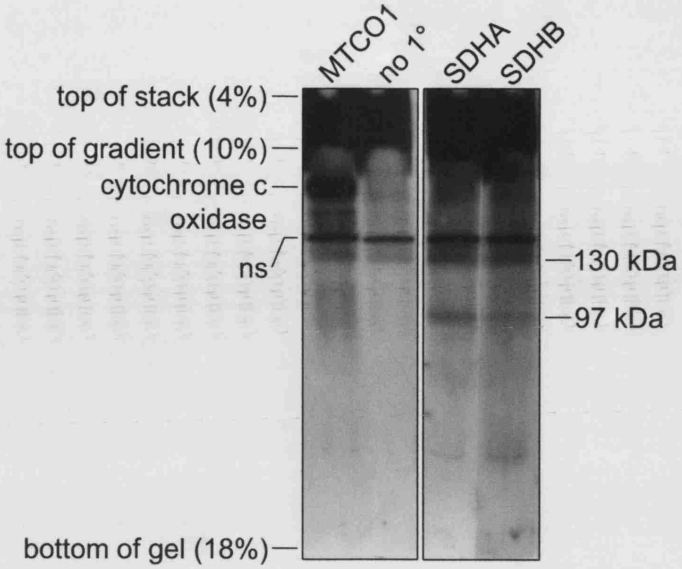

Figure 55 Western blot strips from a 10-18% BN-PAGE gel run with control fibroblast mitoplasts. 10^5 cell equivalents were run per lane. Gel reference points are given to the left of the figure. Also indicated is the migration of the 200 kDa COX monomer and the position of the non-specific secondary antibody signal (ns). Primary antibody targets are given above each strip. Antibodies to SDHA and SDHB both cross react with a fast migrating sub-complex assumed to be an SDHASDHB dimer. The predicted protein molecular mass of this sub-complex, 97 kDa, is given to the right along with the position of holo-complex II (130 kDa).

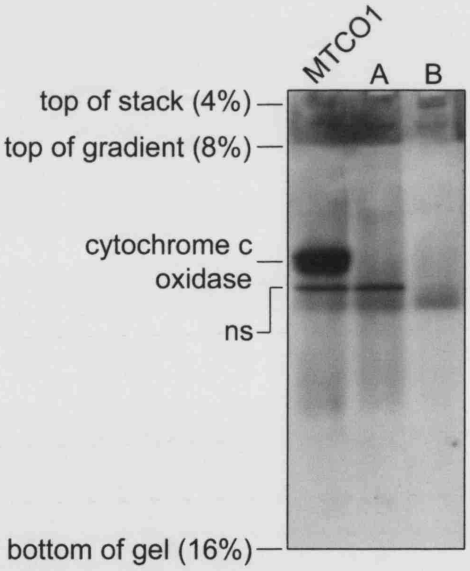

Figure 56 Western blot of an 8-16% BN-PAGE gel run with control fibroblast mitoplasts. 10^5 cell equivalents were run per lane. Gel reference points are given to the left of the figure. Also indicated is the migration of the 200 kDa COX monomer and the non-specific signal seen with certain secondary antibodies (ns). Two different anti-CYCS primary antibodies were used, A: a mouse monoclonal optimised for linearised protein and B: a rabbit poly-clonal optimised for native protein. A strip probed with anti-MTCO1 is shown for reference. The MTCO1 strip was probed with the same secondary antibody as anti-CYCS antibody A and a different secondary antibody was used to detect primary B, hence the sharp non-specific band migrating below the COX holo-complex is not visible in panel B.

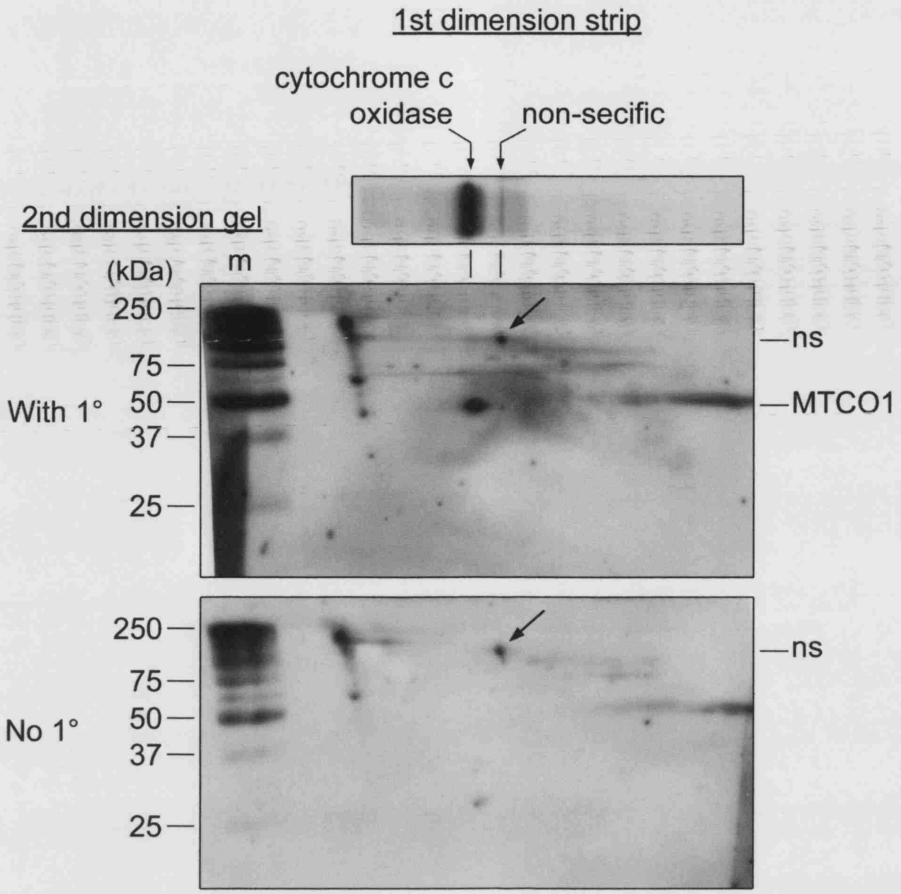

Figure 57 Western blots of 2D BN-PAGE/urea-SDS PAGE gels (8-16%/12.5%) and a strip cut from the same 1st dimension gel. Control mitoplasts from 10^5 cells were run per lane. The 2D blots have been probed with or without anti-MTCO1 as indicated on the left of the figure. The 1st dimension strip was also probed with this primary. The positions of the COX monomer and non-specific secondary antibody signal are indicated on the 1st dimension strip and the MTCO1 signal and non-specific spots on the 2D blots (arrows and "ns"). "m" is 2nd dimension molecular weight markers with masses in kDa. The image is composed from a single autorad exposure.

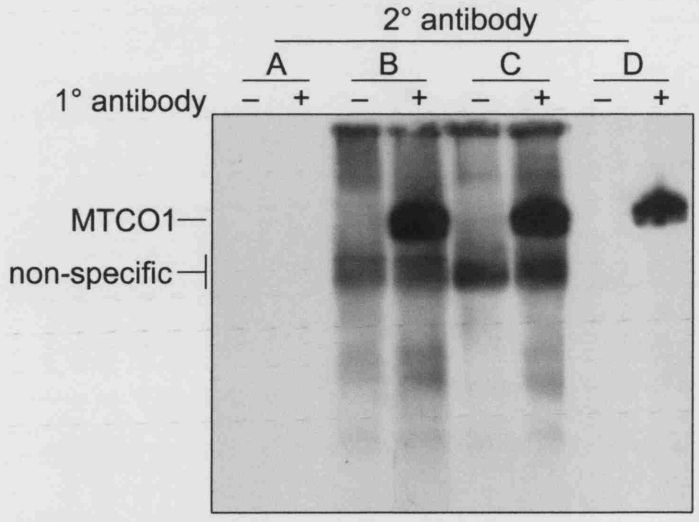

Figure 58 Western blot strips of an 8-16% BN-PAGE gel run with control fibroblast mitoplasts. 10^5 cell equivalents were run per lane. Strips were probed with or without primary antibody against MTCO1 as indicated above each strip. Four different secondary antibodies (A-D) were compared as indicated above each pair of strips. The position of the MTCO1 signal is indicated to the left of the figure as is the major non-specific signal from secondary antibodies B and C.

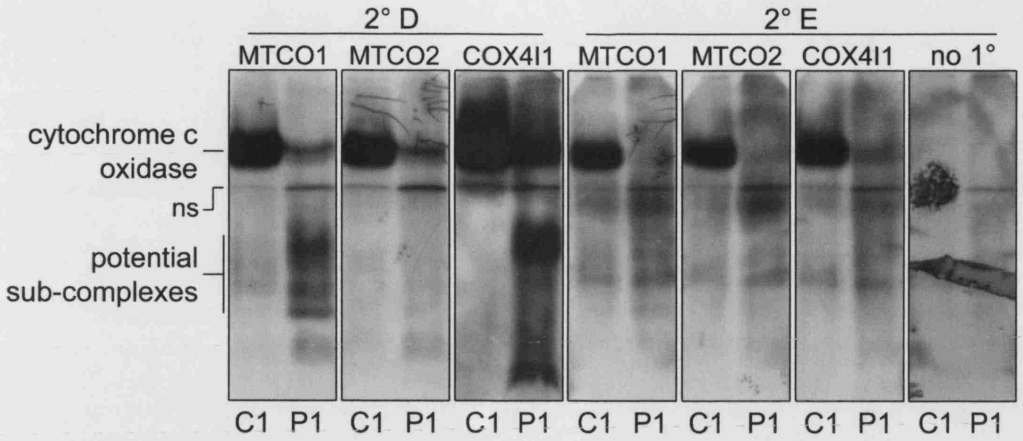

Figure 59 Western blots from 8-16% BN-PAGE gels. Each strip corresponds to a pair of lanes of mitoplasts from a control (C1) and the *SURF1* mutant culture P1 as indicated below each lane. $2x10^5$ cell equivalents were loaded per lane. Secondary antibodies used for each set of strips are given at the top of the figure and primary antibodies are given above each strip. The same dilutions of each primary antibody were used to test both secondary antibodies. The position of the COX monomer, the persistent non-specific signal (ns) and the putative sub-complexes below it are indicated to the left of the figure. A strip probed with secondary E without primary is also shown (no 1°), the dark marks on this strip are due to stains on the autorad. All images are from a single autorad exposure.

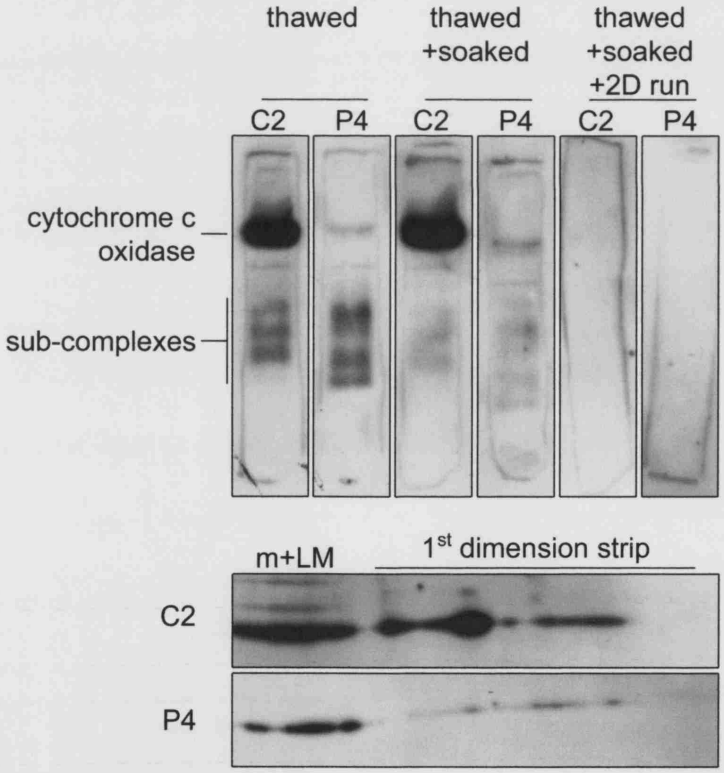

Figure 60 Western blots of gel slices used to test for signal loss during the 2D BN-PAGE protocol. Blots were prepared at various points throughout the protocol as indicated across the top of the figure. Two mitoplast samples were compared, the control C2 and the *SURF1* mutant culture P4. $2x10^5$ cell equivalents were run per lane. All blots were probed with anti-MTCO1. The position of the COX monomer and the sub-complexes are shown on the left of the figure. Gel strip ghosts can be seen as the outline of each strip was marked in ball-point pen prior to probing to facilitate alignment. The lower pair images have been cut from the resulting 2D blot. "m+LM" indicates a molecular weight marker lane including LM extract from a control sample to confirm the position of MTCO1 in the second dimension. All images are taken from a single autorad exposure.

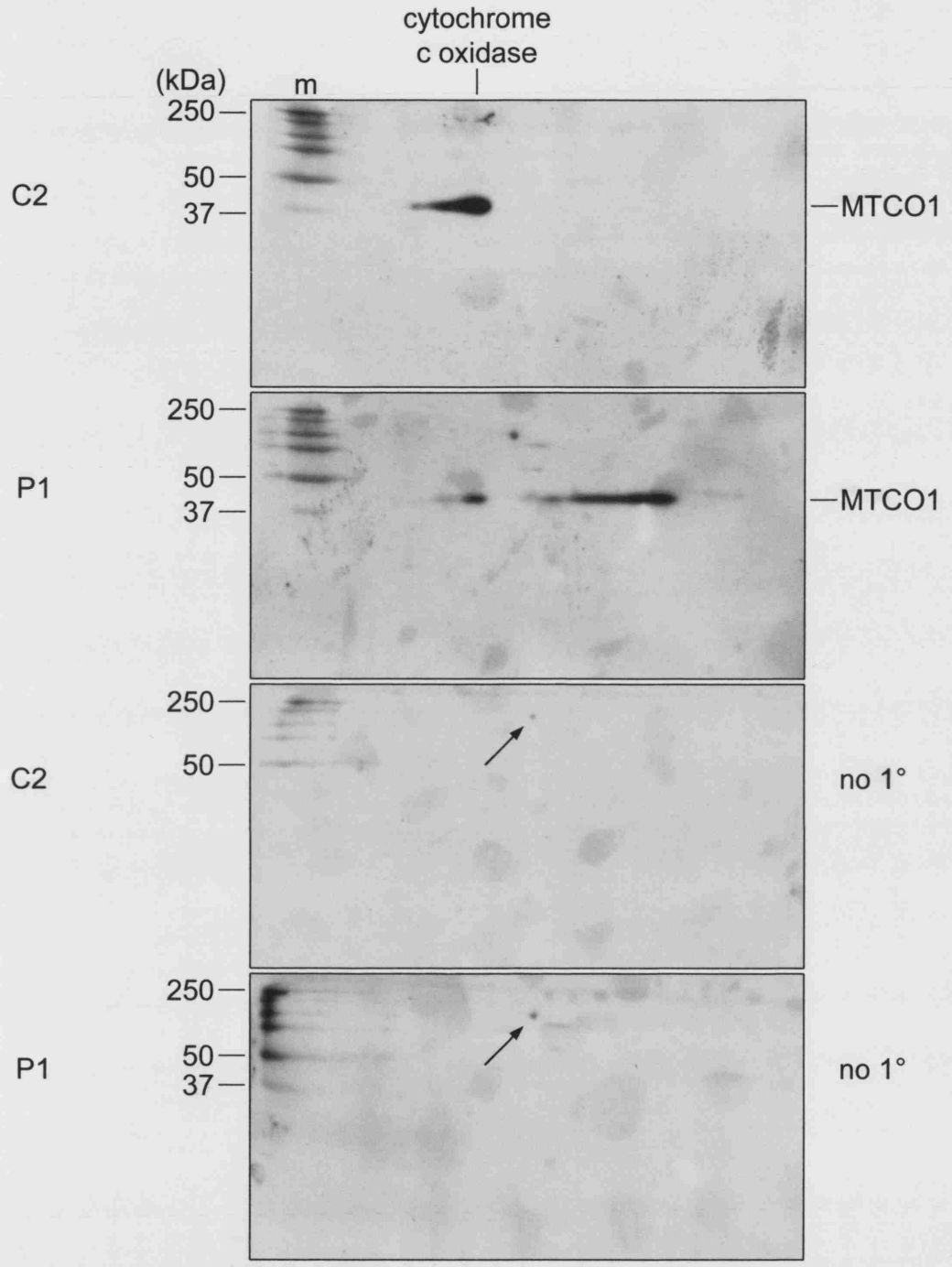

Figure 61 Western blots of 2D BN-PAGE/urea-SDS PAGE gels (8-16%/12.5%). Mitoplasts from $2x10^5$ cells were run per lane. Mitoplast samples from a control fibroblast culture C2 and the *SURF1* mutant culture P1 were compared as indicated on the left. Blots were probed with or without primary antibody to MTCO1 as indicated on the right. The position of the COX monomer in the first dimension is shown at the top of the figure. "m" is the second dimension molecular mass marker lane with masses given in kDa. All images are from a single autorad.

12.1.5 Optimisation of western blotting protocols for 1D and 2D BN-PAGE electrophoresis of human mitoplasts

12.1.5.1 Influence of secondary antibodies

As described in materials and methods all the western blots in this thesis were developed with horse radish peroxidase (HRP) conjugated secondary antibodies combined with enhanced chemiluminescence (ECL). A comparison of a number of different secondary antibodies was carried out to examine the extent to which choice of secondary antibody influenced results.

Four secondary antibodies were compared (figure 58). Secondary A was an anti-HRP-peroxidase conjugate and the lack of signal generated by it indicated that residual, unbound peroxidase was unlikley to contribute to the background signal. Secondary antibodies B, C and D were all anti-[mouse-IgG]-HRP conjugates. A massive amount of non-specific signal was generated by secondary antibodies B and C even in the absence of primary antibody. All blots shown to this point had been developed using secondary antibody B. The very low non-specific signal with secondary antibody D revealed that it was a better choice for use with the native epitope spectrum of BN-PAGE western blots.

12.1.5.2 Initial work with SURF1 mutant samples

Changing to a more specific secondary antibody improved the signal to noise ratio enabling the detection of fainter signal bands. Initial work with patient samples clearly demonstrated the value of this alteration. Figure 59 shows seven blots, each of pairs of lanes of mitoplasts from the *SURF1* mutant culture P1 and a control culture (C) all prepared and run in parallel. Primary antibodies against MTCO1, MTCO2 and COX4I1 were used in conjunction with two different secondary antibodies, D and E. On the set of blots probed with secondary antibody D, bands of signal can be seen below the holo-complex on the blots probed with antibodies against MTCO1 and COX4I1, but not MTCO2. No such bands can be seen on any of the blots probed with secondary antibody E and a large amount of background signal was present on these blots. In particular they contained a dark banding that extended to around two thirds of the way down the gel. The exposure times used to enable visualisation of the sub-complex bands also picked up the sharp non-specific signal see previously running just below COX (figure 59, compare figures 54-58). This experiment confirms the suitability of secondary antibody D

for use in this system and demonstrates its ability to detect specific low abundance bands not detectable using any of the other secondary antibodies. Throughout the remainder of this work secondary antibody D has been used unless stated otherwise.

12.1.5.3 Initial 2D blots of SURF1 mutant samples

The use of secondary antibody D for probing the 2D blots improved results. Comparison of mitoplasts from a control culture, C2, and the *SURF1* mutant culture P1, clearly identified the spot corresponding to the COX holo-complex in both samples with very little background signal (figure 61). In addition, signal could be seen to the right of the holo-complex spot at the appropriate molecular weight for MTCO1. This region of the blot corresponded to species that migrated below the holo-complex in the first dimension. This confirmed that the MTCO1 signal migrating below the holo-complex was a specific MTCO1 signal and could be attributed to MTCO1-containing sub-complexes. The intense, non-specific band seen on 1D blots (figure 59) was also detectable on 2D blots (see arrows; figure 61). It produced a spot above the MTCO1 signal and was present on blots probed without primary antibody confirming the non-specific nature of the signal.

12.1.5.4 Signal loss throughout the 2D BN-PAGE/urea-SDS-PAGE protocol

While altering the choice of secondary antibody improved overall signal strength, 2D blots continued to give variable results. It was felt that the preparation of blots could also be improved. In the original adaptation of the protocol devised by Dr Leo Nijtmans, following frozen storage, gel strips were thawed for use and then soaked for 45 minutes in equilibration buffer with 1% β-mercapto-ethanol*. This was followed by two 15 minute washes in equilibration buffer prior to pouring the second dimension gel around the first dimension strip. Whether or not this might reduce signal strength was examined by blotting gel strips at various points throughout the protocol.

It became clear that there was a large loss of MTCO1 signal from the sub-complex signal bands during the soaking (figure 60). Signal was no doubt also lost from the holo-complex band, however, this was undetectable due to the saturation of dark signals. There was no evidence of MTCO1 signal being retained in the first dimension strip after the second dimension had been run. On the blots of thawed gel strips, banding could be seen below the COX holo-complex in the control sample lane. MTCO1 signal could also

* Dr Leo Nijtmans personal communication.

be seen on 2D blots run from these strips. Importantly, this provided the first indication that sub-complexes containing MTCO1 could also be detected in cells with normal maintenance of COX.

On the basis of the result shown in figure 60, the length of time the first dimension gel strips were soaked in equilibration buffer with β-mercapto-ethanol was reduced from 45 minutes to 15 minutes and the subsequent washes from 15 minutes to 5 minutes. Using this protocol, on blots of control samples probed simultaneously with primary antibodies against MTCO1, MTCO2 and COX4I1, three spots corresponding to components of the COX holo-complex could be seen (figure 62). Spots corresponding the MTCO1 sub-complex bands running below the holo-complex were not detectable.

12.1.5.5 Addition of a tertiary antibody layer

2D blots of patient cell samples prepared and run in parallel with control blots gave very weak signals even when MTCO1 signal was detectable on blots of the same first dimension gel (figure 62). The poor quality of the 2D blots was thought to reflect loss of signal during migration in the second dimension. Therefore, the secondary antibody dilution was reduced from 1/2000 to 1/500 and a peroxidase-conjugated anti-HRP tertiary antibody layer was added at 1/500 (secondary A, see figure 58). These adjustments significantly improved results enabling identification of 2D spots corresponding to all MTCO1, MTCO2 and COX4I1 bands seen on 1D blots (figure 68).

12.2 RESULTS FROM OPTIMISED BN-PAGE PROTOCOLS

12.2.1 1D BN-PAGE PAGE

Distinct patterns of MTCO1 signal could be seen on western blots of 8-16% gels of mitoplast samples from the seven patient cultures and controls (figure 63A). Two bands of MTCO1 signal taken to represent different COX sub-complexes were detected in the control samples migrating below the COX holo-complex. Four clearly defined bands of MTCO1 signal running below the COX holo-complex could be seen in all the samples from fibroblasts derived from the *SURF1* mutant cultures P1, P4, P5 and P7. This confirmed the previous work with single samples (figures 58, 59 & 60). The two central sub-complexes of the four seen in the *SURF1* mutant cultures aligned with the two sub-complex bands seen in controls. The same two central sub-complex bands were also faintly visible in the mitoplasts from P3, P6. A slight variation in the intensity of the

individual sub-complex bands was noticeable between mitoplast samples from the different *SURF1* mutant cultures (figure 63A; e.g. compare $P7_1$ & $P1_1$).

Western blots of 8-16% gels of P1-P7 probed with an antibody to COX4I1 revealed the presence of a faint sub-complex band present in the *SURF1* mutant cultures P1, P4, P5 and P7 but not controls nor the other patient mitoplast samples (figure 63B). Again this confirmed the previous work with single *SURF1* mutant samples (figure 59). Further examination of multiple mitoplast preparations from P1, P4, P5 and P7 showed that bands of MTCO1 signal migrating below the holo-complex were a consistent feature of samples from *SURF1* mutant cultures (figure 64A). When signal patterns from different mitoplast preparations from the same *SURF1* mutant culture were compared it was found that banding patterns remained the same for each sample solubilised from a single mitoplast preparation, however different mitoplast preparations from the same cell culture gave slightly different banding patterns (e.g. compare $P7_1$ and $P7_2$ in figures 63A & 64A). Blots of multiple mitoplast samples from P1, P4, P5 and P7 probed with anti-COX4I1 also confirmed that the COX4I1 signal seen migrating below the COX holo-complex was a consistent feature of *SURF1* mutant samples (figures 63B & 64B). The COX4I1 sub-complex was not detectable in any control samples.

12.2.2 High quality results from pairs of *SURF1* mutant and control samples

High quality blots of 8-16% gels enabled the resolution of multiple bands of MTCO1 signal (figure 65) from *SURF1* mutant cultures. To facilitate description of results these were assigned letters *a-g* downwards from the holo-complex. Using this convention band *ab* denotes the two closely migrating, enzymatically active COX holo-complex bands, band *c* is the sharp non-specific band migrating below it and bands *d*, *e*, *f* and *g* migrate close together in the bottom half of 8-16% gels.

When column-purified human MTCO1 was run alongside a mitoplast sample from culture P1, it migrated between bands *f* and *g* (figure 65). This was repeated three times with identical results. The alignment of bands *e* and *f* between patient cell mitoplasts and control cell mitoplasts was also evident from such blots. The band of COX4I1 signal migrating below the COX holo-complex aligned with MTCO1 signal band *d*. No signal aside from band *c* was detectable below the COX holo-complex in blots probed with antibodies against MTCO2, or COX6C. Comparison of blots run in parallel and probed with anti-SDHA and anti-MTCO1 demonstrated that bands *d*, *e*, *f*, and *g* all migrated below complex II and therefore had apparent molecular weights below 130 kDa.

Speculation on the relative abundance of the sub-complexes between mitoplast samples is generally unreliable as the use of bis-Tris in the protein solubilisation buffer prevented the use of protein assays to balance samples. Loading was balanced on the basis of cell counts prior to mitoplast preparation. This is not a particularly accurate mechanism for balancing samples and it is sensitive to factors such as variation in cell size. Nevertheless, using complex II as a marker for inner-membrane protein solubilisation, the blot probed with anti-SDHA in figure 65 indicates that the patient and control samples in this particular set of blots were fairly well matched.

12.2.3 1D BN-PAGE western blots of *SURF1*, *SCO1* and *COX10* mutant samples

The mitochondrial preparations from P7, P8 and P9 used for denaturing gel western blots (figure 20) were also resolved using 8-16% gels (figure 67). Blots of these gels were probed with primary antibodies against MTCO1, MTCO2, COX4I1 and COX5A. The same anti-MTCO1 cross-reacting bands were present in P7 and C2 as seen previously using mitoplast samples (figures 63A, 64A & 65). This verified that the differences in purification of mitoplasts and mitochondria did not significantly affect the results. The same MTCO1 banding pattern was seen in P8, the *SCO1* mutant culture, as in P7 although relative to the holo-complex (band *ab*) the intensity of the sub-complex bands *c-g* was higher in P7. The MTCO1 banding pattern of mitochondria from P9 matched that of control mitochondria although as expected, the intensity of the holo-complex band, *ab*, was lower in P9.

COX4I1 signal in band *d* was present in P7 mitochondria, as had been seen previously using mitoplasts (figures 63B, 64B & 65) and this signal was also detectable in P8. No anti-COX4I1 signal other than bands *ab* and *c* were identified in P9 or control mitochondria. Using an antibody to COX5A, a weak signal aligning with band *d* was detected in P7. Consistent with all previous work and the denaturing gel western blots, no bands other than weak holo-complex (band *ab*) and band *c* signals could be seen in any of the samples on blots probed with anti-MTCO2.

A band which migrated above band *d* could be seen on some P7 blots, including those probed with anti-MTCO2. The very strong cross reactivity of this band in P7 with an anti-COX5B monoclonal antibody which failed to cross-react with the holo-complex in control samples confirmed that this signal band was caused by a non-specific cross reaction and could be disregarded.

12.2.4 Detection of mitochondrial chaperones

P2 and P3 both showed evidence of multiple OXPHOS complex involvement according to clinical data and denaturing gel western blots (figure 17). It was reasoned that this might stem from defective import and/or maturation of nascent mitochondrial proteins. The matrix chaperones HSPD1 and HSPA9B are both involved in these processes and both function as part of protein complexes. It was hypothesised that defects in the handling of nascent mitochondrial proteins might be manifest as altered migration of HSPD1 or HSPA9E complexes.

Very similar results were obtained using the optimised secondary antibody in conjunction with the HSPD1 and HSPA9B primary antibodies (figure 66A & 66B) as had previously been obtained with the original less sensitive secondary antibody (figure 54). In control mitoplast samples run on 8-16% gels, antibody against HSPD1 generated two sharp major bands of signal towards the top of the gel and a fainter, diffuse band towards the bottom (450, 380 and monomer; figure 66A). The two major bands have been noted by others[684] and calculated to have apparent molecular weights of 450 and 380 kDa. The lower of the three bands, (monomer) was only seen on blots using the optimised secondary antibody and was assumed to represent a minor pool of solubilised monomeric HSPD1 which has a molecular weight of 61 kDa. The same pattern of signal was apparent in samples from culture P3. Samples from culture P2 resulted in very low signal although the two upper bands aligned with those of the control samples.

On blots prepared in parallel, anti-HSPA9B yielded a single strong band migrating towards the bottom of the gel (figure 66B). This was assumed to be the 68.3 kDa HSPA9B monomer. Three fainter bands (1-3) migrating above this could also be detected in control samples using the optimised secondary antibody which had not been seen previously (figure 54). Samples from P3 had an identical banding pattern to controls. As with blots probed with anti-HSPD1, P2 gave very low signal on blots probed with anti-HSPA9B, although the major signal band aligned with that of the control sample. As samples were matched on the basis of cell counts, the intensity of the bands relative to the control could not be taken as an indicator of pathology.

Figure 62

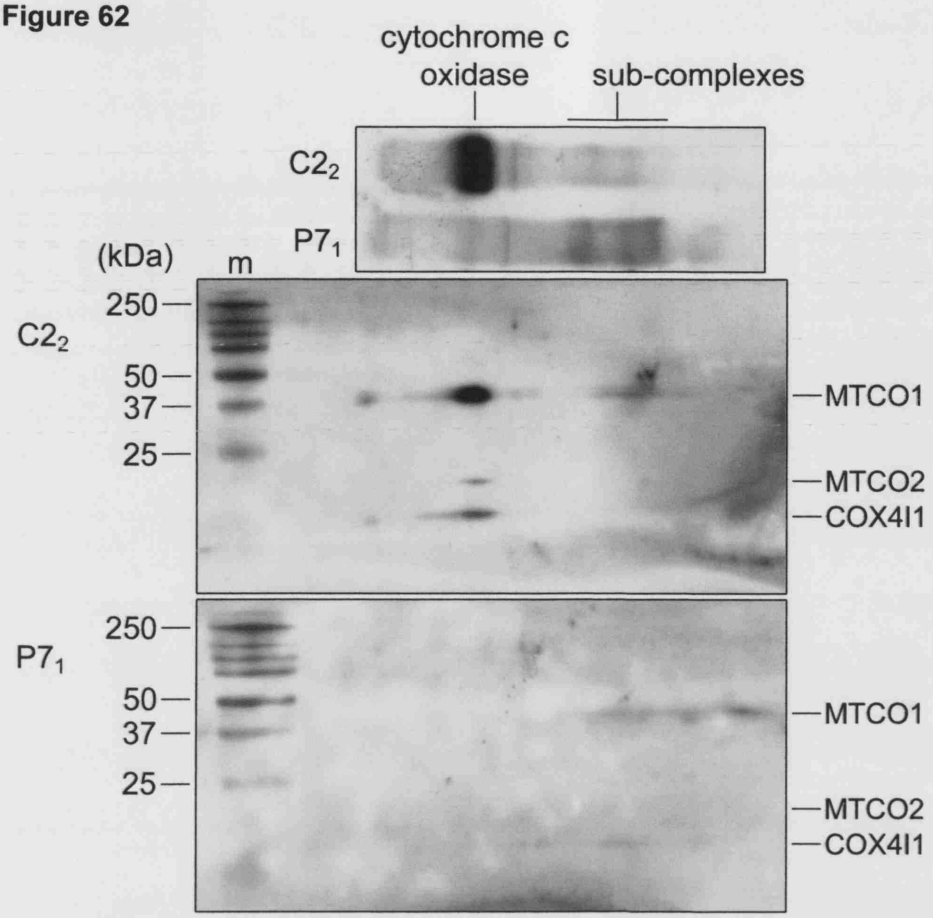

Figure 62 Western blots of a pair of 2D BN-PAGE/urea-SDS PAGE gels (8-16%/12.5%) and a strip cut from a blot of the same first dimension gel. Mitoplast from $2x10^5$ cells were run per lane. The control culture C2 and the patient culture P7 were compared as indicated on the left. Subscript numbering identifies different mitoplast preparations as in figures 63 & 64. 2D blots were probed simultaneously with primary antibodies against MTCO1, MTCO2 and COX4I1. The 1D blot was only probed for MTCO1. The position of the COX monomer and COX sub-complexes are indicated above the 1D blot which has been aligned with the 2D blots. The migration of the COX subunits in the second dimension is shown on the right-hand side of the 2D blots. "m" is a second dimension molecular weight marker with the molecular masses shown to the left in kDa.

Figure 63 Western blots of 8-16% BN-PAGE gels of mitoplast samples from P1-P7 and the controls C1 and C2. Pm is not discussed in this thesis. $2x10^5$ cell equivalents were run per lane. **63A** A blot probed with primary antibody against MTCO1. **63B** A blot probed with primary antibody against COX4I1. The positions of the COX holo-complex monomer and sub-complexes are indicated to the left of each blot. As described in Materials and Methods, mitoplasts from each fibroblast culture were prepared in batches and frozen. Each sample label has a subscript number indicating the identity of the different batches of mitoplasts for that culture. Numbers were assigned arbitrarily and have been used solely to provide a means of tracking individual batches of mitoplasts.

Figure 64 Western blots of 8-16% BN-PAGE gels of mitoplast samples from the *SURF1* mutant fibroblasts P1, P4, P5 and P7 and two samples form the control C1. $2x10^5$ cell equivalents were run per lane. **64A** A blot probed with primary antibody against MTCO1. **64B** An identical blot run in parallel probed with primary antibody against COX4I1. The positions of the COX holo-complex monomer and the sub-complexes are indicated to the left of each blot. As in figure 63, the identity of the different mitoplast preparations from each culture are indicated with subscript numbering.

Figure 63

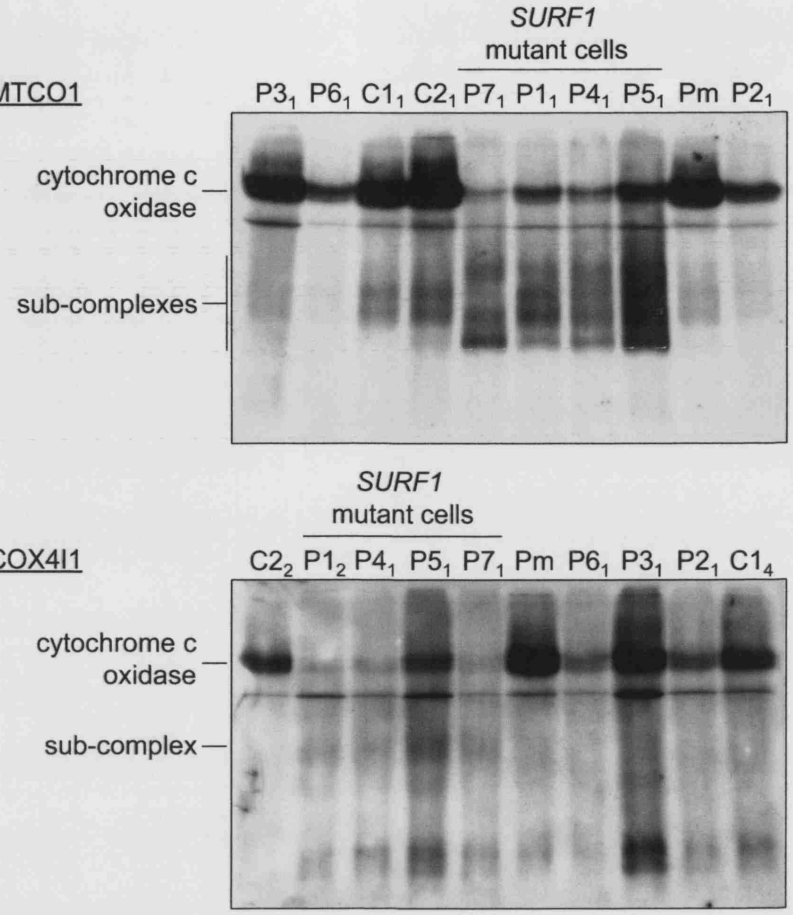

Figure 64

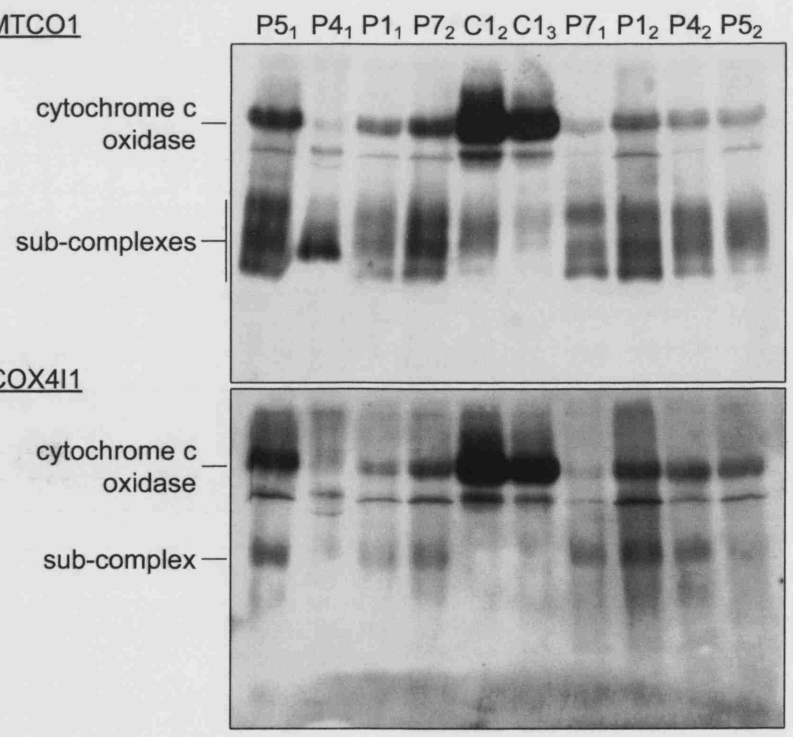

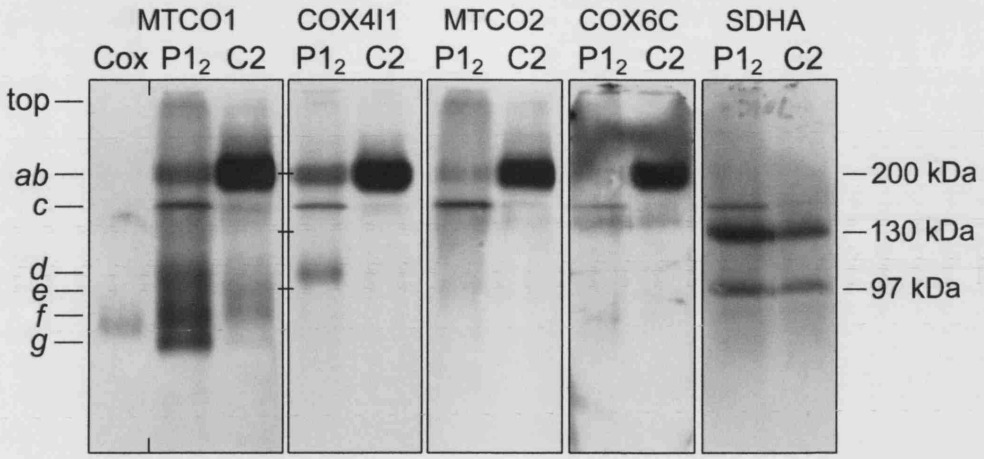

Figure 65 High quality western blots of 8-16% BN-PAGE gels of the *SURF1* mutant culture P1 and the control C2. Mitoplasts from 2x10^5 cells were run per lane. Primary antibody targets are given above each blot. Letters to the left of the figure have been assigned to the bands of anti-MTCO1signal downwards from band *ab* which is the two closely migrating COX holo-complex bands. Band *c* is the non-specific signal seen on previous blots without primary antibody. Bands *d*, *e*, *f* and *g* migrate below these bands. The top of the gel is marked on the left. The apparent molecular weights of the COX holo-complex (200 kDa), complex II (130 kDa) and the putative SDHASDHB dimer (97 kDa) are given on the right. The blot probed with anti-MTCO1 also includes a lane of purified human MTCO1, labelled "Cox". The contrast of the "Cox" lane on the anti-MTCO1 blot (bounded by ticks at the top and bottom) has been enhanced to allow visualisation of the weak signal in this lane. The blots probed with antibodies to COX6C and SDHA were developed using secondary E from figure 59. All images are from a single autorad exposure.

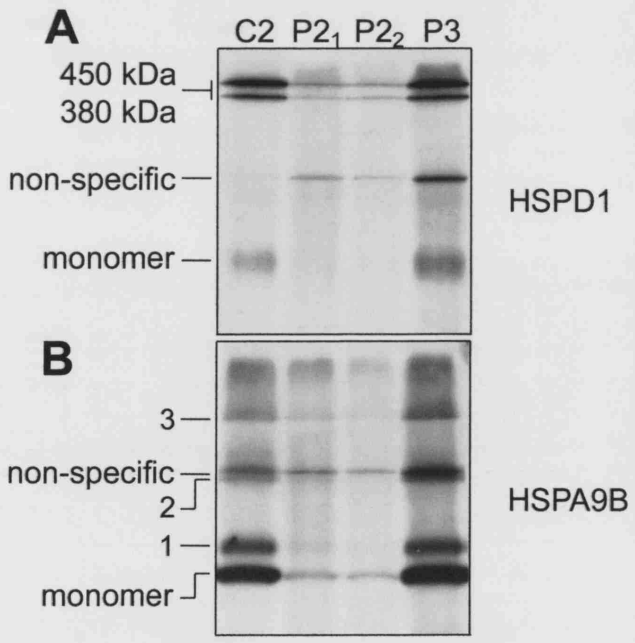

Figure 66 Western blots of 8-16% BN-PAGE gels run with mitoplasts from P2, P3 and the control C2. 2x10^5 cell equivalents were run per lane. Subscript numbering in samples codes identifies different mitoplast preparations as in figures 63 & 64. **66A** A blot probed with a anti-HSPD1. The apparent molecular weights of the two major bands are indicated to the left of the image. A third diffuse band assumed to be free monomeric HSPD1 (61 kDa) is also indicated. **66B** A blot probed with a anti-HSPA9B. The position of the assumed HSPA9B monomer (68.3 kDa) and three slower migrating bands (1-3) are marked on the left of the image. Non-specific cross-reaction of the secondary antibody is indicated on the left of both images.

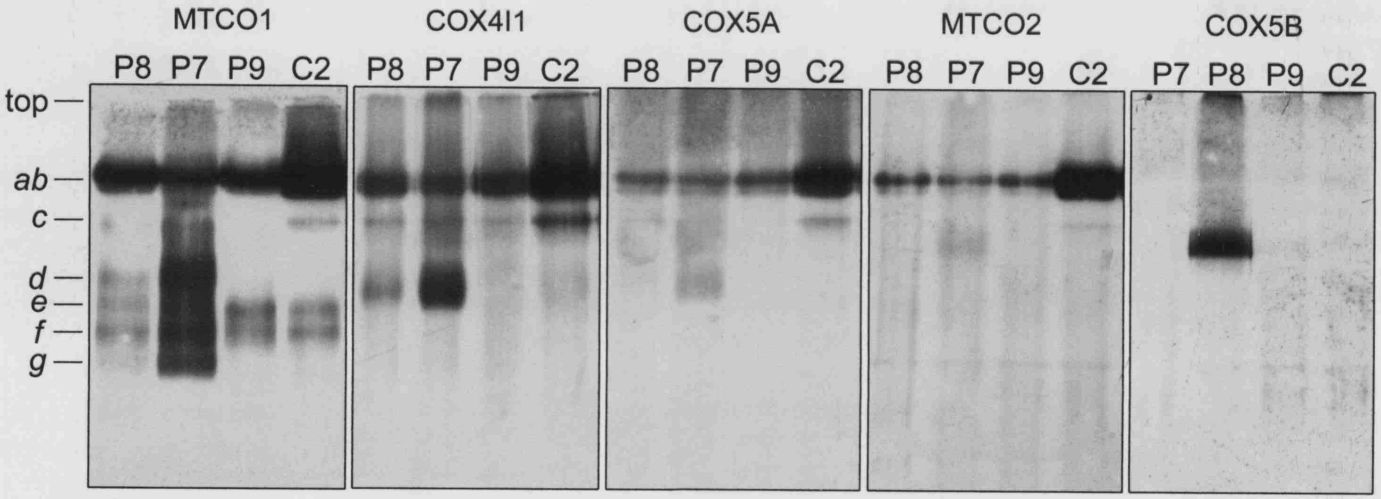

Figure 67 Western blots of 8-16% BN-PAGE gels of mitochondria from the *SURF1* mutant culture P7, the *SCO1* mutant culture P8, the *COX10* mutant culture P9 and the normal control C2. Loading was balanced as in figure 20 but the equivalent of 7.5 µg of C2 protein was loaded per lane. Primary antibody targets are given above each blot. The strong anti-COX5A signal band in P7 aligns with a signal seen on the other P7 blots but not the holo-complex in the C2 indicating this band is a non-specific signal. The top of the gel is indicated on the left of the image along with letters assigned to the various MTCO1 signal bands as in figure 65.

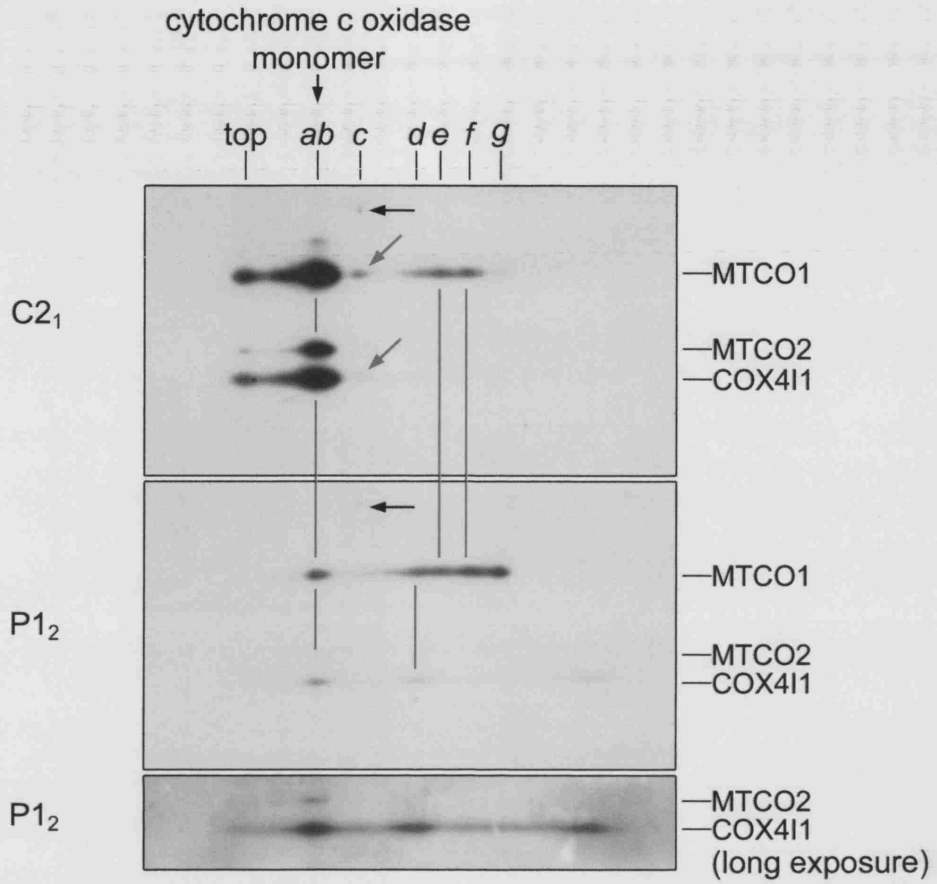

Figure 68 Western blots of 2D BN-PAGE/urea-SDS-PAGE gels (8-16%/12.5%). Mitoplasts from $2x10^5$ cells were run per lane. A control sample C2 and the patient sample P1 were compared. Mitoplasts from $2x10^5$ cells were run on each gel. Blots were probed simultaneously with primary antibodies against MTCO1, MTCO2 and COX4I1 and the positions of the primary antibody signals are marked on the right. The positions of spots corresponding to the six bands of MTCO1 signal (*ab-g*) are marked across the top of the image as in figure 65. Black horizontal arrows indicate the position of the non-specific component of band *c* in on each blot. Blue diagonal arrows on the control blot mark the specific MTCO1 and COX4I1 components of band *c*. The upper two panels are scanned from a single autorad exposure. To allow visualisation of the P1 MTCO2 and COX4I1 signals an additional strip is shown at the bottom of the figure which has been scanned from a longer exposure. Alignments of the various signal spots between the control blot and the patient blot, and the two exposures of the patient blot are shown in red. Blots were developed using a tertiary PAP antibody as described in the text.

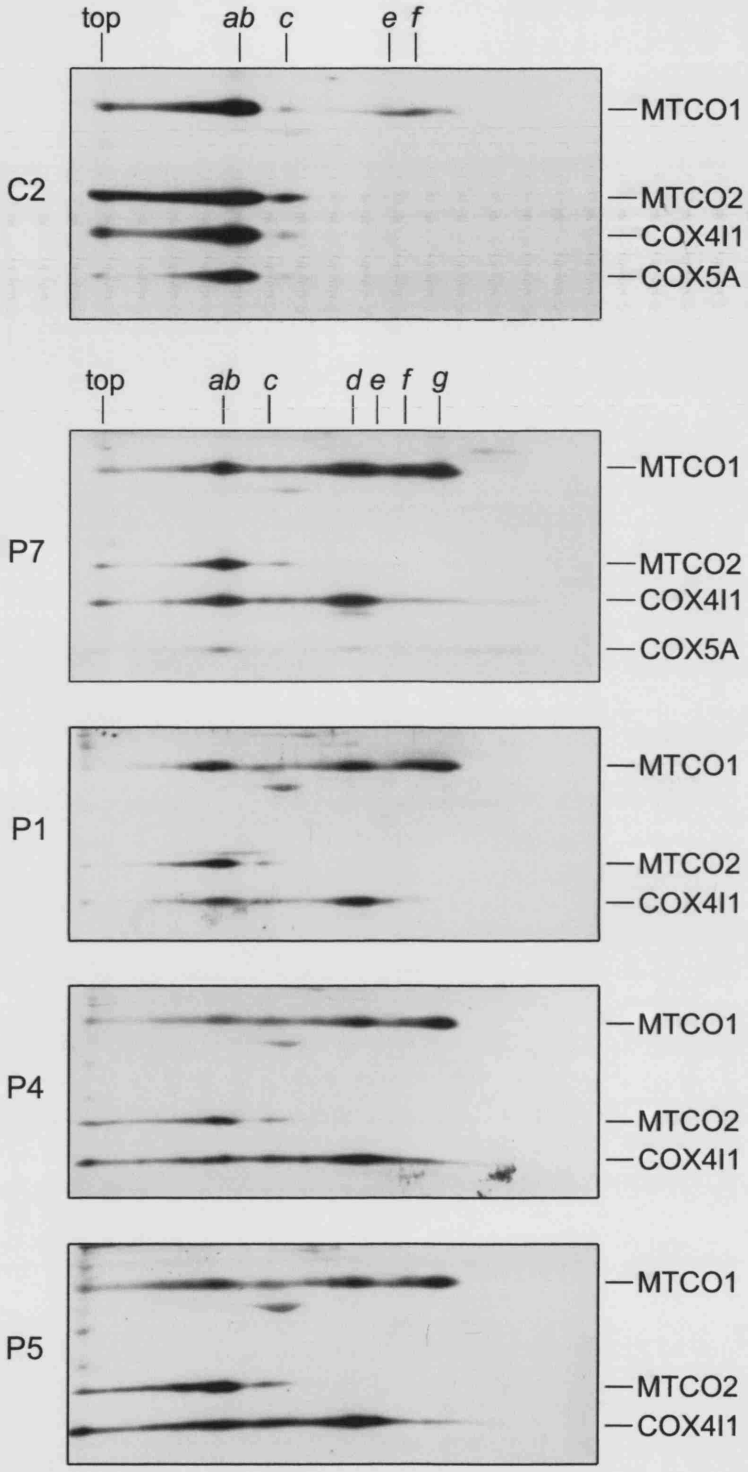

Figure 69 Western blots 2D BN-PAGE/ urea-SDS-PAGE gels (8-16%/13.5%) of mitochondria from the *SURF1* mutant cultures P7, P1, P4 and P5. 50 µg of mitochondrial protein was loaded per lane. Sample names are given to the left of each blot and antibody targets aligned with the appropriate signals are given on the right. The top of the first dimension gel is indicated above the C2 and P7 blots. Letters across the top of these blots correspond to the MTCO1 signal bands as used in previous figures (figure 65). The C2 and P7 blots are the same as those shown in figure 70.

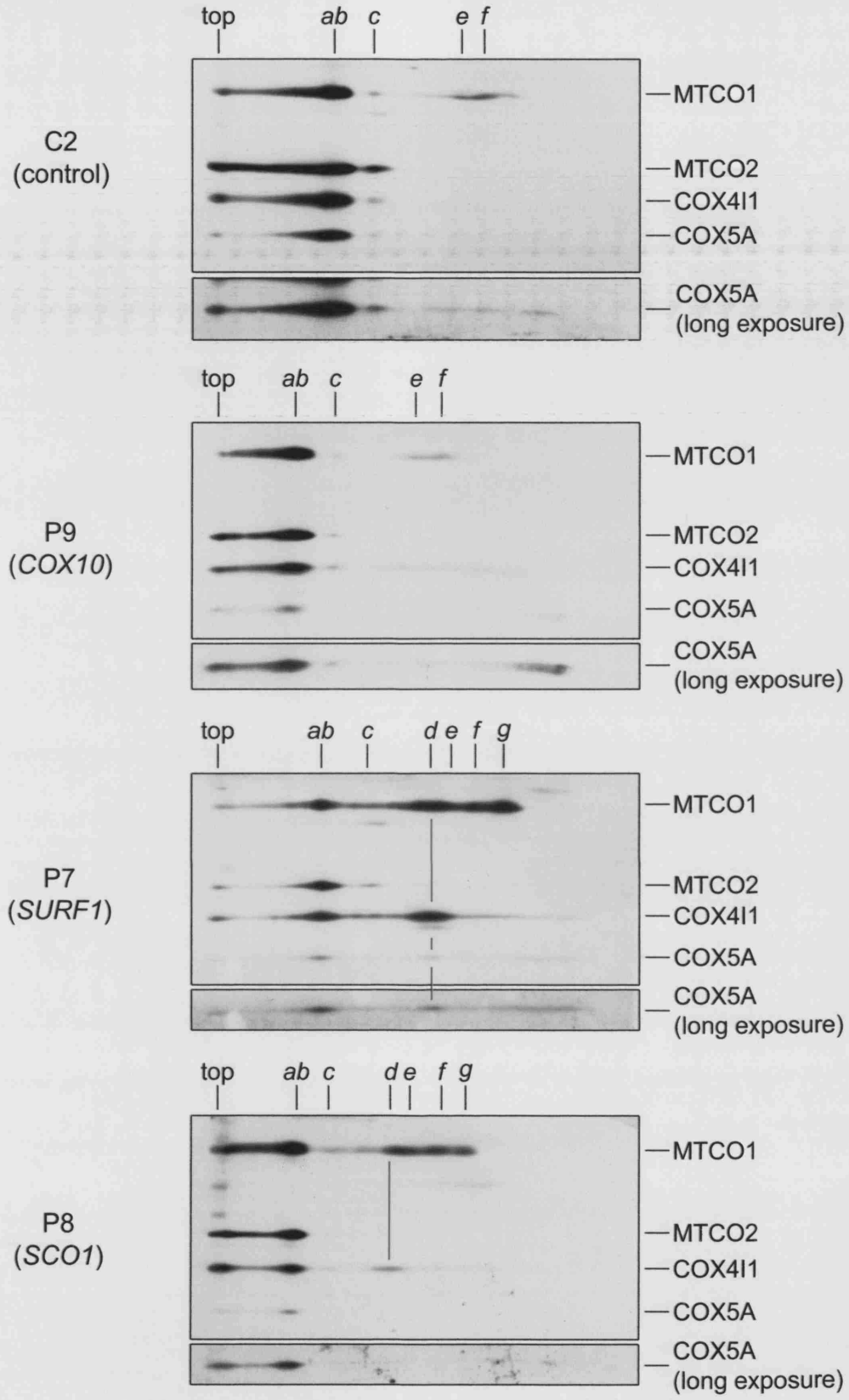

Figure 70 Western blots of 2D BN-PAGE/urea-SDS-PAGE gels (8-16%/13.5%) of mitochondria from P7, P8, P9 and C2 probed with antibodies against COX subunits. 50 µg of mitochondrial protein was loaded per lane. Sample names are given to the left of each blot with mutant genes in parenthesis underneath. The C2 and P7 blots are the same as those shown in figure 69. Antibody signals are indicated on the right of each blot aligned with the appropriate signals and the top of the first dimension gel is indicated above each blot. Letters across the top of each blot correspond to the MTCO1 signal band terminology used previously (figure 65). Alignments of spot *d* are indicated with red lines on the P7 and P8 blots. Longer exposures of each blot are shown below to enable visualisation of the COX5A signal.

12.2.5 Triple-layer development of 2D BN-PAGE/urea-SDS PAGE blots

Blots developed using the triple-layer antibody protocol described above (12.1.5.5) enabled resolution of spots corresponding to all MTCO1 and COX4I1 bands detected using the 1D protocol. In the control sample in the pair of blots shown in figure 68, two spots corresponding to bands *e* and *f* can be seen confirming that both bands represented specific cross-reaction of the MTCO1 antibody. Alignment of the spots corresponding to band *ab*, the COX holo-complex, between the patient and control blots confirmed that bands *e* and *f* were also aligned in *SURF1* mutant and control samples. In addition, the MTCO1 and COX4I1 signals corresponding to band *d* in the *SURF1* mutant samples were also aligned. This indicated that both subunits probably form part of the same sub-complex. No spots corresponding to band *d* were present on the control blot. Low MTCO2 signal on both blots meant that determination of its inclusion in complexes other than band *ab* was unreliable.

Close examination of the blots enabled further determination of the identity of band *c*. Signal in band *c* had already been shown to include a strong non-specific component as it was present on blots probed without primary antibody (figures 54, 55 & 57-59). On the pair of blots shown in figure 68 the same spot migrating above the MTCO1 signal is also visible (see arrows). However, on the control blot a primary antibody-specific signal migrating in line with band *c* could also be seen indicating that band *c* also contained a specific component.

12.2.6 2D Analysis of mitochondria from all *SURF1* mutant cultures

Mitochondria purified from all four *SURF1* mutant cultures (P1, P4, P5 and P7) were resolved using 2D BN-PAGE/urea-SDS-PAGE. Mitochondria were balanced by Dr Taanman according to the SDHA signal on denaturing gel western blots. The higher loading possible using mitochondria improved the signals for all spots compared to previous 2D blots of mitoplasts (compare figures 68 & 69). Alignment of blots probed with antibodies against MTCO1, MTCO2 and COX4I1 yielded very similar patterns of COX sub-complexes in each sample, strengthening the finding that COX sub-complexes are a consistent feature of *SURF1* mutant cells (figure 69). These blots also confirmed that the COX5A signal identified in 1D blots of P7 (figure 67) aligned with the MTCO1 and COX4I1 band *d* spots implying that sub-complex *d* is composed of at least MTCO1•COX4•COX5A. The improved signal strength in these samples also verified the

earlier finding that band *c* contained specific components in addition to the non-specific components seen on 1D blots. On control blots, signal spots from all antibodies aligned with band *c* and signal could also be seen corresponding to MTCO2 in the patient samples. It is assumed that MTCO1 and COX4I1 band *c* spots were masked by smearing in the patient samples.

12.2.7 Comparison of 2D blots of mitochondria from *SURF1*, *SCO1* and *COX10* mutant fibroblasts

2D BN-PAGE/urea-SDS-PAGE western blots were used to confirm the alignment of the bands identified on 1D blots of the disease controls P8 and P9, P7 and a normal control (C2). Blots were simultaneously probed with a cocktail of primary antibodies against MTCO1, MTCO2, COX4I1 and COX5A (figure 70). The spot pattern of the P8 blot matched that of P7, although the intensity of the sub-complex spots was less in P8, in line with the 1D blots (compare figures 70 & 66). Spots of MTCO1 signal could be matched to bands *e-g* seen on 1D blots. As with the *SURF1* mutant samples, a COX4I1 spot aligned with the MTCO1 band *d* spot in P8. No COX5A spot aligning with band *d* could be detected in the P8 sample; however, this would be expected given the low signal strength from the COX5A antibody in general and the low abundance of band *d* in P8 compared to P7 (see COX4I1 signal; figure 70). The spot pattern of P9 matched that of the control mitochondria except that all signals were weaker, in agreement with the 1D blots (figure 67).

12.3 Summary of COX sub-complex abundance, distribution and composition

From a large number of 1D and 2D blots comparing at least one sample from one of the *SURF1* mutant cultures and controls it was surmised that under the solubilisation conditions used, MTCO1 signal bands *d* and *g* were a consistent feature of *SURF1* mutant samples and were not detectable in control samples (n=10*). Two bands, *e* and *f*, were consistently detected in both *SURF1* mutant samples and control samples (n=10). In addition, a band of COX4I1 signal was consistently seen migrating below bands *ab* and *c* in *SURF1* mutant samples (n=6). This band aligned with MTCO1 signal band *d* and was not detectable in controls (n=6). COX5A signal was also detectable on 1D and

* n values correspond to numbers of individual blots of n>1 samples as opposed to total number of samples compared. Values correspond to images shown in this thesis and repeat data not included.

2D blots of purified mitochondria which aligned with band *d* (n=2). No signal other than bands *ab* and *c* was detectable on blots of *SURF1* mutant or control samples probed with antibodies against MTCO2 (n=4) or COX6C (n=3). Assuming that alignment of subunit signals reflects association of constituent subunits as sub-complexes, this data suggests that complexes *ab* (the holo-complex) and sub-complex *c* are composed of all subunits screened, sub-complex *d* is composed of at least MTCO1, COX4I1 and COX5A but not MTCO2 and sub-complexes *e*, *f* and *g* contain at least MTCO1 but not MTCO2, COX4I1 or COX5A. The same sub-complexes as consistently seen in *SURF1* mutant samples were also present in mitochondria from *SCO1* mutant cells although band *ab* was more abundant than bands *d*, *e*, *f* and *g* in the *SCO1* mutant samples (P8; n=2). Only the sub-complexes present in control samples were present in *COX10* mutant samples (P9; n=2), P2 (n=2), P3 (n=2) and P6 (n=2). These data are summarised in table 21.

Table 21 Summary of the relative abundance of MTCO1 signal bands within each sample and minimum components of each signal band according to western blotting. Where known, mutant genes are given in parenthesis under sample names. Figure numbers of figures showing supporting evidence from 1D and 2D blots are listed at the bottom of each column.

	Culture name and genotype if known					Minimum components of sub-complexes according to western blots					
Signal band	Controls	P1, P4, P5, P7 (*SURF1*)	P8 (*SCO1*)	P9 (*COX10*)	P2, P3, P6 unknown	MTCO1	MTCO2	COX4	COX5A	COX6C	Non-specific
a	++	+	+	+	+	●	●	●	●	●	○
b	++	+	+	+	+	●	●	●	●	●	○
c[a]	+	-	-	-	nd	●	●	●	●	nd	●
d		++	+			●	○	●	●	○	○
e	+	++	+	+	-	●	○	○	○	○	○
f	+	++	+	+	-	●	○	○	○	○	○
g		++	+			●	○	○	○	○	○
Evidence from 1D gels	63A, 64A, 65, 66	63A, 64A, 65, 66	66	66	63A	63A, 63B, 64A, 64B, 65, 66					
Evidence from 2D gels	68, 69, 70	68, 69, 70	70	70	nd	68, 69, 70					

Key: Relative abundance, ++= high abundance, += intermediate abundance, -= low abundance, blank cell= band never present, nd= no data. [a] band *c* abundance determined according to MTCO2 signal on 2D blots as non-specific signal co migrated on 1D blots and smearing of MTCO1 signal prevented clear identification on 2D blots. Constituent signals, ●= signal present; ○= signal not present, nd = no data because band *c* could only be detected on 2D blots.

DISCUSSION

PREFACE

Given the dual genetic origin of COX, one of the primary objectives of this study was to determine whether mtDNA was involved in the pathophysiology of the patient fibroblast cultures. A variety of approaches were used to determine that mtDNA could be excluded from the pathophysiology of all of the cultures and the results are discussed in Section 13. Section 14 covers the discovery of mutations in *SURF1* in four of the seven cultures. The *SURF1* mutant fibroblast cultures provided defined genetic models of COX deficiency and their phenotype is carefully examined in Section 15. BN-PAGE was used to examine the presence of COX sub-complexes in the *SURF1* mutant cells. The composition and potential origins of the sub-complexes identified are discussed in Section 16. The overall findings of this study in terms of COX biogenesis and possible functions for SURF1 are covered in Section 17 and the pathophysiology and possible future work on P2, P3 and P6 in which no mutations were found, are discussed in Section 18.

13 ANALYSIS OF MTDNA IN PATIENT-DERIVED PRIMARY DERMAL FIBROBLAST CULTURES

13.1 ANALYSIS OF MTDNA IN PRIMARY DERMAL FIBROBLASTS DERIVED FROM PATIENTS WITH LEIGH'S SYNDROME (P1, P3, P4, P5 & P7)

Although no clinical data was used in the selection of cell cultures for inclusion in this study, P1, P3, P4, P5 and P7 were all derived from patients diagnosed with either Leigh's syndrome or Leigh's-like disease according to the criteria set out by Rahman *et al*[638]. The link between mtDNA mutations and neuromuscular disorders has been apparent since the late 1980's[698] yet at the outset of this project little epidemiological information was available about the incidence of mtDNA lesions or their occurrence in

Leigh's syndrome. No pathological mtDNA lesions were found in any of the fibroblast cultures studied. Aside from the fact that mutations in *SURF1* were identified in P1, P4, P5 and P7, the lack of mtDNA lesions in the cultures derived from patients with Leigh's syndrome is in keeping with the clinical presentations of patients 1, 3, 4, 5 and 7 and the molecular phenotypes of the fibroblast cultures themselves. Arguments in support of this are set out below.

13.1.1 Incidence of mtDNA lesions among Leigh's syndrome patients in relation to the design of this project

It has become clear over the last five years that the most common classes of mtDNA lesion associated with Leigh's syndrome are point mutations in *MTATP6*, followed by point mutations in *MTTK*[638,639,651] (6.2.2.3). The fibroblast cultures described in this thesis were selected for study on the basis of expression of a COX deficiency in culture. Mutations in *MTTK* can cause COX deficiency[103,699-701] and high mutant loads of mt-tRNA mutations, including *MTTK*, can be found in dermal fibroblasts[103,700,701] (vis. the disease control MELAS cultures used in this study). Conversely, while a few rare cases of COX deficiency in muscle have been attributed to 8993T-G in *MTATP6*[651], this mutation is not generally considered a cause of COX deficiency[488,577,578,702], particularly in cultured fibroblasts[702]. It was therefore, extremely unlikely that mutations in *MTATP6* would be present in any of the cultures described in this thesis. Consequently, the design of this study restricted the analysis of mtDNA to screens for classes of mtDNA lesions that are now known to be extremely rare causes of Leigh's syndrome.

13.1.2 The absence of mtDNA lesions in P1, P3, P4, P5 and P7 is consistent with a clinical presentation of Leigh's syndrome

Of the 80 or so mtDNA point mutations in mt-tRNA genes that have been described[573], only five have been associated with Leigh's syndrome or a Leigh's-like disease; 1644G-T (*MTTV*)[703], 3243A-G (*MTTL1*)[648], 5537insT (*MTTW*)[704,705], 8344A-G (*MTTK*)[649,650] and 8363G-A (*MTTK*)[706]. Of these, 8344A-G is most commonly associated with Leigh's syndrome as demonstrated by its appearance in epidemiological studies (6.2.2.3). The other mt-tRNA mutations are either much rarer or far less frequently associated with Leigh's syndrome. Furthermore, although 5537insT[704] and 8363G-A[706] have been documented as causing Leigh's syndrome in infants, in common with most mtDNA-associated disorders, Leigh's syndrome due to mt-tRNA mutations tends to present later in childhood[650,705] or in adulthood[703]. In contrast, patients 1, 3, 4, 5 and 7 all presented

with neurological signs before 2 years of age. Deletions in mtDNA[640] and mtDNA depletion[639,707,708] are also very rare causes of Leigh's syndrome. The disease in such patients tends to be associated with features not commonly seen in Leigh's syndrome[638] such as Pearson's syndrome[709-711] and congenital cataracts[712].

Mutations in *MTCO1*, *MTCO2* or *MTCO3*[573,610,615,616] are also extremely rare[578] (table 6). As with other mtDNA lesions, patients with mutations in *MTCO1*, *MTCO2* or *MTCO3* rarely present with Leigh's syndrome or Leigh's-like disease[573]. A single case of Leigh's-like disease has been attributed to a mutation in a mtDNA-encoded COX subunit gene[619*] and like the majority of *MTCO1*, *MTCO2* or *MTCO3* mutations, the mutation in this patient was determined as being sporadic[573]. In contrast, patients 1, 3 and 4 were from families with affected siblings. Thus the absence of mt-tRNA mutations, mutations in *MTCO1*, *MTCO2* or *MTCO3*, mtDNA deletions or mtDNA depletion in P1, P3, P4, P5 and P7 is entirely consistent with the rarity of such lesions among patients that present with Leigh's syndrome.

13.1.3 The OXPHOS subunit signature of P3 is consistent with disruption of mitochondrial protein synthesis but the involvement of mtDNA can be discounted

The involvement of multiple OXPHOS defects in the pathophysiology of Leigh's syndrome is not uncommon[639] (6.2.2). Biochemistry of muscle from patient 3 identified defects in complexes I, II, III and COX. Biochemistry of P3 confirmed the COX defect but found normal II+III activity[†]. P3 had an OXPHOS subunit signature that was distinct from the other fibroblast cultures derived from Leigh's syndrome patients in that the abundance of subunits from complexes I, III and COX were affected, while subunits from complexes II and V-F_1-portion were unaffected (table 15). Complexes I, III and COX all require proteins encoded by mtDNA for stable assembly and maintenance of normal subunit levels. In contrast, complexes II[180,713] and V-F_1-portion[179,714,715] which do not contain mtDNA-encoded subunits, assemble normally in the absence of mtDNA and subunits are maintained at normal levels. Therefore, the subunit signature of P3 was consistent with a defect of mitochondrial gene expression. Northern blots of *MTCO1* and *MTCO2* mRNA, and the *MTRNR1* and *MTRNR2* rRNAs, did not indicate that mitochondrial transcription was affected in P3, implying that mitochondrial translation may be affected. Similar patterns of OXPHOS complex involvement to that seen in P3

---

* 9537insC in *MTCO3* causing P111X.
† succinate-cytochrome c oxidoreductase activity.

have been noted in skeletal muscle of patients with confirmed defects in mitochondrial translation[716]. A defect in mitochondrial translation in P3 is strongly supported by the fact that an almost identical subunit signature was seen in the disease control MELAS culture which carried a high mutant load of the 3243A-G, *MTTL1* mt-tRNA mutation. mt-tRNA mutations are generally accepted as causing pathology due to the disruption of mitochondrial protein synthesis, although the mechanisms of translation inhibition and associated pathogenesis differ between various mt-tRNA mutations[603,717,718]. The same impact on mitochondrial protein synthesis is also true of large mitochondrial deletions[719,720] which invariably remove mt-tRNA genes and mtDNA depletion, as once a threshold level of mtDNA loss is reached, global effects on steady-state levels of mtDNA-encoded proteins are seen[180,670]. mt-tRNA sequencing and Southern blotting discounted the presence of mt-tRNA mutations, mtDNA deletions and mtDNA depletion in P3.

Mutations in the mitochondrial rRNA genes are also potential candidates for disruption of mitochondrial protein synthesis. Mutations in *MTRNR1* have been associated with amino-glycoside induced deafness[721,722] and mutations in both *MTRNR1* and *MTRNR2* have been associated with cardiomyopathy[723], although there are some questions regarding this association[604]. In agreement with the rarity of mtDNA lesions in Leigh's syndrome, no mutations in mt-rRNA genes have ever been identified in Leigh's syndrome patients[573]. Small regions of *MTRNR1* and *MTRNR2* were sequenced in P3 and no mutations were found. The size and abundance of mitochondrial rRNAs was normal in P3 on northern blots suggesting that there were no defect in processing or stability of mt-rRNAs. Although it is accepted that genetic background and can influence the pathogenicity of mtDNA lesions, strong evidence that mtDNA was normal in P3 comes from the A549 ρ^0 whole cell fusions which demonstrated that P3 mtDNA did not convey a COX defect. This is supported by the fact that the mosaic COX activity and MTCO1 staining patterns seen in the MELAS fibroblasts and often indicative of heteroplasmic mtDNA lesions[78,700] or mtDNA depletion[670], was also absent from P3.

Therefore, while the subunit signature of P3 is indicative of a defect in mitochondrial protein synthesis, and such defects can be caused by a variety of mtDNA lesions, the involvement of mtDNA in the pathophysiology of P3 can be discounted. A more detailed analysis of the wider phenotype of P3 and the speculation on candidate disease mechanisms is given below (18.3).

13.1.4 The involvement of mtDNA can be discounted in the pathophysiology of P1, P4, P5 and P7

P1, P4, P5, and P7 had isolated defects in the maintenance of steady-state COX subunit levels (table 15). This subunit signature is inconsistent with any mechanisms which impact globally on mitochondrial protein synthesis reflecting the absence of mt-tRNA mutations (not sequenced in P7), mtDNA deletions and mtDNA depletion in these cells.

Cybrids, cells or tissues with a high mutant load of mutations in *MTCO1*, *MTCO2* or *MTCO3* do have an isolated reduction in COX activity[481,609,610,612-614,618-620] and reduced abundance of COX subunits[481,609,613,614,618,619] (tables 4 & 17). Although mechanistically the presence of rare mutations in these genes may have been a candidate mechanism for the subunit signatures seen in P1, P4, P5 and P7, the choice of dermal fibroblasts as models for this study meant that such mutations were unlikely to be present. Like many mtDNA lesions, *MTCO1*, *MTCO2* or *MTCO3* mutations often have a restricted tissue distribution[611,614,616,618,618,620]. Fibroblasts from patients with pathogenic 6721T-C[611*], 7671T-A[614†] or 9487del15[618‡] mutations did not have detectable levels of mutant mtDNA, although high levels of 7587T-C[613§] and 9537insC[619**] have been found in fibroblasts. As the fibroblasts selected for this study expressed a COX defect in culture, classes of mtDNA mutation that are not commonly present in the dermal fibroblasts of carriers were also unlikley to be represented among the cohort of cultures selected for study. The absence of *MTCO1*, *MTCO2* and *MTCO3* mutations in P1, P4, P5 and P7 was confirmed by mtDNA sequencing and additionally in P1, P4 and P5 by whole cell fusion with ρ^0 A549 cells. Following the exclusion of the mitochondrial genome in the pathophysiology of P1, P4, P5 and P7 mutations were identified in the nuclear gene *SURF1* in each of the cultures. Analysis of the *SURF1* genotypes and phenotypes of these cells are given below (14;15).

13.1.4.1 The novel base change 15936A-T in P4 is not pathological

A novel base change, 15936A-T in *MTTT* was identified in P4. A number of factors indicated that 15936A-T was not a pathogenic base change. Most obviously, as mentioned above, the clinical presentation of patient 4 and the phenotype of P4 were

---

* *MTCO1*, M273T.
† *MTCO2*, M29K.
‡ *MTCO3*, F95-Δ5.
§ *MTCO2*, M1T.
** *MTCO3*, P111X.

inconsistent with the presence of a pathological mt-tRNA mutation. Aside from this, other data also supports this opinion. Firstly, in agreement with the identification of polymorphisms in three of the five *MTTT* sequences examined here, analysis of sequence variation among human mt-tRNA sequences has shown that *MTTT* contains the highest number of polymorphisms among human mt-tRNAs[699,724]. This implies that mt-tRNA^{Thr} structure is relatively tolerant of sequence alteration and that variation in this region is likely to be non-pathological. The proximity of *MTTT* to the D-loop region, which is the most variable region of mtDNA[78,81], may influence the observed variability. Visual inspection of the *MTTT* sequencing gel suggested 15936A-T was probably homozygous. In contrast, all pathogenic mt-tRNA mutations have been heterozygous albeit with high mutant loads in affected tissues[573]. Alignment of human mt-tRNA^{Thr} sequence to a mammalian consensus map[725] places 15936A-T at position 51 in the centre of the ascending arm of the T-loop stem. Consensus maps of sequence variation within human mt-tRNA structure have revealed that the position of naturally occurring mutations and polymorphisms is random and that it is not possible to predict the pathogenicity of a mutation based on its structural position[724]. There is however, better correlation between the distribution of mutations when compared to evolutionarily conserved nucleotides within each of the 22 mt-tRNA families and 70% of mitochondrial tRNA mutations affect evolutionarily conserved nucleotides[724]. The T-loop stem of mt-tRNA^{Thr} is poorly conserved[725], suggesting that base changes in this region are unlikely to be pathogenic.

13.2 ANALYSIS OF MTDNA IN PRIMARY DERMAL FIBROBLAST CULTURES DERIVED FROM PATIENTS WITHOUT LEIGH'S SYNDROME (P2 & P6)

13.2.1 P2

Mitochondrial dysfunction due to mtDNA lesions is very rare in infants and the very early onset of the disease in patient 2 provided the first indicator that mtDNA lesions were unlikley to be involved in the pathophysiology of P2[573,575] (6.2.2.1). Also, as mentioned above, because complexes II[180,713] and V-F_1-portion[179,714,715] can assemble in the absence of mtDNA, low levels of SDHA, SDHB and ATP5A1, as seen in P2, are not considered markers for the involvement of mtDNA in pathology. The western blotting data is supported by clinical biochemistry which identified low COX and complex II+III activities in P2. In addition, the same OXPHOS defects were noted in muscle, along with defects in activities of complex I, PDH and components of the β-oxidation pathway. Such a wide spectrum of biochemical abnormalities is not generally seen in patients with

mtDNA lesions. The absence of mt-tRNA mutations, mtDNA deletions and mtDNA depletion were all confirmed directly in P2 as in the other cultures. More general evidence that mtDNA was not involved in the pathophysiology of P2 was provided by whole cell fusions and the absence of mosaic COX activity or MTCO1 staining. A more detailed analysis of the wider phenotype of P2 and the speculation on candidate disease mechanisms is given below (18.2).

Four novel base changes were found in P2 mtDNA. Two were synonymous polymorphisms in protein coding genes, one was a missense mutation in an intergenic region, discussed below (13.2.1.1), and the other was a missense mutation in *MTCO1*, also discussed below (13.2.1.2). P2 was derived from a patient of Asian origin. The high number of novel base changes identified in these cells most probably reflects the under-representation of Asian mtDNA sequence data in databases such as MITOMAP which was used as a standard reference for this study. This probably also accounts for the inability to haplotype P2 mtDNA from the sequencing data generated here.

13.2.1.1 5894A-G in the intergenic region between MTTY and MTCO1 is a non-pathological polymorphism

The transition 5894A-G was identified in the intergenic region between *MTTY* and *MTCO1* in P2. During transcript processing this region is cleaved from the 3' end of RNA 6 generating RNA 9, the *MTCO1* mRNA[143,726]. Northern analysis did not indicate problems with the cleavage of RNA 6. A polymorphic $[C]_{12}$ insertion at 5895 has been noted in the Finnish population[727] and 17.6% of pygmies from the Central African Republic[728], hence 5894A-G is very unlikley to be pathogenic.

13.2.1.2 6582G-A in MTCO1 is a non-pathological polymorphism

The base change 6582G-A was identified in *MTCO1* of P2. The base change appeared to be homozygous, providing the first evidence it was unlikely to be pathogenic, although the detection limit of the of the RFLP protocol used was not determined. 6852G-A leads to the amino acid substitution G317S. Ser317 lies between Thr316 and Lys319 which are essential components of the K-channel, required for proton pumping and the transfer of consumed protons during O_2 reduction[44,58,60,729,730] (2.3; table 3A). Missense mutations altering essential K-channel residues in *Rh. sphaeroides* have been shown to reduce enzyme turnover to varying degrees[64,730]. However, the involvement of G317S the pathology of P2 can be ruled out by the presence of 6582G-A in P2-A549 which stained normally for COX activity. As the COX activity stain used to determine the status of

synkaryons does not necessarily require proton pumping activity and specific mutations can cause proton pumping to become uncoupled from electron transport[730], it could be argued that effects of the polymorphism on proton pumping and putative secondary effects on mitochondrial biogenesis were overlooked. However, the presence of this polymorphism in synkaryons with normal COX activity which had been grown for 77 days* demonstrates that even indirectly, G317S does not affect COX biogenesis and implies that maintenance of $\Delta\psi$ must be normal in these cells. This non-pathological nature of this mutation was confirmed by collaboration with Dr Brigitte Meunier who kindly created a yeast model of G317S. Resulting strains had normal growth rates, normal cytochrome c and COX content, normal CN and CO binding, normal haem a_3 environments and normal COX activity[668].

13.2.2 P6

The subunit signature of P6 indicated the involvement of complex III and COX but not complex II and therefore appeared similar to that of P3 and the MELAS culture, in which defect of mitochondrial protein synthesis can be inferred. This is contradicted by the biochemistry carried out by two external laboratories on P6 and patient 6 muscle homogenate which suggested an isolated COX defect (table 8). Moreover, there was no evidence of reduced abundance of *b*- or *c*-type cytochromes in P6 as might be expected with low abundance of complex III. This suggests that the UQCRC2 western blot may not be accurate. As discussed above, a cellular phenotype of reduced mitochondrial gene expression is a reasonable indicator for mtDNA involvement (13.1.3), whereas an isolated COX deficiency is less so (13.1.4). Therefore, the conflicting evidence regarding the OXPHOS involvement in P6 was little help in identifying a genetic origin for the COX defect although the neonatal presentation of patient 6 suggested that mtDNA involvement was unlikely[573,575] (6.2.2.1).

Little mtDNA analysis was carried out on P6. In common with P1-P5, ρ^0 cell fusions strongly indicated that P6 mtDNA did not confer the COX defect present in the parent culture. Again this was supported by the uniform COX activity and MTCO1 stains. Therefore, it is reasonable to assert that from the evidence available, the pathophysiology of P6 was not caused by mtDNA lesions. A more detailed analysis of the wider phenotype of P6 and the speculation on candidate disease mechanisms is given below (18.4).

---

* ~40 passages.

14 ANALYSIS OF *SURF1*

SURF1 (5.2.3.1) emerged as a major candidate gene for COX deficient Leigh's syndrome during the course of this thesis[535,537]. Initially, as data were only available on a small number of patients, the close link between *SURF1* mutations and isolated COX defects in Leigh's syndrome patients[536,578,596,731] was undetermined. Moreover, genotype-phenotype correlations in mitochondrial disorders are not always well defined[573]. Therefore, as all the fibroblast cultures in this study expressed a COX defect in culture and five of the seven cultures were derived from Leigh's syndrome patients, *SURF1* was screened in all samples.

14.1 *SURF1* GENOTYPE-PHENOTYPE RELATIONSHIPS AMONG THE PATIENT FIBROBLAST CULTURES

Mutations in *SURF1* were found in P1, P4, P5, and P7, corresponding to all the cultures derived from Leigh's syndrome patients that expressed an isolated reduction in steady-state COX subunit levels in culture. This finding also sits well with the design of the project as *SURF1* is a ubiquitously expressed housekeeping gene and hence is a good candidate for a disease locus affecting COX expression both *in vitro* in cultured dermal fibroblasts and *in vivo* in differentiated tissues. Although clinical biochemistry supplied with the cells contradicted some of the subunit signatures seen in the *SURF1* mutant cultures, the results generated for this thesis are consistent with the now well recognised relationship between mutant *SURF1* genotypes and a presentation of Leigh's syndrome with an isolated COX deficiency[536,578,596,731] (table 5; 6.2.2.4). In agreement with this, no mutations were found in P3 which was derived from a patient with a confirmed diagnosis of Leigh's syndrome but with biochemistry and an OXPHOS subunit signature which indicated the involvement of complexes I, III and COX. *SURF1* mutations were also absent from P6 and P2. Although there was good biochemical evidence of an isolated COX defect in P6, the presentation of patient 6 was not consistent with Leigh's syndrome. In terms of P2, neither the phenotype of the cells, nor the clinical presentation of patient 2, were consistent with COX deficient Leigh's syndrome.

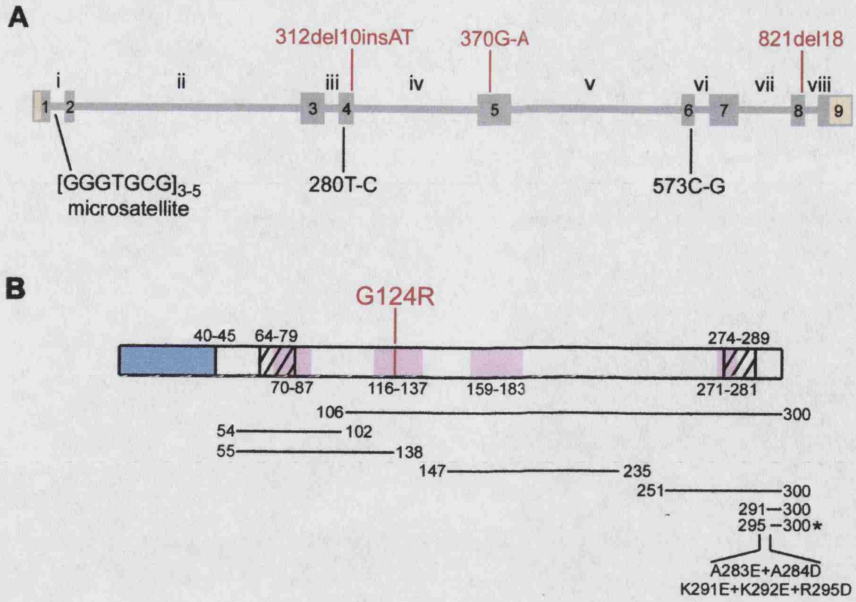

Figure 71A A map of the *SURF1* pre-mRNA showing the locations of the mutations identified in this work (see also figure 8). Exons are numbered in Arabic script and introns in Roman numerals, 5' and 3'UTRs are coloured yellow. Mutations are shown in red and polymorphisms in black. **71B** A map of the SURF1 protein, the N-terminal import sequence is shown in blue, predicted transmembrane domains are cross hatched and conserved regions are shown in pink. The G124R sequence variant identified in P5 is marked in red. Numbering above the protein denotes boundaries of import sequence and predicted transmembrane domains, numbering below denotes conserved regions. Deletions (horizontal lines) and C-terminal substitutions in various recombinant models are given below the sequence map (see text for references). Recombinant protein with the deletion 295-300 marked with an asterisk is the only form able to restore COX activity in *SURF1* null cells.

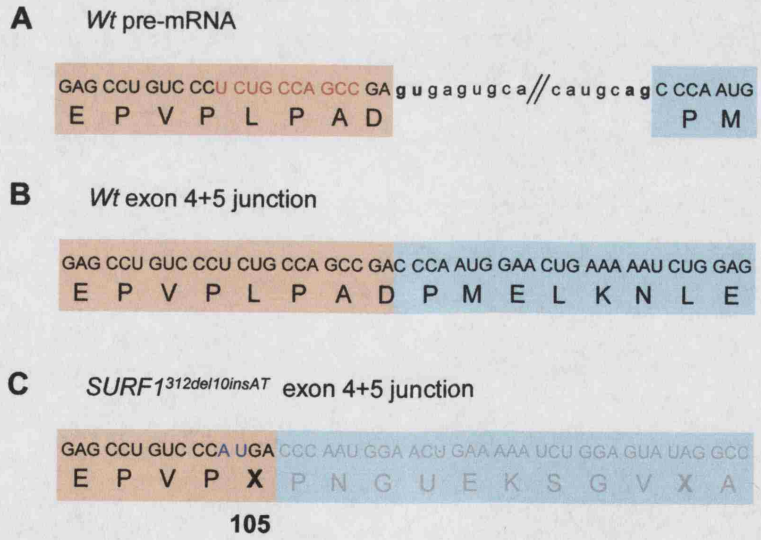

Figure 72 Exon junctions surrounding the 312del10insAT mutation. **72A** Wild type pre-mRNA sequence with bases deleted due to 312del10insAT shown in red. Exon 4 marked by a peach box and exon 5 a blue box. Codons are in upper case triplets with single letter amino acid code below and intronic sequence is in lower case. The intron 4 splice donor and acceptor sites are given in bold font. **72B** Translation of the wild type exon 4+5 junction showing codons and single letter amino acid code. Colouring is as in A. **72C** The *SURF1312del10insAT* exon 4+5 junction. Inserted bases due to 312del10insAT are shown in blue. Colouring as in A except that codons and amino acid sequence downstream of the premature termination codon (X) are in grey. The codon number of the premature termination codon is given underneath (105).

14.2 THE SPECTRUM OF MUTANT *SURF1* ALLELES AND SEQUENCE POLYMORPHISMS IDENTIFIED IN THIS STUDY

A deletion-insertion spanning the 3' boundary of exon 4, 312del10insAT, represented six out of the eight mutant alleles identified in P1, P4, P5 and P7 (figure 71). P1 and P4 were both homozygous for this mutation and P5 and P7 were heterozygous for it. In addition to 312del10insAT, P5 was also heterozygous for the point mutation 370G-A, and P7 was heterozygous for a deletion spanning the 3' boundary of exon 8, 821del18.The high frequency of *SURF1*^{312del10insAT} among the patient group reflects the fact that it is the most common mutant *SURF1* allele[596].

Two synonymous base changes segregated with 312del10insAT; 280T-C and 573C-G, although linkage in P5 and P7 which were heterozygous was not conclusively demonstrated here. Both base-changes have been widely reported as linked to 312del10insAT as features of the *SURF1*^{312del10insAT} allele[596] and it was not felt necessary to study them further. 312del10insAT is also known to segregate with five copies of the [GGGTGCG] heptameric repeat in the microsatellite sequence in intron 1[596]. This correlates with the distribution of five copies of the repeat within the patients studied here. The linkage of each of these features has suggested a common genetic origin for the *SURF1*^{312del10insAT} allele[732]. While it is clear that the *SURF1*^{312del10insAT} allele contains five copies of the intron 1 repeat, a screen of a large number of disease controls and normal controls found that the presence of five copies of the intron 1 microsatellite sequence was not an indicator for the presence of the *SURF1*^{312del10insAT} allele.

14.3 ALLELIC CONSEQUENCES OF THE *SURF1* MUTATIONS IDENTIFIED IN THIS STUDY

14.3.1 312del10insAT is a null allele mediated by non-sense mediated decay

Contrary to persistent speculation[596], the translation of a truncated protein from *SURF1*^{312del10insAT} is extremely unlikely. A northern blot of total RNA from P1-P5 probed for *SURF1* mRNA did not detect any signal from the either of the two *SURF1*^{312del10insAT} homozygous samples, P1 and P4. In accordance with this finding, an intermediate signal was detected P5 which was heterozygous for the *SURF1*^{312del10insAT} allele. mRNA confirmed by sequencing as corresponding to *SURF1*^{312del10insAT} has never been

reported. As there is no reason to suspect that 312del10insAT drastically reduces the activity of the *SURF1* promoter, this suggests that the *SURF1*^{312del10insAT} allele results in a highly unstable transcript[542].

The instability of the *SURF1*^{312del10insAT} transcript is undoubtedly due to the induction of non-sense mediated decay (NMD)[144,252,733-736]. Rapid mRNA turnover via the induction of NMD is a predictable and well accepted consequence of mutations which result in transcripts with premature termination codons[144,252,733-736]. NMD is activated by aberrant mRNAs where in-frame termination codons are created >50 bp 5' to the terminal exon junction[144,252,733-736]. During pre-mRNA processing and mRNP assembly, exon junctions are marked by exon junction complexes (EJCs) which build on pre-mRNAs around 20 bp 5' of exon junctions and are essential for mRNA export[252]. It is believed that a pioneer round of translation reads each transcript prior to cytoplasmic translation, displacing components of EJCs as it progresses[144,252,733-736]. If one or more intact EJCs remains following the pioneer round of translation, the transcript is degraded. There is still considerable debate[733,734,737] as to whether the pioneer round of translation occurs within the nucleus[738] or occurs during or immediately after, nuclear export. In mammalian cells, the major mechanism for the turnover of normal, translationally competent, mRNAs is via de-adenylation followed by 3'-5' degradation by the cytoplasmic exosome concurrent with scavenger decapping[739]. Most NMD-targeted mRNAs are believed to be degraded in, or in close proximity to, the nucleus via a 5'-3' exonucleases, although there is also evidence for the degradation of NMD activating mRNA in the cytoplasm via an accelerated de-adenylation pathway[740]. *In vivo* the primary roles of NMD are to act as a quality control system to remove erroneous splicing products and where present, heterozygous mutant alleles[735], making NMD an essential component of the eukaryotic gene expression machinery.

Although 312del10insAT is very close to the intron 4 splice donor site. *In silico* analysis using three different splice site prediction tools indicated that the mutation was unlikley to affect the strength of the canonical splice donor site in intron 4. Disruption of splice donor sites commonly leads to exon skipping or less often, the activation of cryptic splice donor sites[741-743] due to the loss of sequence elements recognised by the spliceosome. (The possibility that 312del10insAT led to loss of exonic splicing enhancer/silencer (ESE/ESS) elements was not investigated due to the difficulty in predicting such events from genomic sequence data alone[744].)

312del10insAT leads to a frame shift in exon 4 and splicing of exons 4 and 5 of *SURF1*^{312del10insAT} creates a premature stop codon at residue 105 (figure 72). This stop codon is upstream of four exon junctions and therefore is very likely to activate NMD. The complete lack of *SURF1* mRNA signal on the northern blot of total RNA from P1 and P4 which were both homozygous for 312del10insAT supports this assumption. Some mutant transcripts are known to escape NMD[734,735] but the instability of *SURF1*^{312del10insAT} mRNA and the well documented instability of other mutant *SURF1* mRNAs containing premature termination codons[537,542,745-747], indicates that mutant *SURF1* transcripts with premature termination codons are efficient activators of NMD. The rapid turnover of *SURF1*^{312del10insAT} mRNAs by NMD would completely block translation and accumulation of a truncated protein product[144,252,733-736]. Thus, activation of NMD by the premature stop codon at residue 105 efficiently renders 312del10insAT a null, loss of function mutation. Sadly no SURF1 antibody was available to absolutely confirm the presence or absence of SURF1 protein in any of the patient fibroblast cultures. Previous attempts to detect putative truncated proteins from *SURF1*^{312del10insAT} have not been informative due to the use of antibodies generated to SURF1 fragments C-terminal of the premature termination codon[529,533]. Recombinant SURF1$_{STOP105}$, identical to the hypothetical product of *SURF1*^{312del10insAT}, is unable to rescue of COX activity in *SURF1* null cells[529], indicating that the C-terminal region of the protein is essential for function. Therefore, even if *SURF1*^{312del10insAT} mRNA escaped NMD, the truncated protein product is not active.

14.3.2 821del18 is a null allele mediated by non-stop mediated decay

As with 312del10insAT, the novel deletion found in P7 is also predicted to lead to rapid mRNA degradation. The deletion, 821del18, completely removes the 3' boundary of exon 8 and the intron 8 splice donor site. Splicing of pre-mRNAs is carried out by the spliceosome, a dynamic, responsive, ribosome-sized complex composed of many proteins and small nuclear ribonucleoprotein particles (snRNPs)[568]. Following capping, splicing occurs co-transcriptionally and is intimately involved with many aspects of gene expression such as transcript elongation, termination, poly-adenylation[146,748], mRNP assembly and nuclear export[252]. In terms of biochemistry, splicing progresses via two trans-esterification reactions, the first joins the intron branch point to the splice donor site to create the characteristic intron lariat structure, and the second joins the exposed 3' end of the 5' exon to the 3' exon, excising the intron lariat[146,568]. One of the earliest events during splicing reactions is the binding of the U1 snRNP to splice donor sequences which defines the splice donor site and initiates spliceosome assembly[146]. Donor sequence binding is achieved via base-pairing between the U1 RNA and a short

consensus sequence spanning the splice donor site of the nascent transcript[568]. The 821del18 mutation completely removes the U1 binding sequence of intron 8 (figure 73). Because of the directional nature of intron lariat formation, loss of a U1 binding sequence can lead to skipping of the adjoining 5' exon, as the nearest recognised splice donor sequence is that of the preceding exon. More rarely, cryptic splice donor sequences in the vicinity of the original sequence are used leading to the inclusion of intronic sequences or partial loss of the adjoining 5' exon[741-743].

RACE PCR of the 3' end of *SURF1* mRNA from P7 identified two species, one composed of exons 7+8+9, assumed to be the product of the *SURF1*^{312del10insAT} allele, and the other containing only exons 7+9. This confirmed that 821del18 causes the skipping of exon 8 and did not activate any cryptic splice donor sites. Interestingly, translation of the mutant mRNA from the *SURF1*^{821del18} allele found that the frame-shift created a non-stop mRNA without an in-frame stop codon. The mechanism for clearance of non-stop mRNAs is distinct from NMD[749-751]. NMD-targeted mRNAs are degraded in or close to the nucleus 5'-3'. In contrast non-stop mRNAs are degraded by the cytoplasmic exosome 3'-5', after the initiation of normal cytoplasmic translation[749-751].

Despite being exported from the nucleus, non-stop mRNAs are very unstable. In yeast, non-stop mRNAs have a half-life of around 3 minutes which is comparable to that of NMD degraded mRNAs of the same size which have a $t_{½}$ of around 2.5 minutes[749]. Non-stop mediated decay (NXMD) has been demonstrated in mammalian cells[749] and, as with NMD, the major flux through the pathway *in vivo* is believed to be erroneous products of the normal gene expression machinery[749]. Despite the fact that NXMD relies on cytoplasmic translation for in-frame scanning, accumulation of aberrant protein product from *SURF1*^{821del18} is very unlikley. mRNA turnover experiments in yeast indicate that recruitment of the exosome is likely to occur immediately upon ribosomal read-through and efficiently inhibits the accumulation of functional levels of truncated protein product[751]. Even if translation products were to accumulate from *SURF1*^{821del18} mRNA, the truncation removes the terminal 50 amino acids of SURF1, including a predicted C-terminal transmembrane domain. This is very likely to result in an unstable protein. In a recombinant human system where SURF1 missing residues 54-102 or 291-300 could be detected, truncated SURF1 missing the terminal 49 residues was undetectable[529]. The mechanism for this remains unclear, although it is very likely that removal of a transmembrane domain results in aberrant trafficking and/or membrane orientation of the protein. Therefore to summarise, as with *SURF1*^{312del10insAT}, the *SURF1*^{821del18} allele is also a null loss of function allele but in this case induced by rapid NXMD.

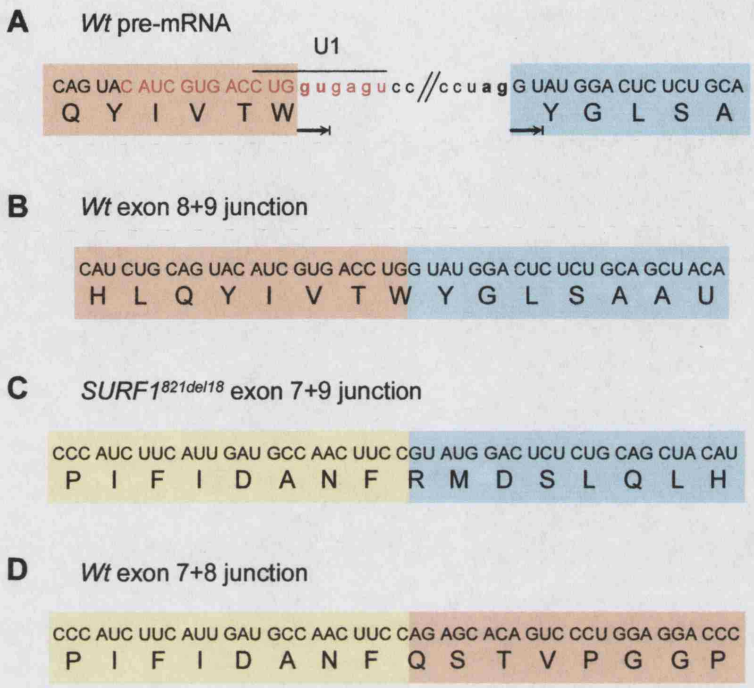

Figure 73 Exon junctions surrounding the 821del18 mutation. **73A** Wild type pre-mRNA sequence with 821del18 deletion shown in red. Exon 8 is marked by a peach box and exon 9 a blue box. Codons are in upper case triplets with single letter amino acid code below and intronic sequence is in lower case. The intron 8 splice donor and acceptor sites are indicated in bold. The U1 snRNP complex binding sequence is marked with a horizontal line above the sequence, incorrectly predicted intron/exon boundaries are marked by blocked arrows under the sequence (see text for details). **73B** Translation of the wild type exon 8+9 junction showing codons and single letter amino acid code. Colouring is as in A. **73C** The *SURF1*^{821del18} exon 7+9 junction. Exon 7 is marked by a yellow box. **73D** The wild type *SURF1* exon 7+8 junction showing the boundary sequence colouring as in B and C.

370G-A is a loss of function allele

The point mutation 370G-A was identified in exon 5 of P5. This transition has been previously described in another compound heterozygous case[540]. Northern analysis of total RNA from P5 identified a weak band corresponding to *SURF1* mRNA. As P5 was compound heterozygous for *SURF1*^{312del10insAT} and *SURF1*$^{370G-A}$, and mRNA from *SURF1*^{312del10insAT} was undetectable in P1 and P4, it was assumed that the *SURF1* signal in P5 was due to *SURF1*$^{370G-A}$ mRNA. This is supported by the intermediate intensity of the *SURF1* mRNA signal in P5 suggesting that it is the product of a single allele. mRNA corresponding to the related mutant allele *SURF1*$^{371G-A}$ has been detectable *in vivo*[542]

strengthening this assumption. Assuming *SURF1*$^{370G-A}$ mRNA is stable, this implies that SURF1 loss of function due to 370G-A is manifest at the protein level.

370G-A leads to the amino acid substitution G124R. 371G-A also substitutes Gly124, giving rise to G124Q. Furthermore, Gly124 is conserved in all known SURF1 sequences[530], providing strong evidence for the pathological nature of disruption of this residue. Western blots of cells compound heterozygous for *SURF1*$^{371G-A}$ and the null allele *SURF1*^{312del10insAT}, failed to detect any SURF1 protein suggesting that loss of Gly124 leads to protein instability[747]. It is reasonable to assume therefore that $SURF1_{G124R}$ is also unstable. Why disruption of Gly124 creates an unstable protein is uncertain, although failure to attain a stably folded form, aberrant protein trafficking or inability to incorporate into stable protein complexes are likely candidate mechanisms.

Despite the fact that an unstable protein is probably translated from *SURF1*$^{370G-A}$, there was no evidence from the work presented here that P5 behaved in any way differently to the other *SURF1* null cultures. This is in agreement with work examining cells from patients heterozygous for 370G-A[540] and 371G-A[542,747] which also found no indication of a phenotypic differences between cells carrying these mutations and those with other *SURF1* mutations. In summary *SURF1*$^{370G-A}$ is another SURF1 loss of function allele although this is likely to be manifest at the level of protein stability in contrast to the null genotypes of *SURF1*^{312del10insAT} and *SURF1*^{821del18} which are mediated via mRNA instability.

14.3.4 Confirmation of the boundaries of intron 8

Direct sequencing of the exon 7+9 mRNA from P7 also enabled confirmation of the 5' boundary of exon 9. This has important implications for prediction of the consequences of exon skipping mutations such as 821del18. In contrast to the NCBI- and ENSEMBL-predicted intron-exon boundaries, Pequignot *et al*[596] has published a transcript map of human *SURF1* with both boundaries of intron 8 slipped 5' by two nucleotides (figure 73). This is undoubtedly due to the choice of exon prediction software, as exon 9 starts with GU, the same two nucleotides as a splice donor site. The GU present at the exon 7+9 junction must originate from exon 9 and not exon 7 as the exon 7+8 junction does not contain the sequence GU. The corrected intron 8 boundaries create canonical short

intron splice donor and acceptor sequences[752] in accordance with all other introns of *SURF1*[596*].

15 PHENOTYPIC FEATURES OF *SURF1* MUTANT FIBROBLAST CULTURES

The identification of mutations in *SURF1* of P1, P4, P5 and P7 enabled the study of human cells with a genetically defined COX deficiency. They provided interesting models of COX deficiency because despite the prevalence of *SURF1* mutations among archives of COX deficient cell cultures, the exact role of SURF1 in COX biogenesis remains unknown. In the following section the phenotype of P1, P4, P5 and P7 is examined and compared to P2, P3 and P6 and other cells with genetically defined COX defects.

15.1 *SURF1* MUTANT FIBROBLASTS EXPRESS AN ISOLATED, UNIFORM COX DEFECT

15.1.1 SURF1 mutant cells express an isolated COX defect

The clinical biochemistry available for P1, P4, P5 and P7 confirmed the presence of severe reductions in COX activity in the cultures and in muscle from the patients they were derived from. However, P1 also had evidence of a complex II+III defect and muscle from patients 1, 4 and 5 also showed defects in complex I, complex II+III and where examined, complex II and PDH. No evidence of defects in OXPHOS complexes other than COX were evident from the subunit signature of these cultures. The disparity between these results possibly reflects poor handling of sensitive mitochondrial preparations. Morphological abnormalities of mitochondria from *SURF1* mutant tissues have been noted under electron microscopy (EM)[539] and these may well contribute to a degree of structural fragility in the organelles from such tissues. It should also be remembered that P1-P5 were established around 20 years ago and that the techniques and proficiency in carrying out biochemical examination of OXPHOS defects have become more reliable over the years. The fact that technical problems occurred in defining the muscle biochemistry in these patients is supported by the wealth of biochemical data demonstrating that *SURF1* defects are associated with isolated COX defects both in cultured cells and tissues such as muscle[534-537,746,753,754] which is in

* see also Ensembl transcript: ENST00000277404 and NCBI surfeit locus genomic sequence: NG_000837.

agreement with the subunit signatures of these cultures. No muscle was available from patients 1-7 for confirmation of OXPHOS biochemistry.

15.1.2 The COX defect in *SURF1* mutant fibroblasts is expressed uniformly

P1, P4, P5 and P7 all stained uniformly negative for COX activity in contrast to P2 where residual activity could be detected and the MELAS fibroblast cell culture which had a mosaic staining pattern. Uniformly negative intracellular staining patterns have been consistently described in *SURF1* mutant primary fibroblast cultures and fibroblast-derived cell lines[529,535,537,542,755,756]. The most common staining pattern reported for muscle from patients with *SURF1* mutations is a uniform, partial loss of COX activity in both type I and type II fibres[753,754,757]. In *SURF1* knock-out mice, a mosaic fibre staining with type II fibres most severely affected has been described[539] and a similar "patchy" loss of COX activity and the appearance of RRF* have also been documented in some patients[542]. The differences in staining patterns between muscle and cultured cells probably reflects a combination of the partial redundancy of SURF1 function, which enables some assembly of normal COX[488,529,533,540,578], and the high level of OXPHOS-related gene expression in differentiated muscle (and type I fibres in particular), compared to that of cultured dermal fibroblasts.

In contrast to P3 and P6, no evidence of increased COX staining was seen in mitotic cells from the *SURF1* mutant cultures. This suggests that the mechanisms that enable redundancy of SURF1 function, i.e. permit COX biogenesis in *SURF1* null cells, are independent of the cell cycle. The uniformity of the COX activity staining of the *SURF1* mutant cells was mirrored by uniform immunohistochemical stains. The normal MTCO1 and COX4I1 immunohistochemical stains undoubtedly reflects differences in the suitability of immunohistochemistry and western blotting for detecting subtle changes in epitope abundance. Immunostaining identified a clear reticular or fragmented, perinuclear, mitochondrial network in all cells. Gross mitochondrial morphology appeared to be normal in all cells and the abnormal mitochondrial morphologies seen in muscle from *SURF1* knock-out mice[539] were not apparent. It is likely that the highly differentiated status of muscle compared to the relatively pleomorphic status of cultured fibroblasts contributed to this finding. The spectrum of mitochondrial morphology seen in the *SURF1* mutant cells was consistent with the normal cycling between a predominantly reticular network during G_1 and more fragmented perinuclear morphology during S-phase[758].

---

* Ragged red fibres.

15.1.3 *SURF1* mutant fibroblasts maintain low levels of normal COX

Residual COX activity has consistently been recorded in *Δshy1* yeast[381,504] and *SURF1* null human[488,529,533,540,578] and murine[539] cells and tissues. Attempts to examine OXPHOS cytochromes using visible spectra of whole cell samples were not particularly successful because at the cell and reductant concentration used, many samples clumped and became unreadable. Where readings could be taken, good results were obtained. The concentration of *b*-type and *c*-type cytochromes in the *SURF1* mutant cultures were all close to normal levels and difference spectra in the 550-580 nm region encompassing these cytochromes were distinct from those seen for ρ^0 disease control samples. This correlates with the normal complex II and III subunit levels seen in the *SURF1* mutant cultures and the normal complex II and III activities documented in cells and tissue from patients with *SURF1* mutations[535,537,664]. In contrast to the normal *c*-type cytochrome levels in human *SURF1* mutant cells, *Δshy1* yeast have two-fold higher levels of cytochrome c than wild-type strains[504]. This suggests there may be differences in the response of mammalian and yeast cells to *SURF1/SHY1* loss of function and may also reflect the differential control of expression of the two cytochrome c isoforms present in yeast[417] compared to the single isoform present in human cells[759].

Measurement of cytochrome aa_3 levels using visible spectra was only possible for P7 and values were around 15% mean control values in accordance with COX activity measurements and published data from other *SURF1* mutant fibroblast cultures[533,534,540,542,664,755*]. Whether or not blue-shifted cytochrome aa_3 α-absorption bands were present in the *SURF1* mutant cultures could not be determined. Tzagoloff has shown that *[COX15/YHA1]* overexpressing, *cyc3* null yeast can accumulate haem A in a form not associated with Cox1p and that these cells have an α-absorption band shifted from 605 nm to 595 nm[495]. Similar blue-shifted α-absorption bands are also seen in yeast *sco1*[760] and *cox17*[761] mutants and also purified COX from *Δcox11 R. sphaeroides* lacking CuB[527]. A blue-shift might have be expected in the *SURF1* mutant cells if significant quantities of haem A were associated with the relatively high levels of residual MTCO1 seen on western blots. HPLC analysis of human cells with *COX10*[492] and *COX15*[505] mutations (which most likely have limited capacity to synthesise haem A) suggests that haem A does not accumulate significantly beyond a level corresponding to COX content. Reports of unpublished HPLC data from *SURF1* mutant cells are said to agree with this finding[492].

---

* n=4 patients including P7 from this study included as p2.

CO laser-flash photolysis provided a much more reliable means for measuring COX abundance in whole cells than visible spectra. The technique has three main advantages: i) it allows examination of the CuB-haem-a_3 binuclear centre separate from other haem A signals; ii) it is extremely sensitive due to the very high absorption co-efficient; iii) the observed rate constant for CO-ligation (κ_{obs}) provides an indicator of disturbances of the CuB-haem-a_3 environment. CO laser-flash photolysis has previously been used to measure the abundance of cytochrome a_3 in human cells with *MTCO1* mutations associated with sideroblastic anaemia[688] and muscle mitochondria carrying a 90% mutant load of an *MTCO2* mutation[614] from a patient with myopathy.

The abundance of cytochrome a_3 binuclear centres in the *SURF1* mutant samples was much lower than controls, falling within a range of 8-18% of control levels. No published values for cytochrome a_3 or aa_3 abundance in *SURF1* null cells or tissues are available for comparison. The cytochrome a_3 abundance in P1, P4 and P5 is similar to the absolute COX activity measured in these cultures of 0%, 6.6% and 0% respectively. The same is also true of the cytochrome a_3 and cytochrome aa_3 levels determined for P7 in comparison to the relative COX/CS ratios of 3.3-14%. The cytochrome a_3 abundance in the *SURF1* mutant cells is also in good agreement with published values for COX activities or relative COX/CS ratios for other *SURF1* null fibroblast cultures or fibroblast-derived transformants (3.5-12.4%[755], 9.6-13.9%[540], 14-17%[542], 15%[533], 18.3%[534], 24.6%[664*]). κ_{obs} values were all within the normal range for all the *SURF1* mutant samples indicating that the cytochrome a_3 environment was normal[666]. The agreement between COX activity measurements and cytochrome a_3 abundance, in addition to the normal rate of CO ligation in the *SURF1* mutant samples, supports the view that the low COX activity in *SURF1* null cells and tissues is the consequence of a low abundance of normal enzyme[529,533,578]. This is in contrast to the reciprocal situation seen in fibroblasts from some other Leigh's syndrome patients which have been found to have reduced COX activity but normal COX abundance as determined by absorbance spectra[762] or steady-state subunit levels[538,597].

15.1.4 COX activity in cells with mutations in other COX assembly factors

COX activities in mitochondria from P7, P8 (*SCO1* mutant) and P9 (*COX10* mutant) were similar and in good agreement with the low abundance of essential subunits such as

* n=4 patients including P7 from this study included as p2.

MTCO2 and MTCO3 seen in each sample on western blots. Other groups studying P9 have failed to detect cytochrome aa_3 signals using visible spectra[589] and COX/CS ratios have been measured at 18% and 40% in *COX10* mutant fibroblasts with different missense mutations[492]. These values are in relatively good agreement with the COX/CS ratio of 9.5% measured in P9 here. No external COX/CS data from *SCO1* mutant fibroblasts is available for direct comparison, although others working on P8 have measured COX activity at ~26% control values[519] which is a reasonably similar to the COX/CS values obtained here. COX/complex II ratios have been measured at 16% in liver and COX/II-III activities at <0.5%, in muscle from patient 8[591] which also compares favourably.

COX/CS ratios have been measured in *SCO2* mutant fibroblasts at 12-30%[523], 50%[592] and 68%[595] control means. Values for muscle from the same patients were 4-18%[523], 0%[592] and 30-50%[595], respectively. Thus there appears to be a wide spread of COX activities measured in *SCO2* mutant cells and tissues, which may reflect complex phenotypes of the different mutant *SCO2* alleles and the different clinical presentation seen in patients with *SCO2* mutations (table 5). This is supported by data which found differences in the folding and Cu^+ binding of various control and mutant isoforms of SCO2[629]. More needs to be known about the specific functions of SCO1 and SCO2 before it can be seen whether valid comparisons can be made between the data from the two mutant cell types, although from the data given above it appears that the COX/CS value of 11.9% determined for P8 is lower than that generally reported for SCO2 mutant cells. Similar to the vales reported for *SCO2* mutant fibroblasts, the absolute COX activities in fibroblasts with mutations in *LRPPRC* are also only marginally reduced, typically falling within 40-50% control values[630]. Overall, the paucity of data relating to *SCO1* and *COX10* mutant cells precludes a definitive comparison but it appears that in cultured fibroblasts residual COX activities and abundance are probably similar in *SURF1*, *SCO1* and *COX10* mutant cells, at the lower end of the patient cell range of ~0-40% control values, whereas SCO2 and LRPPRC mutant cells appear to have higher ranges of ~10-70% and 40-50% respectively.

15.2 THE IMPACT OF *SURF1* LOSS OF FUNCTION ON CELLULAR FITNESS

Growth assays are often used as a measure of cellular fitness and have been employed in screens for genes affecting mitochondrial function[763]. Sugar type and content[690,764], nutrient content[765], pyruvate and uridine availability[97] and CO_2 tension[765] have all been

demonstrated to affect the proliferation of cells with compromised OXPHOS function. Growth assays using different media compositions were used to examine whether *SURF1* loss of function impacted on cellular fitness.

15.2.1 Cell growth was not affected by *SURF1* loss of function under routine growth conditions or by restriction of pyruvate and uridine

ρ^0 cells are dependent on pyruvate and uridine supplementation for growth[97]. *De novo* synthesis of uridine requires the inner-membrane enzyme dihydro-oratate dehydrogenase (*DHODH*) which is dependent on ubiquinone and a functional respiratory chain for activity[766-768]. Uridine supplementation is though to facilitate growth by overcoming the block in *de novo* uridine synthesis at DHODH. The role of pyruvate supplementation remains unclear. To support the growth of cells with diverse, undefined OXPHOS defects, all cultures were routinely grown in high glucose DMEM supplemented with pyruvate and uridine. In such media no difference could be seen between the growth of *SURF1* mutant cultures and control cultures. Therefore, under standard conditions there was no apparent difference in the fitness of *SURF1* mutant cultures compared to controls. When pyruvate and uridine were removed from standard growth media the growth of *SURF1* mutant cultures was not affected. This implies that the residual COX activity in the cells was able to maintain sufficient uridine pools for growth in culture.

15.2.2 *SURF1* mutant fibroblasts are sensitive to blockage of glycolysis

In agreement with previous work on cultures with impaired OXPHOS function[690,764], changing from glucose to galactose as the principle sugar in the culture media reduced the growth of *SURF1* mutant cells relative to controls. Reduced growth of cybrids with an isolated COX defect due to an *MTCO1* mutation has also been noted in such medium[612]. The poor growth of cell cultures with impaired OXPHOS function in medium containing galactose as the primary sugar is thought to be due to the restricted conversion of galactose to glucose-6-phosphate in the early stages of glycolysis[689]. Cultured fibroblasts produce up to five times more ATP via glycolysis than via oxidative phosphorylation in normal glucose-based media[769]. The restriction of glycolysis forces cells to rely on oxidative phosphorylation, using NADH generated by the reduction of pyruvate to lactate as an electron donor via the malate-aspartate shuttle[689] (figure 1A). Clearly, the low COX activity of *SURF1* mutant cells reduces their capacity to carry out oxidative phosphorylation and, hence, their fitness is compromised in glucose free medium.

Although P1, P4 and P5 grew less well than controls in galactose-containing DMEM, they did not reduce in number as was seen for P2, P3 and the MELAS culture, all of which had multiple OXPHOS defects. This matches work showing a correlation between the severity of OXPHOS defects and the sensitivity of cultures to glucose substitution[690] and implies that the isolated COX defect in the *SURF1* mutant cells has less of an impact on cellular fitness than multiple OXPHOS defects.

RPMI has a lower nutrient content than DMEM. Van Den Bogert and co-workers found that cells with chemically-impaired mitochondrial translation are unable to proliferate in RPMI[765]. In contrast, the *SURF1* mutant cultures grew at similar rates to control fibroblast cultures in RPMI containing glucose and restriction of pyruvate and uridine had no effect on growth in RPMI. Again, this result correlates with the low impact of an isolated COX defect. Substitution of glucose with galactose inhibited the growth of all fibroblast cultures, including controls, in RPMI. This was not seen in DMEM and suggests that fibroblasts depend on glucose to a greater extent in low-nutrient media than high nutrient media. The mechanisms behind the poor growth of *SURF1* mutant cells in glucose-free media remain to be investigated but are unlikely to be purely biochemical. The growth assays used in this study only measured total cell number and relationships between proliferation and cell death may have been overlooked. Cells with isolated complex V defects appear to undergo apoptosis at a much higher rate than controls and that this may be linked to ROS* formation[769]. Similar observations were made with complex II deficient cells but not with cells with isolated defects in other OXPHOS complexes. Mitochondrial dysfunction activates cell signalling pathways[183,184] and *SURF1* mutant cells also have differences in the handling of intracellular calcium[770]. Of particular interest to these experiments are data showing that growth inhibition of mtDNA-depleted cells is mediated by CAMK4†-dependent phosphorylation of the transcription factor CREB‡[182]. Growth inhibition in such cells could be removed by inhibition of CAMK4 or expression of dominant-negative form of CREB, indicating that reduced growth was a cellular response to mitochondrial dysfunction and not simply limited by a biochemical defect in oxidative phosphorylation.

---

* Reactive oxygen species.
† Calcium/calmodulin-dependent protein kinase IV.
‡ CRE[cyclic-AMP response element] binding protein.

15.3 *SURF1* LOSS OF FUNCTION DOES NOT IMPACT ON MTDNA GENE EXPRESSION

No evidence was found of gross alterations in the steady-state levels of *MTCO1*, *MTCO2*, *MTRNR1* or *MTRNR2* transcripts in P1, P4 or P5. The lack of influence of *SURF1* loss of function on mitochondrial COX subunit mRNA levels is in agreement with previous work reported for *Δshy1* yeast[478]. Disruption of COX biogenesis due to mutations in *MTCO1*[612] and *MTCO3*[481,619] has also been found not to affect mitochondrial gene expression. These findings are in agreement with the general lack of response in expression levels of OXPHOS subunit genes to aberrant OXPHOS biogenesis (3.1.2.7). In contrast, MSR-like upregulation of *OXA1L*[542] and PHB complex[381] expression has been documented in *SURF1* mutant cells and *Δshy1* yeast, respectively. These findings fit well with the clear MSR noted in *C. elegans* in response to disruption of OXPHOS biogenesis[185] (4.3.4) and suggest that while COX subunit gene expression may not alter in *SURF1* mutant cells, *SURF1* loss of function probably induces an MSR. The general pattern of MSR in the absence of alterations OXPHOS subunit gene expression in cells with aberrant OXPHOS biogenesis provides good evidence that OXPHOS subunit levels are primarily regulated at the protein level under steady-state conditions.

Table 22 Summary of western blot analysis of steady-state COX subunit levels in *SURF1* mutant fibroblasts from this study (see figures 17-20 and table 14) and other groups.

	Reference, patient code[a] and consequence of mutant alleles.									
	This study	538	533	542	534		772			664
Subunit	P1, NMD/NMD P4, NMD/NMD P5, NMD/G124R P7, NMD/NXMD	*p6*, NMD/NMD	*W*, NMD/NMD *Wi*, NMD/NMD *C*, NMD/NMD	*L1*, NMD/I246T *L2*, NMD/NMD *L3*, NMD/G124Q	*P*, NMD G180E	*LS*, NMD NMD	*p3*, NMD NMD	*p4*, S60A NMD	*p5*, μΔi1 μΔi1	*p1*, NMD/NMD *p3*, R192W/NMD *p4*, NMD/NMD
MTCO1	+	-	+	+	+	+	+	+	+	+
MTCO2	-	-	-	+	-	-	-	-	+	-
MTCO3	-	-	nd	nd	-	-	nd	nd	nd	nd
COX4	+	+	+	-	++	++	+	+	++	+
COX5A	+	+	nd	nd	++	++	+	+	++	nd
COX5B	+	++	+	nd	++	++	nd	nd	nd	nd
COX6A1	-[b]	-	nd	nd	-	-	nd	nd	nd	nd
COX6B	-[b]	-	nd	nd	++	+	nd	nd	nd	nd
COX6C	nd	-	nd	nd	+	-	nd	-	+	-

Key: Mutation consequences: NMD, creates a premature stop codon predicted to induce non-sense mediated decay; NXMD, creates non-stop mRNA predicted to induce non-stop mediated decay; μΔi1, 7bp repeat-unit deletion in intron 1 microsatellite sequence with anecdotal evidence for expression of a truncated protein; amino acid substitutions are described using single letter code. Signal summaries: ++, normal or close to normal signal; +, intermediate signal; -, low signal; nd, no data. Where quantified data relative to control signals were available results have been binned in the following way ++ = 100-80%; + = 80-40%; - = 40-0%. [a] Patient codes as described in original paper; [b] data only available for P7.

Table 23 Summary of western blot analysis of COX subunit levels in *SCO2, COX10* and *COX15* mutant cells.

	Reference, tissue, gene and consequence of mutant alleles.						
	This study	521	592	This study	589	538 a	505 b
	Fib-mito	Myoblast	Fibroblast	Fib-mito	Fib-mito	Fib-mito	Fib-mito
	SCO1	*SCO2*	*SCO2*	*COX10*	*COX10*	*COX10*	*COX15*
	P174L	NMD	R171W	N204K	N204K	N204K	R217W
Subunit	NMD	E140K	E140K	N240K	N240K	N240K	ΔEx4
MTCO1	-	nd	nd	-	+	+	-
MTCO2	-	-	++	-	-	+	nd
MTCO3	-	nd	nd	-	+	-	nd
COX4	+	nd	++	+	++	+	-
COX5A	+	nd	nd	+	++	++	nd
COX5B	-	nd	nd	-	++	+	nd
COX6A1	-	nd	nd	-	++	+	nd
COX6B	+	nd	nd	+	+	+	nd
COX6C	nd	nd	nd	nd	+	-	nd

Key: Tissue: fib-mito, fibroblast mitochondria. Mutation consequences: NMD, creates undetectable mRNA; ΔEx4, skipping of exon 4. Signal summaries: ++, normal or close to normal signal; +, intermediate signal; -, low signal; nd, no data. Where quantified data relative to control signals were available results have been binned in the following way ++ = 100-80%; + = 80-40%; - = 40-0%. [a] Patient p16, *COX10* mutations confirmed by personal communication; [b] Data from BN-PAGE western blots.

Table 24 Summary of published western blot analysis of COX subunit levels in tissues with mutations in either *MTCO1*, *MTCO2* or *MTCO3* and cultured ρ^0 cells.

	Reference, tissue, gene and consequence of mutation.						
	609	614	613	618	481	619	180
	Muscle mito	Muscle mito	Fibroblast	Muscle mito	Cybrids 100%	Cybrids 100%	Fibroblast [a]
Subunit	*MTCO1* 42X	*MTCO2* M29K	*MTCO2* M1T	*MTCO3* F94-Δ5	*MTCO3* F94-Δ5	*MTCO3* P111X	ρ^0
MTCO1	-	+	nd	nd	+	+	--
MTCO2	+	-	-	+	-	+	--
MTCO3	++	-	nd	nd	nd	nd	nd
COX4	+	+	+	+	-	++	+
COX5A	nd	+	nd	+	nd	++	+
COX5B	nd	-	nd	+	nd	+	nd
COX6A1	nd	-	nd	nd	nd	-	nd
COX6B	nd	-	nd	+	nd	+	nd
COX6C	nd	-	nd	+	nd	++	-

Key: Tissue: muscle mito, muscle mitochondria; 100%, 100% mutant load. Mutation consequences: 42X, termination codon at residue 42 induced by frame shift from I37; F94-Δ5, in-frame deletion of 5 amino acids starting at 94; [a] MRC5 embryonic lung fibroblasts. Signal summaries: ++, normal or close to normal signal; +, intermediate signal; -, low signal; --, not present; nd, no data. Where quantified data relative to control signals were available results have been binned in the following way ++ = 100-80%; + = 80-40%; - = 40-0%.

15.4 THE COX SUBUNIT SIGNATURE OF *SURF1* MUTANT CELLS

Using immuno-detection by western blotting and immunohistochemistry, P1, P4, P5 and P7 all had identical OXPHOS subunit signatures. As mentioned above this was characterised by an isolated involvement of COX subunits. In each sample the MTCO2, MTCO3 and COX6C* signals were extremely low, whereas the MTCO1, COX4I1 and COX5A signals were reduced compared to controls but intermediate compared to the lowest signals. This division of subunits is to a certain extent supported by crystal structures of bovine COX[45,47,48†] in that MTCO1, COX4I1 and COX5A are closely associated, as are MTCO2 and COX6C. The subunit signature of the *SURF1* mutant cells was distinct from the pattern seen in P2, in which all proteins examined were at lower levels than controls, and P3 and P6 which both showed involvement of other bigenomic complexes. The isolated reduction in COX subunit levels in the *SURF1* mutant samples adds to the consensus of opinion[488,578,731] that SURF1 is specifically involved in maintenance of normal COX holo-complex levels and that loss of *SURF1* function does not impact on the biogenesis of the other OXPHOS complexes.

15.4.1 Comparison to other studies of *SURF1* mutant cells

Comparisons of western blot data between laboratories is an inherently difficult process. The majority of such data is generated using HRP conjugated secondary antibodies to activate chemiluminescent substrates and signals are detected using x-ray film. Even where the same primary antibodies are used, differences in overall sample loading, antibody dilutions, secondary antibody affinities, HRP activity and substrate sensitivity all contribute to making comparisons between sets of data difficult. Fortunately the vast majority of immuno-detection of human OXPHOS subunits uses a battery of monoclonal antibodies developed by the Capaldi laboratory[66,773,774]. This is the same antibody set as used in this study.

The COX subunit signature of the *SURF1* mutant cultures is summarised in table 22 and compared to similar data from six other studies[533,534,538,542,664,772]. All the external data in this table was generated using samples from fibroblasts or fibroblast mitochondria and all groups have used the same primary antibodies[66,773,774]. The relative preservation of the MTCO1, COX4I1, COX5A and COX5B signals and the low MTCO2 and MTCO3 signals seen in this study are also a general feature of results from other studies. Little data are

---

* According to immunohistochemistry.
† PDB files 1OCR, 1OCC and 1OCO available from the Protein Data Bank at http://www.pdb.org/.

available for comparison of the COX6A1 and COX6B signals in P7 mitochondria. Von Kleist-Retzow *et al*[634] also found extremely low signals for both subunits in one study, whereas in another they found low COX6A1 signals but near normal COX6B signals. the variation may reflect a sharp signal response for this antibody.

The spectrum of *SURF1* alleles in the external patient-derived fibroblasts is similar to those in this study. The high frequency of *SURF1* mutations which induce NMD facilitates comparisons as many different *SURF1* mutations are effectively identical null alleles. Indeed, the consistency of the subunit signature of *SURF1* mutant fibroblasts probably reflects the similarities in their genotypes. Key exceptions to the subunit signature seen in this study are the low MTCO1 signal seen in the first study by Von Kleist-Retzow[538], the intermediate MTCO2 signals found by Poyau[542] and in a sample from Hanson[772], and the very low COX4I1 signal again described by Poyau[542]. Culture *p5* described by Hanson was homozygous for a unique microsatellite repeat-unit deletion in intron 1 and unpublished evidence suggests that these cells expressed a truncated form of SURF1 protein[772]. It is therefore likely that the unique subunit signature seen in this culture reflects a unique molecular pathology. The subunit signature identified by Poyau may be due to technical differences as it was found for every culture studied by the group[542] and is quite different from the consensus of other published patterns. Despite these differences, comparison with work from other groups tends to support the initial finding of this study that *SURF1* mutant fibroblasts express a consistent COX subunit signature typified by the cultures examined in this thesis.

15.4.2 Comparison to cells with mutations in other COX assembly factors

Comparison of the subunit signature of the *SURF1* mutant cultures to those of cells with mutations in *SCO1* (P8), *COX10* (P9), or published signatures of cells with mutations in *SCO2*[521,592], *COX10*[538,589], and *COX15*[505] did not identify any similar patterns (table 23). In particular, the MTCO1 and COX6B signals were different in P7 than P8 and P9. Collectively, this implies that mutations in the other COX assembly factor genes create different obstacles for COX biogenesis than *SURF1* loss of function. However, the high frequency of missense mutations in *SCO1*, *SCO2*, *COX10* and *COX15* are also likely to contribute to this observation, as they will lead to more complex phenotypes than the predominantly null genotype of *SURF1* mutant cells. Indeed, western blot analysis has confirmed that P9 expresses low levels of SCO1[519], raising the possibility of aberrant SCO1 activity in these cells. Investigation of wild-type, S225F and E140K forms of SCO2 found that they all have different structures and copper binding capacities[629] supporting

this argument. No data are currently available for comparison of the subunit signature of *LRPPRC* mutant cells[171,555] to those with mutations in *SURF1*.

15.4.3 Comparison to cells with mutations in mtDNA-encoded COX subunit genes and ρ^0 cells

Comparisons with cells carrying mtDNA mutations is complicated by the variability in heteroplasmic mutant loads. **Table 24** summarises published data from tissues and cybrids with mutations in *MTCO1*[609], *MTCO2*[613,614]or *MTCO3*[481,618,619] which were present at sufficiently high levels to lead to a detectable COX deficiency and from a ρ^0 fibroblast cell model[180]. As with the data from COX assembly factors, there is no overall consensus pattern seen in cells with mutations in *MTCO1*, *MTCO2* and *MTCO3*. Assuming that the mutant loads allow a valid comparison, this implies that mutations in these genes lead to genotype-specific molecular pathologies. Interestingly, of all the patterns examined, the subunit signature of muscle mitochondria with the *MTCO2* M29K mutation[614] is the closest to that seen in the *SURF1* mutant cells. The two subunits probed in samples from fibroblasts with the *MTCO2* M1T mutation[613] also fit this pattern. This suggests that there may be some similarity in the molecular pathology of *SURF1* null cells and those with mutations in *MTCO2*. The persistence of COX4I1 and COX5A and the sensitivity of COX6C abundance to disruption of COX biogenesis, as observed in *SURF1* mutant cells, is underlined by the subunit signature of ρ^0 fibroblasts.

15.4.4 The COX subunit signatures of P8 and P9 in comparison to other work

The results obtained in this thesis for P8 provided the first insight into the COX subunit signature of *SCO1* mutant cells. Very recently, Leary and co-workers[519] also studied P8. Only MTCO1 was examined on denaturing gel western blots and in agreement with the results herein, a very low signal was detected. Comparison of the subunit signature of P8 with data from *SCO2* mutant samples is not valid given that SCO1 and SCO2 appear to have unique functions in COX biogenesis (5.2.2.2). In addition, as mentioned previously (15.1.4), the COX activities of *SCO2* mutant fibroblasts appear to have a higher range than those of *SCO1* mutant fibroblasts and hence subunit levels would also be expected to be different. There also appear to be differences in the presentations and affected tissues between patients with *SCO1* and *SCO2* mutations (table 5); However, as pointed out by Valnot *et al*[591], "Whether these differences are significant, fortuitous or related to the small number of reported cases is still debateable."

The subunit signature of P8 was identical to that of the *COX10* mutant culture P9, in agreement with the similar COX/CS values. Two other studies have also examined P9 but have obtained somewhat different subunit signatures (table 23). Aside from the innate difficulty in making comparisons between independent sets of western blots, this may reflect the fact that these cultures expressed a mutant form of COX10 (N204K). If it is accepted that the residual COX activity in P9 reflects partial activity of $COX10_{N204K}$, the differences in data from different labs may simply reflect threshold differences in haem O synthesis by $COX10_{N204K}$ under slightly different cultures conditions. As haem A abundance is rate limiting for COX assembly[474] (5.1.2), conditions which reduce the impact of $COX10_{N204K}$ expression would enable a greater degree of holo-complex assembly and hence increase steady-state subunit levels. In support of this, the relative COX/CS values reported by Valnot[589]were higher than those determined in this study, in agreement with the greater abundance of COX subunits seen in the same study.

16 INVESTIGATION OF CYTOCHROME C OXIDASE SUB-COMPLEXES IN *SURF1* MUTANT CELLS USING BN-PAGE

One of the more interesting findings from the phenotyping of the *SURF1* mutant cells was that their subunit signature showed an imbalance in the abundance of COX subunits. One of the least abundant subunits was MTCO2 (15.4). As it comprises the majority of the cytochrome c binding site and is essential for function, MTCO2 must be present in the pool of holo-enzyme responsible for the residual COX activity in *SURF1* mutant cells (15.1.3). This suggested that subunits with higher steady-state levels than MTCO2, such as MTCO1 and COX4I1, must accumulate in forms that are protected from proteolysis but that are not associated with the holo-enzyme. In agreement with this proposal, during the course of this thesis, a COX sub-complex comprising MTCO1•COX4I1 but not MTCO2 was identified in *SURF1* mutant cells[529]. No such sub-complex has been identified in cells with mutations in *COX10*[492] or *COX15*[505], in agreement with the differences in the subunit signatures seen in cells.

Blue-native PAGE (BN-PAGE) is an electrophoretic technique for resolving protein samples with minimal disruption of tertiary and quaternary structure. The technique has been pioneered by Professor Hermann Schägger of Frankfurt University[31,32,35,682,775] and has been used to investigate OXPHOS complexes in mammals, bacteria, fungi and plants. A BN-PAGE western blotting protocol was devised to investigate COX sub-complexes in the *SURF1* mutant cells and controls. Comparative studies were also

carried out with the other patient fibroblasts and disease controls with mutations in *SCO1* and *COX10*. The results of this study are discussed in the following section.

16.1 DEVELOPMENT OF 1D AND 2D WESTERN BLOTTING PROTOCOLS

A considerable amount of work went into optimising the 1D BN-PAGE and 2D BN-PAGE/urea-SDS-PAGE western blotting protocols. All the alterations made to the protocols were designed to improve detection of target proteins in low abundance sub-complexes and no alterations were made to either the solubilisation protocols or electrophoresis protocols. This was because it was felt that sufficient data relating to the influence of detergent concentrations on mitoplast preparation and solubilisation has previously been presented by Nijtmans[529,681,684-686] and that the reliability of the electrophoresis protocol devised by Schägger[31-34,682,683] was unlikley to be improved within the timeframe of this project.

16.1.1 Optimisation of the 1D BN-PAGE western blotting protocol

16.1.1.1 Removal of excess G250 dye from blotted 1D BN-PAGE membranes

The PVDF membranes used throughout for preparation of western blots efficiently bound the G250 dye used for solubilisation and electrophoresis of BN-PAGE samples and G250 present on the membranes during blocking and probing resulted in massive non-specific signal. This problem was overcome by washing air-dried membranes very briefly in methanol prior to probing in exactly the same manner that air-dried PVDF membranes are normally wetted. As only the upper part of each lane and not other regions of the membrane were affected, inhibition of blocking of non-specific antibody binding to the PVDF was not a cause of the problem. It seems more likely that bound G250 inhibited blocking of non-specific antibody binding to immobilised mitoplast proteins. Why only proteins over a certain size were affected is unclear but it may be that lower regions of gels contained high levels of detergent micelles that competed with the G250.

16.1.1.2 Choice of secondary antibody

Investigation of the influence of secondary antibodies on signal strength and specificity demonstrated that this was of crucial importance to the success of the protocol. Very large differences were apparent in the amount of non-specific signal on blots probed without primary antibody, indicating a high degree of non-specific binding of secondary

antibody or free HRP*. To a certain degree this was not unexpected. The epitope spectrum of a native blot is likely to be closer to that of non-denatured cells or tissues fixed for immunohistochemistry than that of a denaturing gel blot and most HRP-conjugated secondary antibodies developed specifically for western blotting are likely to have been screened for use with conventional denaturing gel systems.

The differences in the ability of some secondary antibodies to detect low abundance bands was also extremely important. Such large differences in sensitivity had not been anticipated and the results validate the care taken in optimising the protocol. While it was beyond the scope of this thesis to investigate these technical differences further, it can be speculated that the specificity, affinity, extent of HRP conjugation and HRP enzyme kinetics are all going to be important factors in selection of commercially available secondary antibodies.

16.1.2 Optimisation of the 2D BN-PAGE western blotting protocol

16.1.2.1 Shortening the pre-soaking of first dimension gel strips

In most 2D BN-PAGE/denaturing-PAGE protocols, first dimension strips cut from BN-PAGE gels are soaked in an equilibration buffer containing 1% SDS and 1% β-mercapto-ethanol to denature samples and reduce disulphide bonds. Using 1.6 mm gel systems, Schägger[32,33,682] advocates soaking first dimension strips in equilibration buffer for 2 hours. The protocol developed by Nijtmans for working with 0.75-1.0 mm thick mini-gel systems recommends soaking first dimension strips in equilibration buffer for between 45-60 minutes[681,684] followed by two washes of 10 minutes in an identical buffer without β-mercapto-ethanol†. Washing steps are included to reduce inhibition acrylamide polymerisation by β-mercapto-ethanol. All protein gels in this project were 0.75 mm thick. Despite initially using the shortened protocol developed by Nijtmans, it was suspected that the high detergent concentration in the equilibration buffer may have encouraged leaching of proteins. A series of blots of first dimension strips made at different stages during the protocol confirmed that signal was lost during the procedure and soaking in equilibration buffer with β-mercapto-ethanol was reduced to 15 minutes and the subsequent washes to 5 minutes. A formal comparison of signals in strips prepared using the 15 minute protocol and that proposed by Nijtmans was not carried out. As no proteins containing disulphide bonds were probed on 2D blots it is unclear whether

---

* Horse radish peroxidase.
† Dr Leo Nijtmans personal communication.

samples were in fact reduced sufficiently, although the very small amount of protein per lane (~10 µg) means that there was likely to have been a massive excess of reducing power in the equilibration buffer. The uniform size distribution of signals for each target protein on 2D blots confirmed that all samples were denatured prior to or during second dimension electrophoresis.

16.1.2.2 Addition of a tertiary antibody layer

In addition to switching to a better secondary antibody, increasing the concentration of secondary antibody and the addition of a tertiary PAP layer significantly improved results on 2D blots. PAP antibodies are commonly used in immunohistochemistry to improve signal strength. There do not appear to be any other reports of the use of tertiary PAP layers in western blotting. One concern with amplifying signal strength so much is the poor linearity of western blotting recorded using ECL and X-ray film and the saturation of strong signals. This was not formally investigated in this study and it is accepted that the difference in signal strength between regions of strong signal, such as the COX holo-complex and weaker regions, such as COX sub-complexes, are likely to have been under represented. Nevertheless, the most important information gained from the 2D blots was the spatial alignment of signal spots and these blots were not used as a primary means to determine relative abundances of sub-complexes or constituent proteins.

16.1.3 Implications of this study for the presence of COX sub-complexes in yeast

A single study by Nijtmans has attempted to examine COX sub-complexes in wild-type and *Δshy1* yeast[381]. No sub-complexes could be identified in either cell type and it was determined by the authors that turnover and stability of these sub-complexes may differ markedly between yeast and human cells. However, this interpretation is probably incorrect as it most likely reflects an inability to detect low abundance sub-complexes rather than a genuine lack of such complexes. In the original figures, signal spots corresponding to the COX holo-complex in *Δshy1* yeast are almost undetectable yet these cells apparently maintained 36% *in gel* COX activity[381]. Using the optimised protocols developed here, holo-complex was easily detected in mitoplasts and mitochondria with COX abundance/activity around 10% control values. Therefore it seems that the failure to detect COX sub-complex in *Δshy1* yeast simply reflects an

inability to detect low abundance signals and the presence of stable COX sub-complexes in *Δshy1* yeast and other yeast Cox-assembly mutants should not be ruled out.

16.2 A COMPLEX II SUB-COMPLEX IS RESOLVED IN MAMMALIAN SAMPLES USING BN-PAGE

OXPHOS complexes were identified from their relative migration in comparison to published work from Schägger[32-34,682], *in gel* enzyme activity stains and western blotting. On longer exposures of blots of rat heart mitochondria probed with anti-ATP5A1 and anti-UQCRC2, minor signal bands could be seen indicating that under the conditions used, these proteins resolved as components of the major OXPHOS complexes and also less abundant complexes of varying sizes. The identity of these potential complexes was not investigated although their presence serves to indicate the complexity of samples resolved using BN-PAGE.

Anti-SDHA cross-reacted with two signal bands in both rat and human samples. In human samples, anti-SDHB also cross-reacted with both bands. *In gel* SDH activity stains using rat heart mitochondria confirmed that complex II was the slower migrating of the two bands. Little analysis of the solubilisation and resolution of complex II using BN-PAGE has been published. Schägger has noted that the uncleaved precursor of SDHD co-migrates with complex II[34], consistent with pre-sequence cleavage occurring after assembly of the complex. On western blots of 5-16% gels of human fibroblast samples, Antonicka and co-workers have identified SDHA signal corresponding to complex II alone in some studies[492,505], while in another they clearly show SDHA signal migrating below complex II[776]. Bands of SDH activity migrating both above and below complex II have been documented in yeast samples resolved using 7-16.5% gels[777,778]. In the samples resolved here, larger complexes were not identified which may reflect differences in the solubility of complex II multimers between yeast and mammalian systems or alternative associations of the yeast enzyme not present in mammals. The lack of SDH activity in the lower band resolved in the rat samples may be due to a number of factors. Clearly, it may reflect a genuine lack of activity but alternatively it could be a result of the complex running close the dye-front. This region of the gel probably contained a lot of G250 and free detergent micelles which may have interfered with activity. In addition, the lower band appears much less abundant than the complex II signal on western blots of rat samples and it may be that there was insufficient activity in the band to register signal.

The presence of Sdh1p and Sdh2p* in each SDH band has been confirmed by western blotting in yeast and this has lead to speculation that the lower band corresponds to an Sdh1p•Sdh2p dimer[777,778†]. This is in agreement with the results of this study. Moreover, the migration of the lower band relative to the OXPHOS complexes and other marker proteins such as HSPA9B, is consistent with the predicted protein molecular weight of 97 kDa for an SDHA•SDHB dimer. Therefore, given the conservation of OXPHOS complex structures and the resolution of an apparently identical complex II sub-complex in human, rat and yeast samples, the faster migrating SDHA signal band has been used as a ~97 kDa molecular weight marker for estimation of the sizes of novel sub-complexes throughout this thesis.

16.3 ABUNDANT COX SUB-COMPLEXES ARE PRESENT IN *SURF1* MUTANT CELLS

COX sub-complexes were identified in all samples, including controls (table 21). Complex *ab* that corresponded to active COX and subcomplexes *c*, *e* and *f* were the only sub-complexes detected in controls, P2, P3, P6 and the *COX10* mutant disease control (P9). In addition to these complexes, sub-complexes *d* and *g* were detected in the *SURF1* mutant cultures (P1, P4, P5 & P7) and the *SCO1* mutant disease control (P8).

16.3.1 The abundance and composition of COX sub-complexes in *SURF1* and *SCO1* mutant cells correlates with COX subunit signatures

The presence of low levels of the COX holo-complex and the accumulation sub-complexes *d* and *g* in the *SURF1* mutant cell cultures provides a basis for the subunit signatures seen in these cells. MTCO1, COX4I1 and COX5A which are components of sub-complexes *d* and *g*, were all present at intermediate levels in the *SURF1* mutant cells. MTCO2 and COX6C which were not detectable in these sub-complexes, were present at very low levels. In comparison to the other patient fibroblasts cultures, the levels of MTCO1 were generally higher in the *SURF1* mutant cultures yet the abundance of the COX holo-complex, as determined using cytochrome a_3 levels or enzyme activity, showed little variation among the patient cultures (with the exception of P6 which was

---

* Homologues of SDHA and SDHB respectively.

† Work by Dibrov and co-workers[779] failed to identify Sdh1p and Sdh2p signal migrating faster than complex II. However no details at all of the BN-PAGE protocol used were published and from the relative migration of complex V, complex II and cytochrome c oxidase in their figures, it appears much lower gel gradients were used consistent with potential Sdh1p•Sdh2p dimers running off their gels.

considerably higher than the other samples). The disparity between relative MTCO1 levels and relative holo-complex levels is therefore explained by the accumulation of MTCO1-containing sub-complexes in the *SURF1* mutant cells. This observation suggests that other subunits found at very low levels in the *SURF1* mutant cells such as MTCO3 and COX6B, are likely to be predominantly present as components of the holo-complex and not sub-complexes. It is difficult to speculate whether the more abundant subunits are components of the same sub-complex as pools of retained subunits are not necessarily associated e.g. MTCO1 was present in sub-complex *d* but also sub-complexes *e*, *f* and *g*. A key finding of this study based on the composition of COX sub-complexes, is that subunits such as MTCO1 and COX4I1 are poor indicators of the abundance of COX holo-enzyme. More suitable markers would be those subunits which were not detected in sub-complexes such as MTCO2, MTCO3 or COX6C.

The fact that the same subunit signature was not seen in the *SURF1* and *SCO1* mutant cells despite accumulating the same COX sub-complexes, reflects the much lower abundance of the COX sub-complexes relative to the holo-complex in the *SCO1* mutant cells. Without knowing more about the function and redundancy of SURF1 and SCO1 and the impact of P174L on SCO1 function, it is difficult to decipher why this was the case. The low levels of MTCO1 in the *COX10* mutant fibroblasts correlates with the low levels of the COX holo-complex and the absence of accumulation of sub-complexes *d* and *g*.

The relative abundance of the COX sub-complexes between the four *SURF1* mutant cultures is difficult to assess because of the variation in the protein loading of the mitoplast samples. Mitoplast samples were loaded on the basis of manual cell counts. As such, intrinsic errors in cell counts and variations in cell size are likely to have affected results. Reductions in cell size, associated with increases in the density of adherent cells, have previously been shown to lead to ~2-fold decrease in rates of oxygen consumption as a function of cell number while in the same samples, oxygen consumption as a function of total protein remained unaltered[780]. Comparison of OXPHOS subunit levels in P1, P4 and P5 indicated that steady-state subunit levels as a function of total protein are similar in *SURF1* mutant cells supporting this assessment and the same must also hold true for the other patient and control mitoplast samples studied. Nevertheless, it should be noted that despite the subtle variation in loading seen on the 1D BN-PAGE blots, the consistent detection of sub-complexes *e* and *f* in all samples confirms that loading was good enough to enable detection of minor signals in

all samples and as such both the 1D and 2D protocols provide a valid assessment of the spectrum of sub-complexes present in the various cell types.

16.3.2 Comparisons with COX sub-complexes previously identified in normal and COX deficient fibroblasts

Comparisons of the relative migration and composition of the sub-complexes identified by Nijtmans and co-workers [477] (5.1.3) to those found in this study suggests that they are the same species. As defined by Nijtmans; S1 contains only MTCO1 which matches sub-complexes *e*, *f*, and *g*, S2 is composed of at least MTCO1 and COX4I1 but not MTCO2 which matches sub-complex *d*, and S3 migrates slightly faster than the holo-complex (S4), which is similar to band *c*.

16.3.2.1 SURF1 mutant cells

Since Nijtmans' study, COX sub-complexes with relative migrations matching S1-S3 have been observed in control and *SURF1* mutant fibroblasts by a number of groups using western blotting. Employing identical methods of mitoplast preparation and solubilisation to those used here, Tiranti *et al* described accumulation of sub-complexes with distributions of MTCO1, MTCO2 and COX4I1 corresponding to S1-S3, although only data regarding MTCO1 was published[529]. Similar results were obtained by Coenen *et al*, looking exclusively at MTCO1 distribution in *SURF1* mutant fibroblasts[540] and MTCO1 signal corresponding to S1-S3 has been identified in fibroblasts derived from *SURF1* knock mice[539]. Sucrose gradient centrifugation has also been used to reveal COX sub-complexes in mitochondria from *SURF1* mutant fibroblasts[772]. Although separation of the complexes was not achieved, western blotting indicated the presence of MTCO1, COX4I1 and COX5A but not MTCO2 sedimenting above the holo-complex. Previously a similar study using glycerol gradient centrifugation demonstrated that Cox1p, Cox3p, Cox5ap* and Cox6p† sediment above the holo-complex in *Δcox4*‡ yeast[781], although the data in this study were not normalised.

The identification of abundant COX sub-complexes resembling assembly-intermediates in *SURF1* mutant cells has led to the widely accepted view that they represent pools of assembly-intermediates which accumulate due to stalled biogenesis of the enzyme[529,540,772]. Although the exact role of SURF1 remains an enigma, *Δshy1* yeast

---

* COX4I1 homologue.
† COX5A homologue.
‡ COX5B homologue.

have a clear defect in the synthesis Cox1p that can be rescued by overexpression of the translational regulator Mss51p[478,541]. This implies that *SURF1* loss of function impacts on the assembly as opposed to the stability of the COX holo-complex. This view is strengthened by the finding in this study that *SCO1* mutant cells accumulate the same spectrum of COX sub-complexes as *SURF1* mutant cells because SCO1 is clearly involved in the assembly of the holo-complex[782-784] (5.2.2.2).

16.3.2.2 SCO1 and SCO2 mutant cells

Very recently, Leary and co-workers published BN-PAGE investigations of *SURF1*, *SCO1* and *SCO2* mutant cells using P8 as their *SCO1* mutant model[519]. COX sub-complexes containing MTCO1 and COX4I1 were found in all the patient cells but not in controls, again emphasising the benefits of optimisation of sub-complex detection in the present work. The sub-complex signal identified by Leary was not resolved as multiple small sub-complexes due to the use of 6-15% gels as opposed to the 8-16% gels employed here. Despite this, their work confirms the findings of this study that COX sub-complexes accumulate in both *SCO1* and *SURF1* mutant cells. This strongly suggests that disruption of CuA synthesis perturbs COX biogenesis at a similar point to loss of SURF1 function and is discussed in further detail below (17.1.4.2; 17.2).

16.3.2.3 COX10 and COX15 mutant cells

In agreement with the results of this study, previous work by Antonicka and co-workers failed to identify abundant COX sub-complexes in *COX10* mutant fibroblasts[492]; however, Antonicka also failed to confirm the presence of COX sub-complexes in control samples. Despite this though not acknowledged in the text of the paper, faint pairs of spots identical to sub-complexes *e* and *f* can be seen in certain control and *COX10* mutant samples resolved in 2D*. Investigation of *COX15* mutant fibroblasts by Antonicka and co-workers also established that these cells do not accumulate COX sub-complexes[505], although here again, sub-complexes were not identified in control samples. These inconsistencies support the optimisation of signal detection carried out in this study (16.1). In spite of these differences, results described above imply that disruption of COX biogenesis at the level of haem A synthesis, does not lead to the accumulation of very abundant COX sub-complexes as seen in *SURF1* mutant cells. This finding is discussed further below (17.1.4.2).

---

* Figure 3.

16.4 Prospective Identities And Origins Of COX Sub-Complexes

On the basis of Nijtmans' metabolic labelling there is clearly evidence for a biological origin for COX sub-complexes, however, assigning purely biological origins to complexes resolved using BN-PAGE overlooks the potential for dissociation of protein complexes during solubilisation and electrophoresis. Solubilisation of any sample, even under ostensibly native conditions, clearly involves disruption of quaternary structure. For instance, separation of the OXPHOS into the five constituent complexes requires dissociation of OXPHOS super-complexes[29,36], bound matrix enzymes[20,22] (1.3) and both COX and complex V dimers. Therefore, the spectrum of protein complexes resolved using BN-PAGE should be considered a combination of both *biological* complexes present *in vivo* and *artefactual* complexes partially denatured during solubilisation.

During the 1980's and 1990's, close scrutiny of the nature of COX preparations demonstrated that the holo-complex dissociates through a series of stable sub-complexes which can be resolved using chromatography or electrophoresis. The relative abundance of these complexes increases under more solubilising conditions[785,786] indicating that they are generated *in vitro*. It was reasoned that sample preparation for BN-PAGE would lead not only to solubilisation of the five OXPHOS complexes, but also the creation of more dissociated complexes, arising as a consequence of the solubilisation procedures. The loss of small, labile subunits from purified bovine complex III during BN-PAGE has previously been noted by Schägger[32]. In the analysis that follows, biological and artefactual origins for the COX sub-complexes resolved in this study are discussed.

16.4.1 Complexes *a* and *b*

The COX holo-complex migrated as a close pair of bands in both the rat heart mitochondria samples and the human samples and the holo-complex signal has been referred to as band *ab*. The individual bands were only clearly discernable on the western blots of human fibroblasts in patient samples as signal was saturated in control samples. The migration of the COX holo-complex as a tight pair of bands has not previously been described in yeast or mammalian samples. Part of the reason for this is probably the paucity of BN-PAGE data generated using gel gradients of 8-16% or higher. The vast majority of published data regarding OXPHOS complex isoforms has been generated using 4/5-13% gradients suitable for resolution of both individual OXPHOS complexes and OXPHOS super-complexes[28,29,34,787]. In published images of 1D gels, the

COX holo-complex is identified as a characteristic broad band of protein[34] or activity stain[492,788,789] and on second dimension gels it generally resolves as a series of broad elliptical spots[34,681,790] as also seen in this study. These findings raise the possibility that the close pair of bands identified here on high resolution 1D blots are not unique.

16.4.1.1 Cytochrome c binding

It was thought that bands *a* and *b* might represent cytochrome c-bound and -unbound forms of the holo-complex but western blotting failed to identify any anti-CYCS cross reactive material. A single study alleges to have resolved of cytochrome c with both complex III and COX in rat heart mitochondria using 2D BN-PAGE/denturing-PAGE[791]; however, cytochrome c has not been identified bound to complex III or COX in any other studies of OXPHOS complexes, even under the mild solubilisation conditions required for resolution of OXPHOS super-complexes[38,792]. This supports the interpretation of the results here that bands *a* and *b* do not originate from binding of residual cytochrome c to a pool COX holo-complex.

16.4.1.2 Speculation on the identity of complexes a and b: Loss of COX6A1 and COX6B is common under conditions similar to BN-PAGE

As has been previously found for complex III[32], loss of small labile subunits provides a good mechanism for the generation of multiple signals for the COX holo-complex. Clues to the likely identity of the missing subunits comes from work examining the stoichiometry of complexes present in COX preparations under conditions similar to those used for BN-PAGE*. In a detailed study of the hetero-dispersed nature of cholate purified COX[687], Heinrichs *et al* resolved five different isoforms of the bovine enzyme[785] (table 25). The complexes were separated using discontinuous pH gradient native-PAGE with low salt buffers† and a range of concentrations of LM or Triton X100. The two largest isoforms they identified were an intact isoform, separated at 12 subunit resolution, and a form lacking COX6A1 and possibly COX6B. Much like the dissociation of the small subunits UQCRFS1 and UQCR from complex III[793] noted by Schägger, the lability of COX6A1 and COX6B has also been noted in high resolution quantitative analysis of bovine COX. Mono-Q fast protein liquid chromatography (FPLC) of purified bovine heart

---

* Rat heart mitochondria were solubilised at 0.2-1.6 mg/ml protein in a buffer containing final concentrations of 37.5 mM bis-Tris (pH 7.0), 0.75 M 6-aminohexanoic acid and 49 mM LM. Crude mitoplast pellets were solubilised at ~0.8 mg/ml protein in a buffer containing final concentrations of 41.5 mM bis-Tris (pH 7.0), 0.83 M 6-aminohexanoic acid and 32.7 mM LM. See Materials and Methods.

† 63 mM Tris-phosphate pH 7.3.

enzyme demonstrated that in various buffers containing 1 mM LM and 400 mM salt, COX eluted from columns as two major peaks, a 13-subunit form and an 11-subunit form missing COX6A1 and COX6B[786]. The lability of these two subunits was found to be sensitive to increases in pH and the type of salt used. Similarly in a study using gel filtration, it was found that COX6B could be selectively removed from the holo-complex solubilised in 1 mM LM by the addition of a high salt concentration (1M KCl) to the elution buffer[794]. The 11-subunit form of the enzyme can also be generated by enzymatic digestion of cardiolipin bound to Triton X100-solubilised enzyme, indicating that retained lipids may be involved in the association of these subunits with the holo-complex[795]. In yeast samples, Triton X100 solubilisation alone is sufficient to remove the homologous subunits[796]. The salt concentrations and the type and concentrations of detergents used in the above examples suggest that loss of COX6A1 and COX6B may well occur during BN-PAGE sample preparation or electrophoresis.

16.4.1.3 Activity and migration of sub-complex b is consistent with loss of COX6A1 and/or COX6B

In agreement with the two sharp bands of COX activity seen in the rat heart mitochondria samples examined in this study, COX6A1 and/or COX6B depleted forms of the enzyme are active. The KCl-treated, COX6B-depleted form of COX has increased activity compared to the holo-enzyme[794], the FPLC-purified 11-subunit form maintains normal activity and biphasic kinetics[786] and the cardiolipin-depleted 11-subunit form maintains around 50% of control activity[795]. In addition, *ΔCox13*[*] yeast retain some COX activity that is near normal at low ionic strength[797, 863]. Thus the proposal that sub-complex *b* may be missing COX6A1 and/or COX6B is compatible with both bands *a* and *b* being enzymatically active.

Complexes *a* and *b* migrated very close together and were thus likely to be very similar in size. The 13-subunit COX holo-complex migrates with an apparent molecular weight of around 200 kDa[32,35]. A human 12-subunit form depleted of either COX6A1 or COX6B would have a protein molecular weight of ~195 kDa and an 11-subunit form depleted of both subunits would have protein molecular weight of ~185 kDa (table 2). At the gel densities and migration of the holo-complex size differences of 5-10% would lead to very small differences in migration and in terms of changes in size the 12- or 11- subunit isoforms are good candidates for the relative migrations observed. The molecular weight

[*] Homologue of COX6A1.

predictions only account for the protein mass of the complexes and do not take into account changes in lipid or detergent association. Alterations in either or both of these could also affect migration, particularly in systems such as BN-PAGE which do not have good relationships between mass and migration[32]. In addition, loss COX6A1 and COX6B does not significantly affect the size of the COX monomer, thus the molecular sieving effects of BN-PAGE[32,682] may not lead to a large difference in migration of the 13 and/or 12- or 11-subunit forms.

16.4.1.4 Evidence of the loss of small subunits from plant COX under BN-PAGE conditions

Further evidence that bands *a* and *b* may result from loss of either or both of COX6A1 and COX6B comes from work examining the plant inner-membrane proteome using BN-PAGE. Eubel and colleagues recently resolved OXPHOS super-complexes from various plants*[29]. In contrast to yeast and bovine samples[28], no super-complexes containing COX were identified, however in digitonin solubilised samples, two isoforms of monomeric COX were found termed complexes *IVa* and *IVb*. They migrated with apparent molecular weights of 300 and 220 kDa and were composed of 12 and 10 subunits respectively. Little is known about the subunit composition of the plant COX holo-complex[29]. Analysis of a 32 kDa protein unique to complex *IVa* found that the C-terminal portion of this protein was homologous to mammalian COX6B (10 kDa). Another <6 kDa protein was also only present in complex *IVa*. Thus, the difference in migration of these two forms of COX was due to loss or absence of two small subunits, one of which is homologous to COX6B. If analogous complexes were present in the human and rat samples analysed here, then the large size of the plant COX6B isoform identified by Eubel, may well account for the much larger difference in relative migration of the two bands in plants.

16.4.1.5 Summary

Given the evidence presented above that COX6A1 and COX6B are easily dissociated from the enzyme under conditions similar to BN-PAGE and that the 11 and 12-subunit isoforms are enzymatically active as seen in the rat samples, it is reasonable to predict that bands *a* and *b* are 13-subunit and 12- or 11-subunit forms of COX (figure 74). Accepting the generally held view that the 13-subunit form of the enzyme is the predominant monomer *in vivo*, it seems likely that potential COX6A1 and/or COX6B

---

* Mustard, *Arabidopsis thaliana*; potato, *Solanum tuberosum*; bean, *Phaseolus vulgaris* and barley *Hordeum vilgare*.

depleted forms are artefacts present as a result of the solubilisation procedure employed for BN-PAGE.

16.4.2 Sub-complex c

On 1D blots of human samples band *c* migrated slightly faster than the COX holo-complex (*ab*) but behind complex II and co-migrated with a persistent non-specific signal. At least one COX subunit spot corresponding to COX sub-complex *c* could be distinguished in all samples on 2D blots with strong signals. The presence of at least one spot, usually MTCO2, in each sample was taken as evidence for the presence of sub-complex *c* as the sensitivity of the primary antibodies used was not homogenous and had subunits been absent from the complex the migration of detectable subunits would not have been consistent. No COX activity could be detected corresponding to sub-complex *c* on *in-gel* activity stains of rat heart mitochondria.

16.4.2.1 The non-specific component of band c

The non-specific component of band *c* on 1D blots may have been due to cross-reaction with collagen. Type I collagen is secreted at high levels by dermal fibroblasts in culture[658] and its production is stimulated by proteases such as thrombin[798] which is present at variable levels in FBS*, and trypsin which was used for passaging cell cultures. The variable intensity of this band both between and within samples suggests that it was a species present at changeable levels in fibroblast which fits well with the inducible, persistent nature of collagen. Hydrophobic and ionic interactions between collagen fibres and IgG antibodies and HRP are well documented[799] and it possible that such interactions were responsible for the non-specific cross-reaction of secondary antibodies with the solubilised, native protein migrating in this band. Type I procollagen has molecular weight of 139 kDa† which is in good agreement with the relative migration of this species on both 1D and 2D blots. During synthesis and maturation, procollagen is present in the ER and secretory vesicles[568] and could have easily co-purified in crude mitoplast preparations. In light of this, it was apparent that the non-specific component of band *c* was less problematic on 1D blots and undetectable on 2D blots, loaded with purified mitochondria.

---

* Foetal bovine serum, all fibroblasts were cultures in media containing 10% FBS. Serum was not heat inactivated during this study.
† COL1A1, NCBI protein database.

Table 25 The relative abundance and components of COX sub-complexes resolved from cholate purified enzyme using DG-PAGE, after Heinrichs *et al*[785]. Band nomenclature is as in original paper.

	Relative abundance as percentage of total signal according to densitometry of DG-PAGE 1st dimension.						Components of band according to presence in denaturing-PAGE 2nd dimension.											
Preparation	None				AEC	Alkali & AEC												
Detergent (mM)	LM		TX100		TX100	TX100												
	10	2	4.5	1.5	1.5	1.5	MTCO1	MTCO2	MTCO3	COX4	COX5A	COX5B	COX6A1	COX6B	COX6C	COX7A2	COX7B/ COX7C	COX8A
Band 1	22	41	24	7	9	2	●	●	●	●	●	●	●	●	●	●	●	●
Band 2	25	10	28	30	28	13	●	●	●	●	●	●	○	○/●	●	●	●	●
Band 3	47	31	34	41	42	58	●	●	○	●	●	●	○	○	●	○	●	●
Band 4	5	17	12	18	21	27	●	●	○	●	●	○	○	○	○/●	○	●	●
Band 5	1	1	2	4	np	np	○	○	○	●	●	○	○	○	○	○	○	○

Key: DG-PAGE= discontinuous pH gradient native-PAGE, AEC= anion exchange chromatography, TX100= Triton X100, LM= lauryl maltoside, np= not present. Components, ●= present; ○= not present, ○/●= present at very low levels.

16.4.2.2 COX subunit components of sub-complex c

As far as can be distinguished by a visual comparison, the migration of sub-complex *c* is identical to that of assembly intermediate S3 identified by Nijtmans, using both western blotting and metabolic labelling[477]. The same sub-complex has been identified using western blotting in control and *SURF1* mutant human fibroblasts[529,540], control and *SURF1* mutant murine fibroblasts[579], tumour cells and *MTCO3* mutant (100%) tumour cell cybrids[619]. All of the afore mentioned studies also identified smaller COX sub-complexes in control and/or mutant samples. Studies which failed to identify small COX sub-complexes using western blotting also fail to attribute signal to S3 confirming the low abundance of this species[492,505].

A similar species to sub-complex *c* has been identified by Schägger on protein stains of 2D BN-PAGE/denaturing-PAGE gels of mitochondria from MOLT4 lymphoblasts[34]. Termed complex *IV'*, it was calculated to migrate with an apparent molecular weight of around 150 kDa. This compares very well with the migrating of sub-complex *c* in comparison to complex II (130 kDa) and COX (200 kDa) and suggests that S3, complex *IV'* and sub-complex *c* are the same species. The second dimension, tricine-SDS-PAGE gels used by both Nijtmans and Schägger do not enable separation of the closely migrating subunits of COX. Thus, neither has presented significant information regarding the composition of the sub-complex as neither was able to separate signal for MTCO2 and MTCO3, nor COX5A and COX5B, nor COX6A1, COX6B and COX6C nor COX7A2, COX7B and COX7C. The analysis presented here that sub-complex *c* contains at least MTCO1, MTCO2, COX4I1 and COX5A does not provide any significant new detail on the composition of this sub-complex.

16.4.2.3 Speculation on the identity of sub-complex c: Loss of MTCO3 is common under conditions similar to BN-PAGE

As with the proposals regarding the identity of bands *a* and *b*, clues to the likely composition of sub-complex *c* come from early work examining the hetero-dispersed nature of solubilised COX preparations and the effects of LM solubilisation on COX. In the work described above from Heinrichs *et al*[785], an abundant isoform of COX depleted of MTCO3, COX6A1, COX6B, COX7A2 was identified in all samples (band 3; table 25). This is testament to the fact that MTCO3 is easily dissociated from the holo-enzyme. Heinrichs and others have demonstrated that it can be removed by alkali treatment[785,800],

chymotrypsin treatment[801], Triton X100 treatment[785] and importantly treatment with LM[785,802-804].

Heinrichs observed a high proportion of MTCO3-depleted enzyme in solutions of COX at 10 mM and 2 mM LM. Mono-dispersed solutions of MTCO3-depleted enzyme can be obtained from rat liver using a chromatographic procedure with no higher than 50 mM LM in any solution[802]. Similarly, preparations of the bovine enzyme can be completely depleted of MTCO3 by overnight incubation at 0.5 mg/ml protein in a buffer of 20 mM Tris (pH 7.8), 1 M NaCl, 1 mM EDTA and an LM concentration of 10-20 mM[803]. Dissociation of MTCO3 has previously been identified as a problem in immuno-precipitation experiments. Substoichiometric amounts of MTCO3 have been recognised for a long time in immuno-precipitated forms of COX[805,806] and specific loss of MTCO3, COX6A1, COX6B and COX7A2 signal has been noted during immuno-precipitation of the holo-complex from samples incubated overnight at ~2 mg/ml protein, ~160 mM salt (PBS) and 30 mM LM[181]. In the above examples the protein, salt and detergent concentrations used to deplete purified COX of MTCO3 are close to those used for BN-PAGE*. It therefore seems very likely that MTCO3-depleted sub-complexes could originate from the solubilisation procedures employed for BN-PAGE.

16.4.2.4 The migration of sub-complex c is similar to that predicted for an MTCO3-depleted sub-complex

In agreement with Heinrichs, Nalecz *et al*[804] also noted that depletion of MTCO3 by LM and KCl was accompanied by loss of COX6A1, COX6B and COX7A2. This pattern of subunit dissociation is supported by the crystal structure of the bovine enzyme as COX6A1, COX6B and COX7A2 all associate closely with MTCO3. An MTCO3•COX6A1•COX6B•COX7A2 depleted monomer has a calculated protein molecular weight of 147.7 kDa (table 2). This figure is very close to values obtained by Ferguson-Miller and colleagues of 152±6 kDa for the LM purified, MTCO3-depleted rat liver enzyme, measured using sedimentation equilibrium[807]. Importantly, this also matches the apparent molecular weight of sub-complex *c* of 150 kDa determined by Schägger. In light of this observation it should be remembered that neither Schägger[34] nor Nijtmans[477] demonstrated the presence of MTCO3 in sub-complex *c*. The assertion by Nijtmans and co-workers that sub-complex *c* has a molecular weight of 180 kDa[477]

---

* Rat heart mitochondria were solubilised at 0.2-1.6 mg/ml protein in a buffer containing 37.5 mM bis-Tris (pH 7.0), 0.75 M 6-aminohexanoic acid and 49 mM LM. Crude mitoplast pellets were solubilised at ~0.8 mg/ml protein in a buffer containing 41.5 mM bis-Tris (pH 7.0), 0.83 M 6-aminohexanoic acid and 32.7 mM LM.

and is missing only COX6A1 and either COX7A2 or COX7B is inconsistent with the relative migration of the complex and their own data which was incapable of resolving most of the COX subunits.

Perhaps the strongest evidence that sub-complex *c* does not contain MTCO3 comes from work looking at tumour cell cybrids with a 100% mutant load of a premature termination codon in *MTCO3*[619]. According to sensitive metabolic labelling experiments, such cells do not maintain any detectable wild-type or truncated MTCO3. Given the complexities of MTCO3 processing involving transition through the OXA1 complex and membrane insertion machinery, membrane chaperones such as prohibitin complex and associated proteases such as the *m*-AAA (4.2.6.2; 4.3.1.3; 4.3.2.2), it is very unlikley that a truncated form of MTCO3 would avoid degradation and be correctly processed into the holo-complex. Moreover, the mutation in question (P111X) removes all the helices required for COX6A1, COX6B and COX7A2 binding, exposing core residues of the protein to proteases. On 2D BN-PAGE/denaturing-PAGE blots probed for MTCO1, the COX holo-complex was not detectable in the mutant *MTCO3* cybrids, whereas an abundant complex aligning with a sub-complex present in controls, which migrates in the same position relative to the holo-complex as sub-complex *c*, was present[619] (described as S3 by the authors). Hence, cells which are incapable of maintaining MTCO3, can accumulate a sub-complex indistinguishable from sub-complex *c*[*].

16.4.2.5 The lack of COX activity of sub-complex c is consistent with loss of MTCO3

Studies of *Rhodobacter sphaeroides* have shown that purified CoxIIIp-depleted and genetically CoxIIIp-deficient (*ΔCoxIII*) forms of COX are very similar. The full complement of COX redox centres are present in both and both have near normal haem environments, CO- and CN-binding characteristics and V_{max} measurements[808]. However, the incomplete enzyme displays rapid suicide inactivation with a half-life around 2% that of the intact enzyme[808]. Rapid inactivation has also been observed for the *Paracoccus denitrificans* enzyme lacking *CoxIII*[809] and although the data remains unpublished, the MTCO3-depleted mammalian enzyme has also been reported to behave similarly[808]. In agreement with these enzymatic findings, homoplasmic human *MTCO3* mutant cybrids,

---

[*] The presence of COX sub-complexes has also been examined by immuno-precipitation in cybrids homoplasmic for a 5 residue deletion in *MTCO3*[481]. No sub-complexes were found in the mutant cybrids; however, as this study also failed to demonstrate significant association of MTCO1, MTCO2 and MTCO3 in control cells this finding can be disregarded.

which are unable to assemble the holo-complex but, as mentioned above, contain a sub-complex similar to sub-complex *c*, have COX activities of around 11% control values[619].

In the present work, *in-gel* activity stains were developed for 1-5 hours at 37°C to generate maximum signal. Suicide inactivation due to absence of MTCO3 offers a good explanation as to why such a large sub-complex containing both MTCO1 and MTCO2 did not stain for COX activity. If the speculation on the identity of sub-complex *c* is correct, the normal CO-binding characteristics described for the CoxIIIp deficient enzyme from *Rh. sphaeroides* are unlikely to have impacted significantly on measurements of haem a_3 abundance on account of the very low relative abundance of sub-complex *c*.

16.4.2.6 Speculation on the origin of sub-complex c

From the information presented above, it is clear that loss of MTCO3•COX6A1•COX6B•COX7A2 can occur under conditions very similar to those used for BN-PAGE[785,802-804], that sub-complexes missing these subunits have a molecular weight[807] that matches the migration of sub-complex *c*[34] and that the lack of activity of sub-complex *c* is consistent with the suicide inactivation of MTCO3-depleted enzymes[808,809]. Therefore, it is reasonable to speculate that sub-complex *c* is an isoform of COX missing MTCO3•COX6A1•COX6B•COX7A2 and that, as is assumed for sub-complex *b*, it could arise as an artefact of the solubilisation procedure employed for BN-PAGE. Yet a biological origin also exists for sub-complex *c* as an assembly intermediate as confirmed by metabolic labelling[477] and its accumulation in cybrids with mutant *MTCO3*[619]. As no confirmation of the presence of MTCO3 or specific small subunits in sub-complex *c* arising as an assembly intermediate has ever been presented, it is entirely possible that this form of sub-complex *c* is also missing MTCO3, COX6A1, COX6B and COX7A2, as has been proposed for solubilisation artefacts. This in agreement with proposals that MTCO3 is incorporated into the holo-complex at a late stage based on the presence of COX redox centres in *ΔCoxIII* strains of *Rh. sphaeroides*[808,810] and the residual COX activity present in *ΔCoxIII* strains of *P. denitrificans*[809,811,812] and human *MTCO3* mutant cybrids[619]. Furthermore in *N. crassa*, nascent Cox3p appears as a component of the holo-complex more rapidly than nascent Cox2p or Cox1p indicating that it is incorporated after these subunits[467].

16.4.2.7 Summary

As dissociation as an artefact of BN-PAGE and late incorporation of MTCO3•COX6A1•COX6B•COX7A2 are indistinguishable and not mutually exclusive, it is

impossible to determine an origin for sub-complex *c* as identified in this study. It is entirely feasible that sub-complex *c* may represent a pool of enzyme lacking MTCO3•COX6A1•COX6B•COX7A2 originating both as a solubilisation artefact and a *bona fide* assembly intermediate (figure 74).

16.4.3 Sub-complexes *d, e, f* and *g*

Sub-complexes *d*, *e*, *f* and *g* all migrated significantly faster than the holo-complex and sub-complex *c*. Sub-complexes *e* and *f* could be detected in all samples, whereas sub-complexes *d* and *g* were only detected in *SURF1* or *SCO1* mutant samples.

16.4.3.1 Overall comparison to small sub-complexes identified by other groups using BN-PAGE

There is considerable variation in published results regarding the identification of small COX sub-complexes resembling sub-complexes *d*, *e*, *f* and *g*. Small COX sub-complexes were first identified in control MOLT4 lymphoblasts by Nijtmans using metabolic labelling and western blotting[34]. In other studies small sub-complexes have not always been detected in control samples. In most cases, studies which detect small sub-complexes in control samples have also detected them in COX deficient samples[281,529,540,619]. Conversely, those studies that fail to detect small sub-complexes in control samples have not found them in COX deficient samples[492,505]. In addition to this variability in detection, only a single previous study has found a size range of small COX sub-complexes in *SURF1* mutant cells different from that of controls[529], as was seen here. In other work, small sub-complexes have either been found over the same size range as controls but at a higher abundance in *SURF1* mutant cells[540] or have only been detected in *SURF1* mutant cells and not controls[539].

As small COX sub-complexes are not abundant species and almost identical sample preparation, gel gradients and electrophoresis protocols have been used by all groups, the inconsistency in detection of small COX sub-complexes is best explained by variation in the ability to detect low intensity signals. This view is supported by the improvements seen in the results of this study following optimisation of signal detection and reduction of signal loss during 2D BN-PAGE (16.1). A conclusion that can be drawn from this is that the unique pattern of small sub-complexes seen in this study reflects better detection of species previously resolved but not detected by other groups and not the isolation of novel COX sub-complexes. The difficulty the field as a whole has had in reproducibly

detecting small COX sub-complexes suggests that their abundance is towards the limit of detection of western blotting using ECL/X-ray film techniques and the loading attainable in BN-PAGE. This underlines the value of parallel investigation of multiple samples as carried out in this thesis.

16.4.3.2 Speculation on the origin and identity of sub-complex d

Sub-complex *d* was only detectable in *SURF1* and *SCO1* mutant samples and was composed of at least MTCO1, COX4I1 and COX5A but did not contain MTCO2 or COX6C. As forms of COX depleted of MTCO2 have not been identified in studies of LM-solubilised enzyme and sub-complex *d* was not found at high levels in control cells, it is unlikely that it originates from artefactual dissociation of the holo-complex. The relative migration of sub-complex *d* matches an assembly intermediate (S2) identified in control MOLT4 cells by Nijtmans[477] and a sub-complex present at high steady-state levels in *SURF1* mutant fibroblasts[529,540,772]. Significantly the results of this study enables a revision of the components of sub-complex *d* to also include COX5A. Sub-complex *d*-like species are considered to represent assembly-intermediates, normally present at very low steady-state levels in control cells, that accumulate to higher levels in cells with disrupted COX biogenesis[529,772]. The results of the present study do not question this hypothesis.

16.4.3.3 Speculation on the origin and identity of sub-complex g

Sub-complex *g* contained full size MTCO1 yet migrated ahead of purified holo-MTCO1. The rapid migration of this sub-complex suggests that is represents a free form of apo-MTCO1. The disparity between the migration of purified holo-MTCO1 and sub-complex *g* is probably due to the use of SDS in the purification of holo-MTCO1. It is also possible that sub-complex *g* is a form apo-MTCO1 without the covalent cross-bridge between His240 and Tyr24 present in holo-MTCO1[49] and that the lack of this structural feature may have affected migration. The timing of formation of this cross-bridge relative to the other aspects of COX biogenesis remains unknown.

At first glance much of the evidence that sub-complex *d* is an accumulated assembly intermediate also holds true for sub-complex *g*. As with accumulation of sub-complex *d*, a fast-migrating MTCO1 signal has consistently been observed in *SURF1* mutant fibroblasts[529,539,540] and sub-complex *g* resembles an assembly intermediate described as a form of nascent MTCO1 by Nijtmans (S1)[477]. However evidence suggest that sub-complex *g* is in fact not analogous to S1. Firstly, sub-complex *g* was not detected in

COX10 mutant cells in this study nor in *COX10* or *COX15* mutant cells examined by others[492,505]. If the form of MTCO1 present in sub-complex *g* originated upstream of the action of COX10 and COX15, i.e. was nascent MTCO1, it would also be expected to accumulate in *COX10* and *COX15* mutant cells due to the downstream disruption of haem A incorporation. Therefore, following the accepted view that haem A incorporation into MTCO1 occurs early in COX assembly and given the evidence that sub-complex *g* accumulates in certain cell types with disrupted COX biogenesis, sub-complex *g* must originate downstream of haem A incorporation.

In both *SURF1* and *SCO1* mutant cells, sub-complexes *d* and *g* were always detected together, implying that the presence of the two sub-complexes was connected. There are a number of possibilities that may account for a connection between the two sub-complexes. Firstly, they may be connected biologically, sub-complex *g* may be a breakdown product of sub-complex *d* or an *off-path* intermediate induced by the accumulation of sub-complex *d*. Alternatively, sub-complex *g* may be derived from artefactual dissociation of sub-complex *d*. In this respect, it is not unreasonable to hypothesize that pools of small assembly-intermediates, that are by definition incomplete, partially denature under solubilising conditions where the vast majority of holo-complex is able to remain intact.

16.4.3.4 Speculation on the origin and identities of sub-complexes e and f

As sub-complexes e and *f* were present in all samples it cannot be ruled out that they were artefactual complexes, representing minor pools of solubilised MTCO1. However, an attractive biological origin for these complexes is that they are analogous to the assembly intermediate S1 identified to Nijtmans[477]. Following the argument above (16.4.3.3) that sub-complex *g* is unlikley to be S1, sub-complexes *e* and *f* are good candidates. In the original metabolic labelling data put forward by Nijtmans, S1 resolved as a broad elliptical spot using 2D BN-PAGE. It is possible that this broad spot represents the two close migrating complexes seen here. Indeed, resolution of the two MTCO1 spots of sub-complexes *e* and *f* was less clear on the 2D blots than the 1D BN-PAGE blots in this study. No marker proteins were probed by Nijtmans to enable comparison of the relative migrations of sub-complexes *e-g* and S1 or S2. The detection of sub-complexes *e-g* in all samples is consistent with the continual synthesis of MTCO1 and its slow incorporation into the holo-complex[467-470] (5.1.1.1).

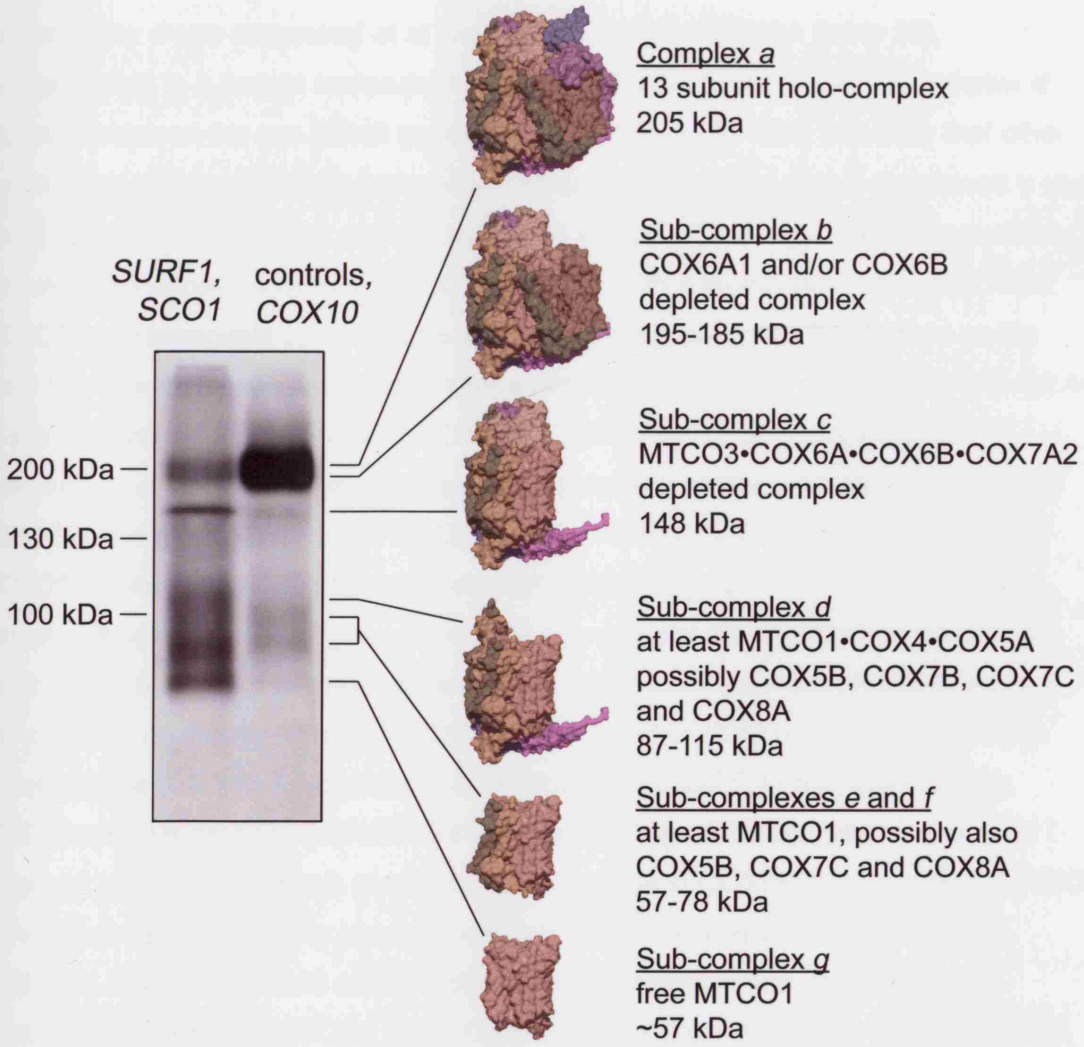

Figure 74 Prospective identities of COX sub-complexes resolved using BN-PAGE. The blot is an anti-MTCO1 blot from figure 65 as an example of banding seen in *SURF1* and *SCO1* mutant samples versus control and *COX10* mutant samples (as labelled above). Apparent protein molecular weights of the COX holo-complex (200 kDa), complex II (130 kDa) and the SDHA•SDHB dimer (approximated to 100 kDa) are given on the left. Models of predicted complexes are given in the centre, generated as in figures 2A & 2B. Descriptions of the potential components of each complex are given on the right.

16.4.3.5 *COX5B, COX7B, COX7C and COX8A are potential components of small COX sub-complexes*

Sub-complex *d* was composed of at least MTCO1•COX4•COX5A (table 25), corresponding to a protein molecular weight of 86.7 kDa (table 2). As sub-complex *d* migrated between the two SDHA signal bands at 130 and 97 kDa, it is likely that other proteins are also present in the complex. The same is also true of sub-complexes *e* and *f* which migrated parallel to or slightly below, the 97 kDa SDHA signal band respectively but were only shown to contain MTCO1 (56 kDa). With a molecular weight of 30 kDa, MTCO3 is a reasonable candidate as a missing protein but it can be rejected on the basis that it is probably incorporated after association of MTCO1 and MTCO2 (16.4.2.4). Of the remaining COX subunits, COX7C and COX8A are good candidates as components of sub-complexes *d*, *e*, and *f*. They have a combined molecular weight of 10.3 kDa and bind exclusively to MTCO1 without making any contact with MTCO2 or MTCO3 (table 1; figure 3). The relatively high COX5B signal in *SURF1* mutant cells indicates that it may also be present in COX sub-complexes. COX5B has a molecular weight of 10.6 kDa and so could potentially be a subunit of sub-complexes *d*, *e* or *f*. A sub-complex containing at least MTCO1, COX4I1 and COX5B has been identified in protein kinase A (PKA)-treated sub-mitochondrial particles[813]. In the holo-complex COX5B contacts MTCO1 and MTCO3 which may suggest incorporation in the latter stages of assembly, although conformational changes in COX5B when bound to MTCO1 in the absence of MTCO3 or changes relating to Zn^{2+} binding cannot be ruled out. COX7B is a good candidate as an undetected component of sub-complex *d* as it contacts predominantly MTCO1 and COX4I1 and has a low molecular weight. COX5B, COX7B, COX7C and COX8A have a combined molecular weight of 27.3 kDa and COX7B, COX7C and COX8A one of 16.7 kDa, both of which could be accommodated by disparity between the *known* protein molecular weight of sub-complex *d* and its migration. The association of these small subunits with sub-complexes *d*, *e*, and *f* is supported by evidence that the small subunits may bind the mtDNA-encoded subunits before the mtDNA-encoded subunits associate with each other[469,471,472] (5.1.1.2).

16.4.3.6 *Chaperones and assembly factors as potential components of the small COX sub-complexes*

Following the assumption that COX sub-complexes are accumulated assembly intermediates, the undetected components of sub-complexes *f-d* might also include chaperones, holdases or assembly factors. Although the most likely scenario is that such

proteins have not yet been characterised, a number of known proteins are reasonable candidates while others can be discounted.

SURF1 can be discounted as a component of sub-complex *e* and *f* because shy1p does not bind Cox1p and the migration of these sub-complexes was not altered in *SURF1* mutant cells. SURF1 can also be discounted as a component of sub-complexes *d* and *g* because their presence in the *SURF1* null cultures. Hsp70 chaperones can be discounted on the basis of size. The same is also true for hsp60 and PHB complex[375-377] chaperones which resolve as large complexes using BN-PAGE. Yeast Oxa1p interacts with nascent Cox1p; however, the OXA1 complex can be ruled out as it remains intact when treated with mild detergents[326*327†] and its large size is not compatible with the migration of any of these sub-complexes. Similarly, the OXA2 complex can be discounted both because it does not appear to associate with nascent Cox1p and it also remains intact when treated with mild detergents[‡340]. Yeast pet309p is also a component of a large 900 kDa complex under BN-PAGE conditions[551] which suggests that LRPPRC and possibly VCY2IP1 (5.2.3.3) can be discounted. Moreover both LRPPRC and VCY2IP1 are too large to be components of sub-complexes *d-f* as monomers. SCO1, and SCO2 are unlikley candidates as components of sub-complexes *d-f* due to their functional role in synthesis of CuA and demonstrated interaction with Cox2p in yeast[518,524].

COX10 (48.9 kDa) and COX15 (43.6/46.0 kDa) are of an appropriate size to be candidates as components of sub-complexes *d-e*, although they are probably too large to be components of sub-complex *f*. No information regarding multimerisation of COX10 and COX15 is available although the proteins do not associate with each other in yeast[495]. Functionally they are attractive candidates as both are required for haem A synthesis which may be regulated by COX assembly[495] (5.2.1). COX11 (31.4 kDa) is also a reasonable size to be considered. Moreover, it is thought to act early in MTCO1 synthesis and maturation (5.2.2.3). However, COX11 appears to be dimeric[519] which may only fit with the migration of sub-complex *e*. If it is accepted that sub-complexes *e* and *f* are analogous to S1, other candidates from yeast are Cox14p (8 kDa) and Mss51p (50 kDa; 5.2.3.4) which bind nascent Cox1p during the first 30 minutes following translation[541]. Barrientos has found that most nascent Cox1p is bound by Cox14p and the small size of the protein makes it a good candidate as a component of sub-

---

* 2 mM LM.
† 0.8 mM Digitonin.
‡ 2 mM LM.

complexes *f-d*. Mss51p could be accommodated in sub-complex e. To date no human homologues or analogues of *MSS51* or *COX14* have been identified and these predictions remain speculative.

16.4.3.7 Summary (figure 74)

- COX5A is also a component of sub-complex *d* which is probably an accumulated form of assembly intermediate S2 proposed by Nijtmans[477].
- Sub-complex *g* represents a free form of MTCO1, the appearance of which may be connected to the accumulation of sub-complex *d*. It is unlikley that sub-complex *g* is analogous to the S1 assembly intermediate identified by Nijtmans[477].
- Sub-complexes *e* and *f* may be analogous to assembly intermediate S1
- COX5B, COX7B, COX7C and COX8A along with chaperones and assembly factors may also be present in sub-complexes *d-f*.
- SURF1 cannot be a component of any of the sub-complexes resolved in this study.

16.4.4 Alternative origins for COX sub-complexes

Despite the general acceptance within the field that COX sub-complexes in patient cells are accumulated assembly-intermediates, without conclusive metabolic labelling studies, it remains possible that they are in fact dissociation intermediates. The presence of dissociation intermediates has never been investigated and as indicated above, may provide an identity for sub-complex *g*. There is evidence from metabolic labelling that around 50-70% of nascent MTCO1, MTCO2 and MTCO3 are digested in the first 12 hours following synthesis with particularly rapid digestion of MTCO2 and MTCO3 during the first 2 hours[481] and similar data has also been shown in yeast[402,478] (5.1.4). The haems and copper ions forming the COX redox centres are potentially toxic species that are carefully handled by the cell[487,506]. Their controlled removal from protein complexes being degraded provides potential rate-limiting steps in holo-complex turnover. Any rate-limiting steps during turnover would result in the presence of pools of dissociation intermediates that if present at sufficient levels, could be resolved and detected using BN-PAGE.

A cautionary note in relation to the identity of COX sub-complexes comes from work looking at the effect of PKA-hyperstimulation on sub-mitochondrial particles[813]. In such

experiments, a COX sub-complex composed of at least MTCO1, COX4I1 and COX5B could be resolved by 1D BN-PAGE. Direct phosphorylation of COX subunits by PKA has previously been reported to regulate enzyme activity[63,73,74] and the PKA regulatory subunit, PRKAR1A, binds COX5B[77] (2.6). Chronic exposure of proliferating myoblasts to azide has also been claimed to lead to dissociation of the holo-complex into MTCO1 containing sub-complexes detectable by BN-PAGE[814], although the resolution in this study was not particularly clear. In summary there are a small number of examples of stimuli which appear to lead to dissociation of the COX holo-complex and it is acknowledged that COX sub-complexes could be dissociation intermediates generated either during or after assembly of the holo-complex.

17 CYTOCHROME C OXIDASE ASSEMBLY AND THE FINDINGS OF THIS THESIS

The following section discusses the results of this study in the light of data on COX biogenesis covered in the Introduction (3, 4 & 5).

17.1 AN IMPROVED MODEL OF COX ASSEMBLY

Current schemes of COX assembly[488,784] tend to be based solely on Nijtmans' work[477] (figure 6B). A more comprehensive model can be provided by also taking into account earlier studies and other models of organellar-protein complex assembly. A modified scheme for the assembly of COX is given below (figure 75). In this model assembly proceeds through the association of four portions of the holo-complex: MTCO1 and associated subunits, COX4I1 and associated subunits, MTCO2 and COX6C, MTCO3 and associated subunits, and is regulated, in part, via control by epistasis of synthesis (CES; 5.3). The basis for these modifications to the current scheme of COX assembly and how they relate to the findings of this study are discussed below. An attempt has also been made to highlight candidate chaperones and proteases that might interact with COX subunits during biogenesis of the holo-complex. With the exception of SURF1 which is discussed below (17.2), the positioning of COX assembly factors in the scheme proposed here is consistent with current models of COX assembly[488,784] and data presented in the introduction (5.2).

Figure 75

Cytochrome c oxidase
holo-complex (dimer)
? CES
MTCO1
synthesis
Haem A
synthesis
B
COX10
FDPS
O
COX15
FDX1
FDRX1
A
COX17
COX11
Cu+
MTCO1
(COX5B)
(COX7C)
(COX8A)
MTCO1
haem a
haem a3
CuB
(COX5B)
(COX7C)
(COX8A)
COX4I1
COX5A
(COX7B)
e/f
d
c
a
2Cu+
COX17
SCO2
SCO1
SURF1
MTCO2
(COX6C)
MTCO1
haem a
haem a3
CuB
(COX5B)
(COX7C)
(COX8A)
COX4I1
COX5A
(COX7B)
MTCO2
CuA
(COX6C)
MTCO3
COX6A1
COX6B
COX7A2
MTCO1
haem a
haem a3
CuB
(COX5B)
(COX7C)
(COX8A)
COX4I1
COX5A
(COX7B)
MTCO2
CuA
(COX6C)
MTCO3
(COX6A1)
(COX6B)
(COX7A2)
Slow ~1-2 hours
Fast ~30 minutes

Figure 75 A proposed scheme of COX assembly updated according to published data and the findings of this study. Assembly of the holo-complex runs left to right as depicted by the grey arrows. Sub-complexes have been labelled using the format employed throughout this study (see also figure 74). Subunits not confirmed to be components of particular sub-complex by western blotting are given in parenthesis. MTCO1 and associated subunits and moieties are coloured purple, MTCO2 and associated subunits and moieties green, and MTCO3 and associated subunits in orange and COX4I1 and associated subunits in blue. Potential sites of action of COX assembly factors are indicated using gene names and points of Cu^{+} insertion are also marked. These have been coloured according to the sub-complexes they interact with. The presumed site of action of SURF1 is highlighted. Potential loops for feedback regulation of the control by epistasis of synthesis (CES) of MTCO1 and haem A synthesis are marked with blue arrows. The chevrons below the scheme indicate possible timings of the assembly process according to published metabolic labelling data.

17.1.1 The staggered association of mtDNA-encoded subunits

Combined metabolic labelling and enzyme purification studies from the 1970's onwards demonstrated that nascent MTCO2 and MTCO3 are incorporated into the COX holo-complex much more rapidly than nascent MTCO1 (5.1.1.1). This data fits nicely with Nijtmans BN-PAGE resolution of metabolically-labelled assembly-intermediates[477] (5.1.3; figures 7A & 7B). Combining the two, it is apparent that the initial MTCO2/MTCO3 signal in S3 and the holo-complex represents labelled, nascent MTCO2/MTCO3 which has been incorporated into complexes containing mature, unlabelled MTCO1. Hence, the slow maturation of MTCO1, through S1 and S2, concurrent with the rapid incorporation of MTCO2 and MTCO3 into S3 and the holo-complex, forms the basis for the staggered association of labelled subunits. The slow maturation of MTCO1 is in agreement with the consistent detection of sub-complexes *e* and *f* in control cells and implies that relatively large pools of these sub-complexes exist under normal conditions. Although not replicated since 1972, Weiss's observation that nascent Cox3p is the most rapidly incorporated subunit correlates with the circumstantial evidence above (16.4.2) that biologically-derived sub-complex *c* is analogous to S3 and that this sub-complex does not contain MTCO3 or its associated small subunits. Sub-complex *c* clearly contained MTCO2 and did not accumulate in the *SCO1* mutant cells, confirming that CuA formation must occur prior to or concurrent with the formation of this sub-complex. The formation of CuA prior to incorporation of MTCO3 is also supported by the presence of residual COX activity in both *MTCO3* mutant cybrids[619] and *ΔCoxIII* strains of *Rh. sphaeroides*[808] (16.4.2.4; 16.4.2.5).

Aside from cells with COX assembly defects, sub-complexes thought to be accumulated assembly-intermediates have also been identified using BN-PAGE in cells with defects in assembly of complex I[776,815], complex III[816] and complex V[686]. Stalled assembly-

intermediates must be relatively stable complexes and probably represent rate limiting steps in the assembly of OXPHOS complexes. In the case of COX, complex I and complex III, the insertion or formation of redox centres are good candidates for rate limiting steps in holo-complex assembly (table 1). This proposal sits well with the scheme of COX assembly proposed below in which sub-complexes *e* and *f* assemble prior to or concurrent with insertion of haem A and CuB, and assembly of sub-complex *d* occurs prior to incorporation of CuA. Incorporation of MTCO3 and associated small subunits, subsequent to the assembly of sub-complex *c*, may also represent a rate limiting step, as following this stage the enzyme is potentially fully active. Careful co-ordination of the final stages of assembly and activation are likely to be required to avoid the production of ROS. Allosteric control of COX activity via phosphorylation (2.6) probably plays an important role in this respect. The point at which dimerisation of the holo-complex occurs remains unknown as COX sub-complexes are generally studied under conditions which cause monomerisation. As MTCO3 and associated subunits form many of the contacts between monomers, dimerisation probably occurs once monomers are fully assembled and contain all the mtDNA-encoded subunits.

Kinetic partitioning[283,284] (4.3.3) provides a platform for the turnover of COX subunits during holo-complex assembly observed in human[481] and yeast cells[402,417,478,479] (5.1.4). As applied to COX assembly, kinetic partitioning dictates that at each stage of the process assembly-intermediates might be channelled either constructively through the assembly pathway or destructively out of the assembly pathway and into proteolytic pathways. Such a model would fit with the slower decline in MTCO1 signal than MTCO2/MTCO3 noted by Hoffbuhr[481], as MTCO1 proceeds slowly through a number of stable assembly-intermediates whereas MTCO2 and MTCO3 are rapidly incorporated into the holo-complex without forming abundant assembly-intermediates.

In terms of protective interactions, homologues of Mss51p, Cox14p and possibly VCY2IP1 may shield nascent MTCO1 from degradation during assembly of the holo-complex. Likewise, the PHB complex appears to play a role in reducing turnover of nascent MTCO3[375]. A possible role for SURF1 in stabilising nascent MTCO2 is discussed below (17.2). With regard to degradation, nascent MTCO1 is probably degraded by the *m*-AAA (4.3.2.2) and by analogy of their overlapping substrate specificities, MPRP-1 and Lon (4.3.2.7;4.3.2.4). Nascent MTCO2 is targeted by the *i*-AAA (4.3.2.2) and potentially PRSS25 which is also resident at the IMS face of the inner-membrane (4.3.2.7). Like MTCO1, nascent MTCO3 appears to be degraded by the *m*-AAA and again Lon and MPRP-1 might also be involved. The mechanisms of turnover of

large assembly-intermediates such as sub-complexes *d* and *c* remain to be determined and it is possible that sub-complexes are dis-assembled and the individual subunits digested by the same proteases that digest nascent subunits. Alternatively, by analogy with cytochrome b_6f assembly in *C. reinhardtii*, ClpXP (4.3.2.6) may be involved in degradation of these larger assemblies[446].

17.1.2 The early incorporation of small nuclear-encoded subunits

Evidence that the association of COX7A2 with MTCO3 occurs before incorporation of MTCO3 into the holo-complex[471] and that nascent COX6A1, COX6B and COX6C are incorporated at the same time as nascent MTCO2 and MTCO3[469] (5.1.1.2) advocate modifications to the scheme proposed by Nijtmans[477] to include earlier incorporation of nuclear-encoded subunits. To expand these observations it cannot be excluded that nascent MTCO2 may be bound by COX6C prior to incorporation and sub-complexes *d-f* might also contain the MTCO1- and/or COX4I1-specific subunits COX5B, COX7B, COX7C and COX8A (16.4.3.5).

The finding that sub-complex *d* contains COX5A sits nicely with data from Saltzgaber-Muller and Schatz[473] that haem incorporation occurs early in MTCO1 maturation. They found that antibodies to Cox6p, the yeast homologue of COX5A, could not immuno-precipitate nascent Cox1p in haem-deficient *hem1* strains, despite the presence of nascent Cox1p in mitochondria from these cells (5.1.1.2). Therefore, in cells that cannot synthesise haem, COX assembly is disrupted upstream of association of Cox6p with Cox1p which, according to the findings of this work, is upstream of the assembly sub-complex *d*. In view of this, it is interesting to note the strong COX5A signal spot corresponding to free COX5A in the *COX10* mutant culture P9 shown in figure 70. Sadly this was not investigated further and it is acknowledged that signals resolving so close to the BN-PAGE dye-front are often unreliable; however, it is possible that in the absence of haem A, nascent COX5A fails of associate with sub-complexes *e* and *f* and that this is responsible for the putative increase in unincorporated COX5A in P9. In the COX holo-complex, COX5A binds COX4I1 but does not contact MTCO1, thus incorporation of COX5A into sub-complex *d* is COX4I1-dependent. The stability of COX4I1 and COX5A in the absence of COX biogenesis has been clearly demonstrated in ρ^0 cells[180] and stable binding between these two subunits in the absence of other subunits has been confirmed using native-PAGE[785]. It is therefore possible that COX4I1, COX5A and potentially COX7B associate prior to MTCO1 binding.

The early incorporation of nuclear-encoded subunits proposed here gives rise to an assembly pathway in which the COX holo-complex assembles via the association of four portions of the holo-complex, MTCO1 and associated subunits, COX4I1 and associated subunits, MTCO2 and COX6C, and MTCO3 and associated subunits. This model differs from that put forward by Nijtmans in which assembly proceeded through the sequential binding of subunits around MTCO1. Membrane-protein complex assembly through the association of independently assembled portions of holo-complexes has many precedents in biology. For instance, the F_1 and F_o portions of complex V assemble independently prior to association[714]. There is also evidence that complex III assembles through the association of a cytochrome *b* sub-complex, a cytochrome c_1 sub-complex and a core-protein sub-complex[816]. Recent work has also identified a number of complex I sub-complexes which appear to associate through a similar branched assembly pathway that is divided such that the assembly of the membrane-intrinsic, membrane-extrinsic and NADH-binding portions of the holo-complex initiate separately[815].

A potential function for the small subunits in COX sub-complexes may be to mark mature, unincorporated mtDNA-encoded subunits. In this way they could either facilitate interaction with the chaperones responsible for bringing MTCO1, MTCO2 and MTCO3 together or protect them from degradation by proteases such as the *m*-AAA, MPRP-1 and the *i*-AAA (4.3.1; 4.3.2). The role of protein-protein interaction in preventing proteolysis by blocking proteolytic signals, so-called *signal masking*, is well documented[817-819]. Mechanisms that ensure the protection of assembly-intermediates from proteolysis are obviously essential to enable accumulation of such sub-complexes in cells with aberrant holo-complex assembly. The small subunits might also act as spatial barriers to prevent electron tunnelling[5] (1) through nascent redox centres that may reduce the potential for reactive oxygen species (ROS) formation.

17.1.3 Import and maturation of nuclear-encoded subunits

Surprisingly, the import and maturation of nuclear-encoded COX subunits is discussed little in relation to COX biogenesis. Nuclear-encoded COX subunits are eukaryotic-type proteins[240] and along with the finding that no COX subunit mRNAs localise to mitochondria in yeast[241] it is likely that all nuclear-encoded subunits are imported post-translationally (4.1.2). Post-translational import relies on cytosolic hsp70s and hsp40s, PPIases and 14-3-3 proteins prior to contact with TOM receptors. In view of this, the presence of phosphorylation sites in the import presequence of COX4I1 provides a potential role for 14-3-3's in regulation of COX4I1 import[74]. A role for hsp90s in the import

of COX subunits is unlikley given the small size of many of these subunits and the fact that most have N-terminal import sequences (table 2) that favours interaction with TOMM20 as opposed to TOMM70A.

Topologically, the nuclear-encoded subunits can be split into three groups, those that span the inner-membrane once in an N_{matrix}-C_{IMS} orientation, those that bind the matrix face of the holo-complex and those that bind the IMS face of the holo-complex (table 2). The prevalence of N-terminal targeting sequences suggests that most, if not all, nuclear-encoded subunits are imported via the TIM23 complex and matrix import motor (4.2.4) and processed by MPP (4.2.5.1). For those subunits that span the inner-membrane, this implies lateral membrane insertion via stop-transfer (4.2.6.1), concurrent with N-terminal presequence removal. The involvement of the OXA1 complex (4.2.6.2) can be excluded as it appears not to handle eukaryotic-type proteins that are orientated N_{matrix}-C_{IMS}. The matrix-face subunits, COX5A and COX5B, are no doubt also imported via the TIM23 pathway and processed by MPP. Evidence from yeast suggests that COX5B is additionally processed by MIPEP[820] (4.2.5.2). The import of the only IMS-face subunit COX6B, is less easily described and may simply require translocation of the outer membrane and release from the TOM complex into the IMS. Recently two related but non-identical proteins, Tim40p[821] and Mia40p[822], have been described in yeast which appear to be involved in the maintenance of the IMS proteome. Human homologues have been identified and provide potential mechanisms for the import of COX6B.

Speculation on the mitochondrial chaperones (4.3.1) that might interact nuclear-encoded COX subunits can only be based on the characteristics of the subunits themselves. The matrix-face subunits COX5A and COX5B are most likely too small to require much assistance in folding from matrix hsp70/hsp40s, hsp60 or hsp90. Proline residues in COX5A and COX5B and the matrix portion of COX4I1, raise the possibility of interaction with mitochondrial PPIases that might also constitute a regulatory aspect of COX assembly[386,823,824]. Like MTCO2 and MTCO3 the membrane spanning subunits may interact with the PHB complex as has recently been shown for some nuclear-encoded complex I subunits[382]. IMS-resident hsp70/hsp40 systems could interact with COX6B but here again the small size of the subunit may suggest otherwise.

The turnover of nuclear-encoded subunits is also a grey area and it is likely that multiple proteases scavenge unincorporated subunits in each mitochondrial compartment. Such a mechanism is necessary to prevent the accumulation of unincorporated nuclear-encoded subunits in COX-assembly mutants. The scavenging of unincorporated protein

complex subunits in multiple cellular compartments probably contributes significantly to the rapid turn-over of much of the nascent proteome[285]. Mitochondrial proteases (4.3.2) that might be involved in the turnover of nuclear-encoded subunits can be proposed on the basis of the mitochondrial compartments in which they are active. Unincorporated subunits in the matrix are probably degraded by Lon and ClpXP and membrane-spanning subunits by the *m*-AAA, *i*-AAA, MPRP-1 and possibly ClpXP following membrane extraction. The scavenging of COX6B in the IMS might involve the *i*-AAA and PRSS25.

17.1.4 A CES model can be applied to COX assembly

In 1998, following their description of CES (5.3), Wollman and colleagues commented on the striking similarity between the patterns of synthesis and turnover of petA, petB and petD in *C. reinhardtii* cytochrome b_6f complex-assembly mutants and patterns of synthesis and turnover of Cox1p, Cox2p and Cox3p in yeast COX-assembly mutants[562]. More recently, Barrientos and co-workers[478,480] have provided considerable evidence to support Wollman's observation. They noted that in *Δshy1* yeast, Cox1p synthesis is lower than controls, although the protein appears stable over a 90-120 minute chase while levels of Cox2p and Cox3p synthesis are normal yet these proteins are rapidly degraded over 30-120 minute chase. After examining other COX-assembly mutants they have also proposed that COX assembly fits Wollman's CES model. The same pattern of low level synthesis of stable Cox1p and normal synthesis of unstable Cox2p and Cox3p is also seen in *Δcox16*, *Δcox18*[479], *Δcox4*[402], *Δcyc1/Δcyc7*[417], *Δsco1*, *ΔMss51*, *ΔCox11*, *ΔOxa1*, *Δcyc3* and *ΔCox5a* strains[480] and has been reported for yeast cells with chemically inhibited cytosolic translation[417]. This wealth of data strongly supports the assertion that in yeast the abundance of the mtDNA-encoded COX subunits is modulated via CES of Cox1p.

The question therefore arises as to whether such a mechanism might also exist in human cells. Although they make no mention of Wollman's work, quantified metabolic labelling by Hoffbuhr and co-workers[481] has provided evidence that CES does apply to COX assembly in human cells (5.1.4). In control cells they noted a rapid and substantial drop in nascent MTCO2 and MTCO3 levels in the 2 hours following translation concurrent with a very small decline in MTCO1 abundance. In cybrids homozygous for an *MTCO3* mutation, they found slightly decreased levels of synthesis of MTCO1,MTCO2 and MTCO3 but the same pattern of a substantial decrease in MTCO2 and MTCO3 levels and smaller decline in MTCO1 abundance in the two hours following

translation. Although the patterns of subunit synthesis are not identical between yeast and humans (possibly because only the human study was quantified), the disparity in turnover of MTCO1 compared to MTCO2/MTCO3 mirrors the CES pattern described by Wollman and seen in the yeast examples given above. It is therefore likely that a CES-type mechanism also controls the abundance of the mtDNA-encoded COX subunits in human cells.

17.1.4.1 Candidate proteins for the regulation of translation of MTCO1

In addition to similarities in the pattern of subunit turnover, Wollman noted that numerous subunit-specific factors needed for the translation of mtDNA-encoded COX subunits had been characterised in yeast and that these could provide a molecular basis for CES[562]. The epistasis of synthesis of petA in *C. reinhardtii* is mediated via inhibition of translation by TCA1[571] and other potential factors that interact both with unincorporated petA and *petA* mRNA (5.3.3). It is reasonable to suppose that CES of MTCO1 might be regulated in a similar manner via factors that interact with nascent MTCO1 and *MTCO1* mRNA. Barrientos and co-workers have suggested that in yeast the best candidates for this function are the Cox1p translational-regulators Mss51p and Cox14p (5.2.3.4). Both interact with nascent Cox1p[480] and Mss51p also interacts with *COX1* UTRs and coding regions[541], functions identical to those proposed for the regulation of PetA synthesis by TCA1[571]. They have proposed a model whereby the initiation and elongation of translation of Cox1p is dependent on the interaction of Mss51p with *COX1* mRNA and nascent Cox1p. Once translation is complete, a complex comprising Cox14p•Cox1p•Mss51p is formed where Cox14p inhibits further stimulation of translation by Mss51p. Under conditions where downstream events are disrupted Mss51p remains sequestered in this complex and translation drops.

As yet no homologues of Mss51p or Cox14p have been identified in humans and if a similar CES strategy exists, it may be that control of MTCO1 synthesis has shifted to other proteins. One candidate, that has been characterised in human cells and is also involved early in MTCO1 synthesis, is the OXA1 complex (4.2.6.2). While not investigated in detail by Barrientos, *Δoxa1/Δcox14* strains were one of the few genotypes in which deletion of *COX14* in a COX-assembly mutant background did not restore Cox1p synthesis. Pet309p (5.2.3.2) is another candidate for involvement in CES of Cox1p in yeast. Like Mss51p, it is also needed for optimum translation Cox1p[549] and like Oxa1p, it also appears to interact genetically with *COX14*[480]. LRPPRC (5.2.3.3) is considered to be the mammalian analogue of Pet309p and is required for maintenance of *MTCO1*, *MTCO2* and *MTCO3* transcripts and control of MTCO1 and MTCO3 synthesis[171]. Interestingly, LRPPRC interacts with both the translational-regulator

HNRNPK (3.1.2.5) and the MTCO1-binding protein VCY2IP1[553,556]. Translational silencing by HNRNPK in the cytosol is mediated via binding to repeated DICE* elements in the 3'UTR of regulated mRNAs[175,825]. While HNRNPK interaction with mitochondrial mRNAs appears to be non-specific[174], it is worth noting that *MTCO1* mRNA is one of only two mammalian mitochondrial mRNAs with a 3'UTR by virtue of the anti-sense *MTSS1* sequence which is not removed during processing (figure 4). Thus candidate proteins are emerging that have the potential to modulate MTCO1 synthesis in human cells and provide a platform for CES.

The question as to which COX sub-complexes or assembly processes might be involved in feedback for CES remains unclear. Evidence for the tight control of haem A synthesis has been presented by Barros and Tzagoloff[495] (5.2.1.3), who have shown that in yeast, haem A synthesis may be auto-regulated by positive feedback at haem B-O and haem O-A conversion. Importantly they have also proposed that haem B-O conversion may also be positively regulated by COX assembly. As Weilburski and Nelson[474] (5.1.2) demonstrated that that the incorporation of MTCO1 is rate-limited by the availability of haem A, this implies COX assembly and haem A synthesis are mutually dependant providing a possible feedback mechanism for CES very early in the assembly process. The accumulation of assembly-intermediates is also a reasonable mechanism and negative feedback from sub-complexes *e-c* could lead to reduced synthesis of MTCO1 in assembly mutants. It might also be that the abundance of intact COX holo-complex provides positive feedback stimulating the synthesis of MTCO1. The ubiquity of reduced synthesis of Cox1p in many types of yeast assembly factor-mutants[402,417,479,480] implies that feedback extends throughout the assembly process and it likely that multiple processes associated within the biogenesis of COX have the potential to influence CES. It is unlikely that any COX sub-complexes identified in this study play any role in electron transport as none contain MTCO2 which forms the majority of the cytochrome c binding patch.

17.1.4.2 The spectrum of COX sub-complexes identified in this study support the modifications to the current model COX assembly

The lack of accumulation of sub-complexes in the *COX10* mutant cells here and in other studies of *COX10*[492] and *COX15*[505] mutant cells supports the positioning of COX10 function early in the assembly process. It is also in agreement with a CES model whereby synthesis of MTCO1 is modulated by the availability of haem A and feedback from downstream in the assembly process. As mentioned above this is supported by the extremely low levels Cox1p synthesis observed in *cox10*[826], *Δcox10* and *Δcox15*[480] yeast

---

* Differentiation control element.

strains. Rapid turnover of nascent MTCO1 could also account for the lack of accumulation of sub-complexes in the *COX10* mutant cells, although this would contradict the evidence above for a CES-type mechanism.

In veiw of the application of a CES model to COX assembly, The disparity between the steady-state MTCO1 levels in the *COX10* mutant and *SURF1* mutant cells can probably be accounted for by the fact SURF1 functions further along the assembly pathway than COX10 and the intervening assembly intermediates appear to be relatively stable in the absence of normal COX assembly. Thus, even if a CES model is accepted, in *SURF1* mutant cells steady-state levels of MTCO1 remain high due to the tolerance of stable assembly intermediates. The disparity between the abundance of sub-complexes in the *SCO1* mutant cells and the *SURF1* mutant cells most likely reflects the partial function of the mutant SCO1 protein[519] in P8, enabling increased flux through the assembly pathway clearing stalled assembly intermediates.

17.2 SPECULATION ON THE ROLE OF SURF1

The finding that the same spectrum of COX sub-complexes are present in *SURF1* and *SCO1* mutant cells sheds light on SURF1 function as it implies that SURF1 functions at a similar point in the COX assembly pathway as SCO1. SCO1 and SCO2 are required for delivery of Cu^+ to MTCO2 for the formation of the CuA centre (5.2.2.2). This suggests that SURF1 may be involved in either the maturation and/or stabilisation of nascent MTCO2, the formation of CuA or the association of MTCO2 with sub-complex *d* (figure 75). Even when considered in isolation, the pattern of sub-complexes seen in *SURF1* mutant cells implies an involvement in the association of MTCO2 with MTCO1 because MTCO2 is absent from sub-complex *d* which accumulates in *SURF1* mutant cells and is therefore likely to be upstream of SURF1 function. Moreover, the subunit signature of the *SURF1* mutant cells was similar to that of fibroblasts carrying an *MTCO2* mutation[614] (M29K; 15.4.3; table 24). Evidence that SURF1 may be directly involved with MTCO2 maturation comes from BN-PAGE of yeast samples that identified Cox2p as a potential component of the 250 kDa Shy1p complex which is also present in human cells[381] (5.2.3.1). The topology of SURF1 is also suitable for involvement in the maturation of MTCO2 and CuA as the majority of the protein is resident in the IMS[533]. This fits very nicely with the topology of MTCO2 (2.1; table 2), SCO1 and SCO2[520,521] which all have large IMS-resident domains enclosing their Cu^+ binding motifs.

The evidence above raises the question as to what the specific function(s) of SURF1 might be. Certain possibilities can probably be discounted. Firstly, a role for SURF1 in export of the C-terminal domain of MTCO2 is unlikely given that this is thought to be carried out by Cox18p in yeast[332] and potentially the OXA2 complex in humans[340] (4.2.6.3). Also, as no metal binding motifs are present in SURF1, a direct role in Cu^+ transfer is unlikely. In yeast, both Sco1p and Sco2p are able to bind the C-terminal domain of Cox2p directly[518,524], ruling out a role for Shy1p/SURF1 as an interface between these proteins. It is possible that SURF1 has chaperone-like role, maintaining MTCO2 in an "open" conformation suitable for insertion of CuA ,although the absence of any known protein motifs in SURF1 sequences prevents any considered analysis of this. Based on the data presented above, the simplest proposal for a function for SURF1 is that at the very least, it prevents proteolytic scavenging of nascent MTCO2 by proteases such as the *i*-AAA (4.3.2.2). It may be that protection of MTCO2 by mechanisms such as signal masking maintains inner-membrane pools of nascent MTCO2 and increases the window for interaction with sub-complex *d* and/or SCO1/SCO2. Whether protection is mediated by SURF1 alone or by SURF1-dependent recruitment of MTCO2 to the 250 kDa SURF1 complex cannot be determined here. A role for SURF1 in maintenance of nascent MTCO2 might also provide a mechanism to regulate COX biogenesis in response to proliferative stimuli. In support of such a mechanism, *SURF1* expression increases in response to serum[548], whereas the expression of COX subunit genes like *COX4I1*[827] does not.

17.3 FUTURE PROSPECTS FOR THE STUDY OF COX ASSEMBLY

The COX assembly pathway proposed in this thesis raises many questions and it is acknowledged that much of the evidence for updates to the model proposed by Nijtmans is circumstantial. Future projects on the biogenesis of COX will no doubt provide answers to some of the uncertainties.

RNA interference (RNAi) is a useful method for impairing expression of nuclear genes[828-831]. The ability to reduce expression of selected COX subunits would provide a means of dissecting those stages of the assembly pathway dependant on the presence of each of the nuclear subunits of the enzyme. RNAi has already been successfully applied to the knock-down of expression of OXPHOS subunit expression in *C. elegans*, an organism particularly amenable to the technique[185]. OXPHOS assembly was not examined in this model, although the induction of an MSR clearly demonstrated a response to the RNAi.

Working on the assumption that loss of a subunit would prevent subsequent steps in the assembly process, in conjunction with BN-PAGE, RNAi might enable determination of whether COX7C and COX8A are components of sub-complexes *e* and *f;* whether COX5B and COX7B are components of sub-complexes *f* and *d;* whether COX6C is required for MTCO2 incorporation and whether COX6A1, COX6B and COX7A2 are required for MTCO3 incorporation. Beyond examination of COX subunits, RNAi could also be applied to assembly factor expression to determine the positioning of factors such as COX17 and COX11 and to determine the effect of clear SCO1/SCO2 loss of function on COX assembly and Cu^{+} metabolism which is currently unknown due to prevalence of missense mutations in patient cells.

Metabolic labelling provides one of the best techniques for determining the temporal position of events in COX assembly. A repeat of Nijtmans experiments[477] with both normal and *SURF1* mutant cells in parallel would help clarify the origin of sub-complex *g* (16.4.3.3) and also whether sub-complexes *e* and *f* are analogous to S1 (16.4.3.4). Another key question is whether sub-complex *c* contains MTCO3. This could be answered by western blotting or application of 3D electrophoresis employing a BN-PAGE first dimension[832]. The potential association of nascent COX4I1 and COX5A described above could easily be investigated using western blots of BN-PAGE gels with higher gradients than those used here or alternatively via immunoprecipitation. It appears unlikely that sub-complexes comprising nascent MTCO2 or MTCO3 bound by their associated small subunits, are abundant enough to be detected by western blotting. It may however be possible to increase their abundance in metabolically labelled cells through the use of protease inhibitors or cycloheximide[480], enabling investigation of the presence of the small subunits via western blotting or potentially peptide fingerprinting.

Dissection of the components of SURF1-complexes would provide valuable insight into the function of SURF1. 3D electrophoresis might provide a means of investigating this further providing sufficient resolution could be obtained in the first dimension. Potentially a 4D protocol could be employed using 2D BN-PAGE/BN-PAGE in place of a BN-PAGE first dimension[28]. Other interesting questions surround the presence or absence of haem A, CuB and CuA in the various COX sub-complexes. *In-gel* haem stains[833] may provide one means of examining this. Background signals from other haems, particularly that of complex II, may cause problems and 2D BN-PAGE/BN-PAGE may improve resolution. Another approach might be to analyse BN-PAGE gel extracts using HPLC and given the unique structures of haems O and A, mass-spectrometry may also be useful.

In terms of cell biology, the increasing number of mitochondrial mRNA-binding proteins that are function in both the cytosol and nucleus suggests an interesting avenue for research. LRPPRC distribution appears to be affected in *LRPPRC* mutant cells derived from patients with French-Canadian Leigh's syndrome[171] and HNRNPK distribution alters in tumour cells and cells undergoing increased cell proliferation[834]. Whether or not the distribution of such proteins is affected in states of mitochondrial stress and aberrant OXPHOS biogenesis might have implications for many aspects of mitochondria-nuclear communication and possibly our understanding of the pathophysiology of mitochondrial disorders.

18 THE PATHOPHYSIOLOGY OF P2, P3 AND P6

The following section discusses the phenotypes of P2, P3 and P6 and covers future work that may provide further information on the pathophysiology of these cell cultures.

18.1 RESOLUTION OF MITOCHONDRIAL CHAPERONES IN P2 AND P3 USING BN-PAGE

The subunit signatures of P2 and P3 both showed evidence of multiple OXPHOS complex involvement. Clinical biochemistry from muscle also suggested an involvement of PDH in both cultures and also components of the β-oxidation pathway in P2. Disturbance of mitochondrial protein import and maturation is a reasonable candidate mechanism for the widespread disruption of OXPHOS subunit levels seen in both these cultures. The hsp60 subunit, HSPD1 (4.3.1.2) and the mitochondrial hsp70, HSPA9B (4.3.1.1), were examined on blots of 8-16% BN-PAGE gels in P2 and P3.

18.1.1 Speculation on the identity of HSPD1 signal bands

In human control mitoplast samples, primary antibody against HSPD1 identified two major bands of signal towards the top of the gel migrating just below complex III. A similar pattern of HSPD1 signal has been reported by Nijtmans using 2D BN-PAGE/denaturing-PAGE[684]. HSPD1 signal has also been identified by peptide fingerprinting, migrating between complex III and COX on gels of rat heart mitochondria[791]. In plant mitochondria samples solubilised using digitonin to enable the resolution of OXPHOS super-complexes, HSP60 migrates as a single band with an apparent molecular weight of about 750 kDa[29]. It is assumed that the two bands seen in

mammalian samples correspond to HSPD1 heptamers with and without heptameric HSPE1 caps. Such complexes would have protein molecular weights of 427 kDa and 504 kDa. According to Nijtmans, the two HSPD1 signal bands migrate with apparent molecular weights 380 and 450 kDa[684]. Although different from the size of the predicted protein complexes, the relative mobilities of the bands measured by Nijtmans are in good agreement with the migration of the bands identified here relative to complex III (500 kDa) and COX (200 kDa). The migration of protein complexes using BN-PAGE is not as clearly related to mass/charge ratio as SDS-PAGE and differences of around 10% between the predicted molecular weights and the relative mobility are consistent with these predictions[32]. On blots probed with a more sensitive secondary antibody a third diffuse band of HSPD1 signal could be seen migrating in the lower half of the gel. This band was assumed to be a minor pool of solubilised monomeric HSPD1 (61 kDa).

18.1.1.1 HSPD1 signal in P2 and P3

Mutations in *HSPD1* have been associated with a form of HSP[634] (6.1.3). No data is available on the influence of *HSPD1* mutations on OXPHOS activity or hsp60 stability[634]. Reduced levels of HSPD1 have previously been reported in fibroblasts derived from infants with certain severe mitochondrial disorders[835-838]. Such cells have wide ranging pathologies including reduced levels of other mitochondrial chaperones[838], disrupted mitochondrial morphology[835,836,839] and reduced activity of PDH[835,836], OXPHOS enzymes[835,836,838] and components of the β-oxidation pathway[835,836]. This spectrum of involvement is similar to that seen in P2 and P3 and muscle from the patients they were derived from.

The two major HSPD1 signal bands seen in controls were also the major HSPD1 signals in P2 and P3. In both cases these bands migrated at the same position as in controls, confirming that there was no alteration in the size or mobility of the major HSPD1 complexes in either patient. As discussed previously, the relative intensity of staining could not be accurately compared between samples because the mitoplast preparations could not be matched for protein content due to the interference of bis-Tris with protein assays[682]. This is an important consideration given the large size of P3 cells. A measure of the imbalance of the P3 mitoplast samples can be gained from comparing the MTCO1 and COX4I1 signals for P3 using BN-PAGE with the matched protein extracts used for the denaturing gel western blots. Given the very low MTCO1 signal on denaturing gel blots compared to the near normal MTCO1 signal in the holo-complex band resolved on BN-PAGE blots, it was clear that mitoplast samples from P3 contained significantly more

protein than the other patient samples, consistent with loading a fixed number of large cells. Moreover, the near normal band *ab* intensity on BN-PAGE blots of P3 contradicts the CO flash-photolysis data that found only 11% control abundance of cytochrome a_3. The samples from P2 seemed slightly better matched on BN-PAGE blots of COX subunits, nevertheless it would be unreliable to used such blots quantitatively and therefore despite the very low intensity of the HSDP1 signal in P2 it is not possible to say that this reflected a deficiency of HSPD1. Moreover, very low signals were also seen when a parallel blot was probed for the matrix chaperone HSPA9B ruling out an isolated reduction in HSPD1 levels.

18.1.2 Speculation on the identity of HSPA9B signal bands

In control samples a fast migrating major signal band was detected and was assumed to be mature monomeric HSPA9B (68.3 kDa). Three minor bands of HSPA9B signal (bands 1-3) were detected above the major band on blots probed with the improved secondary antibody. Although specificity was not confirmed using a second dimension, bands 1-3 may represent solubilised pools of HSPA9B bound by co-chaperones. Binding between mitochondrial hsp70s and their co-factors is stable in the presence of non-ionic detergents and absence of ATP and complexes containing combinations of mitochondrial hsp70s, hsp40s, TIMM44 homologues and GrpEs have been isolated from yeast and rat cells[317,318,840].

Relative to the HSPA9B major signal band, the migration of band 1 was close to that of the lower SDHA signal at around 100 kDa (16.2). Band 2 migrated very close to sub-complex c, at around 150 kDa (16.4.2.4). Band 3 migrated between the lower HSPD1 signal band with an apparent mass 380 kDa[684] and COX at around 200 kDa. An HSPA9B•GRPEL1$_2$ complex would have a protein molecular weight around 112 kDa, HSPA9B•DNAJA3 dimers around 110 kDa and TIMM44•HSPA9B dimers around 115 kDa. All of these potential complexes are representative of known functional interactions are in good agreement with the migration of band 1. A TIMM44•HSPA9B•GRPEL1$_2$ complex would have a molecular weight around 135 kDa and is a reasonable prediction for the identity of band 2. The identity of band 3 is harder to predict, although it would not be unreasonable to speculate that it contains larger assemblies of TIMM44 dimers or additional the components of the TIM23 complex.

18.1.2.1 HSPA9B in P2 and P3

Mutations in *HSPA9B* have not been reported, although low levels of HSPA9B have been found in COX deficient fibroblasts derived from a patient with multiple mitochondrial disease, although these cells also had low levels of HSPD1[838]. HSPA9B was investigated in both cultures using a blot run in parallel with that probed for HSPD1. As with the HSPD1 blot, identical banding could be seen in P3 as the control sample. The signal strength in P2 was again much lower than the other samples ruling out identification of bands 1-3, however, the putative HSPA9B monomer was also the major signal band in P2. These results suggest that aberrant HSPA9B assemblies are not a function of the pathology of P3. The low signal strength in the P2 samples precludes any reliable assessment of whether that is also true of P2.

18.2 SPECULATION ON THE PATHOPHYSIOLOGY AND FUTURE PROSPECTS FOR STUDY OF P2

The pathophysiology of P2 is one of the most unclear of all the cultures examined in this study. Clinical biochemistry indicated multiple enzyme deficiency and in terms of the OXPHOS this was confirmed by western blotting. Genetic analysis excluded the involvement of mtDNA and examination of mitochondrial hsp70 and hsp60 complexes proved inconclusive. Residual COX abundance was similar to that seen in the *SURF1* mutant cells and a weak COX activity stain was apparent. This indicates that the genetic defect in P2 enabled some assembly of COX, either due to total loss of function of a partially redundant protein as seen in the *SURF1* mutant cultures or due to partial loss of function of an essential protein as seen in the *SCO1* and *COX10* mutant cultures.

Given the global defects in mitochondrial function seen in these cells it is likely that the pathophysiology stems from a defect in mitochondrial biogenesis (organellar). Gross mitochondrial abnormalities were not noted in these cells using immuno-florescent stains or COX activity stains and further analysis using EM would be valuable. Disruption of mitochondrial morphology has been noted under EM in cells with *SURF1* mutations[539], disrupted biogenesis of complex V[841] and in *SPG7* knock-out mice[428]. Abnormal mitochondria are also seen *Δyme1*[414] (4.3.2.3) and *ΔPcp1* yeast that lack a mitochondrial rhomboid protease that functions in concert with the *m*-AAA in the activation of Ccp1p[400] and is uniquely required for activation of mitochondrial dynamin-like GTPases involved in

membrane remodelling[842*]. Defects in the function of chaperones or processing peptidases provides a potential model for disruption of mitochondrial biogenesis and this assumption formed the basis for the examination of mitochondrial hsp70 and hsp60. Exactly how screening of chaperones and proteases might be taken further in P2 is unclear. As all mitochondrial proteins appear to be present at low levels in these cells, screening out false negatives would be difficult. Pulse-chase labelling in the presence of cycloheximide could be used to determine whether mitochondrial (organellar) turnover is altered in P2 which might indicate increased autolysis of abnormal mitochondria. More information on the pathophysiology of P2 might be obtained from examination of markers of apoptosis such as flipping of annexin V (*ANXA5*), DNA fragmentation and caspase activation or oxidative damage/stress such as upregulation of superoxide dismutase-1 (*SOD1*), raised glutathione, low aconitase (*ACON1*) activity or increases in protein carbonyls, lipid peroxidation and 8-hydroxyguanine respectively. Increased apoptosis and has been noted in tissues from patients with mitochondrial encephalomyopathy[843] and fibroblasts derived from a NARP patient with a complex V defect that also showed evidence of increased oxidative stress[769].

Another possibility is that the defect in P2 stemmed from abnormal mitochondrial lipid metabolism. The predominantly mitochondrial lipid cardiolipin, is associated with OXPHOS enzymes many inner-membrane carriers[844] and may act as a proton reservoir for the inner membrane[845]. *Δcrd1*[†] yeast which cannot synthesis cardiolipin have multiple OXPHOS defects[846] especially under stress[847] and defects in inner-membrane integrity[848]. Defects in cardiolipin metabolism are seen in Barth's syndrome[‡] patients and others with mutations in *TAZ*[§]. Barth's syndrome is characterised by cardiomyopathy, skeletal muscle hypotonia and neutropenia and affects children and teenagers. It is possible that putative defects in cardiolipin metabolism in patient 2 were more severe than those seen in Barth's syndrome patients and other loci associated with cardiolipin synthesis, such as *CDS1*[**844], might also be candidates for screening. A defect in cardiolipin metabolism causing OXPHOS defects and leading to difficulty in maintaining $\Delta\psi$ may provide a model for further work as this would also affect mitochondrial biogenesis. Examination of mitochondrial lipid spectrums using HPLC, mass spectrometry or thin-layer chromatography would provide a means for initial

---

[*] PCP1 referred to as RBD1.
[†] Cardiolipin synthase.
[‡] OMIM: 300394.
[§] Non-HGNC names: tafazzin, BTHS.
[**] CDP-diacylglycerol synthase (phosphatidate cytidylyltransferase)-1

investigation. Examination of $\Delta\psi$ using fluorescent dyes such as TMRM might also be of value.

Following the exclusion of the involvement of mtDNA, the best prospect for genetic investigation of P2 is probably human cDNA complementation using retroviral vectors. The poor growth of P2 in galactose-containing media suggests it would be suitable for selecting out non-rescued P2 cells. Similar to the overall results of this study, sugar-free RPMI-based media has been used to select complemented clones in screens of cells with mitochondrial dysfunction[849].

18.3 SPECULATION ON THE PATHOPHYSIOLOGY AND FUTURE PROSPECTS FOR STUDY OF P3

The OXPHOS subunit signature of P3 is indicative of a defect in synthesis or maturation of mtDNA-encoded proteins. The lack of accumulation of COX sub-complexes in P3 is also consistent with such a defect. As discussed above, pathogenic mtDNA lesions can be excluded in this culture (13.1.3). Patients with unknown nuclear defects in mitochondrial translation have been identified[716]. More recently patients with mutations in the elongation factor EFG1[861] (3.2.1.2) and the MRP (3.2.1.1) MRPS16[862] have been identified. In terms of a strict defect in mitochondrial translation, proteins involved in tRNA maturation and charging (3.1.2.4), translation initiation, elongation and termination factors (3.2.1.2) and MRPs are obvious candidates, as supported by the identification of these two recent patients. The potential involvement of MRPs in disease has been discussed by O'Brien *et al*[850,851]. Metabolic labelling using either purified mitochondria or whole cells in the presence of cycloheximide, would enable examination of mitochondrial translation in P3, although dissection beyond confirmation or exclusion of a defect may prove difficult.

Another possibility is that the defect in P3 was due not to defective mitochondrial translation but defective processing of mitochondrial translation products. Candidates in this respect might be the inner-membrane insertion machinery (4.2.6) and inner-membrane chaperones such as the PHB complex (4.3.1.3). Although the OXA1 and PHB complexes are also involved in processing of nuclear gene products, missense mutations affecting specific interaction with aspects of the mitochondrial gene expression machinery such as ribosome binding to the OXA1 complex are potential candidate mechanisms. This raises an interesting technical problem, as distinguishing between reduced levels of translation and increased co- or para-translational protein degradation

may prove difficult. Protein degradation of this type has been examined in the cytosol using fusion proteins that contain stable reporter domains[852], although this technique could not currently be applied to mitochondria protein turnover as little is known about the substrate specificities of mitochondrial proteases. Rapid degradation of cytosolic proteins has also been examined using very short (30 second) labelling pulses in combination with different protease inhibitors[285]. This may be more applicable to mitochondrial research, although the kinetics of labelling mitochondrial amino acid pools and the inhibition of mitochondrial proteases are likely to differ from that of the cytosol. Another area that might be examined in P3 would be to assess the extent of ribosomal association with the inner-membrane in comparison to control cells. Evidence for inefficient transfer of nascent mitochondrial proteins to the insertion machinery might be detected in this way.

P3 cells were much larger than the other patient-derived fibroblasts or control fibroblasts and appeared to contain a more granular cytosol. According to passage data supplied with the cells they were a similar age to all the other cultures received (passage 3-7). EM examination of P3 for defects in mitochondrial morphology or the accumulation of partially degraded lysosome-resident mitochondria as lipofuscin[853] would be interesting. An increase in size of fibroblasts carrying mt-tRNA mutations has been noted by other groups[701] although it was not seen in the fibroblasts carrying the *MTTL1* (3243A-G) mutation studied here. The large size of P3 cells may be due to increased mitochondrial proliferation in response to ROS generation due to impaired OXPHOS function. Increased ROS generation is seen in cells with OXPHOS defects[854] and has been associated with an increase in mitochondrial turnover and lipofuscin[853]. A link between ROS and stimulation of mitochondrial proliferation has been described in lung fibroblasts* in which it was noted that treatment with ROS-generating compounds led to an increase in mitochondrial mass as measured using the cardiolipin-specific dye NAO or cellular mtDNA abundance[855]. In support of the above mechanisms acting in P3, increased mitochondrial proliferation in ROS-stimulated cells is insensitive to inhibition of mitochondrial translation[856]. *In vivo* increased mitochondrial proliferation in muscle leads to the formation of characteristic RRF seen in certain mitochondrial myopathies[853]. No details of the muscle morphology of patient 3 were available.

P3 maintained a low residual COX activity that appeared to reflect a low abundance of normal COX. As with P2, this implies that the genetic defect in these cells enabled a

---

* Human, MRC5.

small amount of COX biogenesis. Some mitotic cells in P3 stained positive for COX activity as was also noted in P6, suggesting that the defect in these cells could be rescued by cell cycle-associated changes in gene expression. Cell cycle-dependent alterations in metabolic control of COX are unlikley to be responsible for the staining given the presence of multiple OXPHOS defects in P3 and the fact that the residual COX abundance in P3 was similar to that of the *SURF1* mutant cultures in which no COX positive cells were detected. COX activity increases Mitochondrial mass increases between S- and M-phases of the cell cycle[857] and it is likely that the changes in gene expression associated with this are behind the raised COX activity in these cells. PGC-1 family transcriptional co-activators are important regulators of mitochondrial biogenic cascades[177,178]. Of the three currently identified, PRC appears to be cell cycle-regulated as it is expressed at high levels following serum stimulation and in proliferating cells[827]. Increases in expression of *NRF1* and *CYCS* are seen downstream of *PRC* upregulation, supporting the existence of cell cycle-dependent mitochondrial biogenic cascades. Transient, cell cycle-dependent increases in OXPHOS biogenesis are likely to be modulated via control of assembly factor expression as opposed to OXPHOS subunit gene expression because OXPHOS subunit gene expression does not appear to be cell cycle related and serum stimulation does not increase the expression of genes such as *COX4I1*[827] yet does increase the expression of *SURF1*[548]. Increased expression of positive regulators of mitochondrial protein synthesis and/or maturation in a cell cycle-dependent manner would explain the presence of COX positive mitotic cells in P3. In relation to this it was interesting to note that the SV40 large-T antigen transduced P3 culture, P3tsT, became dependent on pyruvate and uridine for optimal growth in glucose based media. One explanation for this might be that the loss of cell cycle control and block in tumour suppressor function[858] caused by tsT expression led to a rate of proliferation that exceeded the capacity of the residual OXPHOS in P3 to support uridine synthesis. Thus under conditions where uridine was plentiful the cells proliferated well whereas growth was limited when uridine was restricted. Further investigation is necessary, particularly under conditions where pyruvate is present but if this hypothesis turns out to be correct, models such as P3 and P3tsT may be of value for studying the relationship between uridine synthesis and the OXPHOS.

As with P2 the best prospect for identification of the genetic defect in P3 lies with cDNA complementation experiments. P3 grew very poorly in galactose-containing medium, suggesting that enrichment for rescued clones should be possible. The production of P3tsT should facilitate such experiments.

18.4 SPECULATION ON THE PATHOPHYSIOLOGY AND FUTURE PROSPECTS FOR STUDY OF P6

P6 clearly expressed a COX defect in culture and had reduced abundance of COX and COX subunits. As discussed above (13.2.2), the involvement of mtDNA in the pathophysiology of these cells is unlikely. The subunit signature of P6 suggested the possible involvement of complex III but this contradicts biochemical evidence from other labs and the normal *b*- and *c*-type cytochrome abundance measured in these cells. Therefore it is likely that the low UQCRC2 levels detected in these cells is not a reliable result. All western blots of P6 were done at least twice although only a single matched LM extract was used and it seems likely that the combination of a threshold antibody response and a slightly inaccurately balanced sample is responsible for this result. With this in mind it appears that P6 expressed an isolated COX defect.

The pattern of COX sub-complexes detected in P6 is identical the that of controls and P9, the *COX10* mutant culture. This implies that the defect in P6 is probably early in the COX assembly pathway. This suggest screening of *COX10*, *COX15* and possibly *COX11*. Given the proposals above, factors that control the translation of MTCO1 may also be worth examining such as LRPPRC and potential interacting partners. cDNA sequencing may be possible as null mutations resulting in total loss of function are likely to be embryonic lethal and a high frequency of missense alleles has been identified in patients with mutations in these genes (table 23). As with P3, investigation of mitochondrial translation but more specifically *MTCO1*, *MTCO2* and *MTCO3* would also be of value in P6. HPLC of mitochondrial haems might also be of interest as Antonicka *et al* found that haem O is higher in *COX15* mutant cells[505] than controls or cells with mutations in other COX assembly factors[492] including *COX10*, *SCO1* and *SURF1*.

As with P3, COX positive mitotic cells were found in P6. The implications of this finding have been discussed above (18.3). One of the more unexpected results from the study of P6, possibly related to the presence of COX positive mitotic cells, was the rescue of the COX deficient phenotype by transduction with a temperature sensitive form of SV40 large-T antigen (tsT). Expression of SV40 T-Ag leads constitutive expression of many S-phase genes and a block in the function of tumour suppressor function[858]. Bearing in mind the relatively high (>40%) residual COX abundance in P6, it is possible that the COX defect in P6 is caused by a partial loss of activity of a COX assembly factor, the expression of which is modulated during the cell cycle, and that in P6tsT expression of the mutant protein is increased sufficiently to support near normal COX biogenesis. A

model such as this is supported by the serum response of *SURF1* expression[548] and it is probable that other COX assembly factors are also cell cycle regulated. Due to the loss of the severe COX defect in P6tsT, cDNA complementation studies are likely to be of little use in the study of P6 as it is clear that the COX defect in these cells can be rescued by expression of genes which affect cell cycle progression, creating the likelihood that false positives are will to be detected. In the absence of mapping data, genomics-based approaches such as integrative genomics[555,859] are also not applicable thus the candidate gene screening and functional studies mentioned above are likely to provide the best direction for future work with this cell culture.

* * * *

The genetic basis of an increasing number of mitochondrial disorders are now know. The research presented here has sought to demonstrate that when combined with data from model organisms, the study of patient-derived tissues with known genetic defects can provide valuable insight to the mechanisms of OXPHOS biogenesis. In due course such research should improve the diagnosis and genetic counselling of mitochondrial disorders and provide models applicable to the biogenesis of other protein complexes.

19 BIBLIOGRAPHY

1. Nicholls,D.G. & Ferguson S.J. in Bioenergetics 3, Edn. 3 89-155 (Academic Press, Amsterdam London New York; 2002).
2. Mitchell,P. The protonmotive Q cycle: a general formulation. *FEBS Lett.* **59**, 137-139 (1975).
3. Nicholls,D.G. & Ferguson S.J. in Bioenergetics 3, Edn. 3 57-87 (Academic Press, Amsterdam London New York; 2002).
4. Kaim,G. & Dimroth,P. ATP synthesis by F-type ATP synthase is obligatorily dependent on the transmembrane voltage. *EMBO J.* **18**, 4118-4127 (1999).
5. Page,C.C., Moser,C.C., Chen,X., & Dutton,P.L. Natural engineering principles of electron tunnelling in biological oxidation-reduction. *Nature* **402**, 47-52 (1999).
6. Simkovic,M., Degala,G.D., Eaton,S.S., & Frerman,F.E. Expression of human electron transfer flavoprotein-ubiquinone oxidoreductase from a baculovirus vector: kinetic and spectral characterization of the human protein. *Biochem. J.* **364**, 659-667 (2002).
7. Ikeda,Y. & Tanaka,K. Purification and characterization of 2-methyl-branched chain acyl coenzyme A dehydrogenase, an enzyme involved in the isoleucine and valine metabolism, from rat liver mitochondria. *J. Biol Chem.* **258**, 9477-9487 (1983).
8. Stryer,L. in Biochemistry, Edn. 3rd 469-494 (W. H. Freeman and Company, New York; 1987).
9. Wanders,R.J., Duran,M., & Wijburg,F.A. in Mitochondrial Disorders in Neurology 2, Edn. 2nd. eds. Schapira,A.H. & DiMauro,S. 257-297 (Butterworth Heinmann, Boston; 2002).
10. Nicholls,D.G. & Ferguson S.J. in Bioenergetics 3, Edn. 3 17-29 (Academic Press, Amsterdam London New York; 2002).
11. Nicholls,D.G. & Ferguson S.J. in Bioenergetics 3, Edn. 3 219-247 (Academic Press, Amsterdam London New York; 2002).
12. Brisson,D., Vohl,M.C., St Pierre,J., Hudson,T.J., & Gaudet,D. Glycerol: a neglected variable in metabolic processes? *Bioessays* **23**, 534-542 (2001).
13. Nguyen,N.H., Brathe,A., & Hassel,B. Neuronal uptake and metabolism of glycerol and the neuronal expression of mitochondrial glycerol-3-phosphate dehydrogenase. *J. Neurochem.* **85**, 831-842 (2003).
14. Srere,P.A. The Infrastructure of the Mitochondrial Matrix. *Trends Biochem. Sci.* **5**, 120-121 (1980).
15. Lopez-Beltran,E.A., Mate,M.J., & Cerdan,S. Dynamics and environment of mitochondrial water as detected by 1H NMR. *J. Biol Chem.* **271**, 10648-10653 (1996).
16. Garcia-Perez,A.I., Lopez-Beltran,E.A., Kluner,P., Luque,J., Ballesteros,P., & Cerdan,S. Molecular crowding and viscosity as determinants of translational diffusion of metabolites in subcellular organelles. *Arch. Biochem. Biophys.* **362**, 329-338 (1999).
17. Ellis,R.J. Macromolecular crowding: obvious but underappreciated. *Trends Biochem. Sci.* **26**, 597-604 (2001).
18. Ellis,R.J. Macromolecular crowding: an important but neglected aspect of the intracellular environment. *Curr. Opin. Struct. Biol* **11**, 114-119 (2001).
19. Sumegi,B. & Srere,P.A. Complex I binds several mitochondrial NAD-coupled dehydrogenases. *J. Biol. Chem.* **259**, 15040-15045 (1984).
20. Sumegi,B. & Srere,P.A. Binding of the enzymes of fatty acid beta-oxidation and some related enzymes to pig heart inner mitochondrial membrane. *J. Biol. Chem.* **259**, 8748-8752 (1984).
21. Sumegi,B., Porpaczy,Z., & Alkonyi,I. Kinetic advantage of the interaction between the fatty acid beta-oxidation enzymes and the complexes of the respiratory chain. *Biochim. Biophys. Acta* **1081**, 121-128 (1991).
22. Parker,A. & Engel,P.C. Preliminary evidence for the existence of specific functional assemblies between enzymes of the beta-oxidation pathway and the respiratory chain. *Biochem. J.* **345 Pt 3**, 429-435 (2000).
23. Rich,P.R. Electron and proton transfers through quinones and cytochrome bc complexes. *Biochim. Biophys. Acta* **768**, 53-79 (1984).
24. Berry,E.A. & Trumpower,B.L. Isolation of ubiquinol oxidase from Paracoccus denitrificans and resolution into cytochrome bc1 and cytochrome c-aa3 complexes. *J. Biol Chem.* **260**, 2458-2467 (1985).

25. Niebisch,A. & Bott,M. Purification of a cytochrome bc-aa3 supercomplex with quinol oxidase activity from Corynebacterium glutamicum. Identification of a fourth subunity of cytochrome aa3 oxidase and mutational analysis of diheme cytochrome c1. *J. Biol. Chem.* **278**, 4339-4346 (2003).
26. Stroh,A., Anderka,O., Pfeiffer,K., Yagi,T., Finel,M., Ludwig,B., & Schagger,H. Assembly of respiratory complexes I, III, and IV into NADH oxidase supercomplex stabilizes complex I in Paracoccus denitrificans. *J. Biol Chem.* **279**, 5000-5007 (2004).
27. Cruciat,C.M., Brunner,S., Baumann,F., Neupert,W., & Stuart,R.A. The cytochrome bc1 and cytochrome c oxidase complexes associate to form a single supracomplex in yeast mitochondria. *J. Biol Chem.* **275**, 18093-18098 (2000).
28. Schagger,H. & Pfeiffer,K. Supercomplexes in the respiratory chains of yeast and mammalian mitochondria. *EMBO J.* **19**, 1777-1783 (2000).
29. Eubel,H., Jansch,L., & Braun,H.P. New insights into the respiratory chain of plant mitochondria. Supercomplexes and a unique composition of complex II. *Plant Physiol* **133**, 274-286 (2003).
30. Schagger,H. & Pfeiffer,K. The ratio of oxidative phosphorylation complexes I-V in bovine heart mitochondria and the composition of respiratory chain supercomplexes. *J. Biol. Chem.* **276**, 37861-37867 (2001).
31. Schagger,H. & von Jagow,G. Blue native electrophoresis for isolation of membrane protein complexes in enzymatically active form. *Anal. Biochem.* **199**, 223-231 (1991).
32. Schagger,H., Cramer,W.A., & von Jagow,G. Analysis of molecular masses and oligomeric states of protein complexes by blue native electrophoresis and isolation of membrane protein complexes by two-dimensional native electrophoresis. *Anal. Biochem.* **217**, 220-230 (1994).
33. Schagger,H. Quantification of oxidative phosphorylation enzymes after blue native electrophoresis and two-dimensional resolution: normal complex I protein amounts in Parkinson's disease conflict with reduced catalytic activities. *Electrophoresis* **16**, 763-770 (1995).
34. Schagger,H., Bentlage,H., Ruitenbeek,W., Pfeiffer,K., Rotter,S., Rother,C., Bottcher-Purkl,A., & Lodemann,E. Electrophoretic separation of multiprotein complexes from blood platelets and cell lines: technique for the analysis of diseases with defects in oxidative phosphorylation. *Electrophoresis* **17**, 709-714 (1996).
35. Schagger,H. Native electrophoresis for isolation of mitochondrial oxidative phosphorylation protein complexes. *Methods Enzymol.* **260**, 190-202 (1995).
36. Schagger,H. Respiratory chain supercomplexes of mitochondria and bacteria. *Biochim. Biophys. Acta* **1555**, 154-159 (2002).
37. Zhang,M., Mileykovskaya,E., & Dowhan,W. Gluing the respiratory chain together. Cardiolipin is required for supercomplex formation in the inner mitochondrial membrane. *J. Biol. Chem.* **277**, 43553-43556 (2002).
38. Pfeiffer,K., Gohil,V., Stuart,R.A., Hunte,C., Brandt,U., Greenberg,M.L., & Schagger,H. Cardiolipin stabilizes respiratory chain supercomplexes. *J. Biol Chem.* **278**, 52873-52880 (2003).
39. Boumans,H., Grivell,L.A., & Berden,J.A. The respiratory chain in yeast behaves as a single functional unit. *J. Biol. Chem.* **273**, 4872-4877 (1998).
40. Bianchi,C., Genova,M.L., Parenti,C.G., & Lenaz,G. The mitochondrial respiratory chain is partially organized in a supercomplex assembly: kinetic evidence using flux control analysis. *J. Biol Chem.* **279**, 36562-36569 (2004).
41. Schagger,H., De Coo,R., Bauer,M.F., Hofmann,S., Godinot,C., & Brandt,U. Significance of respirasomes for the assembly/stability of human respiratory chain complex I. *J. Biol Chem.* **279**, 36349-36353 (2004).
42. Yoshikawa,S. A cytochrome c oxidase proton pumping mechanism that excludes the O2 reduction site. *FEBS Lett.* **555**, 8-12 (2003).
43. Taanman,J.W. Human cytochrome c oxidase: structure, function, and deficiency. *J. Bioenerg. Biomembr.* **29**, 151-163 (1997).
44. Abramson,J., Svensson-Ek,M., Byrne,B., & Iwata,S. Structure of cytochrome c oxidase: a comparison of the bacterial and mitochondrial enzymes. *Biochim. Biophys. Acta* **1544**, 1-9 (2001).
45. Yoshikawa,S., Shinzawa-Itoh,K., Nakashima,R., Yaono,R., Yamashita,E., Inoue,N., Yao,M., Fei,M.J., Libeu,C.P., Mizushima,T., Yamaguchi,H., Tomizaki,T., & Tsukihara,T. Redox-coupled crystal structural changes in bovine heart cytochrome c oxidase. *Science* **280**, 1723-1729 (1998).
46. Tsukihara,T., Shimokata,K., Katayama,Y., Shimada,H., Muramoto,K., Aoyama,H., Mochizuki,M., Shinzawa-Itoh,K., Yamashita,E., Yao,M., Ishimura,Y., & Yoshikawa,S. The low-spin heme of cytochrome c oxidase as the driving element of the proton-pumping process. *Proc. Natl. Acad. Sci. U. S. A* **100**, 15304-15309 (2003).
47. Tsukihara,T., Aoyama,H., Yamashita,E., Tomizaki,T., Yamaguchi,H., Shinzawa-Itoh,K., Nakashima,R., Yaono,R., & Yoshikawa,S. Structures of metal sites of oxidized bovine heart cytochrome c oxidase at 2.8 A. *Science* **269**, 1069-1074 (1995).
48. Tsukihara,T., Aoyama,H., Yamashita,E., Tomizaki,T., Yamaguchi,H., Shinzawa-Itoh,K., Nakashima,R., Yaono,R., & Yoshikawa,S. The whole structure of the 13-subunit oxidized cytochrome c oxidase at 2.8 A. *Science* **272**, 1136-1144 (1996).

49. Das,T.K., Pecoraro,C., Tomson,F.L., Gennis,R.B., & Rousseau,D.L. The post-translational modification in cytochrome c oxidase is required to establish a functional environment of the catalytic site. *Biochemistry* **37**, 14471-14476 (1998).
50. Musatov,A. & Robinson,N.C. Cholate-induced dimerization of detergent- or phospholipid-solubilized bovine cytochrome C oxidase. *Biochemistry* **41**, 4371-4376 (2002).
51. Robinson,N.C. Functional binding of cardiolipin to cytochrome c oxidase. *J. Bioenerg. Biomembr.* **25**, 153-163 (1993).
52. Lange,C. & Hunte,C. Crystal structure of the yeast cytochrome bc1 complex with its bound substrate cytochrome c. *Proc. Natl. Acad. Sci. U. S. A* **99**, 2800-2805 (2002).
53. Roberts,V.A. & Pique,M.E. Definition of the interaction domain for cytochrome c on cytochrome c oxidase. III. Prediction of the docked complex by a complete, systematic search. *J. Biol. Chem.* **274**, 38051-38060 (1999).
54. Zhen,Y., Hoganson,C.W., Babcock,G.T., & Ferguson-Miller,S. Definition of the interaction domain for cytochrome c on cytochrome c oxidase. I. Biochemical, spectral, and kinetic characterization of surface mutants in subunit ii of Rhodobacter sphaeroides cytochrome aa(3). *J. Biol. Chem.* **274**, 38032-38041 (1999).
55. Wang,K., Zhen,Y., Sadoski,R., Grinnell,S., Geren,L., Ferguson-Miller,S., Durham,B., & Millett,F. Definition of the interaction domain for cytochrome c on cytochrome c oxidase. Ii. Rapid kinetic analysis of electron transfer from cytochrome c to Rhodobacter sphaeroides cytochrome oxidase surface mutants. *J. Biol. Chem.* **274**, 38042-38050 (1999).
56. Trumpower,B.L. A concerted, alternating sites mechanism of ubiquinol oxidation by the dimeric cytochrome bc(1) complex. *Biochim. Biophys. Acta* **1555**, 166-173 (2002).
57. Covian,R., Gutierrez-Cirlos,E.B., & Trumpower,B.L. Anti-cooperative oxidation of ubiquinol by the yeast cytochrome bc1 complex. *J. Biol Chem.* (2004).
58. Yoshikawa,S., Shinzawa-Itoh,K., & Tsukihara,T. X-ray structure and the reaction mechanism of bovine heart cytochrome c oxidase. *J. Inorg. Biochem.* **82**, 1-7 (2000).
59. Wikstrom,M. & Verkhovsky,M.I. Proton translocation by cytochrome c oxidase in different phases of the catalytic cycle. *Biochim. Biophys. Acta* **1555**, 128-132 (2002).
60. Ruitenberg,M., Kannt,A., Bamberg,E., Fendler,K., & Michel,H. Reduction of cytochrome c oxidase by a second electron leads to proton translocation. *Nature* **417**, 99-102 (2002).
61. Bloch,D., Belevich,I., Jasaitis,A., Ribacka,C., Puustinen,A., Verkhovsky,M.I., & Wikstrom,M. The catalytic cycle of cytochrome c oxidase is not the sum of its two halves. *Proc. Natl. Acad. Sci. U. S. A* **101**, 529-533 (2004).
62. Wikstrom,M., Verkhovsky,M.I., & Hummer,G. Water-gated mechanism of proton translocation by cytochrome c oxidase. *Biochim. Biophys. Acta* **1604**, 61-65 (2003).
63. Kadenbach,B., Huttemann,M., Arnold,S., Lee,I., & Bender,E. Mitochondrial energy metabolism is regulated via nuclear-coded subunits of cytochrome c oxidase. *Free Radic. Biol. Med.* **29**, 211-221 (2000).
64. Fetter,J.R., Qian,J., Shapleigh,J., Thomas,J.W., Garcia-Horsman,A., Schmidt,E., Hosler,J., Babcock,G.T., Gennis,R.B., & Ferguson-Miller,S. Possible proton relay pathways in cytochrome c oxidase. *Proc. Natl. Acad. Sci. U. S. A* **92**, 1604-1608 (1995).
65. Huttemann,M., Kadenbach,B., & Grossman,L.I. Mammalian subunit IV isoforms of cytochrome c oxidase. *Gene* **267**, 111-123 (2001).
66. Taanman,J.W., Hall,R.E., Tang,C., Marusich,M.F., Kennaway,N.G., & Capaldi,R.A. Tissue distribution of cytochrome c oxidase isoforms in mammals. Characterization with monoclonal and polyclonal antibodies. *Biochim. Biophys. Acta* **1225**, 95-100 (1993).
67. Schillace,R., Preiss,T., Lightowlers,R.N., & Capaldi,R.A. Developmental regulation of tissue-specific isoforms of subunit VIa of beef cytochrome c oxidase. *Biochim. Biophys. Acta* **1188**, 391-397 (1994).
68. Bonne,G., Seibel,P., Possekel,S., Marsac,C., & Kadenbach,B. Expression of human cytochrome c oxidase subunits during fetal development. *Eur. J. Biochem.* **217**, 1099-1107 (1993).
69. Huttemann,M., Schmidt,T.R., & Grossman,L.I. A third isoform of cytochrome c oxidase subunit VIII is present in mammals. *Gene* **312**, 95-102 (2003).
70. Huttemann,M., Jaradat,S., & Grossman,L.I. Cytochrome c oxidase of mammals contains a testes-specific isoform of subunit VIb--the counterpart to testes-specific cytochrome c? *Mol. Reprod. Dev.* **66**, 8-16 (2003).
71. Taanman,J.W., Turina,P., & Capaldi,R.A. Regulation of cytochrome c oxidase by interaction of ATP at two binding sites, one on subunit VIa. *Biochemistry* **33**, 11833-11841 (1994).
72. Miyazaki,T., Neff,L., Tanaka,S., Horne,W.C., & Baron,R. Regulation of cytochrome c oxidase activity by c-Src in osteoclasts. *J. Cell Biol.* **160**, 709-718 (2003).
73. Bender,E. & Kadenbach,B. The allosteric ATP-inhibition of cytochrome c oxidase activity is reversibly switched on by cAMP-dependent phosphorylation. *FEBS Lett.* **466**, 130-134 (2000).
74. Papa,S., Sardanelli,A.M., Scacco,S., & Technikova-Dobrova,Z. cAMP-dependent protein kinase and phosphoproteins in mammalian mitochondria. An extension of the cAMP-mediated intracellular signal transduction. *FEBS Lett.* **444**, 245-249 (1999).

75. Steenaart,N.A. & Shore,G.C. Mitochondrial cytochrome c oxidase subunit IV is phosphorylated by an endogenous kinase. *FEBS Lett.* **415**, 294-298 (1997).
76. Lee,I., Bender,E., & Kadenbach,B. Control of mitochondrial membrane potential and ROS formation by reversible phosphorylation of cytochrome c oxidase. *Mol. Cell Biochem.* **234-235**, 63-70 (2002).
77. Yang,W.L., Iacono,L., Tang,W.M., & Chin,K.V. Novel function of the regulatory subunit of protein kinase A: regulation of cytochrome c oxidase activity and cytochrome c release. *Biochemistry* **37**, 14175-14180 (1998).
78. Taanman,J.W. The mitochondrial genome: structure, transcription, translation and replication. *Biochim. Biophys. Acta* **1410**, 103-123 (1999).
79. Boore,J.L. Animal mitochondrial genomes. *Nucleic Acids Res.* **27**, 1767-1780 (1999).
80. Barrell,B.G., Anderson,S., Bankier,A.T., de Bruijn,M.H., Chen,E., Coulson,A.R., Drouin,J., Eperon,I.C., Nierlich,D.P., Roe,B.A., Sanger,F., Schreier,P.H., Smith,A.J., Staden,R., & Young,I.G. Different pattern of codon recognition by mammalian mitochondrial tRNAs. *Proc. Natl. Acad. Sci. U. S. A* **77**, 3164-3166 (1980).
81. Taanman,J.W. in Genetics of Mitochondrial Diseases, Edn. 1. ed. Holt,I.J. 27-46 (Oxford University Press, Oxford; 2003).
82. Yang,M.Y., Bowmaker,M., Reyes,A., Vergani,L., Angeli,P., Gringeri,E., Jacobs,H.T., & Holt,I.J. Biased incorporation of ribonucleotides on the mitochondrial L-strand accounts for apparent strand-asymmetric DNA replication. *Cell* **111**, 495-505 (2002).
83. Grossman,L.I., Watson,R., & Vinograd,J. The presence of ribonucleotides in mature closed-circular mitochondrial DNA. *Proc. Natl. Acad. Sci. U. S. A* **70**, 3339-3343 (1973).
84. Lonsdale,D.M. & Jones,I.G. Ribonuclease-sensitivity of covalently closed rat liver mitochondrial deoxyribonucleic acid. *Biochem. J.* **141**, 155-158 (1974).
85. Lonsdale,D.M. & Jones,I.G. Localization of the ribonucleotide sites in rat liver mitochondrial deoxyribonucleic acid. *Biochem. J.* **169**, 79-85 (1978).
86. Miyaki,M., Koide,K., & Ono,T. RNase and alkali sensitivity of closed circular mitochondrial DNA of rat ascites hepatoma cells. *Biochem. Biophys. Res. Commun.* **50**, 252-258 (1973).
87. Nass,M.M. Mitochondrial DNA. II. Structure and physicochemical properties of isolated DNA. *J. Mol. Biol.* **42**, 529-545 (1969).
88. Wong-Staal,F., Mendelsohn,J., & Goulian,M. Ribonucleotides in closed circular mitochondrial DNA from HeLa cells. *Biochem. Biophys. Res. Commun.* **53**, 140-148 (1973).
89. Kajander,O.A., Rovio,A.T., Majamaa,K., Poulton,J., Spelbrink,J.N., Holt,I.J., Karhunen,P.J., & Jacobs,H.T. Human mtDNA sublimons resemble rearranged mitochondrial genoms found in pathological states. *Hum. Mol. Genet.* **9**, 2821-2835 (2000).
90. Kajander,O.A., Karhunen,P.J., & Jacobs,H.T. The relationship between somatic mtDNA rearrangements, human heart disease and aging. *Hum. Mol. Genet.* **11**, 317-324 (2002).
91. Maarouf,N., Arno,G., Carter,N.D., Syrris,P., Yusuf,S., Camm,A.J., Poleiniki,J., & Al Saady,N.M. Quantitation of mitochondrial sublimons in human fibrillating atria. *Clin. Sci. (Lond)* (2004).
92. Kraytsberg,Y., Schwartz,M., Brown,T.A., Ebralidse,K., Kunz,W.S., Clayton,D.A., Vissing,J., & Khrapko,K. Recombination of human mitochondrial DNA. *Science* **304**, 981 (2004).
93. Trounce,I., Schmiedel,J., Yen,H.C., Hosseini,S., Brown,M.D., Olson,J.J., & Wallace,D.C. Cloning of neuronal mtDNA variants in cultured cells by synaptosome fusion with mtDNA-less cells. *Nucleic Acids Res.* **28**, 2164-2170 (2000).
94. Nekhaeva,E., Bodyak,N.D., Kraytsberg,Y., McGrath,S.B., van Orsouw,N.J., Pluzhnikov,A., Wei,J.Y., Vijg,J., & Khrapko,K. Clonally expanded mtDNA point mutations are abundant in individual cells of human tissues. *Proc. Natl. Acad. Sci. U. S. A* **99**, 5521-5526 (2002).
95. Khrapko,K., Nekhaeva,E., Kraytsberg,Y., & Kunz,W. Clonal expansions of mitochondrial genomes: implications for in vivo mutational spectra. *Mutat. Res.* **522**, 13-19 (2003).
96. Kraytsberg,Y., Nekhaeva,E., Bodyak,N.B., & Khrapko,K. Mutation and intracellular clonal expansion of mitochondrial genomes: two synergistic components of the aging process? *Mech. Ageing Dev.* **124**, 49-53 (2003).
97. King,M.P. & Attardi,G. Human cells lacking mtDNA: repopulation with exogenous mitochondria by complementation. *Science* **246**, 500-503 (1989).
98. Jazayeri,M., Andreyev,A., Will,Y., Ward,M., Anderson,C.M., & Clevenger,W. Inducible expression of a dominant negative DNA polymerase-gamma depletes mitochondrial DNA and produces a rho0 phenotype. *J. Biol Chem.* **278**, 9823-9830 (2003).
99. Garrido,N., Griparic,L., Jokitalo,E., Wartiovaara,J., van der Bliek,A.M., & Spelbrink,J.N. Composition and dynamics of human mitochondrial nucleoids. *Mol. Biol Cell* **14**, 1583-1596 (2003).
100. Legros,F., Malka,F., Frachon,P., Lombes,A., & Rojo,M. Organization and dynamics of human mitochondrial DNA. *J. Cell Sci.* **Pt**, (2004).
101. Iborra,F.J., Kimura,H., & Cook,P.R. The functional organization of mitochondrial genomes in human cells. *BMC. Biol* **2**, 9 (2004).

102. Capaldi,R.A., Aggeler,R., Gilkerson,R., Hanson,G., Knowles,M., Marcus,A., Margineantu,D., Marusich,M., Murray,J., Oglesbee,D., Remington,S.J., & Rossignol,R. A replicating module as the unit of mitochondrial structure and functioning. *Biochim. Biophys. Acta* **1555**, 192-195 (2002).
103. Cavelier,L., Johannisson,A., & Gyllensten,U. Analysis of mtDNA copy number and composition of single mitochondrial particles using flow cytometry and PCR. *Exp. Cell Res.* **259**, 79-85 (2000).
104. Margineantu,D.H., Cox,W.G., Sundell,L., Sherwood,S.W., Beechem,J.A., & Capaldi,R.A. Cell cycle dependent morphology changes and associated mitochondrial DNA redistribution in mitochondria of human cell lines. *Mitochondrion* **1**, 425-435 (2002).
105. Bustin,M. Regulation of DNA-dependent activities by the functional motifs of the high-mobility-group chromosomal proteins. *Mol. Cell Biol.* **19**, 5237-5246 (1999).
106. Takamatsu,C., Umeda,S., Ohsato,T., Ohno,T., Abe,Y., Fukuoh,A., Shinagawa,H., Hamasaki,N., & Kang,D. Regulation of mitochondrial D-loops by transcription factor A and single-stranded DNA-binding protein. *EMBO Rep.* **3**, 451-456 (2002).
107. Shadel,G.S. & Clayton,D.A. Mitochondrial DNA maintenance in vertebrates. *Annu. Rev. Biochem.* **66**, 409-435 (1997).
108. Meeusen,S., Tieu,Q., Wong,E., Weiss,E., Schieltz,D., Yates,J.R., & Nunnari,J. Mgm101p is a novel component of the mitochondrial nucleoid that binds DNA and is required for the repair of oxidatively damaged mitochondrial DNA. *J. Cell Biol.* **145**, 291-304 (1999).
109. Meeusen,S. & Nunnari,J. Evidence for a two membrane-spanning autonomous mitochondrial DNA replisome. *J. Cell Biol* **163**, 503-510 (2003).
110. Kaufman,B.A., Newman,S.M., Hallberg,R.L., Slaughter,C.A., Perlman,P.S., & Butow,R.A. In organello formaldehyde crosslinking of proteins to mtDNA: identification of bifunctional proteins. *Proc. Natl. Acad. Sci. U. S. A* **97**, 7772-7777 (2000).
111. Kaufman,B.A., Kolesar,J.E., Perlman,P.S., & Butow,R.A. A function for the mitochondrial chaperonin Hsp60 in the structure and transmission of mitochondrial DNA nucleoids in Saccharomyces cerevisiae. *J. Cell Biol* **163**, 457-461 (2003).
112. Baumann,F., Milisav,I., Neupert,W., & Herrmann,J.M. Ecm10, a novel hsp70 homolog in the mitochondrial matrix of the yeast Saccharomyces cerevisiae. *FEBS Lett.* **487**, 307-312 (2000).
113. Sakasegawa,Y., Hachiya,N.S., Tsukita,S., & Kaneko,K. Ecm10p localizes in yeast mitochondrial nucleoids and its overexpression induces extensive mitochondrial DNA aggregations. *Biochem. Biophys. Res. Commun.* **309**, 217-221 (2003).
114. Liu,T., Lu,B., Lee,I., Ondrovicova,G., Kutejova,E., & Suzuki,C.K. DNA and RNA binding by the mitochondrial Lon protease is regulated by nucleotide and protein substrates. *J. Biol Chem.* (2004).
115. Spelbrink,J.N., Li,F.Y., Tiranti,V., Nikali,K., Yuan,Q.P., Tariq,M., Wanrooij,S., Garrido,N., Comi,G., Morandi,L., Santoro,L., Toscano,A., Fabrizi,G.M., Somer,H., Croxen,R., Beeson,D., Poulton,J., Suomalainen,A., Jacobs,H.T., Zeviani,M., & Larsson,C. Human mitochondrial DNA deletions associated with mutations in the gene encoding Twinkle, a phage T7 gene 4-like protein localized in mitochondria. *Nat. Genet.* **28**, 223-231 (2001).
116. Boldogh,I.R., Nowakowski,D.W., Yang,H.C., Chung,H., Karmon,S., Royes,P., & Pon,L.A. A protein complex containing Mdm10p, Mdm12p, and Mmm1p links mitochondrial membranes and DNA to the cytoskeleton-based segregation machinery. *Mol. Biol Cell* **14**, 4618-4627 (2003).
117. Sesaki,H., Southard,S.M., Hobbs,A.E., & Jensen,R.E. Cells lacking Pcp1p/Ugo2p, a rhomboid-like protease required for Mgm1p processing, lose mtDNA and mitochondrial structure in a Dnm1p-dependent manner, but remain competent for mitochondrial fusion. *Biochem. Biophys. Res. Commun.* **308**, 276-283 (2003).
118. Alam,T.I., Kanki,T., Muta,T., Ukaji,K., Abe,Y., Nakayama,H., Takio,K., Hamasaki,N., & Kang,D. Human mitochondrial DNA is packaged with TFAM. *Nucleic Acids Res.* **31**, 1640-1645 (2003).
119. Youngman,M.J., Hobbs,A.E., Burgess,S.M., Srinivasan,M., & Jensen,R.E. Mmm2p, a mitochondrial outer membrane protein required for yeast mitochondrial shape and maintenance of mtDNA nucleoids. *J. Cell Biol* **164**, 677-688 (2004).
120. Hobbs,A.E., Srinivasan,M., McCaffery,J.M., & Jensen,R.E. Mmm1p, a mitochondrial outer membrane protein, is connected to mitochondrial DNA (mtDNA) nucleoids and required for mtDNA stability. *J. Cell Biol.* **152**, 401-410 (2001).
121. Kondo-Okamoto,N., Shaw,J.M., & Okamoto,K. Mmm1p spans both the outer and inner mitochondrial membranes and contains distinct domains for targeting and foci formation. *J. Biol Chem.* **278**, 48997-49005 (2003).
122. Shadel,G.S. Coupling the mitochondrial transcription machinery to human disease. *Trends Genet.* **20**, 513-519 (2004).
123. Ohsato,T., Muta,T., Fukuoh,A., Shinagawa,H., Hamasaki,N., & Kang,D. R-Loop in the replication origin of human mitochondrial DNA is resolved by RecG, a Holliday junction-specific helicase. *Biochem. Biophys. Res. Commun.* **255**, 1-5 (1999).
124. Lee,D.Y. & Clayton,D.A. Initiation of mitochondrial DNA replication by transcription and R-loop processing. *J. Biol. Chem.* **273**, 30614-30621 (1998).

125. Sbisa,E., Tanzariello,F., Reyes,A., Pesole,G., & Saccone,C. Mammalian mitochondrial D-loop region structural analysis: identification of new conserved sequences and their functional and evolutionary implications. *Gene* **205**, 125-140 (1997).
126. Tiranti,V., Savoia,A., Forti,F., D'Apolito,M.F., Centra,M., Rocchi,M., & Zeviani,M. Identification of the gene encoding the human mitochondrial RNA polymerase (h-mtRPOL) by cyberscreening of the Expressed Sequence Tags database. *Hum. Mol. Genet.* **6**, 615-625 (1997).
127. Small,I.D. & Peeters,N. The PPR motif - a TPR-related motif prevalent in plant organellar proteins. *Trends Biochem. Sci.* **25**, 46-47 (2000).
128. Falkenberg,M., Gaspari,M., Rantanen,A., Trifunovic,A., Larsson,N.G., & Gustafsson,C.M. Mitochondrial transcription factors B1 and B2 activate transcription of human mtDNA. *Nat. Genet.* (2002).
129. McCulloch,V., Seidel-Rogol,B., & Shadel,G.S. A human mitochondrial transcription factor is related to RNA adenine methyltransferases and binds S-adenosylmethionine. *Mol Cell Biol* **26**, 1116-1125 (2002).
130. McCulloch,V. & Shadel,G.S. Human mitochondrial transcription factor B1 interacts with the C-terminal activation region of h-mtTFA and stimulates transcription independently of its RNA methyltransferase activity. *Mol. Cell Biol* **23**, 5816-5824 (2003).
131. Seidel-Rogol,B.L., McCulloch,V., & Shadel,G.S. Human mitochondrial transcription factor B1 methylates ribosomal RNA at a conserved stem-loop. *Nat. Genet.* **33**, 23-24 (2003).
132. Hixson,J.E. & Clayton,D.A. Initiation of transcription from each of the two human mitochondrial promoters requires unique nucleotides at the transcriptional start sites. *Proc. Natl. Acad. Sci. U. S. A* **82**, 2660-2664 (1985).
133. Montoya,J., Gaines,G.L., & Attardi,G. The pattern of transcription of the human mitochondrial rRNA genes reveals two overlapping transcription units. *Cell* **34**, 151-159 (1983).
134. Gaines,G., Rossi,C., & Attardi,G. Markedly different ATP requirements for rRNA synthesis and mtDNA light strand transcription versus mRNA synthesis in isolated human mitochondria. *J. Biol. Chem.* **262**, 1907-1915 (1987).
135. Kantharaj,G.R., Bhat,K.S., & Avadhani,N.G. Mode of transcription and maturation of ribosomal ribonucleic acid in vitro in mitochondria from Ehrlich ascites cells. *Biochemistry* **22**, 3151-3156 (1983).
136. Attardi,G., Chomyn,A., King,M.P., Kruse,B., Polosa,P.L., & Murdter,N.N. Regulation of mitochondrial gene expression in mammalian cells. *Biochem. Soc. Trans.* **18**, 509-513 (1990).
137. Duborjal,H., Beugnot,R., Mousson De Camaret,B., & Issartel,J.P. Large functional range of steady-state levels of nuclear and mitochondrial transcripts coding for the subunits of the human mitochondrial OXPHOS system. *Genome Res.* **12**, 1901-1909 (2002).
138. Christianson,T.W. & Clayton,D.A. In vitro transcription of human mitochondrial DNA: accurate termination requires a region of DNA sequence that can function bidirectionally. *Proc. Natl. Acad. Sci. U. S. A* **83**, 6277-6281 (1986).
139. Enriquez,J.A., Fernandez-Silva,P., Garrido-Perez,N., Lopez-Perez,M.J., Perez-Martos,A., & Montoya,J. Direct regulation of mitochondrial RNA synthesis by thyroid hormone. *Mol. Cell Biol.* **19**, 657-670 (1999).
140. Chrzanowska-Lightowlers,Z.M., Temperley,R.J., Smith,P.M., Seneca,S.H., & Lightowlers,R.N. Functional polypeptides can be synthesized from human mitochondrial transcripts lacking termination codons. *Biochem. J.* **377**, 725-731 (2004).
141. Asin-Cayuela,J., Helm,M., & Attardi,G. A monomer-to-trimer transition of the human mitochondrial transcription termination factor (mTERF) is associated with a loss of in vitro activity. *J. Biol Chem.* **279**, 15670-15677 (2004).
142. Prieto-Martin,A., Montoya,J., & Martinez-Azorin,F. Phosphorylation of rat mitochondrial transcription termination factor (mTERF) is required for transcription termination but not for binding to DNA. *Nucleic Acids Res.* **32**, 2059-2068 (2004).
143. Ojala,D., Montoya,J., & Attardi,G. tRNA punctuation model of RNA processing in human mitochondria. *Nature* **290**, 470-474 (1981).
144. Moore,M.J. Nuclear RNA turnover. *Cell* **108**, 431-434 (2002).
145. Anderson,S., Bankier,A.T., Barrell,B.G., de Bruijn,M.H., Coulson,A.R., Drouin,J., Eperon,I.C., Nierlich,D.P., Roe,B.A., Sanger,F., Schreier,P.H., Smith,A.J., Staden,R., & Young,I.G. Sequence and organization of the human mitochondrial genome. *Nature* **290**, 457-465 (1981).
146. Proudfoot,N.J., Furger,A., & Dye,M.J. Integrating mRNA processing with transcription. *Cell* **108**, 501-512 (2002).
147. Grohmann,K., Amairic,F., Crews,S., & Attardi,G. Failure to detect "cap" structures in mitochondrial DNA-coded poly(A)-containing RNA from HeLa cells. *Nucleic Acids Res.* **5**, 637-651 (1978).
148. Ojala,D. & Attardi,G. Identification and partial characterization of multiple discrete polyadenylic acid containing RNA components coded for by HeLa cell mitochondrial DNA. *J. Mol. Biol.* **88**, 205-219 (1974).

149. Temperley,R.J., Seneca,S.H., Tonska,K., Bartnik,E., Bindoff,L.A., Lightowlers,R.N., & Chrzanowska-Lightowlers,Z.M. Investigation of a pathogenic mtDNA microdeletion reveals a translation-dependent deadenylation decay pathway in human mitochondria. *Hum. Mol. Genet.* (2003).
150. Gagliardi,D., Stepien,P.P., Temperley,R.J., Lightowlers,R.N., & Chrzanowska-Lightowlers,Z.M. Messenger RNA stability in mitochondria: different means to an end. *Trends Genet.* **20**, 260-267 (2004).
151. Dever,T.E. Gene-specific regulation by general translation factors. *Cell* **108**, 545-556 (2002).
152. Ofengand,J. & Bakin,A. Mapping to nucleotide resolution of pseudouridine residues in large subunit ribosomal RNAs from representative eukaryotes, prokaryotes, archaebacteria, mitochondria and chloroplasts. *J. Mol. Biol* **266**, 246-268 (1997).
153. Dubin,D.T., Montoya,J., Timko,K.D., & Attardi,G. Sequence analysis and precise mapping of the 3' ends of HeLa cell mitochondrial ribosomal RNAs. *J. Mol. Biol.* **157**, 1-19 (1982).
154. Xiao,S., Scott,F., Fierke,C.A., & Engelke,D.R. Eukaryotic ribonuclease P: a plurality of ribonucleoprotein enzymes. *Annu. Rev. Biochem.* **71**, 165-189 (2002).
155. Dubrovsky,E.B., Dubrovskaya,V.A., Levinger,L., Schiffer,S., & Marchfelder,A. Drosophila RNase Z processes mitochondrial and nuclear pre-tRNA 3' ends in vivo. *Nucleic Acids Res.* **32**, 255-262 (2004).
156. Levinger,L., Jacobs,O., & James,M. In vitro 3'-end endonucleolytic processing defect in a human mitochondrial tRNA(Ser(UCN)) precursor with the U7445C substitution, which causes non-syndromic deafness. *Nucleic Acids Res.* **29**, 4334-4340 (2001).
157. Nagaike,T., Suzuki,T., Tomari,Y., Takemoto-Hori,C., Negayama,F., Watanabe,K., & Ueda,T. Identification and characterization of mammalian mitochondrial tRNA nucleotidyltransferases. *J. Biol. Chem.* **276**, 40041-40049 (2001).
158. Yasukawa,T., Suzuki,T., Ishii,N., Ohta,S., & Watanabe,K. Wobble modification defect in tRNA disturbs codon-anticodon interaction in a mitochondrial disease. *EMBO J.* **20**, 4794-4802 (2001).
159. Mudge,S.J., Williams,J.H., Eyre,H.J., Sutherland,G.R., Cowan,P.J., & Power,D.A. Complex organisation of the 5'-end of the human glycine tRNA synthetase gene. *Gene* **209**, 45-50 (1998).
160. Tolkunova,E., Park,H., Xia,J., King,M.P., & Davidson,E. The human lysyl-tRNA synthetase gene encodes both the cytoplasmic and mitochondrial enzymes by means of an unusual alternative splicing of the primary transcript. *J. Biol Chem.* **275**, 35063-35069 (2000).
161. Shimada,N., Suzuki,T., & Watanabe,K. Dual mode recognition of two isoacceptor tRNAs by mammalian mitochondrial seryl-tRNA synthetase. *J. Biol Chem.* **276**, 46770-46778 (2001).
162. Yokogawa,T., Shimada,N., Takeuchi,N., Benkowski,L., Suzuki,T., Omori,A., Ueda,T., Nishikawa,K., Spremulli,L.L., & Watanabe,K. Characterization and tRNA recognition of mammalian mitochondrial seryl-tRNA synthetase. *J. Biol Chem.* **275**, 19913-19920 (2000).
163. Takeuchi,N., Vial,L., Panvert,M., Schmitt,E., Watanabe,K., Mechulam,Y., & Blanquet,S. Recognition of tRNAs by Methionyl-tRNA transformylase from mammalian mitochondria. *J. Biol Chem.* **276**, 20064-20068 (2001).
164. Koc,E.C. & Spremulli,L.L. RNA-binding proteins of mammalian mitochondria. *Mitochondrion* **2**, 277-291 (2003).
165. Minczuk,M., Piwowarski,J., Papworth,M.A., Awiszus,K., Schalinski,S., Dziembowski,A., Dmochowska,A., Bartnik,E., Tokatlidis,K., Stepien,P.P., & Borowski,P. Localisation of the human hSuv3p helicase in the mitochondrial matrix and its preferential unwinding of dsDNA. *Nucleic Acids Res.* **30**, 5074-5086 (2002).
166. Preiss,T. & Lightowlers,R.N. Post-transcriptional regulation of tissue-specific isoforms. A bovine cytosolic RNA-binding protein, COLBP, associates with messenger RNA encoding the liver-form isopeptides of cytochrome c oxidase. *J. Biol. Chem.* **268**, 10659-10667 (1993).
167. Preiss,T., Chrzanowska-Lightowlers,Z.M., & Lightowlers,R.N. The tissue-specific RNA-binding protein COLBP is differentially regulated during myogenesis. *Biochim. Biophys. Acta* **1221**, 286-289 (1994).
168. Preiss,T., Sang,A.E., Chrzanowska-Lightowlers,Z.M., & Lightowlers,R.N. The mRNA-binding protein COLBP is glutamate dehydrogenase. *FEBS Lett.* **367**, 291-296 (1995).
169. Brennan,L.E., Nakagawa,J., Egger,D., Bienz,K., & Moroni,C. Characterisation and mitochondrial localisation of AUH, an AU-specific RNA-binding enoyl-CoA hydratase. *Gene* **228**, 85-91 (1999).
170. Mili,S. & Pinol-Roma,S. LRP130, a pentatricopeptide motif protein with a noncanonical RNA-binding domain, is bound in vivo to mitochondrial and nuclear RNAs. *Mol. Cell Biol.* **23**, 4972-4982 (2003).
171. Xu,F., Morin,C., Mitchell,G., Ackerley,C., & Robinson,B.H. The role of the LRPPRC (leucine-rich pentatricopeptide repeat cassette) gene in cytochrome oxidase assembly: mutation causes lowered levels of COX (cytochrome c oxidase) I and COX III mRNA. *Biochem. J.* **382**, 331-336 (2004).
172. Habelhah,H., Shah,K., Huang,L., Ostareck-Lederer,A., Burlingame,A.L., Shokat,K.M., Hentze,M.W., & Ronai,Z. ERK phosphorylation drives cytoplasmic accumulation of hnRNP-K and inhibition of mRNA translation. *Nat. Cell Biol.* **3**, 325-330 (2001).

173. Ostrowski,J., Kawata,Y., Schullery,D.S., Denisenko,O.N., & Bomsztyk,K. Transient recruitment of the hnRNP K protein to inducibly transcribed gene loci. *Nucleic Acids Res.* **31**, 3954-3962 (2003).
174. Ostrowski,J., Wyrwicz,L., Rychlewski,L., & Bomsztyk,K. Heterogeneous nuclear ribonucleoprotein K protein associates with multiple mitochondrial transcripts within the organelle. *J. Biol. Chem.* **277**, 6303-6310 (2002).
175. Ostareck,D.H., Ostareck-Lederer,A., Wilm,M., Thiele,B.J., Mann,M., & Hentze,M.W. mRNA silencing in erythroid differentiation: hnRNP K and hnRNP E1 regulate 15-lipoxygenase translation from the 3' end. *Cell* **89**, 597-606 (1997).
176. Mili,S., Shu,H.J., Zhao,Y., & Pinol-Roma,S. Distinct RNP complexes of shuttling hnRNP proteins with pre-mRNA and mRNA: candidate intermediates in formation and export of mRNA. *Mol. Cell Biol.* **21**, 7307-7319 (2001).
177. Scarpulla,R.C. Transcriptional activators and coactivators in the nuclear control of mitochondrial function in mammalian cells. *Gene* **286**, 81-89 (2002).
178. Scarpulla,R.C. Nuclear activators and coactivators in mammalian mitochondrial biogenesis. *Biochim. Biophys. Acta* **1576**, 1-14 (2002).
179. Buchet,K. & Godinot,C. Functional F1-ATPase essential in maintaining growth and membrane potential of human mitochondrial DNA-depleted rho degrees cells. *J. Biol. Chem.* **273**, 22983-22989 (1998).
180. Marusich,M.F., Robinson,B.H., Taanman,J.W., Kim,S.J., Schillace,R., Smith,J.L., & Capaldi,R.A. Expression of mtDNA and nDNA encoded respiratory chain proteins in chemically and genetically-derived Rho0 human fibroblasts: a comparison of subunit proteins in normal fibroblasts treated with ethidium bromide and fibroblasts from a patient with mtDNA depletion syndrome. *Biochim. Biophys. Acta* **1362**, 145-159 (1997).
181. Nijtmans,L.G., Spelbrink,J.N., Van Galen,M.J., Zwaan,M., Klement,P., & Van den Bogert,C. Expression and fate of the nuclearly encoded subunits of cytochrome-c oxidase in cultured human cells depleted of mitochondrial gene products. *Biochim. Biophys. Acta* **1265**, 117-126 (1995).
182. Arnould,T., Vankoningsloo,S., Renard,P., Houbion,A., Ninane,N., Demazy,C., Remacle,J., & Raes,M. CREB activation induced by mitochondrial dysfunction is a new signaling pathway that impairs cell proliferation. *EMBO J.* **21**, 53-63 (2002).
183. Biswas,G., Adebanjo,O.A., Freedman,B.D., Anandatheerthavarada,H.K., Vijayasarathy,C., Zaidi,M., Kotlikoff,M., & Avadhani,N.G. Retrograde Ca2+ signaling in C2C12 skeletal myocytes in response to mitochondrial genetic and metabolic stress: a novel mode of inter-organelle crosstalk. *EMBO J.* **18**, 522-533 (1999).
184. Biswas,G., Anandatheerthavarada,H.K., Zaidi,M., & Avadhani,N.G. Mitochondria to nucleus stress signaling: a distinctive mechanism of NF{kappa}B/Rel activation through calcineurin-mediated inactivation of I{kappa}B{beta}. *J. Cell Biol.* **161**, 507-519 (2003).
185. Kuzmin,E.V., Karpova,O.V., Elthon,T.E., & Newton,K.J. Mitochondrial respiratory deficiencies signal up-regulation of genes for heat shock proteins. *J. Biol Chem.* **279**, 20672-20677 (2004).
186. Chrzanowska-Lightowlers,Z.M., Preiss,T., & Lightowlers,R.N. Inhibition of mitochondrial protein synthesis promotes increased stability of nuclear-encoded respiratory gene transcripts. *J. Biol. Chem.* **269**, 27322-27328 (1994).
187. Bai,Y., Shakeley,R.M., & Attardi,G. Tight control of respiration by NADH dehydrogenase ND5 subunit gene expression in mouse mitochondria. *Mol. Cell Biol.* **20**, 805-815 (2000).
188. Clayton,D.A. Replication of animal mitochondrial DNA. *Cell* **28**, 693-705 (1982).
189. Collins,M.L., Eng,S., Hoh,R., & Hellerstein,M.K. Measurement of mitochondrial DNA synthesis in vivo using a stable isotope-mass spectrometric technique. *J. Appl. Physiol* **94**, 2203-2211 (2003).
190. Bogenhagen,D. & Clayton,D.A. Mouse L cell mitochondrial DNA molecules are selected randomly for replication throughout the cell cycle. *Cell* **11**, 719-727 (1977).
191. Magnusson,J., Orth,M., Lestienne,P., & Taanman,J.W. Replication of mitochondrial DNA occurs throughout the mitochondria of cultured human cells. *Exp. Cell Res.* **289**, 133-142 (2003).
192. Tang,Y., Schon,E.A., Wilichowski,E., Vazquez-Memije,M.E., Davidson,E., & King,M.P. Rearrangements of human mitochondrial DNA (mtDNA): new insights into the regulation of mtDNA copy number and gene expression. *Mol. Biol. Cell* **11**, 1471-1485 (2000).
193. Berk,A.J. & Clayton,D.A. Mechanism of mitochondrial DNA replication in mouse L-cells: asynchronous replication of strands, segregation of circular daughter molecules, aspects of topology and turnover of an initiation sequence. *J. Mol. Biol.* **86**, 801-824 (1974).
194. Shearman,C.W. & Kalf,G.F. DNA replication by a membrane-DNA complex from rat liver mitochondria. *Arch. Biochem. Biophys.* **182**, 573-586 (1977).
195. Korhonen,J.A., Pham,X.H., Pellegrini,M., & Falkenberg,M. Reconstitution of a minimal mtDNA replisome in vitro. *EMBO J.* **23**, 2423-2429 (2004).
196. Bogenhagen,D.F. & Clayton,D.A. Concluding remarks: The mitochondrial DNA replication bubble has not burst. *Trends Biochem. Sci.* **28**, 404-405 (2003).
197. Bogenhagen,D.F. & Clayton,D.A. The mitochondrial DNA replication bubble has not burst. *Trends Biochem. Sci.* **28**, 357-360 (2003).

198. Holt,I.J. & Jacobs,H.T. Response: The mitochondrial DNA replication bubble has not burst. *Trends Biochem. Sci.* **28**, 355-356 (2003).
199. Robberson,D.L., Kasamatsu,H., & Vinograd,J. Replication of mitochondrial DNA. Circular replicative intermediates in mouse L cells. *Proc. Natl. Acad. Sci. U. S. A* **69**, 737-741 (1972).
200. Bowmaker,M., Yang,M.Y., Yasukawa,T., Reyes,A., Jacobs,H.T., Huberman,J.A., & Holt,I.J. Mammalian mitochondrial DNA replicates bidirectionally from an initiation zone. *J. Biol Chem.* **278**, 50961-50969 (2003).
201. Holt,I.J., Lorimer,H.E., & Jacobs,H.T. Coupled leading- and lagging-strand synthesis of mammalian mitochondrial DNA. *Cell* **100**, 515-524 (2000).
202. Han,z. & Stachow,c. Analysis of *Schizosaccharmyces pombe* mitochondrial DNA replication by two dimensional gel electrophoresis. *Chromosoma* **103**, 162-170 (1994).
203. Mayhook,A.G., Rinaldi,A.M., & Jacobs,H.T. Replication origins and pause sites in sea urchin mitochondrial DNA. *Proc. R. Soc. Lond B Biol. Sci.* **248**, 85-94 (1992).
204. Preiser,P.R., Wilson,R.J., Moore,P.W., McCready,S., Hajibagheri,M.A., Blight,K.J., Strath,M., & Williamson,D.H. Recombination associated with replication of malarial mitochondrial DNA. *EMBO J.* **15**, 684-693 (1996).
205. Koike,K. & Wolstenholme,D.R. Evidence for discontinuous replication of circular mitochondrial DNA molecules from Novikoff rat ascites hepatoma cells. *J. Cell Biol.* **61**, 14-25 (1974).
206. Suzuki,T., Terasaki,M., Takemoto-Hori,C., Hanada,T., Ueda,T., Wada,A., & Watanabe,K. Structural compensation for the deficit of rRNA with proteins in the mammalian mitochondrial ribosome. Systematic analysis of protein components of the large ribosomal subunit from mammalian mitochondria. *J. Biol Chem.* **276**, 21724-21736 (2001).
207. Suzuki,T., Terasaki,M., Takemoto-Hori,C., Hanada,T., Ueda,T., Wada,A., & Watanabe,K. Proteomic analysis of the mammalian mitochondrial ribosome. Identification of protein components in the 28 S small subunit. *J. Biol Chem.* **276**, 33181-33195 (2001).
208. Koc,E.C., Burkhart,W., Blackburn,K., Moyer,M.B., Schlatzer,D.M., Moseley,A., & Spremulli,L.L. The large subunit of the mammalian mitochondrial ribosome. Analysis of the complement of ribosomal proteins present. *J. Biol Chem.* **276**, 43958-43969 (2001).
209. Koc,E.C., Burkhart,W., Blackburn,K., Koc,H., Moseley,A., & Spremulli,L.L. Identification of four proteins from the small subunit of the mammalian mitochondrial ribosome using a proteomics approach. *Protein Sci.* **10**, 471-481 (2001).
210. O'Brien,T.W. Properties of human mitochondrial ribosomes. *IUBMB Life* **55**, 505-513 (2003).
211. Kenmochi,N., Suzuki,T., Uechi,T., Magoori,M., Kuniba,M., Higa,S., Watanabe,K., & Tanaka,T. The human mitochondrial ribosomal protein genes: mapping of 54 genes to the chromosomes and implications for human disorders. *Genomics* **77**, 65-70 (2001).
212. Sharma,M.R., Koc,E.C., Datta,P.P., Booth,T.M., Spremulli,L.L., & Agrawal,R.K. Structure of the mammalian mitochondrial ribosome reveals an expanded functional role for its component proteins. *Cell* **115**, 97-108 (2003).
213. Cavdar,K.E., Burkhart,W., Blackburn,K., Moseley,A., & Spremulli,L.L. The small subunit of the mammalian mitochondrial ribosome. Identification of the full complement of ribosomal proteins present. *J. Biol Chem.* **276**, 19363-19374 (2001).
214. Spirina,O., Bykhovskaya,Y., Kajava,A.V., O'Brien,T.W., Nierlich,D.P., Mougey,E.B., Sylvester,J.E., Graack,H.R., Wittmann-Liebold,B., & Fischel-Ghodsian,N. Heart-specific splice-variant of a human mitochondrial ribosomal protein (mRNA processing; tissue specific splicing). *Gene* **261**, 229-234 (2000).
215. Cavdar,K.E., Ranasinghe,A., Burkhart,W., Blackburn,K., Koc,H., Moseley,A., & Spremulli,L.L. A new face on apoptosis: death-associated protein 3 and PDCD9 are mitochondrial ribosomal proteins. *FEBS Lett.* **492**, 166-170 (2001).
216. Liu,M. & Spremulli,L. Interaction of mammalian mitochondrial ribosomes with the inner membrane. *J. Biol Chem.* **275**, 29400-29406 (2000).
217. Marzuki,S. & Hibbs,A.R. Are all mitochondrial translation products synthesized on membrane-bound ribosomes? *Biochim. Biophys. Acta* **866**, 120-124 (1986).
218. Sanchirico,M.E., Fox,T.D., & Mason,T.L. Accumulation of mitochondrially synthesized Saccharomyces cerevisiae Cox2p and Cox3p depends on targeting information in untranslated portions of their mRNAs. *EMBO J.* **17**, 5796-5804 (1998).
219. Lodish,H., Berk,A., Zipursky,S.L., Matsudaira,P., Baltimore,D., & Darnell,J.E. in Molecular Cell Biology, Edn. 4th 101-137 (W.H. Freeman and Company, New York; 2000).
220. Farwell,M.A., Schirawski,J., Hager,P.W., & Spremulli,L.L. Analysis of the interaction between bovine mitochondrial 28 S ribosomal subunits and mRNA. *Biochim. Biophys. Acta* **1309**, 122-130 (1996).
221. Liao,H.X. & Spremulli,L.L. Effects of length and mRNA secondary structure on the interaction of bovine mitochondrial ribosomes with messenger RNA. *J. Biol Chem.* **265**, 11761-11765 (1990).
222. Liao,H.X. & Spremulli,L.L. Interaction of bovine mitochondrial ribosomes with messenger RNA. *J. Biol Chem.* **264**, 7518-7522 (1989).

223. Ma,L. & Spremulli,L.L. Cloning and sequence analysis of the human mitochondrial translational initiation factor 2 cDNA. *J. Biol Chem.* **270**, 1859-1865 (1995).
224. Bonner,D.S., Wiley,J.E., & Farwell,M.A. Assignment1 of the mitochondrial translational initiation factor 2 gene (MTIF2) to human chromosome 2 bands p16-->p14 by in situ hybridization and with somatic cell hybrids. *Cytogenet. Cell Genet.* **83**, 80-81 (1998).
225. Overman,R.G., Jr., Enderle,P.J., Farrow,J.M., III, Wiley,J.E., & Farwell,M.A. The human mitochondrial translation initiation factor 2 gene (MTIF2): transcriptional analysis and identification of a pseudogene. *Biochim. Biophys. Acta* **1628**, 195-205 (2003).
226. Koc,E.C. & Spremulli,L.L. Identification of mammalian mitochondrial translational initiation factor 3 and examination of its role in initiation complex formation with natural mRNAs. *J. Biol Chem.* **277**, 35541-35549 (2002).
227. Shah,Z.H., Migliosi,V., Miller,S.C., Wang,A., Friedman,T.B., & Jacobs,H.T. Chromosomal locations of three human nuclear genes (RPSM12, TUFM, and AFG3L1) specifying putative components of the mitochondrial gene expression apparatus. *Genomics* **48**, 384-388 (1998).
228. Vernon,J.L., Burr,P.C., Wiley,J.E., & Farwell,M.A. Assignment of the mitochondrial translation elongation factor Ts gene (TSFM) to human chromosome 12 bands q13-->q14 by in situ hybridization and with somatic cell hybrids. *Cytogenet. Cell Genet.* **89**, 145-146 (2000).
229. Gao,J., Yu,L., Zhang,P., Jiang,J., Chen,J., Peng,J., Wei,Y., & Zhao,S. Cloning and characterization of human and mouse mitochondrial elongation factor G, GFM and Gfm, and mapping of GFM to human chromosome 3q25.1-q26.2. *Genomics* **74**, 109-114 (2001).
230. Hammarsund,M., Wilson,W., Corcoran,M., Merup,M., Einhorn,S., Grander,D., & Sangfelt,O. Identification and characterization of two novel human mitochondrial elongation factor genes, hEFG2 and hEFG1, phylogenetically conserved through evolution. *Hum. Genet.* **109**, 542-550 (2001).
231. He,H., Chen,M., Scheffler,N.K., Gibson,B.W., Spremulli,L.L., & Gottlieb,R.A. Phosphorylation of mitochondrial elongation factor Tu in ischemic myocardium: basis for chloramphenicol-mediated cardioprotection. *Circ. Res.* **89**, 461-467 (2001).
232. Andersen,G.R., Thirup,S., Spremulli,L.L., & Nyborg,J. High resolution crystal structure of bovine mitochondrial EF-Tu in complex with GDP. *J. Mol Biol* **297**, 421-436 (2000).
233. Cai,Y.C., Bullard,J.M., Thompson,N.L., & Spremulli,L.L. Interaction of mitochondrial elongation factor Tu with aminoacyl-tRNA and elongation factor Ts. *J. Biol Chem.* **275**, 20308-20314 (2000).
234. Hansen,L.L., Jorgensen,R., & Justesen,J. Assignment of the human mitochondrial translational release factor 1 (MTRF1) to chromosome 13q14.1-->q14.3 and of the human mitochondrial ribosome recycling factor (MRRF) to chromosome 9q32-->q34.1 with radiation hybrid mapping. *Cytogenet. Cell Genet.* **88**, 91-92 (2000).
235. Piwowarski,J., Grzechnik,P., Dziembowski,A., Dmochowska,A., Minczuk,M., & Stepien,P.P. Human polynucleotide phosphorylase, hPNPase, is localized in mitochondria. *J. Mol. Biol* **329**, 853-857 (2003).
236. Leszczyniecka,M., Su,Z.Z., Kang,D.C., Sarkar,D., & Fisher,P.B. Expression regulation and genomic organization of human polynucleotide phosphorylase, hPNPase(old-35), a Type I interferon inducible early response gene. *Gene* **316**, 143-156 (2003).
237. Taylor,S.W., Fahy,E., Zhang,B., Glenn,G.M., Warnock,D.E., Wiley,S., Murphy,A.N., Gaucher,S.P., Capaldi,R.A., Gibson,B.W., & Ghosh,S.S. Characterization of the human heart mitochondrial proteome. *Nat. Biotechnol.* **21**, 281-286 (2003).
238. Taylor,S.W., Fahy,E., & Ghosh,S.S. Global organellar proteomics. *Trends Biotechnol.* **21**, 82-88 (2003).
239. Gellerfors,P., Wielburski,A., & Nelson,B.D. Synthesis of mitochondrial proteins in isolated rat hepatocytes. *FEBS Lett.* **108**, 167-170 (1979).
240. Karlberg,O., Canback,B., Kurland,C.G., & Andersson,S.G. The dual origin of the yeast mitochondrial proteome. *Yeast* **17**, 170-187 (2000).
241. Marc,P., Margeot,A., Devaux,F., Blugeon,C., Corral-Debrinski,M., & Jacq,C. Genome-wide analysis of mRNAs targeted to yeast mitochondria. *EMBO Rep.* **3**, 159-164 (2002).
242. Ades,I.Z. & Butow,R.A. The products of mitochondria-bound cytoplasmic polysomes in yeast. *J. Biol Chem.* **255**, 9918-9924 (1980).
243. Fujiki,M. & Verner,K. Coupling of cytosolic protein synthesis and mitochondrial protein import in yeast. Evidence for cotranslational import in vivo. *J. Biol. Chem.* **268**, 1914-1920 (1993).
244. Beddoe,T. & Lithgow,T. Delivery of nascent polypeptides to the mitochondrial surface. *Biochim. Biophys. Acta* **1592**, 35-39 (2002).
245. Lithgow,T. Targeting of proteins to mitochondria. *FEBS Lett.* **476**, 22-26 (2000).
246. Sylvestre,J., Margeot,A., Jacq,C., Dujardin,G., & Corral-Debrinski,M. The role of the 3' untranslated region in mRNA sorting to the vicinity of mitochondria is conserved from yeast to human cells. *Mol. Biol Cell* **14**, 3848-3856 (2003).
247. Izquierdo,J.M. & Cuezva,J.M. Control of the translational efficiency of beta-F1-ATPase mRNA depends on the regulation of a protein that binds the 3' untranslated region of the mRNA. *Mol Cell Biol* **17**, 5255-5268 (1997).

248. MacKenzie,J.A. & Payne,R.M. Ribosomes specifically bind to mammalian mitochondria via protease-sensitive proteins on the outer membrane. *J. Biol Chem.* **279**, 9803-9810 (2004).
249. Crowley,K.S. & Payne,R.M. Ribosome binding to mitochondria is regulated by GTP and the transit peptide. *J. Biol Chem.* **273**, 17278-17285 (1998).
250. Ellis,E.M. & Reid,G.A. The Saccharomyces cerevisiae MTS1 gene encodes a putative RNA-binding protein involved in mitochondrial protein targeting. *Gene* **132**, 175-183 (1993).
251. Gratzer,S., Beilharz,T., Beddoe,T., Henry,M.F., & Lithgow,T. The mitochondrial protein targeting suppressor (mts1) mutation maps to the mRNA-binding domain of Npl3p and affects translation on cytoplasmic polysomes. *Mol Microbiol.* **35**, 1277-1285 (2000).
252. Reed,R. & Hurt,E. A conserved mRNA export machinery coupled to pre-mRNA splicing. *Cell* **108**, 523-531 (2002).
253. Corral-Debrinski,M., Belgareh,N., Blugeon,C., Claros,M.G., Doye,V., & Jacq,C. Overexpression of yeast karyopherin Pse1p/Kap121p stimulates the mitochondrial import of hydrophobic proteins in vivo. *Mol Microbiol.* **31**, 1499-1511 (1999).
254. Gautschi,M., Lilie,H., Funfschilling,U., Mun,A., Ross,S., Lithgow,T., Rucknagel,P., & Rospert,S. RAC, a stable ribosome-associated complex in yeast formed by the DnaK-DnaJ homologs Ssz1p and zuotin. *Proc. Natl. Acad. Sci. U. S. A* **98**, 3762-3767 (2001).
255. Wiedmann,B., Sakai,H., Davis,T.A., & Wiedmann,M. A protein complex required for signal-sequence-specific sorting and translocation. *Nature* **370**, 434-440 (1994).
256. Beatrix,B., Sakai,H., & Wiedmann,M. The alpha and beta subunit of the nascent polypeptide-associated complex have distinct functions. *J. Biol Chem.* **275**, 37838-37845 (2000).
257. George,R., Walsh,P., Beddoe,T., & Lithgow,T. The nascent polypeptide-associated complex (NAC) promotes interaction of ribosomes with the mitochondrial surface in vivo. *FEBS Lett.* **516**, 213-216 (2002).
258. Deshaies,R.J., Koch,B.D., Werner-Washburne,M., Craig,E.A., & Schekman,R. A subfamily of stress proteins facilitates translocation of secretory and mitochondrial precursor polypeptides. *Nature* **332**, 800-805 (1988).
259. Terada,K., Ueda,I., Ohtsuka,K., Oda,T., Ichiyama,A., & Mori,M. The requirement of heat shock cognate 70 protein for mitochondrial import varies among precursor proteins and depends on precursor length. *Mol Cell Biol* **16**, 6103-6109 (1996).
260. Artigues,A., Iriarte,A., & Martinez-Carrion,M. Binding to chaperones allows import of a purified mitochondrial precursor into mitochondria. *J. Biol Chem.* (2002).
261. Yaffe,M.B. How do 14-3-3 proteins work?-- Gatekeeper phosphorylation and the molecular anvil hypothesis. *FEBS Lett.* **513**, 53-57 (2002).
262. Tzivion,G. & Avruch,J. 14-3-3 proteins: active cofactors in cellular regulation by serine/threonine phosphorylation. *J. Biol Chem.* **277**, 3061-3064 (2002).
263. Brunet,A., Kanai,F., Stehn,J., Xu,J., Sarbassova,D., Frangioni,J.V., Dalal,S.N., DeCaprio,J.A., Greenberg,M.E., & Yaffe,M.B. 14-3-3 transits to the nucleus and participates in dynamic nucleocytoplasmic transport. *J. Cell Biol* **156**, 817-828 (2002).
264. Komiya,T., Rospert,S., Schatz,G., & Mihara,K. Binding of mitochondrial precursor proteins to the cytoplasmic domains of the import receptors Tom70 and Tom20 is determined by cytoplasmic chaperones. *EMBO J.* **16**, 4267-4275 (1997).
265. Komiya,T., Sakaguchi,M., & Mihara,K. Cytoplasmic chaperones determine the targeting pathway of precursor proteins to mitochondria. *EMBO J.* **15**, 399-407 (1996).
266. Young,J.C., Hoogenraad,N.J., & Hartl,F.U. Molecular chaperones Hsp90 and Hsp70 deliver preproteins to the mitochondrial import receptor Tom70. *Cell* **112**, 41-50 (2003).
267. May,T. & Soll,J. 14-3-3 proteins form a guidance complex with chloroplast precursor proteins in plants. *Plant Cell* **12**, 53-64 (2000).
268. Yano,M., Terada,K., & Mori,M. AIP is a mitochondrial import mediator that binds to both import receptor Tom20 and preproteins. *J. Cell Biol* **163**, 45-56 (2003).
269. Hachiya,N., Mihara,K., Suda,K., Horst,M., Schatz,G., & Lithgow,T. Reconstitution of the initial steps of mitochondrial protein import. *Nature* **376**, 705-709 (1995).
270. Owens-Grillo,J.K., Czar,M.J., Hutchison,K.A., Hoffmann,K., Perdew,G.H., & Pratt,W.B. A model of protein targeting mediated by immunophilins and other proteins that bind to hsp90 via tetratricopeptide repeat domains. *J. Biol Chem.* **271**, 13468-13475 (1996).
271. Scheufler,C., Brinker,A., Bourenkov,G., Pegoraro,S., Moroder,L., Bartunik,H., Hartl,F.U., & Moarefi,I. Structure of TPR domain-peptide complexes: critical elements in the assembly of the Hsp70-Hsp90 multichaperone machine. *Cell* **101**, 199-210 (2000).
272. Yano,M., Terada,K., & Mori,M. Mitochondrial import receptors Tom20 and Tom22 have chaperone-like activity. *J. Biol Chem.* (2003).
273. Frydman,J. Folding of newly translated proteins in vivo: the role of molecular chaperones. *Annu. Rev. Biochem.* **70**, 603-647 (2001).
274. Young,J.C., Moarefi,I., & Hartl,F.U. Hsp90: a specialized but essential protein-folding tool. *J. Cell Biol* **154**, 267-273 (2001).

275. Becker,J., Walter,W., Yan,W., & Craig,E.A. Functional interaction of cytosolic hsp70 and a DnaJ-related protein, Ydj1p, in protein translocation in vivo. *Mol. Cell Biol.* **16**, 4378-4386 (1996).
276. Caplan,A.J., Cyr,D.M., & Douglas,M.G. YDJ1p facilitates polypeptide translocation across different intracellular membranes by a conserved mechanism. *Cell* **71**, 1143-1155 (1992).
277. Caplan,A.J., Tsai,J., Casey,P.J., & Douglas,M.G. Farnesylation of YDJ1p is required for function at elevated growth temperatures in Saccharomyces cerevisiae. *J. Biol Chem.* **267**, 18890-18895 (1992).
278. Terada,K. & Mori,M. Human DnaJ homologs dj2 and dj3, and bag-1 are positive cochaperones of hsc70. *J. Biol. Chem.* **275**, 24728-24734 (2000).
279. Gollub,E.G. & Dayan,J. Regulation by heme of the synthesis of cytochrome C oxidase subunits V and VII in yeast. *Biochem. Biophys. Res. Commun.* **128**, 1447-1454 (1985).
280. Reid,G.A. & Schatz,G. Import of proteins into mitochondria. Yeast cells grown in the presence of carbonyl cyanide m-chlorophenylhydrazone accumulate massive amounts of some mitochondrial precursor polypeptides. *J. Biol Chem.* **257**, 13056-13061 (1982).
281. Ugalde,C., Coenen,M.J.H., Farhoud,M.H., Gilinsky,S., Koopman,W.J.H., Van Den Heuvel,L.P., Smeitink,J.A.M., & Nijtmans,L.G.J. New perspectives on the assembly process of mitochondrial respiratory chain complex cytochrome c oxidase. *Mitochondrion* **2**, 117-128 (2002).
282. Thorsness,P.E., White,K.H., & Fox,T.D. Inactivation of YME1, a member of the ftsH-SEC18-PAS1-CDC48 family of putative ATPase-encoding genes, causes increased escape of DNA from mitochondria in Saccharomyces cerevisiae. *Mol. Cell Biol* **13**, 5418-5426 (1993).
283. Wickner,S., Maurizi,M.R., & Gottesman,S. Posttranslational quality control: folding, refolding, and degrading proteins. *Science* **286**, 1888-1893 (1999).
284. Hohfeld,J., Cyr,D.M., & Patterson,C. From the cradle to the grave: molecular chaperones that may choose between folding and degradation. *EMBO Rep.* **2**, 885-890 (2001).
285. Schubert,U., Anton,L.C., Gibbs,J., Norbury,C.C., Yewdell,J.W., & Bennink,J.R. Rapid degradation of a large fraction of newly synthesized proteins by proteasomes. *Nature* **404**, 770-774 (2000).
286. Rapaport,D. Biogenesis of the mitochondrial TOM complex. *Trends Biochem. Sci.* **27**, 191-197 (2002).
287. Endo,T., Yamamoto,H., & Esaki,M. Functional cooperation and separation of translocators in protein import into mitochondria, the double-membrane bounded organelles. *J. Cell Sci.* **116**, 3259-3267 (2003).
288. Truscott,K.N., Brandner,K., & Pfanner,N. Mechanisms of protein import into mitochondria. *Curr. Biol* **13**, R326-R337 (2003).
289. Pfanner,N. & Chacinska,A. The mitochondrial import machinery: preprotein-conducting channels with binding sites for presequences. *Biochim. Biophys. Acta* **1592**, 15-24 (2002).
290. Endo,T. & Kohda,D. Functions of outer membrane receptors in mitochondrial protein import. *Biochim. Biophys. Acta* **1592**, 3-14 (2002).
291. Abe,Y., Shodai,T., Muto,T., Mihara,K., Torii,H., Nishikawa,S., Endo,T., & Kohda,D. Structural basis of presequence recognition by the mitochondrial protein import receptor Tom20. *Cell* **100**, 551-560 (2000).
292. Model,K., Prinz,T., Ruiz,T., Radermacher,M., Krimmer,T., Kuhlbrandt,W., Pfanner,N., & Meisinger,C. Protein translocase of the outer mitochondrial membrane: role of import receptors in the structural organization of the TOM complex. *J. Mol Biol* **316**, 657-666 (2002).
293. Pfanner,N. & Geissler,A. Versatility of the mitochondrial protein import machinery. *Nat. Rev. Mol. Cell Biol.* **2**, 339-349 (2001).
294. Hoogenraad,N.J., Ward,L.A., & Ryan,M.T. Import and assembly of proteins into mitochondria of mammalian cells. *Biochim. Biophys. Acta* **1592**, 97-105 (2002).
295. Koehler,C.M. The small Tim proteins and the twin Cx3C motif. *Trends Biochem. Sci.* **29**, 1-4 (2004).
296. Vasiljev,A., Ahting,U., Nargang,F.E., Go,N.E., Habib,S.J., Kozany,C., Panneels,V., Sinning,I., Prokisch,H., Neupert,W., Nussberger,S., & Rapaport,D. Reconstituted TOM core complex and Tim9/Tim10 complex of mitochondria are sufficient for translocation of the ADP/ATP carrier across membranes. *Mol. Biol Cell* **15**, 1445-1458 (2004).
297. Muhlenbein,N., Hofmann,S., Rothbauer,U., & Bauer,M.F. Organization and function of the small Tim complexes acting along the import pathway of metabolite carriers into mammalian mitochondria. *J. Biol Chem.* **279**, 13540-13546 (2004).
298. Rehling,P., Model,K., Brandner,K., Kovermann,P., Sickmann,A., Meyer,H.E., Kuhlbrandt,W., Wagner,R., Truscott,K.N., & Pfanner,N. Protein insertion into the mitochondrial inner membrane by a twin-pore translocase. *Science* **299**, 1747-1751 (2003).
299. Kovermann,P., Truscott,K.N., Guiard,B., Rehling,P., Sepuri,N.B., Muller,H., Jensen,R.E., Wagner,R., & Pfanner,N. Tim22, the essential core of the mitochondrial protein insertion complex, forms a voltage-activated and signal-gated channel. *Mol Cell* **9**, 363-373 (2002).
300. Truscott,K.N., Kovermann,P., Geissler,A., Merlin,A., Meijer,M., Driessen,A.J., Rassow,J., Pfanner,N., & Wagner,R. A presequence- and voltage-sensitive channel of the mitochondrial preprotein translocase formed by Tim23. *Nat. Struct. Biol* **8**, 1074-1082 (2001).

301. Donzeau,M., Kaldi,K., Adam,A., Paschen,S., Wanner,G., Guiard,B., Bauer,M.F., Neupert,W., & Brunner,M. Tim23 links the inner and outer mitochondrial membranes. *Cell* **101**, 401-412 (2000).
302. Yamamoto,H., Esaki,M., Kanamori,T., Tamura,Y., Nishikawa,S., & Endo,T. Tim50 is a subunit of the TIM23 complex that links protein translocation across the outer and inner mitochondrial membranes. *Cell* **111**, 519-528 (2002).
303. Geissler,A., Chacinska,A., Truscott,K.N., Wiedemann,N., Brandner,K., Sickmann,A., Meyer,H.E., Meisinger,C., Pfanner,N., & Rehling,P. The mitochondrial presequence translocase: an essential role of Tim50 in directing preproteins to the import channel. *Cell* **111**, 507-518 (2002).
304. Rehling,P., Pfanner,N., & Meisinger,C. Insertion of hydrophobic membrane proteins into the inner mitochondrial membrane--a guided tour. *J: Mol. Biol* **326**, 639-657 (2003).
305. Hoogenraad,N.J. & Ryan,M.T. Translocation of proteins into mitochondria. *IUBMB. Life* **51**, 345-350 (2001).
306. Koehler,C.M. Protein translocation pathways of the mitochondrion. *FEBS Lett.* **476**, 27-31 (2000).
307. Paschen,S.A. & Neupert,W. Protein import into mitochondria. *IUBMB. Life* **52**, 101-112 (2001).
308. Pfanner,N. & Truscott,K.N. Powering mitochondrial protein import. *Nat. Struct. Biol* **9**, 234-236 (2002).
309. Huang,S., Ratliff,K.S., & Matouschek,A. Protein unfolding by the mitochondrial membrane potential. *Nat. Struct. Biol* **9**, 301-307 (2002).
310. Voisine,C., Craig,E.A., Zufall,N., Von Ahsen,O., Pfanner,N., & Voos,W. The protein import motor of mitochondria: unfolding and trapping of preproteins are distinct and separable functions of matrix Hsp70. *Cell* **97**, 565-574 (1999).
311. Liu,Q., D'Silva,P., Walter,W., Marszalek,J., & Craig,E.A. Regulated cycling of mitochondrial Hsp70 at the protein import channel. *Science* **300**, 139-141 (2003).
312. Okamoto,K., Brinker,A., Paschen,S.A., Moarefi,I., Hayer-Hartl,M., Neupert,W., & Brunner,M. The protein import motor of mitochondria: a targeted molecular ratchet driving unfolding and translocation. *EMBO J.* **21**, 3659-3671 (2002).
313. Horst,M., Oppliger,W., Feifel,B., Schatz,G., & Glick,B.S. The mitochondrial protein import motor: dissociation of mitochondrial hsp70 from its membrane anchor requires ATP binding rather than ATP hydrolysis. *Protein Sci.* **5**, 759-767 (1996).
314. Moro,F., Okamoto,K., Donzeau,M., Neupert,W., & Brunner,M. Mitochondrial protein import: molecular basis of the ATP-dependent interaction of MtHsp70 with Tim44. *J. Biol Chem.* **277**, 6874-6880 (2002).
315. D'Silva,P.D., Schilke,B., Walter,W., Andrew,A., & Craig,E.A. J protein cochaperone of the mitochondrial inner membrane required for protein import into the mitochondrial matrix. *Proc. Natl. Acad. Sci. U. S. A* **100**, 13839-13844 (2003).
316. Frazier,A.E., Dudek,J., Guiard,B., Voos,W., Li,Y., Lind,M., Meisinger,C., Geissler,A., Sickmann,A., Meyer,H.E., Bilanchone,V., Cumsky,M.G., Truscott,K.N., Pfanner,N., & Rehling,P. Pam16 has an essential role in the mitochondrial protein import motor. *Nat. Struct. Mol. Biol* **11**, 226-233 (2004).
317. Horst,M., Oppliger,W., Rospert,S., Schonfeld,H.J., Schatz,G., & Azem,A. Sequential action of two hsp70 complexes during protein import into mitochondria. *EMBO J.* **16**, 1842-1849 (1997).
318. Ishihara,N. & Mihara,K. Identification of the protein import components of the rat mitochondrial inner membrane, rTIM17, rTIM23, and rTIM44. *J. Biochem. (Tokyo)* **123**, 722-732 (1998).
319. Lim,J.H., Martin,F., Guiard,B., Pfanner,N., & Voos,W. The mitochondrial Hsp70-dependent import system actively unfolds preproteins and shortens the lag phase of translocation. *EMBO J.* **20**, 941-950 (2001).
320. Gakh,O., Cavadini,P., & Isaya,G. Mitochondrial processing peptidases. *Biochim. Biophys. Acta* **1592**, 63-77 (2002).
321. Petek,E., Windpassinger,C., Vincent,J.B., Cheung,J., Boright,A.P., Scherer,S.W., Kroisel,P.M., & Wagner,K. Disruption of a novel gene (IMMP2L) by a breakpoint in 7q31 associated with Tourette syndrome. *Am. J. Hum. Genet.* **68**, 848-858 (2001).
322. Stuart,R.A. Insertion of proteins into the inner membrane of mitochondria: the role of the Oxa1 complex. *Biochim. Biophys. Acta* **1592**, 79-87 (2002).
323. Folsch,H., Guiard,B., Neupert,W., & Stuart,R.A. Internal targeting signal of the BCS1 protein: a novel mechanism of import into mitochondria. *EMBO J.* **15**, 479-487 (1996).
324. Folsch,H., Gaume,B., Brunner,M., Neupert,W., & Stuart,R.A. C- to N-terminal translocation of preproteins into mitochondria. *EMBO J.* **17**, 6508-6515 (1998).
325. Herrmann,J.M. & Neupert,W. Protein insertion into the inner membrane of mitochondria. *IUBMB Life* **55**, 219-225 (2003).
326. Nargang,F.E., Preuss,M., Neupert,W., & Herrmann,J.M. The Oxa1 protein forms a homooligomeric complex and is an essential part of the mitochondrial export translocase in Neurospora crassa. *J. Biol Chem.* **277**, 12846-12853 (2002).

327. Preuss,M., Leonhard,K., Hell,K., Stuart,R.A., Neupert,W., & Herrmann,J.M. Mba1, a novel component of the mitochondrial protein export machinery of the yeast Saccharomyces cerevisiae. *J. Cell Biol* **153**, 1085-1096 (2001).
328. Szyrach,G., Ott,M., Bonnefoy,N., Neupert,W., & Herrmann,J.M. Ribosome binding to the Oxa1 complex facilitates co-translational protein insertion in mitochondria. *EMBO J.* **22**, 6448-6457 (2003).
329. Hell,K., Herrmann,J.M., Pratje,E., Neupert,W., & Stuart,R.A. Oxa1p, an essential component of the N-tail protein export machinery in mitochondria. *Proc. Natl. Acad. Sci. U. S. A* **95**, 2250-2255 (1998).
330. Hell,K., Neupert,W., & Stuart,R.A. Oxa1p acts as a general membrane insertion machinery for proteins encoded by mitochondrial DNA. *EMBO J.* **20**, 1281-1288 (2001).
331. He,S. & Fox,T.D. Membrane translocation of mitochondrially coded Cox2p: distinct requirements for export of N and C termini and dependence on the conserved protein Oxa1p. *Mol. Biol Cell* **8**, 1449-1460 (1997).
332. Saracco,S.A. & Fox,T.D. Cox18p Is Required for Export of the Mitochondrially Encoded Saccharomyces cerevisiae Cox2p C-Tail and Interacts with Pnt1p and Mss2p in the Inner Membrane. *Mol Biol Cell* **13**, 1122-1131 (2002).
333. Baumann,F., Neupert,W., & Herrmann,J.M. Insertion of bitopic membrane proteins into the inner membrane of mitochondria involves an export step from the matrix. *J. Biol Chem.* **277**, 21405-21413 (2002).
334. Meyer,W., Bomer,U., & Pratje,E. Mitochondrial inner membrane bound Pet1402 protein is rapidly imported into mitochondria and affects the integrity of the cytochrome oxidase and ubiquinol-cytochrome c oxidoreductase complexes. *Biol Chem.* **378**, 1373-1379 (1997).
335. Bonnefoy,N., Kermorgant,M., Groudinsky,O., Minet,M., Slonimski,P.P., & Dujardin,G. Cloning of a human gene involved in cytochrome oxidase assembly by functional complementation of an oxa1- mutation in Saccharomyces cerevisiae. *Proc. Natl. Acad. Sci. U. S. A* **91**, 11978-11982 (1994).
336. Dalbey,R.E. & Kuhn,A. Evolutionarily related insertion pathways of bacterial, mitochondrial, and thylakoid membrane proteins. *Annu. Rev. Cell Dev. Biol* **16**, 51-87 (2000).
337. Luirink,J., Samuelsson,T., & de Gier,J.W. YidC/Oxa1p/Alb3: evolutionarily conserved mediators of membrane protein assembly. *FEBS Lett.* **501**, 1-5 (2001).
338. Yen,M.R., Harley,K.T., Tseng,Y.H., & Saier,M.H., Jr. Phylogenetic and structural analyses of the oxa1 family of protein translocases. *FEMS Microbiol. Lett.* **204**, 223-231 (2001).
339. Jia,L., Dienhart,M., Schramp,M., McCauley,M., Hell,K., & Stuart,R.A. Yeast Oxa1 interacts with mitochondrial ribosomes: the importance of the C-terminal region of Oxa1. *EMBO J.* **22**, 6438-6447 (2003).
340. Funes,S., Nargang,F.E., Neupert,W., & Herrmann,J.M. The Oxa2 protein of Neurospora crassa plays a critical role in the biogenesis of cytochrome oxidase and defines a ubiquitous subbranch of the Oxa1/YidC/Alb3 protein family. *Mol. Biol Cell* **15**, 1853-1861 (2004).
341. Rotig,A., Parfait,B., Heidet,L., Dujardin,G., Rustin,P., & Munnich,A. Sequence and structure of the human OXA1L gene and its upstream elements. *Biochim. Biophys. Acta* **1361**, 6-10 (1997).
342. Rep,M. & Grivell,L.A. MBA1 encodes a mitochondrial membrane-associated protein required for biogenesis of the respiratory chain. *FEBS Lett.* **388**, 185-188 (1996).
343. Young,J.C., Barral,J.M., & Ulrich,H.F. More than folding: localized functions of cytosolic chaperones. *Trends Biochem. Sci.* **28**, 541-547 (2003).
344. Laloraya,S., Dekker,P.J., Voos,W., Craig,E.A., & Pfanner,N. Mitochondrial GrpE modulates the function of matrix Hsp70 in translocation and maturation of preproteins. *Mol. Cell Biol* **15**, 7098-7105 (1995).
345. Liu,Q., Krzewska,J., Liberek,K., & Craig,E.A. Mitochondrial Hsp70 Ssc1: role in protein folding. *J. Biol. Chem.* **276**, 6112-6118 (2001).
346. Voisine,C., Schilke,B., Ohlson,M., Beinert,H., Marszalek,J., & Craig,E.A. Role of the mitochondrial Hsp70s, Ssc1 and Ssq1, in the maturation of Yfh1. *Mol. Cell Biol.* **20**, 3677-3684 (2000).
347. Craig,E.A. & Marszalek,J. A specialized mitochondrial molecular chaperone system: a role in formation of Fe/S centers. *Cell Mol. Life Sci.* **59**, 1658-1665 (2002).
348. Voos,W. & Rottgers,K. Molecular chaperones as essential mediators of mitochondrial biogenesis. *Biochim. Biophys. Acta* **1592**, 51-62 (2002).
349. Wadhwa,R., Taira,K., & Kaul,S.C. An Hsp70 family chaperone, mortalin/mthsp70/PBP74/Grp75: what, when, and where? *Cell Stress. Chaperones.* **7**, 309-316 (2002).
350. Singh,B., Soltys,B.J., Wu,Z.C., Patel,H.V., Freeman,K.B., & Gupta,R.S. Cloning and some novel characteristics of mitochondrial Hsp70 from Chinese hamster cells. *Exp. Cell Res.* **234**, 205-216 (1997).
351. Ran,Q., Wadhwa,R., Kawai,R., Kaul,S.C., Sifers,R.N., Bick,R.J., Smith,J.R., & Pereira-Smith,O.M. Extramitochondrial localization of mortalin/mthsp70/PBP74/GRP75. *Biochem. Biophys. Res. Commun.* **275**, 174-179 (2000).

352. Syken,J., De Medina,T., & Munger,K. TID1, a human homolog of the Drosophila tumor suppressor l(2)tid, encodes two mitochondrial modulators of apoptosis with opposing functions. *Proc. Natl. Acad. Sci. U. S. A* **96**, 8499-8504 (1999).
353. Terada,K., Kanazawa,M., Bukau,B., & Mori,M. The human DnaJ homologue dj2 facilitates mitochondrial protein import and luciferase refolding. *J. Cell Biol.* **139**, 1089-1095 (1997).
354. Hanai,R. & Mashima,K. Characterization of two isoforms of a human DnaJ homologue, HSJ2. *Mol. Biol Rep.* **30**, 149-153 (2003).
355. Sarkar,S., Pollack,B.P., Lin,K.T., Kotenko,S.V., Cook,J.R., Lewis,A., & Pestka,S. hTid-1, a human DnaJ protein, modulates the interferon signaling pathway. *J. Biol Chem.* **276**, 49034-49042 (2001).
356. Choglay,A.A., Chapple,J.P., Blatch,G.L., & Cheetham,M.E. Identification and characterization of a human mitochondrial homologue of the bacterial co-chaperone GrpE. *Gene* **267**, 125-134 (2001).
357. Naylor,D.J., Stines,A.P., Hoogenraad,N.J., & Hoj,P.B. Evidence for the existence of distinct mammalian cytosolic, microsomal, and two mitochondrial GrpE-like proteins, the Co-chaperones of specific Hsp70 members. *J. Biol Chem.* **273**, 21169-21177 (1998).
358. Da Cruz,S., Xenarios,I., Langridge,J., Vilbois,F., Parone,P.A., & Martinou,J.C. Proteomic analysis of the mouse liver mitochondrial inner membrane. *J. Biol Chem.* **278**, 41566-41571 (2003).
359. Schonfeld,H.J., Schmidt,D., Schroder,H., & Bukau,B. The DnaK chaperone system of Escherichia coli: quaternary structures and interactions of the DnaK and GrpE components. *J. Biol. Chem.* **270**, 2183-2189 (1995).
360. Borges,J.C., Fischer,H., Craievich,A.F., Hansen,L.D., & Ramos,C.H.I. Free human mitochondrial GrpE is a symmetric dimer in solution. *Journal of Biological Chemistry* **278**, 35337-35344 (2003).
361. Richardson,A., Landry,S.J., & Georgopoulos,C. The ins and outs of a molecular chaperone machine. *Trends Biochem. Sci.* **23**, 138-143 (1998).
362. Hartl,F.U. & Hayer-Hartl,M. Molecular chaperones in the cytosol: from nascent chain to folded protein. *Science* **295**, 1852-1858 (2002).
363. Brinker,A., Pfeifer,G., Kerner,M.J., Naylor,D.J., Hartl,F.U., & Hayer-Hartl,M. Dual function of protein confinement in chaperonin-assisted protein folding. *Cell* **107**, 223-233 (2001).
364. Heyrovska,N., Frydman,J., Hohfeld,J., & Hartl,F.U. Directionality of polypeptide transfer in the mitochondrial pathway of chaperone-mediated protein folding. *Biol Chem.* **379**, 301-309 (1998).
365. Manning-Krieg,U.C., Scherer,P.E., & Schatz,G. Sequential action of mitochondrial chaperones in protein import into the matrix. *EMBO J.* **10**, 3273-3280 (1991).
366. Rospert,S., Looser,R., Dubaquie,Y., Matouschek,A., Glick,B.S., & Schatz,G. Hsp60-independent protein folding in the matrix of yeast mitochondria. *EMBO J.* **15**, 764-774 (1996).
367. Dubaquie,Y., Looser,R., Funfschilling,U., Jeno,P., & Rospert,S. Identification of in vivo substrates of the yeast mitochondrial chaperonins reveals overlapping but non-identical requirement for hsp60 and hsp10. *EMBO J.* **17**, 5868-5876 (1998).
368. Cabiscol,E., Belli,G., Tamarit,J., Echave,P., Herrero,E., & Ros,J. Mitochondrial Hsp60, resistance to oxidative stress, and the labile iron pool are closely connected in Saccharomyces cerevisiae. *J. Biol Chem.* **277**, 44531-44538 (2002).
369. Chandra,D. & Tang,D.G. Mitochondrially localized active caspase-9 and caspase-3 result mostly from translocation from the cytosol and partly from caspase-mediated activation in the organelle. Lack of evidence for Apaf-1-mediated procaspase-9 activation in the mitochondria. *J. Biol Chem.* **278**, 17408-17420 (2003).
370. Samali,A., Cai,J., Zhivotovsky,B., Jones,D.P., & Orrenius,S. Presence of a pre-apoptotic complex of pro-caspase-3, Hsp60 and Hsp10 in the mitochondrial fraction of jurkat cells. *EMBO J.* **18**, 2040-2048 (1999).
371. Xanthoudakis,S., Roy,S., Rasper,D., Hennessey,T., Aubin,Y., Cassady,R., Tawa,P., Ruel,R., Rosen,A., & Nicholson,D.W. Hsp60 accelerates the maturation of pro-caspase-3 by upstream activator proteases during apoptosis. *EMBO J.* **18**, 2049-2056 (1999).
372. Gupta,S. & Knowlton,A.A. Cytosolic heat shock protein 60, hypoxia, and apoptosis. *Circulation* **106**, 2727-2733 (2002).
373. Soltys,B.J. & Gupta,R.S. Immunoelectron microscopic localization of the 60-kDa heat shock chaperonin protein (Hsp60) in mammalian cells. *Exp. Cell Res.* **222**, 16-27 (1996).
374. Hansen,J.J., Bross,P., Westergaard,M., Nielsen,M.N., Eiberg,H., Borglum,A.D., Mogensen,J., Kristiansen,K., Bolund,L., & Gregersen,N. Genomic structure of the human mitochondrial chaperonin genes: HSP60 and HSP10 are localised head to head on chromosome 2 separated by a bidirectional promoter. *Hum. Genet.* **112**, 71-77 (2003).
375. Steglich,G., Neupert,W., & Langer,T. Prohibitins regulate membrane protein degradation by the m-AAA protease in mitochondria. *Mol. Cell Biol.* **19**, 3435-3442 (1999).
376. Nijtmans,L.G., de Jong,L., Artal Sanz,M., Coates,P.J., Berden,J.A., Back,J.W., Muijsers,A.O., van der,S.H., & Grivell,L.A. Prohibitins act as a membrane-bound chaperone for the stabilization of mitochondrial proteins. *EMBO J.* **19**, 2444-2451 (2000).

377. Nijtmans,L.G., Artal Sanz,M., Grivell,L.A., & Coates,P.J. The mitochondrial PHB complex: roles in mitochondrial respiratory complex assembly, ageing and degenerative disease. *Cell Mol Life Sci.* **59**, 143-155 (2002).
378. Berger,K.H. & Yaffe,M.P. Prohibitin family members interact genetically with mitochondrial inheritance components in Saccharomyces cerevisiae. *Mol. Cell Biol.* **18**, 4043-4052 (1998).
379. Ikonen,E., Fiedler,K., Parton,R.G., & Simons,K. Prohibitin, an antiproliferative protein, is localized to mitochondria. *FEBS Lett.* **358**, 273-277 (1995).
380. Back,J.W., Artal Sanz,M., de Jong,L., De Koning,L.J., Nijtmans,L.G., De Koster,C.G., Grivell,L.A., van der,S.H., & Muijsers,A.O. A structure for the yeast prohibitin complex: Structure prediction and evidence from chemical crosslinking and mass spectrometry. *Protein Sci.* **11**, 2471-2478 (2002).
381. Nijtmans,L.G., Artal Sanz,M., Bucko,M., Farhoud,M.H., Feenstra,M., Hakkaart,G.A., Zeviani,M., & Grivell,L.A. Shy1p occurs in a high molecular weight complex and is required for efficient assembly of cytochrome c oxidase in yeast. *FEBS Lett.* **498**, 46-51 (2001).
382. Bourges,I., Ramus,C., Mousson,D.C., Beugnot,R., Remacle,C., Cardol,P., Hofhaus,G., & Issartel,J.P. Structural organization of mitochondrial human complex I: role of the ND4 and ND5 mitochondria-encoded subunits and interaction with the prohibitin. *Biochem. J.* **Pt**, (2004).
383. Matouschek,A., Rospert,S., Schmid,K., Glick,B.S., & Schatz,G. Cyclophilin catalyzes protein folding in yeast mitochondria. *Proc. Natl. Acad. Sci. U. S. A* **92**, 6319-6323 (1995).
384. Von Ahsen,O., Tropschug,M., Pfanner,N., & Rassow,J. The chaperonin cycle cannot substitute for prolyl isomerase activity, but GroEL alone promotes productive folding of a cyclophilin-sensitive substrate to a cyclophilin-resistant form. *EMBO J.* **16**, 4568-4578 (1997).
385. Rassow,J., Mohrs,K., Koidl,S., Barthelmess,I.B., Pfanner,N., & Tropschug,M. Cyclophilin 20 is involved in mitochondrial protein folding in cooperation with molecular chaperones Hsp70 and Hsp60. *Mol. Cell Biol.* **15**, 2654-2662 (1995).
386. Crompton,M. On the involvement of mitochondrial intermembrane junctional complexes in apoptosis. *Curr. Med. Chem.* **10**, 1473-1484 (2003).
387. Felts,S.J., Owen,B.A., Nguyen,P., Trepel,J., Donner,D.B., & Toft,D.O. The hsp90-related protein TRAP1 is a mitochondrial protein with distinct functional properties. *J. Biol Chem.* **275**, 3305-3312 (2000).
388. Cechetto,J.D. & Gupta,R.S. Immunoelectron microscopy provides evidence that tumor necrosis factor receptor-associated protein 1 (TRAP-1) is a mitochondrial protein which also localizes at specific extramitochondrial sites. *Exp. Cell Res.* **260**, 30-39 (2000).
389. Wurthner,J.U., Frank,D.B., Felici,A., Green,H.M., Cao,Z., Schneider,M.D., McNally,J.G., Lechleider,R.J., & Roberts,A.B. Transforming growth factor-beta receptor-associated protein 1 is a Smad4 chaperone. *J. Biol Chem.* **276**, 19495-19502 (2001).
390. Owen,B.A., Sullivan,W.P., Felts,S.J., & Toft,D.O. Regulation of heat shock protein 90 ATPase activity by sequences in the carboxyl terminus. *J. Biol Chem.* **277**, 7086-7091 (2002).
391. Confalonieri,F. & Duguet,M. A 200-amino acid ATPase module in search of a basic function. *Bioessays* **17**, 639-650 (1995).
392. Neuwald,A.F., Aravind,L., Spouge,J.L., & Koonin,E.V. AAA+: A class of chaperone-like ATPases associated with the assembly, operation, and disassembly of protein complexes. *Genome Res.* **9**, 27-43 (1999).
393. Leonhard,K., Herrmann,J.M., Stuart,R.A., Mannhaupt,G., Neupert,W., & Langer,T. AAA proteases with catalytic sites on opposite membrane surfaces comprise a proteolytic system for the ATP-dependent degradation of inner membrane proteins in mitochondria. *EMBO J.* **15**, 4218-4229 (1996).
394. Arnold,I. & Langer,T. Membrane protein degradation by AAA proteases in mitochondria. *Biochim. Biophys. Acta* **1592**, 89-96 (2002).
395. Langer,T., Kaser,M., Klanner,C., & Leonhard,K. AAA proteases of mitochondria: quality control of membrane proteins and regulatory functions during mitochondrial biogenesis. *Biochem. Soc. Trans.* **29**, 431-436 (2001).
396. Leonhard,K., Guiard,B., Pellecchia,G., Tzagoloff,A., Neupert,W., & Langer,T. Membrane protein degradation by AAA proteases in mitochondria: Extraction of substrates from either membrane surface. *Molecular Cell* **5**, 629-638 (2000).
397. Guelin,E., Rep,M., & Grivell,L.A. Afg3p, a mitochondrial ATP-dependent metalloprotease, is involved in degradation of mitochondrially-encoded Cox1, Cox3, Cob, Su6, Su8 and Su9 subunits of the inner membrane complexes III, IV and V. *Febs Letters* **381**, 42-46 (1996).
398. Pearce,D.A. & Sherman,F. Degradation of cytochrome oxidase subunits in mutants of yeast lacking cytochrome c and suppression of the degradation by mutation of yme1. *J. Biol Chem.* **270**, 20879-20882 (1995).
399. Pellegrini,L., Passer,B.J., Canelles,M., Lefterov,I., Ganjei,J.K., Fowlkes,B.J., Koonin,E.V., & D'Adamio,L. PAMP and PARL, two novel putative metalloproteases interacting with the COOH-terminus of Presenilin-1 and -2. *J. Alzheimers. Dis.* **3**, 181-190 (2001).

400. Esser,K., Tursun,B., Ingenhoven,M., Michaelis,G., & Pratje,E. A novel two-step mechanism for removal of a mitochondrial signal sequence involves the mAAA complex and the putative rhomboid protease Pcp1. *J. Mol. Biol* **323**, 835-843 (2002).
401. Arlt,H., Tauer,R., Feldmann,H., Neupert,W., & Langer,T. The YTA10-12 complex, an AAA protease with chaperone-like activity in the inner membrane of mitochondria. *Cell* **85**, 875-885 (1996).
402. Nakai,T., Yasuhara,T., Fujiki,Y., & Ohashi,A. Multiple genes, including a member of the AAA family, are essential for degradation of unassembled subunit 2 of cytochrome c oxidase in yeast mitochondria. *Mol. Cell Biol.* **15**, 4441-4452 (1995).
403. Shotland,Y., Koby,S., Teff,D., Mansur,N., Oren,D.A., Tatematsu,K., Tomoyasu,T., Kessel,M., Bukau,B., Ogura,T., & Oppenheim,A.B. Proteolysis of the phage lambda CII regulatory protein by FtsH (HflB) of Escherichia coli. *Mol. Microbiol.* **24**, 1303-1310 (1997).
404. Krzywda,S., Brzozowski,A.M., Verma,C., Karata,K., Ogura,T., & Wilkinson,A.J. The crystal structure of the AAA domain of the ATP-dependent protease FtsH of Escherichia coli at 1.5 A resolution. *Structure (Camb.)* **10**, 1073-1083 (2002).
405. Karata,K., Inagawa,T., Wilkinson,A.J., Tatsuta,T., & Ogura,T. Dissecting the role of a conserved motif (the second region of homology) in the AAA family of ATPases. Site-directed mutagenesis of the ATP-dependent protease FtsH. *J. Biol Chem.* **274**, 26225-26232 (1999).
406. Korbel,D., Wurth,S., Kaser,M., & Langer,T. Membrane protein turnover by the m-AAA protease in mitochondria depends on the transmembrane domains of its subunits. *EMBO Rep.* **5**, 698-703 (2004).
407. Rep,M., van Dijl,J.M., Suda,K., Schatz,G., Grivell,L.A., & Suzuki,C.K. Promotion of mitochondrial membrane complex assembly by a proteolytically inactive yeast Lon. *Science* **274**, 103-106 (1996).
408. Savel'ev,A.S., Novikova,L.A., Kovaleva,I.E., Luzikov,V.N., Neupert,W., & Langer,T. ATP-dependent proteolysis in mitochondria - m-AAA protease and PIM1 protease exert overlapping substrate specificities and cooperate with the mtHsp70 system. *Journal of Biological Chemistry* **273**, 20596-20602 (1998).
409. Kaser,M., Kambacheld,M., Kisters-Woike,B., & Langer,T. Oma1, a novel membrane-bound metallopeptidase in mitochondria with activities overlapping with the m-AAA protease. *J. Biol Chem.* **278**, 46414-46423 (2003).
410. Leonhard,K., Stiegler,A., Neupert,W., & Langer,T. Chaperone-like activity of the AAA domain of the yeast Yme1 AAA protease. *Nature* **398**, 348-351 (1999).
411. Paul,M.F. & Tzagoloff,A. Mutations in RCA1 and AFG3 inhibit F1-ATPase assembly in Saccharomyces cerevisiae. *FEBS Lett.* **373**, 66-70 (1995).
412. Tzagoloff,A., Yue,J., Jang,J., & Paul,M.F. A new member of a family of ATPases is essential for assembly of mitochondrial respiratory chain and ATP synthetase complexes in Saccharomyces cerevisiae. *J. Biol. Chem.* **269**, 26144-26151 (1994).
413. Arlt,H., Steglich,G., Perryman,R., Guiard,B., Neupert,W., & Langer,T. The formation of respiratory chain complexes in mitochondria is under the proteolytic control of the m-AAA protease. *EMBO J.* **17**, 4837-4847 (1998).
414. Campbell,C.L., Tanaka,N., White,K.H., & Thorsness,P.E. Mitochondrial morphological and functional defects in yeast caused by yme1 are suppressed by mutation of a 26S protease subunit homologue. *Mol. Biol Cell* **5**, 899-905 (1994).
415. Campbell,C.L. & Thorsness,P.E. Escape of mitochondrial DNA to the nucleus in yme1 yeast is mediated by vacuolar-dependent turnover of abnormal mitochondrial compartments. *J. Cell Sci.* **111 (Pt 16)**, 2455-2464 (1998).
416. Nakai,T., Mera,Y., Yasuhara,T., & Ohashi,A. Divalent metal ion-dependent mitochondrial degradation of unassembled subunits 2 and 3 of cytochrome c oxidase. *J. Biochem. (Tokyo)* **116**, 752-758 (1994).
417. Barrientos,A., Pierre,D., Lee,J., & Tzagoloff,A. Cytochrome oxidase assembly does not require catalytically active cytochrome c. *J. Biol. Chem.* (2003).
418. Lemaire,C., Hamel,P., Velours,J., & Dujardin,G. Absence of the mitochondrial AAA protease Yme1p restores F0-ATPase subunit accumulation in an oxa1 deletion mutant of Saccharomyces cerevisiae. *J. Biol. Chem.* **275**, 23471-23475 (2000).
419. Shah,Z.H., Hakkaart,G.A.J., Arku,B., de Jong,L., van der Spek,H., Grivell,L.A., & Jacobs,H.T. The human homologue of the yeast mitochondrial AAA metalloprotease Yme1p complements a yeast yme1 disruptant. *Febs Letters* **478**, 267-270 (2000).
420. Klanner,C., Prokisch,H., & Langer,T. MAP-1 and IAP-1, two novel AAA proteases with catalytic sites on opposite membrane surfaces in mitochondrial inner membrane of Neurospora crassa. *Mol. Biol Cell* **12**, 2858-2869 (2001).
421. Kolodziejczak,M., Kolaczkowska,A., Szczesny,B., Urantowka,A., Knorpp,C., Kieleczawa,J., & Janska,H. A higher plant mitochondrial homologue of the yeast m-AAA protease. Molecular cloning, localization, and putative function. *J. Biol Chem.* **277**, 43792-43798 (2002).

422. Banfi,S., Bassi,M.T., Andolfi,G., Marchitiello,A., Zanotta,S., Ballabio,A., Casari,G., & Franco,B. Identification and characterization of AFG3L2, a novel paraplegin-related gene. *Genomics* **59**, 51-58 (1999).
423. Casari,G., De Fusco,M., Ciarmatori,S., Zeviani,M., Mora,M., Fernandez,P., De Michele,G., Filla,A., Cocozza,S., Marconi,R., Durr,A., Fontaine,B., & Ballabio,A. Spastic paraplegia and OXPHOS impairment caused by mutations in paraplegin, a nuclear-encoded mitochondrial metalloprotease. *Cell* **93**, 973-983 (1998).
424. Atorino,L., Silvestri,L., Koppen,M., Cassina,L., Ballabio,A., Marconi,R., Langer,T., & Casari,G. Loss of m-AAA protease in mitochondria causes complex I deficiency and increased sensitivity to oxidative stress in hereditary spastic paraplegia. *J. Cell Biol* **163**, 777-787 (2003).
425. Settasatian,C., Whitmore,S.A., Crawford,J., Bilton,R.L., Cleton-Jansen,A.M., Sutherland,G.R., & Callen,D.F. Genomic structure and expression analysis of the spastic paraplegia gene, SPG7. *Hum. Genet.* **105**, 139-144 (1999).
426. Kremmidiotis,G., Gardner,A.E., Settasatian,C., Savoia,A., Sutherland,G.R., & Callen,D.F. Molecular and functional analyses of the human and mouse genes encoding AFG3L1, a mitochondrial metalloprotease homologous to the human spastic paraplegia protein. *Genomics* **76**, 58-65 (2001).
427. Coppola,M., Pizzigoni,A., Banfi,S., Bassi,M.T., Casari,G., & Incerti,B. Identification and characterization of YME1L1, a novel paraplegin-related gene. *Genomics* **66**, 48-54 (2000).
428. Ferreirinha,F., Quattrini,A., Pirozzi,M., Valsecchi,V., Dina,G., Broccoli,V., Auricchio,A., Piemonte,F., Tozzi,G., Gaeta,L., Casari,G., Ballabio,A., & Rugarli,E.I. Axonal degeneration in paraplegin-deficient mice is associated with abnormal mitochondria and impairment of axonal transport. *J. Clin. Invest* **113**, 231-242 (2004).
429. van Dyck,L., Pearce,D.A., & Sherman,F. PIM1 encodes a mitochondrial ATP-dependent protease that is required for mitochondrial function in the yeast Saccharomyces cerevisiae. *J. Biol Chem.* **269**, 238-242 (1994).
430. Stahlberg,H., Kutejova,E., Suda,K., Wolpensinger,B., Lustig,A., Schatz,G., Engel,A., & Suzuki,C.K. Mitochondrial Lon of Saccharomyces cerevisiae is a ring-shaped protease with seven flexible subunits. *Proc. Natl. Acad. Sci. U. S. A* **96**, 6787-6790 (1999).
431. Wagner,I., van Dyck,L., Savel'ev,A.S., Neupert,W., & Langer,T. Autocatalytic processing of the ATP-dependent PIM1 protease: crucial function of a pro-region for sorting to mitochondria. *EMBO J.* **16**, 7317-7325 (1997).
432. van Dijl,J.M., Kutejova,E., Suda,K., Perecko,D., Schatz,G., & Suzuki,C.K. The ATPase and protease domains of yeast mitochondrial Lon: roles in proteolysis and respiration-dependent growth. *Proc. Natl. Acad. Sci. U. S. A* **95**, 10584-10589 (1998).
433. van Dyck,L., Neupert,W., & Langer,T. The ATP-dependent PIM1 protease is required for the expression of intron-containing genes in mitochondria. *Genes Dev.* **12**, 1515-1524 (1998).
434. Lu,B., Liu,T., Crosby,J.A., Thomas-Wohlever,J., Lee,I., & Suzuki,C.K. The ATP-dependent Lon protease of Mus musculus is a DNA-binding protein that is functionally conserved between yeast and mammals. *Gene* **306**, 45-55 (2003).
435. Wagner,I., Arlt,H., van Dyck,L., Langer,T., & Neupert,W. Molecular chaperones cooperate with PIM1 protease in the degradation of misfolded proteins in mitochondria. *EMBO J.* **13**, 5135-5145 (1994).
436. Bota,D.A. & Davies,K.J. Lon protease preferentially degrades oxidized mitochondrial aconitase by an ATP-stimulated mechanism. *Nat. Cell Biol* **4**, 674-680 (2002).
437. Hori,O., Ichinoda,F., Tamatani,T., Yamaguchi,A., Sato,N., Ozawa,K., Kitao,Y., Miyazaki,M., Harding,H.P., Ron,D., Tohyama,M., Stern,M., & Ogawa,S. Transmission of cell stress from endoplasmic reticulum to mitochondria: enhanced expression of Lon protease. *J. Cell Biol* **157**, 1151-1160 (2002).
438. Fu,G.K. & Markovitz,D.M. The human LON protease binds to mitochondrial promoters in a single-stranded, site-specific, strand-specific manner. *Biochemistry* **37**, 1905-1909 (1998).
439. Luciakova,K., Sokolikova,B., Chloupkova,M., & Nelson,B.D. Enhanced mitochondrial biogenesis is associated with increased expression of the mitochondrial ATP-dependent Lon protease. *FEBS Lett.* **444**, 186-188 (1999).
440. de Sagarra,M.R., Mayo,I., Marco,S., Rodriguez-Vilarino,S., Oliva,J., Carrascosa,J.L., & Casta n JG Mitochondrial localization and oligomeric structure of HClpP, the human homologue of E. coli ClpP. *J. Mol. Biol* **292**, 819-825 (1999).
441. Santagata,S., Bhattacharyya,D., Wang,F.H., Singha,N., Hodtsev,A., & Spanopoulou,E. Molecular cloning and characterization of a mouse homolog of bacterial ClpX, a novel mammalian class II member of the Hsp100/Clp chaperone family. *J. Biol. Chem.* **274**, 16311-16319 (1999).
442. Bross,P., Andresen,B.S., Knudsen,I., Kruse,T.A., & Gregersen,N. Human ClpP protease: cDNA sequence, tissue-specific expression and chromosomal assignment of the gene. *FEBS Lett.* **377**, 249-252 (1995).

443. Corydon,T.J., Bross,P., Holst,H.U., Neve,S., Kristiansen,K., Gregersen,N., & Bolund,L. A human homologue of Escherichia coli ClpP caseinolytic protease: recombinant expression, intracellular processing and subcellular localization. *Biochem. J.* **331 (Pt 1)**, 309-316 (1998).
444. Corydon,T.J., Wilsbech,M., Jespersgaard,C., Andresen,B.S., Borglum,A.D., Pedersen,S., Bolund,L., Gregersen,N., & Bross,P. Human and mouse mitochondrial orthologs of bacterial ClpX. *Mamm. Genome* **11**, 899-905 (2000).
445. Kang,S.G., Ortega,J., Singh,S.K., Wang,N., Huang,N.N., Steven,A.C., & Maurizi,M.R. Functional proteolytic complexes of the human mitochondrial ATP-dependent protease, hClpXP. *J. Biol Chem.* **277**, 21095-21102 (2002).
446. Majeran,W., Wollman,F.A., & Vallon,O. Evidence for a role of ClpP in the degradation of the chloroplast cytochrome b(6)f complex. *Plant Cell* **12**, 137-150 (2000).
447. Damerau,K. & St John,A.C. Role of Clp protease subunits in degradation of carbon starvation proteins in Escherichia coli. *J. Bacteriol.* **175**, 53-63 (1993).
448. Jarosch,E., Geiss-Friedlander,R., Meusser,B., Walter,J., & Sommer,T. Protein dislocation from the endoplasmic reticulum--pulling out the suspect. *Traffic.* **3**, 530-536 (2002).
449. Mayer,T.U., Braun,T., & Jentsch,S. Role of the proteasome in membrane extraction of a short-lived ER-transmembrane protein. *EMBO J.* **17**, 3251-3257 (1998).
450. Chillaron,J. & Haas,I.G. Dissociation from BiP and retrotranslocation of unassembled immunoglobulin light chains are tightly coupled to proteasome activity. *Mol. Biol Cell* **11**, 217-226 (2000).
451. Dougan,D.A., Mogk,A., Zeth,K., Turgay,K., & Bukau,B. AAA+ proteins and substrate recognition, it all depends on their partner in crime. *FEBS Lett.* **529**, 6-10 (2002).
452. Bao,Y.C., Tsuruga,H., Hirai,M., Yasuda,K., Yokoi,N., Kitamura,T., & Kumagai,H. Identification of a human cDNA sequence which encodes a novel membrane-associated protein containing a zinc metalloprotease motif. *DNA Res.* **10**, 123-128 (2003).
453. Groll,M. & Clausen,T. Molecular shredders: how proteasomes fulfill their role. *Curr. Opin. Struct. Biol* **13**, 665-673 (2003).
454. Clausen,T., Southan,C., & Ehrmann,M. The HtrA family of proteases: implications for protein composition and cell fate. *Mol. Cell* **10**, 443-455 (2002).
455. Maurizi,M.R. Love it or cleave it: tough choices in protein quality control. *Nat. Struct. Biol* **9**, 410-412 (2002).
456. De Luca,A., De Falco,M., Severino,A., Campioni,M., Santini,D., Baldi,F., Paggi,M.G., & Baldi,A. Distribution of the serine protease HtrA1 in normal human tissues. *J. Histochem. Cytochem.* **51**, 1279-1284 (2003).
457. Jones,J.M., Datta,P., Srinivasula,S.M., Ji,W., Gupta,S., Zhang,Z., Davies,E., Hajnoczky,G., Saunders,T.L., Van Keuren,M.L., Fernandes-Alnemri,T., Meisler,M.H., & Alnemri,E.S. Loss of Omi mitochondrial protease activity causes the neuromuscular disorder of mnd2 mutant mice. *Nature* **425**, 721-727 (2003).
458. Antonsson,B. Mitochondria and the Bcl-2 family proteins in apoptosis signaling pathways. *Mol. Cell Biochem.* **256-257**, 141-155 (2004).
459. Kuwana,T. & Newmeyer,D.D. Bcl-2-family proteins and the role of mitochondria in apoptosis. *Curr. Opin. Cell Biol* **15**, 691-699 (2003).
460. Gregersen,N., Bross,P., Andrese,B.S., Pedersen,C.B., Corydon,T.J., & Bolund,L. The role of chaperone-assisted folding and quality control in inborn errors of metabolism: protein folding disorders. *J. Inherit. Metab Dis.* **24**, 189-212 (2001).
461. Rottgers,K., Zufall,N., Guiard,B., & Voos,W. The ClpB homolog Hsp78 is required for the efficient degradation of proteins in the mitochondrial matrix. *J. Biol Chem.* **277**, 45829-45837 (2002).
462. Saijo,T., Welch,W.J., & Tanaka,K. Intramitochondrial folding and assembly of medium-chain acyl-CoA dehydrogenase (MCAD). Demonstration of impaired transfer of K304E-variant MCAD from its complex with hsp60 to the native tetramer. *J. Biol Chem.* **269**, 4401-4408 (1994).
463. Pedersen,C.B., Bross,P., Winter,V.S., Corydon,T.J., Bolund,L., Bartlett,K., Vockley,J., & Gregersen,N. Misfolding, degradation, and aggregation of variant proteins. The molecular pathogenesis of short chain acyl-CoA dehydrogenase (SCAD) deficiency. *J. Biol Chem.* **278**, 47449-47458 (2003).
464. Saijo,T. & Tanaka,K. Isoalloxazine ring of FAD is required for the formation of the core in the Hsp60-assisted folding of medium chain acyl-CoA dehydrogenase subunit into the assembly competent conformation in mitochondria. *J. Biol Chem.* **270**, 1899-1907 (1995).
465. Zhao,Q., Wang,J., Levichkin,I.V., Stasinopoulos,S., Ryan,M.T., & Hoogenraad,N.J. A mitochondrial specific stress response in mammalian cells. *EMBO J.* **21**, 4411-4419 (2002).
466. Martinus,R.D., Garth,G.P., Webster,T.L., Cartwright,P., Naylor,D.J., Hoj,P.B., & Hoogenraad,N.J. Selective induction of mitochondrial chaperones in response to loss of the mitochondrial genome. *Eur. J. Biochem.* **240**, 98-103 (1996).
467. Schwab,A.J., Sebald,W., & Weiss,H. Different pool sizes of the precursor polypeptides of cytochrome oxidase from Neurospora crassa. *Eur. J. Biochem.* **30**, 511-516 (1972).

468. Wielburski,A., Kuzela,S., & Nelson,B.D. Studies on the assembly of cytochrome oxidase in isolated rat hepatocytes. *Biochem. J.* **204**, 239-245 (1982).
469. Wielburski,A. & Nelson,B.D. Evidence for the sequential assembly of cytochrome oxidase subunits in rat liver mitochondria. *Biochem. J.* **212**, 829-834 (1983).
470. Mariottini,P., Chomyn,A., Doolittle,R.F., & Attardi,G. Antibodies against the COOH-terminal undecapeptide of subunit II, but not those against the NH2-terminal decapeptide, immunoprecipitate the whole human cytochrome c oxidase complex. *J. Biol. Chem.* **261**, 3355-3362 (1986).
471. Woodrow,G. & Schatz,G. The role of oxygen in the biosynthesis of cytochrome c oxidase of yeast mitochondria. *J. Biol Chem.* **254**, 6088-6093 (1979).
472. Mason,T.L. & Schatz,G. Cytochrome c oxidase from bakers' yeast. II. Site of translation of the protein components. *J. Biol Chem.* **248**, 1355-1360 (1973).
473. Saltzgaber-Muller,J. & Schatz,G. Heme is necessary for the accumulation and assembly of cytochrome c oxidase subunits in Saccharomyces cerevisiae. *J. Biol Chem.* **253**, 305-310 (1978).
474. Wielburski,A. & Nelson,B.D. Heme a induces assembly of rat liver cytochrome c oxidase subunits I--III in isolated mitochondria. *FEBS Lett.* **177**, 291-294 (1984).
475. Hundt,E., Trapp,M., & Kadenbach,B. Biosynthesis of cytochrome c oxidase in isolated rat hepatocytes. *FEBS Lett.* **115**, 95-99 (1980).
476. Capaldi,R.A. Structure and assembly of cytochrome c oxidase. *Arch. Biochem. Biophys.* **280**, 252-262 (1990).
477. Nijtmans,L.G., Taanman,J.W., Muijsers,A.O., Speijer,D., & Van den Bogert,C. Assembly of cytochrome-c oxidase in cultured human cells. *Eur. J. Biochem.* **254**, 389-394 (1998).
478. Barrientos,A., Korr,D., & Tzagoloff,A. Shy1p is necessary for full expression of mitochondrial COX1 in the yeast model of Leigh's syndrome. *EMBO J.* **21**, 43-52 (2002).
479. Carlson,C.G., Barrientos,A., Tzagoloff,A., & Glerum,D.M. COX16 Encodes a Novel Protein Required for the Assembly of Cytochrome Oxidase in Saccharomyces cerevisiae. *J. Biol. Chem.* **278**, 3770-3775 (2003).
480. Barrientos,A., Zambrano,A., & Tzagoloff,A. Mss51p and Cox14p jointly regulate mitochondrial Cox1p expression in Saccharomyces cerevisiae. *EMBO J.* **23**, 3472-3482 (2004).
481. Hoffbuhr,K.C., Davidson,E., Filiano,B.A., Davidson,M., Kennaway,N.G., & King,M.P. A pathogenic 15-base pair deletion in mitochondrial DNA-encoded cytochrome c oxidase subunit III results in the absence of functional cytochrome c oxidase. *J. Biol. Chem.* **275**, 13994-14003 (2000).
482. Saikumar,P. & Kurup,C.K. Effect of administration of 2-methyl-4-dimethylaminoazobenzene on the half-lives of rat liver mitochondria and cytochrome oxidase. *Biochim. Biophys. Acta* **840**, 127-133 (1985).
483. Nair,N. & Kurup,C.K. Effect of administration of diethylhexyl phthalate on the function and turnover of rat hepatic mitochondria. *Biochim. Biophys. Acta* **925**, 332-340 (1987).
484. Ip,M.M., Chee,P.Y., & Swick,R.W. Turnover of hepatic mitochondrial ornithine aminotransferase and cytochrome oxidase using (14C)carbonate as tracer. *Biochim. Biophys. Acta* **354**, 29-38 (1974).
485. Aschenbrenner,B., Druyan,R., Albin,R., & Rabinowitz,M. Haem a, cytochrome c and total protein turnover in mitochondria from rat heart and liver. *Biochem. J.* **119**, 157-160 (1970).
486. Hare,J.F. & Hodges,R. Turnover of mitochondrial inner membrane proteins in hepatoma monolayer cultures. *J. Biol. Chem.* **257**, 3575-3580 (1982).
487. Ryter,S.W. & Tyrrell,R.M. The heme synthesis and degradation pathways: role in oxidant sensitivity. Heme oxygenase has both pro- and antioxidant properties. *Free Radic. Biol. Med.* **28**, 289-309 (2000).
488. Barrientos,A., Barros,M.H., Valnot,I., Rotig,A., Rustin,P., & Tzagoloff,A. Cytochrome oxidase in health and disease. *Gene* **286**, 53-63 (2002).
489. Tzagoloff,A., Nobrega,M., Gorman,N., & Sinclair,P. On the functions of the yeast COX10 and COX11 gene products. *Biochem. Mol. Biol. Int.* **31**, 593-598 (1993).
490. Glerum,D.M. & Tzagoloff,A. Isolation of a human cDNA for heme A:farnesyltransferase by functional complementation of a yeast cox10 mutant. *Proc. Natl. Acad. Sci. U. S. A* **91**, 8452-8456 (1994).
491. Saiki,K., Mogi,T., Hori,H., Tsubaki,M., & Anraku,Y. Identification of the functional domains in heme O synthase. Site-directed mutagenesis studies on the cyoE gene of the cytochrome bo operon in Escherichia coli. *J. Biol Chem.* **268**, 26927-26934 (1993).
492. Antonicka,H., Leary,S.C., Guercin,G.H., Agar,J.N., Horvath,R., Kennaway,N.G., Harding,C.O., Jaksch,M., & Shoubridge,E.A. Mutations in COX10 result in a defect in mitochondrial heme A biosynthesis and account for multiple, early onset clinical phenotypes associated with isolated COX deficiency. *Hum. Mol. Genet.* (2003).
493. Murakami,T., Reiter,L.T., & Lupski,J.R. Genomic structure and expression of the human heme A:farnesyltransferase (COX10) gene. *Genomics* **42**, 161-164 (1997).

494. Glerum,D.M., Muroff,I., Jin,C., & Tzagoloff,A. COX15 codes for a mitochondrial protein essential for the assembly of yeast cytochrome oxidase. *J. Biol. Chem.* **272**, 19088-19094 (1997).
495. Barros,M.H. & Tzagoloff,A. Regulation of the heme A biosynthetic pathway in Saccharomyces cerevisiae. *FEBS Lett.* **516**, 119-123 (2002).
496. Barros,M.H., Carlson,C.G., Glerum,D.M., & Tzagoloff,A. Involvement of mitochondrial ferredoxin and Cox15p in hydroxylation of heme O. *FEBS Lett.* **492**, 133-138 (2001).
497. Barros,M.H., Nobrega,F.G., & Tzagoloff,A. Mitochondrial ferredoxin is required for heme A synthesis in Saccharomyces cerevisiae. *J. Biol Chem.* **277**, 9997-10002 (2002).
498. Degtyarenko,K.N. & Kulikova,T.A. Evolution of bioinorganic motifs in P450-containing systems. *Biochem. Soc. Trans.* **29**, 139-147 (2001).
499. Muhlenhoff,U. & Lill,R. Biogenesis of iron-sulfur proteins in eukaryotes: a novel task of mitochondria that is inherited from bacteria. *Biochim. Biophys. Acta* **1459**, 370-382 (2000).
500. Lange,H., Kaut,A., Kispal,G., & Lill,R. A mitochondrial ferredoxin is essential for biogenesis of cellular iron-sulfur proteins. *Proc. Natl. Acad. Sci. U. S. A* **97**, 1050-1055 (2000).
501. Brown,K.R., Brown,B.M., Hoagland,E., Mayne,C.L., & Hegg,E.L. Heme A synthase does not incorporate molecular oxygen into the formyl group of heme A. *Biochemistry* **43**, 8616-8624 (2004).
502. Brown,K.R., Allan,B.M., Do,P., & Hegg,E.L. Identification of novel hemes generated by heme A synthase: evidence for two successive monooxygenase reactions. *Biochemistry* **41**, 10906-10913 (2002).
503. Petruzzella,V., Tiranti,V., Fernandez,P., Ianna,P., Carrozzo,R., & Zeviani,M. Identification and characterization of human cDNAs specific to BCS1, PET112, SCO1, COX15, and COX11, five genes involved in the formation and function of the mitochondrial respiratory chain. *Genomics* **54**, 494-504 (1998).
504. Mashkevich,G., Repetto,B., Glerum,D.M., Jin,C., & Tzagoloff,A. SHY1, the yeast homolog of the mammalian SURF-1 gene, encodes a mitochondrial protein required for respiration. *J. Biol. Chem.* **272**, 14356-14364 (1997).
505. Antonicka,H., Mattman,A., Carlson,C.G., Glerum,D.M., Hoffbuhr,K.C., Leary,S.C., Kennaway,N.G., & Shoubridge,E.A. Mutations in COX15 produce a defect in the mitochondrial heme biosynthetic pathway, causing early-onset fatal hypertrophic cardiomyopathy. *Am. J. Hum. Genet.* **72**, 101-114 (2003).
506. Huffman,D.L. & O'Halloran,T.V. Function, structure, and mechanism of intracellular copper trafficking proteins. *Annu. Rev. Biochem.* **70**, 677-701 (2001).
507. Prohaska,J.R. & Gybina,A.A. Intracellular copper transport in mammals. *J. Nutr.* **134**, 1003-1006 (2004).
508. Rae,T.D., Schmidt,P.J., Pufahl,R.A., Culotta,V.C., & O'Halloran,T.V. Undetectable intracellular free copper: the requirement of a copper chaperone for superoxide dismutase. *Science* **284**, 805-808 (1999).
509. Cobine,P.A., Ojeda,L.D., Rigby,K.M., & Winge,D.R. Yeast contain a non-proteinaceous pool of copper in the mitochondrial matrix. *J. Biol Chem.* **279**, 14447-14455 (2004).
510. Beers,J., Glerum,D.M., & Tzagoloff,A. Purification, characterization, and localization of yeast Cox17p, a mitochondrial copper shuttle. *J. Biol. Chem.* **272**, 33191-33196 (1997).
511. Heaton,D.N., George,G.N., Garrison,G., & Winge,D.R. The mitochondrial copper metallochaperone Cox17 exists as an oligomeric, polycopper complex. *Biochemistry* **40**, 743-751 (2001).
512. Heaton,D., Nittis,T., Srinivasan,C., & Winge,D.R. Mutational analysis of the mitochondrial copper metallochaperone Cox17. *J. Biol. Chem.* **275**, 37582-37587 (2000).
513. Maxfield,A.B., Heaton,D.N., & Winge,D.R. Cox17 is functional when tethered to the mitochondrial inner membrane. *J. Biol Chem.* **279**, 5072-5080 (2004).
514. Horng,Y.C., Cobine,P.A., Maxfield,A.B., Carr,H.S., & Winge,D.R. Specific copper transfer from the Cox17 metallochaperone to both Sco1 and Cox11 in the assembly of yeast cytochrome C oxidase. *J. Biol Chem.* **279**, 35334-35340 (2004).
515. Takahashi,Y., Kako,K., Arai,H., Ohishi,T., Inada,Y., Takehara,A., Fukamizu,A., & Munekata,E. Characterization and identification of promoter elements in the mouse COX17 gene. *Biochim. Biophys. Acta* **1574**, 359-364 (2002).
516. Kako,K., Tsumori,K., Ohmasa,Y., Takahashi,Y., & Munekata,E. The expression of Cox17p in rodent tissues and cells. *Eur. J. Biochem.* **267**, 6699-6707 (2000).
517. Paret,C., Ostermann,K., Krause-Buchholz,U., Rentzsch,A., & Rodel,G. Human members of the SCO1 gene family: complementation analysis in yeast and intracellular localization. *FEBS Lett.* **447**, 65-70 (1999).
518. Lode,A., Paret,C., & Rodel,G. Molecular characterization of Saccharomyces cerevisiae Sco2p reveals a high degree of redundancy with Sco1p. *Yeast* **19**, 909-922 (2002).
519. Leary,S.C., Kaufman,B.A., Pellecchia,G., Guercin,G.H., Mattman,A., Jaksch,M., & Shoubridge,E.A. Human SCO1 and SCO2 have independent, cooperative functions in copper delivery to cytochrome c oxidase. *Hum. Mol. Genet.* **13**, 1839-1848 (2004).

520. Nittis,T., George,G.N., & Winge,D.R. Yeast Sco1, a protein essential for cytochrome c oxidase function is a Cu(I)-binding protein. *J. Biol. Chem.* **276**, 42520-42526 (2001).
521. Jaksch,M., Paret,C., Stucka,R., Horn,N., Muller-Hocker,J., Horvath,R., Trepesch,N., Stecker,G., Freisinger,P., Thirion,C., Muller,J., Lunkwitz,R., Rodel,G., Shoubridge,E.A., & Lochmuller,H. Cytochrome c oxidase deficiency due to mutations in SCO2, encoding a mitochondrial copper-binding protein, is rescued by copper in human myoblasts. *Hum. Mol. Genet.* **10**, 3025-3035 (2001).
522. Glerum,D.M., Shtanko,A., & Tzagoloff,A. SCO1 and SCO2 act as high copy suppressors of a mitochondrial copper recruitment defect in Saccharomyces cerevisiae. *J. Biol. Chem.* **271**, 20531-20535 (1996).
523. Papadopoulou,L.C., Sue,C.M., Davidson,M.M., Tanji,K., Nishino,I., Sadlock,J.E., Krishna,S., Walker,W., Selby,J., Glerum,D.M., Coster,R.V., Lyon,G., Scalais,E., Lebel,R., Kaplan,P., Shanske,S., De Vivo,D.C., Bonilla,E., Hirano,M., DiMauro,S., & Schon,E.A. Fatal infantile cardioencephalomyopathy with COX deficiency and mutations in SCO2, a COX assembly gene. *Nat. Genet.* **23**, 333-337 (1999).
524. Lode,A., Kuschel,M., Paret,C., & Rodel,G. Mitochondrial copper metabolism in yeast: interaction between Sco1p and Cox2p. *FEBS Lett.* **485**, 19-24 (2000).
525. Tzagoloff,A., Capitanio,N., Nobrega,M.P., & Gatti,D. Cytochrome oxidase assembly in yeast requires the product of COX11, a homolog of the P. denitrificans protein encoded by ORF3. *EMBO J.* **9**, 2759-2764 (1990).
526. Carr,H.S., George,G.N., & Winge,D.R. Yeast Cox11, a protein essential for cytochrome c oxidase assembly, is a Cu(I)-binding protein. *J. Biol. Chem.* **277**, 31237-31242 (2002).
527. Hiser,L., Di Valentin,M., Hamer,A.G., & Hosler,J.P. Cox11p is required for stable formation of the Cu(B) and magnesium centers of cytochrome c oxidase. *J. Biol. Chem.* **275**, 619-623 (2000).
528. Banci,L., Bertini,I., Cantini,F., Ciofi-Baffoni,S., Gonnelli,L., & Mangani,S. Solution structure of Cox11, a novel type of beta-immunoglobulin-like fold involved in CuB site formation of cytochrome c oxidase. *J. Biol Chem.* **279**, 34833-34839 (2004).
529. Tiranti,V., Galimberti,C., Nijtmans,L., Bovolenta,S., Perini,M.P., & Zeviani,M. Characterization of SURF-1 expression and Surf-1p function in normal and disease conditions. *Hum. Mol. Genet.* **8**, 2533-2540 (1999).
530. Poyau,A., Buchet,K., & Godinot,C. Sequence conservation from human to prokaryotes of Surf1, a protein involved in cytochrome c oxidase assembly, deficient in Leigh syndrome. *FEBS Lett.* **462**, 416-420 (1999).
531. Ikeda,M., Arai,M., Lao,D.M., & Shimizu,T. Transmembrane topology prediction methods: a re-assessment and improvement by a consensus method using a dataset of experimentally-characterized transmembrane topologies. *In Silico. Biol* **2**, 19-33 (2002).
532. Lao,D.M., Arai,M., Ikeda,M., & Shimizu,T. The presence of signal peptide significantly affects transmembrane topology prediction. *Bioinformatics.* **18**, 1562-1566 (2002).
533. Yao,J. & Shoubridge,E.A. Expression and functional analysis of SURF1 in Leigh syndrome patients with cytochrome c oxidase deficiency. *Hum. Mol. Genet.* **8**, 2541-2549 (1999).
534. Von Kleist-Retzow,J.C., Yao,J., Taanman,J.W., Chantrel,K., Chretien,D., Cormier-Daire,V., Rotig,A., Munnich,A., Rustin,P., & Shoubridge,E.A. Mutations in SURF1 are not specifically associated with Leigh syndrome. *J. Med. Genet.* **38**, 109-113 (2001).
535. Tiranti,V., Hoertnagel,K., Carrozzo,R., Galimberti,C., Munaro,M., Granatiero,M., Zelante,L., Gasparini,P., Marzella,R., Rocchi,M., Bayona-Bafaluy,M.P., Enriquez,J.A., Uziel,G., Bertini,E., Dionisi-Vici,C., Franco,B., Meitinger,T., & Zeviani,M. Mutations of SURF-1 in Leigh disease associated with cytochrome c oxidase deficiency. *Am. J. Hum. Genet.* **63**, 1609-1621 (1998).
536. Tiranti,V., Jaksch,M., Hofmann,S., Galimberti,C., Hoertnagel,K., Lulli,L., Freisinger,P., Bindoff,L., Gerbitz,K.D., Comi,G.P., Uziel,G., Zeviani,M., & Meitinger,T. Loss-of-function mutations of SURF-1 are specifically associated with Leigh syndrome with cytochrome c oxidase deficiency. *Ann. Neurol.* **46**, 161-166 (1999).
537. Zhu,Z., Yao,J., Johns,T., Fu,K., De,B., I, Macmillan,C., Cuthbert,A.P., Newbold,R.F., Wang,J., Chevrette,M., Brown,G.K., Brown,R.M., & Shoubridge,E.A. SURF1, encoding a factor involved in the biogenesis of cytochrome c oxidase, is mutated in Leigh syndrome. *Nat. Genet.* **20**, 337-343 (1998).
538. Von Kleist-Retzow,J.C., Vial,E., Chantrel-Groussard,K., Rotig,A., Munnich,A., Rustin,P., & Taanman,J.W. Biochemical, genetic and immunoblot analyses of 17 patients with an isolated cytochrome c oxidase deficiency. *Biochim. Biophys. Acta* **1455**, 35-44 (1999).
539. Agostino,A., Invernizzi,F., Tiveron,C., Fagiolari,G., Prelle,A., Lamantea,E., Giavazzi,A., Battaglia,G., Tatangelo,L., Tiranti,V., & Zeviani,M. Constitutive knockout of Surf1 is associated with high embryonic lethality, mitochondrial disease and cytochrome c oxidase deficiency in mice. *Hum. Mol. Genet.* **12**, 399-413 (2003).
540. Coenen,M.J., Van Den Heuvel,L.P., Nijtmans,L.G., Morava,E., Marquardt,I., Girschick,H.J., Trijbels,F.J., Grivell,L.A., & Smeitink,J.A. SURFEIT-1 gene analysis and two-dimensional blue

native gel electrophoresis in cytochrome c oxidase deficiency. *Biochem. Biophys. Res. Commun.* **265**, 339-344 (1999).

541. Perez-Martinez,X., Broadley,S.A., & Fox,T.D. Mss51p promotes mitochondrial Cox1p synthesis and interacts with newly synthesized Cox1p. *EMBO J.* **22**, 5951-5961 (2003).
542. Poyau,A., Buchet,K., Bouzidi,M.F., Zabot,M.T., Echenne,B., Yao,J., Shoubridge,E.A., & Godinot,C. Missense mutations in SURF1 associated with deficient cytochrome c oxidase assembly in Leigh syndrome patients. *Hum. Genet.* **106**, 194-205 (2000).
543. Duhig,T., Ruhrberg,C., Mor,O., & Fried,M. The human Surfeit locus. *Genomics* **52**, 72-78 (1998).
544. Gaston,K. & Fried,M. YY1 is involved in the regulation of the bi-directional promoter of the Surf-1 and Surf-2 genes. *FEBS Lett.* **347**, 289-294 (1994).
545. Gaston,K. & Fried,M. CpG methylation and the binding of YY1 and ETS proteins to the Surf-1/Surf-2 bidirectional promoter. *Gene* **157**, 257-259 (1995).
546. Gaston,K. & Fried,M. CpG methylation has differential effects on the binding of YY1 and ETS proteins to the bi-directional promoter of the Surf-1 and Surf-2 genes. *Nucleic Acids Res.* **23**, 901-909 (1995).
547. Cole,E.G. & Gaston,K. A functional YY1 binding site is necessary and sufficient to activate Surf-1 promoter activity in response to serum growth factors. *Nucleic Acids Res.* **25**, 3705-3711 (1997).
548. Vernon,E.G. & Gaston,K. Myc and YY1 mediate activation of the Surf-1 promoter in response to serum growth factors. *Biochim. Biophys. Acta* **1492**, 172-179 (2000).
549. Manthey,G.M. & McEwen,J.E. The product of the nuclear gene PET309 is required for translation of mature mRNA and stability or production of intron-containing RNAs derived from the mitochondrial COX1 locus of Saccharomyces cerevisiae. *EMBO J.* **14**, 4031-4043 (1995).
550. Manthey,G.M., Przybyla-Zawislak,B.D., & McEwen,J.E. The Saccharomyces cerevisiae Pet309 protein is embedded in the mitochondrial inner membrane. *Eur. J. Biochem.* **255**, 156-161 (1998).
551. Krause,K., Lopes,D.S., Roberts,D.G., & Dieckmann,C.L. The mitochondrial message-specific mRNA protectors Cbp1 and Pet309 are associated in a high-molecular weight complex. *Mol. Biol Cell* (2004).
552. Naithani,S., Saracco,S.A., Butler,C.A., & Fox,T.D. Interactions among COX1, COX2, and COX3 mRNA-specific Translational Activator Proteins on the Inner Surface of the Mitochondrial Inner Membrane of Saccharomyces cerevisiae. *Mol. Biol. Cell* **14**, 324-333 (2003).
553. Liu,L., Amy,V., Liu,G., & McKeehan,W.L. Novel complex integrating mitochondria and the microtubular cytoskeleton with chromosome remodeling and tumor suppressor RASSF1 deduced by in silico homology analysis, interaction cloning in yeast, and colocalization in cultured cells. *In Vitro Cell Dev. Biol. Anim* **38**, 582-594 (2002).
554. Tsuchiya,N., Fukuda,H., Sugimura,T., Nagao,M., & Nakagama,H. LRP130, a protein containing nine pentatricopeptide repeat motifs, interacts with a single-stranded cytosine-rich sequence of mouse hypervariable minisatellite Pc-1. *Eur. J. Biochem.* **269**, 2927-2933 (2002).
555. Mootha,V.K., Lepage,P., Miller,K., Bunkenborg,J., Reich,M., Hjerrild,M., Delmonte,T., Villeneuve,A., Sladek,R., Xu,F., Mitchell,G.A., Morin,C., Mann,M., Hudson,T.J., Robinson,B., Rioux,J.D., & Lander,E.S. Identification of a gene causing human cytochrome c oxidase deficiency by integrative genomics. *Proc. Natl. Acad. Sci. U. S. A* **100**, 605-610 (2003).
556. Liu,L. & McKeehan,W.L. Sequence analysis of LRPPRC and its SEC1 domain interaction partners suggests roles in cytoskeletal organization, vesicular trafficking, nucleocytosolic shuttling, and chromosome activity. *Genomics* **79**, 124-136 (2002).
557. Wong,E.Y.M., Tse,J.Y.M., Yao,K.-M., Lui,V.C.H., Tam,P.-C., & Yeung,W.S.B. Identification and Characterization of Human VCY2-Interacting Protein: VCY2IP-1, a Microtubule-Associated Protein-Like Protein. *Biol. Reprod.* **70**, 775-784 (2004).
558. Faye,G. & Simon,M. Analysis of a yeast nuclear gene involved in the maturation of mitochondrial pre-messenger RNA of the cytochrome oxidase subunit I. *Cell* **32**, 77-87 (1983).
559. Glerum,D.M., Koerner,T.J., & Tzagoloff,A. Cloning and characterization of COX14, whose product is required for assembly of yeast cytochrome oxidase. *J. Biol. Chem.* **270**, 15585-15590 (1995).
560. Siep,M., van Oosterum,K., Neufeglise,H., van der,S.H., & Grivell,L.A. Mss51p, a putative translational activator of cytochrome c oxidase subunit-1 (COX1) mRNA, is required for synthesis of Cox1p in Saccharomyces cerevisiae. *Curr. Genet.* **37**, 213-220 (2000).
561. Choquet,Y. & Wollman,F.A. Translational regulations as specific traits of chloroplast gene expression. *FEBS Lett.* **529**, 39-42 (2002).
562. Choquet,Y., Stern,D.B., Wostrikoff,K., Kuras,R., Girard-Bascou,J., & Wollman,F.A. Translation of cytochrome f is autoregulated through the 5' untranslated region of petA mRNA in Chlamydomonas chloroplasts. *Proc. Natl. Acad. Sci. U. S. A* **95**, 4380-4385 (1998).
563. Choquet,Y., Wostrikoff,K., Rimbault,B., Zito,F., Girard-Bascou,J., Drapier,D., & Wollman,F.A. Assembly-controlled regulation of chloroplast gene translation. *Biochem. Soc. Trans.* **29**, 421-426 (2001).

564. Kuras,R. & Wollman,F.A. The assembly of cytochrome b6/f complexes: an approach using genetic transformation of the green alga Chlamydomonas reinhardtii. *EMBO J.* **13**, 1019-1027 (1994).
565. Choquet,Y. & Vallon,O. Synthesis, assembly and degradation of thylakoid membrane proteins. *Biochimie* **82**, 615-634 (2000).
566. Choquet,Y., Zito,F., Wostrikoff,K., & Wollman,F.A. Cytochrome f translation in Chlamydomonas chloroplast is autoregulated by its carboxyl-terminal domain. *Plant Cell* **15**, 1443-1454 (2003).
567. Stroebel,D., Choquet,Y., Popot,J.L., & Picot,D. An atypical haem in the cytochrome b(6)f complex. *Nature* **426**, 413-418 (2003).
568. Lodish,H., Berk,A., Zipursky,S.L., Matsudaira,P., Baltimore,D., & Darnell,J.E. in Molecular Cell Biology, Edn. 4th 101-137 (W.H. Freeman and Company, New York; 2000).
569. Nicholls,D.G. & Ferguson S.J. Bioenergetics 3. (Academic Press, Amsterdam London New York; 2002).
570. Gumpel,N.J., Ralley,L., Girard-Bascou,J., Wollman,F.A., Nugent,J.H., & Purton,S. Nuclear mutants of Chlamydomonas reinhardtii defective in the biogenesis of the cytochrome b6f complex. *Plant Mol. Biol.* **29**, 921-932 (1995).
571. Wostrikoff,K., Choquet,Y., Wollman,F.A., & Girard-Bascou,J. TCA1, a single nuclear-encoded translational activator specific for petA mRNA in Chlamydomonas reinhardtii chloroplast. *Genetics* **159**, 119-132 (2001).
572. Hart,P.E., De Vivo,D.C., & Schapira,A.H. in Mitochondria Disorders in Neurology 2, Edn. 2nd. eds. Schapira,A.H. & DiMauro,S. 35-68 (Butterworth Heinmann, Boston; 2002).
573. Schon,E.A., Hirano,M., & DiMauro,S. in Mitochondria Disorders in Neurology 2, Edn. 2nd. eds. Schapira,A.H. & DiMauro,S. 69-113 (Butterworth Heinmann, Boston; 2002).
574. Caruso,U., Adami,A., Bertini,E., Burlina,A.B., Carnevale,F., Cerone,R., Dionisi-Vici,C., Giordano,G., Leuzzi,E., Parenti,G., Savasta,S., Uziel,G., & Zeviani,M. Respiratory-chain and pyruvate metabolism defects: Italian collaborative survey on 72 patients. *J. Inherit. Metab Dis.* **19**, 143-148 (1996).
575. Darin,N., Oldfors,A., Moslemi,A.R., Holme,E., & Tulinius,M. The incidence of mitochondrial encephalomyopathies in childhood: clinical features and morphological, biochemical, and DNA anbormalities. *Ann. Neurol.* **49**, 377-383 (2001).
576. Von Kleist-Retzow,J.C., Cormier-Daire,V., de Lonlay,P., Parfait,B., Chretien,D., Rustin,P., Feingold,J., Rotig,A., & Munnich,A. A high rate (20%-30%) of parental consanguinity in cytochrome-oxidase deficiency. *Am. J. Hum. Genet.* **63**, 428-435 (1998).
577. Robinson,B.H. Human cytochrome oxidase deficiency. *Pediatr. Res.* **48**, 581-585 (2000).
578. Shoubridge,E.A. Cytochrome c oxidase deficiency. *Am. J. Med. Genet.* **106**, 46-52 (2001).
579. Agostino,A., Valletta,L., Chinnery,P.F., Ferrari,G., Carrara,F., Taylor,R.W., Schaefer,A.M., Turnbull,D.M., Tiranti,V., & Zeviani,M. Mutations of ANT1, Twinkle, and POLG1 in sporadic progressive external ophthalmoplegia (PEO). *Neurology* **60**, 1354-1356 (2003).
580. Kaukonen,J., Juselius,J.K., Tiranti,V., Kyttala,A., Zeviani,M., Comi,G.P., Keranen,S., Peltonen,L., & Suomalainen,A. Role of adenine nucleotide translocator 1 in mtDNA maintenance. *Science* **289**, 782-785 (2000).
581. Van Goethem,G., Dermaut,B., Lofgren,A., Martin,J.J., & Van Broeckhoven,C. Mutation of POLG is associated with progressive external ophthalmoplegia characterized by mtDNA deletions. *Nat. Genet.* **28**, 211-212 (2001).
582. Lamantea,E., Tiranti,V., Bordoni,A., Toscano,A., Bono,F., Servidei,S., Papadimitriou,A., Spelbrink,H., Silvestri,L., Casari,G., Comi,G.P., & Zeviani,M. Mutations of mitochondrial DNA polymerase gammaA are a frequent cause of autosomal dominant or recessive progressive external ophthalmoplegia. *Ann. Neurol.* **52**, 211-219 (2002).
583. Naviaux,R.K. & Nguyen,K.V. POLG mutations associated with Alpers' syndrome and mitochondrial DNA depletion. *Ann. Neurol.* **55**, 706-712 (2004).
584. Nishino,I., Spinazzola,A., & Hirano,M. Thymidine phosphorylase gene mutations in MNGIE, a human mitochondrial disorder. *Science* **283**, 689-692 (1999).
585. Saada,A., Shaag,A., Mandel,H., Nevo,Y., Eriksson,S., & Elpeleg,O. Mutant mitochondrial thymidine kinase in mitochondrial DNA depletion myopathy. *Nature Genetics* **29**, 342-344 (2001).
586. Mandel,H., Szargel,R., Labay,V., Elpeleg,O., Saada,A., Shalata,A., Anbinder,Y., Berkowitz,D., Hartman,C., Barak,M., Eriksson,S., & Cohen,N. The deoxyguanosine kinase gene is mutated in individuals with depleted hepatocerebral mitochondrial DNA. *Nat. Genet.* **29**, 337-341 (2001).
587. Holthofer,H., Ahola,H., Solin,M.L., Wang,S., Palmen,T., Luimula,P., Miettinen,A., & Kerjaschki,D. Nephrin localizes at the podocyte filtration slit area and is characteristically spliced in the human kidney. *Am. J. Pathol.* **155**, 1681-1687 (1999).
588. Solin,M.L., Pitkanen,S., Taanman,J.W., & Holthofer,H. Mitochondrial dysfunction in congenital nephrotic syndrome. *Lab Invest* **80**, 1227-1232 (2000).
589. Valnot,I., Von Kleist-Retzow,J.C., Barrientos,A., Gorbatyuk,M., Taanman,J.W., Mehaye,B., Rustin,P., Tzagoloff,A., Munnich,A., & Rotig,A. A mutation in the human heme

A:farnesyltransferase gene (COX10) causes cytochrome c oxidase deficiency. *Hum. Mol. Genet.* **9**, 1245-1249 (2000).

590. Oquendo,C.E., Antonicka,H., Shoubridge,E.A., Reardon,W., & Brown,G.K. Functional and genetic studies demonstrate that mutation in the COX15 gene can cause Leigh syndrome. *J. Med. Genet.* **41**, 540-544 (2004).
591. Valnot,I., Osmond,S., Gigarel,N., Mehaye,B., Amiel,J., Cormier-Daire,V., Munnich,A., Bonnefont,J.P., Rustin,P., & Rotig,A. Mutations of the SCO1 gene in mitochondrial cytochrome c oxidase deficiency with neonatal-onset hepatic failure and encephalopathy. *Am. J. Hum. Genet.* **67**, 1104-1109 (2000).
592. Jaksch,M., Ogilvie,I., Yao,J., Kortenhaus,G., Bresser,H.G., Gerbitz,K.D., & Shoubridge,E.A. Mutations in SCO2 are associated with a distinct form of hypertrophic cardiomyopathy and cytochrome c oxidase deficiency. *Hum. Mol. Genet.* **9**, 795-801 (2000).
593. Tarnopolsky,M.A., Bourgeois,J.M., Fu,M.H., Kataeva,G., Shah,J., Simon,D.K., Mahoney,D., Johns,D., MacKay,N., & Robinson,B.H. Novel SCO2 mutation (G1521A) presenting as a spinal muscular atrophy type I phenotype. *Am. J. Med. Genet.* **125A**, 310-314 (2004).
594. Salviati,L., Sacconi,S., Rasalan,M.M., Kronn,D.F., Braun,A., Canoll,P., Davidson,M., Shanske,S., Bonilla,E., Hays,A.P., Schon,E.A., & DiMauro,S. Cytochrome c oxidase deficiency due to a novel SCO2 mutation mimics Werdnig-Hoffmann disease. *Arch. Neurol.* **59**, 862-865 (2002).
595. Jaksch,M., Horvath,R., Horn,N., Auer,D.P., Macmillan,C., Peters,J., Gerbitz,K.D., Kraegeloh-Mann,I., Muntau,A., Karcagi,V., Kalmanchey,R., Lochmuller,H., Shoubridge,E.A., & Freisinger,P. Homozygosity (E140K) in SCO2 causes delayed infantile onset of cardiomyopathy and neuropathy. *Neurology* **57**, 1440-1446 (2001).
596. Pequignot,M.O., Dey,R., Zeviani,M., Tiranti,V., Godinot,C., Poyau,A., Sue,C., Di Mauro,S., Abitbol,M., & Marsac,C. Mutations in the SURF1 gene associated with Leigh syndrome and cytochrome C oxidase deficiency. *Hum. Mutat.* **17**, 374-381 (2001).
597. Rahman,S., Lake,B.D., Taanman,J.W., Hanna,M.G., Cooper,J.M., Schapira,A.H., & Leonard,J.V. Cytochrome oxidase immunohistochemistry: clues for genetic mechanisms. *Brain* **123 Pt 3**, 591-600 (2000).
598. Adams,P.L., Lightowlers,R.N., & Turnbull,D.M. Molecular analysis of cytochrome c oxidase deficiency in Leigh's syndrome. *Ann. Neurol.* **41**, 268-270 (1997).
599. Jaksch,M., Hofmann,S., Kleinle,S., Liechti-Gallati,S., Pongratz,D.E., Muller-Hocker,J., Jedele,K.B., Meitinger,T., & Gerbitz,K.D. A systematic mutation screen of 10 nuclear and 25 mitochondrial candidate genes in 21 patients with cytochrome c oxidase (COX) deficiency shows tRNA(Ser)(UCN) mutations in a subgroup with syndromal encephalopathy. *J. Med. Genet.* **35**, 895-900 (1998).
600. Chinnery,P.F., Thorburn,D.R., Samuels,D.C., White,S.L., Dahl,H.M., Turnbull,D.M., Lightowlers,R.N., & Howell,N. The inheritance of mitochondrial DNA heteroplasmy: random drift, selection or both? *Trends Genet.* **16**, 500-505 (2000).
601. Chinnery,P.F. Inheritance of mitochondrial disorders. *Mitochondrion* **2**, 149-155 (2002).
602. Bodnar,A.G., Cooper,J.M., Holt,I.J., Leonard,J.V., & Schapira,A.H. Nuclear complementation restores mtDNA levels in cultured cells from a patient with mtDNA depletion. *Am. J. Hum. Genet.* **53**, 663-669 (1993).
603. Jacobs,H.T. Disorders of mitochondrial protein synthesis. *Hum. Mol. Genet.* **12 Spec No 2**, R293-R301 (2003).
604. Jacobs,H.T. in Genetics of Mitochondrial Diseases, Edn. 1. ed. Holt,I.J. 125-144 (Oxford University Press, Oxford; 2003).
605. Rossmanith,W. & Karwan,R.M. Impairment of tRNA processing by point mutations in mitochondrial tRNA(Leu)(UUR) associated with mitochondrial diseases. *FEBS Lett.* **433**, 269-274 (1998).
606. Yasukawa,T., Suzuki,T., Ohta,S., & Watanabe,K. Wobble modification defect suppresses translational activity of tRNAs with MERRF and MELAS mutations. *Mitochondrion* **2**, 129-141 (2002).
607. Yasukawa,T., Suzuki,T., Ueda,T., Ohta,S., & Watanabe,K. Modification defect at anticodon wobble nucleotide of mitochondrial tRNAs(Leu)(UUR) with pathogenic mutations of mitochondrial myopathy, encephalopathy, lactic acidosis, and stroke-like episodes. *J. Biol. Chem.* **275**, 4251-4257 (2000).
608. Karadimas,C.L., Greenstein,P., Sue,C.M., Joseph,J.T., Tanji,K., Haller,R.G., Taivassalo,T., Davidson,M.M., Shanske,S., Bonilla,E., & DiMauro,S. Recurrent myoglobinuria due to a nonsense mutation in the COX I gene of mitochondrial DNA. *Neurology* **55**, 644-649 (2000).
609. Comi,G.P., Bordoni,A., Salani,S., Franceschina,L., Sciacco,M., Prelle,A., Fortunato,F., Zeviani,M., Napoli,L., Bresolin,N., Moggio,M., Ausenda,C.D., Taanman,J.W., & Scarlato,G. Cytochrome c oxidase subunit I microdeletion in a patient with motor neuron disease. *Ann. Neurol.* **43**, 110-116 (1998).

610. Varlamov,D.A., Kudin,A.P., Vielhaber,S., Schroder,R., Sassen,R., Becker,A., Kunz,D., Haug,K., Rebstock,J., Heils,A., Elger,C.E., & Kunz,W.S. Metabolic consequences of a novel missense mutation of the mtDNA CO I gene. *Hum. Mol. Genet.* **11**, 1797-1805 (2002).
611. Gattermann,N., Retzlaff,S., Wang,Y.L., Hofhaus,G., Heinisch,J., Aul,C., & Schneider,W. Heteroplasmic point mutations of mitochondrial DNA affecting subunit I of cytochrome c oxidase in two patients with acquired idiopathic sideroblastic anemia. *Blood* **90**, 4961-4972 (1997).
612. Bruno,C., Martinuzzi,A., Tang,Y., Andreu,A.L., Pallotti,F., Bonilla,E., Shanske,S., Fu,J., Sue,C.M., Angelini,C., DiMauro,S., & Manfredi,G. A stop-codon mutation in the human mtDNA cytochrome c oxidase I gene disrupts the functional structure of complex IV. *Am. J. Hum. Genet.* **65**, 611-620 (1999).
613. Clark,K.M., Taylor,R.W., Johnson,M.A., Chinnery,P.F., Chrzanowska-Lightowlers,Z.M., Andrews,R.M., Nelson,I.P., Wood,N.W., Lamont,P.J., Hanna,M.G., Lightowlers,R.N., & Turnbull,D.M. An mtDNA mutation in the initiation codon of the cytochrome C oxidase subunit II gene results in lower levels of the protein and a mitochondrial encephalomyopathy. *Am. J. Hum. Genet.* **64**, 1330-1339 (1999).
614. Rahman,S., Taanman,J.W., Cooper,J.M., Nelson,I., Hargreaves,I., Meunier,B., Hanna,M.G., Garcia,J.J., Capaldi,R.A., Lake,B.D., Leonard,J.V., & Schapira,A.H. A missense mutation of cytochrome oxidase subunit II causes defective assembly and myopathy. *Am. J. Hum. Genet.* **65**, 1030-1039 (1999).
615. Uusimaa,J., Finnila,S., Vainionpaa,L., Karppa,M., Herva,R., Rantala,H., Hassinen,I.E., & Majamaa,K. A mutation in mitochondrial DNA-encoded cytochrome c oxidase II gene in a child with Alpers-Huttenlocher-like disease. *Pediatrics* **111**, e262-e268 (2003).
616. Horvath,R., Scharfe,C., Hoeltzenbein,M., Do,B.H., Schroder,C., Warzok,R., Vogelgesang,S., Lochmuller,H., Muller-Hocker,J., Gerbitz,K.D., Oefner,P.J., & Jaksch,M. Childhood onset mitochondrial myopathy and lactic acidosis caused by a stop mutation in the mitochondrial cytochrome c oxidase III gene. *J. Med. Genet.* **39**, 812-816 (2002).
617. Horvath,R., Lochmuller,H., Hoeltzenbein,M., Muller-Hocker,J., Schoser,B.G., Pongratz,D., & Jaksch,M. Spontaneous recovery of a childhood onset mitochondrial myopathy caused by a stop mutation in the mitochondrial cytochrome c oxidase III gene. *J. Med. Genet.* **41**, e75 (2004).
618. Keightley,J.A., Hoffbuhr,K.C., Burton,M.D., Salas,V.M., Johnston,W.S., Penn,A.M., Buist,N.R., & Kennaway,N.G. A microdeletion in cytochrome c oxidase (COX) subunit III associated with COX deficiency and recurrent myoglobinuria. *Nat. Genet.* **12**, 410-416 (1996).
619. Tiranti,V., Corona,P., Greco,M., Taanman,J.W., Carrara,F., Lamantea,E., Nijtmans,L., Uziel,G., & Zeviani,M. A novel frameshift mutation of the mtDNA COIII gene leads to impaired assembly of cytochrome c oxidase in a patient affected by Leigh-like syndrome. *Hum. Mol. Genet.* **9**, 2733-2742 (2000).
620. Hanna,M.G., Nelson,I.P., Rahman,S., Lane,R.J., Land,J., Heales,S., Cooper,M.J., Schapira,A.H., Morgan-Hughes,J.A., & Wood,N.W. Cytochrome c oxidase deficiency associated with the first stop-codon point mutation in human mtDNA. *Am. J. Hum. Genet.* **63**, 29-36 (1998).
621. Manfredi,G., Schon,E.A., Moraes,C.T., Bonilla,E., Berry,G.T., Sladky,J.T., & DiMauro,S. A new mutation associated with MELAS is located in a mitochondrial DNA polypeptide-coding gene. *Neuromuscul. Disord.* **5**, 391-398 (1995).
622. Parfait,B., Percheron,A., Chretien,D., Rustin,P., Munnich,A., & Rotig,A. No mitochondrial cytochrome oxidase (COX) gene mutations in 18 cases of COX deficiency. *Hum. Genet.* **101**, 247-250 (1997).
623. Taanman,J.W., Muddle,J.R., & Muntau,A.C. Mitochondrial DNA depletion can be prevented by dGMP and dAMP supplementation in a resting culture of deoxyguanosine kinase-deficient fibroblasts. *Hum. Mol. Genet.* **12**, 1839-1845 (2003).
624. Korhonen,J.A., Gaspari,M., & Falkenberg,M. TWINKLE Has 5' -> 3' DNA helicase activity and is specifically stimulated by mitochondrial single-stranded DNA-binding protein. *J. Biol. Chem.* **278**, 48627-48632 (2003).
625. Koziell,A., Grech,V., Hussain,S., Lee,G., Lenkkeri,U., Tryggvason,K., & Scambler,P. Genotype/phenotype correlations of NPHS1 and NPHS2 mutations in nephrotic syndrome advocate a functional inter-relationship in glomerular filtration. *Hum. Mol. Genet.* **11**, 379-388 (2002).
626. Liu,L., Done,S.C., Khoshnoodi,J., Bertorello,A., Wartiovaara,J., Berggren,P.O., & Tryggvason,K. Defective nephrin trafficking caused by missense mutations in the NPHS1 gene: insight into the mechanisms of congenital nephrotic syndrome. *Hum. Mol. Genet.* **10**, 2637-2644 (2001).
627. Sanders,C.R. & Myers,J.K. Disease-related misassembly of membrane proteins. *Annu. Rev. Biophys. Biomol. Struct.* **33**, 25-51 (2004).
628. Mogi,T., Saiki,K., & Anraku,Y. Biosynthesis and functional role of haem O and haem A. *Mol. Microbiol.* **14**, 391-398 (1994).
629. Foltopoulou,P.F., Zachariadis,G.A., Politou,A.S., Tsiftsoglou,A.S., & Papadopoulou,L.C. Human recombinant mutated forms of the mitochondrial COX assembly Sco2 protein differ from wild-type in physical state and copper binding capacity. *Mol. Genet. Metab* **81**, 225-236 (2004).

630. Merante,F., Petrova-Benedict,R., MacKay,N., Mitchell,G., Lambert,M., Morin,C., De Braekeleer,M., Laframboise,R., Gagne,R., & Robinson,B.H. A biochemically distinct form of cytochrome oxidase (COX) deficiency in the Saguenay-Lac-Saint-Jean region of Quebec. *Am. J. Hum. Genet.* **53**, 481-487 (1993).
631. Morin,C., Mitchell,G., Larochelle,J., Lambert,M., Ogier,H., Robinson,B.H., & De Braekeleer,M. Clinical, metabolic, and genetic aspects of cytochrome C oxidase deficiency in Saguenay-Lac-Saint-Jean. *Am. J. Hum. Genet.* **53**, 488-496 (1993).
632. Hazan,J., Fonknechten,N., Mavel,D., Paternotte,C., Samson,D., Artiguenave,F., Davoine,C.S., Cruaud,C., Durr,A., Wincker,P., Brottier,P., Cattolico,L., Barbe,V., Burgunder,J.M., Prud'homme,J.F., Brice,A., Fontaine,B., Heilig,B., & Weissenbach,J. Spastin, a new AAA protein, is altered in the most frequent form of autosomal dominant spastic paraplegia. *Nat. Genet.* **23**, 296-303 (1999).
633. McDermott,C.J., Taylor,R.W., Hayes,C., Johnson,M., Bushby,K.M., Turnbull,D.M., & Shaw,P.J. Investigation of mitochondrial function in hereditary spastic paraparesis. *Neuroreport* **14**, 485-488 (2003).
634. Hansen,J.J., Durr,A., Cournu-Rebeix,I., Georgopoulos,C., Ang,D., Nielsen,M.N., Davoine,C.S., Brice,A., Fontaine,B., Gregersen,N., & Bross,P. Hereditary spastic paraplegia SPG13 is associated with a mutation in the gene encoding the mitochondrial chaperonin Hsp60. *Am. J. Hum. Genet.* **70**, 1328-1332 (2002).
635. Koehler,C.M., Leuenberger,D., Merchant,S., Renold,A., Junne,T., & Schatz,G. Human deafness dystonia syndrome is a mitochondrial disease. *Proc. Natl. Acad. Sci. U. S. A* **96**, 2141-2146 (1999).
636. Tranebjaerg,L., Hamel,B.C., Gabreels,F.J., Renier,W.O., & Van Ghelue,M. A de novo missense mutation in a critical domain of the X-linked DDP gene causes the typical deafness-dystonia-optic atrophy syndrome. *Eur. J. Hum. Genet.* **8**, 464-467 (2000).
637. Rothbauer,U., Hofmann,S., Muhlenbein,N., Paschen,S.A., Gerbitz,K.D., Neupert,W., Brunner,M., & Bauer,M.F. Role of the deafness dystonia peptide 1 (DDP1) in import of human Tim23 into the inner membrane of mitochondria. *J. Biol Chem.* **276**, 37327-37334 (2001).
638. Rahman,S., Blok,R.B., Dahl,H.H., Danks,D.M., Kirby,D.M., Chow,C.W., Christodoulou,J., & Thorburn,D.R. Leigh syndrome: clinical features and biochemical and DNA abnormalities. *Ann. Neurol.* **39**, 343-351 (1996).
639. Morris,A.A., Leonard,J.V., Brown,G.K., Bidouki,S.K., Bindoff,L.A., Woodward,C.E., Harding,A.E., Lake,B.D., Harding,B.N., Farrell,M.A., Bell,J.E., Mirakhur,M., & Turnbull,D.M. Deficiency of respiratory chain complex I is a common cause of Leigh disease. *Ann. Neurol.* **40**, 25-30 (1996).
640. Pulkes,T. & Hanna,M.G. Human mitochondrial DNA diseases. *Adv. Drug Deliv. Rev.* **49**, 27-43 (2001).
641. Wallace,D.C. Mitochondrial diseases in man and mouse. *Science* **283**, 1482-1488 (1999).
642. Loeffen,J., Smeitink,J., Triepels,R., Smeets,R., Schuelke,M., Sengers,R., Trijbels,F., Hamel,B., Mullaart,R., & Van den Heuvel,L.P. The first nuclear-encoded complex I mutation in a patient with Leigh syndrome. *Am. J. Hum. Genet.* **63**, 1598-1608 (1998).
643. Triepels,R.H., Van Den Heuvel,L.P., Loeffen,J.L., Buskens,C.A., Smeets,R.J., Rubio Gozalbo,M.E., Budde,S.M., Mariman,E.C., Wijburg,F.A., Barth,P.G., Trijbels,J.M., & Smeitink,J.A. Leigh syndrome associated with a mutation in the NDUFS7 (PSST) nuclear encoded subunit of complex I. *Ann. Neurol.* **45**, 787-790 (1999).
644. Bourgeron,T., Rustin,P., Chretien,D., Birch-Machin,M., Bourgeois,M., Viegas-Pequignot,E., Munnich,A., & Rotig,A. Mutation of a nuclear succinate dehydrogenase gene results in mitochondrial respiratory chain deficiency. *Nat. Genet.* **11**, 144-149 (1995).
645. Parfait,B., Chretien,D., Rotig,A., Marsac,C., Munnich,A., & Rustin,P. Compound heterozygous mutations in the flavoprotein gene of the respiratory chain complex II in a patient with Leigh syndrome. *Hum. Genet.* **106**, 236-243 (2000).
646. Chinnery,P.F., Johnson,M.A., Wardell,T.M., Singh-Kler,R., Hayes,C., Brown,D.T., Taylor,R.W., Bindoff,L.A., & Turnbull,D.M. The epidemiology of pathogenic mitochondrial DNA mutations. *Ann. Neurol.* **48**, 188-193 (2000).
647. Herrnstadt,C., Elson,J.L., Fahy,E., Preston,G., Turnbull,D.M., Anderson,C., Ghosh,S.S., Olefsky,J.M., Beal,M.F., Davis,R.E., & Howell,N. Reduced-median-network analysis of complete mitochondrial DNA coding-region sequences for the major African, Asian, and European haplogroups. *Am. J. Hum. Genet.* **70**, 1152-1171 (2002).
648. Sue,C.M., Bruno,C., Andreu,A.L., Cargan,A., Mendell,J.R., Tsao,C.Y., Luquette,M., Paolicchi,J., Shanske,S., DiMauro,S., & De Vivo,D.C. Infantile encephalopathy associated with the MELAS A3243G mutation. *J. Pediatr.* **134**, 696-700 (1999).
649. Santorelli,F.M., Tanji,K., Shanske,S., Krishna,S., Schmidt,R.E., Greenwood,R.S., DiMauro,S., & De Vivo,D.C. The mitochondrial DNA A8344G mutation in Leigh syndrome revealed by analysis in paraffin-embedded sections: revisiting the past. *Ann. Neurol.* **44**, 962-964 (1998).

650. Silvestri,G., Ciafaloni,E., Santorelli,F.M., Shanske,S., Servidei,S., Graf,W.D., Sumi,M., & DiMauro,S. Clinical features associated with the A-->G transition at nucleotide 8344 of mtDNA ("MERRF mutation"). *Neurology* **43**, 1200-1206 (1993).
651. Makino,M., Horai,S., Goto,Y., & Nonaka,I. Mitochondrial DNA mutations in Leigh syndrome and their phylogenetic implications. *J. Hum. Genet.* **45**, 69-75 (2000).
652. Pecina,P., Houstkova,H., Hansikova,H., Zeman,J., & Houstek,J. Genetic defects of cytochrome c oxidase assembly. *Physiol Res.* **53 Suppl 1**, S213-S223 (2004).
653. Salviati,L., Freehauf,C., Sacconi,S., DiMauro,S., Thoma,J., & Tsai,A.C. Novel SURF1 mutation in a child with subacute encephalopathy and without the radiological features of Leigh Syndrome. *Am. J. Med. Genet.* **128A**, 195-198 (2004).
654. Das,A.M., Schweitzer-Krantz,S., Byrd,D.J., & Brodehl,J. Absence of cytochrome c oxidase activity in a boy with dysfunction of renal tubules, brain and muscle. *Eur. J. Pediatr.* **153**, 267-270 (1994).
655. Ogier,H., Lombes,A., Scholte,H.R., Poll-The BT, Fardeau,M., Alcardi,J., Vignes,B., Niaudet,P., & Saudubray,J.M. de Toni-Fanconi-Debre syndrome with Leigh syndrome revealing severe muscle cytochrome c oxidase deficiency. *J. Pediatr.* **112**, 734-739 (1988).
656. Lonlay-Debeney,P., Von Kleist-Retzow,J.C., Hertz-Pannier,L., Peudenier,S., Cormier-Daire,V., Berquin,P., Chretien,D., Rotig,A., Saudubray,J.M., Baraton,J., Brunelle,F., Rustin,P., Van Der,K.M., & Munnich,A. Cerebral white matter disease in children may be caused by mitochondrial respiratory chain deficiency. *J. Pediatr.* **136**, 209-214 (2000).
657. Blake,J.C., Taanman,J.W., Morris,A.M., Gray,R.G., Cooper,J.M., McKiernan,P.J., Leonard,J.V., & Schapira,A.H. Mitochondrial DNA depletion syndrome is expressed in amniotic fluid cell cultures. *Am. J. Pathol.* **155**, 67-70 (1999).
658. Xu,S., Vancheeswaran,R., Bou-Gharios,G., O'Hare,M.J., Olsen,I., Abraham,D., & Black,C. Scleroderma-derived human fibroblasts retain abnormal phenotypic and functional characteristics following retroviral transduction with the SV40 tsT antigen. *Exp. Cell Res.* **220**, 407-414 (1995).
659. Cepko,C.L., Roberts,B.E., & Mulligan,R.C. Construction and applications of a highly transmissible murine retrovirus shuttle vector. *Cell* **37**, 1053-1062 (1984).
660. Stamps,A.C., Davies,S.C., Burman,J., & O'Hare,M.J. Analysis of proviral integration in human mammary epithelial cell lines immortalized by retroviral infection with a temperature-sensitive SV40 T-antigen construct. *Int. J. Cancer* **57**, 865-874 (1994).
661. Jat,P.S. & Sharp,P.A. Cell lines established by a temperature-sensitive simian virus 40 large-T-antigen gene are growth restricted at the nonpermissive temperature. *Mol. Cell Biol.* **9**, 1672-1681 (1989).
662. Seligman,A.M., Karnovsky,M.J., Wasserkrug,H.L., & Hanker,J.S. Nondroplet ultrastructural demonstration of cytochrome oxidase activity with a polymerizing osmiophilic reagent, diaminobenzidine (DAB). *J. Cell Biol* **38**, 1-14 (1968).
663. Villani,G. & Attardi,G. In vivo control of respiration by cytochrome c oxidase in wild-type and mitochondrial DNA mutation-carrying human cells. *Proc. Natl. Acad. Sci. U. S. A* **94**, 1166-1171 (1997).
664. Pecina,P., Capkova,M., Chowdhury,S.K., Drahota,Z., Dubot,A., Vojti, skova,A., Hansi, kova,H., Houst'kova,H., Zeman,J., Godinot,C., & Houstek,J. Functional alteration of cytochrome c oxidase by SURF1 mutations in Leigh syndrome. *Biochim. Biophys. Acta* **1639**, 53-63 (2003).
665. Lyon,H. in Cell Biology, A Laboratory Handbook, Vol. 2. ed. Celis,J.E. 239-244 (Academic Press, London; 1994).
666. Brown,S., Colson,A.M., Meunier,B., & Rich,P.R. Rapid screening of cytochromes of respiratory mutants of Saccharomyces cerevisiae. Application to the selection of strains containing novel forms of cytochrome-c oxidase. *Eur. J. Biochem.* **213**, 137-145 (1993).
667. Meunier,B. & Rich,P.R. Quantitation and characterization of cytochrome c oxidase in complex systems. *Anal. Biochem.* **260**, 237-243 (1998).
668. Meunier,B. Site-directed mutations in the mitochondrially encoded subunits I and III of yeast cytochrome oxidase. *Biochem. J.* **354**, 407-412 (2001).
669. Capaldi,R.A., Marusich,M.F., & Taanman,J.W. Mammalian cytochrome-c oxidase: characterization of enzyme and immunological detection of subunits in tissue extracts and whole cells. *Methods Enzymol.* **260**, 117-132 (1995).
670. Taanman,J.W., Bodnar,A.G., Cooper,J.M., Morris,A.A., Clayton,P.T., Leonard,J.V., & Schapira,A.H. Molecular mechanisms in mitochondrial DNA depletion syndrome. *Hum. Mol. Genet.* **6**, 935-942 (1997).
671. Davis,R.E., Miller,S., Herrnstadt,C., Ghosh,S.S., Fahy,E., Shinobu,L.A., Galasko,D., Thal,L.J., Beal,M.F., Howell,N., & Parker,W.D., Jr. Mutations in mitochondrial cytochrome c oxidase genes segregate with late-onset Alzheimer disease. *Proc. Natl. Acad. Sci. U. S. A* **94**, 4526-4531 (1997).
672. Davis, R. E., Miller, S., Herrnstadt, C., Ghosh, S. S., Fahy, E., Shinobu, L. A., Galasko, D., Thal, L. J., Beal, M. F., Howell, N., and Parker, W. D., Jr. Retraction. Proc.Natl.Acad.Sci.U.S.A 95[20], 12069. 2004.

673. Herrnstadt,C., Clevenger,W., Ghosh,S.S., Anderson,C., Fahy,E., Miller,S., Howell,N., & Davis,R.E. A novel mitochondrial DNA-like sequence in the human nuclear genome. *Genomics* **60**, 67-77 (1999).
674. Chomczynski,P. & Sacchi,N. Single-step method of RNA isolation by acid guanidinium thiocyanate-phenol-chloroform extraction. *Anal. Biochem.* **162**, 156-159 (1987).
675. Cheng,S., Higuchi,R., & Stoneking,M. Complete mitochondrial genome amplification. *Nat. Genet.* **7**, 350-351 (1994).
676. Pulkes,T., Liolitsa,D., Nelson,I.P., & Hanna,M.G. Classical mitochondrial phenotypes without mtDNA mutations: the possible role of nuclear genes. *Neurology* **61**, 1144-1147 (2003).
677. Cassio,D. in Cell Biology, A Laboratory Handbook, Vol. 2. ed. Celis,J.E. 422-427 (Academic Press, London; 1994).
678. Wilson,G.N., Hollar,B.A., Waterson,J.R., & Schmickel,R.D. Molecular analysis of cloned human 18S ribosomal DNA segments. *Proc. Natl. Acad. Sci. U. S. A* **75**, 5367-5371 (1978).
679. Henke,W., Herdel,K., Jung,K., Schnorr,D., & Loening,S.A. Betaine improves the PCR amplification of GC-rich DNA sequences. *Nucleic Acids Res.* **25**, 3957-3958 (1997).
680. Bourgeron,T., Chretien,D., Rotig,A., Munnich,A., & Rustin,P. Isolation and characterization of mitochondria from human B lymphoblastoid cell lines. *Biochem. Biophys. Res. Commun.* **186**, 16-23 (1992).
681. Klement,P., Nijtmans,L.G., Van den Bogert,C., & Houstek,J. Analysis of oxidative phosphorylation complexes in cultured human fibroblasts and amniocytes by blue-native-electrophoresis using mitoplasts isolated with the help of digitonin. *Anal. Biochem.* **231**, 218-224 (1995).
682. Schagger,H. Blue-native gels to isolate protein complexes from mitochondria. *Methods Cell Biol.* **65**, 231-244 (2001).
683. Bentlage,H., De Coo,R., ter Laak,H., Sengers,R., Trijbels,F., Ruitenbeek,W., Schlote,W., Pfeiffer,K., Gencic,S., von Jagow,G., & . Human diseases with defects in oxidative phosphorylation. 1. Decreased amounts of assembled oxidative phosphorylation complexes in mitochondrial encephalomyopathies. *Eur. J. Biochem.* **227**, 909-915 (1995).
684. Nijtmans,L.G., Henderson,N.S., & Holt,I.J. Blue Native electrophoresis to study mitochondrial and other protein complexes. *Methods* **26**, 327-334 (2002).
685. Henderson,N.S., Nijtmans,L.G., Lindsay,J.G., Lamantea,E., Zeviani,M., & Holt,I.J. Separation of intact pyruvate dehydrogenase complex using blue native agarose gel electrophoresis. *Electrophoresis* **21**, 2925-2931 (2000).
686. Nijtmans,L.G., Henderson,N.S., Attardi,G., & Holt,I.J. Impaired ATP synthase assembly associated with a mutation in the human ATP synthase subunit 6 gene. *J. Biol. Chem.* **276**, 6755-6762 (2001).
687. Steffens,G.J. & Buse,G. Studies on Cytochrome c Oxidase, I: Purification and Characterisation of the Enzyme from Bovine Heart and Identification of Peptide Chains in the Complex. *Hoppe Seylers. Z. Physiol Chem.* **357**, 1126-1137 (1976).
688. Broker,S., Meunier,B., Rich,P., Gattermann,N., & Hofhaus,G. MtDNA mutations associated with sideroblastic anaemia cause a defect of mitochondrial cytochrome c oxidase. *Eur. J. Biochem.* **258**, 132-138 (1998).
689. Robinson,B.H. Use of fibroblast and lymphoblast cultures for detection of respiratory chain defects. *Methods Enzymol.* **264**, 454-464 (1996).
690. Petrova-Benedict,R., Buncic,J.R., Wallace,D.C., & Robinson,B.H. Selective killing of cells with oxidative defects in galactose medium: a screening test for affected patient fibroblasts. *J. Inherit. Metab Dis.* **15**, 943-944 (1992).
691. Finnila,S., Lehtonen,M.S., & Majamaa,K. Phylogenetic network for European mtDNA. *Am. J. Hum. Genet.* **68**, 1475-1484 (2001).
692. Andrews,R.M., Kubacka,I., Chinnery,P.F., Lightowlers,R.N., Turnbull,D.M., & Howell,N. Reanalysis and revision of the Cambridge reference sequence for human mitochondrial DNA. *Nat. Genet.* **23**, 147 (1999).
693. Ingman,M., Kaessmann,H., Paabo,S., & Gyllensten,U. Mitochondrial genome variation and the origin of modern humans. *Nature* **408**, 708-713 (2000).
694. Taanman,J.W., Herzberg,N.H., De Vries,H., Bolhuis,P.A., & Van den Bogert,C. Steady-state transcript levels of cytochrome c oxidase genes during human myogenesis indicate subunit switching of subunit VIa and co-expression of subunit VIIa isoforms. *Biochim. Biophys. Acta* **1139**, 155-162 (1992).
695. Pertea,M., Lin,X., & Salzberg,S.L. GeneSplicer: a new computational method for splice site prediction. *Nucleic Acids Res.* **29**, 1185-1190 (2001).
696. Hebsgaard,S.M., Korning,P.G., Tolstrup,N., Engelbrecht,J., Rouze,P., & Brunak,S. Splice site prediction in Arabidopsis thaliana pre-mRNA by combining local and global sequence information. *Nucleic Acids Res.* **24**, 3439-3452 (1996).

697. Reese,M.G., Eeckman,F.H., Kulp,D., & Haussler,D. Improved splice site detection in Genie. *J. Comput. Biol.* **4**, 311-323 (1997).
698. DiMauro,S. & Andreu,A.L. Mutations in mtDNA: are we scraping the bottom of the barrel? *Brain Pathol.* **10**, 431-441 (2000).
699. Sternberg,D., Chatzoglou,E., Laforet,P., Fayet,G., Jardel,C., Blondy,P., Fardeau,M., Amselem,S., Eymard,B., & Lombes,A. Mitochondrial DNA transfer RNA gene sequence variations in patients with mitochondrial disorders. *Brain* **124**, 984-994 (2001).
700. Antonicka,H., Floryk,D., Klement,P., Stratilova,L., Hermanska,J., Houstkova,H., Kalous,M., Drahota,Z., Zeman,J., & Houstek,J. Defective kinetics of cytochrome c oxidase and alteration of mitochondrial membrane potential in fibroblasts and cytoplasmic hybrid cells with the mutation for myoclonus epilepsy with ragged-red fibres ('MERRF') at position 8344 nt. *Biochem. J.* **342 Pt 3**, 537-544 (1999).
701. James,A.M., Wei,Y.H., Pang,C.Y., & Murphy,M.P. Altered mitochondrial function in fibroblasts containing MELAS or MERRF mitochondrial DNA mutations. *Biochem. J.* **318 (Pt 2)**, 401-407 (1996).
702. Vazquez-Memije,M.E., Shanske,S., Santorelli,F.M., Kranz-Eble,P., Davidson,E., DeVivo,D.C., & DiMauro,S. Comparative biochemical studies in fibroblasts from patients with different forms of Leigh syndrome. *J. Inherit. Metab Dis.* **19**, 43-50 (1996).
703. Chalmers,R.M., Lamont,P.J., Nelson,I., Ellison,D.W., Thomas,N.H., Harding,A.E., & Hammans,S.R. A mitochondrial DNA tRNA(Val) point mutation associated with adult-onset Leigh syndrome. *Neurology* **49**, 589-592 (1997).
704. Santorelli,F.M., Tanji,K., Sano,M., Shanske,S., El Shahawi,M., Kranz-Eble,P., DiMauro,S., & De Vivo,D.C. Maternally inherited encephalopathy associated with a single-base insertion in the mitochondrial tRNATrp gene. *Ann. Neurol.* **42**, 256-260 (1997).
705. Tulinius,M., Moslemi,A.R., Darin,N., Westerberg,B., Wiklund,L.M., Holme,E., & Oldfors,A. Leigh syndrome with cytochrome-c oxidase deficiency and a single T insertion nt 5537 in the mitochondrial tRNATrp gene. *Neuropediatrics* **34**, 87-91 (2003).
706. Shtilbans,A., Shanske,S., Goodman,S., Sue,C.M., Bruno,C., Johnson,T.L., Lava,N.S., Waheed,N., & DiMauro,S. G8363A mutation in the mitochondrial DNA transfer ribonucleic acidLys gene: another cause of Leigh syndrome. *J. Child Neurol.* **15**, 759-761 (2000).
707. Absalon,M.J., Harding,C.O., Fain,D.R., Li,L., & Mack,K.J. Leigh syndrome in an infant resulting from mitochondrial DNA depletion. *Pediatr. Neurol.* **24**, 60-63 (2001).
708. Morris,A.A., Taanman,J.W., Blake,J., Cooper,J.M., Lake,B.D., Malone,M., Love,S., Clayton,P.T., Leonard,J.V., & Schapira,A.H. Liver failure associated with mitochondrial DNA depletion. *J. Hepatol.* **28**, 556-563 (1998).
709. Santorelli,F.M., Barmada,M.A., Pons,R., Zhang,L.L., & DiMauro,S. Leigh-type neuropathology in Pearson syndrome associated with impaired ATP production and a novel mtDNA deletion. *Neurology* **47**, 1320-1323 (1996).
710. Yamadori,I., Kurose,A., Kobayashi,S., Ohmori,M., & Imai,T. Brain lesions of the Leigh-type distribution associated with a mitochondriopathy of Pearson's syndrome: light and electron microscopic study. *Acta Neuropathol. (Berl)* **84**, 337-341 (1992).
711. Rotig,A., Cormier,V., Koll,F., Mize,C.E., Saudubray,J.M., Veerman,A., Pearson,H.A., & Munnich,A. Site-specific deletions of the mitochondrial genome in the Pearson marrow-pancreas syndrome. *Genomics* **10**, 502-504 (1991).
712. Bene,J., Nadasi,E., Kosztolanyi,G., Mehes,K., & Melegh,B. Congenital cataract as the first symptom of a neuromuscular disease caused by a novel single large-scale mitochondrial DNA deletion. *Eur. J. Hum. Genet.* **11**, 375-379 (2003).
713. Hargreaves,P., Rahman,S., Guthrie,P., Taanman,J.W., Leonard,J.V., Land,J.M., & Heales,S.J. Diagnostic value of succinate ubiquinone reductase activity in the identification of patients with mitochondrial DNA depletion. *J. Inherit. Metab Dis.* **25**, 7-16 (2002).
714. Nijtmans,L.G., Klement,P., Houstek,J., & Van den Bogert,C. Assembly of mitochondrial ATP synthase in cultured human cells: implications for mitochondrial diseases. *Biochim. Biophys. Acta* **1272**, 190-198 (1995).
715. Appleby,R.D., Porteous,W.K., Hughes,G., James,A.M., Shannon,D., Wei,Y.H., & Murphy,M.P. Quantitation and origin of the mitochondrial membrane potential in human cells lacking mitochondrial DNA. *Eur. J. Biochem.* **262**, 108-116 (1999).
716. Sasarman,F., Karpati,G., & Shoubridge,E.A. Nuclear genetic control of mitochondrial translation in skeletal muscle revealed in patients with mitochondrial myopathy. *Hum. Mol. Genet.* **11**, 1669-1681 (2002).
717. Borner,G.V., Zeviani,M., Tiranti,V., Carrara,F., Hoffmann,S., Gerbitz,K.D., Lochmuller,H., Pongratz,D., Klopstock,T., Melberg,A., Holme,E., & Paabo,S. Decreased aminoacylation of mutant tRNAs in MELAS but not in MERRF patients. *Hum. Mol. Genet.* **9**, 467-475 (2000).
718. Florentz,C. Molecular investigations on tRNAs involved in human mitochondrial disorders. *Bioscience Reports* **22**, 81-98 (2002).

719. Morgan-Hughes,J.A. & Hanna,M.G. Mitochondrial encephalomyopathies: the enigma of genotype versus phenotype. *Biochim. Biophys. Acta* **1410**, 125-145 (1999).
720. Hayashi,J., Ohta,S., Kikuchi,A., Takemitsu,M., Goto,Y., & Nonaka,I. Introduction of disease-related mitochondrial DNA deletions into HeLa cells lacking mitochondrial DNA results in mitochondrial dysfunction. *Proc. Natl. Acad. Sci. U. S. A* **88**, 10614-10618 (1991).
721. Prezant,T.R., Agapian,J.V., Bohlman,M.C., Bu,X., Oztas,S., Qiu,W.Q., Arnos,K.S., Cortopassi,G.A., Jaber,L., Rotter,J.I., & . Mitochondrial ribosomal RNA mutation associated with both antibiotic-induced and non-syndromic deafness. *Nat. Genet.* **4**, 289-294 (1993).
722. Torroni,A., Cruciani,F., Rengo,C., Sellitto,D., Lopez-Bigas,N., Rabionet,R., Govea,N., Lopez,D.M., Sarduy,M., Romero,L., Villamar,M., del,C., I, Moreno,F., Estivill,X., & Scozzari,R. The A1555G mutation in the 12S rRNA gene of human mtDNA: recurrent origins and founder events in families affected by sensorineural deafness. *Am. J. Hum. Genet.* **65**, 1349-1358 (1999).
723. Arbustini,E., Diegoli,M., Fasani,R., Grasso,M., Morbini,P., Banchieri,N., Bellini,O., Dal Bello,B., Pilotto,A., Magrini,G., Campana,C., Fortina,P., Gavazzi,A., Narula,J., & Vigano,M. Mitochondrial DNA mutations and mitochondrial abnormalities in dilated cardiomyopathy. *Am. J. Pathol.* **153**, 1501-1510 (1998).
724. Florentz,C. & Sissler,M. Disease-related versus polymorphic mutations in human mitochondrial tRNAs. Where is the difference? *EMBO Rep.* **2**, 481-486 (2001).
725. Helm,M., Brule,H., Friede,D., Giege,R., Putz,D., & Florentz,C. Search for characteristic structural features of mammalian mitochondrial tRNAs. *RNA.* **6**, 1356-1379 (2000).
726. Chomyn,A., Hunkapiller,M.W., & Attardi,G. Alignment of the amino terminal amino acid sequence of human cytochrome c oxidase subunits I and II with the sequence of their putative mRNAs. *Nucleic Acids Res.* **9**, 867-877 (1981).
727. Vilkki,J., Savontaus,M.L., Kalimo,H., & Nikoskelainen,E.K. Mitochondrial DNA polymorphism in Finnish families with Leber's hereditary optic neuroretinopathy. *Hum. Genet.* **82**, 208-212 (1989).
728. Chen,Y.S., Torroni,A., Excoffier,L., Santachiara-Benerecetti,A.S., & Wallace,D.C. Analysis of mtDNA variation in African populations reveals the most ancient of all human continent-specific haplogroups. *Am. J. Hum. Genet.* **57**, 133-149 (1995).
729. Branden,M., Sigurdson,H., Namslauer,A., Gennis,R.B., Adelroth,P., & Brzezinski,P. On the role of the K-proton transfer pathway in cytochrome c oxidase. *Proc. Natl. Acad. Sci. U. S. A* **98**, 5013-5018 (2001).
730. Pawate,A.S., Morgan,J., Namslauer,A., Mills,D., Brzezinski,P., Ferguson-Miller,S., & Gennis,R.B. A mutation in subunit I of cytochrome oxidase from Rhodobacter sphaeroides results in an increase in steady-state activity but completely eliminates proton pumping. *Biochemistry* **41**, 13417-13423 (2002).
731. Zeviani,M., Spinazzola,A., & Carelli,V. Nuclear genes in mitochondrial disorders. *Curr. Opin. Genet. Dev.* **13**, 262-270 (2003).
732. Brown, R. M., Humphreys, C. P. A, Dorricott, H. D., Sage, E. K., Slater, J. H., and Brown, G. K. SURF1 mutations in cytochrome c oxidase deficient Leigh disease: Two prevalent mutations, one with a common genetic origin. 1999. 4th European Meeting on Mitochondrial Pathology (EUROMIT 4). Conference Proceeding
733. Brogna,S. Pre-mRNA processing: insights from nonsense. *Curr. Biol.* **11**, R838-R841 (2001).
734. Schell,T., Kulozik,A.E., & Hentze,M.W. Integration of splicing, transport and translation to achieve mRNA quality control by the nonsense-mediated decay pathway. *Genome Biol.* **3**, REVIEWS1006 (2002).
735. Frischmeyer,P.A. & Dietz,H.C. Nonsense-mediated mRNA decay in health and disease. *Hum. Mol. Genet.* **8**, 1893-1900 (1999).
736. Mendell,J.T. & Dietz,H.C. When the message goes awry: disease-producing mutations that influence mRNA content and performance. *Cell* **107**, 411-414 (2001).
737. Wilkinson,M.F. & Shyu,A.B. RNA surveillance by nuclear scanning? *Nat. Cell Biol.* **4**, E144-E147 (2002).
738. Iborra,F.J., Jackson,D.A., & Cook,P.R. Coupled transcription and translation within nuclei of mammalian cells. *Science* **293**, 1139-1142 (2001).
739. Wang,Z. & Kiledjian,M. Functional link between the mammalian exosome and mRNA decapping. *Cell* **107**, 751-762 (2001).
740. Chen,C.Y. & Shyu,A.B. Rapid deadenylation triggered by a nonsense codon precedes decay of the RNA body in a mammalian cytoplasmic nonsense-mediated decay pathway. *Mol. Cell Biol.* **23**, 4805-4813 (2003).
741. Berget,S.M. Exon recognition in vertebrate splicing. *J. Biol. Chem.* **270**, 2411-2414 (1995).
742. Krawczak,M., Reiss,J., & Cooper,D.N. The mutational spectrum of single base-pair substitutions in mRNA splice junctions of human genes: causes and consequences. *Hum. Genet.* **90**, 41-54 (1992).
743. Nakai,K. & Sakamoto,H. Construction of a novel database containing aberrant splicing mutations of mammalian genes. *Gene* **141**, 171-177 (1994).

744. Cartegni,L., Chew,S.L., & Krainer,A.R. Listening to silence and understanding nonsense: exonic mutations that affect splicing. *Nat. Rev. Genet.* **3**, 285-298 (2002).
745. Head,R.A., Brown,R.M., & Brown,G.K. Diagnostic difficulties with common SURF1 mutations in patients with cytochrome oxidase-deficient Leigh syndrome. *J. Inherit. Metab Dis.* **27**, 57-65 (2004).
746. Pequignot,M.O., Desguerre,I., Dey,R., Tartari,M., Zeviani,M., Agostino,A., Benelli,C., Fouque,F., Prip-Buus,C., Marchant,D., Abitbol,M., & Marsac,C. New splicing-site mutations in the SURF1 gene in Leigh syndrome patients. *J. Biol. Chem.* **276**, 15326-15329 (2001).
747. Dubot,A., Hervouet,E., Mandon,G., Zabot,M.T., & Godinot,C. Pathogenicity of missense mutations in *SURF1* deficiency inducing the Leigh syndrome. Importance in diagnosis. *Mitochondrion* **4**, 41-47 (2004).
748. Orphanides,G. & Reinberg,D. A unified theory of gene expression. *Cell* **108**, 439-451 (2002).
749. Frischmeyer,P.A., van Hoof,A., O'Donnell,K., Guerrerio,A.L., Parker,R., & Dietz,H.C. An mRNA surveillance mechanism that eliminates transcripts lacking termination codons. *Science* **295**, 2258-2261 (2002).
750. Maquat,L.E. Molecular biology. Skiing toward nonstop mRNA decay. *Science* **295**, 2221-2222 (2002).
751. van Hoof,A., Frischmeyer,P.A., Dietz,H.C., & Parker,R. Exosome-mediated recognition and degradation of mRNAs lacking a termination codon. *Science* **295**, 2262-2264 (2002).
752. Lim,L.P. & Burge,C.B. A computational analysis of sequence features involved in recognition of short introns. *Proc. Natl. Acad. Sci. U. S. A* **98**, 11193-11198 (2001).
753. Teraoka,M., Yokoyama,Y., Ninomiya,S., Inoue,C., Yamashita,S., & Seino,Y. Two novel mutations of SURF1 in Leigh syndrome with cytochrome c oxidase deficiency. *Hum. Genet.* **105**, 560-563 (1999).
754. Santoro,L., Carrozzo,R., Malandrini,A., Piemonte,F., Patrono,C., Villanova,M., Tessa,A., Palmeri,S., Bertini,E., & Santorelli,F.M. A novel SURF1 mutation results in Leigh syndrome with peripheral neuropathy caused by cytochrome c oxidase deficiency. *Neuromuscul. Disord.* **10**, 450-453 (2000).
755. Munaro,M., Tiranti,V., Sandona,D., Lamantea,E., Uziel,G., Bisson,R., & Zeviani,M. A single cell complementation class is common to several cases of cytochrome c oxidase-defective Leigh's syndrome. *Human Molecular Genetics* **6**, 221-228 (1997).
756. Tiranti,V., Munaro,M., Sandona,D., Lamantea,E., Rimoldi,M., DiDonato,S., Bisson,R., & Zeviani,M. Nuclear DNA origin of cytochrome c oxidase deficiency in Leigh's syndrome: genetic evidence based on patient's-derived rho degrees transformants. *Hum. Mol. Genet.* **4**, 2017-2023 (1995).
757. Sue,C.M., Karadimas,C., Checcarelli,N., Tanji,K., Papadopoulou,L.C., Pallotti,F., Guo,F.L., Shanske,S., Hirano,M., De Vivo,D.C., Van Coster,R., Kaplan,P., Bonilla,E., & DiMauro,S. Differential features of patients with mutations in two COX assembly genes, SURF-1 and SCO2. *Ann. Neurol.* **47**, 589-595 (2000).
758. Gilkerson,R.W., Margineantu,D.H., Capaldi,R.A., & Selker,J.M. Mitochondrial DNA depletion causes morphological changes in the mitochondrial reticulum of cultured human cells. *FEBS Lett.* **474**, 1-4 (2000).
759. Zhang,Z. & Gerstein,M. The human genome has 49 cytochrome c pseudogenes, including a relic of a primordial gene that still functions in mouse. *Gene* **312**, 61-72 (2003).
760. Dickinson,E.K., Adams,D.L., Schon,E.A., & Glerum,D.M. A human SCO2 mutation helps define the role of Sco1p in the cytochrome oxidase assembly pathway. *J. Biol. Chem.* **275**, 26780-26785 (2000).
761. Punter,F.A. & Glerum,D.M. Mutagenesis reveals a specific role for Cox17p in copper transport to cytochrome oxidase. *J. Biol. Chem.* (2003).
762. Zimmermann,P. & Kadenbach,B. Modified structure and kinetics of cytochrome-c oxidase in fibroblasts from patients with Leigh syndrome. *Biochim. Biophys. Acta* **1180**, 99-106 (1992).
763. Steinmetz,L.M., Scharfe,C., Deutschbauer,A.M., Mokranjac,D., Herman,Z.S., Jones,T., Chu,A.M., Giaever,G., Prokisch,H., Oefner,P.J., & Davis,R.W. Systematic screen for human disease genes in yeast. *Nat. Genet.* **31**, 400-404 (2002).
764. Robinson,B.H., Petrova-Benedict,R., Buncic,J.R., & Wallace,D.C. Nonviability of cells with oxidative defects in galactose medium: a screening test for affected patient fibroblasts. *Biochem. Med. Metab Biol.* **48**, 122-126 (1992).
765. Van den Bogert,C., Spelbrink,J.N., & Dekker,H.L. Relationship between culture conditions and the dependency on mitochondrial function of mammalian cell proliferation. *J. Cell Physiol* **152**, 632-638 (1992).
766. Ullrich,A., Knecht,W., Fries,M., & Loffler,M. Recombinant expression of N-terminal truncated mutants of the membrane bound mouse, rat and human flavoenzyme dihydroorotate dehydrogenase. A versatile tool to rate inhibitor effects? *Eur. J. Biochem.* **268**, 1861-1868 (2001).

767. Loffler,M., Jockel,J., Schuster,G., & Becker,C. Dihydroorotat-ubiquinone oxidoreductase links mitochondria in the biosynthesis of pyrimidine nucleotides. *Mol. Cell Biochem.* **174**, 125-129 (1997).
768. Rawls,J., Knecht,W., Diekert,K., Lill,R., & Loffler,M. Requirements for the mitochondrial import and localization of dihydroorotate dehydrogenase. *Eur. J. Biochem.* **267**, 2079-2087 (2000).
769. Geromel,V., Kadhom,N., Cebalos-Picot,I., Ouari,O., Polidori,A., Munnich,A., Rotig,A., & Rustin,P. Superoxide-induced massive apoptosis in cultured skin fibroblasts harboring the neurogenic ataxia retinitis pigmentosa (NARP) mutation in the ATPase-6 gene of the mitochondrial DNA. *Hum. Mol. Genet.* **10**, 1221-1228 (2001).
770. Wasniewska,M., Karczmarewicz,E., Pronicki,M., Piekutowska-Abramczuk,D., Zablocki,K., Popowska,E., Pronicka,E., & Duszynski,J. Abnormal calcium homeostasis in fibroblasts from patients with Leigh disease. *Biochem. Biophys. Res. Commun.* **283**, 687-693 (2001).
771. Clark,K.M., Brown,T.A., Davidson,M.M., Papadopoulou,L.C., & Clayton,D.A. Differences in nuclear gene expression between cells containing monomer and dimer mitochondrial genomes. *Gene* **286**, 91-104 (2002).
772. Hanson,B.J., Carrozzo,R., Piemonte,F., Tessa,A., Robinson,B.H., & Capaldi,R.A. Cytochrome c oxidase-deficient patients have distinct subunit assembly profiles. *J. Biol. Chem.* **276**, 16296-16301 (2001).
773. Hanson,B.J., Marusich,M.F., & Capaldi,R.A. Antibody-based approaches to diagnosis and characterization of oxidative phosphorylation diseases. *Mitochondrion* **1**, 237-248 (2001).
774. Taanman,J.W., Burton,M.D., Marusich,M.F., Kennaway,N.G., & Capaldi,R.A. Subunit specific monoclonal antibodies show different steady-state levels of various cytochrome-c oxidase subunits in chronic progressive external ophthalmoplegia. *Biochim. Biophys. Acta* **1315**, 199-207 (1996).
775. Schagger,H. Electrophoretic techniques for isolation and quantification of oxidative phosphorylation complexes from human tissues. *Methods Enzymol.* **264**, 555-566 (1996).
776. Antonicka,H., Ogilvie,I., Taivassalo,T., Anitori,R.P., Haller,R.G., Vissing,J., Kennaway,N.G., & Shoubridge,E.A. Identification and characterization of a common set of complex I assembly intermediates in mitochondria from patients with complex I deficiency. *J. Biol. Chem.* (2003).
777. Bullis,B.L. & Lemire,B.D. Isolation and characterization of the Saccharomyces cerevisiae SDH4 gene encoding a membrane anchor subunit of succinate dehydrogenase. *J. Biol Chem.* **269**, 6543-6549 (1994).
778. Robinson,K.M. & Lemire,B.D. Flavinylation of succinate: ubiquinone oxidoreductase from Saccharomyces cerevisiae. *Methods Enzymol.* **260**, 34-51 (1995).
779. Dibrov,E., Fu,S., & Lemire,B.D. The Saccharomyces cerevisiae TCM62 gene encodes a chaperone necessary for the assembly of the mitochondrial succinate dehydrogenase (complex II). *J. Biol. Chem.* **273**, 32042-32048 (1998).
780. Villani,G., Greco,M., Papa,S., & Attardi,G. Low reserve of cytochrome c oxidase capacity in vivo in the respiratory chain of a variety of human cell types. *J. Biol. Chem.* **273**, 31829-31836 (1998).
781. Dowhan,W., Bibus,C.R., & Schatz,G. The cytoplasmically-made subunit IV is necessary for assembly of cytochrome c oxidase in yeast. *EMBO J.* **4**, 179-184 (1985).
782. Schulze,M. & Rodel,G. SCO1, a yeast nuclear gene essential for accumulation of mitochondrial cytochrome c oxidase subunit II. *Mol. Gen. Genet.* **211**, 492-498 (1988).
783. Krummeck,G. & Rodel,G. Yeast SCO1 protein is required for a post-translational step in the accumulation of mitochondrial cytochrome c oxidase subunits I and II. *Curr. Genet.* **18**, 13-15 (1990).
784. Carr,H.S. & Winge,D.R. Assembly of cytochrome c oxidase within the mitochondrion. *Acc. Chem. Res.* **36**, 309-316 (2003).
785. Heinrichs,M. & Schonert,H. Identification of different quaternary structures of beef heart cytochrome-c oxidase by two-dimensional polyacrylamide gel electrophoresis. *FEBS Lett.* **223**, 255-261 (1987).
786. Liu,Y.C., Sowdal,L.H., & Robinson,N.C. Separation and quantitation of cytochrome c oxidase subunits by Mono-Q fast protein liquid chromatography and C18 reverse-phase high-performance liquid chromatography. *Arch. Biochem. Biophys.* **324**, 135-142 (1995).
787. Arnold,I., Pfeiffer,K., Neupert,W., Stuart,R.A., & Schagger,H. Yeast mitochondrial F1F0-ATP synthase exists as a dimer: identification of three dimer-specific subunits. *EMBO J.* **17**, 7170-7178 (1998).
788. Van Coster,R., Smet,J., George,E., De Meirleir,L., Seneca,S., Van Hove,J., Sebire,G., Verhelst,H., De Bleecker,J., Van Vlem,B., Verloo,P., & Leroy,J. Blue native polyacrylamide gel electrophoresis: a powerful tool in diagnosis of oxidative phosphorylation defects. *Pediatr. Res.* **50**, 658-665 (2001).
789. Jung,C., Higgins,C.M., & Xu,Z. Measuring the quantity and activity of mitochondrial electron transport chain complexes in tissues of central nervous system using blue native polyacrylamide gel electrophoresis. *Anal. Biochem.* **286**, 214-223 (2000).

790. Devreese,B., Vanrobaeys,F., Smet,J., Van Beeumen,J., & Van Coster,R. Mass spectrometric identification of mitochondrial oxidative phosphorylation subunits separated by two-dimensional blue-native polyacrylamide gel electrophoresis. *Electrophoresis* **23**, 2525-2533 (2002).
791. Brookes,P.S., Pinner,A., Ramachandran,A., Coward,L., Barnes,S., Kim,H., & Darley-Usmar,V.M. High throughput two-dimensional blue-native electrophoresis: a tool for functional proteomics of mitochondria and signaling complexes. *Proteomics.* **2**, 969-977 (2002).
792. Schagger,H. Respiratory chain supercomplexes. *IUBMB. Life* **52**, 119-128 (2001).
793. Engel,W.D., Michalski,C., & von Jagow,G. Reconstitution of the ubiquinol: cytochrome c reductase from a bc1 subcomplex and the 'Rieske' iron-sulfur protein isolated by a new method. *Eur. J. Biochem.* **132**, 395-407 (1983).
794. Weishaupt,A. & Kadenbach,B. Selective Removal of Subunit-Vib Increases the Activity of Cytochrome-C-Oxidase. *Biochemistry* **31**, 11477-11481 (1992).
795. Sedlak,E. & Robinson,N.C. Phospholipase A(2) digestion of cardiolipin bound to bovine cytochrome c oxidase alters both activity and quaternary structure. *Biochemistry* **38**, 14966-14972 (1999).
796. Taanman,J.W. & Capaldi,R.A. Purification of yeast cytochrome c oxidase with a subunit composition resembling the mammalian enzyme. *J. Biol. Chem.* **267**, 22481-22485 (1992).
797. Taanman,J.W. & Capaldi,R.A. Subunit VIa of yeast cytochrome c oxidase is not necessary for assembly of the enzyme complex but modulates the enzyme activity. Isolation and characterization of the nuclear-coded gene. *J. Biol. Chem.* **268**, 18754-18761 (1993).
798. Chambers,R.C., Dabbagh,K., McAnulty,R.J., Gray,A.J., Blanc-Brude,O.P., & Laurent,G.J. Thrombin stimulates fibroblast procollagen production via proteolytic activation of protease-activated receptor 1. *Biochem. J.* **333 (Pt 1)**, 121-127 (1998).
799. Boenisch,T., Farmilo,A.J., Stead,R.H., Key,M., Welcher,R., Harvey,R., & Atwood,K.N. Immunological Staining Methods. (Dakocytomation, Carpinteria; 2001).
800. Saraste,M., Penttila,T., & Wikstrom,M. Quaternary structure of bovine cytochrome oxidase. *Eur. J. Biochem.* **115**, 261-268 (1981).
801. Puettner,I., Carafoli,E., & Malatesta,F. Spectroscopic and functional properties of subunit III-depleted cytochrome oxidase. *J. Biol. Chem.* **260**, 3719-3723 (1985).
802. Thompson,D.A. & Ferguson-Miller,S. Lipid and subunit III depleted cytochrome c oxidase purified by horse cytochrome c affinity chromatography in lauryl maltoside. *Biochemistry* **22**, 3178-3187 (1983).
803. Hill,B.C. & Robinson,N.C. Cyanide binding to bovine heart cytochrome c oxidase depleted of subunit III by treatment with lauryl maltoside. *J. Biol. Chem.* **261**, 15356-15359 (1986).
804. Nalecz,K.A., Bolli,R., Ludwig,B., & Azzi,A. The role of subunit III in bovine cytochrome c oxidase. Comparison between native, subunit III-depleted and Paracoccus denitrificans enzymes. *Biochim. Biophys. Acta* **808**, 259-272 (1985).
805. Kolarov,J., Kuzela,S., Wielburski,A., & Nelson,B.D. The characterization of mitochondrial translation products in rat liver and rat hepatoma cells. *FEBS Lett.* **126**, 61-65 (1981).
806. Ludwig,B., Downer,N.W., & Capaldi,R.A. Labeling of cytochrome c oxidase with [35S]diazobenzenesulfonate. Orientation of this electron transfer complex in the inner mitochondrial membrane. *Biochemistry* **18**, 1401-1407 (1979).
807. Suarez,M.D., Revzin,A., Narlock,R., Kempner,E.S., Thompson,D.A., & Ferguson-Miller,S. The functional and physical form of mammalian cytochrome c oxidase determined by gel filtration, radiation inactivation, and sedimentation equilibrium analysis. *J. Biol. Chem.* **259**, 13791-13799 (1984).
808. Bratton,M.R., Pressler,M.A., & Hosler,J.P. Suicide inactivation of cytochrome c oxidase: catalytic turnover in the absence of subunit III alters the active site. *Biochemistry* **38**, 16236-16245 (1999).
809. Haltia,T., Semo,N., Arrondo,J.L., Goni,F.M., & Freire,E. Thermodynamic and structural stability of cytochrome c oxidase from Paracoccus denitrificans. *Biochemistry* **33**, 9731-9740 (1994).
810. Bratton,M.R., Hiser,L., Antholine,W.E., Hoganson,C., & Hosler,J.P. Identification of the structural subunits required for formation of the metal centers in subunit I of cytochrome c oxidase of Rhodobacter sphaeroides. *Biochemistry* **39**, 12989-12995 (2000).
811. Haltia,T., Saraste,M., & Wikstrom,M. Subunit III of cytochrome c oxidase is not involved in proton translocation: a site-directed mutagenesis study. *EMBO J.* **10**, 2015-2021 (1991).
812. Haltia,T., Finel,M., Harms,N., Nakari,T., Raitio,M., Wikstrom,M., & Saraste,M. Deletion of the gene for subunit III leads to defective assembly of bacterial cytochrome oxidase. *EMBO J.* **8**, 3571-3579 (1989).
813. Vijayasarathy,C., Damle,S., Lenka,N., & Avadhani,N.G. Tissue variant effects of heme inhibitors on the mouse cytochrome c oxidase gene expression and catalytic activity of the enzyme complex. *Eur. J. Biochem.* **266**, 191-200 (1999).
814. Leary,S.C., Hill,B.C., Lyons,C.N., Carlson,C.G., Michaud,D., Kraft,C.S., Ko,K., Glerum,D.M., & Moyes,C.D. Chronic treatment with azide in situ leads to an irreversible loss of cytochrome c oxidase activity via holoenzyme dissociation. *J. Biol. Chem.* **277**, 11321-11328 (2002).

815. Ugalde,C., Vogel,R., Huijbens,R., Van Den,H.B., Smeitink,J., & Nijtmans,L. Human mitochondrial complex I assembles through the combination of evolutionary conserved modules; a framework to interpret complex I deficiencies. *Hum. Mol. Genet.* (2004).
816. Zara,V., Palmisano,I., Conte,L., & Trumpower,B.L. Further insights into the assembly of the yeast cytochrome bc1 complex based on analysis of single and double deletion mutants lacking supernumerary subunits and cytochrome b. *Eur. J. Biochem.* **271**, 1209-1218 (2004).
817. Johnson,P.R., Swanson,R., Rakhilina,L., & Hochstrasser,M. Degradation signal masking by heterodimerization of MATalpha2 and MATa1 blocks their mutual destruction by the ubiquitin-proteasome pathway. *Cell* **94**, 217-227 (1998).
818. Keller,S.H., Lindstrom,J., Ellisman,M., & Taylor,P. Adjacent basic amino acid residues recognized by the COP I complex and ubiquitination govern endoplasmic reticulum to cell surface trafficking of the nicotinic acetylcholine receptor alpha-Subunit. *J. Biol Chem.* **276**, 18384-18391 (2001).
819. Obin,M., Lee,B.Y., Meinke,G., Bohm,A., Lee,R.H., Gaudet,R., Hopp,J.A., Arshavsky,V.Y., Willardson,B.M., & Taylor,A. Ubiquitylation of the transducin betagamma subunit complex. Regulation by phosducin. *J. Biol Chem.* **277**, 44566-44575 (2002).
820. Branda,S.S. & Isaya,G. Prediction and identification of new natural substrates of the yeast mitochondrial intermediate peptidase. *J. Biol Chem.* **270**, 27366-27373 (1995).
821. Naoe,M., Ohwa,Y., Ishikawa,D., Ohshima,C., Nishikawa,S.I., Yamamoto,H., & Endo,T. Identification of Tim40 that mediates protein sorting to the mitochondrial intermembrane space. *J. Biol Chem.* (2004).
822. Chacinska,A., Pfannschmidt,S., Wiedemann,N., Kozjak,V., Sanjuan Szklarz,L.K., Schulze-Specking,A., Truscott,K.N., Guiard,B., Meisinger,C., & Pfanner,N. Essential role of Mia40 in import and assembly of mitochondrial intermembrane space proteins. *EMBO J.* (2004).
823. Halestrap,A.P. & Brennerb,C. The adenine nucleotide translocase: a central component of the mitochondrial permeability transition pore and key player in cell death. *Curr. Med. Chem.* **10**, 1507-1525 (2003).
824. Ratajczak,T., Ward,B.K., & Minchin,R.F. Immunophilin chaperones in steroid receptor signalling. *Curr. Top. Med. Chem.* **3**, 1348-1357 (2003).
825. Ostareck-Lederer,A., Ostareck,D.H., Standart,N., & Thiele,B.J. Translation of 15-lipoxygenase mRNA is inhibited by a protein that binds to a repeated sequence in the 3' untranslated region. *EMBO J.* **13**, 1476-1481 (1994).
826. Nobrega,M.P., Nobrega,F.G., & Tzagoloff,A. COX10 codes for a protein homologous to the ORF1 product of Paracoccus denitrificans and is required for the synthesis of yeast cytochrome oxidase. *J. Biol. Chem.* **265**, 14220-14226 (1990).
827. Andersson,U. & Scarpulla,R.C. PGC-I-related coactivator, a novel, serum-inducible coactivator of nuclear respiratory factor 1-dependent transcription in mammalian cells. *Molecular and Cellular Biology* **21**, 3738-3749 (2001).
828. Tijsterman,M. & Plasterk,R.H. Dicers at RISC; the mechanism of RNAi. *Cell* **117**, 1-3 (2004).
829. Downward,J. RNA interference. *BMJ* **328**, 1245-1248 (2004).
830. Holen,T. & Mobbs,C.V. Lobotomy of genes: use of RNA interference in neuroscience. *Neuroscience* **126**, 1-7 (2004).
831. Mittal,V. Improving the efficiency of RNA interference in mammals. *Nat. Rev. Genet.* **5**, 355-365 (2004).
832. Werhahn,W. & Braun,H.P. Biochemical dissection of the mitochondrial proteome from Arabidopsis thaliana by three-dimensional gel electrophoresis. *Electrophoresis* **23**, 640-646 (2002).
833. Kuras,R., de Vitry,C., Choquet,Y., Girard-Bascou,J., Culler,D., Buschlen,S., Merchant,S., & Wollman,F.A. Molecular genetic identification of a pathway for heme binding to cytochrome b6. *J. Biol. Chem.* **272**, 32427-32435 (1997).
834. Ostrowski,J. & Bomsztyk,K. Nuclear shift of hnRNP K protein in neoplasms and other states of enhanced cell proliferation. *Br. J. Cancer* **89**, 1493-1501 (2003).
835. Agsteribbe,E., Huckriede,A., Veenhuis,M., Ruiters,M.H., Niezen-Koning,K.E., Skjeldal,O.H., Skullerud,K., Gupta,R.S., Hallberg,R., van Diggelen,O.P., & . A fatal, systemic mitochondrial disease with decreased mitochondrial enzyme activities, abnormal ultrastructure of the mitochondria and deficiency of heat shock protein 60. *Biochem. Biophys. Res. Commun.* **193**, 146-154 (1993).
836. Briones,P., Vilaseca,M.A., Ribes,A., Vernet,A., Lluch,M., Cusi,V., Huckriede,A., & Agsteribbe,E. A new case of multiple mitochondrial enzyme deficiencies with decreased amount of heat shock protein 60. *J. Inherit. Metab Dis.* **20**, 569-577 (1997).
837. Huckriede,A. & Agsteribbe,E. Decreased synthesis and inefficient mitochondrial import of hsp60 in a patient with a mitochondrial encephalomyopathy. *Biochim. Biophys. Acta* **1227**, 200-206 (1994).
838. Rungi,A.A., Primeau,A., Nunes,C.L., Gordon,J.W., Robinson,B.H., & Hood,D.A. Events upstream of mitochondrial protein import limit the oxidative capacity of fibroblasts in multiple mitochondrial disease. *Biochim. Biophys. Acta* **1586**, 146-154 (2002).

839. Huckriede,A., Heikema,A., Sjollema,K., Briones,P., & Agsteribbe,E. Morphology of the mitochondria in heat shock protein 60 deficient fibroblasts from mitochondrial myopathy patients. Effects of stress conditions. *Virchows Arch.* **427**, 159-165 (1995).
840. Kronidou,N.G., Oppliger,W., Bolliger,L., Hannavy,K., Glick,B.S., Schatz,G., & Horst,M. Dynamic interaction between Isp45 and mitochondrial hsp70 in the protein import system of the yeast mitochondrial inner membrane. *Proc. Natl. Acad. Sci. U. S. A* **91**, 12818-12822 (1994).
841. Paumard,P., Vaillier,J., Coulary,B., Schaeffer,J., Soubannier,V., Mueller,D.M., Brethes,D., di Rago,J.P., & Velours,J. The ATP synthase is involved in generating mitochondrial cristae morphology. *EMBO J.* **21**, 221-230 (2002).
842. McQuibban,G.A., Saurya,S., & Freeman,M. Mitochondrial membrane remodelling regulated by a conserved rhomboid protease. *Nature* **423**, 537-541 (2003).
843. Mirabella,M., Di Giovanni,S., Silvestri,G., Tonali,P., & Servidei,S. Apoptosis in mitochondrial encephalomyopathies with mitochondrial DNA mutations: a potential pathogenic mechanism. *Brain* **123 (Pt 1)**, 93-104 (2000).
844. Schlame,M., Rua,D., & Greenberg,M.L. The biosynthesis and functional role of cardiolipin. *Prog. Lipid Res.* **39**, 257-288 (2000).
845. Haines,T.H. & Dencher,N.A. Cardiolipin: a proton trap for oxidative phosphorylation. *FEBS Lett.* **528**, 35-39 (2002).
846. Jiang,F., Ryan,M.T., Schlame,M., Zhao,M., Gu,Z., Klingenberg,M., Pfanner,N., & Greenberg,M.L. Absence of cardiolipin in the crd1 null mutant results in decreased mitochondrial membrane potential and reduced mitochondrial function. *J. Biol. Chem.* **275**, 22387-22394 (2000).
847. Koshkin,V. & Greenberg,M.L. Oxidative phosphorylation in cardiolipin-lacking yeast mitochondria. *Biochem. J.* **347 Pt 3**, 687-691 (2000).
848. Koshkin,V. & Greenberg,M.L. Cardiolipin prevents rate-dependent uncoupling and provides osmotic stability in yeast mitochondria. *Biochem. J.* **364**, 317-322 (2002).
849. de Lonlay,P., Mugnier,C., Sanlaville,D., Chantrel-Groussard,K., Benit,P., Lebon,S., Chretien,D., Kadhom,N., Saker,S., Gyapay,G., Romana,S., Weissenbach,J., Munnich,A., Rustin,P., & Rotig,A. Cell complementation using Genebridge 4 human:rodent hybrids for physical mapping of novel mitochondrial respiratory chain deficiency genes. *Hum. Mol. Genet.* **11**, 3273-3281 (2002).
850. O'Brien,T.W. Evolution of a protein-rich mitochondrial ribosome: implications for human genetic disease. *Gene* **286**, 73-79 (2002).
851. Sylvester,J.E., Fischel-Ghodsian,N., Mougey,E.B., & O'Brien,T.W. Mitochondrial ribosomal proteins: candidate genes for mitochondrial disease. *Genet. Med.* **6**, 73-80 (2004).
852. Turner,G.C. & Varshavsky,A. Detecting and measuring cotranslational protein degradation in vivo. *Science* **289**, 2117-2120 (2000).
853. James,A.M. & Murphy,M.P. in Genetics of Mitochondrial Diseases, Edn. 1. ed. Holt,I.J. 209-228 (Oxford University Press, Oxford; 2003).
854. James,A.M. & Murphy,M.P. How mitochondrial damage affects cell function. *J. Biomed. Sci.* **9**, 475-487 (2002).
855. Lee,H.C., Yin,P.H., Lu,C.Y., Chi,C.W., & Wei,Y.H. Increase of mitochondria and mitochondrial DNA in response to oxidative stress in human cells. *Biochem. J.* **348 Pt 2**, 425-432 (2000).
856. Lee,H.C., Yin,P.H., Chi,C.W., & Wei,Y.H. Increase in mitochondrial mass in human fibroblasts under oxidative stress and during replicative cell senescence. *J. Biomed. Sci.* **9**, 517-526 (2002).
857. Sanger,N., Strohmeier,R., Kaufmann,M., & Kuhl,H. Cell cycle-related expression and ligand binding of peripheral benzodiazepine receptor in human breast cancer cell lines. *Eur. J. Cancer* **36**, 2157-2163 (2000).
858. Butel,J.S. & Lednicky,J.A. Cell and molecular biology of simian virus 40: implications for human infections and disease. *J. Natl. Cancer Inst.* **91**, 119-134 (1999).
859. Tiranti,V., D'Adamo,P., Briem,E., Ferrari,G., Mineri,R., Lamantea,E., Mandel,H., Balestri,P., Garcia-Silva,M.T., Vollmer,B., Rinaldo,P., Hahn,S.H., Leonard,J., Rahman,S., Dionisi-Vici,C., Garavaglia,B., Gasparini,P., & Zeviani,M. Ethylmalonic encephalopathy is caused by mutations in ETHE1, a gene encoding a mitochondrial matrix protein. *Am. J. Hum. Genet.* **74**, 239-252 (2004).
860. Acin-Perez,R., Bayona-Bafaluy,M.P., Fernandez-Silva,P., Moreno-Loshuertos,R., Perez-Martos,A., Bruno,C., Moraes,C.T., & Enriquez,J.A. Respiratory complex III is required to maintain complex I in mammalian mitochondria. *Mol. Cell* **13**, 805-815 (2004).
861. Coenen,M.J., Antonicka,H., Ugalde,C., Sasarman,F., Rossi,R., Heister,J.G., Newbold,R.F., Trijbels,F.J., Van Den Heuvel,L.P., Shoubridge,E.A., & Smeitink,J.A. Mutant mitochondrial elongation factor G1 and combined oxidative phosphorylation deficiency. *N. Engl. J. Med.* **351**, 2080-2086 (2004).
862. Miller,C., Saada,A., Shaul,N., Shabtai,N., Ben Shalom,E., Shaag,A., Hershkovitz,E., & Elpeleg,O. Defective mitochondrial translation caused by a ribosomal protein (MRPS16) mutation. *Ann. Neurol.* **56**, 734-738 (2004).
863. Taanman,J.W. & Capaldi,R.A. Subunit VIa of yeast cytochrome c oxidase is not necessary for assembly of the enzyme complex but modulates the enzyme activity. Isolation and characterization of the nuclear-coded gene. *J. Biol. Chem.* **268**, 18754-18761 (1993).